



Carlos Luís de Oliveira Macedo Serra

Mestre em Engenharia Civil

**Prediction of dam concrete structural properties
based on wet-screened test results and
mesoscale modelling**

Dissertação para obtenção do Grau de Doutor em

Engenharia Civil

Orientador: António Lopes Batista, Professor Associado
Convidado, Universidade Nova de Lisboa

Co-orientador: Nuno Monteiro Azevedo, Investigador Auxiliar,
Laboratório Nacional de Engenharia Civil

Júri

Presidente: Prof. Doutor Fernando Manuel Anjos Henriques

Arguentes: Prof. Doutor Jorge Manuel Vinagre Alfaiate
Prof. Doutor António Manuel Pinho Ramos

Vogais: Doutor José Vieira de Lemos
Prof. Doutor António Lopes Batista
Prof. Doutor Miguel Ângelo Dias Azenha
Prof. Doutor Carlos Manuel Chastre Rodrigues

Carlos Luís de Oliveira Macedo Serra

**Prediction of dam concrete structural properties based
on wet-screened test results and mesoscale modelling**

A elaboração desta tese beneficiou do regime de isenção de propinas, no âmbito do Protocolo de Cooperação existente entre a Faculdade de Ciências e Tecnologia da Universidade Nova de Lisboa e o Laboratório Nacional de Engenharia Civil

Dezembro, 2017

Prediction of dam concrete structural properties based on wet-screened test results and mesoscale modelling

Copyright © Carlos Luís de Oliveira Macedo Serra, Faculdade de Ciências e Tecnologia, Universidade NOVA de Lisboa.

A Faculdade de Ciências e Tecnologia e a Universidade NOVA de Lisboa têm o direito, perpétuo e sem limites geográficos, de arquivar e publicar esta dissertação através de exemplares impressos reproduzidos em papel ou de forma digital, ou por qualquer outro meio conhecido ou que venha a ser inventado, e de a divulgar através de repositórios científicos e de admitir a sua cópia e distribuição com objetivos educacionais ou de investigação, não comerciais, desde que seja dado crédito ao autor e editor.

To my mother.

Acknowledgements

First of all I would like to thank my advisor and Head of the Concrete Dams Department, Dr. António Lopes Batista, and co-advisor, Dr. Nuno Monteiro Azevedo, for their guidance throughout the development of this work. My sincere thanks to Dr. António Lopes Batista for his support and confidence in my decisions, since my early years as an engineer. To Dr. Nuno Monteiro Azevedo goes all my appreciation and admiration for the knowledge, help and understanding during these four years. I also would like to acknowledge the Head of the Monitoring Unit, Dr. António Tavares de Castro, and the members of the Board of Directors of the National Laboratory for Civil Engineering (LNEC), Eng. Carlos Pina, Dr. Maria Alzira Santos and Eng. Maria de Lurdes Antunes, for enabling the available resources at LNEC and granting me the fellowship and the time to carry out this thesis.

My acknowledgements goes to the Coordinator of the Doctoral Programme at the "Faculdade de Ciências e Tecnologia" of the NOVA University of Lisbon (FCT/UNL), Professor Válter Lúcio, to Professor Corneliu Cismasiu and Professor Carlos Chastre Rodrigues for the interactions during the development of the doctoral courses and to the two member of the "Comissão de Acompanhamento de Tese"(CAT), Professor António Pinho Ramos and Professor Jorge Alfaiate, for their feedback and time.

I would like to thank the colleagues at LNEC with which I had scientific and technical collaboration/interaction during the last four years, providing their expertise, knowledge and hard work which were directly or indirectly related to this thesis: Fernando Marques, Dr. João Custódio, Dr. Juan Mata, Dr. Luísa Braga, Manuel Andrade, Dr. Noemi Schclar and Eng. Renato Pereira. Thanks also to: Alexandre Pinheiro, André Cordeiro, Dr. António Bettencourt Ribeiro, Dr. António Santos Silva, António Tavares, Carlos Resende, Dr. Carlos Santos, Daniel Vicente, Eng. David Pereira, Francisco Morganho, Eng. Gil Rosa, Eng. Gustavo Coelho, Hélder Vitória, Hernani Brum, Hugo Soares, João Amante, João Balsinha, Jorge Gião, Dr. Jorge Pereira Gomes, Dr. José Muralha, Dr. José Piteira Gomes, Dr. José Vieira de Lemos, Dr. Laura Caldeira, Dr. Luís Martins, Dr. Luís Oliveira Santos,

Manuel Bernardino, Dr. Manuel Vieira, Maria Teresa Pereira, Paula Miguel, Dr. Paulo Morais, Ricardo Oliveira, Rogério Pereira, Tiago Gomes, Eng. Tiago Henriques, Vitor Fialho. Thanks are also due to the administrative staff of DBB, namely Alexandrina Domingues, Maria de São José Januário, Lucília Marmeleira and Leonor Siragusa for their valuable work and support. Through my personal interaction with LNEC's researchers and technicians it was possible to see their dedication to technological development and recognise the large range of expertise available in this institution.

A special acknowledgement goes to Dr. Ana Fonseca and Dr. Maria João Henriques for providing the access to the "LabImagem" computers and Eloísa Castilho and Ivo Dias's help on the demanding numerical simulations.

I would like to thank also the support of the remaining colleagues and friends from LNEC: Dr. Eliane Portela, Fernando Garcia, Eng. Francisco Borralho, Eng. Hugo Pernet, Hugo Silva, Dr. João Casaca, Eng. João Saraiva, Eng. José Mora Ramos, José Moreira, Dr. Luís Lamas, Eng. Nádia Braz, Dr. Nuno Lima, Eng. Pedro Miranda, Pedro Pavia, Dr. Ricardo Resende, Dr. Romano Câmara, Dr. Sérgio Oliveira; and, particularly, Ana Vasconcelos, André Paixão, Andrea Brito, António Cabaço, Carlos Pereira, Dora Roque, Eloísa Castilho, Fátima Gouveia, Ivo Dias, João Coelho, João Manso, João Reis, João Rico, João Silva, Lourenço Sasseti, Luís Miranda, Margarida Espada, Mariline Candeias, Miguel Rodrigues, Pedro Marcelino, Ricardo Santos and Rute Ramos.

Thanks are due to "Energias de Portugal" (EDP) and "Hidroeléctrica de Cahora Bassa" (HCB) for the permission to publish data relative to the concrete composition and test results.

Finally, my most special gratitude belongs to my mother, father, brothers and friends, who's unconditional encouragement was key to the success of this work. This success is mainly due to a team effort in which my wife, Francisca, and my son, Duarte, played a significant role of keeping my mind focused on what is important and my spirit always uplifted. Thank you!

Abstract

Dam or full-mixed concrete is produced with large aggregates which implies the use of large specimens, heavy laboratory equipment and non-standard embedding monitoring devices. The wet-screened concrete, obtained from the full-mixed concrete by sieving the larger aggregates while the concrete is still fresh, is used to cast smaller specimens and embed standard monitoring devices.

This thesis focuses on the prediction of the structural properties of dam concrete based on wet-screened concrete experimental results, analytical models and detailed particle models in which the mesostructure is represented.

In order to study the effect of wet-screening, an *in situ* experimental setup and a series of laboratory tests were carried out for both dam and wet-screened concretes. Three sets of creep cells were installed in a dam which allowed for the improvement of the experimental setup and the testing procedures, aiming to reduce costs, to facilitate the installation *in situ* and to increase the reliability of the results. The test results revealed the differences between the two types of concrete and the influence of the coarse aggregate on the deformability and strength properties.

Different analytical models based on composite models, on the equivalent age method, on size effect and on the Abrams law were developed to describe the instantaneous and delayed behaviour of concrete using the composition data and to establish a practical relationship between dam and wet-screened concrete behaviour. Similarly, a numerical solution based on the discrete element method applied to particle models was developed to predict the behaviour of dam concrete. A new fast numerical procedure for long-term analysis taking into account the aging viscoelastic behaviour of cementitious material is proposed. Particle models are especially suited for modelling dam concrete since the coarse aggregate structure can be explicitly represented, allowing the study of stress

distribution inside the specimen and the study of complex failure patterns both in tension and compression. For the two types of approaches, the obtained experimental results were used to calibrate the main parameters and to validate the analytical and numerical prediction models.

The experimental results and the development of physically-based models highlighted the particular properties of dam concrete, allowed for a significant contribution to the analysis of concrete instantaneous and delayed behaviour and presented new approaches for the prediction of dam concrete behaviour based on the wet-screened properties.

Keywords: Dam concrete, Wet-screened concrete, Structural properties, Experimental work, Analytical models, Numerical models

Resumo

O betão de barragens ou betão integral é produzido com agregados de grandes dimensões que implicam a utilização de grandes provetes, equipamentos de laboratório de grande capacidade e dispositivos de medição embebidos especiais. O betão crivado, obtido do betão integral através da crivagem dos agregados maiores enquanto o betão ainda está fresco, é utilizado para betonar provetes de menores dimensões e embeber dispositivos de medição de tamanho *standard*.

Esta tese centra-se na previsão das propriedades estruturais do betão integral de barragens com base nos resultados experimentais do betão crivado, considerando modelos analíticos e modelos detalhados de partículas em que a mesoestrutura do betão é representada.

No sentido de estudar o efeito da crivagem, um programa experimental *in situ* e uma série de ensaios de laboratório envolvendo o betão de barragens e o betão crivado foram utilizados neste estudo. Foram instalados três conjuntos de células de fluência numa barragem onde foram introduzidos melhoramentos da instalação experimental e dos procedimentos de ensaio com o objetivo de reduzir custos, facilitar a instalação *in situ* e melhorar a qualidade dos resultados. Os resultados obtidos apresentam as diferenças entre os dois tipos de betão e a influência do agregado grosso nas propriedades de deformabilidade e de resistência.

Diferentes modelos analíticos baseados em modelos compósitos, no método da idade equivalente, na lei de escala e na lei de Abrams foram desenvolvidos para representar o comportamento instantâneo e diferido do betão considerando a sua composição e para encontrar expressões de correlação entre o comportamento do betão de barragens e o betão crivado. Da mesma forma, a solução numérica adoptada nesta tese consiste na utilização de modelos de partículas para a previsão do comportamento do betão de barragens. Um

procedimento numérico foi desenvolvido para análises a longo prazo em que o comportamento viscoelástico com endurecimento é tido em consideração. Os modelos de partículas são particularmente adequados para a modelação do betão de barragens uma vez que a estrutura dos agregados pode ser explicitamente representada, permitindo o estudo da distribuição de tensões no interior do provete e o estudo de modelos de fratura complexos, em tração e em compressão. Nos dois tipos de abordagem, os resultados experimentais foram utilizados para a calibração dos parâmetros e para a validação dos modelos analíticos e numéricos.

Os resultados experimentais e o desenvolvimento de metodologias de previsão com base em fenómenos físicos evidenciou as principais propriedades de deformabilidade e de resistência do betão de barragens ao longo do tempo, contribuiu significativamente para a análise do comportamento instantâneo e diferido do betão e apresentou novas abordagens para a previsão do comportamento do betão de barragens a partir das propriedades do betão crivado.

Palavras-chave: Betão de barragens, Betão crivado, Propriedades estruturais, Trabalho experimental, Modelos analíticos, Modelos numéricos

Contents

List of Figures	xxi
List of Tables	xxxiii
List of Acronyms	xxxvii
List of Symbols	xliii
1 Introduction	1
1.1 Research problem	1
1.2 Objectives and methodology	4
1.3 Numerical and graphical tools used for the development of the thesis	7
1.4 Thesis outline	8
2 Structural properties of hardened dam concrete	11
2.1 Introduction	11
2.2 Concrete material properties	13
2.2.1 General aspects	13
2.2.2 Dam concrete	15
2.3 Concrete structural behaviour	17
2.3.1 General aspects	17
2.3.2 Development of strains and stresses in concrete	19
2.3.3 Deformation properties	25
2.3.4 Strength properties	28
2.3.5 Effect of <i>in situ</i> conditions on hardened dam concrete rheological properties	32
2.3.6 Construction method, casting schedule and concrete types	36
2.3.7 Effect of wet-screening on hardened dam concrete structural properties	41

2.4	Modelling concrete behaviour	54
2.4.1	Analytical models for the prediction of concrete structural properties	54
2.4.2	Discrete models for the study of concrete behaviour considering its mesostructure	59
3	Experimental characterization of the structural properties of dam concrete	69
3.1	Introduction	69
3.2	Properties of dam concrete placed on Portuguese large dams	70
3.2.1	Introductory note	70
3.2.2	Composition and properties	70
3.2.3	Fit of creep test results to the logarithmic creep function	75
3.2.4	Correlation between full-mixed and wet-screened concrete deformability	77
3.3	Case study: Baixo Sabor dam	80
3.3.1	General description of the dam	80
3.3.2	Characterization of the concretes placed in Baixo Sabor dam	80
3.3.3	Composition of each type of prescribed concrete	81
3.3.4	Composition of the concrete placed in the creep cells	85
3.3.5	Maturing conditions of concrete placed <i>in situ</i>	86
3.4	Procedures for the laboratory testing of structural properties of mortar and concrete	88
3.5	Procedures for the <i>in situ</i> testing of deformability properties of concrete	92
3.5.1	Proposed improvements for creep cell installation	92
3.5.2	Creep cell setup used in the case study	95
3.6	Structural properties of the rock used for the aggregates	97
3.7	Structural properties of the mortar and concrete placed in the dam	98
3.7.1	General aspects	98
3.7.2	Laboratory deformability test results	98
3.7.3	<i>In situ</i> deformability test results	103
3.7.4	Laboratory compressive strength test results	107
3.7.5	Laboratory splitting tensile strength test results	111
3.7.6	Correlation between concrete properties	113
3.8	Concluding remarks	117

4	Analytical modelling of the dam concrete structural properties	119
4.1	Introduction	119
4.2	Prediction of dam concrete modulus of elasticity	120
4.2.1	Introductory note	120
4.2.2	Proposed methodology	121
4.2.3	Maturity method application and fit to <i>in situ</i> test results	122
4.2.4	Composite models for the characterization of the elastic properties	125
4.2.5	Prediction of the dam concrete modulus of elasticity based on experimental tests of wet-screened concrete	126
4.3	Prediction of dam concrete creep in compression	130
4.3.1	Introductory note	130
4.3.2	Proposed methodology	130
4.3.3	Prediction model for the concrete creep strains	132
4.3.4	Age-adjusted effective modulus method	135
4.3.5	Composite model for the characterization of the long-term properties	137
4.3.6	Prediction of dam concrete creep strains under compression based on experimental tests of wet-screened concrete	140
4.4	Prediction of dam concrete compressive and splitting tensile strength	148
4.4.1	Introductory note	148
4.4.2	Proposed methodology	148
4.4.3	Conversion of specimen size based on size effect law	149
4.4.4	Abrams law for the prediction of concrete strength	150
4.4.5	Prediction of dam concrete strength based on wet-screened test results	155
4.5	Proposed framework for dam concrete quality control based on analytical models	158
4.6	Concluding remarks	166
5	Numerical modelling of the concrete structural properties using particle models	169
5.1	Introduction	169
5.2	Discrete element method applied to rigid particle	170
5.3	General aspects	170
5.3.1	Force-displacement law	172
5.3.2	Law of motion	176

5.3.3	Stability of the solution in explicit integration schemes	181
5.3.4	Adaptive dynamic relaxation	184
5.3.5	Convergence criteria	185
5.3.6	Micro-macro approximations	185
5.3.7	Energy terms	186
5.4	Random assemblies of concrete	188
5.5	Contact constitutive models for the analysis of long-term behaviour of concrete	189
5.5.1	Hooke's model	189
5.5.2	Numerical formulation of solidification theory	190
5.5.3	Proposed calibration procedure for the macro-micro relationship of elastic and aging viscoelastic properties	193
5.5.4	Proposed fast numerical procedure for long-term analysis using DEM and validation of the aging viscoelastic contact model	196
5.5.5	Validation of the aging viscoelastic contact model using the proposed fast numerical procedure	197
5.6	Analysis of the long-term behaviour of concrete considering its mesostructure	205
5.6.1	Mortar, aggregate and concrete test results and fit to B3 model . .	205
5.6.2	Modelling the instantaneous behaviour of the aggregates and the long-term behaviour of the mortar	207
5.6.3	Modelling the long-term behaviour of the concrete considering the effect of the interfacial transition zone (ITZ)	209
5.7	Contact constitutive models for the analysis of failure behaviour of concrete	217
5.7.1	Mohr-Coulomb model with a tension cut-off (brittle model)	217
5.7.2	Mohr-Coulomb model with softening in tension and shear	218
5.7.3	Validation of Mohr-Coulomb contact models (brittle and softening)	224
5.8	Analysis of the failure behaviour of concrete considering its mesostructure	227
5.8.1	Particle model properties and parametric study	227
5.8.2	Modelling the tensile and compressive instantaneous stress-strain behaviour	234
5.9	Concluding remarks	239

6	Numerical modelling of the dam concrete structural properties using particle models	243
6.1	Introduction	243
6.2	Prediction of dam concrete deformability properties using particle models	245
6.2.1	Particle model definitions	245
6.2.2	Prediction of mortar's creep compliance based on the concrete properties	251
6.2.3	Calibration of micro parameters of the contacts for the aggregates and for the mortar	254
6.2.4	Generation of wet-screened and dam concrete's aggregate structure	256
6.2.5	Influence of the aggregate content and maximum size of aggregate on the behaviour of concrete	259
6.2.6	Influence of temperature on the development of the mechanical properties	262
6.2.7	Prediction of wet-screened concrete long-term deformability properties	264
6.2.8	Prediction of dam concrete long-term deformability properties . .	269
6.2.9	Study of the normal and shear force distribution inside the concrete mesostructure	276
6.3	Prediction of dam concrete strength properties using particle models . . .	281
6.3.1	Correlation between modulus of elasticity and strength results of mortar and aggregate	281
6.3.2	Micro-macro approximations for contact strength	283
6.3.3	Calibration of micro parameters of the contacts for the mortar and aggregates	284
6.3.4	Prediction of wet-screened and dam concrete strength properties .	286
6.4	Concluding remarks	302
7	Conclusions and future developments	305
7.1	Summary and main conclusions	305
7.2	General recommendations and future developments	312
7.3	List of publications during the development of the Ph.D. thesis	317
7.3.1	Technical papers in international journals (with peer review) . . .	317
7.3.2	Technical papers in national journals	317

CONTENTS

7.3.3	International proceedings papers	317
7.3.4	National proceedings papers	318
7.3.5	Technical reports	319
	Bibliography	321
A	Properties of the cement and of the fly ash used in Baixo Sabor dam	353
B	Scientific papers published in national and international journals during the Ph.D.	355
C	C++ computational structure of the 2D particle model for the behaviour analysis	363

List of Figures

1.1	Schematic view of the approach used in this work combining the three main scientific areas: experimental work; analytical modelling; and, numerical modelling	6
2.1	Influencing factors of concrete strength (Mehta and Monteiro 2006)	15
2.2	Representation of stress-strain curve of concrete in compression for a given t' : a) instantaneous loading; b) sustained loading. Adapted from (ICOLD 2008))	20
2.3	Representation of stress-strain-time behaviour of concrete for instantaneous and sustained compressive loading: a) stress-strain behaviour; b) strain-time behaviour; c) stress-time behaviour	22
2.4	Definition of strain components in the strain-time representation	23
2.5	Strain and stress behaviour over time with respect to loading, restraining and curing conditions (Mehta and Monteiro 2006)	24
2.6	Stress-strain behaviour of concrete under compressive and tensile uniaxial stresses and illustration of the cracking development around the coarse aggregates	31
2.7	Comparison between compressive stress-strain curves of rock, cement paste and concrete with several coarse aggregate contents (Coutinho and Gonçalves 1994)	31
2.8	Comparison of creep strain development for standard curing temperature and constant elevated temperatures. Adapted from (Bažant and Kim 1992) . . .	33
2.9	Influence of casting and curing temperature on concrete strength (Mehta and Monteiro 2006)	34
2.10	Influence of curing conditions on strength (USBR 1988)	35
2.11	Effect of <i>in situ</i> conditions on dam concrete properties: a) Compressive strength; b) Modulus of elasticity (ICOLD 2008)	36
2.12	Representation of the types of concrete placed in a cross section of an arch dam	37

2.13 Construction phases and placement of each type of concrete. Example with strainmeter instalation.	38
2.14 Construction phases and placement of each type of concrete. Example with gallery	40
2.15 Effect of wet-screening and size of specimen on the compressive strength of concrete (Blanks and McNamara 1935)	42
2.16 Test results of wet-screened and full-mixed concrete: a) compressive strength; b) modulus of elasticity (Soares de Pinho <i>et al.</i> 1988)	43
2.17 Total specific strains of full-mixed and wet-screened concrete measured <i>in situ</i> and in laboratory (points) and fit to B3 model (grey surface). Adapted from (Soares de Pinho <i>et al.</i> 1988)	44
2.18 Ratios between dam concrete compressive strengths in seal-cured cylinders and wet-screened compressive strengths (USBR 1988)	45
2.19 Effect of aggregate maximum size on cement content. Adapted from (Higginson <i>et al.</i> 1962; ICOLD 2008)	50
2.20 Effect of aggregate maximum size on compressive strength. Adapted from (Higginson <i>et al.</i> 1962; ICOLD 2008)	51
2.21 Effect of maximum size aggregate on concrete strength. Adapted from (Cordon and Gillespie 1963)	51
2.22 Correlation between compressive strength of mortar and concrete. Adapted from (Neville 1983)	52
2.23 Correlation between compressive strength of mortar and concrete. Adapted from (Larrard and Belloc 1997)	53
2.24 Representation of the lattice mesh: a) computer generated aggregate structure; b) detailed properties of each frame (Lilliu and Mier 2003a)	62
2.25 Failure patterns of concrete DEM particle models under compression using uniform and heterogeneous contact properties and circular and polygonal aggregates (Monteiro Azevedo and Vieira de Lemos 2006)	64
2.26 Schematic illustration of the different failure patterns considering different aggregate strength properties (F^{0a}) and ITZ strength properties (F^{0am}) (Piotrowska 2013)	66

3.1	Wet-screened concrete modulus of elasticity results of several dams obtained from laboratory tests	74
3.2	Wet-screened concrete compressive strength results of several dams obtained from laboratory tests	74
3.3	Creep test results: a) full-mixed concrete of Baixo Sabor <i>in situ</i> ; b) full-mixed concrete of Torrão dam <i>in situ</i> ; c) concrete of Crestuma dam, loading at age of 35 days; d) concrete of Fronhas dam, loading at age of 28 days	75
3.4	Representation of the creep strains fitted to laboratory creep test results of wet-screened concrete at the age of 28 days	76
3.5	Correlation between deformability properties of dam and wet-screened concrete with granitic aggregates obtained in laboratory and <i>in situ</i> : a) modulus of elasticity; b) creep coefficient for 1000 days under loading for several loading ages	77
3.6	Correlation between compressive strength properties of dam and wet-screened concrete obtained in laboratory	79
3.7	Baixo Sabor dam during construction in May 2013	80
3.8	Wet-screened concrete contents using different maximum size of aggregate (MSA) ("a" represents the total aggregate, "g" the coarse aggregate, "s" the fine aggregate, "c" the cement, "f" the fly-ash, "b" the binder and "w" the water contents)	83
3.9	Sieve analysis of the Baixo Sabor dam concretes	85
3.10	Sieve analysis of DAM concrete, SCR76 wet-screened concrete and SCR38 wet-screened concrete placed in creep cell CC1 and comparison with the prescribed concretes (Core-DAM, Core-SCR76 and Core-SCR38)	86
3.11	Measured temperatures inside Baixo Sabor dam at several levels of the central block (G39 is a embedded strainmeter, MJ12, MJ88 and MJ129 are embedded jointmeters and CF12 is a strainmeter embedded in a creep cell).	88
3.12	Specimens used for the determination of the compressive and splitting tensile strength and deformability of each type of concrete and of the mortar	91
3.13	Components of an active creep cell (CC-A) by the traditional creep cell design (a)) and by the proposed creep cell design (b))	93
3.14	Creep cell installation	95

3.15	Representation of the active and non-stress creep cells for both full-mixed and wet-screened concrete and placement of creep cells on the dam's body.	96
3.16	Creep cells (CC) dimensions and maximum size aggregate (MSA)	96
3.17	Placement of the strainmeters inside the creep cells	97
3.18	Modulus of elasticity results of dam and wet-screened concretes and for the core and the face concretes obtained in laboratory	100
3.19	Compressive creep test results for the prismatic specimen cast with #38 (SCR38) concrete at the age of 28 days (P #38-CC1)	102
3.20	Experimental compressive creep compliances for the prismatic specimens in laboratory at different loading ages	102
3.21	Stress-strain diagram and modulus of elasticity determination for <i>in situ</i> tests	104
3.22	Compressive creep test results for the creep cell cast with full-mixed concrete at the age of 28 days (DAM-CC1)	106
3.23	Experimental compressive creep compliances for the creep cells at several loading ages	107
3.24	Compressive strength results of DAM and SCR concretes for Core, Face and Reinforcement placements and of mortar	110
3.25	Splitting tensile strength results of DAM and SCR concretes for Core, Face and Reinforcement placements and of mortar	112
3.26	Correlation between the compressive strength obtained in cubes and the compressive strength obtained in cylinders	114
3.27	Correlation between the compressive strength and the modulus of elasticity .	114
3.28	Correlation between the compressive strength and the splitting tensile strength	115
3.29	Correlation between wet-screened and dam concrete properties	116
4.1	Global approach used for the prediction of dam concrete modulus of elasticity in compression	122
4.2	Measured temperature in CC1-150-A and the equivalent age calculated with the maturity method	124
4.3	Logarithmic fit to modulus of elasticity test results obtained <i>in situ</i> and the estimate for reference conditions using maturity method (CC1)	125
4.4	Adapted composite model for wet-screening procedure	127

4.5	Prediction of dam concrete modulus of elasticity development using experimental results of SCR76 wet-screened concrete (composite 1)	129
4.6	Prediction of dam concrete modulus of elasticity development using experimental results of SCR38 wet-screened concrete (composite 2)	130
4.7	Procedure for the validation of the equivalent composite model for dam concrete compressive creep strains	131
4.8	Schematic representation of the composite model: (a) volume of aggregate, V_a , lower than the maximum compactness of aggregate, $V_{a,max}$ considered as a model with a series and parallel portions; b) volume of aggregate, V_a , equal to the maximum compactness of aggregate, $V_{a,max}$ yielding a model with parallel coupling	138
4.9	Compressive creep test results of #38 concrete at several ages and fit to model B3 for elevated constant temperature (<i>in situ</i> conditions) and constant reference temperature conditions	142
4.10	Compressive creep test results of #76 concrete at several ages and fit to model B3 for elevated constant temperature (<i>in situ</i> conditions) and constant reference temperature conditions	143
4.11	Compressive creep test results of dam concrete at several ages and fit to model B3 for elevated constant temperature (<i>in situ</i> conditions) and constant reference temperature conditions	143
4.12	Adapted composite model for wet-screening procedure	144
4.13	Percentage difference between the prediction using the equivalent composite and the experimental results for several values of β	146
4.14	Prediction of full-mixed concrete creep compliance under compression using #76 mm equivalent composite model ($\beta = 0.5$)	146
4.15	Prediction of full-mixed concrete creep compliance under compression using #38 mm equivalent composite model ($\beta = 0.6$)	147
4.16	Prediction of #76 concrete creep compliance under compression using #38 mm equivalent composite model ($\beta = 0.3$)	147
4.17	Schematic view of the proposed methodology for the prediction of the dam concrete strength properties	148
4.18	Size effect laws for the compressive and splitting tensile strengths	150

4.19	Extended Abrams law for the compressive strength at the age of 90 days of Baixo Sabor dam concrete	154
4.20	Extended Abrams law for the splitting tensile strength at the age of 90 days of Baixo Sabor dam concrete	155
4.21	Ratios between full-mixed and wet-screened compressive and splitting tensile strength	157
4.22	Proposed procedure for dam concrete quality control concerning the comparison between dam and wet-screened results	161
4.23	Illustration of the conversion procedure for the deformability properties including the determination of the proportions of wet-screened (SCR) and full-mixed (DAM) concretes and of the composite model parameters	162
4.24	Number and size of specimens for the calibration of the composite model parameter, β^{MSA} and of the extended Abrams law's parameters, A , B and α_d .	162
4.25	Illustration of the conversion procedure for the strength properties including the determination of the the water-cement ratio of wet-screened (SCR) and full-mixed (DAM) concretes, of the Abram's law parameters and of the size effect parameters	163
4.26	Number and size of specimens for the calibration of the size effect law parameters, K_1 and K_2	163
4.27	Number and size of specimens for the determination of the effect of the supplementary cementitious materials	164
4.28	Number and size of specimens for the calibration of the equivalent age method	164
5.1	General DEM cycle	171
5.2	Contact point definition in particle models	172
5.3	Contact point velocity definition in particle models	174
5.4	Incremental linear contact model in particle models	174
5.5	Correction of shear contact force in particle models	175
5.6	Transmission of contact force to particle forces and moments in particle models	176
5.7	Graphical representation of the central difference scheme	179
5.8	Equivalent elastic beam in particle models	186
5.9	Mechanical representation of the elastic model: a) Force-overlap diagram; b) Development of contact forces and overlap over time	189

5.10	DEM cycle with the proposed numerical scheme for viscoelastic behaviour with incremental contact forces	196
5.11	Assemblies for the validation of the aging viscoelastic models	198
5.12	Comparison between the analytical solution of the creep compliance based on the solidification theory, the numerical solution obtained from the fully explicit DEM formulation with damping and the numerical solution using the proposed fast numerical procedure and three different time discretizations	200
5.13	Contact force development for the numerical solution obtained from the original DEM formulation using the adaptive dynamic relaxation method (ADR) for the instantaneous deformation and the aging viscoelastic constitutive model for the delayed deformation and the numerical solution using the numerical incremental procedure for creep model applied to the solidification theory . .	201
5.14	Comparison between the solidification theory analytical solution, the fully explicit DEM formulation with ADR and the proposed fast numerical procedure considering three time internals (N=2, 5 and 10) for a two particle, one contact assembly	203
5.15	Comparison between the solidification theory analytical solution, the fully explicit DEM formulation with ADR and the proposed fast numerical procedure considering three time internals (N=2, 5 and 10) for 10×10 particle assembly with hexagonal arrangement and for a large random assembly	204
5.16	Fit of B3 model to Ward's creep test results of mortar and concrete using genetic algorithm (GA) (Ward <i>et al.</i> 1969)	206
5.17	Results of the calibration procedure of the $\alpha_{n,mortar}$ and $\alpha_{s,mortar}$ for a loading age of 7 days	208
5.18	Results of the parametric study for the determination of the influence of ITZ on the behaviour of concrete	211
5.19	Description of the detailed particle model for the study of concrete's long-term behaviour	213
5.20	Comparison between the experimental concrete creep test results by Ward, the fit to B3 model and the results of the long-term analysis of concrete using the DEM applied to particle model using the proposed fast numerical procedure with five and ten time intervals (N=5 and 10) and for two loading times ($t-t'=365$ and 3650 days) (average of 5 numerical samples)	215

5.21	Normal contact force distributions after loading ($t=7.01$ days) and after one year under constant loading ($t=372$ days)	216
5.22	Mohr-Coulomb model with tension cut-off	218
5.23	Mohr-Coulomb model with softening in tension and shear	221
5.24	Description of the normal contact force path under softening	222
5.25	Description of the shear contact forces path under softening	223
5.26	Assemblies for the validation of the Mohr-coulomb models	225
5.27	Contact force-displacement law for the 2×1 assembly under tension and compression loading considering brittle (left) and softening (right) contact model	225
5.28	Contact force-displacement law for the 10×10 assembly under tension loading considering brittle (left) and softening (right) contact model	226
5.29	Global and contact force-displacement law for the 2×2 assembly under shear loading considering brittle (left) and softening (right) contact model	226
5.30	Global and contact force-displacement law for the 2×2 assembly under compression and shear loading considering brittle (left) and softening (right) contact model	227
5.31	Specimen size and type of loading of the concrete particle models	228
5.32	Influence of the modulus of elasticity of the aggregate in the stress-strain behaviour in tension and compression	231
5.33	Influence of the contact strength properties of the mortar in the stress-strain behaviour in tension and compression	231
5.34	Influence of the contact cohesion of the mortar in the stress-strain behaviour in tension and compression	232
5.35	Influence of the ratio between contact strength properties of the ITZ and the mortar in the stress-strain behaviour in tension and compression	232
5.36	Influence of the contact fracture energy in the stress-strain behaviour in tension and compression	233
5.37	Influence of the lateral restraint of the walls in the stress-strain behaviour in tension and compression	234
5.38	Development of cracking pattern and correspondence to the stress-strain behaviour under tensile stress	236

5.39	Results of direct tensile strength tests of the concrete particle model including the stress-strain behaviour and the development of the modulus of elasticity and Poisson's ratio, of the number of normal and shear contact breaks and of the work and kinetic energy	237
5.40	Results of compressive strength tests of the concrete particle model including the stress-strain behaviour and the development of the modulus of elasticity and Poisson's ratio, of the number of normal and shear contact breaks and of the work and kinetic energy	238
5.41	Development of cracking pattern and correspondence to the stress-strain behaviour under compressive stress	239
6.1	Schematic representation of the proposed approach for the prediction of dam concrete properties using particle models	245
6.2	Representation of the loading conditions at the top wall and the boundary conditions of the particle model	247
6.3	Calibration of the deformability properties of each component of concrete and modelling of #38 wet-screened concrete	250
6.4	Calibration of the deformability properties of each component of concrete and modelling of dam concrete	250
6.5	Validation of the composite model for the prediction of mortar's creep compliance based on the #38 wet-screened concrete	253
6.6	Generation of concrete's aggregate structure for the analysis of particle models	257
6.7	Comparison between the sieve analysis of DAM and SCR38 concretes and of the generated assemblies for the DEM analysis	259
6.8	Types of simple particle models for the studying the influence of the aggregate content and maximum size of aggregate	261
6.9	Results of each type of simple particle model	262
6.10	Validation of the temperature effect on the development of the creep strains .	264
6.11	Results of SCR38 concrete particle model based on the mortar's and aggregate's deformability mean properties and considering a constant temperature of 20 °C	266
6.12	Results of SCR76 concrete particle model based on the mortar's and aggregate's deformability mean properties and considering a constant temperature of 20 °C	266

6.13	Results of SCR76 concrete particle model based on the mortar's and aggregate's deformability mean properties and considering the measured temperature inside the creep cell	268
6.14	Results of SCR38 concrete particle model based on the mortar's and aggregate's deformability mean properties and considering the measured temperature inside the creep cell	268
6.15	Results of DAM concrete particle model based on the mortar's and aggregate's deformability mean properties and considering a constant temperature of 20 °C	270
6.16	Results of DAM concrete particle model using different aggregate's modulus of elasticity	272
6.17	Results of DAM concrete particle model using different aggregate's modulus of elasticity	273
6.18	Results of DAM concrete particle model based on the mortar's deformability, considering the crushed aggregates	274
6.19	Results of DAM concrete particle model based on the mortar's deformability, considering the aggregate's deformability variability and the measured temperature inside the creep cells	276
6.20	Comparison between compressive and tensile normal contact forces in rounded coarse aggregate structure and crushed coarse aggregate structure for the DAM concrete particle model	277
6.21	Development of the maximum and minimum normal contact forces over time for each contact type considering a rounded particle model and the measured temperature inside the creep cells	278
6.22	Localization and results of each analyzed cross section of DAM concrete specimen	279
6.23	Stress distribution over the cross section CS-H-1 of the DAM concrete specimen loaded at the age of 7 days	280
6.24	Stress distribution over the cross section CS-V-2 of the DAM concrete specimen loaded at the age of 7 days	281
6.25	Correlation between splitting tensile strength and the modulus of elasticity and fit to mortar and aggregate test results	282
6.26	Tensile and compressive stress-strain curves of mortar for three different loading ages	285

6.27	Cracking pattern, normal and shear contact damage for direct tensile test of mortar at the age of 7 days	286
6.28	Cracking pattern, normal and shear contact damage for compressive test of mortar at the age of 7 days	286
6.29	Comparison between stress-strain curves of the two sets of strength properties of ITZ (reduced $F_{t,n,max}^{ITZ}$ and reduced C^{ITZ}) for the prediction compressive strength of SCR38 concrete	288
6.30	Stress-strain curves of SCR38 concrete considering ITZ's properties half of mortar's properties	290
6.31	Cracking pattern and normal contact damage for tensile test of SCR38 concrete at the age of 90 days considering ITZ's properties half of mortar's properties	291
6.32	Cracking pattern and normal contact damage for compressive test of SCR38 concrete at the age of 90 days considering ITZ's properties half of mortar's properties	291
6.33	Stress-strain curves of SCR38 concrete considering ITZ's properties half of mortar's properties with and without lateral restraint	292
6.34	Comparison of failure patterns for compressive loading with (right) and without (left) lateral restraint of the walls	292
6.35	Stress-strain curves of DAM concrete considering ITZ's properties half of mortar's properties and no lateral restraint	294
6.36	Stress-strain curves of DAM concrete considering ITZ's properties half of mortar's properties with and without lateral restraint	294
6.37	Cracking pattern and normal contact damage for tensile test of DAM concrete at the age of 90 days considering ITZ's properties half of mortar's properties	295
6.38	Cracking pattern and normal contact damage for compressive test of DAM concrete at the age of 90 days considering ITZ's properties half of mortar's properties and without lateral restraint of the walls	295
6.39	Cracking pattern and normal contact damage for compressive test of DAM concrete at the age of 90 days considering ITZ's properties half of mortar's properties and with lateral restraint of the walls	296
6.40	Distribution of tensile contact forces of DAM concrete near the peak strength	296
6.41	Distribution of tensile contact forces of DAM concrete after peak strength	297

6.42	Distribution of compressive contact forces of DAM concrete near the peak strength	297
6.43	Distribution of compressive contact forces of DAM concrete after peak strength	297
6.44	Comparison between stress-strain curves of SCR38 concrete tested in small and large specimens	298
6.45	Comparison between stress-strain curves of SCR38 and DAM concrete tested in large specimens	299
6.46	Comparison between cracking patterns of tensile tests of SCR38 concrete (left) and DAM concrete (right) using the same specimen size	300
6.47	Comparison between cracking patterns of compressive tests of DAM concrete (top) and SCR38 concrete (bottom) using the same specimen size	301
C.1	C++ discrete element method code flowchart	367
C.2	C++ classes	368

List of Tables

2.1	Ratios between full-mixed and wet-screened concretes for compressive and splitting tensile strengths obtained from experimental results	47
3.1	Concrete composition of several Portuguese dams	73
3.2	Maximum aggregate sizes (MSA) used in the DAM concretes	82
3.3	Average composition data of DAM concretes and mortar and the estimated composition data for SCR concretes	84
3.4	Sieve analysis of DAM concretes and mortar and the estimated sieve analysis for SCR concretes	84
3.5	Average composition of dam concrete and estimated compositions of SCR76 (#76 mm) and SCR38 (#38 mm) wet-screened concretes used in the creep cells	86
3.6	Experimental setup data for quality control procedures and for the specific tests	90
3.7	Mechanical properties of the rock used for the aggregates	97
3.8	Modulus of elasticity results of dam and wet-screened concretes and for the core and the face concretes obtained in laboratory	99
3.9	Creep test results obtained from prisms in laboratory (average of two specimens P #38-CC1 and P #38-CC2)	101
3.10	Average values and standard deviations of modulus of elasticity obtained from creep cells <i>in situ</i>	103
3.11	Compressive creep test results obtained from creep cells <i>in situ</i>	105
3.12	Compressive strength results of DAM and SCR concretes for Core, Face and Reinforcement placements and of mortar	109
3.13	Splitting tensile strength results of DAM and SCR concretes for Core, Face and Reinforcement placements and of mortar	111
4.1	Logarithmic fit to CC1-A creep cell results	124

4.2	Composite data for the estimation of the modulus of elasticity of dam concrete (part 1)	127
4.3	Composite data for the estimation of the modulus of elasticity of dam concrete (part 2)	127
4.4	Fitted parameters for the dam concrete modulus of elasticity prediction using the two types of adopted composite models	129
4.5	Coefficients for the extension of model B3 to basic creep at constant elevated temperature	141
4.6	Equivalent age and equivalent loading time used in the analysis	142
4.7	Parameters obtained by the optimization procedure	142
4.8	Properties used for the equivalent composite model analysis	144
4.9	Comparison between estimate of β given by Caquot law and the by the fit to the experimental results	147
4.10	Baixo Sabor dam data for the fit to the extended Abrams law	152
4.11	Parameters of the extended Abrams law	153
4.12	Prediction of the dam concrete based on the proposed relationship and on the test results of wet-screened concrete (part 1)	157
4.13	Prediction of the dam concrete based on the proposed relationship and on the test results of wet-screened concrete (part 2)	158
4.14	List of parameters, variables, type and number of specimens proposed for the calibration of the different effects	165
4.15	List of parameters, variables, type and number of specimens proposed for the calibration of the different models	165
5.1	Real and scaled system properties	184
5.2	Parameters for the particle model validation	198
5.3	Comparison of performance results of the original DEM formulation without damping, with local non-viscous damping and using the adaptive dynamic relaxation method (ADR) and of the numerical incremental procedure for creep model applied to the solidification theory	200
5.4	Description of the three types of particle assemblies and contact properties	202
5.5	Comparison of calculation times for three types of particle assemblies for both fully explicit DEM and the proposed fast numerical procedure	203

5.6	Properties and composition of the aggregate, the mortar and of the concrete	206
5.7	Parameters of B3 model fit to Ward’s creep test results of mortar and concrete using genetic algorithm (GA)	206
5.8	Optimum parameters α_n^{opt} and α_s^{opt} of the mortar and the aggregate	208
5.9	Optimum coefficients obtained from the minimization of the quadratic model to fit the concrete behaviour	211
5.10	Aggregate distribution, total aggregate volumes and number of particles of the concrete compact assemblies (average of five numerical samples)	213
5.11	Results of the long-term analysis of concrete using DEM particle model and five time intervals (N=5)	214
5.12	224
5.13	Concrete composition of Vonk (1992) tests	228
5.14	Definition of variables for the sensitivity study	230
5.15	Parameters used for the concrete particle model	235
5.16	Results of tensile and compressive numerical tests of concrete particle models	235
6.1	Particle model properties for the representation of concrete behaviour	248
6.2	Calibration scheme for each type of concrete considering its different components	251
6.3	Parameters of B3 model for Core-SCR38 wet-screened concrete (#38)	252
6.4	Calculation of β_{Caquot} based on the properties of Core-SCR38 concrete	253
6.5	Parameters of B3 model for the mortar	253
6.6	Calibration micro parameters for the modelling of each aggregate’s deformability properties	255
6.7	Calibration micro parameters for the modelling of mortar’s deformability properties	255
6.8	Influence of the minimum particle radius on the size of the concrete particle assembly	256
6.9	Sieve analysis for each type of concrete placed in Baixo Sabor dam	258
6.10	Properties of each type of concrete and of concrete particle models	258
6.11	Results of each type of single aggregate particle model	261
6.12	Results of SCR76 and SCR38 concrete particle model based on the mortar’s and aggregate’s deformability mean properties and considering a constant temperature of 20 °C	265

6.13	Results of SCR76 and SCR38 concrete particle model based on the mortar's and aggregate's deformability mean properties and considering the measured temperature inside the creep cells	269
6.14	Results of DAM concrete particle model based on the mortar's and aggregate's deformability mean properties and considering a constant temperature of 20 °C	269
6.15	Results of DAM concrete particle model using different aggregate's modulus of elasticity (part 1)	271
6.16	Results of DAM concrete particle model using different aggregate's modulus of elasticity (part 2)	271
6.17	Results of DAM concrete particle model using different ITZ's modulus of elasticity	273
6.18	Results of DAM concrete particle model based on the mortar's deformability properties and considering crushed aggregates	274
6.19	Results of DAM concrete particle model based on the mortar's and aggregate's deformability properties and considering the measured temperature inside the creep cells	275
6.20	Identification and properties of each analysed cross section of DAM concrete specimen	279
6.21	Correlation parameters fitted to experimental results of mortar and aggregate	282
6.22	Parameters of MORTAR particle model for the prediction of strength properties	285
6.23	Strength results of MORTAR particle model	285
6.24	Parameters of mortar, ITZ and aggregate contact model for the prediction of strength properties of concrete	288
6.25	Strength results of SCR38 and DAM concrete particle model	289
6.26	Comparison between analytical and numerical predictions	299
A.1	Chemical characteristics of the cement and fly ashes	354
A.2	Physical characteristics of the cement and fly ashes	354

List of Acronyms

Abbreviations

#38	Sieve aperture of 38 mm or wet-screened concrete with #38 mm maximum size of aggregate
#76	Sieve aperture of 76 mm or wet-screened concrete with #38 mm maximum size of aggregate
<i>CC #38 – A</i>	Active creep cell cast with wet-screened concrete obtained by screening the dam concrete placed in the dam’s core with a 38 mm aperture sieve
<i>CC #38 – N</i>	Non-stress creep cell cast with wet-screened concrete obtained by screening the dam concrete placed in the dam’s core with a 38 mm aperture sieve
<i>CC #76 – A</i>	Active creep cell cast with wet-screened concrete obtained by screening the dam concrete placed in the dam’s core with a 76 mm aperture sieve
<i>CC #76 – N</i>	Non-stress creep cell cast with wet-screened concrete obtained by screening the dam concrete placed in the dam’s core with a 76 mm aperture sieve
<i>CC 150 – A</i>	Active creep cell cast with full-mixed concrete
<i>CC 150 – N</i>	Non-stress creep cells cast with full-mixed concrete
<i>P #38</i>	Prismatic specimen cast with wet-screened concrete obtained by screening the dam concrete placed in the dam’s core with a 38 mm aperture sieve

LIST OF ACRONYMS

2D	Two dimensional
3D	Three dimensional
AAR	Alkali-aggregate reactions
AEMM	Age-adjusted effective modulus method
ASR	Alkali-silicate reactions
C2S	Dicalcium silicates
C3A	Tricalcium aluminate
C3S	Tricalcium silicate
C4AF	Tetracalcium aluminoferrite
CAT	Comissão de Acompanhamento de Tese
CC	Creep cell
Composite #76-Dam	Composite model for the prediction of deformability properties of dam concrete based on the results of SCR76/#76 concrete
Composite #38-Dam	Composite model for the prediction of deformability properties of dam concrete based on the results of SCR38/#38 concrete
Composite #38-#76	Composite model for the prediction of deformability properties of SCR76/#76 concrete based on the results of SCR38/#38 concrete
Core-SCR76	Wet-screened concrete obtained by screening the dam concrete placed in the dam's core with a 76 mm aperture sieve
Core-SCR38	Wet-screened concrete obtained by screening the dam concrete placed in the dam's core with a 38 mm aperture sieve
Core-DAM	Dam or full-mixed concrete obtained from the concrete production on site and placed in the dam's core
CSH	Calcium silicate hydrate

DAM	Dam or full-mixed concrete obtained from the concrete production on site and placed in the dam
DEM	Discrete element method
EN	European standard
EPS	Expanded polystyrene
Face-SCR38	Wet-screened concrete obtained by screening the dam concrete placed in the dam's up and downstream faces with a 38 mm aperture sieve
Face-DAM	Dam or full-mixed concrete obtained from the concrete production on site and placed in the dam's up and downstream faces
FEM	Finite element method
FM	Fineness modulus of coarse and fine aggregate
FPZ	Fracture process zone
GA	Genetic algorithm
HCB	Hidroeléctrica de Cahora Bassa
HWST	Horizontal wedge splitting test method
IER	Internal expansion reactions
ISR	Internal sulfate reactions
ITZ	Interfacial transition zone
MC	Measurement circle
MDEM	Modified distinct or discrete element method
MPT	Maximum paste thickness
MSA	Maximum size of aggregates
PM	Particle model
Reinforcement-DAM	Dam or full-mixed concrete obtained from the concrete production on site and placed in the reinforced areas

LIST OF ACRONYMS

RH	Relative humidity
SCM	Supplementary cementing materials
SCR38	Wet-screened concrete obtained by screening the dam concrete with a 38 mm aperture sieve
SCR76	Wet-screened concrete obtained by screening the dam concrete with a 76 mm aperture sieve
SDA	Strong Discontinuity Approach
SDT	Stiffness damage test
TC	Technical committee
UCS	Uniaxial compressive strength
X-FEM	Extended Finite Element Method

Official Bodies

ACI	American Concrete Institute
ASCE	American Society of Civil Engineers
ASTM	American Society for Testing and Materials
CEB	Comité Européen du Béton (European Committee for Concrete)
CEN	European Committee for Standardization
DBB	Departamento de Barragens de Betão (Concrete Dams Department)
DIN	Deutsches Institut für Normung (German Institute for Standardization)
EDP	Energias de Portugal
FIB	Fédération Internationale du Béton (International Federation for Structural Concrete)
FIP	Fédération Internationale de la Précontrainte (International Federation for Prestressing)

ICOLD	International Commission on Large Dams
LNEC	Laboratório Nacional de Engenharia Civil (National Laboratory for Civil Engineering)
RILEM	Réunion Internationale des Laboratoires et Experts des Matériaux, systèmes de construction et ouvrages (International Union of Laboratories and Experts in Construction Materials, Systems and Structures)
USBR	United States Bureau of Reclamation

List of Symbols

Alphanumeric

a	Aggregate content measured in weight per unit volume
a_v	Coarse aggregate content measured in volume per unit volume
A	Length side of a cube
$a_{i,agg}$	Calibration parameters for aggregate contact properties
$a_{i,mortar}$	Calibration parameters for mortar contact properties
a, b	Parameters of the fit to logarithmic function over time
A, B	Coefficients of analytical models for the development of compressive strength over time
A, B, α_d	Parameters of the proposed extended Abrams law
$a_{dam}^{*,comp}, b_{dam}^{*,comp}$	Parameters of the fit to logarithmic function over time adjusted to the composite models
A_g	Volume of aggregate per unit volume of concrete
A_{agg}	Calibration parameter for aggregate contact properties
$A_{g,max} = V_{a,max}$	Maximum volume of aggregate per unit volume of concrete
A_{mortar}	Calibration parameter for mortar contact properties
b	Binder content measured in weight per unit volume
$b_{1,agg}$	Calibration parameter for aggregate contact properties
$b_{1,mortar}$	Calibration parameter for mortar contact properties

LIST OF SYMBOLS

b, c	Coefficients of empirical expressions for the correlation of concrete's modulus of elasticity and compressive strength
b_v	Binder content measured in volume per unit volume
c	Cement content measured in weight per unit volume
C	Cohesion
$C_{residual}$	Residual cohesion
$C_0(t, t')$	Basic creep compliance
$c_{i,agg}$	Calibration parameters for aggregate contact properties
$c_{i,mortar}$	Calibration parameters for mortar contact properties
$\dot{C}_0(t, t')$	Creep compliance rate
$C_d(t, t')$	Drying creep compliance
c	Damping
c_c	Critical damping
c_v	Cement content measured in volume per unit volume
d	Euclidean distance between the centres of gravity of two particles
d	Contact damage
d_{av}	Average diameter between sieves
Δt_{crit}	Critical time step
d_n^+	Contact normal damage in tension
d_s	Contact shear damage
$E(t) = E_c(t)$	Modulus of elasticity of concrete in compression at time t
E_a	Activation energy
$E''(t, t')$	Age-adjusted effective modulus
$E''_{am}(t, t')$	Age-adjusted modulus of the parallel portion of aggregate and matrix/mortar
$E''_m(t, t')$	Age-adjusted modulus of the matrix or mortar

E_{agg}	Modulus of elasticity of aggregate
E_{agg}^{macro}	Macroscopic modulus of elasticity of aggregate
E_c^*	Modulus of elasticity obtained by fitting a logarithmic function over time
$E_{c,dam}^{*,composite}$	Modulus of elasticity of dam concrete predicted by composite model
$E_{c,eq.bin}^*$	Modulus of elasticity of equivalent binder
E_c^{exp}	Modulus of elasticity obtained experimentally
$E_{DAM,IN SITU}(t')$	Modulus of elasticity of dam concrete obtained <i>in situ</i>
$E_{DAM,LAB}(t')$	Modulus of elasticity of dam concrete obtained in laboratory
E_{mortar}^{DEM}	Modulus of elasticity of aggregate particle model using DEM
E_{eff}^{DEM}	Effective modulus of concrete particle model using DEM
$E_{exp}(t)$	Modulus of elasticity obtained from experimental tests
$E_{inst}(t)$	Instantaneous modulus of elasticity at time t
E_m	Modulus of elasticity of matrix
E_{eff}^{DEM}	Effective modulus of mortar M6 obtained experimentally
E_m	Maximum efficiency of secondary material
e^{model}	Deviations between experimental and predicted values of modulus of elasticity
E_n	Modulus of elasticity in the normal direction
$E_{SCR,IN SITU}(t')$	Modulus of elasticity of wet-screened concrete obtained <i>in situ</i>
$E_{SCR,LAB}(t')$	Modulus of elasticity of wet-screened concrete obtained in laboratory
$E_{sust}(t)$	Sustained modulus of elasticity at time t
f	Fly ash content measured in weight per unit volume

LIST OF SYMBOLS

f_v	Fly ash content measured in volume per unit volume
$\mathbf{F}^{[C]}$	Force vector of contact C
$\mathbf{F}_s^{[C]}$	Shear force vector of contact C
$\mathbf{F}_t^{unbalanced}$	Unbalanced force at time t
$f_c = f_{c,max}$	Uniaxial compressive strength
$f_c^{DAM} = f_{c,dam}$	Uniaxial compressive strength of DAM concrete
$f_c^{SCR} = f_{c,wet-screened}$	Uniaxial compressive strength of SCR38 concrete
$f_{c,28}$	Uniaxial compressive strength at the age of 28 days
$f_{c,cubes}$	Uniaxial compressive strength obtained in cubic specimens
$f_{c,cylinders}$	Uniaxial compressive strength obtained in cylindrical specimens
$f_{c,k}$	Characteristic uniaxial compressive strength
$f_{c,\phi}$	Uniaxial compressive strength obtained using a cylinder specimen with diameter ϕ
f_{c,ϕ_0}	Uniaxial compressive strength obtained using a reference cylinder specimen with diameter ϕ_0
$f_{c,triaxial}$	Axial compressive strength in triaxial stress test
$f_{c,u}$	Ultimate uniaxial compressive strength
\mathbf{F}^d	Translational damping force
\mathbf{F}_t^{int}	Force at the centre of a particle at time t
$F_n^{[C]}$	Normal force of contact C
$F_n^{[C],old}$	Normal force of contact C at the previous time step
$F_{n,predicted}$	Predicted normal contact force
$F_{n,t,max}$	Maximum tensile normal contact force
$\mathbf{F}^{[C],old}$	Force vector of contact C at the previous time step
$\mathbf{F}_t^{[\phi]}$	Force vector acting at the centre of particle ϕ at time t
$\mathbf{F}_s^{[C],corrected}$	Corrected shear force vector of contact C

$F_{s,max}$	Maximum shear contact force
$\mathbf{F}_{s,predicted}$	Predicted normal contact force
$F_{s,residual}$	Residual shear contact force
f_t	Tensile strength obtained from direct tensile test
$f_{t,m}$	Mean tensile strength obtained from direct tensile test
$f_{t,flexural}$	Tensile strength obtained from flexural test
$f_{t,flexural,m}$	Mean tensile strength obtained from flexural test
f_{tol}	Force tolerance
$f_{t,splitting} = f_{t,spl}$	Tensile strength obtained from splitting test (Brazilian test)
$f_{t,spl}^{DAM}$	Tensile strength of DAM concrete obtained from splitting test (Brazilian test)
$f_{t,spl}^{SCR}$	Tensile strength of SCR38 concrete obtained from splitting test (Brazilian test)
$f_{t,splitting,m}$	Mean tensile strength obtained from splitting test (Brazilian test)
f_{t,spl,ϕ_0}	Splitting tensile strength obtained using a reference cylinder specimen with diameter ϕ_0
$f_{t,spl,\phi}$	Splitting tensile strength obtained using a cylinder with diameter ϕ
s	Coarse aggregate content measured in weight per unit volume
$G_{f,n}$	Normal fracture energy
$G_{e,n}$	Normal elastic energy
$G_{f,s}$	Shear fracture energy
$G_{e,s}$	Shear elastic energy
$h(t)$	Volume fraction growth associated to the viscous behaviour
H	Height of a cylindrical specimen

LIST OF SYMBOLS

I	Inertia of a particle
I_{scaled}	Equivalent inertia of the scaled system
$J(t, t')$	Creep compliance at time t for a loading at time t'
$J_{\#38}(t, t')$	Creep compliance of SCR38 or #38 concrete
$J_{\#76}(t, t')$	Creep compliance of SCR76 or #76 concrete
$J_{B3}(t, t')$	Creep compliance by model B3
$J_{Composite}^{\beta}(t, t')$	Creep compliance obtained from the composite model using β parameter
$J_{Dam}(t, t')$	Creep compliance of DAM concrete
$J_{concrete}^{DEM}(t, t')$	Creep compliance of concrete particle model using DEM
$J_{exp}^{C4}(t, t')$	Creep compliance of concrete C4 obtained experimentally
J_{mortar}^{DEM}	Creep compliance of mortar particle model using DEM
$J_{exp}(t, t')$	Creep compliance obtained from experimental tests
$J_{ITZ}(t, t')$	Creep compliance of ITZ
$J_m(t, t')$	Creep compliance of the matrix or mortar
J^{macro}	Macroscopic creep compliance
$J_n(t, t')$	Normal contact creep compliance
J_n^{micro}	Microscopic creep compliance in the normal direction
J_s^{micro}	Microscopic creep compliance in the shear direction
k	Stiffness of an elementary system
$K_1^{agg}, K_2^{agg}, n1^{agg}$	Coefficients of empirical expressions for the correlation of concrete's modulus of elasticity and compressive strength of aggregates
$K_1^{mortar}, K_2^{mortar}, n1^{mortar}$	Coefficients of empirical expressions for the correlation of concrete's modulus of elasticity and compressive strength of mortar

K_0	Coefficients of empirical expressions for the correlation of concrete's modulus of elasticity and compressive strength
K, A	Coefficients of strength prediction laws
$KITZ_{qi}$	Coefficients for establishing the relation between the ITZ's and the mortar's creep compliance
$k_{\mu,n}$	Normal stiffness of the Kelvin chain μ
k_n	Contact normal stiffness
$k_{n,agg}$	Contact stiffness of aggregate
k_n^{wall}	Wall stiffness in the normal direction
k_{rot}	Rotational stiffness of a particle
k_s	Contact shear stiffness
k_s^{wall}	Wall stiffness in the shear direction
k_t	Overall cementing efficiency at the age, t
K, t_0, τ	Coefficients of analytical models for the development of compressive strength over time
k_{trans}	Translational stiffness of a particle
m	Mass of a particle
m_{scaled}	Equivalent mass of the scaled system
$M_{3,t}^{[\phi]}$	Moment acting at the centre of particle ϕ at time t
n	Lime fixation factor
$N_c = N_{contacts}$	Number of contacts in the particle assembly
N_{chains}	Number of Kelvin chains in the rheological model
N_{coord}	Coordination number or number of contacts of a given particle
$N_{particles}$	Number of particles in an assembly
N_{steps}	Number of steps of the DEM calculations
\mathbf{n}	Unit normal to the contact plane

LIST OF SYMBOLS

\mathbf{n}^{old}	Unit normal to the contact plane at the previous time step
p_c	Ratio between the cement content and the sum of the cement and secondary cementitious materials contents (by weight)
p_f	Ratio between the fly ash content and the sum of the cement and secondary cementitious materials contents (by weight)
q_1, q_2, q_3, q_4	Parameters of model B3
$q_{i,ITZ}$	Parameters of model B3 related to the ITZ's creep compliance
q_i^{macro}	Parameters of model B3 related to the macroscopic creep compliance
$q_i^{mortar-SCR38}$	Parameters of model B3 related to the macroscopic creep compliance of mortar obtained by the SCR38 concrete using composite models
$q_{n,i}^{micro}$	Parameters of model B3 related to the microscopic creep compliance in the normal direction
$q_{s,i}^{micro}$	Parameters of model B3 related to the microscopic creep compliance in the shear direction
$R(t, t')$	Relaxation function at time t for a loading at time t'
R	Gas constant
R^2	Coefficient of determination of a regression model
R_{adj}^2	Adjusted coefficient of determination of a regression model
r_C	Relation between mortar's and ITZ's cohesion
r_F	Relation between mortar's and ITZ's maximum normal contact forces
$r_{G,n}$	Relation between fracture and elastic energy in the normal direction

$r_{G,s}$	Relation between fracture and elastic energy in the shear direction
R_{max}	Maximum radius between two particles
R_{mean}	Mean radius between two particles
R_{min}	Minimum radius between two particles
$R^{[\phi]}$	Radius of particle ϕ
s	Fine aggregate content measured in weight per unit volume
s_v	Fine aggregate content measured in volume per unit volume
s	Coefficients of analytical models for the development of compressive strength over time
SF	Silica fume content measured in weight per unit volume
SF_v	Silica fume content measured in volume per unit volume
t	Time or age of concrete
$T(t)$	Temperature at time t
t'	Age at loading
t	Thickness of the particle disk
T	Measured temperature
T	Real time
$\tan \phi$	Coefficient of friction
T_{calc}	Calculation time
t_e	Equivalent time
t'_e	Equivalent loading age
T_{ref}	Reference temperature
$t_T - t'_e$	Equivalent time under loading
\mathbf{u}	Displacement
U_c	Activation energy related to the acceleration of creep rate
U'_c	Activation energy related to the magnification of creep

LIST OF SYMBOLS

U^{el}	Internal elastic strain energy
U_h	Activation energy related to cement hydration reactions
U^{inel}	Internal energy dissipated by inelastic deformation
U^k	Kinetic energy
U_n	Overlap distance between two particles
$U_{n,t,max}$	Maximum normal overlap in tension
$U_{n,t,Fmax}$	Normal overlap at maximum normal contact force in tension
$U_{s,max}$	Maximum shear overlap
u_{tol}	Displacement tolerance
V	Volume
$V_{2.4-4.75}^{2D}$	Fraction volume of the 2.4-4.75 coarse aggregate in a 2D plane
$V_{4.75-10}^{2D}$	Fraction volume of the 4.75-10 coarse aggregate in a 2D plane
$V_{coarse\ agg}^{2D}$	Fraction volume of the coarse aggregate in a 2D plane
V_{mortar}^{2D}	Fraction volume of the mortar in a 2D plane
$V_{\#38}$	Fraction volume of SCR38 or #38 concrete with respect to the volume of DAM concrete
$V_{\#76}$	Fraction volume of SCR76 or #76 concrete with respect to the volume of DAM concrete
$V_{a>38}$	Fraction volume of the removed aggregates for obtaining SCR38 or #38 concrete with respect to the volume of DAM concrete
$V_{a>76}$	Fraction volume of the removed aggregates for obtaining SCR76 or #76 concrete with respect to the volume of DAM concrete
$V_{a,coarse}$	Volume of coarse aggregates in a given concrete specimen

$V_{a,fine}$	Volume of fine aggregates in a given concrete specimen
V_{agg}	Fraction volume of aggregate
$V_{a,total}$	Volume of aggregates in a given concrete specimen
$V_{eq.bin}$	Fraction volume of equivalent binder
$v_f(t)$	Volume fraction growth associated to the viscoelastic behaviour in the shear direction
V_m	Fraction volume of matrix
$v_n(t)$	Volume fraction growth associated to the viscoelastic behaviour in the normal direction
V_{spec}	Volume of concrete specimen
v_x^{wall}	Wall velocity in the horizontal direction
v_y^{wall}	Wall velocity in the vertical direction
w	Water content measured in weight per unit volume
w_v	Water content measured in volume per unit volume
W	Unit weight of concrete
W	Energy term for the total energy of the system
w_{add}	Water content added to the mixture
w_{agg}	Water content in the aggregates (moisture)
W^{damp}	Work done by the damping forces
W^{ext}	Work done by the external forces
W^{global}	Work done by the global damping forces
W^{local}	Work done by the local damping forces
$\mathbf{x}^{[\phi]}$	Position vector of particle ϕ
X	Random variable X
$\ddot{\mathbf{x}}^{[\phi]}$	Translational acceleration vector of particle ϕ
$\ddot{\mathbf{x}}^{[C]}$	Translational acceleration vector of contact C
$\dot{\mathbf{x}}^{[\phi]}$	Translational velocity vector of particle ϕ

LIST OF SYMBOLS

$\dot{\mathbf{x}}^{[C]}$	Translational velocity vector of contact C
$\left(\dot{\mathbf{x}}^{[C]}\right)_\phi$	Translational velocity vector of particle ϕ at contact point C
$X_{95\%}$	Value of random variable X for 95% confidence values
$x_n^{creep}(t)$	Normal contact creep displacement
$x_n^{inst}(t)$	Normal contact instantaneous displacement
$x_n^F(t)$	Normal contact stress-dependent displacement

Greek letters

α	Parameter of B3 model
α, β	Coefficients of analytical models for the development of compressive strength over time
α, β	Parameters of (Granger and Bažant 1995) composite model
β_{Caquot}	Parameter β of (Granger and Bažant 1995) composite model proposed by Caquot
α	Non-viscous damping coefficient
α	Coefficient of strength prediction laws
$\alpha_{n,agg}$	Calibration parameter for aggregate contact properties
$\alpha_{n,mortar}$	Calibration parameter for mortar contact properties
$\alpha_{s,agg}$	Calibration parameter for aggregate contact properties
$\alpha_{s,mortar}$	Calibration parameter for mortar contact properties
$\alpha_{s,agg,0}$	Calibration parameter for aggregate contact properties
$\beta_{\#38-Dam}$	Parameters of the composite model used for the prediction of DAM concrete deformability based on the results of SCR38 or #38 concrete
$\beta_{\#38-Dam}$	Parameters of the composite model used for the prediction of SCR76 or #76 concrete deformability based on the results of SCR38 or #38 concrete

$\beta_{\#76-Dam}$	Parameters of the composite model used for the prediction of DAM concrete deformability based on the results of SCR76 or #76 concrete
β_{fit}	Parameters of the composite model fitted to the experimental results
$\chi(t, t')$	Age-adjusted coefficient
η	Coarseness characteristic
ΔE	Absolute deviation of concrete modulus of elasticity
$\Delta \varepsilon(t, t')$	Total strain increment
$\Delta \varepsilon''(t, t')$	Viscoelastic strain increment
$\Delta \varepsilon_n$	Normal strain increment
$\Delta E_{\sigma(E_{agg})}$	Absolute deviation of concrete modulus of elasticity for the study of the influence of modulus of elasticity variability of the aggregate
$\Delta \mathbf{F}^{[C]}$	Force increment vector of contact C
$\Delta F_n^{[C]}$	Normal force increment of contact C
ΔF_n^{eq}	Equivalent normal contact force increment
$\Delta \mathbf{F}_s^{[C]}$	Shear force increment vector of contact C
$\Delta \mathbf{F}_s^{[C], corrected}$	Corrected shear force increment vector of contact C
$\Delta \mathbf{F}_s^{[C], old}$	Shear force increment vector of contact C at the previous time step
$\Delta \mathbf{x}_s^{eq}$	Equivalent normal contact force increment
$\Delta \gamma_n(t)$	Total increment of viscoelastic microstrain
ΔJ	Absolute deviation of concrete creep compliance
$\Delta J_{\sigma(E_{agg})}$	Absolute deviation of concrete creep compliance for the study of the influence of modulus of elasticity variability of the aggregate
Δt	Time increment

LIST OF SYMBOLS

ΔT	Real time increment
$\Delta \mathbf{u}$	Displacement increment of a particle
$\Delta \mathbf{x}^{[C]}$	Displacement increment vector of contact C
$\Delta x_n^{[C]}$	Normal displacement increment of contact C
$\Delta x_n^f(t)$	Normal contact viscous displacement increment
$\Delta x_n^v(t)$	Normal contact viscoelastic displacement increment
$\Delta x_{n,visco}$	Aging viscoelastic normal displacement increment
$\Delta \mathbf{x}_s^{[C]}$	Shear displacement increment vector of contact C
$\Delta \mathbf{x}_{s,visco}$	Aging viscoelastic shear displacement increment
ε^f	Viscous strain
$\varepsilon(t, t')$	Total axial strain at time t for a loading at time t'
$\varepsilon^0(t)$	Stress-independent strain at time t
$\varepsilon^c(t, t') = \varepsilon_{creep}(t, t')$	Creep strain at time t for a loading at time t'
$\varepsilon^{cr}(t')$	Cracking strain for a loading at time t'
ϵ_E	Percentage error between numerical and analytical results of modulus of elasticity
ϵ_E	Percentage deviation of concrete modulus of elasticity
ϵ_E^{exp}	Percentage error between numerical and experimental results of modulus of elasticity
$\epsilon_{E_{\sigma(E_{agg})}}$	Percentage deviation of concrete modulus of elasticity for the study of the influence of modulus of elasticity variability of the aggregate
$\varepsilon^i(t')$	Instantaneous strain for a loading at time t'
ϵ_J	Percentage error between numerical and analytical results of creep compliance
ϵ_J	Percentage deviation of concrete creep compliance

ϵ_J^{exp}	Percentage error between numerical and experimental results of creep compliance
$\epsilon_{J_{\sigma(E_{agg})}}$	Percentage deviation of concrete creep compliance for the study of the influence of modulus of elasticity variability of the aggregate
$\epsilon_{lateral}(t, t')$	Total lateral strain at time t for a loading at time t'
$\epsilon^{sh}(t)$	Shrinkage strain at time t
$\epsilon^T(t)$	Thermal strain at time t
$\epsilon_{spec}(t, t')$	Specific creep strains obtained from experimental tests
ϵ_{ijk}	Permutation symbol
ϵ^v	Viscoelastic strain
$\eta_{\mu, n}$	Normal viscosities of the Kelvin chain μ
γ	Density or unit weight of concrete
ΔM_3^d	Rotational damping force
$\mu(X)$	Mean value of random variable X
ν_{agg}^{DEM}	<i>Poisson's</i> of aggregate particle model using DEM
ν_{mortar}^{DEM}	<i>Poisson's</i> of mortar particle model using DEM
ω	Natural angular frequency
ω_0	Lowest angular frequency of the undamped structural system
$\omega_3^{[\phi]}$	Rotational velocity of particle ϕ
$\dot{\omega}_3^{[\phi]}$	Rotational acceleration of particle ϕ
ω^{max}	Highest angular frequency of the undamped structural system
ω^{model}	Standardized deviations between experimental and predicted values of modulus of elasticity
$\phi(t, t')$	Creep coefficient

LIST OF SYMBOLS

ϕ	Diameter of a cylindrical specimen
ϕ_0	Diameter of a reference cylinder specimen
$\phi_{DAM,IN\ SITU}(t')$	Modulus of elasticity of dam concrete obtained <i>in situ</i>
$\phi_{DAM,LAB}(t')$	Modulus of elasticity of dam concrete obtained in laboratory
$\phi_m(t, t')$	Creep coefficient of the matrix or mortar
ϕ_{max}	Maximum size of aggregate (MSA)
ϕ_{max}^0	Reference maximum size of aggregate (MSA)
$\Phi_n(t)$	Microscopic compliance for the incremental normal displacements of non-aging material related to the viscoelastic deformation
$\phi_{SCR,IN\ SITU}(t')$	Modulus of elasticity of wet-screened concrete obtained <i>in situ</i>
$\phi_{SCR,LAB}(t')$	Modulus of elasticity of wet-screened concrete obtained in laboratory
$\Psi_n(t)$	Microscopic compliance for the incremental normal displacements of non-aging material related to the viscous deformation
ρ^*	Spectral ratio
$\sigma(t)$	Stress at time t
σ_n	Normal stress
$\sigma(X)$	Standard deviation of random variable X
$\theta^{[\phi]}$	Rotation of particle ϕ
ξ	Damping ratio

Introduction

1.1 Research problem

The infrastructures related to water storage and supply, flood control and sustainable energy production are of great importance. Due to climate change, the role of dams is becoming more relevant, especially in Mediterranean countries which are being affected by more intense periods of drought (López-Moreno *et al.* 2009; Ho *et al.* 2017).

The safety and durability of structures are the basis of structural design and the control of these two factors is specially relevant in dam engineering due to the potential damage related to the failure of a dam. Additionally, maintenance and rehabilitation issues related to existing dams and the demanding challenges of new construction require technological advances for more efficient, sustainable and safe structures.

Concrete dam design aims the definition of shapes that guarantee moderate compressive stresses and, approximately, zero tensile stresses, during service life. Conventional concrete dams are built in individual blocks of about 15-m length and, usually, with 2-m lift. During the construction period the main safety concern is the cracking risk during hardening and heat dissipation of each lift. During service life, the behaviour of dams is usually monitored and analysed in order to evaluate the structural response and assess if the global safety is maintained. Numerical structural models are often used to aid the behaviour analysis and concrete structural properties are important input parameters. Uncertainty in the determination of dam concrete properties is one of the reasons for the use of higher safety

factors, when compared with other structures.

A classification of structural creep sensitivity places dams as a level 4, in a range of 1 to 5, being 5 the most sensitive (Bažant 2000). Extreme examples of the importance of this matter are several examples of excessive bridge deflections (Bažant *et al.* 2011) and the collapse of Koror-Babeldaob bridge in the Republic of Palau (Bažant and Li 2008; Bažant *et al.* 2009) which are known to be related to poor estimates of concrete behaviour. According to ICOLD (2008) and USBR (2005), aging of concrete, including creep and shrinkage phenomena and also deterioration processes of concrete, such as swelling or poor resistance to freezing and thawing, are known to be the cause of dam deterioration, which can lead to failure or to a partial or full dam replacement.

Further understanding and prediction of dam or full-mixed concrete behaviour requires a comprehensive testing programme, however, dam concrete experimental characterization has particular challenges. The use of large size aggregates implies larger specimens, and, therefore, it is common to remove the aggregates after mixing and, with the remaining wet-screened concrete, cast smaller specimens and embed monitoring devices. Several studies show that the structural properties of dam concrete differs from the wet-screened concrete, both for instantaneous and delayed behaviour (Soares de Pinho *et al.* 1988; Vilardell *et al.* 1998; ICOLD 2008; Zhou *et al.* 2010).

Additionally, the further understanding of material behaviour and the development of adequate semi-empirical and numerical models can lead to the improvement of the design guidelines, to a better behaviour interpretation during the structure lifetime and, therefore, a more accurate safety control and rehabilitation procedures, as well as more sustainable and economic solutions. Moreover, reliable relationships between dam concrete and wet-screened concrete should be used during design phase, for concrete quality control during construction and for safety control and monitoring data analysis throughout service life.

In this particular case, additionally to the experimental characterization and to empirical knowledge, numerical modelling of concrete behaviour can be of great use. When validated with experimental tests, numerical models are suitable to estimate mechanical properties of concrete based on the behaviour of its components (Jennings *et al.* 2008). This advantage would, for example, reduce the number of specimens necessary to characterize the concrete properties and improve the interpretation of *in situ* monitored data over time, for different loading scenarios and environmental conditions, which is especially

relevant for the analysis of dam concrete behaviour.

The former experience is key to achieve a durable, structurally capable and sustainable design. Correlations between the main early-age and long-term properties, determined whether from test results from other dams, whether from trial mix programmes, can be of great aid. These correlations are important to the designer when specifying the required safety factors and to the contractor improving quality control, to insure early error detection and to verify property conformity throughout the work's construction. It is also relevant to the owner and the regulator to evaluate the dam's response during the first filling and to interpret the dam structural behaviour for several decades, insuring the overall safety of the structure (Batista 1998; ICOLD 2008).

Due to geometric conditions and structural and economical requirements, dam concrete is considered to be a mass concrete (ACI Committee 207 2005) with a poor cement content, of about 100 to 200 kg/m³ and large additions content, up to 50% of the cement content. It has also a large aggregate content and the aggregate's maximum size can reach 150 mm or 200 mm. Due to its large placement volume, the heat production and dissipation, the temperature gradients during the hardening process and, consequently, the cracking risk at early ages are the main concerns of mass concrete. The strength properties are often taken as a secondary requirement for the composition design (ACI Committee 207 2005). However, the strength properties are important for the evaluation of the cracking risk at early ages and for long-term deterioration assessment scenario, which can occur due to seismic loads and potentially alkali-reactive aggregates (Nixon and Sims 2016).

For cracking risk assessment it is necessary to accurately determine the mechanical properties development, as well as the stress development during the heat dissipation. In dam concrete the cement is often replaced by fly ash to cope with the temperature rise effect and to control future swelling effects related with alkali-aggregate reactions (ACI Committee 207 2005). Results show that dam concrete's elastic and strength properties have a slower development, lower maximum strengths and slightly higher modulus of elasticity (ICOLD 2008), when compared with conventional concretes.

As mentioned, dam concrete is usually made with large size coarse aggregates, for which common mould dimension and laboratory equipment are not suitable. As a result of these difficulties, concrete quality control and concrete characterization are sometimes based on results from wet-screened concrete obtained from the full-mixed mass concrete. In addition, several embedded monitoring devices are cast with wet-screened concrete due

to its small size when compared to the maximum size of aggregate (MSA) of full-mixed concrete. Wet-screened concrete is traditionally obtained by removing the larger aggregates, usually greater than 38 mm (#38 wet-screened concrete), from the original concrete mix while it is still fresh (Blanks and McNamara 1935). The wet-screening procedure implies a significant change in the composition of dam concrete but, due to dam concrete specific use and despite the extensive experimental work and research developed worldwide concerning concrete behaviour, correlations between the behaviour of full-mixed and wet-screened concretes are still to be determined (USBR 1988; Soares de Pinho *et al.* 1988; Vilardell *et al.* 1998; ICOLD 2008; Elices and Rocco 2008; Serra *et al.* 2012).

Experimental testing of the produced concrete carried out for quality control and for properties characterization is a key element for this type of structures. The complexity of concrete response, from viscoelastic to fracture behaviour, implies different tests to determine the instantaneous behaviour, both in tension and compression, and time-dependent behaviour of wet-screened and full-mixed concrete. Usually, the instantaneous behaviour is characterized by modulus of elasticity determination tests, tensile and compressive strength determination tests carried out at several ages. The time-dependent behaviour is evaluated from *in situ* and laboratory compressive creep tests using different loading ages (RILEM TC 107-CSP 1998).

1.2 Objectives and methodology

Dam structural design practice often considers material properties based on estimates provided by experimental data available in the literature or from other works and on preliminary test results obtained from trial compositions (ICOLD 2008). Since it is difficult to test dam concrete, scientific methods to material property prediction are a useful aid to the design phase and for construction and maintenance procedures. This thesis contributes to technological developments of concrete engineering and to aid maintenance, safety control and lifetime prediction issues, with focus on the material properties characterization.

The first main goal of this work is to better understand the behaviour of dam concrete over time through experimental results and to develop both analytical and numerical prediction models. The second main goal is to obtain accurate estimates of dam concrete's main structural properties considering the wet-screened concrete test results and the composition data. A secondary goal is the development of generic analytical and numerical

models suited for the study of any type of concrete and that could be used for the prediction of complex structural behaviours.

A reliable concrete structural property prediction model based on the wet-screened results and physically-based prediction models at the mesoscale can give additional information on the structural behaviour of concrete, further understanding of the differences between the two types of concrete and reveal the main effects of wet-screening on deformability and strength properties. The combination of physically-based expressions and numerical models, based on test results, can help to:

- Reduce the number of tests of full-mixed concrete using large specimens, which are known to be costly;
- Guarantee, during the construction phase, that the concrete strength, evaluated from wet-screened concrete samples meets the design requirements of the dam concrete;
- Calculate stresses in dam concrete using the strains measured in strainmeter groups placed in the dam's body but embedded in wet-screened concrete;
- Improve structural property estimates, lowering uncertainty levels and safety factors. This, ultimately, will lead to more efficient structures and less unnecessary material consumption;
- Obtain better estimates of strength and deformability development at early ages allowing for more reliable decisions about cracking risk management, such as temperature control, volume changes, curing and lift scheduling;
- Improve long-term behaviour interpretation of concrete dams, accurately identifying differences between "normal" behaviour and unusual behaviour (a tool for health monitoring) and, therefore, achieve a more reliable safety control (USBR 2005; Nixon and Sims 2016).

The approach used for this work is to study and combine the features of three main scientific areas: experimental characterization and definition of statistical relationships; semi-empirical expressions and simple rheological models for the concrete behaviour based on general expressions; and, numerical analysis prediction of concrete behaviour. As described in Figure 1.1, each approach is not self-contained since it can either supply information or be influenced by the results obtained in other approach. For example, test results can be used to calibrate the prediction models. Additionally, a good model can be also used to test hypothesis, to interpret and validate test results. Models can also help to

better define experimental procedures or to study and test new experimental techniques without additional costs.

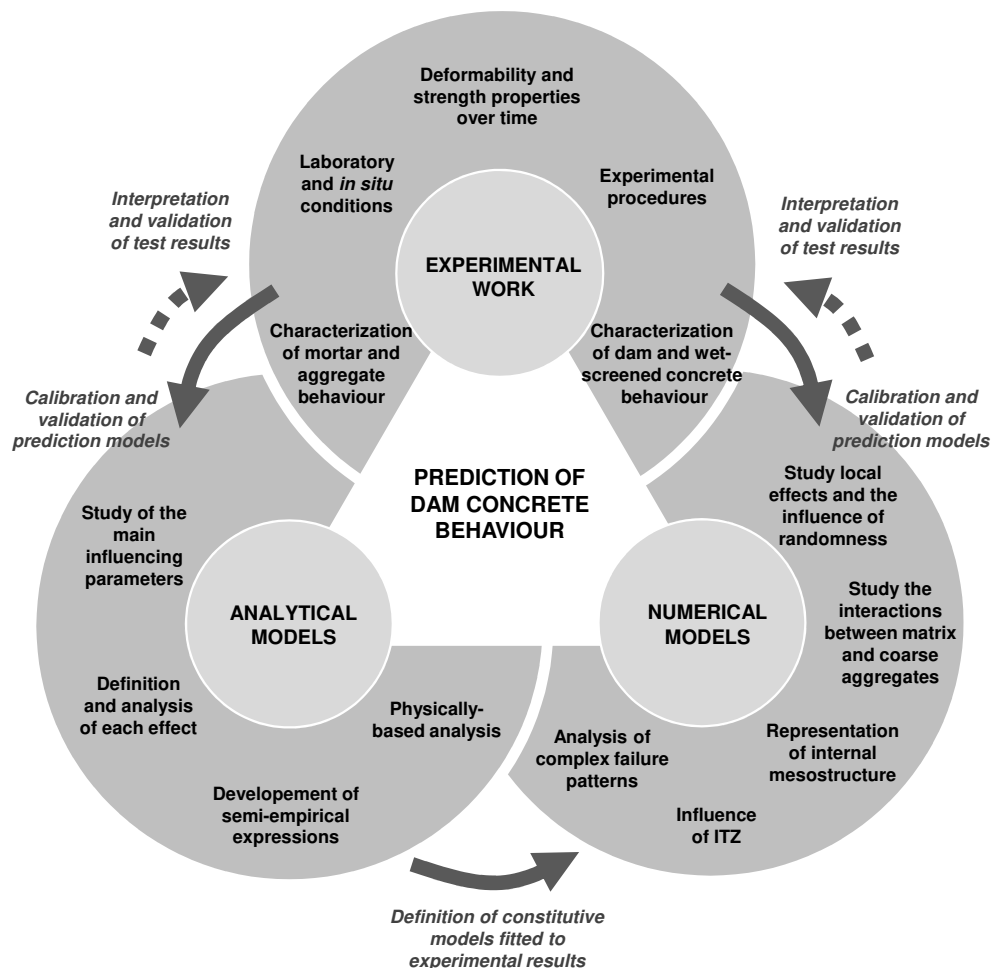


Figure 1.1: Schematic view of the approach used in this work combining the three main scientific areas: experimental work; analytical modelling; and, numerical modelling

The experimental work sets the base for this research in which different structural properties of dam and wet-screened concretes, mortar and aggregates, were determined for laboratory and on site conditions. This allowed for the definition and identification of the overall behaviour of the materials and establish statistical correlations between the composition and the development of the main structural properties.

The experimental results, obtained for limited conditions, were used to fit different types of analytical prediction models which can be then used for several testing conditions, for example different loading ages and different curing temperatures. These type of models were built on physically-based concepts which are of great aid for understanding the behaviour of concrete and, especially, of dam concrete. This advantage was key to model

the effect of the wet-screening procedure on dam concrete properties and to establish new analytical models based on semi-empirical expressions for the behaviour prediction.

The final part of the work focuses on the development of a numerical solution based on a structural system of rigid particles to study the behaviour of concrete taking into account its internal mesostructure. The main heterogeneity in concrete is due to the different behaviours of coarse aggregate and mortar and the effect of their interactions. The mesoscale modelling can give an important insight on how each component interact inside the concrete and how they can affect the mechanical properties over time, considering the concrete composition and the external environmental conditions.

The analytical models, calibrated with experimental results, are used to define the behaviour of each numerical model component, *i.e.* the behaviour of each type of contact between particles. The concrete particle models require thorough validation using simple examples in which the input conditions can be controlled. The expected behaviour of concrete can be checked using established examples considering more complex problems, available in the literature. This validation sets the basis for the goal of this work and for the application to the case study: the prediction of Baixo Sabor dam concrete behaviour and the simulation of the wet-screening procedure, for both instantaneous and delayed structural properties.

The work developed in this thesis aims to contribute to technological developments of concrete dam engineering providing improved experimental procedures, relevant test results and new analytical and numerical prediction tools to support safety control issues related to the structural properties determination.

This work was done within the framework of P2I/LNEC DamConcrete research project, entitled "Caraterização experimental e modelação numérica das propriedades reológicas do betão de barragens".

1.3 Numerical and graphical tools used for the development of the thesis

The work presented in this thesis has been developed using different platforms and tools. Firstly, the experimental results have been handled using both MATLAB (The Mathworks Inc. 2010) and R (R Development Core Team 2017) languages for analytical manipulation and as a graphical tool. The statistical analyses of the test results, which included the use

of linear and nonlinear regressions, multiple linear regressions and parameter-fitting using optimization methods, such as genetic algorithms, relied on the opensource R language (R Development Core Team 2017) which is a powerful statistical computing and graphical software environment.

The numerical modelling using Discrete Element Method (DEM) applied to particle models was implemented in C++ language, using the Visual Studio C++ 2010 Express platform (Microsoft Corporation 2010b). This type of language enables easy and fast computational processing based on object-oriented programming. The particle assembly generator was developed by Monteiro Azevedo during his Ph.D. work (Monteiro Azevedo 2003) and it was developed in C language. The visualisation of the particle assemblies geometry and of the graphical results of the numerical models relies on opensource Paraview (Ayachit 2015)

The design and detailing of creep cells experimental setup and some schematic figures throughout the thesis were done using the graphical platform AutoCAD (Autodesk 2016).

1.4 Thesis outline

This thesis has seven chapters, including this Introduction, in which the work's framework and research problem are presented, and the Conclusions chapter.

The second chapter presents a literature review on the structural behaviour of concrete with particular focus on dam concrete, on its composition, types, production and testing issues and *in situ* conditions. A review on the different types of analytical and discrete models is presented. Special attention is given to semi-empirical or analytical models which try to explain concrete behaviour based on its composition, for example on the properties of the aggregates. Similarly, the review focuses on discrete models considering the mesostructure of concrete. Several basic structural concepts are introduced in this chapter in order to complement the methodologies and models used throughout the thesis.

The third chapter presents the developed experimental characterization of dam concrete based on laboratory and *in situ* tests. The case study is the Baixo Sabor dam concrete due to its structural importance and, therefore, to the extensive concrete characterization performed during construction of both dam and wet-screened concretes. Three sets of creep cells were installed in Baixo Sabor dam which allowed for the improvement of the experimental setup and the testing procedures, aiming to reduce costs, to facilitate the

installation and to increase the accuracy of the results. The test results revealed the main differences between the two types of concrete and the influence of the coarse aggregate on the main structural properties. The test results of the main structural properties of the aggregates and the mortar are also presented.

The fourth chapter presents three different methodologies for the prediction of dam concrete properties based on the wet-screened test results using simple analytical models based on semi-empirical laws. The chapter is divided into three main parts: the first relates to the use of two-phase composite models and the equivalent age method to explain the relationship between the modulus of elasticity of dam concrete and the modulus of elasticity of wet-screened concrete; the second part, similarly to the first, establishes a procedure for the prediction of creep strain development of dam concrete based on a two-phase composite model, on the age-adjusted effective modulus (AAEM) method, on the equivalent age method and on the *in situ* test results of wet-screened concrete; and the third part proposes a semi-empirical expression for the prediction of concrete compressive and splitting tensile strength based on the water to cementitious materials ratio and on the maximum size of aggregate (MSA). Combining this expression with the size effect law, a relationship between strength results of dam concrete obtained in large specimens and strength results of wet-screened concrete obtained in standard size specimens is proposed. This chapter proposes also a framework for the quality control procedures concerning the conformity check of dam and wet-screened concrete test results obtained during construction.

The fifth chapter describes the application of the discrete element method (DEM) to 2D rigid particle models (PM) including the developed contact models, the Hooke model, the aging viscoelastic model based on the solidification theory and the Mohr-Coulomb model with cut-off and with linear softening. A new fast numerical procedure for the long-term analysis of cementitious materials is proposed and validated. Due to the time step constraints of DEM, long-term analysis can be very time consuming, therefore the proposed fast numerical procedure separates the calculation time and the real time in order to increase computational efficiency. The fast numerical procedure is validated using simple particle assemblies for different loading scenarios and used in a practical application for the prediction of concrete's aging viscoelastic behaviour based on the properties of its components, the aggregate, the mortar and the interfacial transition zone (ITZ). A specific parametric study combined with an optimization process is used to estimate the

aging viscoelastic properties of the ITZ. The second part of the fifth chapter relates to the implementation of the Mohr-Coulomb model considering brittle failure and linear softening. Similarly to the first part, simple particle assemblies are used to validate the contact behaviour both in tensile and compressive loadings. A practical application to literature results of concrete are also used to further validate the models and perform a parametric study for the main input variables.

The sixth chapter presents the methodology and application of DEM for the prediction of dam concrete structural properties based on the results of wet-screened concrete. This chapter highlights the combination of some of the analytical models used in the third chapter with the particle modelling, namely for the definition of the long-term aging viscoelastic behaviour of mortar. The chapter is divided into the prediction of the long-term behaviour and the prediction of the strength properties of dam concrete. For both parts, the prediction methodology relies on the calibration of the contact micro properties in order to describe the behaviour of the main components of concrete, *i.e.* aggregates, mortar and ITZ, based on the available test results and analytical model predictions. The contact micro properties are then used for the prediction of the wet-screened concrete behaviour, in which the concrete model is further validated, and for the prediction of dam concrete behaviour. The concrete particle models are composed by the coarse aggregates which follow the size distribution of each type of concrete and by the mortar. To take into account the contribution of each component to the overall macroscopic behaviour, the smallest particle in the assembly is restraint to the smallest coarse aggregate. The effect of temperature variations on the development of deformability properties is also considered using the equivalent time method in order to predict the *in situ* behaviour of concrete.

Structural properties of hardened dam concrete

2.1 Introduction

For an accurate safety control related to cracking risk assessment, it is necessary to determine the development of concrete structural properties, as well as the stress and strain histories during construction and the first years (Cervera *et al.* 2000b; Noorzaei *et al.* 2006). Moreover, to interpret the structural behaviour for several decades, both instantaneous and time-dependent properties are key to assess the overall safety of the structure and make reliable lifetime predictions (Naus and Johnston 2001; Charlwood 2009; Schrefler *et al.* 2010; Jia 2010). The main structural properties are the ones related to the deformability, the strength and the thermal expansion coefficient. The deformability properties concern the creep compliance, which includes the instantaneous modulus of elasticity or Young's modulus and the Poisson's ratio. The strength properties are related to the failure mode and the compressive and tensile strengths are the most commonly used for the characterization of concrete.

The large number of variables involved in the production, placing and curing of concrete makes it difficult to have an accurate prediction of its mechanical properties without any previous experimental results. The most common approach to predict the development of the mechanical properties is to use empirical or semi-empirical expressions (Granger

and Bažant 1995; Bažant and Baweja 2000; Hwang *et al.* 2004) but several studies also rely on numerical models to simulate the complex behaviour of concrete considering its mesostructure (Roelfstra *et al.* 1985; Qiu and Zhang 2017). New approaches rely on multiscale analysis in order to explain the influence of each component at different scale lengths (Jennings and Bullard 2011; Honorio *et al.* 2016).

This chapter presents a literature review concerning the dam concrete behaviour, the models used to predict concrete structural properties and it is divided into three main parts. The first part concerns the concrete material properties, focusing on its composition and on the specific material properties of dam concrete. The second part presents a review on the structural properties of hardened dam concrete, mainly the deformability and strength properties. Special focus is given to several experimental results concerning the effect of the coarse aggregate on concrete behaviour and to the research on the effect of wet-screening. The third part of this review relates to the modelling of concrete behaviour and presents several types of approaches for the prediction of the main mechanical properties using both analytical models and more complex numerical models. The analytical models, which include both empirical and semi-empirical models, are based on the observed behaviour of concrete and have the advantage of being very simple to use and give an important reference for the interpretation of new test results. The use of the name "analytical model" for this type of prediction tool relates to the fact that they are based on analytical expressions which are known to describe the behaviour of the material.

For the prediction of long-term behaviour, several types of semi-empirical models have been developed throughout the last decades to obtain the creep behaviour of concrete based on the components contents and on its compressive strength (Neville *et al.* 1983). These type of models can be calibrated using a large creep test database (Bažant and Li 2008) and, more recently, relying also on the long-term structural effects (Wendner *et al.* 2013; RILEM TC-242-MDC 2015).

Other semi-empirical models describe the global effect of the decrease of strength as the water to cement ratio increases (Abrams 1918; Bolomey 1936). For example, the physical explanation of the Abrams law is related with the observation that the amount of water is related with the cement paste quality and with its pore structure. As the quality of the cement paste decreases the strength of the concrete also decreases. The Abram's model parameters depend on the type of strength, the type of cement and aggregates, the admixtures, the curing and testing conditions and the age of concrete.

The numerical models are used for the analysis of complex structural systems for which there is no theoretical solution. Usually, they combine a large variety of material properties and can be used for different geometric shapes and different boundary and loading conditions in order to obtain the structural response. Numerical models imply the discretization of space and time. Each discretized element have a predefined behaviour and, for a given boundary and loading conditions and insuring the compatibility between elements, an approximate solution can be obtained. This literature review concerns only the numerical models based on the discrete element method, which will be used throughout the thesis.

Additionally, a special focus will be given to the use of numerical models for the study of concrete considering its mesostructure. The mesoscale is defined as the intermediate scale between the study of cementitious materials (microscale) and the study of large scale structural systems (macroscale) (Jennings and Bullard 2011). It is usual to consider mesoscale analysis as the study of mortar or concrete in which the fine or coarse aggregates are explicitly taken into account, which in this case defines the scale length between 1 mm to 1 m, *i.e.* at the specimen level.

2.2 Concrete material properties

2.2.1 General aspects

Concrete is an hydraulic composite material made from aggregates with different sizes and a cement-based matrix. It is a manufactured material with significant structural strength and reduced production and placement cost. The cement grains, when in contact with water, react and form a load bearing structure, generally called the cement paste, capable of agglutinating the aggregates together. The composite nature is one of the main features of concrete and determines its behaviour. The heterogeneity of concrete is due to the composition, *i.e.* cement, aggregates, water, air, additions or supplementary cementing materials (SCM) and admixtures.

Due to its profound dissemination and good mechanical characteristics when mixed with water, the most used type of cement is the artificial Portland cement, known just as Portland cement. The Portland cement results from the grinding and calcination of a mixture of about 80% limestone (calcium carbonate) and 20% clay (iron and aluminium silicates). During calcination, the elementary components react and originate the main

crystalline structures of cement, being the tricalcium silicate ($3\text{CaO}\cdot\text{SiO}_2$ or C3S), the dicalcium silicate ($2\text{CaO}\cdot\text{SiO}_2$ or C2S), the tricalcium aluminate ($3\text{CaO}\ \text{Al}_2\text{O}_3$ or C3A) and tetracalcium aluminoferrite ($4\text{CaO}\ \text{Al}_2\text{O}_3\text{Fe}_2\text{O}_3$ or C4AF) the most commons products. The product is called the clinker which is grinded into a fine powder made of small cement particles. The chemical components, mainly C3S and C2S, when in contact with water, react to form new hydrated amorphous structures, the calcium silicate hydrate gel (CSH gel) and the calcium hydroxide ($\text{Ca}(\text{OH})_2$). These exothermic reactions are generally known as the cement hydration. The reaction rate, the type of structures obtained and the interaction between products are still not fully understood (Taylor 1997).

The cement paste agglutinates the aggregates and develops its bearing capacity over time. The aggregates, considered in the past as "inert filling", are recognized today as an important element to the mechanical properties of concrete (Alexander and Mindess 2010). Besides their contribution to the behaviour as a part of a composite material, nowadays it is known that some types of aggregates develop alkali-aggregate reactions in the interface between the paste and the aggregate (AAR). The product of these reactions is a hydrated gel with higher volume than the reactants, which leads to an overall expansion effect in the concrete (Rajabipour *et al.* 2015). The purpose of aggregates in concrete is to be a good filler, with good mechanical properties and well graded, in order to reduce the cement content, keeping acceptable levels of workability and reducing costs (ACI Committee 207 2005). Besides the mechanical properties and grading of the aggregates, the porosity, the water absorption, the size, the shape and the roughness have an important role in the behaviour of the composite material (Alexander and Mindess 2010).

Additions are compounds that replace, within some extent, the Portland cement as the main binder, in order to enhance a particular property or to reduce the heat generated during hydration reactions of the cement. These products, natural or artificial, are divided into two main groups: the pozzolans and the blast-furnace slag (Coutinho and Gonçalves 1994). Within the Portuguese context, and particularly for dam concrete production, pozzolans and fly-ash have been widely used, replacing up to 50% of the Portland cement (Serra *et al.* 2014a). As pointed out by Coutinho and Gonçalves (1994), one advantage of the pozzolan replacement is a reduction of the hydration heat, without the strength decreasing in the same proportion. Another advantage is the control of the AAR potential (ACI Committee 207 2005).

It is generally accepted that the mechanical properties of the hardened concrete, especially the strength properties, are determined by shape and curing conditions of the specimen, the type of loading and the properties of each concrete component: i) the properties, content and distribution of the aggregate in the concrete matrix; ii) the properties and content of the cement paste matrix of binder and water; and, iii) the properties of the interface between cement paste and aggregate surface, the interfacial transition zone, ITZ (Mitsui *et al.* 1994; Ollivier *et al.* 1995; Scrivener *et al.* 2004; Dolado and Breugel 2011). Figure 2.1 shows the different factors that influence the concrete strength, divided into the three main groups (Mehta and Monteiro 2006).

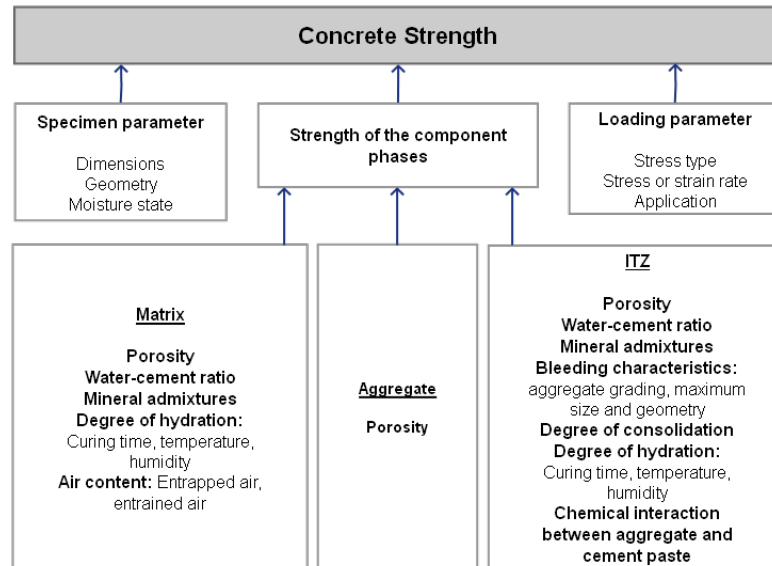


Figure 2.1: Influencing factors of concrete strength (Mehta and Monteiro 2006)

The diversity of concretes available, from self-compacting concrete to high-strength and mass concrete, results in different mechanical property values and development over time. Each type of concrete has its particular applications, according to the required strength, plastic specifications, geometric conditions and practical applications.

2.2.2 Dam concrete

The design of a prescribed composition for a given concrete was, until the end of the nineteenth century, empirical and based on former experience (Coutinho 1988; Flatt *et al.* 2012). Since then, several developments were done, namely related to: a larger variety of products; more information about the effect of each component on the behaviour;

better procedures for optimum proportioning. When prescribing a concrete, specially dam concrete, the experience and the experimental results obtained from former structures are, still, an important aid for the concrete design.

Due to its specific requirements, it is usual, in Europe, to design dam concrete as a prescribed concrete according to the European standard EN 206-1 (NP EN 206 2005). The strength and durability requirements as well as the composition of concrete are specified in order to obtain the desired behaviour over time and trial tests are often carried out in order to define the final concrete composition.

Mass concrete implies the placement of large concrete volumes that requires the adoption of special measures to reduce the generation of heat during hydration reactions, to control volume changes and to minimize the cracking risk at early ages (ACI Committee 207 1997; ACI Committee 207 2005).

Dam concrete is usually produced with large size aggregates in order to reduce the production costs. The grading and cement content are obtained to achieve maximum compaction, complete coating of aggregates and maximum strength. The maximum size of aggregates (MSA) can be 150 mm and the total aggregate percentage can be up to 60% of the total volume (ICOLD 2008). The cement and other cementitious materials content (binder content) in this type of concrete is, therefore, low (100 to 300 kg/m³). Contrary to other concretes, due to the thermal cracking risk, the composition of dam concrete is customized in order to decrease the heat generation, taking the strength properties as a secondary requirement (ACI Committee 207 1997; ACI Committee 207 2005).

Added difficulties are the constraints associated with the production of large volumes of concrete at remote locations and the high rate of construction which implies also a high rate of materials supply. It is very common to use rock quarries placed next to the dam, preferably placed in the reservoir, for the aggregate supply. The rock provided by these quarries has to be tested in order to comply with the necessary requirements for the concrete production. The compromise between the quality of the aggregate and the transportation costs has a great impact on the dam concrete design since the effect of the aggregate properties on most of the mechanical properties is very important. The use of local rock quarries and local aggregates is usually associated with larger property variations over the construction period.

Recent developments of concrete technology are mainly related with the use of new materials and construction procedures. For example, in Portugal, technological advances

lead to an increase of fly ash content added during the mix and a decrease of cement content (from 300 kg/m³ in 1980 to 100 kg/m³ in 2012). It should be noted that the type of cement used in the past, type IV according to ASTM C150 (ASTM 2017) and type II and IV according to EN 197-1:2012 (CEN 2012), had also a percentage of supplementary cementitious materials, such as pozzolanic materials, but in smaller amounts. The use of powerful superplasticizers, water-reducing and air-entraining admixtures also influence the properties of fresh and hardened concrete, increasing the workability for the same water to cementitious materials ratio and producing a more compact product.

In modern concrete dams, the dam concrete is made, in general, with low cement content (between 150 to 200 kg/m³), with fly ash addition and a maximum size of the aggregates (MSA) of 150 mm.

Concrete dam design must respect safety factors based on a specified minimum compressive and tensile strengths, taking into account a maximum heat generation. The reference age for the evaluation of compressive strength can be 90, 180 or 365 days since casting (the International Committee on Large Dams (ICOLD) recommends the age of 180 days or later (ICOLD 2008)). The use of late testing ages refers to the development of significant stress only months or years after casting. Besides, with the use of additions, such as pozzolans, the strength development after 90 days is still substantial (in average, strength can increase 40% from 90 to 365 days, (ICOLD 2008)).

2.3 Concrete structural behaviour

2.3.1 General aspects

Due to its particular application and despite the extensive experimental work and research developed worldwide, general correlations between wet-screened and dam or full-mixed concrete properties are still to be determined (Soares de Pinho *et al.* 1988; Vilardell *et al.* 1998; ICOLD 2008; Serra *et al.* 2012).

ICOLD published a bulletin with a comprehensive review on the physical properties of hardened conventional concrete in dams (ICOLD 2008). This report presents an extensive literature review concerning the development of most relevant mechanical properties, the main factors that influence those properties and also the mathematical models used for the behaviour analysis.

As mentioned before, dam concrete has its particular properties which are greatly

dependent of local materials supply and of environmental conditions and can have large variations from work to work. ICOLD (2008) presents a wide range of test results obtained from several decades of experience in dam construction around the world. Despite the importance of this type of test data, estimates obtained from the other case studies have to be used carefully. The report focuses also on the compressive, tensile and shear strengths, the static and dynamic modulus of elasticity, the creep response, the drying shrinkage, the thermal properties, the water permeability, the frost resistance and the fracture energy. The *in situ* behaviour of dam concrete is also addressed throughout the report. Due to the difficulties associated to dam concrete testing, it is very usual to have a large number of wet-screened concrete test results and very few of full-mixed concrete.

Despite the cast volumes, the placement rates and specific composition, it is necessary to guarantee the design requirements of *in situ* dam concrete. An efficient quality control based on available information of properties of concrete constituents, on simple tests for determining properties of fresh concrete, on placement procedures and on hardened concrete testing, is key to meet the expected structural properties (ICOLD 2009).

Experimental testing of the produced concrete carried out for quality control and for properties characterization, are key elements for this type of structures. The complexity of concrete response, from viscoelastic to fracture behaviour, implies different tests to determine the instantaneous, both in tension and compression, and time-dependent behaviour of wet-screened and full-mixed concrete. Usually, the instantaneous behaviour is characterized by modulus of elasticity determination tests, tensile and compression strength determination tests, carried out at several ages. The time-dependent behaviour is evaluated from *in situ* and laboratory compression creep tests using different loading ages (RILEM TC 107-CSP 1998).

Other key reference is the United States Bureau of Reclamation (USBR) report that includes the main features concerning the production and testing of concrete, with special focus on dam concrete (USBR 2005).

As described, dam concrete can be produced using large size coarse aggregates with maximum size aggregate (MSA) up to 150 mm. As a result, ordinary specimen sizes and laboratory equipment are not suitable to characterize dam concrete with large MSA. The characterization of this large aggregate concretes implies the cast of very large specimens and the use of heavy testing equipment with an added cost to the work. Since the access to these types of equipments is limited, only a few tests are done using this type of concrete

during the dam construction, compromising the concrete characterization and the quality control assessment.

In order to overcome these difficulties, concrete quality control and concrete characterization rely, in a great extent, on wet-screened concrete laboratory results obtained from the full-mixed mass concrete (dam concrete), placed *in situ*. Wet-screened concrete is obtained by removing the larger aggregates, usually greater than 38 mm (#38 wet-screened concrete or SCR38), from the original dam concrete mix while it is still fresh. Several monitoring devices, such as strainmeters, are embedded in wet-screened concrete due to its small dimensions when compared with the MSA.

For a preliminary design, the USBR (1977) recommends the use of average values for the main concrete properties: values between 20.7 and 34.5 MPa for the compressive strength; 5% to 6% of the compressive strength for the tensile strength (1.0 MPa to 2.1 MPa); 0.2 for the Poisson's ratio; 34.5 GPa for the instantaneous modulus of elasticity; 20.7 GPa for the sustained modulus of elasticity, E_{sust} ($E_{sust} = \frac{E_{inst}}{1+\chi\phi}$, in which $E_{inst} = E(t')$ is the instantaneous modulus of elasticity, $\phi = \phi(t, t')$ is the creep coefficient and $\chi = \chi(t, t')$ is the age-adjusted coefficient (Bažant 1988)); $9.0 \times 10^{-6}/^{\circ}\text{C}$ for the thermal expansion coefficient; and, 2402.8 kg/m³ for the unit mass.

2.3.2 Development of strains and stresses in concrete

Considering plain concrete under a sustained stress, $\sigma(t')$, and temperature, $T(t)$, the total strains, $\varepsilon(t, t')$, can be represented by the addition of several terms (Equation 2.1).

$$\varepsilon(t, t') = \varepsilon^i(t') + \varepsilon^c(t, t') + \varepsilon^{cr}(t') + \varepsilon^{sh}(t) + \varepsilon^T(t) \quad (2.1)$$

where t is a given time after cast, t' is the age at loading, $\varepsilon(t, t')$ is the total strain, composed by the sum of instantaneous strain, $\varepsilon^i(t')$, creep strain, $\varepsilon^c(t, t')$, strain due to cracking, $\varepsilon^{cr}(t, t')$, shrinkage, $\varepsilon^{sh}(t)$ and strain due to thermal variations, $\varepsilon^T(t)$. Stress-dependent strains in undamaged concrete are usually divided into instantaneous and creep or delayed, whether the duration of the load is "fast" or sustained over time. The separation between instantaneous and creep strains is not unique since it depends on the load duration and often leads to misinterpretations of the concrete behaviour (Bažant and Baweja 2000). Despite that, this division is of great use for structural analysis and for the interpretation of experimental test results and monitored structural data. When loading is considered to

be instantaneous and temperature is assumed constant, creep strains are small, thermal strain is zero and shrinkage during that period is negligible. The total strains are only age dependent, although it is known that both instantaneous and cracking strains depend also on the loading duration, $t - t'$,

$$\varepsilon(t') = \varepsilon^i(t') + \varepsilon^{cr}(t') \quad (2.2)$$

Concrete can be considered as a time-dependent linear viscoelastic material provided that stress is less than 40% of the compressive strength and that large sign inversion, large cyclic strains or even significant changes in water content and temperature do not occur (Bažant 1988). As a consequence of this hypothesis, we can use the principle of superposition given by the Stieltjes integral,

$$\varepsilon(t, t') - \varepsilon^0(t) = \int_0^t J(t, t') \frac{d\sigma(t')}{dt'} dt' = \int_0^t J(t, t') d\sigma(t') \quad (2.3)$$

where $\varepsilon^0(t)$ is the sum of the shrinkage and thermal strains.

The instantaneous strains of undamaged concrete are related to the modulus of elasticity or Young's modulus which can be obtained from standard laboratory tests. It is known that different values of modulus of elasticity can be obtained from different testing conditions, mainly due to the loading rate, load duration and magnitude of loading. Figure 2.2 shows the different possible values of modulus of elasticity, from tangent to secant modulus at a given stress-strain curve point, for instantaneous loading (Figure 2.2 a)). For viscous materials and for sustained loading, higher the load duration, lower the modulus of elasticity values (Figure 2.2 b)).

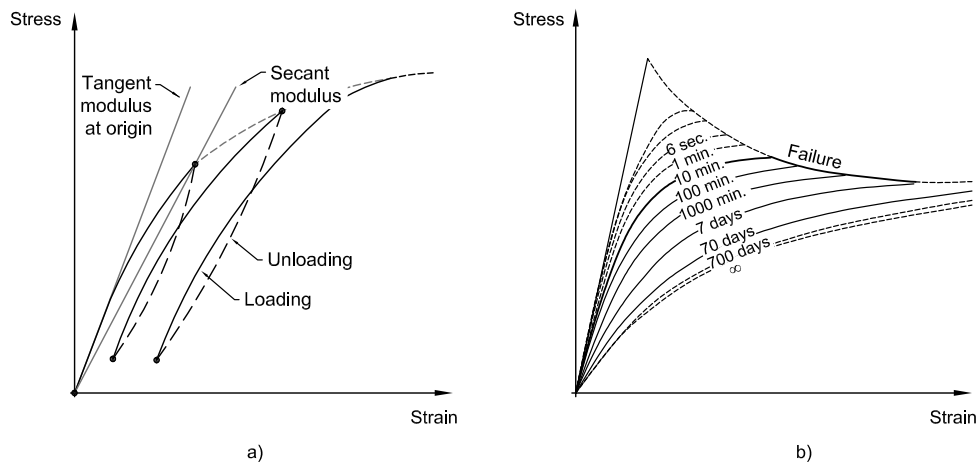


Figure 2.2: Representation of stress-strain curve of concrete in compression for a given t' : a) instantaneous loading; b) sustained loading. Adapted from (ICOLD 2008))

Strains can also be divided into two main types: stress-dependent strains and stress-independent strains. Regarding Equation 2.1, $\varepsilon^i(t')$, $\varepsilon^c(t, t')$ and $\varepsilon^{cr}(t, t')$ are stress-dependent and $\varepsilon^{sh}(t)$ and $\varepsilon^T(t)$ are stress-independent strains. As the instantaneous load increases, local areas in concrete start to crack yielding the global nonlinear behaviour. Small microcracks can increase in size and length and start to merge into large cracks. From this point on, the cracking strains increase significantly until the specimen cannot withstand more load. Figure 2.3 shows the instantaneous and delayed behaviour of concrete for the complete compressive strain range. The stress-strain-time representation allows for the correspondence between each type of deformation (black lines represents the instantaneous behaviour and the grey lines represent the delayed behaviour).

The black continuous line in Figure 2.3 a) describes the instantaneous behaviour, considering that no creep strains develop: points 1 and 2 refer to elastic behaviour (until 30% to 40% of the maximum strength, $1 \approx 1^i$ and $2 \approx 2^i$); point 3 already exhibits some inelastic behaviour, shown by the development of cracking strains (difference between point 3 and point 3^i , in which the superscript “i” refers to the instantaneous part of the deformation); point 4 refers to the maximum compressive strength ($f_{c,max}$); and point 5 defines the concrete failure. The post-peak behaviour, in which the stress capacity decreases as the strain increases, after point 4 is known as softening and refers to the nonuniform distribution of internal stresses due to the heterogeneity of concrete and to the nonuniform initial internal stresses that can be found at the mesoscale (Vonk 1992).

The grey dashed line in Figure 2.3 a) corresponds to the equivalent stress-strain for sustained loading (points 1^* , 2^* and 3^*), in which instantaneous, creep and cracking strains occur simultaneously. Considering the strain-time behaviour (Figure 2.3 b)) it is possible to obtain the strains development over time. The grey continuous lines refer to the total strains ($\varepsilon(t, t')$) and the grey dashed lines refer to the instantaneous strains over time, for different loading intensities at time, t' . Primary, secondary and tertiary creep develop according to the level of applied stress. Primary creep occurs for low stress levels and is defined by the decreasing creep rate with time. Secondary creep occurs when creep strains develop at a constant rate. Tertiary creep occurs when the creep rate increases with time due to high levels of stress. Tertiary creep only occurs for high stresses above 40% to 50% of the maximum compressive strength, $f_{c,max}$. At high stresses, close to the maximum strength, the progression of microcracking seem to induce the apparent increase of creep (tertiary creep) and lead ultimately to failure.

CHAPTER 2. STRUCTURAL PROPERTIES OF HARDENED DAM CONCRETE

By its turn, creep strains can be classified also as basic creep and drying creep, according to the curing conditions of concrete. Basic creep refers to the increase of deformation of concrete under hygrometric equilibrium (sealed specimen or moisture cured), due to constant stress. Drying creep is the increase of deformation of concrete induced by the moisture exchange, due to constant stress.

Figure 2.4 shows the different strain development over time for a sustained loading since t' , under constant temperature and subjected to drying. Due to the hardening process of concrete, the modulus of elasticity values increase with time and, therefore, the real elastic strain decreases. It is usual to consider the nominal elastic strain as the obtained at time of loading, t' .

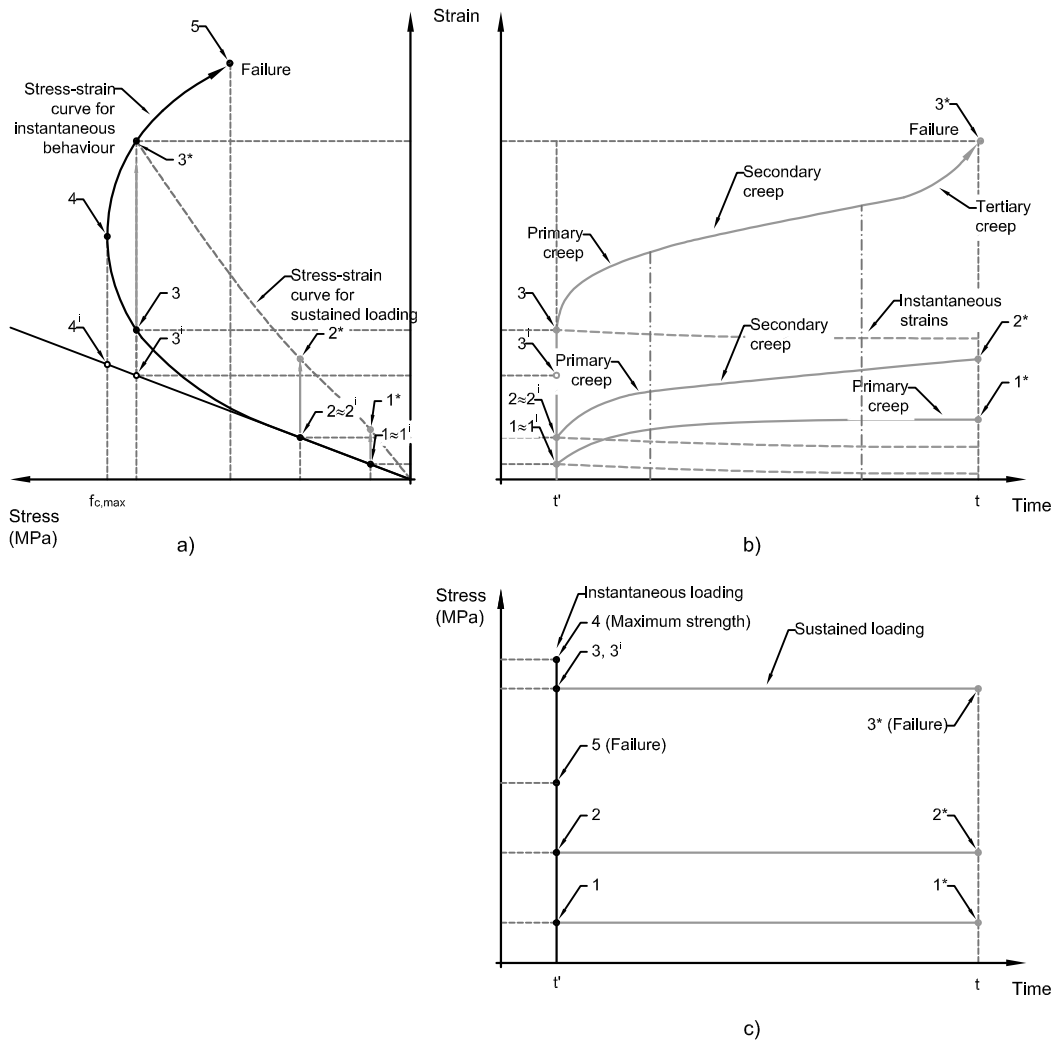


Figure 2.3: Representation of stress-strain-time behaviour of concrete for instantaneous and sustained compressive loading: a) stress-strain behaviour; b) strain-time behaviour; c) stress-time behaviour

After the loading is removed the real elastic strain is immediately recovered and the strain slowly decrease following the creep recovery which can be smaller or, for very long-term loadings, equal to the creep compliance. Usually, an irreversible strain remains after the loading is removed which relates to the irreversible deformations that occur over time (Neville *et al.* 1983). Shrinkage strains develop over time due to cement hydration (autogenous shrinkage), water movement due to drying (drying shrinkage) and hydrated cement carbonation (carbonation shrinkage) (Oliveira Santos 2006).

Figures 2.4 and 2.5 show a schematic view of the different types of deformations and stresses associated with the different types of loadings (constant stress or constant strain), restraints and curing conditions (with and without moisture movement between concrete and the environment).

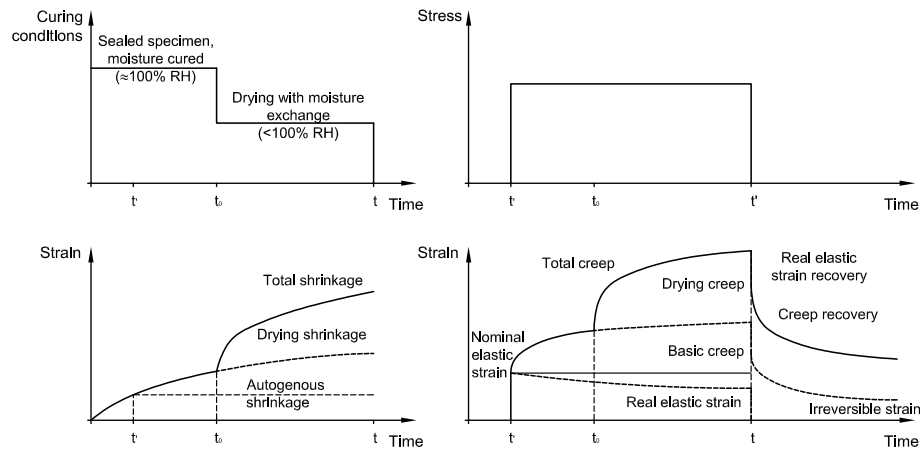


Figure 2.4: Definition of strain components in the strain-time representation

Strength properties are related to the maximum stress obtained when the load is applied without any creep development (instantaneous or short-term loading). Deformability properties relate both to the elastic part of the stress-strain curve for instantaneous loading and to the delayed deformations due to sustained or long-term loading.

CHAPTER 2. STRUCTURAL PROPERTIES OF HARDENED DAM CONCRETE

Mechanism	Diagram	Strain vs. Time	Stress vs. Time	Notes
Basic Creep				No moisture movement between concrete and ambient (no drying shrinkage) Constant stress over time
Stress Relaxation				Constant strain over time
Drying Shrinkage (Unrestrained)				The member is free to move No stresses are generated
Drying Shrinkage (Restrained)				Development of tensile stress
Drying Shrinkage (Under constant strain)				The previous example is a particular case with $\sigma_0 = 0$
Creep + Drying Shrinkage				The total strain is not the sum of the elastic, basic creep, and drying shrinkage strain. the strain due to drying creep should be included.
Drying Shrinkage + Stress Relaxation (Restrained)				The relaxation stress opposed the stress due to drying shrinkage
Drying Shrinkage + Stress Relaxation (Under constant strain)				Shrinkage and relaxation stress act in the same direction

Figure 2.5: Strain and stress behaviour over time with respect to loading, restraining and curing conditions (Mehta and Monteiro 2006)

2.3.3 Deformation properties

Concrete deformability properties can also be divided into instantaneous and delayed properties, *i.e.*, modulus of elasticity or Young's modulus, creep and relaxation. The complete deformability behaviour can be described by a creep compliance or creep function, $J(t, t')$, from which the elastic modulus, $E(t')$, and the relaxation function, $R(t, t')$, can be obtained (Bažant 1972; Bažant *et al.* 1979; Bažant *et al.* 2013).

The modulus of elasticity at the age t' , $E(t')$, can be defined as the uniform stress, $\sigma(t')$, needed to obtain a unit strain, $\varepsilon(t')$, $\left(E(t') = \frac{\sigma(t')}{\varepsilon(t')}\right)$ which can be defined as the slope of the stress-strain curve. For characterizing the approximate linear behaviour of concrete, the experimental value of modulus of elasticity is usually obtained from the secant between a predefined lower and upper stress. For example, as specified in (LNEC 1993a), the lower stress is taken as 0.6 MPa and the upper stress is taken as a third of the maximum stress, obtained in cylinders.

The viscoelastic and viscous properties of concrete also influence the value of the modulus of elasticity. The instantaneous properties are defined with an arbitrary criteria which is related to the time under loading. Very short loading times, yield higher instantaneous modulus and larger loading times allow for the development of the creep strains and yield lower instantaneous modulus. Dynamic modulus of elasticity is obtained for a very high loading rate and it is usually used for dynamic analysis. The criteria for the definition of the time under loading can be very different from standard to standard. The Portuguese standard E397 (LNEC 1993a) specifies a sustained load during 30 seconds after the upper stress is achieved. The time-dependence makes the comparison between several experimental sources of modulus of elasticity very difficult.

The Poisson's ratio, defined as the ratio between the lateral strains, $\varepsilon_{lateral}(t, t')$, and the axial strains, $\varepsilon(t, t')$, for a uniform axial stress, $\sigma(t')$, is usually considered to vary between 0.15 and 0.20 and invariant in time (ICOLD 2008). Most of structural analysis considers the value of 0.20 although some studies report the existence of a creep and relaxation Poisson's ratio which are specially relevant for tridimensional stress states (Gopalakrishnan *et al.* 1969).

Creep strain is defined as the increase of strain under constant stress and the stress relaxation is the decrease of stress under constant strain. Although several studies concerning concrete creep were carried out throughout the last decades in a structural and

material level, the physical and chemical phenomena are yet to be fully understood (Acker 2001; Vandamme and Ulm 2009).

Creep and relaxation effects relate to the same material phenomena, which is thought to be due to displacement diffusion mechanism, adsorbed water movements on the surface of the hydrated cement, viscous deformation of the hardened cement, solubility increase with the applied stress and atomic rearrangement at the nanoscale (Coutinho 1977; Neville *et al.* 1983; Vandamme and Ulm 2009). The systematic and comprehensive work of Neville (Neville and Meyers 1964; Neville *et al.* 1983; Neville 1983; Neville and Brooks 2010) and Coutinho (Coutinho 1977; Coutinho and Gonçalves 1994) are key for the study of concrete creep. The complexity of the phenomena and the variety of components of concrete makes it impracticable a comprehensive study about the origin of creep (Neville *et al.* 1983). Concrete creep is influenced by intrinsic factors such as, the properties of each component, the mix proportions and the concreting conditions, as well as by external factors, such as for example, the loading age, the temperature and humidity levels, the intensity and type of loading (Neville and Meyers 1964; Soares de Pinho 1989).

The viscoelastic properties of concrete are mainly due to the time-dependent behaviour of the cement paste but the composite nature of concrete has a large influence on the development of creep strains over time. The aggregates, which, for this type of deformation and stress range, are considered elastic, restraint the development of creep strains of the cement paste and introduces a nonuniform stress state at the mesoscale.

It is usual to associate the strength of concrete with creep since as the quality of the cement paste increases, *i.e.* as the water to cement ratio decreases, the creep strains also decrease. As a general rule, Neville stated that "for constant mix proportions and the same type of aggregate, creep is proportional to the applied stress and inversely proportional to the strength at the time of application of load" (Neville 1959). As concrete ages the instantaneous and creep strains are bound to decrease due to the progression of cement hydration and water consumption. For usual cement contents between 300 kg/m³ and 400 kg/m³, creep strains decrease as the cement and the aggregate content increase (Coutinho and Gonçalves 1994). Similarly, higher modulus of elasticity of the aggregates reduces significantly the creep strain development due to the restraint of the creep potential of the cement paste. The larger absorption and porosity of the aggregates eases the water movements around the aggregates leading to an increase of creep (Neville *et al.* 1983). It is also believed that the microcracking and slip, especially near the interface between the

aggregates and the cement paste, the interfacial transition zone (ITZ), can be an important factor for the development of creep (Neville *et al.* 1983). Ramos (1985) refers to the effect of moisture and temperature as the two most important external factors. Concrete drying leads to a significant increase of creep (drying creep) and to differential creep development inside the specimen or structural element. Temperature variations have opposite effects on creep strains.

Although its experimental difficulties, the study of creep in tension has particular interest for assessment of cracking. The main difficulties are associated with the measurement of very small strains, the correct measurement of shrinkage and the application of a pure tension stress state. Although some contradictory results, it is generally believed that creep in tension has similar development of creep in compression, except for the early ages where the creep rate are higher for tensile loadings (Coutinho and Gonçalves 1994).

Concrete shrinkage is defined as the decrease in size of unloaded specimens and is mainly due to the desaturation of the cement paste pores which introduces internal contraction forces and the subsequent size reduction (Coutinho and Gonçalves 1994). Other types of shrinkage, such as the chemical, plastic and carbonation shrinkages, also occur. The desaturation can occur from the loss of evaporable pore water due to its consumption during the hydration of cement (autogenous shrinkage or self-dessication) and from the exchange of moisture content between the internal structure of concrete into the environment. Similarly to creep, the cement type and content, the aggregate properties and the water to cement ratio are the main factors influencing shrinkage strains (Coutinho and Gonçalves 1994). The curing conditions, particularly the moisture differential between the specimen and the external environment, and the thickness of concrete specimen or structural element have a significant effect on the development of drying shrinkage (Coutinho and Gonçalves 1994).

Deformation properties are important parameters for the study of short and long-term behaviour of concrete dams. The stress relaxation is specially relevant for the construction period in which the temperature variations are most significant and when the stress relief is especially important. Over time, the development of the creep strains translate into the increase of the global structural displacements over time. An accurate estimate of the concrete creep compliance is key for interpretation of the normal behaviour and for the identification of possible deterioration scenarios.

Dam concrete should be designed in order to have a moderate creep strain development and avoid an excessively rigid material. Concretes with a small creep strain development

and with a limited capacity of stress relaxation are more likely to develop cracks (ICOLD 2008). The specific composition of dam concrete, with large fly ash content and large aggregates, requires further research regarding the hydration and aging processes based on dam concrete experimental results.

For dam concrete, the service stresses are, most of the time, below 30% to 40% of the maximum compressive strength and, therefore, only primary creep develops. Additionally, since water diffusion in concrete is very slow, it is usually considered that the dam body remains in autogenous conditions, without drying or with no moisture exchanges (sealed conditions). This assumption implies that the main dam's body only develops basic creep strains and autogenous shrinkage over time.

Experimental studies concerning deformability properties of dam concrete are limited and creep test results are even more scarce due to the testing difficulties. Since dam concrete is largely constraint to the geographic and logistic conditions and the creep strain development depends on a large number of variables, it is difficult to find a standard behaviour. Generally, dam concrete has lower creep strain development when compared with standard concrete used for conventional structures, such as buildings and bridges. The lower values are due to the large aggregate content and the use of small cement content. Creep test results of dam concrete, placed on site, are available (USBR 1955; Pukhov 1978; Pukhov and Kuleshov 1981; Ramos and Soares de Pinho 1981; Ramos 1985; Soares de Pinho *et al.* 1988; Soares de Pinho 1989; Smith and Hammons 1993; ICOLD 2008; Serra *et al.* 2012; Serra *et al.* 2016a). The work of Portuguese researchers in this subject, from LNEC (1968) and Silveira and Florentino (1971) to Coutinho (1977) and Soares Pinho (Silveira *et al.* 1981; ICOLD 2008) in the eighties and nineties, is noteworthy and recognized internationally.

2.3.4 Strength properties

The ultimate concrete properties are related to the fracture modes involved which depend on specimen geometry, internal aggregate structure, boundary and loading conditions (Van Mier and Nooru-Mohamed 1990; Vonk 1992). Taking also into account the different properties of the concrete components, it is possible to understand the difficulties of predicting the strength of concrete and of comparing test results from different origins.

One of the most important factor influencing the compressive and tensile strength is the porosity of the cement paste, especially of the interfacial transition zone (ITZ). A

more porous material is likely to have a lower ultimate strength due to more and larger voids (that can be seen as defects). Directly related to the porosity is the water-cement ratio or, when other cementitious materials are used, water-binder ratio (considering the binder as the sum of cement and additions).

Since the set of concrete, the strength properties increase continuously to a maximum value as the cementitious materials react with the available water. The strength development over time can be fast or slow. The strength gain depends on the type and fineness of cement, the presence of additions and admixtures and the curing conditions. For example, the use of pozzolanic materials is known to slow the global hydration process since this type of materials remains inactive during the early ages and start to react at latter ages providing significant strength increases over the first year (Ganesh Babu and Siva Nageswara Rao 1996).

The main strength properties for the analysis of concrete structures are the tensile and compressive strengths. There are several experimental methods for the determination of these properties which should be taken into account. Tensile strength can be obtained directly by pure tension tests or indirectly using flexural beam tests and splitting tensile tests (or Brazilian tests). The pure tension test, although more expensive and technically demanding, gives the real tensile strength associated with fracture mode type I (Coutinho and Gonçalves 1994). Other indirect tensile strength tests depend on the testing conditions, such as the specimen size and shape, the boundary and loading conditions.

Similarly to indirect tensile strength tests, compressive strength tests depend also on the testing conditions. It is known that the failure of quasi-brittle materials, such as concrete, is size-dependent due to the development of a finite volume of a fracture process zone (FPZ) (Bažant 1994). The relationship between the volume of the FPZ and the size of the specimen determines the amount of damaged area and the cracking progression in the specimen. For this type of material with post-peak softening, larger specimens yield lower strength properties (Kim *et al.* 1999).

The characteristics of the testing machine are also important for obtaining different types of failure modes in compression (Coutinho and Gonçalves 1994). For example, the friction between the steel loading platens on the concrete specimen introduces local lateral restraint and a confined volume at both ends of the specimen which is known to greatly influence the maximum compressive strength and the post-peak response (Mier *et al.* 1997). The existence of these confined zones due to frictional restraint implies also the height of

the specimen as an important factor for the compressive strength.

For both types of strength, the softening response is linked to the measurement length and location of the strain gauges. This factor is especially relevant for tensile strength due to the localization of damage in a narrow crack (Vonk 1992).

Figure 2.6 presents the generic stress-strain behaviour of concrete under compressive and tensile uniaxial stresses and describes the cracking development around the aggregates. For instantaneous compressive loads, until 30% to 40% of the maximum stress, one can consider a linear behaviour (①), from this stress to 70% of the maximum stress, microcracking starts to develop, specially in the weakest areas, the ITZ, and the curve yields some curvature (② and ③), from 90% to the maximum stress, microcracking propagates to visible cracking and the Poisson's ratio varies significantly (④). Under constant strain velocity loading and special testing conditions (Hudson *et al.* 1972; Vonk 1992; Mier *et al.* 1997), the specimen still bears load and the strain increase rapidly after maximum stress (⑤). The development of a stable descendent curve, known as softening, is due to the remaining plastic bond and to the shear strength between crack surfaces, in which aggregate interlocking can have an important contribution (Walraven 1980; Vonk 1992). Softening occurs both for compressive and tensile loadings and is especially sensitive to the loading conditions. For compressive loadings, platens with low frictional restraint and tall specimens yield more brittle responses (steeper softening curve, ⑤¹ and ⑤²). For tensile loadings, due to the damage localization in a very small volume, large measurement lengths yield more brittle global responses (⑥¹ and ⑥²).

The composite nature of concrete is present in the compressive stress-strain curves, where it is possible to study the material behaviour in all of its strain capacity. As investigated by Gilkey and Murphy (Coutinho and Gonçalves 1994), the nonlinear behaviour of concrete is mostly due to the presence of aggregates. Both bulk behaviour of rock and cement paste have a longer linear behaviour. Although several other factors affect the behaviour, their work showed that compressive stress-strain curves of concretes with different coarse aggregate contents yield different nonlinear degrees (Figure 2.7).

This behaviour is due to small sliding and microcracking development in the cement paste around the aggregate, which turns into craking and failure. As referred by Vonk (1992), "stiff aggregates act as stress concentrators" and that the load capacity is transferred mainly from coarse aggregate to coarse aggregate, from the top loading platen to the bottom loading platen. The internal forces are not straight due to the random distribution of

2.3. CONCRETE STRUCTURAL BEHAVIOUR

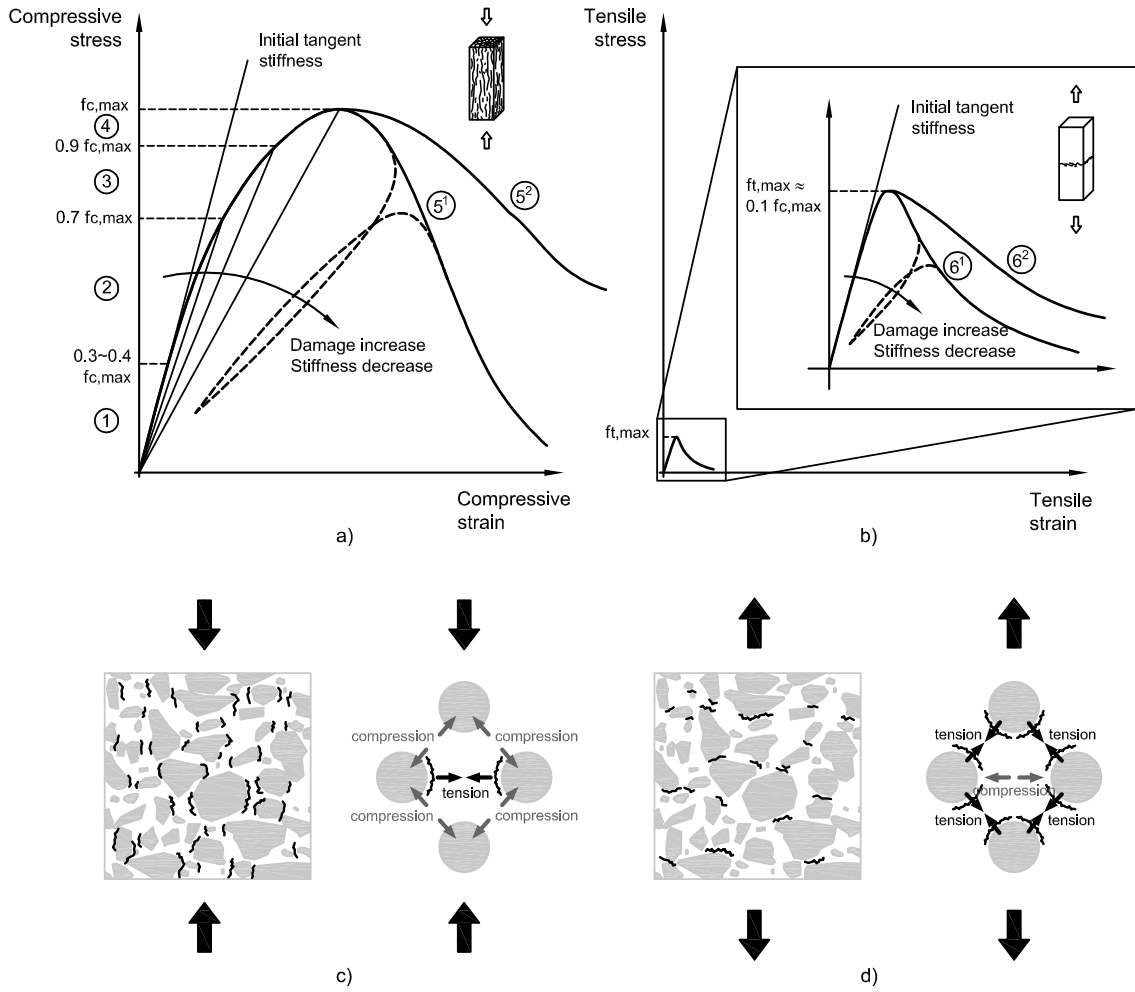


Figure 2.6: Stress-strain behaviour of concrete under compressive and tensile uniaxial stresses and illustration of the cracking development around the coarse aggregates

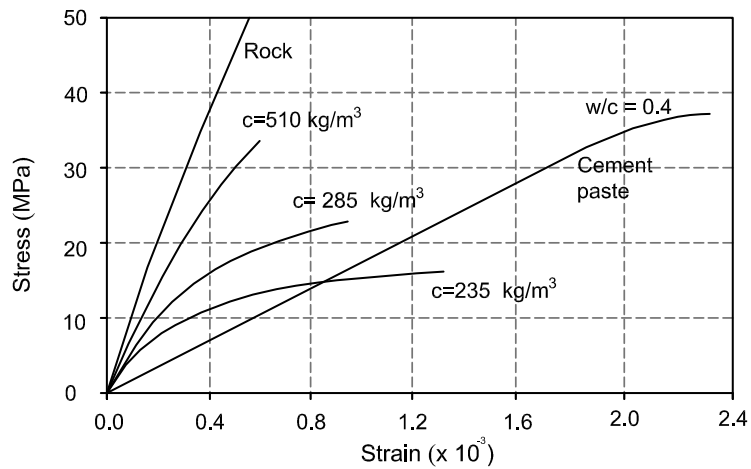


Figure 2.7: Comparison between compressive stress-strain curves of rock, cement paste and concrete with several coarse aggregate contents (Coutinho and Gonçalves 1994)

aggregates which introduces balanced lateral tensile forces inside the specimen between aggregates (Figure 2.6). Since the interfacial transition zone has weaker properties, the lateral bond between the cement paste and the aggregates is firstly damaged.

2.3.5 Effect of *in situ* conditions on hardened dam concrete rheological properties

Concrete properties depend on local conditions which can vary widely from work to work and during the hardening process and often differ from the ones obtained from laboratory standard procedures. Therefore, it is important to obtain and understand the relationship between *in situ* and laboratory test results. *In situ* conditions refer mainly to the temperature and moisture content variations.

The casting, compaction and curing procedures on site can introduce significant variations on the main structural properties. The effect of temperature and moisture content histories should be considered since it affects the development of the hydration processes and of the cement's internal structure (Coutinho and Gonçalves 1994).

One of the most important factors is the effect of temperature variations on creep strain and strength development over time. As previously described, higher curing temperature increases the rate of hydration, the load bearing cementitious structure grows faster and stiffer over time.

Elevated temperatures before the load application imply smaller short-term creep strains since temperature accelerates the chemical reactions of the cement hydration. On the other hand, higher temperatures also produce higher creep rates due to the viscosity reduction, the acceleration of the water movements and water pressure inside the cement paste pores (Nasser and Neville 1967; Silveira and Florentino 1971; Neville 1983). The global effect of these opposite mechanisms is an increase of creep strains over time. A comprehensive study on the effect of elevated temperature on the creep development is the work of Kommendant *et al.* in 1976 presented in (Bažant and Kim 1992). The results show the increase of creep rate since the early ages for the curing temperatures of 43°C and 71°C and for several loading ages (Figure 2.8).

Since higher curing temperatures accelerate the hydration reactions it leads to higher strength rates over time but reduces the ultimate maximum values for both compressive and tensile strengths (Coutinho and Gonçalves 1994; Kim *et al.* 2002a). Figure 2.9 shows the results of USBR experimental work on the development of strength considering different

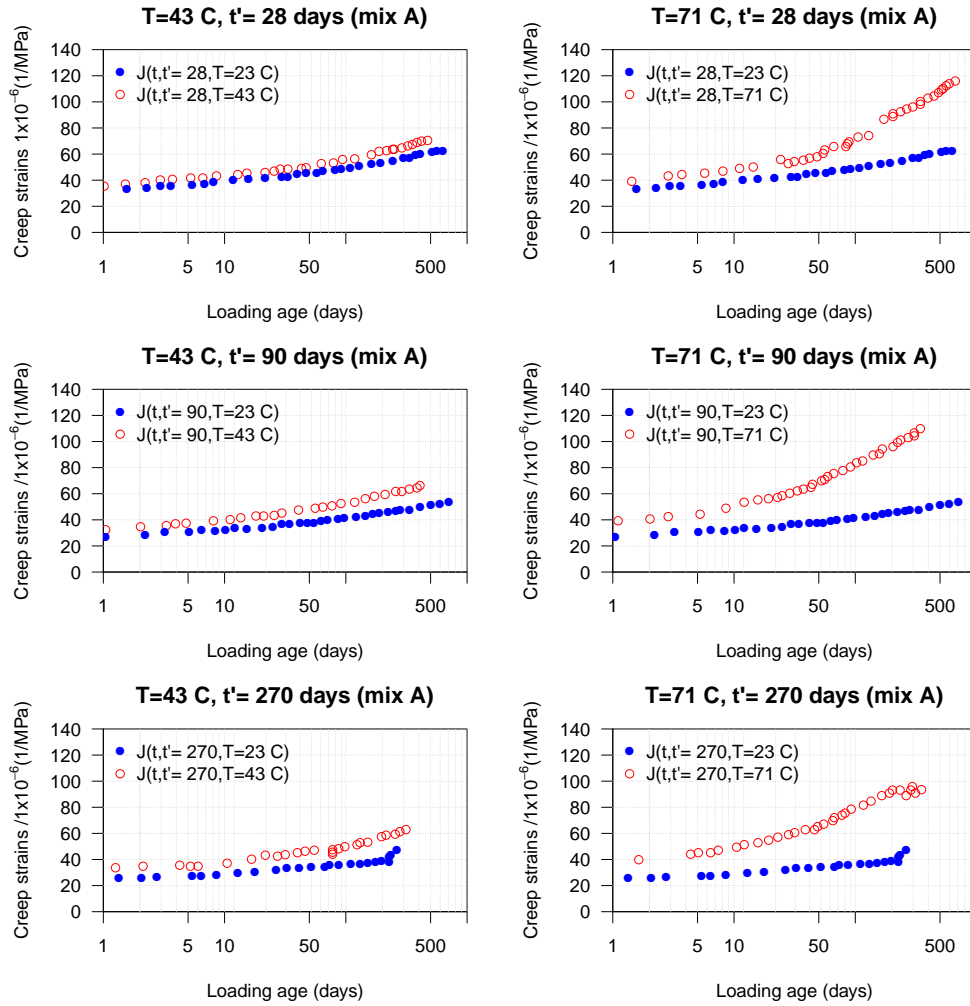


Figure 2.8: Comparison of creep strain development for standard curing temperature and constant elevated temperatures. Adapted from (Bažant and Kim 1992)

testing conditions with a wide temperature range (between -9°C and 46°C). It is shown that higher temperatures at early ages are bound to compromise the potential maximum strength due the fast and more nonuniform hydration in the beginning of the hardening process (Figure 2.9 b)). Low temperatures reduce hydration rates as long as the water does not freeze in which case the reactions can not occur and the concrete will not develop its strength properties (Figure 2.9 c)).

Concrete's moisture content is known to have two opposite effects on strength. It is generally accepted that, for normal concretes with usual water-cement ratio, moist-cured concrete yields higher strength since there is an unlimited access to water for hydration reactions (Mehta and Monteiro 2006). Figure 2.10 shows the results of the work of the USBR considering different curing conditions, including the two extreme situations, specimens

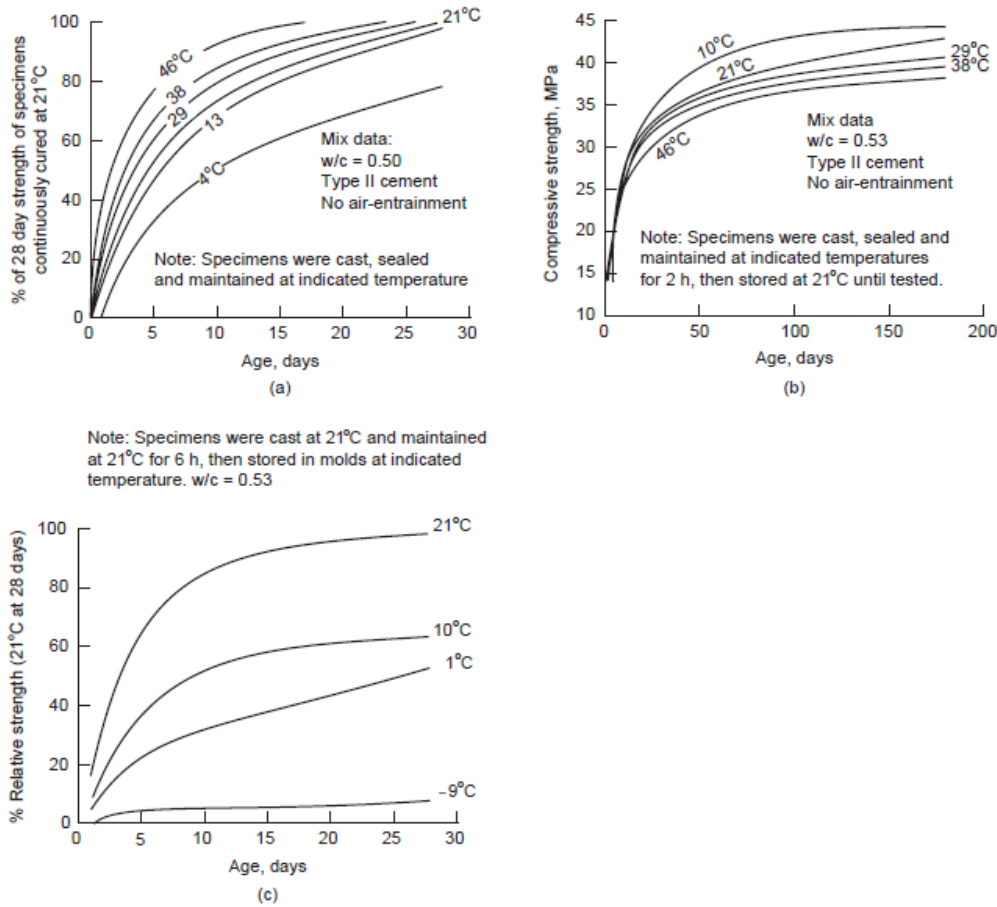


Figure 2.9: Influence of casting and curing temperature on concrete strength (Mehta and Monteiro 2006)

stored continuously in laboratory air and specimens continuously moist cured, and some intermediate conditions with initial moist cured followed by drying (USBR 1988). The results show that initial moist cured conditions increase the maximum compressive strength when compared with a continuously drying specimen. Drying shrinkage at the early ages can introduce microcracking to concrete reducing the ultimate maximum strength, hence the importance of water curing in the first days (Popovics 1986). Popovics (1986) concludes that the moisture distribution inside concrete can have a stronger effect on compressive strength than the global moisture content. Popovics also hypothesises about the beneficial confinement effect of a drying outside layer of concrete to explain large compressive strengths for drying concrete which was previously kept in a wet environment. More recent research also shows the effect of drying on the increase of the capillary suction and the an increase of concrete strength (Yurtdas *et al.* 2004; Burlion *et al.* 2005).

Figure 2.11 shows the results from wet-screened laboratory specimens and dam cores

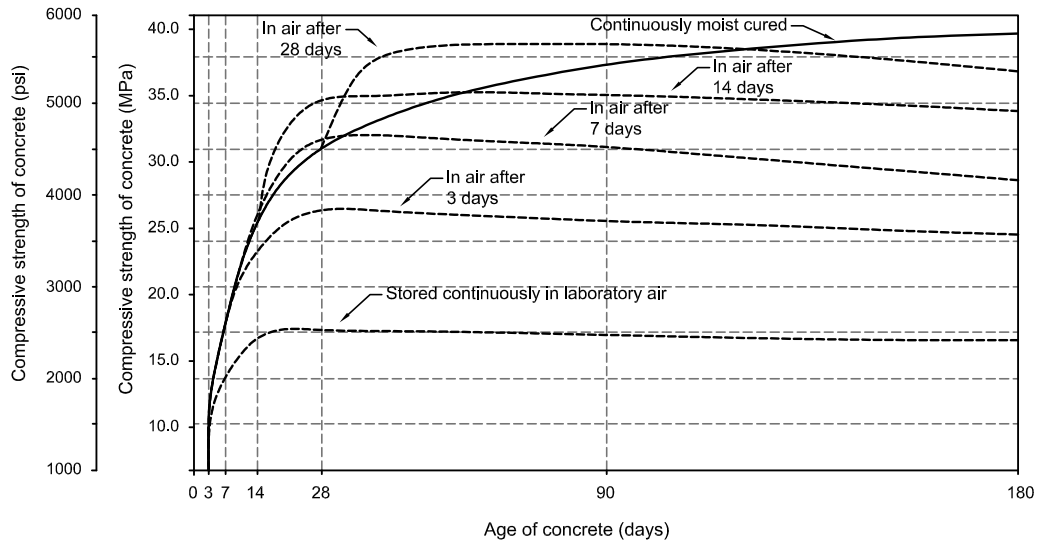


Figure 2.10: Influence of curing conditions on strength (USBR 1988)

for compressive strength and modulus of elasticity (ICOLD 2008). It seems that the development rate of the *in situ* properties is smaller for older ages. The curing conditions of dam concrete depends on the type of dam (for example, its thickness), the mix of concrete (with higher or lower heat generation) and the placement rates (influencing heat dissipation rate). Generally, one can consider that the main dam body does not have moisture exchanges with the environment and, during the first years of age, the core temperatures can vary from 50°C to 10°C. The large thickness of concrete dams allows for the hypothesis of hygrometric equilibrium within the dams body. It is considered that drying only occurs in a small thickness of the downstream face, which can be negligible for the study of long-term behaviour. The dam body is considered, therefore, to have no water exchange with the environment. In order to simulate those conditions is usual to seal the specimens with rolled lead sheet or, if that is not possible, the specimens are maintained at 100% relative humidity.

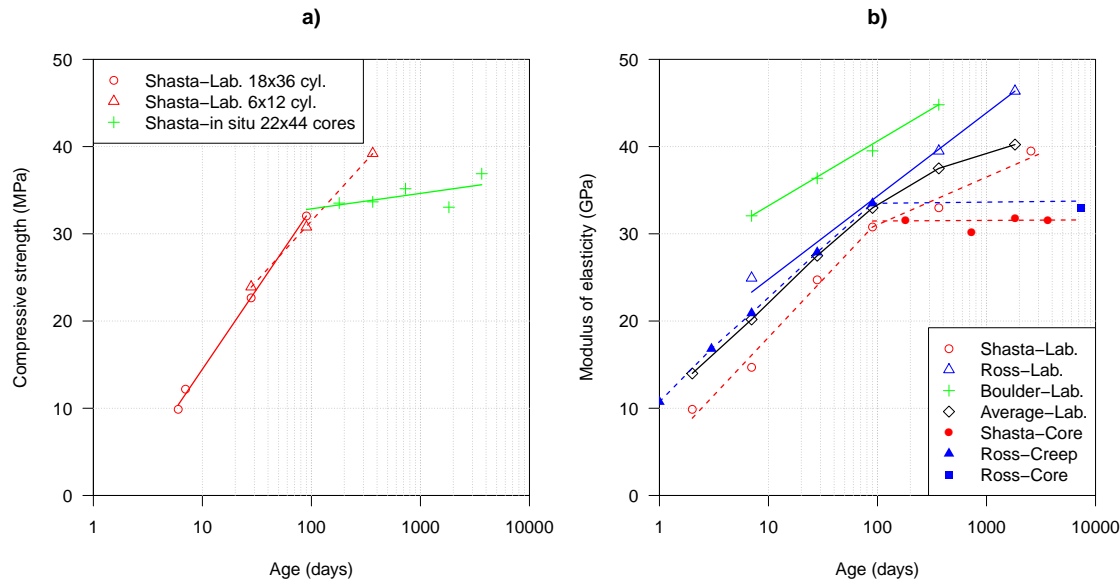


Figure 2.11: Effect of *in situ* conditions on dam concrete properties: a) Compressive strength; b) Modulus of elasticity (ICOLD 2008)

2.3.6 Construction method, casting schedule and concrete types

Conventional concrete dams are built using the block construction method (Jansen 2012). The usual block dimensions are 15-m width and are cast in 2.0-m height lift until the crest is reached. In each of the lifts, different types of concretes are cast in different areas of the block. For example, since the exposed upstream and downstream faces are subjected to higher temperature variations and higher stresses than the dam's core, these areas have higher quality concrete.

Dam concrete can be classified as Core concrete, Face concrete and Reinforcement concrete, depending on the placement location in the dam. Core is the concrete placed in the interior of the dam (MSA of 152 mm), Face is the concrete placed in the upstream and downstream faces of the dam (1.0 to 1.5 m in thickness and has a MSA of 76 mm) and Reinforcement is the concrete placed in the reinforced areas (MSA of 38 mm). Singularities inside the dam's body, such as galleries and large holes, introduce local tensile stresses thus the use of reinforcement bars next to these elements.

Dam concrete types can be further divided into dam concrete and wet-screened concrete, from now on also referred to as DAM and SCR concretes. DAM concrete is produced and placed on site and the SCR concrete is obtained by sieving the aggregates with a diameter larger than 38 mm, after mixing. The wet-screened concrete is used for embedding

monitoring devices, such as strainmeters. The concrete quality control includes both the dam and the wet-screened concretes but, due to testing constraints, the latter has a much higher testing frequency of sampling.

The combination of these two types of classes defines the type of concrete and its characteristics, as well as the location in the dam's body (Figure 2.12), for example Core-SCR is the the wet-screened concrete obtained from the dam concrete placed on the dam's core.

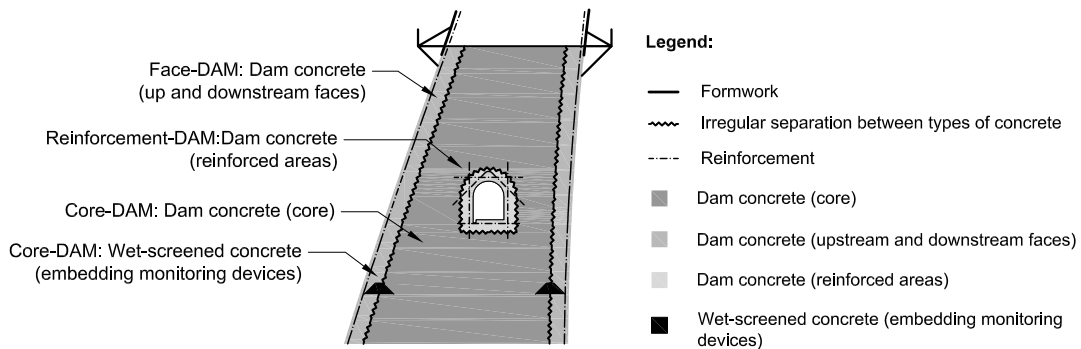


Figure 2.12: Representation of the types of concrete placed in a cross section of an arch dam

Figure 2.13 shows the construction sequence of a block with the installation of three strainmeter sets (two at the up and downstream faces and one in the mid section, represented as black trapezia). At a given level, after the strainmeter spiders are installed and previously to the cast of the lift, the produced dam concrete is wet-screened and the volumes surrounding the strainmeters spiders are cast with the aid of a removable pyramidal formwork. Then, the bedding mortar is placed in a thin layer across the area of the block. This bedding mortar is a high cement content grout that increases the strength capacity of the lift joints. The cast of the block begins by the placement and compaction of consecutive placements of 0.5-m height, firstly of the core concrete (dark grey) and secondly of the up and downstream concrete (light grey), until the 2.0-m height lift is completed. The core concrete is placed 1 to 1.5 meters away from the formwork. The remaining volumes next to the formwork are cast with the up and downstream concretes. The connection between the two concrete is done with the concrete still fresh and it is represented by a *zigzag* line in Figure 2.12 and 2.13.

The compaction of the large volume of concrete, specially with large aggregates and dry consistency, uses a set of 4 to 6 large internal vibrators in a backhoe for the open areas

CHAPTER 2. STRUCTURAL PROPERTIES OF HARDENED DAM CONCRETE

of the block. In special areas, such as the reinforcement areas, the up and downstream faces and around the strainmeter spiders, a single internal vibrator is often used. Usually 12 hours after the last placement, a surface treatment of the horizontal construction joint is done in order to remove the thin and weak layer of segregated cement paste and to disclose the surface of the aggregates. After 72 hours the formwork is ready to be removed and elevated to the next lift.

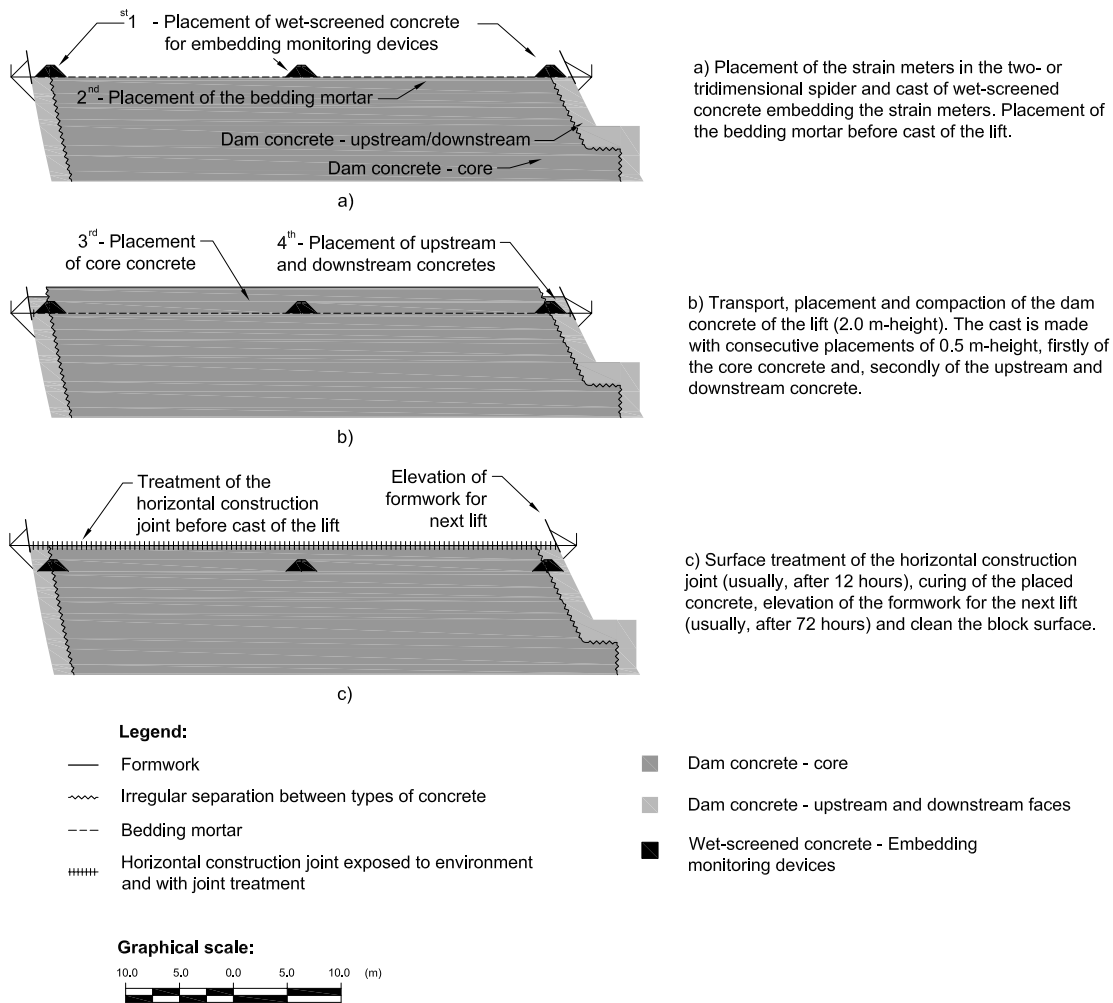


Figure 2.13: Construction phases and placement of each type of concrete. Example with strainmeter instalation.

Figure 2.14 shows a generic sequence of the construction of other lifts considering the inclusion of a gallery and the use of reinforcement in the up and downstream faces. In this case, after the treatment of the horizontal construction lift joint and the rise of formwork, the up and downstream face reinforcement and the formwork and the reinforcement of the gallery can be placed, extended to the next lift. Then, the bedding mortar, the dam and reinforcement concretes are placed in the block considering the construction of the formwork and the specific reinforcement surrounding the gallery.

The construction sequences of these two particular cases show the use of each type of concrete in the structure. Due to the large placement volumes in the core of the dam, a larger MSA can be used. In particular areas, such as the up and downstream faces, a more durable, higher strength and easier to compact concrete is recommended. This can be obtained increasing the cement content and reducing the aggregate's maximum size. The reinforcement areas implies the use of smaller aggregates and, since they are subjected to higher stresses, a higher cement content concrete is used. The strainmeters spiders, with small measurement length (standard Carlson strainmeters have 25.4 cm), are embedded with wet-screened concrete, obtained from the core or up and downstream concrete by sieving the aggregates higher than 38 mm.

Further details on mixing, handling and compaction procedures of dam concrete are described in (ICOLD 2008; ICOLD 2009).

CHAPTER 2. STRUCTURAL PROPERTIES OF HARDENED DAM CONCRETE

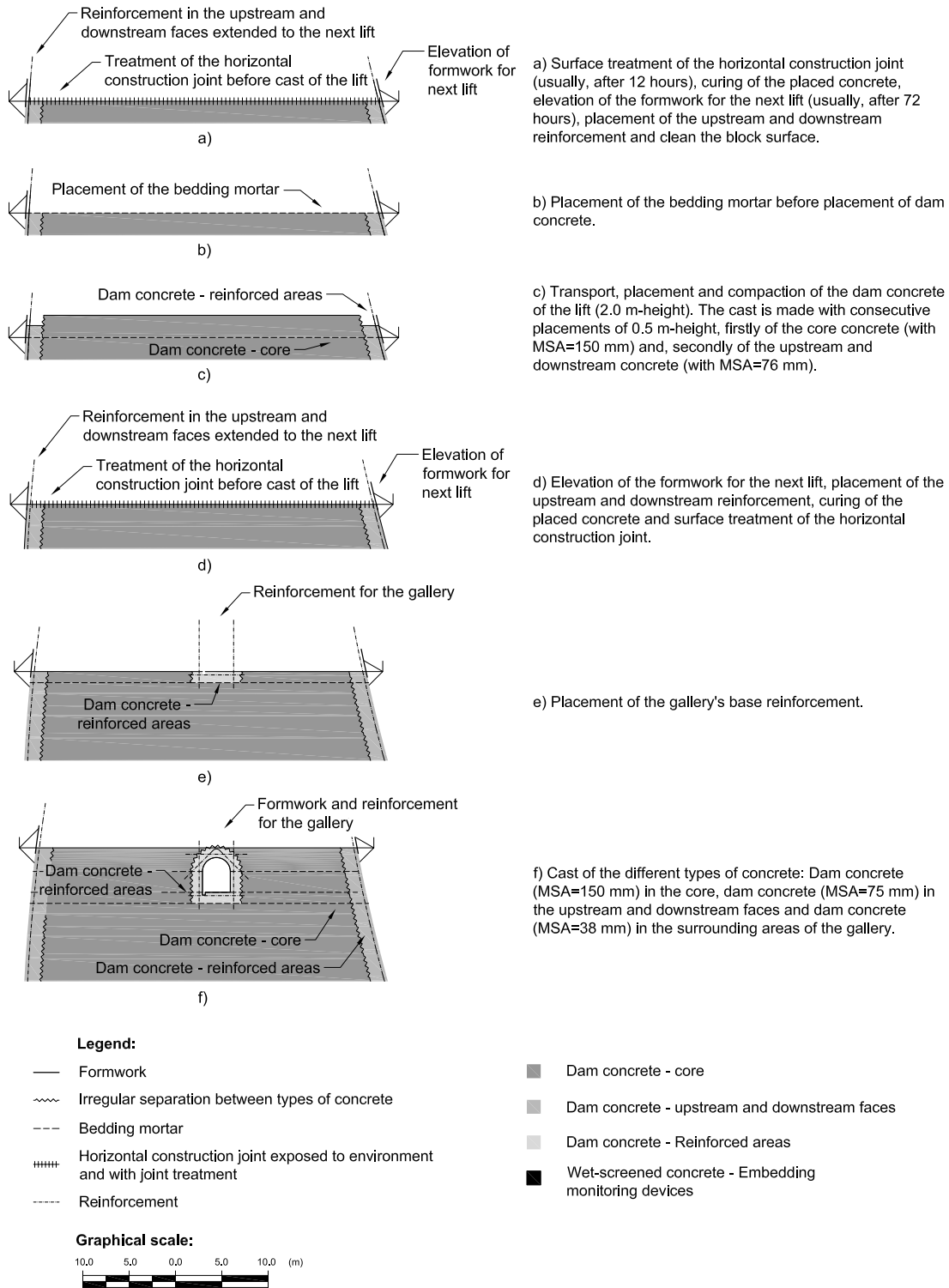


Figure 2.14: Construction phases and placement of each type of concrete. Example with gallery

2.3.7 Effect of wet-screening on hardened dam concrete structural properties

Dam concrete is usually made with large size coarse aggregates for which common specimen dimension and laboratory equipment are not suitable. As previously described, wet-screened concrete is obtained by removing the larger aggregates, usually greater than 38 mm (#38 wet-screened concrete), from the produced dam concrete mix, while it is still fresh. The wet-screened concrete is widely used for concrete characterization, quality control procedures and for embedding the monitoring devices, such as strain and stress meters (USBR 1988; ACI Committee 207 2005). Although both concrete types are made from the same materials, the mix proportions are significantly different (Blanks and McNamara 1935) and it is expected that the main mechanical properties of full-mixed and wet-screened concrete also differ over time.

The wet-screening issues date to the beginning of the twentieth century with the construction of Hoover dam (known at the time as Boulder dam) in the United States of America and to the intensive research of the USBR on the construction methods and dam concrete properties (Blanks and McNamara 1935; Dolen 2010; Bartojay and Joy 2010). Blanks and McNamara (1935) experimental work focused not only on the effect of wet-screening but also on the effect of composition on the main structural properties, of the specimen size, of the maximum size of aggregate and of the curing conditions. The study concluded that the wet-screened concrete obtained from sieving the larger aggregates or a pseudo-wet-screened concrete mixed with the smaller aggregates had similar strengths but very different slump values (being the slump of wet-screened concrete larger). Test results show that the modulus of elasticity of full-mixed concrete is larger than the obtained wet-screened since the aggregate content is largely reduced. It was concluded that, for the Boulder or Hoover dam concrete, the isolated effect of wet-screening is negligible (dashed line in Figure 2.15). The compressive strength of both full-mixed and wet-screened concretes obtained using the same specimen sizes are very close. The strength reduction due to the use of different specimen sizes, which are usually proportional to the size of the largest aggregate, is the main effect to take into account (Blanks and McNamara 1935).

In Portugal several researchers discussed the advantages and difficulties of wet-screening dam concrete in the Symposium of Concretes Placed in Large Masses ("Simposium de Betões em Grandes Massas") from 1952 (Novais Ferreira 1952). Some researchers argued

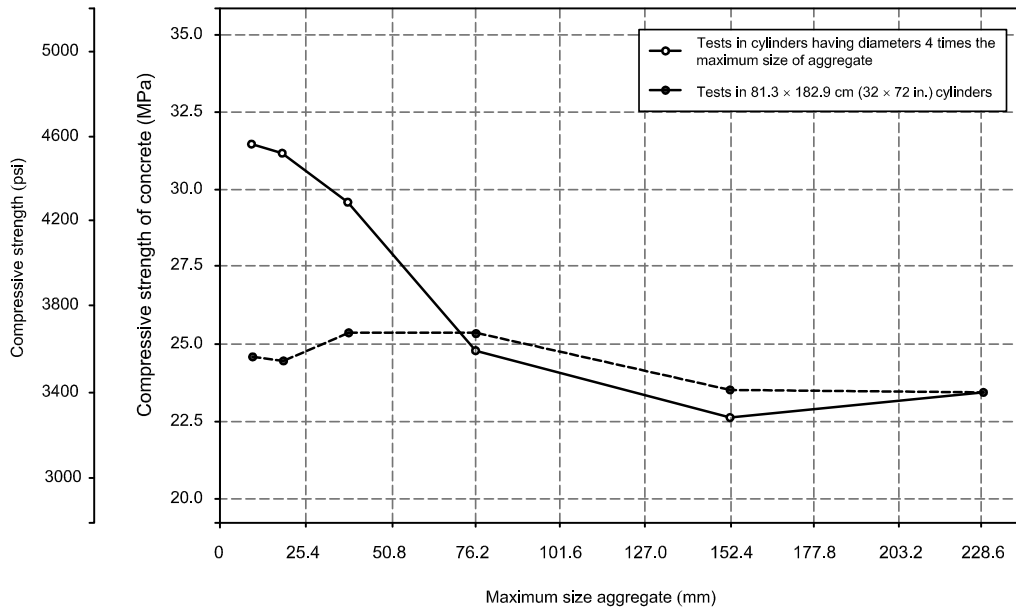


Figure 2.15: Effect of wet-screening and size of specimen on the compressive strength of concrete (Blanks and McNamara 1935)

that it is not possible to establish correlations between full-mixed and wet-screening concrete due to the significant changes in the composition, namely the distribution and content of the aggregates. It was also concluded that the addition of other cementitious materials and the use of admixtures influence the relationship between the two types of concrete. Experimental studies at LNEC showed differences up to 50% between the compressive strength of full-mixed and the wet-screened concrete (Novais Ferreira 1952).

Significant work was done at the National Laboratory for Civil Engineering in the 1980's concerning the investigation of the influence of wet-screening on the properties of dam concrete. The work of Soares de Pinho, summarized in (Soares de Pinho *et al.* 1988), gives a general insight about the relationship between wet-screened concrete and dam concrete properties, for the experimental point of view.

Figure 2.16 shows compressive strength and modulus of elasticity test results obtained for full-mixed and the for the corresponding wet-screened concrete. These results validate the overall behaviour of lower compressive strength and higher modulus of elasticity of the full-mixed concrete compared with the wet-screened concrete, for different ages.

Figure 2.17 shows the fit of a creep function, $J(t, t')$, to the total creep test results for wet-screened concrete maintained in laboratory, for wet-screened and full-mixed concrete placed *in situ*. Creep function is age-dependent and time-dependent, *i.e.*, total creep strain

vary with the age of the concrete when the loading is applied and with the duration of the loading. It is observed that wet-screened concrete has lower delayed deformability than the original full-mixed concrete and that *in situ* conditions seem to increase the modulus of elasticity for a given age.

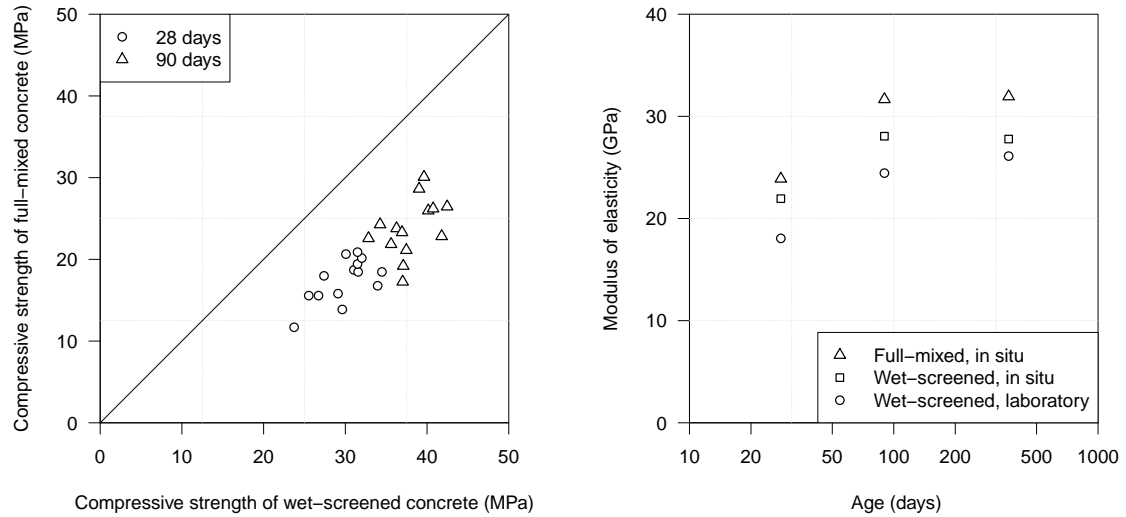


Figure 2.16: Test results of wet-screened and full-mixed concrete: a) compressive strength; b) modulus of elasticity (Soares de Pinho *et al.* 1988)

Focused on the long-term behaviour of dam concrete Serra *et al.* (2012) present several *in situ* creep test results of full-mixed and wet-screened concrete. Despite the large scatter, the results show the general trend measured by Soares de Pinho (1989).

Based on the work of Dreux and Gorisse in 1981, Ramos (1985) shows the effect of wet-screening for the Portuguese practices and predicts that the relationship between the full-mixed and the wet-screened concrete strength obtained from a 76 mm and a 38 mm screen is 0.84 and 0.78, respectively. The justification for the increase of strength as the sieve aperture decreases is the increase of cement content as a consequence of wet-screening.

The practical conversion between full-mixed and wet-screened compressive strength often relies on the work of the United States Bureau of Reclamation (USBR) from 1988 (USBR 1988) and/or on specific experimental programme. Figure 2.18 shows the compressive strength test results for different ages and reveals that the ratio between full-mixed and wet-screened concrete compressive strengths, $f_{c,dam}$ and $f_{c,wet-screened}$, respectively, decreases with the age of the wet-screened concrete. It is possible to acknowledge that, except for the early ages of wet-screened concrete, the ratio is below unit, meaning that

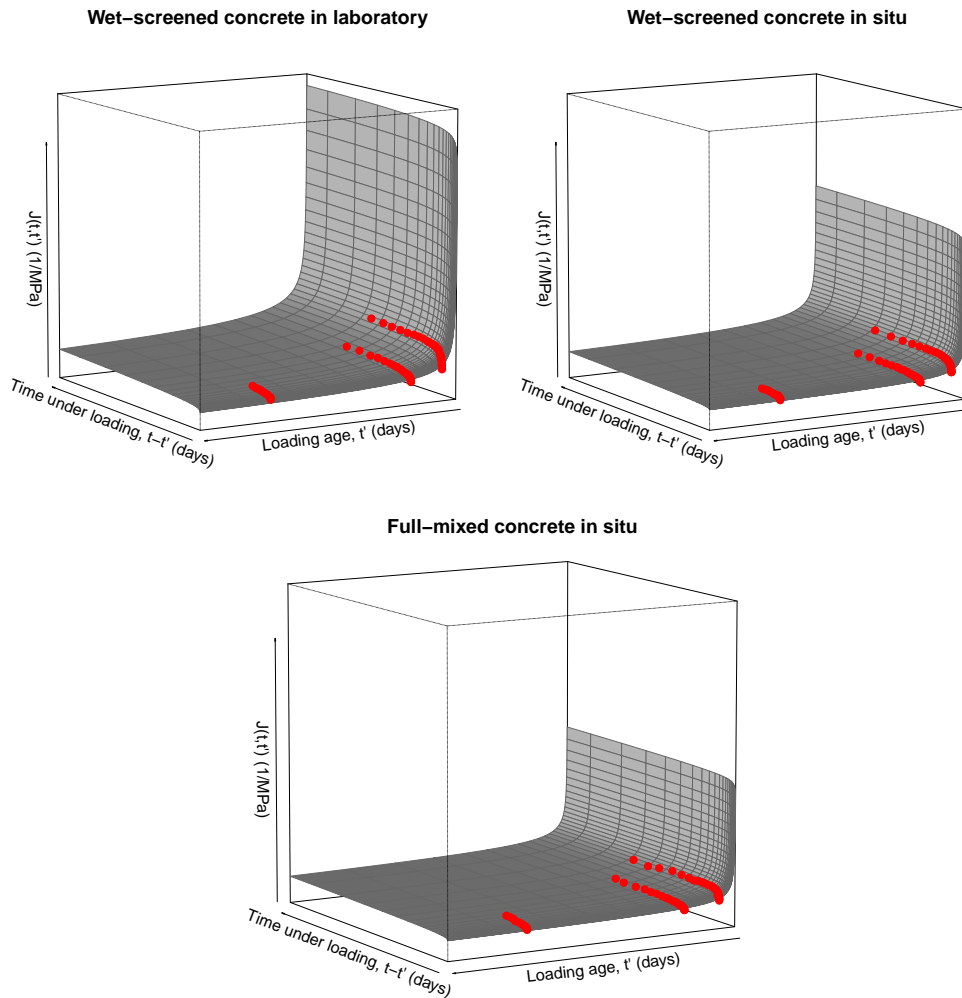


Figure 2.17: Total specific strains of full-mixed and wet-screened concrete measured *in situ* and in laboratory (points) and fit to B3 model (grey surface). Adapted from (Soares de Pinho *et al.* 1988)

compressive strength of full-mixed concrete is lower than compressive strength of wet-screened concrete. This work also mentions the importance of the effect of the specimen size on the prediction of full-mixed concrete based on the results of wet-screened test results, which are often obtained from smaller specimens.

Vilardell *et al.* (1998) presents stress-strain curves of mortar, wet-screened concrete and full-mixed concrete (dam concrete) obtained for different loading ages. The results show the different development over time of each material and the relationship between the modulus of elasticity of mortar, of wet-screened concrete and of dam concrete. The modulus of elasticity increases as the maximum size of aggregate increases, which is usually associated with the increase of the aggregate content. This work focused also on the prediction of the modulus of elasticity using different composite models.

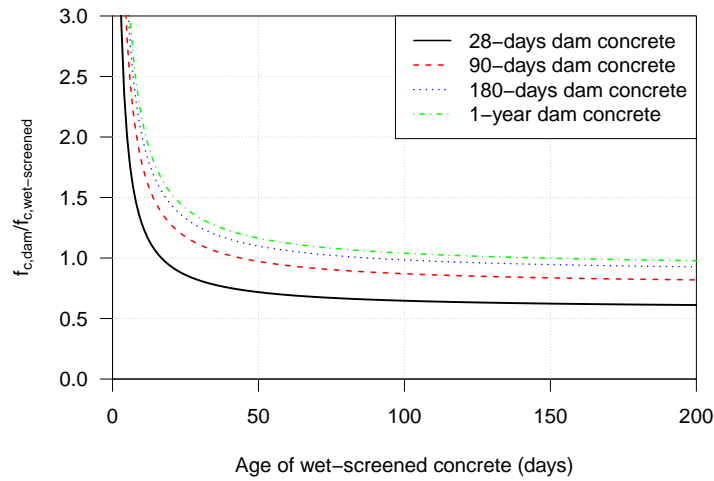


Figure 2.18: Ratios between dam concrete compressive strengths in seal-cured cylinders and wet-screened compressive strengths (USBR 1988)

Sajna and Linsbauer (1998) present an experimental work related specifically to the wet-screening and size effect on fracture energy of concrete using the Horizontal Wedge Splitting Test method (HWST) and different specimen sizes. It was concluded that the size effect has a much larger influence on the fracture mechanics characteristics (fracture toughness and fracture energy associated to the mode I fracture in pure tension (Mehta and Monteiro 2006)) than the maximum size of the aggregates. Similar work has been developed by Ghaemmaghami and Ghaemian (2006) concerning the fracture properties of dam concrete and ranging the maximum size of aggregate between 20 mm and 65 mm. The main finding is the effect of the aggregate size on the fracture energy and that this property depends on the nature, size and properties of the aggregates (Ghaemmaghami and Ghaemian 2006).

The comprehensive experimental work of Li *et al.* (2004) and Deng *et al.* (2008) is noteworthy not only for the comparison of the effect of two types of aggregates (oval-shaped aggregates and crushed aggregates) on different concrete properties at several concrete ages but also to the specific study of dam and wet-screened concrete, using large and small specimens, respectively. Using specific uniaxial tensile and compressive tests procedures it was possible to obtain the complete stress-strain response for each type of concrete and specimen and, therefore, extract a large number of variables, such as the tensile and compressive strengths, the secant modulus of elasticity in tension and in compression, the

strain at peak tensile and compressive stress and the fracture energy. The dam or full-mixed concretes yield higher modulus of elasticity, higher fracture energy but lower tensile and compressive strengths (obtained from different specimens). The authors propose empirical expressions for the prediction of dam and wet-screened tensile strength based on the compressive strengths.

The experimental results of Zhou *et al.* (2010) contradict the general tendency for the compressive strength at younger ages. Although it was concluded that the average compressive strength of full-mixed concrete was higher than the wet-screened concrete, this conclusion could be due to the very larger result scatter. The work of Zhao *et al.* (2015) also differs from the general tendency with respect to the fracture energy under direct tensile test.

More recent work confirms the general relationship between dam and wet-screened concrete compressive and tensile strengths (Kumar *et al.* 2015; Guan *et al.* 2016; Yang *et al.* 2016) but it also indicates lower modulus of elasticity for the full-mixed concrete (Guan *et al.* 2016). Shen *et al.* (2017) show that dynamic strength of full-mixed concrete is also lower than its wet-screened concrete under the same loading conditions.

Yang *et al.* (2016) give some insight on the physical mechanisms of the effect of the aggregate size on the strength of concrete. It is argued that the maximum size of aggregate has a positive and a negative effect on the strength properties. The positive effect relates to the reduction of the interfacial transition zone, the weaker material inside the concrete specimen, as the size of the aggregate increases. The negative effect is due to the quality reduction of the cement paste, especially of the interfacial transition zone, due to the decrease of workability and compaction difficulties.

Table 2.1 presents a summary of the ratios between dam and wet-screened (SCR) concretes for compressive and splitting tensile strengths, f_c and $f_{t,spl}$, obtained from the experimental results available in the literature. The dam or full-mixed concrete results were obtained with large specimens and the wet-screened concrete results were obtained with small specimens.

Table 2.1: Ratios between full-mixed and wet-screened concretes for compressive and splitting tensile strengths obtained from experimental results

Age (days)	Specimen size (f_c)		Specimen size ($f_{t,spl}$)		$\frac{f_c^{DAM}}{f_c^{SCR}}$	$\frac{f_{t,spl}^{DAM}}{f_{t,spl}^{SCR}}$	Reference
	DAM	SCR	DAM	SCR			
28					0.75	-	
90	24 × 48 (in.)	6 × 12 (in.)	-	-	0.68	-	(Blanks and McNamara 1935)
365			-	-	0.68	-	
28					0.93	-	
90	24 × 48 (in.)	6 × 12 (in.)	-	-	0.92	-	(Higginson <i>et al.</i> 1962)
365			-	-	0.87	-	
28					0.7-0.8	-	
90	18 × 36 (in.)	6 × 12 (in.)	-	-	0.65-0.75	-	(USBR 1988)
180			-	-	0.65-0.77	-	
28					0.58	-	
90	450 × 900 (mm)	20 × 20 × 20 (mm)	-	-	0.60	-	(Soares de Pinho <i>et al.</i> 1988)
28					0.53*	0.70*	
90	450 × 450 × 450 (mm)	150 × 150 × 150 (mm)	450 × 450 × 900 (mm)	150 × 150 × 550 (mm)	0.51*	0.88*	(Li <i>et al.</i> 2004; Deng <i>et al.</i> 2008)
365			-	-	0.50*	0.98*	
28					1.1	0.83	
90	450 × 450 × 450 (mm)	-	450 × 450 × 1800 (mm)	-	1.01	0.74	(Zhou <i>et al.</i> 2010)
180			-	-	0.99	0.75	
90	450 × 450 × 450 (mm)	150 × 150 × 150 (mm)	-	-	0.88	-	(Kumar <i>et al.</i> 2015)
90	-	-	-	-	0.85	0.77	(Guan <i>et al.</i> 2016)
7					1.12	0.68	
28			450 × 450 × 450 (mm)		0.86	0.63	
90					0.89	0.71	(Yang <i>et al.</i> 2016)
365					0.84	0.70	

*The ratios were obtained using the fit to the experimental results

Due to its particular application, its prescribed composition (NP EN 206 2005) and despite the extensive experimental work and research developed worldwide concerning conventional concrete, correlations between the behaviour of wet-screened and full-mixed concrete are limited and concern only specific concrete ages. ACI Committee 207, for example, refers briefly that the compressive strength of large specimens of full mass concrete is 80 to 90% of the compressive strength of wet-screened concrete, evaluated in smaller specimens (ACI Committee 207 2005).

The relationship between full-mixed and wet-screened concrete mechanical properties has been studied in the past mainly through experimental testing. However, a general physically-based correlation between wet-screened and full-mixed dam concrete properties has not yet been proposed. The need of reliable relationships between full-mixed concrete and wet-screened concrete is required for design, concrete quality control during construction, monitoring and data analysis and for safety control throughout service life (USBR 1988; ACI Committee 207 2005; ICOLD 2008).

In order to understand the effect of wet-screening, research studies focused on the influence of the properties, gradation and content of aggregates on the structural properties of concrete are also relevant.

Several experimental studies investigated the influence of aggregate content, size and type on the fracture behaviour of concrete, including the modulus of elasticity (Walker and Bloem 1960; Hirsch 1962; Counto 1964; Alexander and Mindess 2010), the maximum strength (Walker and Bloem 1960; Tsiskreli and Dzhevakhidze 1970; Scholer and Baker 1973; Zhou *et al.* 1995; Kozul and Darwin 1997; Sizov 1997; Özturan and Çeçen 1997; Akçaoğlu *et al.* 2004; Vu *et al.* 2011) and the fracture energy (Kozul and Darwin 1997; Sajna and Linsbauer 1998; Khaloo *et al.* 2009; Rocco and Elices 2009; Beygi *et al.* 2014; Nikbin *et al.* 2014).

Strength of concrete is strongly related to damage in the interface between cement paste and aggregates, where a weaker material is formed, the ITZ. The shape, dimension, content, surface roughness, strength and deformability of the aggregate are important factors for the properties and development of the ITZ (Scholer 1967; Mitsui *et al.* 1994; Ollivier *et al.* 1995; Scrivener *et al.* 2004; Akçaoğlu *et al.* 2004).

Based on experimental tests, Walker and Bloem (1960) showed the influence of grading and MSA on compressive and tensile strengths with an extensive and comprehensive experimental study using several cement contents and considering non air-entrained and

air-entrained concretes. The aggregate maximum size ranged from 9.5 to 63.5 mm (3/8 to 2 1/2 inches) and cement content ranged from 223.8 to 447.5 kg/m³ (4 to 8 sacks per cubic yard; 1 sack/yd³ = 94.3 pounds/yd³ = 55.9 kg/m³). The results indicated, as previously stated by other authors, that strength decreases when larger aggregates are used, for the most specimens, and that this effect is more pronounced for higher cement contents.

The study of Tsiskreli and Dzhavakhidze (1970) concerned the concrete compressive and tensile strengths and the effect of size and fraction volume of coarse aggregate for the concrete of the arch dam at the Ingur hydroelectric station. The approach was to obtain an empirical expression for strength values based on a sensitive criterion of aggregate size, the "coarseness characteristic", $\eta = \sum V d_{av}$, where d_{av} is the average diameter between sieves and V is their volume per unit volume of concrete. This parameter has the advantage of considering both the size and the fraction volume of each coarse aggregate component and of being more sensitive to study strength. Results showed that for small cement contents, the compressive strength increased with the MSA and that this effect diminishes as cement content increases. The opposite effect was obtained for tensile strength, from splitting and flexural tests. Tensile strength decreases with the "coarseness characteristic".

Another important study concerning the effect of MSA on the strength properties of concrete is the experimental work of Higginson *et al.* (1962). This investigation compared a series of test results varying the maximum size of the aggregate and the cement content. Due to its comprehensiveness, as recommend by the authors, the obtained results constitute, still nowadays, a "general guide in designing concrete mixes for average conditions" (Higginson *et al.* 1962; ACI Committee 207 1997; ACI Committee 207 2005; ICOLD 2008).

This study refers to the use of the aggregate size and the cement content to obtain high, medium and low strength concretes. For dam concrete, low stresses imply the use of low strength values and, therefore, large MSA are recommended in order to optimize the cement content. Figure 2.19 presents the strength contour lines of a set of experimental tests of concrete made from aggregates with dimensions ranging from 9.5 to 152.4 mm (3/8 to 6 inches) and with several cement contents, ranging from 167.8 to 391.6 kg/m³ (282.9 to 660.0 pounds/yd³). The conclusions are significant and show a nonlinear behaviour when increasing MSA for a given cement content. For low cement contents, strength increases with MSA but with a decreasing rate. For higher cement contents, it seems to be an optimum line for which strength does not increase with the MSA. The study explains also that the aggregate surface area has a positive and negative effect in compressive strength.

Small MSA implies a greater surface area and larger space between aggregates, therefore, requires more mortar paste to coat the surface and to fill the spaces (positive effect to strength). Small MSA implies also the use of higher water-cement ratios which increases porosity and reduces strength. It was also mentioned in this work that the failure of low cement content mass concrete were due to lack of bond between aggregates and mortar.

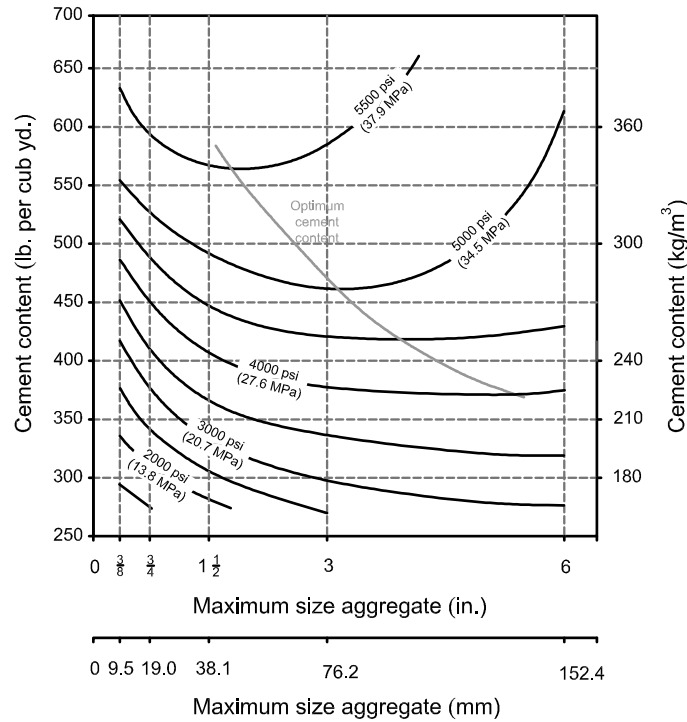


Figure 2.19: Effect of aggregate maximum size on cement content. Adapted from (Higginson *et al.* 1962; ICOLD 2008)

Cordon and Gillespie (1963) also focused on the effect of the MSA on the compressive strength of concrete for different water cement ratios. Figure 2.21 shows that compressive strength decreases as the MSA increases. This comprehensive experimental work has significant results and it had great importance for understanding the influence of each component on the strength of concrete but the conclusions should be carefully analysed. Since the small aggregate concretes have larger water and cement requirements, the effect of the MSA is not entirely clear from this type of representation (Figure 2.21) and the slump results. Additionally, although at the time the size effect was not fully studied, the decrease in strength in some results could be due to the increase of the specimen size for the concretes with larger aggregates (152.4 mm \times 300.8 mm cylinders were used for concrete with aggregates up to 38 mm and 203.2 mm \times 406.4 mm were used for concrete

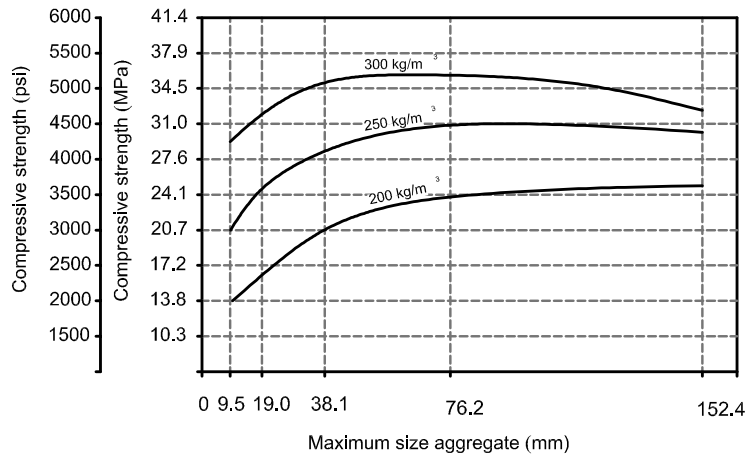


Figure 2.20: Effect of aggregate maximum size on compressive strength. Adapted from (Higginson *et al.* 1962; ICOLD 2008)

with aggregates with MSA=76 mm).

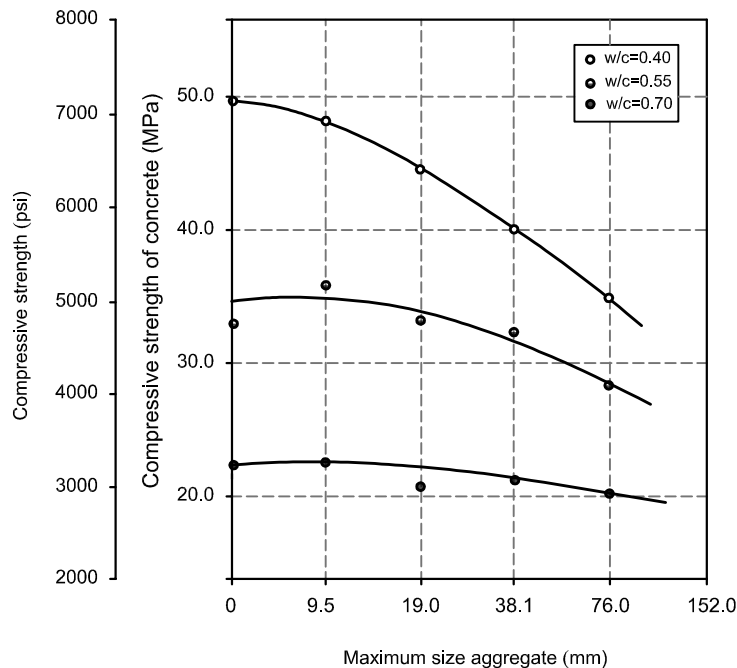


Figure 2.21: Effect of maximum size aggregate on concrete strength. Adapted from (Cordon and Gillespie 1963)

The experimental work of Scholer and Baker (1973) was based on a series of gradations which were produced based on the variations measured in highways. The fineness index was taken as the independent variable explaining the effect of the gradation.

Despite the complex behaviour of concrete, Neville *et al.* (1983) show that there is a

strong age-independent correlation between concrete and mortar's compressive strength for different loading ages and that, compared to mortar, concrete has higher compressive strength (Figure 2.22). The coarse aggregates introduce strong strength and stiffness heterogeneities into concrete but, according to these results, it seems to increase the bearing capacity of the material due to interlocking of the aggregates (Kaplan 1959). On the other hand, regarding the tensile strength, Kaplan (1959) and Neville *et al.* (1983) refer that mortar strength results are bound to be higher than the concrete, due to the strong influence of ITZ.

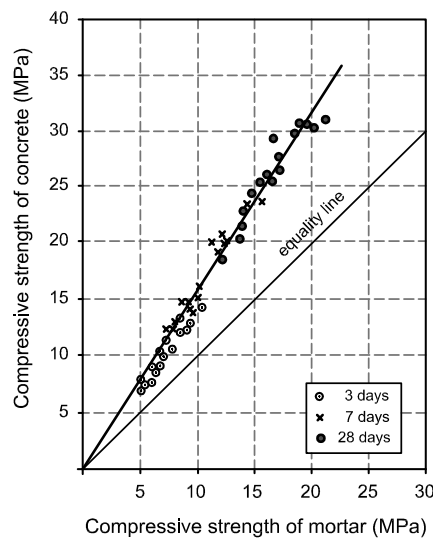


Figure 2.22: Correlation between compressive strength of mortar and concrete. Adapted from (Neville 1983)

Larrard and Belloc (1997) and Larrard (1999) present a different approach on the prediction of concrete strength using a unique physical parameter, the maximum paste thickness (MPT), which comprises topological and mechanical aspects. This parameter is capable of describing the two contradictory effects of the MSA on concrete strength, already described by other authors (Walker and Bloem 1960; Higginson *et al.* 1962; Stock *et al.* 1979): "for a given amount of cement, increasing the MSA tends to reduce the water demand, while the strength obtained for a given w/c is lower" (Larrard and Belloc 1997). Larrard and Belloc (1997) also present several experimental results of paste, mortar and concrete and conclude that there is a relationship between compressive strength of mortar and concrete for different types of aggregate, but the strength values of concrete are always lower than the mortar, due to the weaker ITZ (Figure 2.23). The results show the different

interactions between normal and high-strength cement paste and normal and very good quality aggregates and its effect on the ultimate properties.

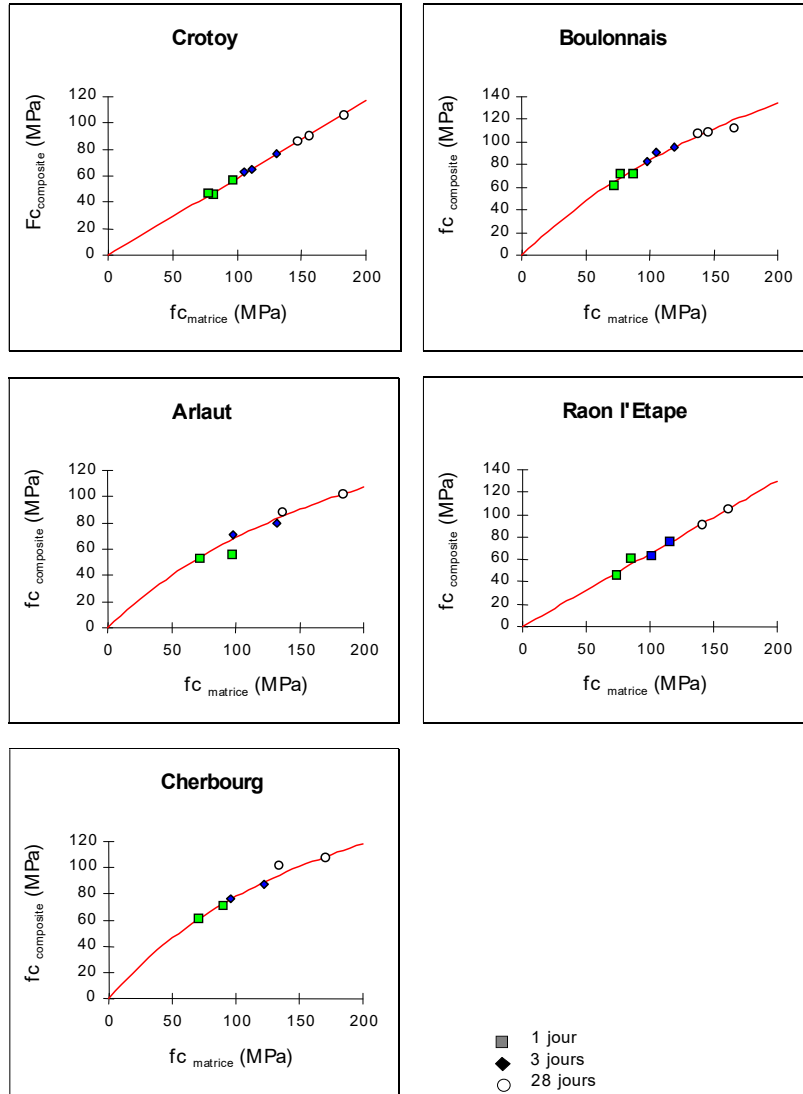


Figure 2.23: Correlation between compressive strength of mortar and concrete. Adapted from (Larrard and Belloc 1997)

Although some contradictory results require further study, these type of correlation are especially useful for the characterization of dam concrete strength properties since mortar specimens are easier to test and can be used to add some insight on the behaviour of concrete.

Other works focused on the influence of coarse aggregate on strength properties, each one focused on a particular factor and mechanical property: the effect of aggregate size on the use of the cylinder splitting test as a measure of tensile strength (Hannant *et al.* 1973); the effect of the coarse aggregate size on the ITZ (Akçaoğlu *et al.* 2004); experimental

work with large specimens for studying the influence on fracture energy (Kozul and Darwin 1997; Khaloo *et al.* 2009); and, the triaxial behaviour (Vu *et al.* 2011).

2.4 Modelling concrete behaviour

2.4.1 Analytical models for the prediction of concrete structural properties

2.4.1.1 General aspects

According to Neville *et al.* (1983) the study of materials can be divided into three levels: the empirical, the phenomenological (semi-empirical or engineering level) and the molecular (theoretical or structural). Each one is focused on different perspectives of the same behaviour. The empirical level is based on experimental results for which empirical expressions are used to characterize the behaviour. The phenomenological level considers simple physical models in order to understand the material behaviour which can be adapted or influenced by experimental evidences. The molecular level aims to include the processes at the molecular or atomic level and leads to an explanation of the physical problem. In civil engineering it is usual to rely on semi-empirical expressions to predict the macroscopic behaviour of concrete and use them in the structural analysis (Fib 2010).

As pointed out by USBR (1988), this type of analytical models can be used to "troubleshoot, evaluate, predict, or estimate concrete strengths", bearing in mind that "strengths calculated by any method must always be considered subject to revision on the basis of experience with field or trial batches".

2.4.1.2 Prediction of deformability properties

Prediction of concrete creep and shrinkage goes back to the beginning of the twentieth century, when Woolson and Hatt registered what it seemed to be a "flow" of concrete (Neville *et al.* 1983). Since then, several mathematical laws were developed to establish the relationship between strain and stress over time (Bažant 1975; Fib 2010; Briffaut *et al.* 2012).

Several studies have been focused on the prediction of the creep strain development based on other structural properties, such as the compressive strength, or on composition data, such as the cement and water contents. The different prediction models for the delayed behaviour have been developed by Bažant throughout the years: BaP model

(Bažant and Osman 1976); BP-KX model (Bažant and Kim 1991); and the most recent, B3 model (Bažant and Baweja 1995a) and B4 model (Bažant *et al.* 2013). The *Fédération Internationale du Béton* (FIB) also proposes simple prediction models in the fib Model Code 90 (CEB-FIP 1990) and in the fib Model Code 2010 (Fib 2010). Similarly, the American Concrete Institute (ACI) proposes other expressions in their standards, ACI 209R-92 (ACI Committee 209 1992). Gardner and Lockman (2001) propose the GL2000 model for the prediction of shrinkage and creep of concrete. The logarithmic expression has been also proposed in past studies for the dam concrete creep function considering only basic creep strains (Ramos 1985; Soares de Pinho 1989).

The heterogeneity of concrete can be studied using models in which the mesostructure is taken into account. Composite models allow for the prediction of the deformability properties taking into account the concrete composition and considering concrete as coarse aggregate inclusions embedded in a matrix of mortar. The first composite models applied to concrete concerned the elastic behaviour using approaches based on uniaxial rheological models (Hirsch 1962; Hansen 1965; Counto 1964). Other type of models are based on homogenization techniques, such as the variational approach considering spherical inclusions (Hashin-Shtrickman bounds) (Hashin 1963), the self-consistent model considering ellipsoidal inclusions (Hill 1965) and the Mori-Tanaka method (Benveniste 1987).

The two-phase composite models applied to concrete are usually used for determining the elastic properties, considering the bond between binder paste or mortar and the coarse aggregates. The hypothesis of these types of models are the assumption of elastic linear behaviour, the assumption of isotropy of each component. Further, the Poisson's ratio effect and the interface behaviour between inclusions and matrix are neglected (Counto 1964).

Several authors proposed two-phase composite models for the determination of the instantaneous deformability properties (Hashin 1962; Hirsch 1962; Counto 1964; Hansen 1965) with specific applications (Vilardell *et al.* 1998; Topçu 2005). The prediction of the aging viscoelastic behaviour of the materials using composite model was developed with the work of Counto and Popovics (Counto 1964; Popovics 1987) and later with Granger, Bažant and Baweja (Granger and Bažant 1995; Baweja *et al.* 1998), based on the uniaxial rheological models, and, more recently, Sanahuja and Lavergne, using homogenization concepts (Sanahuja 2013; Lavergne *et al.* 2015). Recent studies relate to the development of three-, four- and n-phase (Li *et al.* 1999; Zheng *et al.* 2012) composite models in order

to take into account the different types of material properties inside the concrete matrix, particularly the properties and behaviour of the interfacial transition zone (Hashin and Monteiro 2002; Grondin and Matallah 2014).

2.4.1.3 Prediction of strength properties

Over the years several authors and institutions proposed different analytical models for the development of compressive strength over time in order to describe the behaviour from setting to complete hardening. These expressions have parameters which can be fitted to experimental results at a given concrete age and used for the compressive prediction for later ages.

International institutions, such as the American Concrete Institute (ACI) and the International Federation for Structural Concrete (FIB), recommend general development laws composed by a time dependent expression and the compressive strength at reference age, usually 28 days. The expressions proposed by Carino and Lew (2001) are frequently used since it links the cement hydration to the development of mechanical properties (Schutter and Taerwe 1996; Cervera *et al.* 1999). The hydration of cement has an upper limit related to cement and water content and due to diffusion of water through C-S-H new products of hydration around the unhydrated cement particles. These studies, similarly to the hydration of cement, consider a limit for the strength of concrete and, therefore, the use of hyperbolic functions with an ultimate strength to simulate the development of strength over time. Yeh (2006) describes four methodologies for determining the compressive strength as a function of the water-other cementitious materials ratio and time, using Abrams and Power's formula. A set of generalized formulas is proposed.

Based on the experimental studies, different authors developed empirical expressions which represent the relationship between two different structural properties, for example, the concrete's modulus of elasticity and the compressive strength (Teychenne *et al.* 1978; ACI Committee 363 1992; ACI Committee 318 1995; Noguchi *et al.* 2009; Fib 2010) and different types of tensile strengths and the compressive strength of concrete (Carino and Lew 1982; Oluokun *et al.* 1991; ACI Committee 318 1995; Larrard 1999; Arıoğlu *et al.* 2006; Fib 2010). This type of expressions can be used to reduce the number of specimens in a given experimental programme and are particularly relevant for the prediction of tensile strength.

Concerning ultimate structural properties, there are different expressions that relate

the strength of concrete with other properties of concrete based on the composition data. These expressions generally describe the behaviour of concrete and its parameters can be found by fitting to experimental results.

One of the first expressions to be developed was the formula of Feret from 1892 (Bolomey 1936),

$$f_c = K \left(\frac{c_v}{c_v + w_v + v_v} \right)^2 \quad (2.4)$$

where c_v , w_v and v_v are the volume of cement, water and voids, respectively, per unit volume of concrete and K is a constant coefficient that includes other factors affecting the strength of concrete ¹.

Due to the difficulties in obtaining the exact volumes of cement, water, aggregates and voids, these prediction expressions are not used in practice. The most used are the Abrams law (Equation 2.5), the Graf law (Equation 2.6) and the Bolomey law (Equation 2.7).

$$f_c = \frac{K}{A^x} \quad (2.5)$$

where x is the ratio between the volume of mixing water and the apparent volume of cement (considering the apparent density of cement equal to 1.5) and K and A are coefficients dependent on the quality of the cement, the curing duration and conditions ².

Later in 1923, Graf adapted the Abrams law to take into account the european testing conditions and proposed the expression:

$$f_c = \frac{f_{c,28}}{400} \left(\frac{A}{7^{2w/c}} + \alpha \right) \quad (2.6)$$

where $f_{c,28}$ is the compressive strength at the age of 28 days, A is a coefficient dependent on the quality of the cement, the curing duration and conditions ³, w/c is the ratio, in weight, between water content and cement content and α is a coefficient that varies between 20 and 40.

Based on the Feret formula and for compact concretes, Bolomey (1936) proposed the following expression:

¹For compressive strength at the age of 28 days, the value of K may vary from 3000 lbf/in² (206.8 MPa) and 4500 lbf/in² (310.3 MPa).

²For the compressive strength at the age of 28 days of cylinders with 15 cm in diameter and 30 cm of height, Abrams refers $K=985$ and $A=7$.

³For the compressive strength at the age of 28 days, A can vary from 1300 and 2600, with an average of 1640.

$$f_c = K \left(\frac{c}{w} - 0.50 \right) \quad (2.7)$$

which is a particular case of the general expression:

$$f_c = \left[\left(\frac{\gamma}{2.35} \right)^2 \left(\frac{c}{w} \right) \right]^B \frac{K}{2} \quad (2.8)$$

where f_c is the compressive strength in kg/cm², γ is the density of the concrete in kg/m³, c/w is the ratio, in weight, between cement and water contents, B is a coefficient dependent of the type of cement and can vary between 1.2 and 2.0 ⁴ and K is a coefficient dependent on the quality of the cement, the curing duration and conditions ⁵.

The concrete strength predictions are often related to the water-cementitious materials ratio which is the base of the most common empirical law, the Abrams law (Abrams 1918). Although this empirical relationship is widely used, it is not valid for all range water to cement ratio (Gilkey 1961). For very low water to cement ratios the quality of the cement paste inside the concrete is compromised by the compaction difficulties (Mehta and Monteiro 2006).

The recommendation of USBR (1988), based on the formula of Feret, includes also the influence of secondary cementitious materials and chemical admixtures:

$$f_c = K \left[1 + \left(\frac{E_m p_c (1 - p_c)^n}{1 - p_c} \right) \right] \left(\frac{c_v}{c_v + w_v + v_v} \right)^2 \quad (2.9)$$

$$p = \frac{c_w}{c_w + f_w} \quad (2.10)$$

where E_m is the maximum efficiency of the secondary material, n is the lime fixation factor, p_c is the ratio between the weight of cement and the sum of the weight of cement and the secondary cementitious materials, c_w and f_w are the weight of cement and secondary cementitious material, respectively, per unit volume of concrete. USBR (1988) proposes values for E_m and n as a function of the type of cementitious material and recommends the evaluation of the two values based on test results considering two percentages of secondary material. It also considers that $n = 1$ can be an appropriate value for the fly ash and,

⁴In general, for Portland cements, B=1.5.

⁵Considering B=1.5 and normal cements, the values of K can vary from 140 to 180 for the age of 7 days and between 180 and 250 for the age of 28 days.

therefore, the value of E_m can be obtained from one type of concrete. If there is not any information available, USBR recommends the value of 1.25 for E_m .

Some studies focused on the importance of the cement content, the water content and the maximum aggregate size (Higginson *et al.* 1962; Stock *et al.* 1979; Akçaoğlu *et al.* 2004; Popovics and Ujhelyi 2008). For example, in order to predict concrete strength based on composition, Popovics and Ujhelyi (2008) proposed an adaptation of the Abrams law by including the cement content, the water content and the concrete consistency (measured as slump flow or Vebê time) as additional variables of the model. Although recognizing the importance of the maximum particle size in concrete strength, this variable was not taken into account (Popovics and Ujhelyi 2008). Similarly to Popovics work, other studies developed new models considering specific approaches (Rao 2001; Çolak 2006) or variables, such as age (Yeh 2006; Abd elaty 2014) and the fly ash content (Rajamane *et al.* 2007).

As previously described, one important model which relies on a more comprehensive parameter is the prediction model proposed by Larrard (1999). The parameter is the maximum paste thickness (MPT), *i.e.* the mean distance between two adjacent coarse aggregates includes the effect of aggregate volume and the effect of MSA and, according to the author, determines the magnitude of concrete strength since this is where the higher stresses will occur. Other effects are also taken into consideration in his study in order to have a general model for the prediction of compressive strength of concrete (effect of the properties of the aggregates, the effect of time, the effect of additions and the effect of fillers).

2.4.2 Discrete models for the study of concrete behaviour considering its mesostructure

Mesoscale analyses focus on the study of the behaviour of concrete, on the interactions between coarse or fine aggregates and on the maturing mortar or cement paste in order to evaluate the main mechanical properties and their deterioration over time (Alnaggar *et al.* 2013; Giorla *et al.* 2015; Pan *et al.* 2017). Several types of models and approaches have been used for the prediction of concrete behaviour and to study the influence of coarse aggregate mainly on the fracture properties (Monteiro Azevedo and Vieira de Lemos 2006; Grassl *et al.* 2012). The approaches can be divided into continuum and discrete frameworks.

Fracture of concrete have been modelled using several types of approaches based on the finite element method, which are known as classical strain localization methods. One

type of models, based on the strong discontinuity approach (SDA) uses discontinuous displacements into the elements (Simo *et al.* 1993; Costa *et al.* 2010; Dias *et al.* 2017) (embedded-discontinuities) or into the nodes (extended finite element method, X-FEM) (Moës and Belytschko 2002) in order to simulate the crack opening. Other type of fracture models are often referred to as "smeared" crack models or weak discontinuous models since it distributes strain softening and reduces the material strength and stiffness of the finite elements in which the tensile strength is exceeded (Cervera and Chiumenti 2006).

The work of Roelfstra *et al.* (1985) from 1985 shows the advantages of using finite element models to describe the different phenomena occurring inside the concrete during hardening, focusing on the deformation properties, such as elasticity and shrinkage. Practical mesoscopic applications for the prediction of concrete behaviour or for the study of a specific effect or property using continuum models are presented by Carol *et al.* (2001) and Wang *et al.* (2016), in which interface elements in a finite element mesh define the fracture behaviour at the ITZ. The work of Benboudjema *et al.* (2004), Xotta *et al.* (2013), and Havlásek and Jirásek (2015), consider the creep properties, the behaviour of ITZ, the effect of drying and a damage model coupled with softening plasticity (Benboudjema *et al.* 2004). Both examples show the importance of the ITZ behaviour on the properties of concrete and the effect of local damage on the development of the cracking patterns and, ultimately on the failure mode. The work of Wriggers and Moftah (2006) focuses on the effective properties of concrete and shows the agreement between experimental results, composite and numerical model results considering the aggregate size distribution. The representation of the mesostructure of concrete allows for a more detailed research of specific studies, such as the coupling between creep and damage in which the physical explanation takes place at the mesoscale (Saliba *et al.* 2012), the development of internal self-balanced stresses that occur during hydration and hardening of concrete (Briffaut *et al.* 2013; Xu *et al.* 2017) and the study of stress development on concrete with alkali-silica reactions (Giorla *et al.* 2015). It is known that stiff aggregates restrain the deformations, introduces a non-uniform stress field inside concrete in which there are highly stressed areas and that creep has a significant role in the relaxation of these stresses (Briffaut *et al.* 2013; Giorla *et al.* 2015).

Other type of model based on a continuum domain is the microplane model in which the relationships between strains and stresses are not defined by tensors but by vectors acting on an arbitrary plane. At a given point, strains and stresses are defined as the

summation of strain and stress vectors calculated on several microplanes with different orientations, in order to describe the material microstructure (Bažant *et al.* 1996).

However, the quasi-brittle behaviour of some heterogeneous materials, such as concrete, is considered to be poorly simulated by traditional continuous approaches that disregard the material microstructure and the randomness of material heterogeneity (Cusatis 2001; Monteiro Azevedo 2003). The damage and fracture processes of this type of materials are complex and sensitive to the volume where the energy is dissipating and, therefore, numerical models should consider this effect (Bažant 2002).

Discrete models are able to introduce some type of microstructure and randomness into the material representation and the cracking zone is explicitly taken into consideration. This feature is known to be better suited to simulate fracture in quasi-brittle materials (Monteiro Azevedo 2003). By considering the material as a randomly produced assembly of discrete rigid particles in contact with each other and, for those contacts, consider a simple interaction model, it is possible to study the behaviour of concrete taking into account its mesostructure.

The discrete or distinct element method (DEM), initially developed for modelling granular materials (Cundall 1971), is an important tool for modelling heterogeneous materials undergoing generalized micro-cracking through the material and large macro-cracking patterns. Rigid particle models (PM) are being used to reproduce the overall behaviour of quasi-brittle materials, such as rock and concrete, and have been shown to reproduce several macroscopic phenomena, such as elasticity, viscoelasticity, post-peak behaviour, crack propagation and strength increase with confinement (Monteiro Azevedo 2003).

The use of DEM was first applied to the study of geotechnical materials of granular nature. Cundall described the basis for the DEM simulation by considering the movement and interaction of rock blocks (Cundall 1971) and of 2D circular elements (Cundall and Strack 1979). Later on, cracking was taken into account for geomaterials, such as rock, with very simple contact models between rigid elements (Zubelewicz and Mróz 1983; Plesha 1983). Plesha (1983) focused on the importance of the rock microstructure and proposed a model explicitly considering the microstructure into the interaction of discrete rigid polygons or polyhedra. Meguro and Hakuno (1989) proposed an extended version of DEM, the modified discrete element method, MDEM, with the intent of simulating the behaviour of concrete under extreme dynamic events adopting a nonlinear interaction model between the rigid particles for the normal and shear directions, called the "pore-strings". At a larger

scale problem, Vieira de Lemos (1987) applied the method to the dynamic analysis of rock mass of dam foundations using polyhedra and Cundall is still now actively working in modelling the behaviour of rock mass (Mas Ivars *et al.* 2011).

Bažant *et al.* (1990) proposed a lattice model where pin-jointed frames are connected to the centres of the coarse aggregates and, therefore, the dimension of the frames is directly linked to the mesostructure of the concrete. Cusatis (2001) presented a tridimensional particle model in which each coarse aggregate is explicitly modelled as a rigid particle and the interaction between the particles simulates the cement paste or mortar behaviour.

The lattice models considering bending frames (Schlangen and Mier 1992) differ from the lattice discrete particle model proposed by Cusatis (2001) and Smith *et al.* (2015) since the first uses the finite element method (FEM) and the second uses DEM for obtaining the structural response. The first type of models solves the structural system by assembling the stiffness matrix, at each time step. The DEM is based on a numerical time integration scheme for solving the equations of motion and for the definition of contact interaction between elements.

In lattice models the fracture behaviour is obtained by removing the frames that reach a maximum strength stress as load increases (Schlangen and Mier 1992). The dimension and properties of the frames are constraint to the heterogeneity of the material (Figure 2.24).

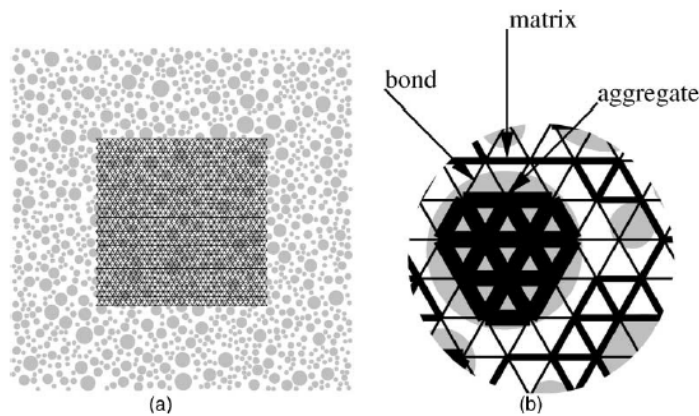


Figure 2.24: Representation of the lattice mesh: a) computer generated aggregate structure; b) detailed properties of each frame (Lilliu and Mier 2003a)

Some applications of the lattice models relate to the study the influence of the beam length, the effect of the aggregate structure, content and properties (Mier *et al.* 2002; Lilliu and Mier 2003b) and the fracture process zone (FPZ) (Grassl and Jirásek 2010), the size effect (Grassl *et al.* 2012), the influence of irregular shaped aggregates (Qian and

Schlangen 2013) and, more recently, to study the drying shrinkage damage and the early age behaviour which includes a lattice moisture model with the usual lattice fracture model (Luković *et al.* 2016; Šavija and Schlangen 2016; Pan *et al.* 2017). This type of models are mesh dependent for regular trusses, introduce local instabilities when a frame is removed and the global behaviour is affected by the mesh spacing the same way as for continuous models (Schlangen and Garboczi 1997).

Rigid body spring models have been also used to model the overall behaviour of structures (Kawai 1978) and the behaviour of concrete (Bolander and Saito 1998). These models require the definition of the interaction springs between rigid bodies at their interface. Advances have been done regarding the study of concrete fracture using the rigid body spring model in which the component's properties, such as the water to cement ratio, are taken into account to predict the behaviour of the mortar binding the aggregates and empirical correlations between the main structural properties are analysed (Nagai *et al.* 2004). A 3D extension and other applications have been also proposed: simulation of impact loads (Yamamoto *et al.* 2016) and effect of expansions inside the concrete (Eddy *et al.* 2017).

DEM particle modelling is especially suited for detailed simulations due to its computational simplicity, when compared with finite element method formulations (Giorla *et al.* 2015). A detailed DEM particle model including the particles representing the mortar allows for the contact constitutive models to be less complex when compared with other particle models that do not have the same degree of discretization (Alnaggar *et al.* 2013; Pan *et al.* 2017).

Several particle models were developed throughout the years, mainly based on the original Cundall's DEM (Cundall 1971; Cundall and Strack 1979) as the solving method, but using different interaction models for different types of problems. Hassani (1998) compared the results of an assembly of circular particles with a visco-elastic model (Voigt-Kelvin model) and particular failure criteria with the results of a one-shear test. In the rigid particle model, the constitutive models used at contact involved only interaction at one point of contact and only forces were developed at each contact. However, materials such as rock present some kind of cemented granular nature which can be considered by introducing a bending stiffness at the contact. Failure occurs when maximum tensile and shear stresses at the contact, due to both force and moment developed at the contact, are exceeded (Potyondy and Cundall 2004). This enhancement is known to improve the main

physical behaviour of rock, such as elasticity, micro-cracking and peak strength, for several test configurations: Brazilian test, uniaxial and triaxial compressive test. Other approaches to simulate this type of materials is to increase the number of contacts of a given particle (coordination number) establishing an additional bond between close particles that are not physically in contact (Oñate *et al.* 2015).

Monteiro Azevedo (2003) proposed a rigid particle model based on DEM for the analysis of plain and reinforced concrete, in which both aggregates and reinforcement are explicitly considered and a multiple contact point model is implemented. The post-peak tensile and shear behaviour at contact can be considered using brittle, linear or bi-linear constitutive models. Monteiro Azevedo and Vieira de Lemos (2006) and Monteiro Azevedo *et al.* (2008) present DEM particle model applications to evaluate the influence of the properties of coarse aggregates (aggregate shape and modulus of elasticity) on the development of stress-strain behaviour. These studies show that the heterogeneity of the assemblies and/or contact properties and the contact friction behaviour are key factors for representing the failure patterns and to increase post-peak ductility both in tension and in compression (Figure 2.25).

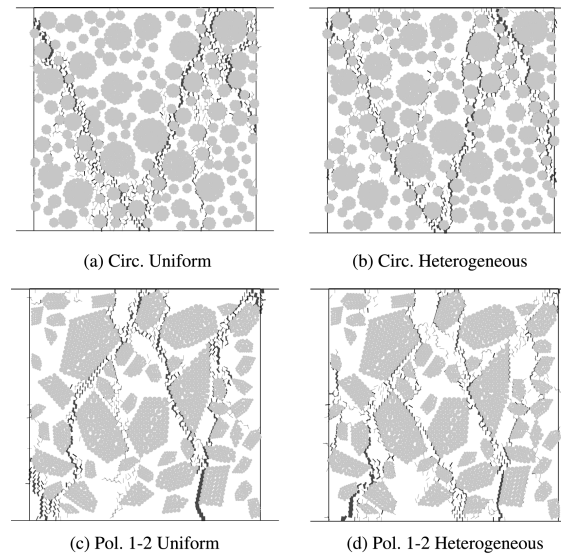


Figure 2.25: Failure patterns of concrete DEM particle models under compression using uniform and heterogeneous contact properties and circular and polygonal aggregates (Monteiro Azevedo and Vieira de Lemos 2006)

Although roughness is known to have a role in the cracking pattern and force-displacement curve, polygonal particles are difficult to deal with and the contact detection during calculations is computationally expensive, and, therefore, circular or spherical particles have

been widely used (Monteiro Azevedo 2003).

To simulate the specific microstructure in granular material, Jensen *et al.* (1999) used cluster particles, which are a group of circular particles in which the translations between them are constraint. Additionally, focused on improving the relationship between compressive and tensile strength and post-peak behaviour, Cho *et al.* (2007) propose a clumped particle model for the simulation of rock in combination with bonded contact model. A clump is similar to a cluster particle, but the rotation between particles intra-clump is also restrained, as rigid bodies. In order to simulate the granular nature of rock, Potyondy (2010) proposed a model in which the nonlinear behaviour is implemented in a fictitious interface, a smooth-joint contact, in order to reproduce the specific microstructure of Äspö diorite. The overall response of the material is a combination of a network of interfaces defining the microstructure and the behaviour of a grain like assembly surrounded by interface joints and considering a bond contact in the intra-grain particles. The goal of this type of adaptations is to include a more realistic representation of the microstructure of rock in order to improve geometry-based properties, such as dilation and interlocking friction (Cho *et al.* 2007).

One of the main disadvantages of DEM is the need for the calibration of the micro properties at contact level in order to obtain the macroscopic properties of the particle assembly that represent the mechanical behaviour of the material. As described by Oñate *et al.* (2015) and Rojek *et al.* (2012) two main approaches have been used. The first is a global approach in which the micro parameters are set equal to every contact, regardless of the particle size or packing, in order to establish analytical expressions for the relationship between micro and macro properties (Labra and Oñate 2009). The second approach uses a physical concept to introduce the influence of the particle radius (Potyondy and Cundall 2004). Combining the two approaches, some authors have developed general analytical expressions that are calibrated to describe the relationship between the micro and the macro properties (Wang and Tonon 2009; Kazerani and Zhao 2010).

More recently, different mesoscale studies have been developed focusing on the use of DEM applied to particle models for the prediction of concrete behaviour, for example, the study of the dynamic behaviour, namely the effect of rate strain (Qin and Zhang 2011) and the prediction of hard impact (Tavarez and Plesha 2007; Antoniou *et al.* 2017), the study of local failure mechanics, size effect (Nitka and Tejchman 2015), the effect of aspect ratio and of friction between the specimen and the platens (Sinaie 2017) and the decrease

of the main mechanical properties due to high temperature damage (Sinaie *et al.* 2016).

These studies highlight the need for more detailed and realistic models in order to better represent the fracture behaviour of concrete, such as, the fracture toughness, the pre-peak and pos-peak ductility, the debonding between aggregate and cement past or the fracture of aggregate particles, the identification and study of the fracture process zone. DEM particle model applications, in which the detailed mesostructure is explicitly taken into account, can be found in (Piotrowska 2013; Nitka and Tejchman 2017; Suchorzewski *et al.* 2017). Piotrowska (2013) studied the influence of aggregate and ITZ properties on the fracture of concrete using a detailed particle model and presents a schematic graph illustrating the possible failure patterns (Figure 2.26). A weak aggregate concrete yields continuous and straight cracks throughout the specimen, whereas a strong aggregate concrete forces the crack path through weak ITZ around the aggregate particles or through the mortar between the aggregate particles.

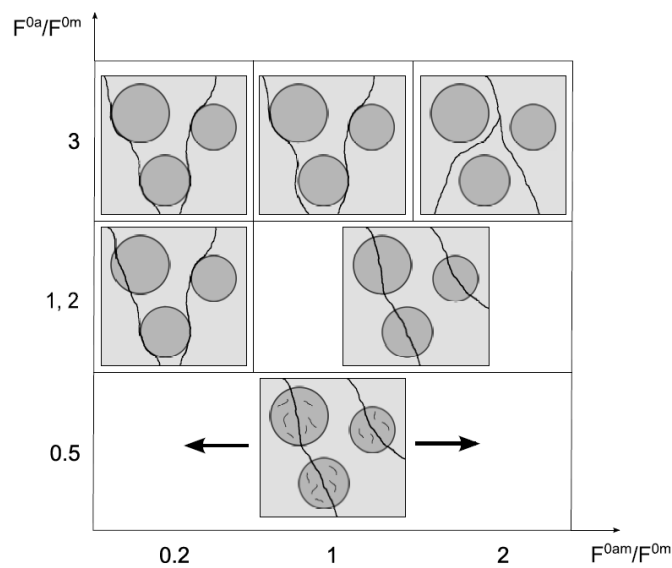


Figure 2.26: Schematic illustration of the different failure patterns considering different aggregate strength properties (F^{0a}) and ITZ strength properties (F^{0am}) (Piotrowska 2013)

The studies using DEM are usually confined to the prediction of the short-term properties of concrete and the aging viscoelasticity is often disregarded (Donzé and Magnier 1995; Cusatis 2001; Potyondy and Cundall 2004; Monteiro Azevedo *et al.* 2008). The development of stiffness in the early ages, the high increase of deformation due to stress and the drop of stress due to an imposed strain related to the rate of loading are main features of the behaviour of concrete and should be included into a constitutive model.

Rate-type effects, such as creep, have been considered for dynamic analysis in a simplified manner for short-term analysis (Cusatis *et al.* 2001) and, more recently, were taken into account in lattice models (Abdellatef *et al.* 2015; Pan *et al.* 2017). Other example of a short time-dependent analysis using discrete models are the studies of asphalt mixtures with DEM using non-aging viscoelastic contact models (Liu *et al.* 2009; Ma *et al.* 2016). Given that detailed particle DEM based models are computationally intensive due to the restrictions of the time step, long-term analysis is usually prohibitive.

Experimental characterization of the structural properties of dam concrete

3.1 Introduction

This chapter describes the experimental characterization procedures of the main structural properties of dam concrete and presents the results of deformability and strength tests of the concrete used in the case study, the Baixo Sabor dam.

Firstly, a general overview of the properties of dam concrete placed on Portuguese large dams is presented. Composition data, deformability and strength test results of several concretes are showcased, allowing the comparison with the test results obtained in the case study. The importance and difficulties of dam concrete characterization are also highlighted. A preliminary relationship between wet-screened and dam concrete deformability properties can be drawn based on the analysis of these results.

The case study is the concrete placed in the Baixo Sabor dam. This chapter presents the main features of the arch dam, describes the materials used for the production of concrete, the construction method, the casting schedule and the types of concrete cast in the dam's body. The composition data of dam and wet-screened concretes is also presented. Based on these results, a procedure for obtaining the wet-screened composition data is proposed.

The first set of tests relate to the main experimental work developed in this thesis.

The experimental programme included the planning, installation and maintenance of specific equipments placed on site, the creep cells, for the determination of the *in situ* creep strains and of standard laboratory creep tests. The experimental procedures for the characterization of dam concrete properties are described in detail. The *in situ* experimental programme using creep cells focused on the correlation between dam and wet-screened concrete properties.

In order to complement the results obtained from creep cells, the test results obtained in quality control during construction, provided by the dam's owner, were also analysed. The concrete results concern standard laboratory tests of the main mechanical properties of dam and wet-screened concretes at several loading ages.

The test results include the mechanical properties of the rock used for the aggregates, the dam and wet-screened concretes and the mortar binding the aggregates. The studied mechanical properties are the modulus of elasticity at different ages, the creep compliance in compression, the uniaxial compressive strength and the splitting tensile strength, determined at different ages.

The detailed description of each individual result obtained in the creep cells is available in two technical reports (LNEC 2013; LNEC 2014b). The raw data and a statistical analysis of the test results concerning the quality control laboratory testing is presented in other technical report (LNEC 2017).

3.2 Properties of dam concrete placed on Portuguese large dams

3.2.1 Introductory note

The content of this section was published in a scientific paper in the national journal "Revista Portuguesa de Engenharia de Estruturas" with the title "Análise integrada dos resultados dos ensaios de deformabilidade do betão de grandes barragens portuguesas" (Serra *et al.* 2015a) (Appendix B).

3.2.2 Composition and properties

In this section an overview of the properties of the concrete placed in several Portuguese large dams is presented. The available data was obtained from different sources, such as technical reports and specific studies (Ramos and Soares de Pinho 1983; Soares de Pinho

et al. 1988; Batista 1998; Serra *et al.* 2010; Vieira 2012; Serra *et al.* 2014b). Unfortunately, some properties and results are often incomplete, especially for older dams. The deformability results are more frequent than the strength results due to LNEC's effort on experimental studies using creep cells.

The collected data of composition and deformability test results of the concrete of several Portuguese dams, built since 1951, allowed the establishment of correlations between the deformability properties of the full-mixed and the wet-screened concrete used in dam construction. Taking into account the laboratory and *in situ* testing, correlations between creep coefficients of wet-screened and full-mixed concrete were obtained.

The type of aggregates vary according to the dam's geographic areas. Most of the large concrete dams are located in the Northern part of Portugal where good quality granitic rock is available. The maximum size of aggregate is usually 150 mm. The cement content has been decreasing with time mainly due to the addition of supplementary materials (mainly fly ash) when mixing. The water-binder ratio varied from 0.70 on Picote dam (built in 1958) to 0.34 on Torrão dam (built in 1988). Table 3.1 presents the available composition properties from each studied dam concrete of a total of nineteen dams.

Figure 3.1 shows the modulus of elasticity test results of 15 dams (Castelo do Bode, Venda Nova, Picote, Cabril, Régua, Vilarinho das Furnas, Cahora Bassa, Aguieira, Pracana, Torrão, Fronhas, Crestuma, Alqueva, Baixo Sabor and Alto Ceira II) over a large period of time. The presented results were obtained from laboratory tests of the wet-screened concrete. Generally, the modulus of elasticity varies, approximately, between 23 GPa to 35 GPa at the age of 90 days, and between 27 GPa to 40 GPa at the age of 365 days, except for the results from Alqueva and Cabril dam, which have extreme values. The major variability of this mechanical property is due to the modulus of elasticity of the coarse aggregates and to its content. The majority of the analysed dams used granitic aggregates (70%), but the modulus of elasticity of granitic rocks can vary widely also (Alexander and Mindess 2010). An important feature of this type of concrete is the significant development rate at latter ages (between 90 and 365 days of age).

The available creep tests results are organized by dam, type of concrete (wet-screened and full-mixed), maturing conditions (laboratory and *in situ*) and loading age. Figure 3.3 presents the obtained experimental creep compliance, $J_{exp}(t, t')$, for a selection of tests and the fit to the logarithmic creep function (solid lines). The results show the large scatter in magnitude and development of creep strains over time.

CHAPTER 3. EXPERIMENTAL CHARACTERIZATION OF THE STRUCTURAL PROPERTIES OF DAM CONCRETE

Figure 3.2 presents compressive strength test results of wet-screened concrete obtained from the dam concrete placed in some Portuguese dams. Similarly to the modulus of elasticity results, the compressive strength show large variations, varying between 27.8 MPa in Aguieira dam (built in 1981) and 55.3 MPa in Foz Tua dam (built in 2015), for the age of 365 days.

3.2. PROPERTIES OF DAM CONCRETE PLACED ON PORTUGUESE
LARGE DAMS

Table 3.1: Concrete composition of several Portuguese dams

Dam	Year	Aggregate type	Φ_{max} (mm)	c	f	w	a	g	s	Proportions b : c : f : w : a : g : s
Castelo de Bode	1951	Gravel from Zêzere river	n.a.	220	0	n.a.	2147	1611	536	1.0 : 1.0 : 0.0 : n.a. : 9.8 : 7.3 : 2.4
Venda Nova	1951	Granite	n.a.	225	0	n.a.	2130	1675	455	1.0 : 1.0 : 0.0 : n.a. : 9.5 : 7.4 : 2
Salomonde	1953	Granite	n.a.	250	0	n.a.	1992	1554	438	1.0 : 1.0 : 0.0 : n.a. : 8.0 : 6.2 : 1.8
Cábril	1954	Granite	150	220	0	130	2064	1652	411	1.0 : 1.0 : 0.0 : 0.59 : 9.4 : 7.5 : 1.9
Caniçada	1955	Granite	n.a.	250	0	n.a.	2080	1680	400	1.0 : 1.0 : 0.0 : n.a. : 8.3 : 6.7 : 1.6
Bouça	1955	Metamorphic	n.a.	250	0	n.a.	n.a.	n.a.	n.a.	1.0 : 1.0 : 0.0 : n.a. : n.a. : n.a. : n.a.
Picote (w/c=0.5)	1958	Granite	n.a.	200	0	100	n.a.	n.a.	n.a.	1.0 : 1.0 : 0.0 : 0.50 : n.a. : n.a. : n.a.
Picote (w/c=0.7)	1958	Granite	n.a.	200	0	140	n.a.	n.a.	n.a.	1.0 : 1.0 : 0.0 : 0.70 : n.a. : n.a. : n.a.
Vilarinho das Furnas	1972	Granite	150	225	0	n.a.	n.a.	n.a.	n.a.	1.0 : 1.0 : 0.0 : n.a. : n.a. : n.a. : n.a.
Rêgua	1973	Gravel	75	210	0	105	2010	1604	405	1.0 : 1.0 : 0.0 : 0.50 : 9.6 : 7.6 : 1.9
Cahora Bassa	1975	Gneiss	150	215	0	127	2165	1716	449	1.0 : 1.0 : 0.0 : 0.59 : 10.1 : 8 : 2.1
Aguieira	1981	Granite	150	225	0	113	2104	1703	401	1.0 : 1.0 : 0.0 : 0.50 : 9.4 : 7.6 : 1.8
Fronhas	1985	Gravel from Alva river	100	220	0	80	2075	1670	405	1.0 : 1.0 : 0.0 : 0.36 : 9.4 : 7.6 : 1.8
Crestuma	1985	Gravel	38	300	0	150	1920	1437	483	1.0 : 1.0 : 0.0 : 0.50 : 6.4 : 4.8 : 1.6
Torrão	1988	Granite	150	185	0	63	2122	1568	554	1.0 : 1.0 : 0.0 : 0.34 : 11.5 : 8.5 : 3.0
Alto Lindoso	1992	Granite	150	150	0	77	2187	1554	633	1.0 : 1.0 : 0.0 : 0.51 : 14.6 : 10.4 : 4.2
			150	150	0	63	2187	1554	633	1.0 : 1.0 : 0.0 : 0.42 : 14.6 : 10.4 : 4.2
			150	180	0	83	2187	1554	633	1.0 : 1.0 : 0.0 : 0.46 : 12.2 : 8.6 : 3.5
			150	150	0	73	2187	1554	633	1.0 : 1.0 : 0.0 : 0.49 : 14.6 : 10.4 : 4.2
Alqueva	2002	Green schist	150	158	39	102	2288	1638	650	1.0 : 0.8 : 0.2 : 0.52 : 11.6 : 8.3 : 3.3
			150	157	41	75	2407	1712	695	1.0 : 0.8 : 0.2 : 0.38 : 12.2 : 8.6 : 3.5
			150	164	41	104	2317	1667	650	1.0 : 0.8 : 0.2 : 0.51 : 11.3 : 8.1 : 3.2
			150	158	39	102	2288	1638	650	1.0 : 0.8 : 0.2 : 0.52 : 11.6 : 8.3 : 3.3
			150	159	40	71	2352	1663	689	1.0 : 0.8 : 0.2 : 0.36 : 11.8 : 8.4 : 3.5
Alto Ceira II	2013	Granite	63	117	143	151	1970	1193	777	1.0 : 0.5 : 0.6 : 0.60 : 7.6 : 4.6 : 3
Baixo Sabor	2014	Granite	150	111	110	129	1955	1434	521	1.0 : 0.5 : 0.5 : 0.58 : 8.9 : 6.5 : 2.4
			150	110	110	128	1962	1434	528	1.0 : 0.5 : 0.5 : 0.58 : 8.9 : 6.5 : 2.4
			150	110	110	133	2041	1431	610	1.0 : 0.5 : 0.5 : 0.60 : 9.3 : 6.5 : 2.8
Maximum value			150	300	143	151	2407	1716	777	-
Minimum value			38	110	0	63	1920	1193	400	-

Note: ϕ_{max} – maximum size aggregate (MSA); b – binder content (b=c+f); c – cement content; f – fly ash content; w – water content; a – aggregate content; g – coarse aggregate content; s – fine aggregate content; n.a. – not available

CHAPTER 3. EXPERIMENTAL CHARACTERIZATION OF THE STRUCTURAL PROPERTIES OF DAM CONCRETE

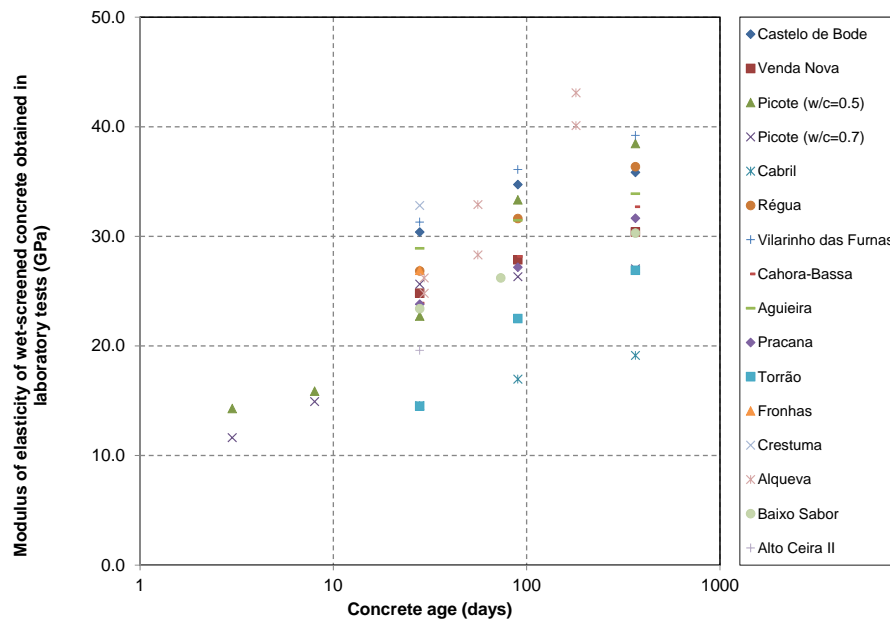


Figure 3.1: Wet-screened concrete modulus of elasticity results of several dams obtained from laboratory tests

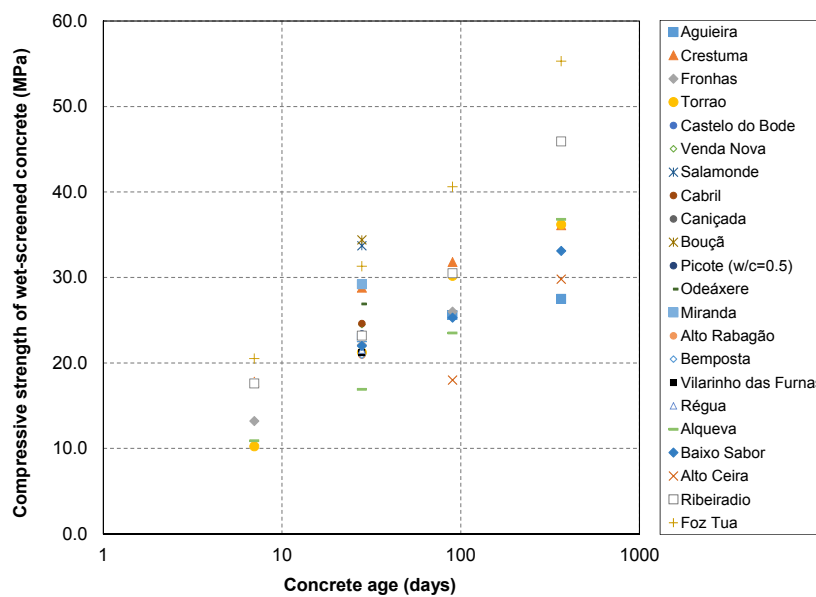


Figure 3.2: Wet-screened concrete compressive strength results of several dams obtained from laboratory tests

3.2. PROPERTIES OF DAM CONCRETE PLACED ON PORTUGUESE LARGE DAMS

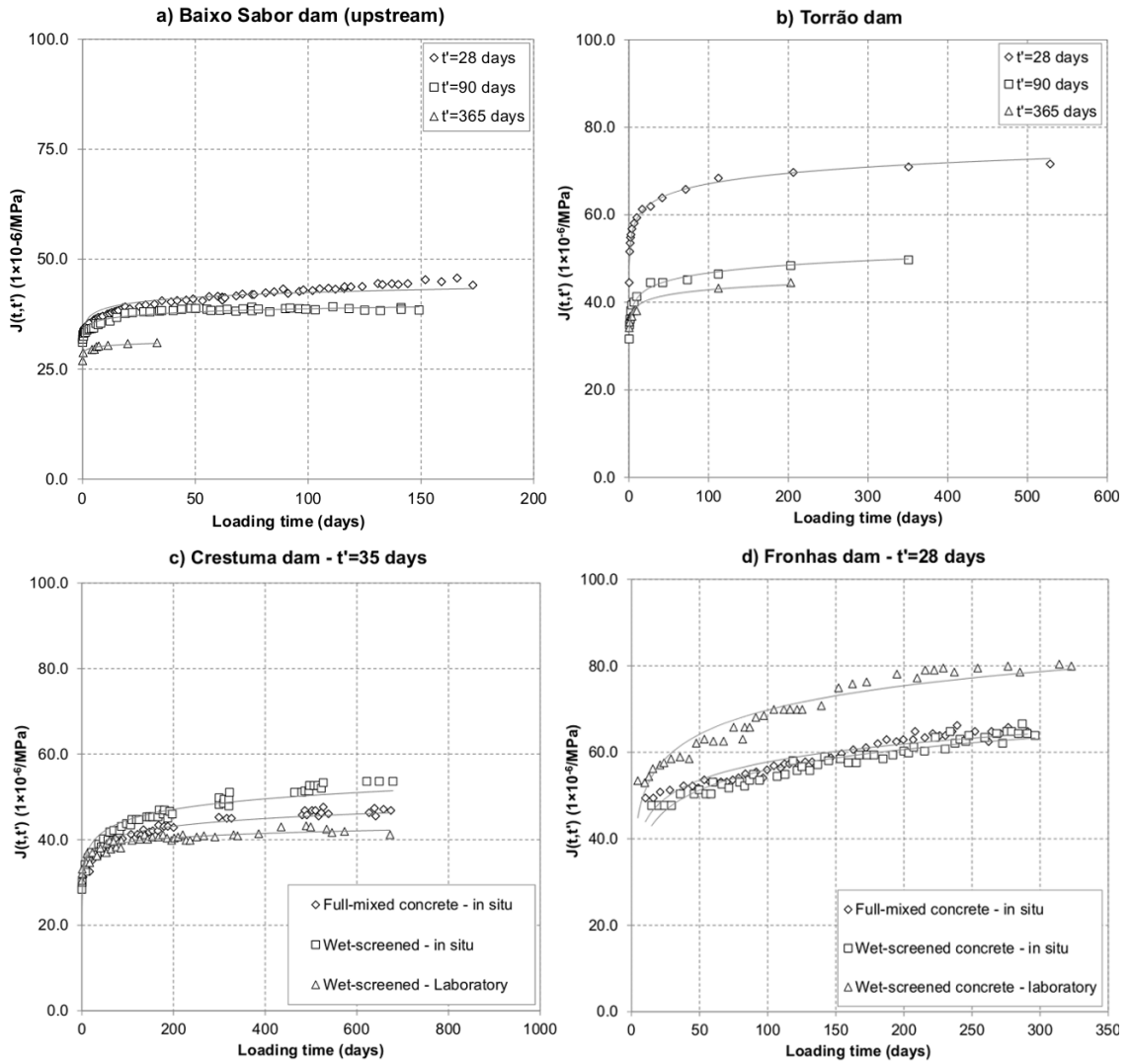


Figure 3.3: Creep test results: a) full-mixed concrete of Baixo Sabor *in situ*; b) full-mixed concrete of Torrão dam *in situ*; c) concrete of Crestuma dam, loading at age of 35 days; d) concrete of Fronhas dam, loading at age of 28 days

3.2.3 Fit of creep test results to the logarithmic creep function

The specific conditions to which dam concrete is subjected, close to hygrometrical isolation and with low stresses (usually below 30% to 40% of the maximum strength), imply the development of only primary and basic creep strains, for service loads (Neville *et al.* 1983). The logarithmic expression for the dam concrete creep function or creep compliance, $J(t, t')$, has been proposed in past studies (Ramos 1985; Soares de Pinho 1989) (Equation 3.1).

$$J(t, t') = K(t') + F(t') \times \log(t) \quad (3.1)$$

where t and t' are the age of concrete and loading age and $K(t')$ and $F(t')$ are time-dependent coefficients. The advantages of this expression are the low number of parameters that need to be determined, the fact that those parameters can be obtained through simple experimental tests and that it predicts a good fit to primary and basic creep. The disadvantages are the poor fit in all the range of loading time (difficulties to fit for early ages) and that requires the parameters definition on each loading age, t' . The fit of the available experimental results to the logarithmic creep function allowed for a direct comparison of the delayed deformability properties of several dam concretes and the study of the influence of maturation conditions, in laboratory and *in situ*, on the strain development over time.

Figure 3.4 presents the creep functions and the correspondent creep strains fitted to experimental results obtained in laboratory tests of wet-screened concrete at the age of 28 days, for several dams (the dashed lines are the extrapolation values to 3000 days under loading). The creep function values are scattered mainly due to the variation of the modulus of elasticity, which influences the instantaneous part of the deformation ($1/E(t')$). For the majority of the creep test results, the values of delayed strains, ε_{creep} , after 1500 days under loading (about 4 years) range between $5 \times 10^{-6}/\text{MPa}$ to $25 \times 10^{-6}/\text{MPa}$ (excluding the exceptional cases of Cabril, Régua and Cahora Bassa dam concretes).

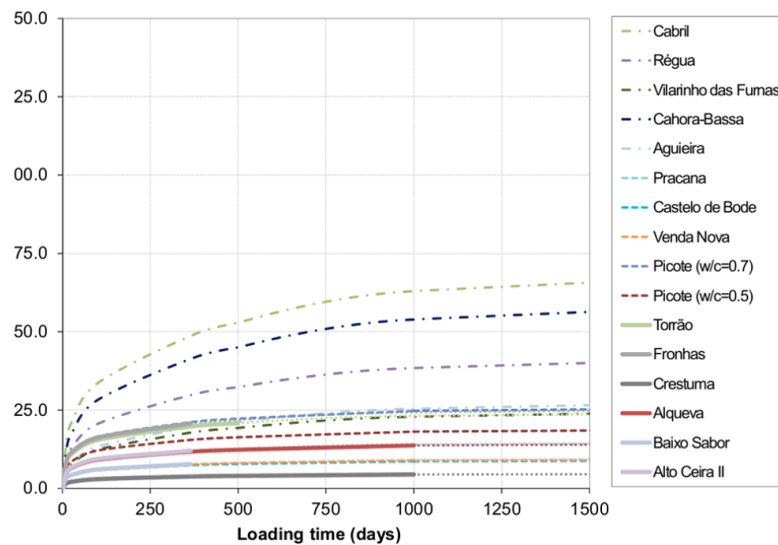


Figure 3.4: Representation of the creep strains fitted to laboratory creep test results of wet-screened concrete at the age of 28 days

A summary of the fitted parameters of the logarithmic function to the experimental results of the total strains (sum of instantaneous strains and the creep strains) is available in (Serra *et al.* 2015b). The parameter values of $K(t')$ and $F(t')$ and, therefore, of creep

compliance, $J(1000, t')$, and creep coefficient, $\phi(1000, t')$, after 1000 days under loading have a large variation due mainly to the different compositions and components used over the years. For example, for the full-mixed concrete *in situ*, the creep coefficient for a loading age of 365 days and 1000 days under loading, varied from 0.16 to 0.67.

3.2.4 Correlation between full-mixed and wet-screened concrete deformability

The available data, obtained from the tests performed in creep cells installed in Torrão, Fronhas, Alto Lindoso and Baixo Sabor dams, enabled the establishment of a correlation between wet-screened (SCR) concrete deformability properties, obtained in laboratory tests, and wet-screened (SCR) and dam concrete deformability properties, obtained from *in situ* tests (Figure 3.5). For this comparison only concretes with granitic aggregates were considered.

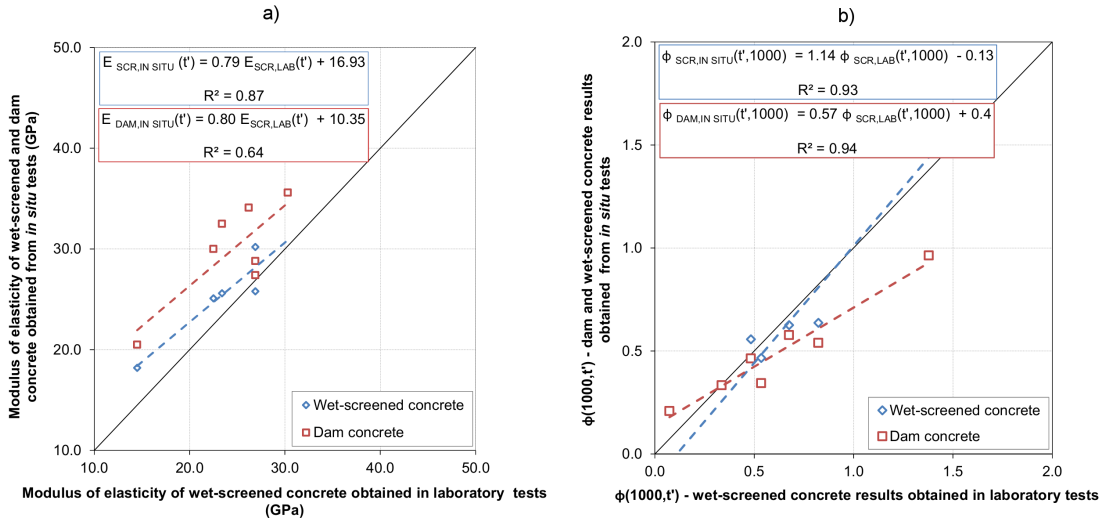


Figure 3.5: Correlation between deformability properties of dam and wet-screened concrete with granitic aggregates obtained in laboratory and *in situ*: a) modulus of elasticity; b) creep coefficient for 1000 days under loading for several loading ages

It is shown that, despite the variability of the concrete compositions, of the properties of each component and, especially, of the water-binder ratio and the fly ash content, there is a good correlation between the deformability of wet-screened concrete and the dam concrete from which it was obtained. The correlations present a large coefficient of determination, R^2 , except for the *in situ* modulus of elasticity of the full-mixed concrete, where the coefficient of determination is 0.64. Based on these results, it is possible to conclude that the *in situ* modulus of elasticity of the full-mixed concrete is always

greater than those obtained for the laboratory wet-screened concrete, due, mainly, to the larger aggregate content. The dam concrete creep coefficients are, in general, smaller than the creep coefficients of laboratory wet-screened concrete, especially for older ages. Equations 3.2 to 3.5 present the statistical correlation between the studies properties of dam and wet-screened concretes.

$$E_{SCR,IN\ SITU}(t') = 0.79 E_{SCR,LAB}(t') + 16.93 \quad (3.2)$$

$$E_{DAM,IN\ SITU}(t') = 0.80 E_{DAM,LAB}(t') + 10.35 \quad (3.3)$$

$$\phi_{SCR,IN\ SITU}(t' + 1000, t') = 1.14 \phi_{SCR,LAB}(t' + 1000, t') - 0.13 \quad (3.4)$$

$$\phi_{DAM,IN\ SITU}(t' + 1000, t') = 0.57 \phi_{DAM,LAB}(t' + 1000, t') + 0.40 \quad (3.5)$$

where $E_{SCR,IN\ SITU}(t')$, $E_{SCR,LAB}(t')$ and $E_{DAM,IN\ SITU}(t')$ are the modulus of elasticity of wet-screened concrete obtained *in situ*, the modulus of elasticity of wet-screened concrete obtained in laboratory and the modulus of elasticity of dam concrete obtained *in situ*, respectively, and $\phi_{SCR,IN\ SITU}(t, t')$, $\phi_{SCR,LAB}(t, t')$ and $\phi_{DAM,IN\ SITU}(t, t')$ are the creep coefficient of wet-screened concrete obtained *in situ*, the creep coefficient of wet-screened concrete obtained in laboratory and the creep coefficient of dam concrete obtained *in situ*.

A similar correlation can be obtained between the laboratory compressive strength of wet-screened, $f_{c,SCR}(t')$, and dam concrete, $f_{c,DAM}(t')$, based on the available results of Portuguese dams (Figure 3.6). Note that this correlation is based on the average experimental results of small specimens of wet-screened concrete and large specimens of dam concrete. The results show that dam concrete has a smaller compressive strength when compared with the wet-screened concrete.

$$f_{c,DAM}(t') = 0.42 f_{c,SCR}(t') + 9.94 \quad (3.6)$$

The linear fits presented in Figure 3.5 can be used for a preliminary prediction of the dam concrete deformability based on wet-screened test results, which are easier and often

3.2. PROPERTIES OF DAM CONCRETE PLACED ON PORTUGUESE LARGE DAMS

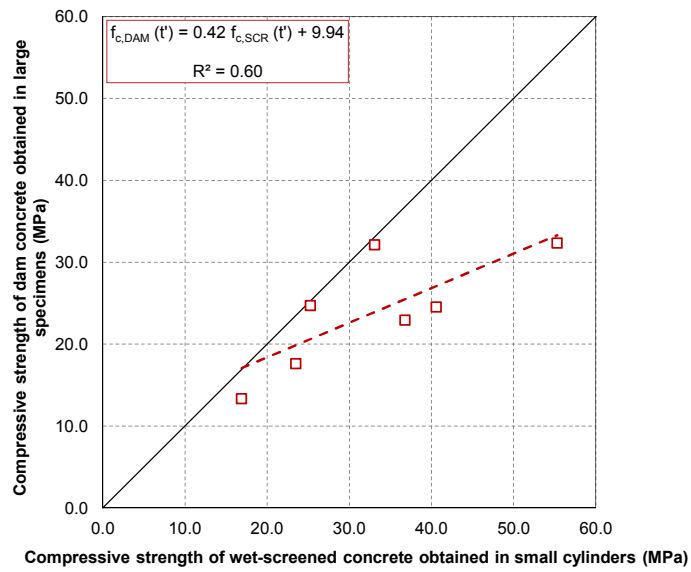


Figure 3.6: Correlation between compressive strength properties of dam and wet-screened concrete obtained in laboratory

used for concrete design studies.

3.3 Case study: Baixo Sabor dam

3.3.1 General description of the dam

Baixo Sabor dam, on Sabor river, located in the north eastern Portugal, is a double curvature thick arch dam with a height of 123.0 m and a crest development and thickness of 505 m and 6.00 m, respectively. Baixo Sabor dam has a total concrete volume of, approximately, 670,000 m³. Due to the large volume placement of concrete, arch dams are usually built using the block construction method (Jansen 2012). The structure is divided into 32 blocks with approximately a 15-m width near the right and the left banks and with 17.00 m width in the central blocks. The blocks are separated by vertical contraction joints and cast in 2.0-m height lifts. During construction, the contraction joints were grouted to obtain a monolithic structure, after forced cooling of the concrete blocks. The dam construction began in 2012 and ended in 2014 and the first filling of the reservoir was completed in April 2016. Figure 3.7 shows the downstream face of Baixo Sabor dam during the construction, in May 2013.



Figure 3.7: Baixo Sabor dam during construction in May 2013

3.3.2 Characterization of the concretes placed in Baixo Sabor dam

3.3.2.1 Properties of the materials

Cementitious materials

The cementitious materials are a portland cement CEM I 42.5R (IPQ 2012a), type I according to ASTM C150/C150M (ASTM 2009), and a class F fly ash, according to ASTM C618 (ASTM 2012), provided by the Compostilla thermoelectric powerplant, in

Spain. Both materials meet or exceed the chemical and physical requirements set in the applicable standards. Furthermore, the fly ash has low lime and alkali contents ($<8\%$ CaO and $<4\%$ $\text{Na}_2\text{O}_{eq.}$), as recommended in (ASTM 2014) and (Nixon and Sims 2016). The cement and fly ash average density are 3120 kg/m^3 and 2480 kg/m^3 , respectively, using the test method described in NP EN 196-6:2010 (IPQ 2014).

A chemical analysis was performed to both the cement and fly ash used in the dam concrete. The chemical analysis of the cement was carried out according to NP EN 196-2:2014 (IPQ 2014); the characterization of the fly ash followed the methods recommended in NP EN 450-1:2012 (IPQ 2012b). The determination of the fly ash alkali content, not covered by NP EN 450-1, was done using a LNEC Internal Method. The fly ash iron oxide content was determined following LNEC Specification E 406:1993 (LNEC 1993d). The replacement ratio of the cement by fly ash for the Baixo Sabor dam is 50%.

The results obtained and the specific test methods used for each property are presented in Appendix A.

Aggregates

The fine and the coarse aggregates are granitic, with an average bulk density of 2644 kg/m^3 . Both the fine and coarse aggregate characteristics were checked against LNEC Specification E 373:1993 (LNEC 1993b) and their use followed the recommendations of ACI 221.R (ACI Committee 221 2001).

Water and admixtures

The water used in the production of the concrete was obtained from the Sabor river which meets the requirements of (LNEC 1993c).

Two different admixtures, Pozzolith 398N and TechniFlow 91, were used as water reducers and superplasticizers (Table 3.3). These types of water reducer increases the flow of concrete for a given w/cm and eases the workability for large placements. The use of superplasticizers, since it has a higher power of water reduction, was used in the reinforced areas where the stresses are higher. Both admixtures followed the required specifications of NP EN 934 (IPQ 2001).

3.3.3 Composition of each type of prescribed concrete

The composition of dam concrete was customized to the available conditions and materials. The cementitious materials content and water-cementitious material ratio were designed,

firstly, to control the temperature rise and, secondly, to obtain the required strength and durability properties (ACI Committee 207 2005; CEN 2005).

This section presents the prescribed composition of each type of concrete and the estimated proportions for the wet-screened concretes placed in Baixo Sabor dam. From now on the full-mixed or dam concrete will also be referred as DAM and the wet-screened concrete will also be referred as SCR (SCR76 using the sieve with an aperture of 76 mm, #76 mm, and SCR38 using the sieve with an aperture of 38 mm, #38 mm). Also to define the placement, the names Core, Face and Reinforcement, will be used to identify the concretes placed in the dam's core, near the dam's surfaces and in the reinforced zones of the dam, respectively. Table 3.2 presents the maximum size of aggregates used for each type of concrete used in the different dam structural elements (EDP 2005).

Table 3.2: Maximum aggregate sizes (MSA) used in the DAM concretes

MSA (in.)	MSA (mm)	Placement	Acronym
6	150	Dam's core	Core
3	76	Upstream and downstream faces Core and surface of the spillway	Face
1 ½	38	Reinforced concrete in the dam's body	Reinforcement
¾	19	Reinforced walls, columns and beams	-

The wet-screened concrete is used when the dimensions of the aggregates are incompatible with the specimens dimensions or with the monitoring device dimensions. The wet-screened concrete is obtained from the produced dam concrete by removing the aggregates larger than a given sieve aperture. The 38 mm aperture sieve is usually adopted for wet-screening the full-mixed concrete. The wet-screening procedure is done after mixing, while the concrete is still fresh. The wet-screening procedure changes the composition of the original concrete, mainly the coarse aggregate content. Since the volume of the removed aggregate is replaced with less coarse aggregate, the remaining components content increase, but the water to cementitious materials ratio remains approximately constant (Blanks and McNamara 1935).

The estimated wet-screened concrete contents were calculated by removing the volume of the sieved aggregates and considering a simplified spherical geometry for the aggregates (model 1 - dashed lines in Figure 3.8). Since the wet-screening is done after mixing using the fresh dam concrete, a small amount of mortar is also lost with the larger aggregates. Therefore, the estimated contents were improved by considering the removal of a thin layer

of mortar coating the screened aggregates (model 2 - thick continuous lines in Figure 3.8). Taking into account the estimate of the coarse aggregate volume removed when wet-screening the dam concrete and the estimate of the volume of mortar that is lost with the sieved aggregates, it was possible to define the contents of the wet-screened concretes (model 2), obtaining a better agreement with the experimental results (points in Figure 3.8).

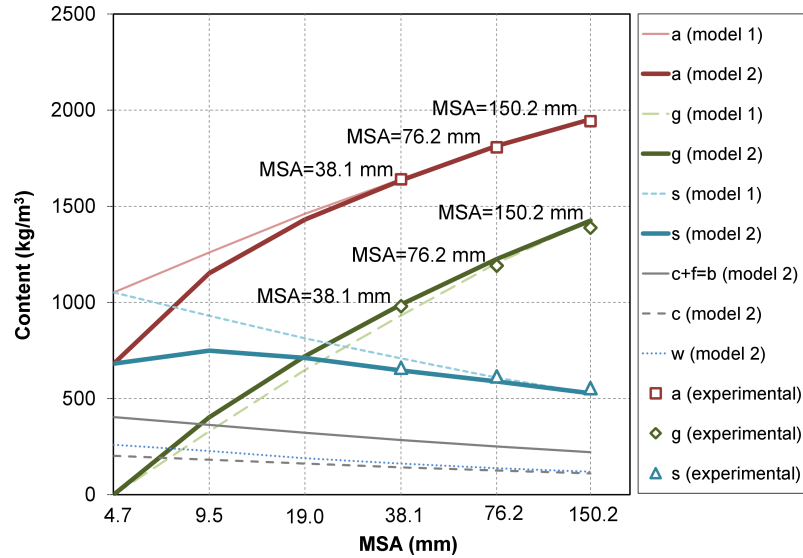


Figure 3.8: Wet-screened concrete contents using different maximum size of aggregate (MSA) ("a" represents the total aggregate, "g" the coarse aggregate, "s" the fine aggregate, "c" the cement, "f" the fly-ash, "b" the binder and "w" the water contents)

Tables 3.3 and 3.4 show the composition of the concrete types placed *in situ*. The main differences between each type of concrete are the MSA, the coarse and fine aggregate contents, the cementitious materials content and the water content. The Face and Reinforcement concretes have a lower water-cementitious material ratio and higher strength properties to cope with higher tensile stresses in the upstream and downstream faces and around the galleries. The water content provided by the aggregate's moisture was obtained considering the moisture percentage of the aggregates (9.1% for fine aggregates and 1.4% for coarse aggregates, average values) and the average water absorption for fine and coarse aggregates (0.44% for fine aggregates and 0.6% for coarse aggregates).

Figure 3.9 shows the particle size distribution of the coarse aggregates of each concrete. The cumulative weight percentages retained in each sieve of the wet-screened concretes are estimated values. The estimated wet-screened concrete components contents were calculated removing the volume of the sieved aggregates, considering a simplified spherical geometry for the aggregates and the removal of a thin layer of mortar coating the screened

CHAPTER 3. EXPERIMENTAL CHARACTERIZATION OF THE
STRUCTURAL PROPERTIES OF DAM CONCRETE

aggregates, as described in previous work (Serra *et al.* 2016a). One can perceive that, although the SCR38 concretes have the same MSA and similar gradation as the Reinforcement concrete (Figure 3.9), the properties of the mortar are different and their mechanical properties cannot be directly compared.

Besides the concrete tests, a specific experimental study was carried out including the characterization of the mortar, produced in laboratory using the same material components as the ones used in Baixo Sabor dam concretes (Tables 3.3 and 3.4). The amount of water used in the production of the mortar was calculated in order to take into account the humidity of the coarse aggregates of the concrete.

Table 3.3: Average composition data of DAM concretes and mortar and the estimated composition data for SCR concretes

Type of concrete	Content (kg/m ³)							
	Cement I 42.5 R	Fly ash	Fine aggregate 0/4.75	Coarse aggregate 4.75/150	Total water water	Water- cementitious material ratio	Pozzoloth 398 N	Admixtures TechniFlow 91
Core-DAM	110.0	110.0	527.0	1425.0	124.0	0.56	0.88	-
Core-SCR38R	141.5	141.5	674.9	988.3	158.8	0.56	1.26	-
Face-DAM	130.0	130.0	637.0	1293.0	143.0	0.55	1.04	-
Face-SCR38	149.7	149.7	730.9	1049.4	164.1	0.55	1.29	-
Reinforcement-DAM	175.0	175.0	798.0	781.0	174.0	0.50	-	3.5
MORTAR	220.6	220.1	1147.4	-	229.1	0.52	1.7	-

Note: Total water is the water added to the mix and the water from the aggregate's moisture. The water content provided by the aggregate's moisture was obtained considering the moisture percentage of the aggregates (9.1% for fine aggregates and 1.4% for coarse aggregates, average values) and the average water absorption for fine and coarse aggregates (0.44% for fine aggregates and 0.6% for coarse aggregates).

Table 3.4: Sieve analysis of DAM concretes and mortar and the estimated sieve analysis for SCR concretes

Type of concrete	Content (kg/m ³)						
	Fine aggregate			Coarse aggregate			
	0/4.75	4.75/9.5	9.5/19.0	19.0/37.5	37.5/76	76/150	
Core-DAM	527.0	186.0	234.0	273.0	351.0	381.0	
Core-SCR38	674.9	265.4	333.8	389.5	-	-	
Face-DAM	637.0	212.0	271.0	366.0	444.0	-	
Face-SCR38	730.9	262.0	335.0	452.4	-	-	
Reinforcement-DAM	798.0	233.0	301.0	518.0	-	-	
MORTAR	1147.4	-	-	-	-	-	

Note: The cumulative weight percentages retained in each sieve of the wet-screened concretes were calculated based on removal of the aggregate volume retained in the 38 mm sieve and considering that a portion of the mortar was also lost in the wet-screening.

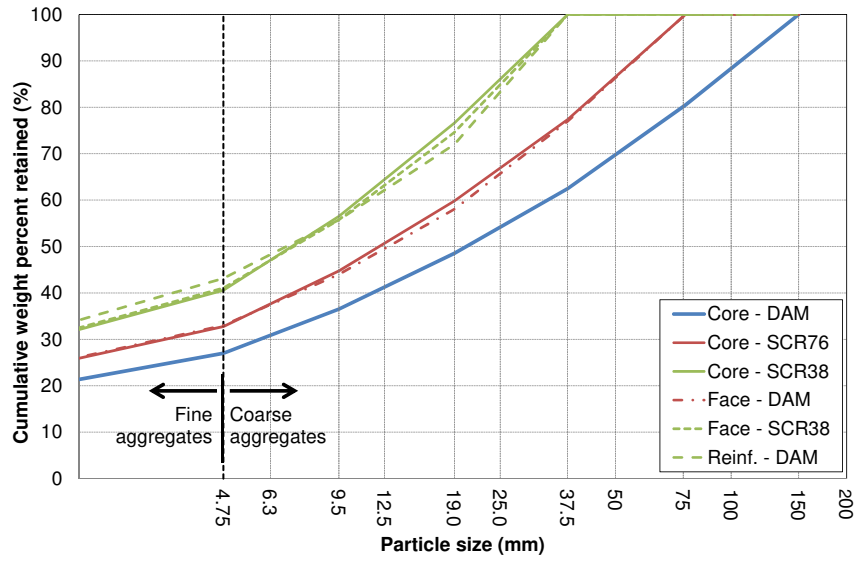


Figure 3.9: Sieve analysis of the Baixo Sabor dam concretes

3.3.4 Composition of the concrete placed in the creep cells

It is also relevant to highlight the composition data of the concrete placed in the experimental setup of the creep cells on Baixo Sabor dam. The specific studies concerning the results of creep tests are based on the proportions of its cast concrete and not the average prescribed composition, presented in the previous section.

Table 3.5 presents the composition of the dam concrete, with MSA of 150 mm, and an estimate of the compositions of the wet-screened concretes, #76 (SCR76) and #38 (SCR38), placed in the creep cells. The cumulative weight percentages retained in each sieve of the wet-screened concretes are measured values of a sieve analysis after mixing. In Figure 3.10 the solid dark lines represent the prescribed coarse aggregate proportions defined by the designer for the overall structure and the dashed grey lines are the sieve analysis, obtained experimentally for the creep cell CC1. The weight percentages of the wet-screened concretes (SCR76 and SCR38) were obtained by weighting the remaining aggregates in these concretes after wet-screening, respectively, by the 76 mm and 38 mm aperture sieve. Only the cumulative weight related to the coarse aggregates are presented due to its importance to the analysis at the mesoscale considering the mortar as an homogeneous material.

Table 3.5: Average composition of dam concrete and estimated compositions of SCR76 (#76 mm) and SCR38 (#38 mm) wet-screened concretes used in the creep cells

Type of concrete	Content (kg/m ³)								
	<i>c</i>	<i>f</i>	<i>b</i>	<i>w_{add}</i>	<i>w_{agg}</i>	<i>w</i>	<i>g</i>	<i>s</i>	<i>a</i>
DAM	110.3	110.2	220.4	62.2	57.9	120.1	1441.9	556.4	1998.3
SCR76	125.6	125.3	250.8	71.3	66.3	137.6	1225.5	644.0	1869.5
SCR38	143.0	142.6	285.6	83.9	78.1	162.0	988.7	710.7	1699.4

c=cement content; *f*=fly ash content; *b*=binder content; *w_{add}*=added water content; *w_{agg}*=content of water in aggregate (moisture); *w*=total water content; *g*=coarse aggregate content; *s*=fine aggregate content; *a*=total aggregate content

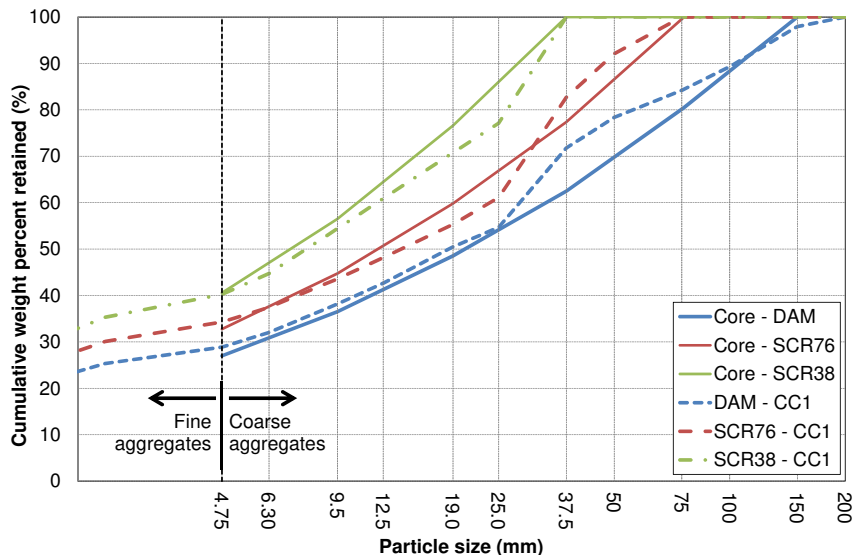


Figure 3.10: Sieve analysis of DAM concrete, SCR76 wet-screened concrete and SCR38 wet-screened concrete placed in creep cell CC1 and comparison with the prescribed concretes (Core-DAM, Core-SCR76 and Core-SCR38)

3.3.5 Maturing conditions of concrete placed *in situ*

In concrete dams the heat of hydration dissipation during the set and hardening process and the early age cracking risk are a main concern. For the cracking risk assessment, it is necessary to know the development of the mechanical properties of the concrete placed *in situ*.

Laboratory tests allow the characterization of the behaviour of concrete in controlled conditions of temperature and humidity. *In situ*, concrete temperatures vary over time and can range from up to 50°C, at the early ages, to low temperatures, in the winter time. The large thickness of concrete dams allows for the hypothesis of hygrometric equilibrium within the dam's body (Bentur 2002; Schrefler *et al.* 2010). It is considered that drying

only occurs in a small part near the upstream and downstream surfaces, which can be negligible. Most of the dam's body is considered, therefore, to have no water exchange with the environment. In order to simulate those conditions the specimens are usually sealed with rolled lead sheet or, if that is not possible, the specimens are maintained at 100% relative humidity.

Temperature variations influence the development of the mechanical properties (higher temperatures increase the hardening rate) (Carino and Tank 1992; Han *et al.* 2003; Kim *et al.* 2002a) and is specially important at younger ages, when most of the cement hydration reactions take place.

In the particular case of dams, due to the large placements of concrete and to the low thermal conductivity of concrete, the hydration heat does not dissipate sufficiently fast and the temperatures inside the dam's core increase significantly and can maintain high temperatures for several months. Also, for arch dams, in order to obtain a monolithic structure it is possible to grout the vertical contraction joints with the aid of a forced cooling system which drops the temperature in the core to low values. The forced cooling is achieved by circulating cooled water through cooling pipes, installed during construction.

The combination of elevated temperatures and forced cooling can result in high temperature gradients and, therefore, stresses that can exceed the strength capacity at a given age. With the later development of the mechanical properties due to the addition of fly ash, this issue can be specially relevant in the early ages.

Figure 3.11 shows the measured temperatures in several devices embedded in the concrete of Baixo Sabor dam, placed at different levels during the construction of the central block. As pointed out before, the temperatures can reach very high temperatures (40-50°C) and in the period of one year can drop to very low values (8-10°C). This effect is especially relevant for the thicker parts of the dam, where the heat of hydration has more difficulty to dissipate.

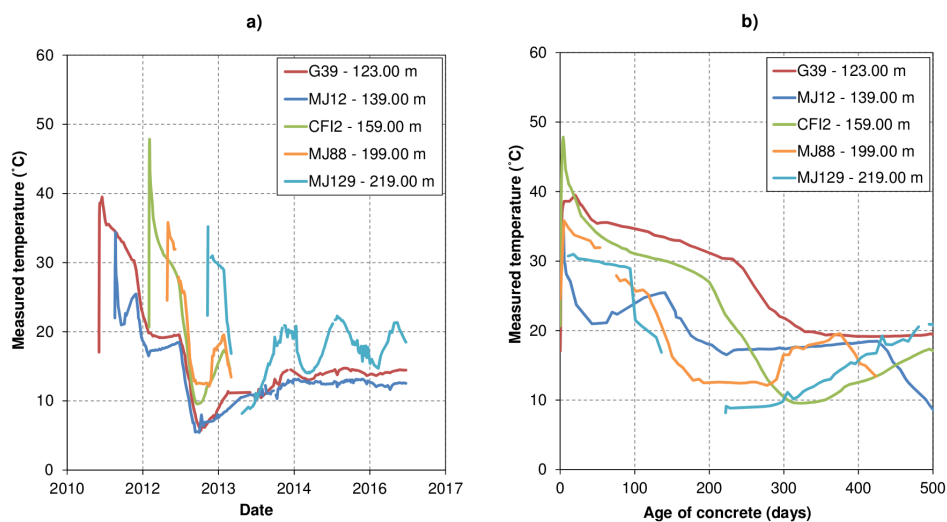


Figure 3.11: Measured temperatures inside Baixo Sabor dam at several levels of the central block (G39 is a embedded strainmeter, MJ12, MJ88 and MJ129 are embedded jointmeters and CF12 is a strainmeter embedded in a creep cell).

3.4 Procedures for the laboratory testing of structural properties of mortar and concrete

The strength properties of concrete were obtained from an experimental programme carried out during the construction period. A set of tests and periodicity were defined by the dam's owner in order to fully characterize the mechanical behaviour of the concretes placed on site and to guarantee the quality control criteria.

In the concrete production, the main parameter to control was the water to cementitious materials (binder) ratio. After mixing, the visual inspection of the quality of the concrete, including inspection for signs of segregation, exudation and lack of cohesion, the specific unit weight, the consistency and the placement temperature were also criteria to be met when the concrete was still fresh. This type of control was done for every mix on site.

After hardening, the specific unit weight, the permeability, the modulus of elasticity, the compressive and tensile strengths were evaluated. The frequency of tests are different for each type of test and for each type of concrete. For example, the specific unit weight was evaluated for every specimen, the compressive strength of wet-screened is obtained in a daily basis and the compressive strength of dam concrete (full-mixed concrete) was only obtained twice a week. The specimens were cast on site after mixing and stored in controlled conditions until the test date. The temperature should be kept at 20°C and the

3.4. PROCEDURES FOR THE LABORATORY TESTING OF STRUCTURAL PROPERTIES OF MORTAR AND CONCRETE

relative humidity should be 100%. The saturated state was required in order to meet the *in situ* condition of the dam's core.

The large volume of dam concrete specimens associated with the high testing frequency required the use of large storage installation. The storage in controlled conditions was key for a good property evaluation and comparison between several mixes. Large temperature variations and drying of the concrete can produce microcracks inside the specimen and influence the ultimate strength values. The designed minimum compressive strength was checked, usually at the age of 90 days, and, in case of a non-conformity, corrective measures were introduced to the composition.

The testing procedures, concerning mixing, handling, compaction, casting, the shape and requirements of the moulds and curing and testing conditions followed a prescribed standard, according with the type of test and the type of concrete (DIN 1991; NP EN 206 2005).

The experimental laboratory results presented in this thesis are divided into two groups. The first group relates to the test results concerning the characterization and quality control procedures prescribed by the dam's owner and executed by the contractor. This group includes strength, modulus of elasticity tests of wet-screened and dam concretes placed during construction and it has a large sampling. The second group includes specific tests, within the framework of this thesis, such as the test for the full characterization of the mortar and of the dam and wet-screened concretes related to the installation of the creep cells. The characterization of the creep cell's concrete included *in situ* and laboratory modulus of elasticity and compressive creep tests.

Table 3.6 presents the overall experimental setup under the scope of the quality control procedures and the specific studies for the development of this thesis. The presented information relates to the type of concrete, the age of testing, the type of specimen, the testing conditions, the responsible entity for the execution of the tests and the standard or recommendation used. Although large amount of tests, the tests related to the quality control during construction had a limited testing age range, being the age of reference 90 days. In the scope of the specific tests, done for this thesis, more testing ages were included.

Table 3.6: Experimental setup data for quality control procedures and for the specific tests

Scope	Type of concrete	Property	Age of testing (days)	Type of specimen	Testing conditions	Responsible	Standard
Quality control	Core-DAM	E_c	28, 90	Cylindrical	Laboratory, moisture cured	Contractor	DIN 1048-5
		f_c	90, 365	Cylindrical			
		$f_{t,spl}$	90, 365	Cylindrical			
Quality control	Face - DAM	E_c	28, 90	Cylindrical	Laboratory, moisture cured	Contractor	DIN 1048-5
		f_c	90, 365	Cylindrical			
		$f_{t,spl}$	90, 365	Cylindrical			
Quality control	Core-SCR38	E_c	90, 365	Cylindrical	Laboratory, moisture cured	Contractor	DIN 1048-5
		f_c	28, 90, 365	Cylindrical			
		f_c	1-365	Cubic			
Quality control	Face-SCR38	$f_{t,spl}$	90	Cylindrical	Laboratory, moisture cured	Contractor	DIN 1048-5
		E_c	90, 365	Cylindrical			
		f_c	28, 90, 365	Cylindrical			
Quality control	Reinforcement-DAM	f_c	1-365	Cubic	Laboratory, moisture cured	Contractor	DIN 1048-5
		$f_{t,spl}$	90	Cylindrical			
		E_c	90	Cylindrical			
This work	Core-DAM	E_c	1-365	Cylindrical	<i>In situ</i>	LNEC	LNEC's internal recommendations
		J_c	28, 90, 365	Cylindrical			
		E_c	1-365	Cylindrical			
This work	Core-SCR76	J_c	28, 90, 365	Cylindrical	<i>In situ</i>	LNEC	LNEC's internal recommendations
		E_c	1-365	Cylindrical			
		J_c	28, 90, 365	Cylindrical			
This work	Core-SCR38	E_c	1-365	Cylindrical	<i>In situ</i>	LNEC	LNEC's internal recommendations
		J_c	28, 90, 365	Cylindrical			
		E_c	1-365	Cylindrical			
This work	Core-SCR38	E_c	1-365	Prismatic	Laboratory, moisture cured	LNEC	LNEC's internal recommendations
		E_c	28, 90, 365	Prismatic			
		J_c	28, 90, 365	Prismatic			
This work	MORTAR	E_c	7, 28, 90	Cylindrical	Laboratory, moisture cured	LNEC	LNEC E397
		f_c	7, 28, 90	Cylindrical			

3.4. PROCEDURES FOR THE LABORATORY TESTING OF STRUCTURAL PROPERTIES OF MORTAR AND CONCRETE

Figure 3.12 shows the specimen shapes and sizes used in the compressive and tensile strength tests and their relationship with the maximum size of aggregate. The diameter of the cylinders for the strength tests are constraint to the MSA of each type of concrete. For determining the wet-screened concrete compressive strength, a 15 cm in diameter and 30 cm-height cylinders (15×30 cm) were used. For determining the compressive strength of dam concrete, with MSA larger than 38 mm, larger specimens, with 45 cm in diameter and 90 cm-height cylinders (45×90 cm) were used. As for the tensile strength determination, due to the difficulties and cost of direct tension tests, the tensile strength was obtained from splitting strength test (or Brazilian test). The ratio between the smaller specimen dimension (ϕ) and the MSA is recommended to be larger then 4 (ASTM 2006). However, for the Core-DAM concrete with MSA of 152 mm, this ratio is only 3.0 due to the limited capacity of the testing equipment. The other types of concrete had higher ϕ -MSA ratio due to the lower values of MSA: the Face-DAM concrete had a ratio of 6; the Core-SCR had a ratio of 4; and, MORTAR had a ratio of 22. The slenderness ratio (H/ϕ) was 2, except for the mortar specimens and for the splitting tensile tests of dam concrete.


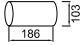
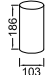
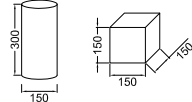
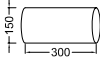
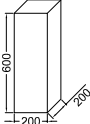
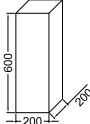
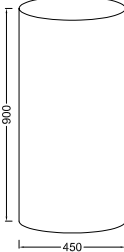
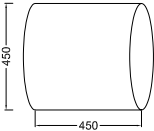
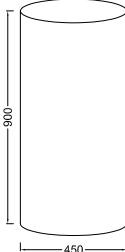
Type of concrete	Uniaxial compressive strength, f_c	Splitting tensile strength, $f_{r,spl}$	Modulus of elasticity, E_c	Creep compliance, $J_c(t,t')$
Mortar binding the coarse aggregates (MORTAR)				
Wet-screened concrete (SCR) Concrete for embedding monitoring devices 38 mm				
Dam concrete (DAM) Core concrete 150 mm Upstream and downstream concrete 76 mm				

Figure 3.12: Specimens used for the determination of the compressive and splitting tensile strength and deformability of each type of concrete and of the mortar

3.5 Procedures for the *in situ* testing of deformability properties of concrete

3.5.1 Proposed improvements for creep cell installation

Creep cells are a specific technique for the *in situ* characterization of instantaneous and delayed behaviour of concrete. Creep cells are concrete cylinders embedded in the dam body, subjected to the same thermohygro-metric conditions as the dam body, since the top of the cell is in contact with the structural concrete, but isolated from the stress field. With the aid of a flat-jack, it is possible to apply a given normal stress to the cell and the strains are recorded with embedded strain meters. The loading system allows for instantaneous deformability tests (used to determine the modulus the elasticity) and for creep tests, maintaining constant stress over time. The use of creep cells had its first developments in the Portuguese Carrapatelo dam, in 1967, and it is still usual nowadays to install these type of devices on important dams, since it allows for testing under the same thermohygro-metric conditions of the structural concrete.

Generally, there are two types of creep cells, the full-mixed concrete cells (structural concrete) and the wet-screened concrete cells. Besides characterizing the deformability of full-mixed concrete, it is possible to study its relation with the wet-screened concrete and, also, the influence of the *in situ* conditions.

For the investigation of the *in situ* instantaneous and delayed deformability properties of the full-mixed concrete and for the evaluation of the influence of wet-screening an improved experimental setup was developed.

The cylindrical specimens were moulded by expanded polystyrene (EPS) hollow cylinders that create a gap between the cell and the dam's concrete. In the past, the gap has been obtained by a double face copper mould (Soares de Pinho *et al.* 1988). This new type of mould allows for a reduction of stiffness and cost. The change was also motivated by the re-design of the flat-jacks and the introduction of two rigid platen interfaces, above and below each flat-jack. This rigid element guaranteed a more uniform transfer of oil pressure from the flat-jack to the bottom of the concrete specimen (Figure 3.13).

The experimental apparatus is composed by a creep cell subjected to a controlled stress, known as "active cell", and by another that allows free deformation, known as "non-stress cell" (Figure 3.15). The active cell registers the total strain variations over time, including the stress-dependent strains, and the "non-stress cell" measures the stress-independent

3.5. PROCEDURES FOR THE *IN SITU* TESTING OF DEFORMABILITY PROPERTIES OF CONCRETE

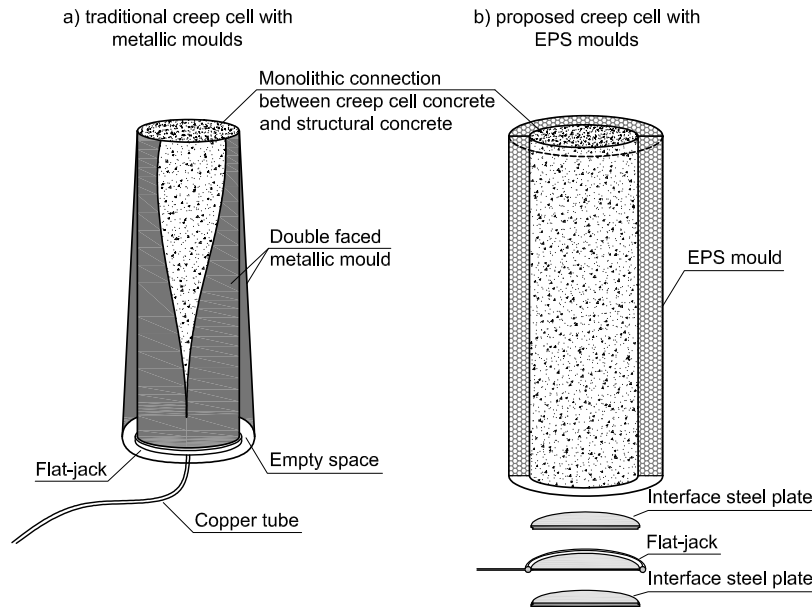


Figure 3.13: Components of an active creep cell (CC-A) by the traditional creep cell design (a)) and by the proposed creep cell design (b))

strains, known as the autogeneous and thermal strains. Both cells are instrumented with embedded Carlson strain meters. Since both cells are casted with the same material, at the same time and are placed next to each other, it is assumed that they are subjected to the same environmental conditions and, therefore, that their behaviour can be compared.

The loading system of the active cells is composed by a closed hydraulic circuit which controls the applied pressure on a flat jack on the basis of the concrete specimen. The pressure can be kept constant with the aid of a mixture of oil and nitrogen stored close to the creep cells. This loading system allows fast stress variations in order to determine the modulus of elasticity at a given age and ensures constant load for long periods of time. Similar experimental work was used for the study of the influence of *in situ* conditions on the delayed deformability properties of concrete placed in a nuclear containment structure (Trivedi and Singh 2014) and in an arch dam (Serra *et al.* 2012).

This type of experimental setup was developed in the past by the National Laboratory for Civil Engineering (LNEC) (Soares de Pinho *et al.* 1988; Serra *et al.* 2012) and adapted for this Ph.D. experimental work. The traditional creep cells have a double-sided metallic mould in order to guaranteed the separation between the concrete inside the specimen and the concrete of the lift and the flat-jack is placed directly below the concrete specimen (Figure 3.13 a)). The use of metallic moulds *in situ*, in addition to its high cost and stiffness, it is very difficult to transport. Besides, creep test results of other dams suggest

that the oil pressure was not full applied to the specimen due to lack of rigidity of the flat-jack (Serra *et al.* 2012).

The re-design of the proposed creep cells included several technical improvements which were implemented in Baixo Sabor dam: i) the use of a standard flat-jack (with rigid interface platens), larger in diameter (ϕ) and increasing the ϕ -MSA ratio of dam concrete specimen (Figure 3.16); ii) the use of three measurement devices in the dam concrete specimen for a more reliable strain measurements; and, iii) the use of expanded polystyrene (EPS) hollow cylinder as the mould to separate the concrete specimen from the dam's body (instead of metallic moulds use in the past, with higher rigidity). The procedure for the experimental installation was: i) placement of the loading system (the storage device in the visiting gallery and the flat-jack of each creep cells) and purge the hydraulic circuit; ii) placement of the measuring devices inside the active and non-active cells and the electric cables; iii) wet-screening of the dam concrete; iv) cast of each creep cell with dam concrete and wet-screened concrete; v) setting the initial reading values in each creep cell; and, vi) cast the surrounding lift.

Figure 3.14 illustrates the procedure for the installation of creep cells, with the placement of the flat-jack in the base of each active creep cell (a), the instrumentation embedded inside the creep cells (b), the overall experimental set prior to casting (c) and the casting of the creep cells and of a concrete lift (d).

The advantage of creep cells is the possibility to characterize the deformability properties over time in the environmental conditions of the dam's core. They also allow the testing of large specimens, suited for the dam concrete and its large aggregates, since the surrounding mass concrete is used as the reaction frame.

The curing conditions of moisture cured specimens followed the usual standard sequence procedures: casting; transportation with moist geotextile; storage in a controlled temperature (20 °C) and moist cured conditions ($RH \approx 100\%$) until testing. The curing conditions of sealed specimens included the sealing of the specimen immediately after casting, using a lead sheet, and the storage in a controlled temperature room (20 °C).

These recent developments in the creep cell setup were successfully installed in Baixo Sabor dam (three sets of creep cells) and in Ribeiradio dam (two sets of creep cells). A further development, designed to enable the access to the flat-jack, was installed in Foz Tua dam (two sets of creep cells). The first type of creep cells, described in §3.5.2, are the main focus of this work and a more detailed description is available in (Serra *et al.* 2014a).

3.5. PROCEDURES FOR THE *IN SITU* TESTING OF DEFORMABILITY PROPERTIES OF CONCRETE

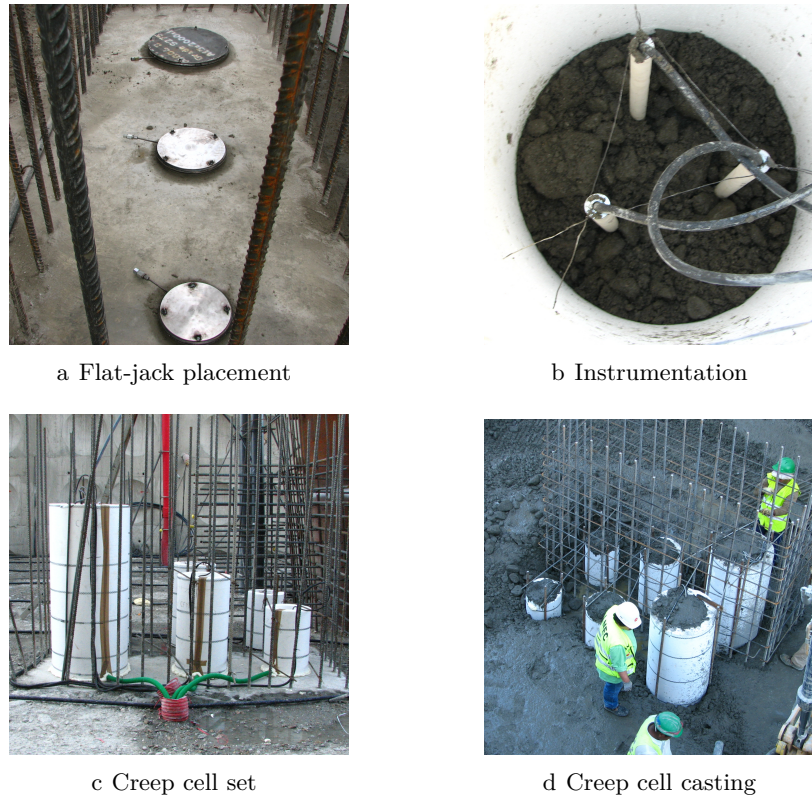


Figure 3.14: Creep cell installation

3.5.2 Creep cell setup used in the case study

The experimental *in situ* installation used for Baixo Sabor dam follows the setup discussed previously in §3.5. The dam has three sets of creep cells, CC1, CC2 and CC3, in three different blocks, several meters apart. Each set has one full-mixed creep cell (CC 150-A, where the "150" stands for MSA and "A" for active cell) and one full-mixed non-stress cell (CC 150-N, "N" referring to non-stress cell), one wet-screened #76 mm creep cell (CC #76-A) and one wet-screened #76 mm non-stress cell (CC #76-N) and one wet-screened #38 mm creep cell (CC #38-A) and one wet-screened #38 mm non-stress cell (CC #38-N).

Due to geometrical and testing equipment limitations, only #38 wet-screened concrete prismatic specimens were used for laboratory testing (P #38). These prismatic specimens were sealed with a lead sheet covering lateral and top faces of the prisms (in order to have no water exchanges with the environment) and maintained with controlled temperature of $20 \pm 1^\circ\text{C}$. The laboratory specimens were sealed with wrapped sheet, previously lining the mould, and soldered immediately after casting. Figure 3.15 illustrate the different types of creep cells in Baixo Sabor dam. The casting of the three sets were made within a month

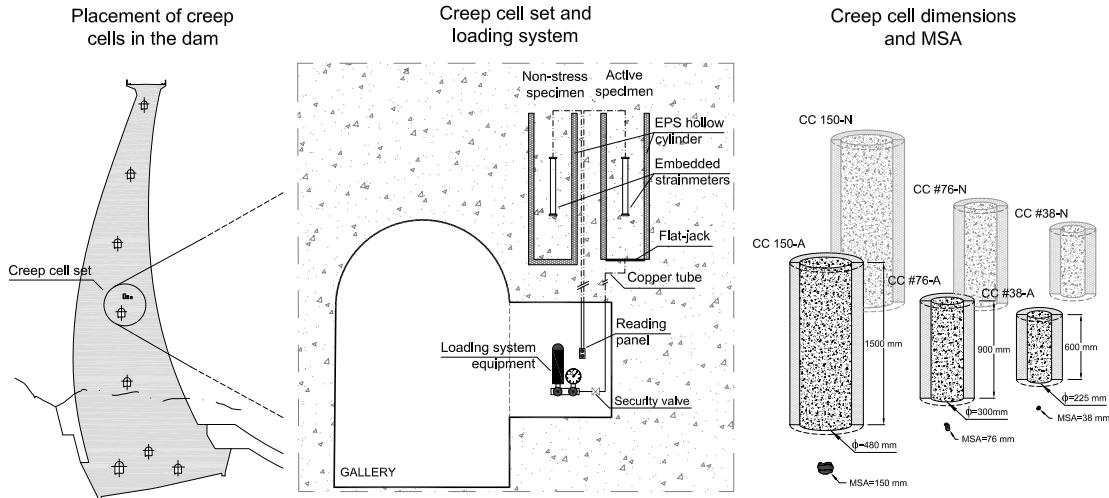


Figure 3.15: Representation of the active and non-stress creep cells for both full-mixed and wet-screened concrete and placement of creep cells on the dam's body.

with close concrete compositions. Figure 3.16 shows the dimensions of the creep cells in correspondence with the MSA used for each type of concrete. The diameter of the EPS cylinders (ϕ) was constrained by the maximum size aggregate of the concrete to be casted and by the maximum diameter of the flat-jack used in the loading system. The ratios ϕ /MSA are 3.2 for the full-mixed concrete, 3.9 for the #76 concrete and 5.9 for the #38 concrete.

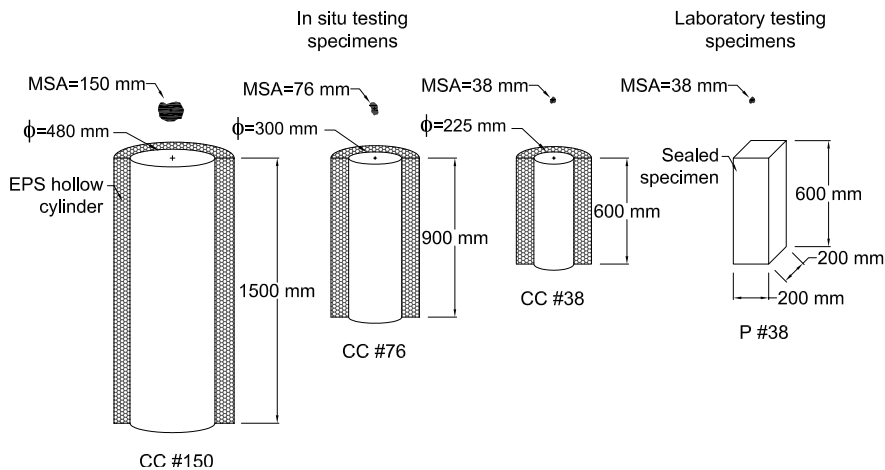


Figure 3.16: Creep cells (CC) dimensions and maximum size aggregate (MSA)

Standard A10 Carlson strainmeters, with a measurement length of 25.4 cm (10"), are not suited for the Core-DAM concrete, due to the size of the aggregates. In this particular

3.6. STRUCTURAL PROPERTIES OF THE ROCK USED FOR THE AGGREGATES

case, special A20 Carlson strainmeters were used, which have a measurement length of 50.8 cm (20"). In order to investigate the distribution of strain inside the larger specimens, three A20 Carlson strainmeters were installed in the Core-DAM concrete specimens. In the remaining specimens only one A10 Carlson strainmeter was installed (Figure 3.17).

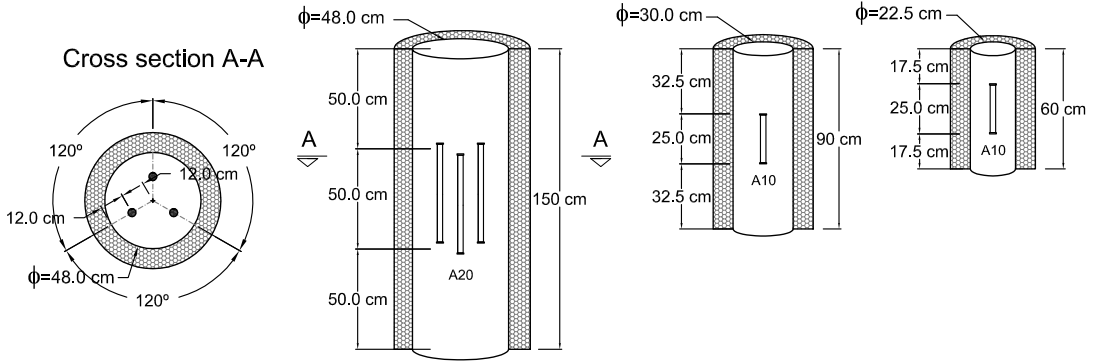


Figure 3.17: Placement of the strainmeters inside the creep cells

Further details about this type of experimental installation are published in LNEC's technical reports (LNEC 2013; LNEC 2014a).

3.6 Structural properties of the rock used for the aggregates

The average and standard deviations of the modulus of elasticity, compressive strength and splitting tensile strength of the intact rock used for the aggregate were obtained from a specific study (EDP 2005). The results are presented in Table 3.7. The results were provided by the dam's owner and were obtained from the material characterization of the rock quarries. Only the materials classified as W1 and W2, regarding their weathering, were considered for the production of concrete.

Table 3.7: Mechanical properties of the rock used for the aggregates

	Density (mean(st.dev.)) (kg/m ³)	E_c (mean(st.dev.)) (GPa)	f_c (mean(st.dev.)) (MPa)	$f_{t,spl}$ (mean(st.dev.)) (MPa)
Granite	2640 (100)	46.3 (5.2)	99.5 (4.0)	7.3 (0.8)

The strength results are compatible with the type of rock used for concrete aggregates, with high values. The modulus of elasticity average value is considered adequate for a good quality granite (Alexander and Mindess 2010). The scatter is considered high for this type of test indicating some heterogeneity in the quarries.

3.7 Structural properties of the mortar and concrete placed in the dam

3.7.1 General aspects

The results related to the quality control were obtained during the construction of the dam. The results related to LNEC were obtained from a specific testing program for the characterization of the mortar taken place at the National Laboratory for Civil Engineering (LNEC) after the dam construction. The mortar was produced with the same materials of the studied dam concretes.

A statistical analysis was done for each structural property, type of concrete and loading age in order to find the distribution parameters that best fit the test results (LNEC 2017). The goal was to describe the raw data, to interpret the behaviour of each set of data and to evaluate its fitness to the Normal, log-Normal and Weibul distributions. This analysis was motivated by the large standard deviations obtained for each property and was found to improve the characterization of the test results, particularly the characterization of the scatter for younger ages (LNEC 2017).

3.7.2 Laboratory deformability test results

3.7.2.1 Modulus of elasticity test results

The curing conditions related to the "Quality control" are the ones defined by the standard DIN 1048-5 (DIN 1991), which is moisture cured until testing. For the study developed in this thesis, "LNEC", prismatic specimens were sealed immediately after casting and stored at a controlled room until testing. The use of sealed specimens, although more expensive, ensures a more similar curing conditions to the dam's core, several meters from a drying surface. Moisture cured conditions imply a continuous supply of water to the hydration reaction and the sealed conditions imply that there is no exchange of moisture between the specimen and the environment.

Table 3.8 and Figure 3.18 present the modulus of elasticity test results for each type of concrete and for the mortar at several ages and for different curing conditions. As expected, the standard deviations for the modulus of elasticity are lower than for the strength properties, but even so, considered high when compared with conventional concrete (ICOLD 2008). The overall obtained results show very similar behaviour between concretes,

3.7. STRUCTURAL PROPERTIES OF THE MORTAR AND CONCRETE PLACED IN THE DAM

with values ranging between 25.4 GPa for the wet-screened concrete and 27.9 GPa for the Face-DAM concrete, at the age of 90 days. Dam concrete's modulus of elasticity are expected to be higher than their wet-screened concretes (27.9 GPa for Core-SCR and 27.6 for Core-DAM). These results do not show the established relationship between aggregate content and the values of modulus of elasticity. In Figure 3.18 the grey areas and error bars represent the confidence interval of each sample for a given testing age, *i.e.* the upper and lower 95% confidence values ($X_{95\%} = \mu(X) \pm 1.96 \times \sigma(X)$, in which $\mu(X)$ and $\sigma(X)$ are the mean and standard deviation of the variable X, respectively). This representation of the confidence values show a measure of the dispersion of the results and highlights the need for a good quality control of dam concrete to ensure that the minimum designed strength values is achieved.

Table 3.8: Modulus of elasticity results of dam and wet-screened concretes and for the core and the face concretes obtained in laboratory

Type of concrete	Type of specimen	Testing conditions	Age (days)	<i>N</i>	E_c (mean(st.dev.)) (GPa)
Core - DAM	$\phi = 450$ mm, $H = 900$ mm	Quality control	90	134	27.6 (3.5)
			365	57	28.7 (3.2)
Core - SCR	$\phi = 150$ mm, $H = 300$ mm	Quality control	28	77	23.3 (3.0)
			90	62	27.9 (3.1)
Face - DAM	$\phi = 450$ mm, $H = 900$ mm	Quality control	90	108	27.9 (3.5)
			365	28	31.5 (2.5)
Face - SCR	$\phi = 150$ mm, $H = 300$ mm	Quality control	28	63	23.1 (3.6)
			90	63	27.9 (3.0)
Reinf - DAM	$\phi = 150$ mm, $H = 300$ mm	Quality control	28	36	24.8 (3.9)
			90	84	29.5 (2.9)
Core - SCR	$200 \times 200 \times 600$ mm	LNEC - sealed	14	9	20.4 (2.7)
			28	9	22.1 (3.2)
			90	6	25.4 (1.0)
			365	7	34.1 (3.7)
Core - SCR	$200 \times 200 \times 600$ mm	LNEC - moisture cured	14	8	19.5 (1.6)
			28	8	20.4 (1.8)
			90	7	25.4 (1.3)
			365	4	30.0 (1.1)
MORTAR	$\phi = 103$ mm, $H = 186$ mm	LNEC - moisture cured	7	3	12.7 (0.5)
			28	3	14.9 (0.2)
			90	3	22.7 (0.8)

Note: *N* is the number of tested specimens

CHAPTER 3. EXPERIMENTAL CHARACTERIZATION OF THE STRUCTURAL PROPERTIES OF DAM CONCRETE

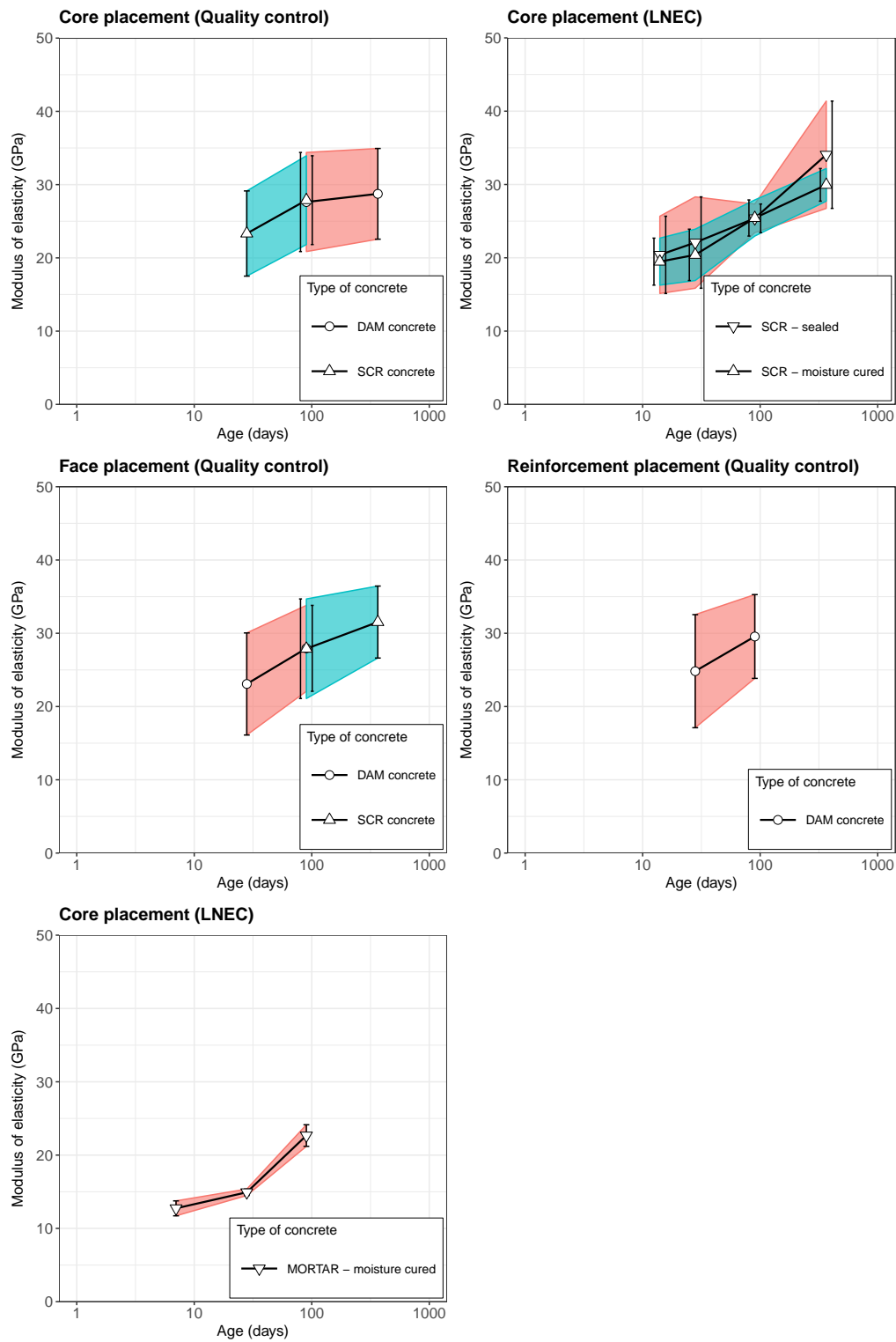


Figure 3.18: Modulus of elasticity results of dam and wet-screened concretes and for the core and the face concretes obtained in laboratory

3.7.2.2 Compressive creep strains development over time

For the specific study concerning the determination of the creep function, a standard laboratory setup (Neville 1983) was used to obtain experimental results of delayed deformations under approximately constant environmental conditions (20 ± 2 °C) for the same concrete batch used for the cast of the creep cells. The wet-screened concrete obtained from creep cells was cast using $200 \times 200 \times 600$ (mm) prisms for specific creep tests (Figure 3.12). The specimens were sealed with a lead sheet in order to maintain the moisture content similar to the dam's core.

Table 3.9 and Figures 3.19 and 3.20 present the experimental results obtained in laboratory for both loading age of 28 and 90 days and for approximately one year under loading (P #38), including the experimental creep compliance, $J_{exp}(t, t')$, or specific strain, $\varepsilon_{spec}(t, t')$.

The experimental creep compliance, $J_{exp}(t, t')$, at time t for a loading age of t' , considered to be a measurement of creep if the stress is kept constant, are obtained by subtracting the free strains, $\varepsilon_{non-stress}(t, t')$, measured in the non-stress cell, from the total strains, $\varepsilon_{active}(t, t')$, measured in the active cell, and dividing by the applied stress (Equation 3.7).

$$\varepsilon_{spec}(t, t') = J_{exp}(t, t') = \frac{\varepsilon_{active}(t, t') - \varepsilon_{non-stress}(t, t')}{\sigma(t')} \quad (3.7)$$

If stress is maintained constant since the first load and the temperature is kept constant, one can compare experimental creep compliance, $J_{exp}(t, t')$, with theoretical creep compliance, $J(t, t')$.

Figures 3.19 a) and b) present the temperature and stress inside the specimen over time, and Figures 3.19 c) and d) show the strain development on the active and non-stress specimens and the increase of the creep strains over time.

The modulus of elasticity results obtained in these specimens, LNEC-sealed, show a good agreement with the results obtained for the quality control purposes (Core-SCR), despite the different curing conditions (Table 3.8).

CHAPTER 3. EXPERIMENTAL CHARACTERIZATION OF THE STRUCTURAL PROPERTIES OF DAM CONCRETE

Table 3.9: Creep test results obtained from prisms in laboratory (average of two specimens P #38-CC1 and P #38-CC2)

Type of concrete	Creep cell batch	Specimen name	t' (days)	$t-t'$ (days)	$T(t')$ (°C)	$\sigma(t')$ (MPa)	$E_{exp}(t')$ (GPa)	$J_{exp}(t, t')$ ($10^{-6}/\text{MPa}$)
SCR38	CC1	P#38-CC1	27.5	362	20.3	5.7	22.1	64.2
	CC2	P#38-CC2	73.5	320	20.5	5.7	25.4	56.3

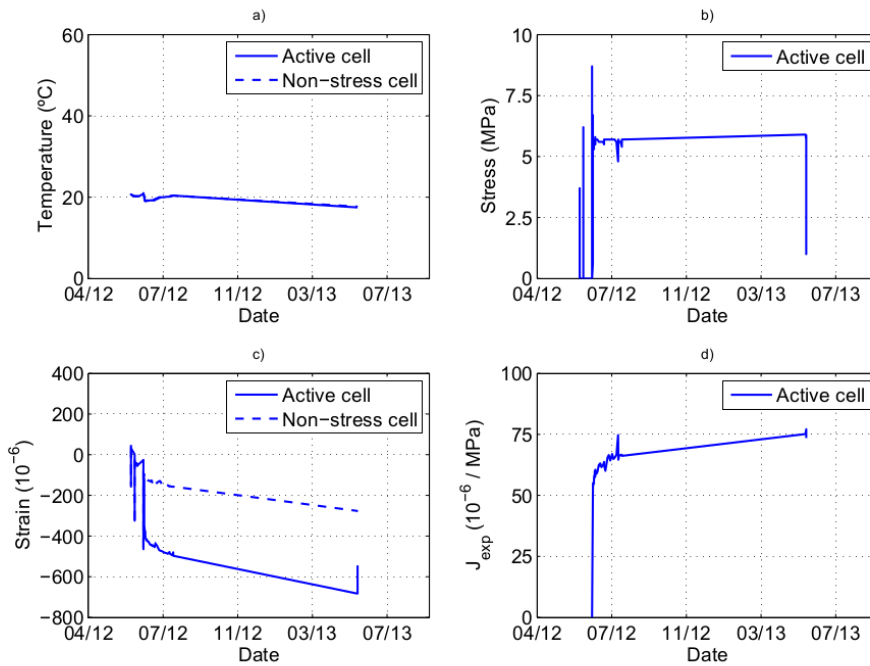


Figure 3.19: Compressive creep test results for the prismatic specimen cast with #38 (SCR38) concrete at the age of 28 days (P #38-CC1)

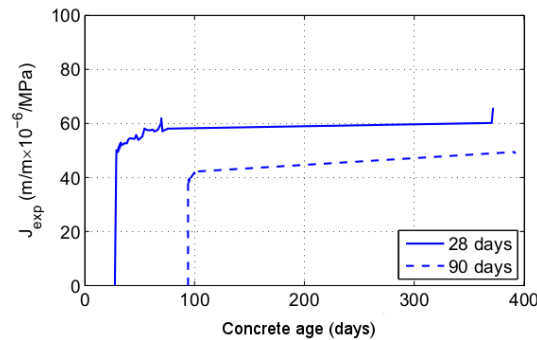


Figure 3.20: Experimental compressive creep compliances for the prismatic specimens in laboratory at different loading ages

3.7.3 *In situ* deformability test results

3.7.3.1 Modulus of elasticity test results

Creep cells allow for modulus of elasticity determination tests and for creep tests at a given age after casting. The modulus of elasticity was determined at the ages of 7, 14, 28, 90 and 365 days for every creep cell set. Due to the particularities of the experimental *in situ* installation, the tests followed an adjusted procedure based on the usual standards (DIN 1991). The *in situ* experimental test procedures for the determination of the modulus of elasticity of concrete were similar to the procedures used for rock mass foundation where loading and unloading cycles are used to determine its elastic properties (Hudson 1993). The maximum testing load, defined as one third of the maximum strength, was divided into small loading steps and, for each one, the strain variation was measured. The loading rate was kept constant and similar to the one used in standard laboratory procedures (approximately 20 kN/s). A stress-strain diagram allows the analysis of the quality of the results (Figure 3.21). For small loads it was observed that the readings were not reliable since the flat-jack was adjusting to the creep cell. For higher loads the behaviour is considered linear and represents the elastic behaviour of the concrete (since the flat-jack total area is considered to be in contact with the specimen). To minimize measurement errors it is usual to use a regression analysis for the linear portion of the unloading stage and subsequent loads (ignoring the lower stress values). The modulus of elasticity at a given age was obtained from the average of three loading cycles. The modulus of elasticity, E_c , is obtained from the harmonic average of the loading and unloading slopes from the stress-strain diagram. Table 3.10 presents the test results obtained for the defined testing ages for each type of creep cell.

Table 3.10: Average values and standard deviations of modulus of elasticity obtained from creep cells *in situ*

Age (days)	E_c (mean(st.dev.)) (GPa)			
	Aggregate	DAM	SCR76	SCR38
7		31.3 (3.4)	26.2 (2.1)	25.1 (1.3)
14		31.9 (3.0)	27.2 (0.7)	25.4 (0.2)
28	46.3 (5.2)	31.5 (1.7)	27.8 (0.5)	26.0 (0.5)
90		33.5 (1.9)	29.7 (1.2)	27.9 (0.1)
365		36.3 (2.5)	31.8 (0.8)	29.9 (-)

From a preliminary qualitative analysis it is possible to conclude that the moduli

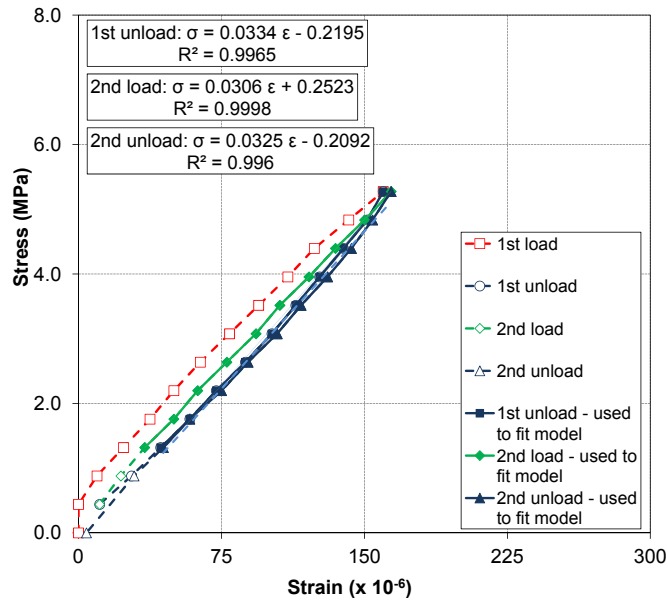


Figure 3.21: Stress-strain diagram and modulus of elasticity determination for *in situ* tests

of elasticity have high values, especially for the full-mixed concrete at the younger ages, which can be explained by the higher coarse aggregate content, when compared with wet-screened concrete, and by the maturing conditions (with temperature higher than the temperature of 20°C, currently used in laboratory testing). The large fly ash content has an important role in the properties development (Ghosh and Timusk 1981; Popovics 1982; Smith and Hammons 1993; Hwang *et al.* 2004; Kar *et al.* 2013), since it "delays" the hardening process (high development rate between the age of 90 and 365 days). The large standard deviations are consistent with the difficulties of characterizing dam concrete and wet-screened concrete, mainly because: i) the maximum aggregate size is considered large for the specimen diameter, even for the wet-screened concrete; ii) the casting conditions are difficult to control due to the rheology of the fresh concrete, with low workability; and, iii) the *in situ* determination procedure involves more unknowns than standard testing in laboratory.

3.7.3.2 Compressive creep strains development over time

Three compressive creep tests were performed at the ages of 28, 90 and 365 days, for the creep cells sets CC1, CC2 and CC3, respectively. As mentioned, the pressure was maintained constant with the aid of a closed hydraulic system of oil and nitrogen. The applied oil pressure was limited to 60 bar in order to ensure linear and primary creep

3.7. STRUCTURAL PROPERTIES OF THE MORTAR AND CONCRETE PLACED IN THE DAM

strains, similar to the dam service conditions, and constraint by the loading capacity of the hydraulic system. The applied stress is related to the flat-jack contact area with the creep cell.

Figure 3.22 shows an example of the creep test results obtained for the creep cell casted with full-mixed concrete at the age of 28 days. The full set of results is published in a LNEC's technical report (LNEC 2014a). The measured temperature shows a quick rise until the 3 days of age, followed by a decrease to about 30°C at the age of 25 days (Figure 3.22 a)). Due to the subsequent concrete lifts of the block, the temperature in the creep cell was almost constant during a period of 4 months and then it dropped from about 30 °C to approximately 10 °C in February 2013 and was kept cool during a long period of time (3 months) for the grout filling of the vertical contraction joint. The applied stress (Figure 3.22 b)) was kept approximately constant for the creep test at the age of 28 days, except for the execution of the modulus of elasticity tests, with loading and unloading cycles at predefined ages. Figure 3.22 c) presents the development of the total strains, measured both in the active creep cell and the non-stress creep cell. The main variations are due to temperature and, after 28 days, due to the applied stress at the active cell. Figure 3.22 d) shows the specific strains calculated for the loading time, since 28 days of age. The specific strains increased rapidly in the first days, followed by a decrease in the rate of development until the beginning of the forced cooling, where a small decrease was measured.

Table 3.11: Compressive creep test results obtained from creep cells *in situ*

Type of concrete	Creep cell	t' (days)	$t-t'$ (days)	$T(t')$ (°C)	$\sigma(t-t')$ (MPa)	$E_{exp}(t')$ (GPa)	$J_{exp}(t, t')$ ($10^{-6}/\text{MPa}$)
DAM	CC1	27.5	362	32.3	5.3	32.5	37.2
	CC2	89.0	320	32.0	5.3	35.2	39.3
	CC3	364.4	33	9.4	5.3	37.8	32.3
SCR76	CC1	27.8	362	31.6	5.2	28.4	48.2
	CC2	89.1	320	30.5	5.2	31.0	39.8
	CC3	364.6	33	9.2	5.2	32.7	38.5
SCR38	CC1	27.8	362	31.2	5.0	25.6	62.1
	CC2	90.0	320	-	-	-	-
	CC3	365.0	33	-	-	-	-

Table 3.11 presents the main results obtained in the creep cells installed in Baixo Sabor dam, for the dam, the #76 and the #38 concretes. For each loading age, t' , and for each type of concrete, the measured temperature at that age, $T(t')$, the applied stress, $\sigma(t')$, the experimental modulus of elasticity, $E_{exp}(t')$ and the experimental creep compliance,

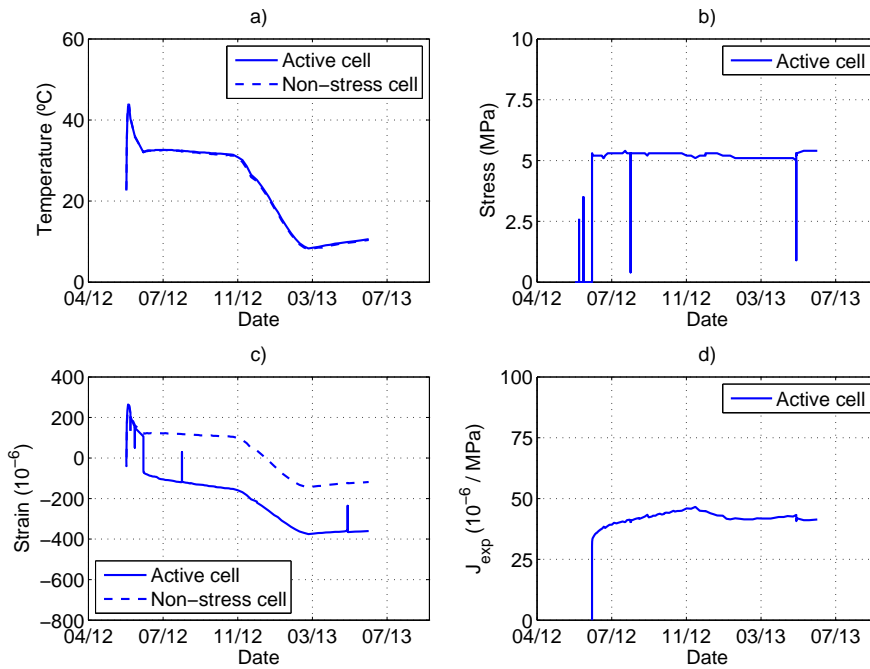


Figure 3.22: Compressive creep test results for the creep cell cast with full-mixed concrete at the age of 28 days (DAM-CC1)

$J_{exp}(t, t')$ or specific strain, $\varepsilon_{spec}(t, t')$ for the time under loading, $t - t'$, are presented. Since the temperature on site varies over time, at each loading age the measured temperature was different (approximately 30 °C for the loading ages of 28 and 90 days and 9.4 °C for the loading age of 365 days). For the #38 concrete only the test results for the loading age of 28 days are available, due to leak on the embedded loading system of both CC2 and CC3 that was detected after installation during testing.

Results show that concretes wet-screened with lower aperture of the screening sieve give higher specific strains, for every loading ages. This conclusion follows the known behaviour since the wet-screened concrete has a lower content of coarse aggregate and a higher content of cement paste compared with the full-mixed concrete from which it was obtained.

The creep test results reveal also the small values of specific strains obtained *in situ*, especially for the full-mixed concrete in which the creep strains after one year are only about 20% of the instantaneous strains at the beginning of the creep test. The behaviour of wet-screened #38 mm concrete *in situ* is similar to the the behaviour of wet-screened #38 mm concrete tested in laboratory, which despite a lower modulus of elasticity at the loading ages, gives approximately the same specific strains development over time.

3.7. STRUCTURAL PROPERTIES OF THE MORTAR AND CONCRETE PLACED IN THE DAM

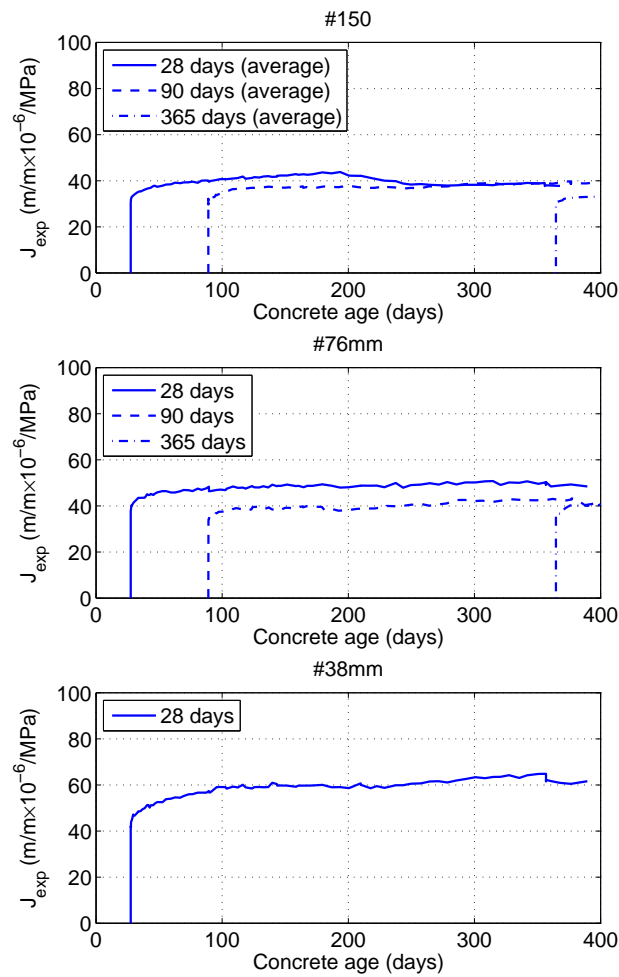


Figure 3.23: Experimental compressive creep compliances for the creep cells at several loading ages

3.7.4 Laboratory compressive strength test results

The testing ages of the laboratory compressive strength tests were defined by the dam's owner and only the compressive strength obtained from cubic specimens have a significant number of results at several ages. These results are useful to define the full range of development from 1 day to 1 year. Despite the limited data, the results show the development of strength over time of the different types of concrete and the strong rate for later ages (after 28 days). Conventional concrete without the addition of other cementitious materials, does not has a significant increase of strength after the age of 28 days. This rate can be explained by the large content of fly ash which has slower hydration process (Santos Silva 2006). The increase of strength from 28 days to 365 days of age can reach 70% for the Face-SCR concrete. The results obtained using cubic specimens have larger strength values, which is due to the larger confinement in this type of specimen, when

compared with cylindrical specimens. The strength values are higher for the Reinforcement placements and smaller for the Core placements, which has lower cement content. Generally, the wet-screened concrete have slightly higher strength values. The strength values of the mortar are smaller than the concretes but its development over time is higher. Table 3.12 and Figure 3.24 present the compressive strength test results for each type of concrete and for the mortar at several ages, considering 95% confidence intervals).

The concrete results are related to the quality control procedures during the 4-year construction period, hence the high number of tested specimens (N). The results related to LNEC tests were obtained from a additional experimental program for the characterization of the mortar, taken place at the LNEC. The large standard deviations are considered to be usual values for this type of concrete and taking into account the construction duration (Zhou *et al.* 2010). The standard deviations can reach as much as 20% of the mean values, even for wet-screened concrete with smaller aggregates, except for the younger ages (less than 7 days), in which this percentage can be higher.

Although the composition remained the same over time, there can be a variation of the material properties during construction, especially the properties of the aggregates. The significant scatter can also be due to the use of large aggregates (Khaloo *et al.* 2009) which are significantly larger than in conventional concrete. Furthermore, for dam concrete results, the ratio between the size of aggregates and the size of the specimen can introduce significant deviations during testing.

For the development of this work and for the sake of uniformity, it is considered that the strength values obtained for over 3 days of age follow a Normal distribution (LNEC 2017).

3.7. STRUCTURAL PROPERTIES OF THE MORTAR AND CONCRETE PLACED IN THE DAM

Table 3.12: Compressive strength results of DAM and SCR concretes for Core, Face and Reinforcement placements and of mortar

Type of concrete	Type of specimen	Testing conditions	Age (days)	N	f_c (mean(st.dev.)) (MPa)			
Core-DAM	$\phi = 450$ mm, $H = 900$ mm	Quality control	90	134	24.7 (4.2)			
			365	57	32.1 (4.5)			
Core-SCR	$\phi = 150$ mm, $H = 300$ mm	Quality control	28	77	22.0 (4.5)			
			90	256	25.3 (5.2)			
Core-SCR	$A = 150$ mm	Quality control	365	53	33.1 (5.1)			
			1	43	4.1 (3.6)			
			2	71	11.0 (3.6)			
			3	75	13.4 (3.0)			
			4	47	15.4 (3.7)			
			5	28	16.9 (3.5)			
			6	16	15.4 (2.1)			
			7	451	18.0 (3.2)			
			28	482	25.5 (4.3)			
			90	813	31.7 (5.3)			
Face-DAM	$\phi = 450$ mm, $H = 900$ mm	Quality control	180	34	37.6 (5.2)			
			365	122	41.1 (6.5)			
			90	108	26.3 (4.0)			
			365	28	36.9 (5.1)			
			Face-SCR	$\phi = 150$ mm, $H = 300$ mm	Quality control	28	63	21.9 (4.6)
						90	260	26.9 (5.5)
			Face-SCR	$A = 150$ mm	Quality control	365	45	37.2 (6.2)
						1	194	4.1 (3.3)
						2	352	10.4 (3.0)
						3	1	11.5 (-)
4	152	15.5 (3.5)						
5	108	16.9 (3.2)						
6	60	17.9 (3.1)						
7	874	18.3 (3.7)						
28	863	25.9 (4.8)						
90	1238	32.0 (5.6)						
Reinforcement-DAM	$\phi = 150$ mm, $H = 300$ mm	Quality control	365	137	41.7 (7.4)			
			28	36	27.0 (5.2)			
Reinforcement-DAM	$A = 150$ mm	Quality control	90	84	36.7 (5.9)			
			1.0	10	8.2 (3.5)			
			1.5	8	12.1 (6.6)			
			2.0	19	13.5 (2.8)			
			2.5	31	15.3 (2.5)			
			3.0	385	16.6 (2.9)			
			3.5	2	17.8 (1.5)			
			6.0	3	23.6 (4.5)			
			7.0	876	22.7 (3.3)			
			28.0	873	31.7 (4.7)			
MORTAR	$\phi = 103$ mm, $H = 186$ mm	LNEC	90.0	865	42.9 (5.5)			
			7	3	14.6 (0.7)			
			28	3	20.1 (1.0)			
			90	3	32.9 (0.6)			

Note: N is the number of tested specimens

CHAPTER 3. EXPERIMENTAL CHARACTERIZATION OF THE STRUCTURAL PROPERTIES OF DAM CONCRETE

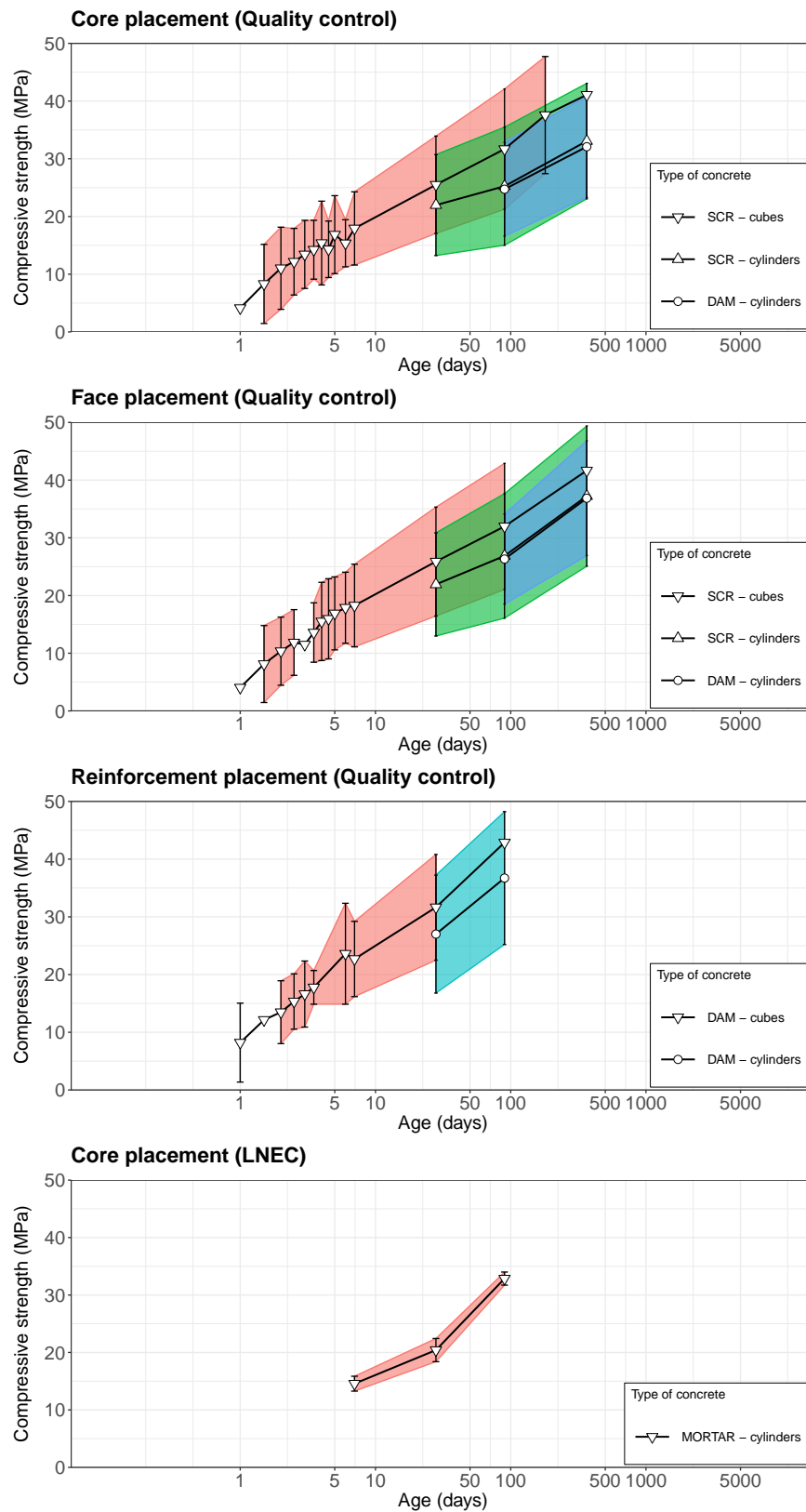


Figure 3.24: Compressive strength results of DAM and SCR concretes for Core, Face and Reinforcement placements and of mortar

3.7. STRUCTURAL PROPERTIES OF THE MORTAR AND CONCRETE PLACED IN THE DAM

3.7.5 Laboratory splitting tensile strength test results

Table 3.13 and Figure 3.25 present the splitting tensile strength test results for each type of concrete and for the mortar at several ages. The experimental programme focused essentially on the reference age of 90 days. The standard deviations are as high as the ones obtained for the compressive strength. Similarly to the compressive strength results, the 95% confidence intervals are also plotted.

The splitting strength results are higher for the Reinforcement dam concrete when compared with the Core concrete. The wet-screened concrete results obtained using small specimens are higher than their original dam concrete, tested using larger specimens. The mortar splitting strength results are also higher than the Core-DAM concrete, at the age of 90 days.

Table 3.13: Splitting tensile strength results of DAM and SCR concretes for Core, Face and Reinforcement placements and of mortar

Type of concrete	Type of specimen	Testing conditions	Age (days)	N	$f_{t,spl}$ (mean(st.dev.)) (MPa)
Core-DAM	$\phi = 450$ mm, $H = 450$ mm	Quality control	90	94	2.2 (0.3)
			365	22	2.8 (0.3)
Core-SCR	$\phi = 150$ mm, $H = 300$ mm	Quality control	90	66	2.7 (0.4)
Face-DAM	$\phi = 450$ mm, $H = 450$ mm	Quality control	90	43	2.2 (0.4)
Face-SCR	$\phi = 150$ mm, $H = 300$ mm	Quality control	90	65	2.8 (0.4)
Reinforcement-DAM	$\phi = 150$ mm, $H = 300$ mm	Quality control	90	80	3.5 (0.4)
MORTAR	$\phi = 103$ mm, $H = 186$ mm	LNEC	7	3	1.9 (0.1)
			28	3	2.4 (0.1)
			90	3	2.9 (0.5)

Note: N is the number of tested specimens

CHAPTER 3. EXPERIMENTAL CHARACTERIZATION OF THE STRUCTURAL PROPERTIES OF DAM CONCRETE

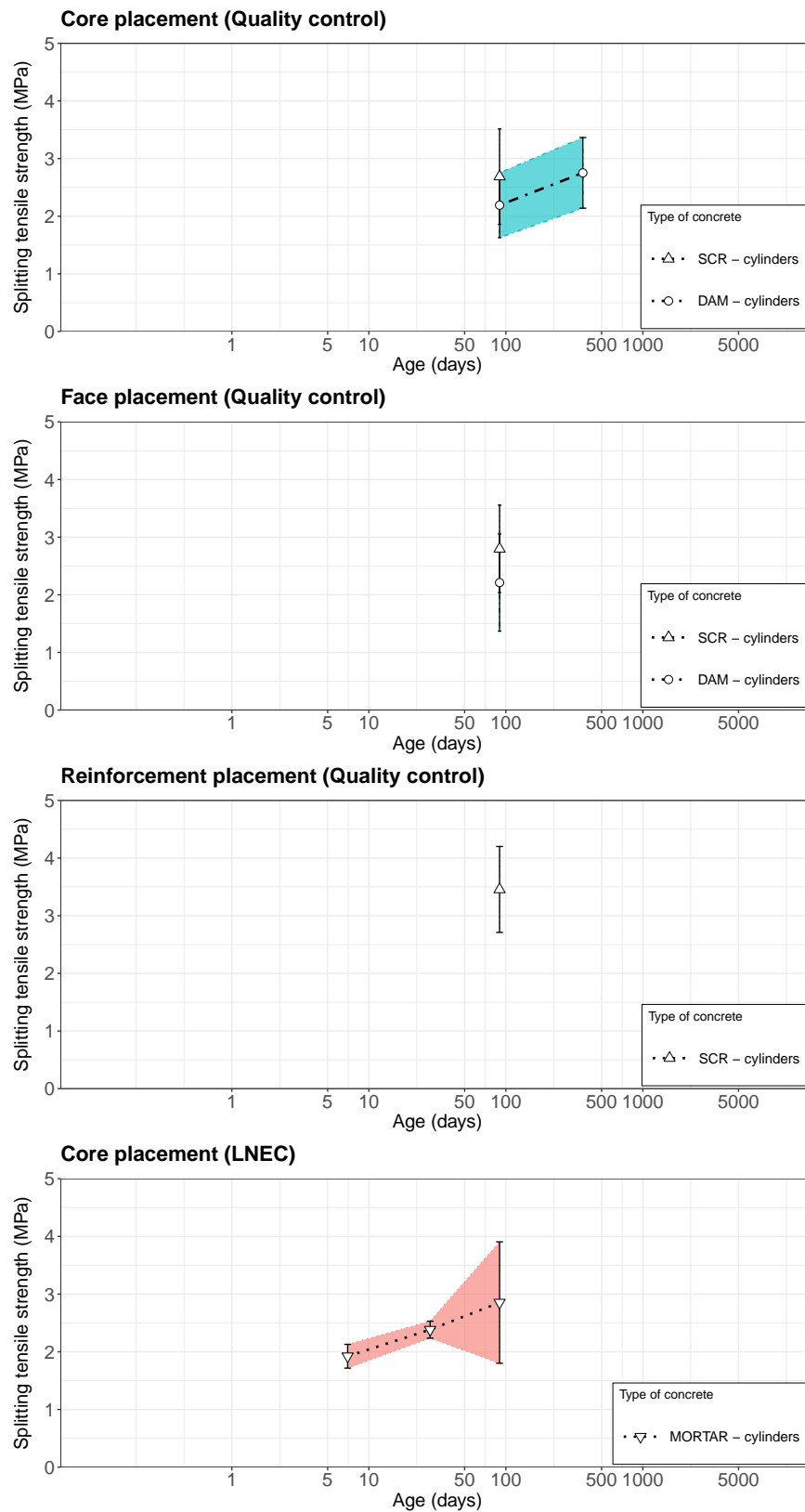


Figure 3.25: Splitting tensile strength results of DAM and SCR concretes for Core, Face and Reinforcement placements and of mortar

3.7.6 Correlation between concrete properties

In this section a preliminary correlation between the test results for each type of concrete is presented. This type of correlation can be useful for the statistical prediction of a property given another property, based on prior experimental results and to cross-check and validate a given test result.

The first analysis concerns the correlation between concrete properties, namely the compressive strength obtained using cubes and using cylinders, the compressive strength and the modulus of elasticity, and the compressive strength and the splitting tensile strength. Several standards define empirical expressions for this type of correlation which can be fitted to experimental results (ACI Committee 318 1995; Fib 2010). This type of empirical expressions can be used when there are limited results of one type of tests. For example, non-destructive tests, such as the modulus of elasticity tests can be used to estimate the strength properties based on a fitted empirical expression.

Figure 3.26 shows the correlation between compressive strength obtained using cubes and using cylinders. As pointed out before, the cylinder test results yield lower values of compressive strength when compared with results obtained using cubical specimens. This type of behaviour is documented in the literature and is due to the higher confinement effect on the top and bottom of the cubical specimens, increasing the peak strength (Mier 1998). The right plot in Figure 3.26 shows two outlier values that highlight some type of error associated with the curing, the testing conditions or the analysis. This type of result should be removed from the database since their correlation do not follow the established behaviour.

The plot of the compressive strength and the modulus of elasticity results (Figure 3.27) shows a strong correlation between the two properties. Although some scatter, the compressive strength has higher rate of development over time than the modulus of elasticity. This is more pronounced for the Reinforcement-DAM concrete. The behaviour of wet-screened concretes is similar to the one obtained for the respective dam concrete.

Figure 3.28 shows the correlation between the compressive strength obtained in cylinders and the splitting tensile strength from the same concrete batch. The general idea is that the direct tensile strength is, approximately, one tenth of the the compressive strength (Coutinho and Gonçalves 1994) and 90% of the splitting tensile strength (Fib 2010). Therefore, the splitting tensile strength is 10% of the compressive strength. The

CHAPTER 3. EXPERIMENTAL CHARACTERIZATION OF THE STRUCTURAL PROPERTIES OF DAM CONCRETE

results of Baixo Sabor dam are coherent with this estimate, despite the usual large scatter.

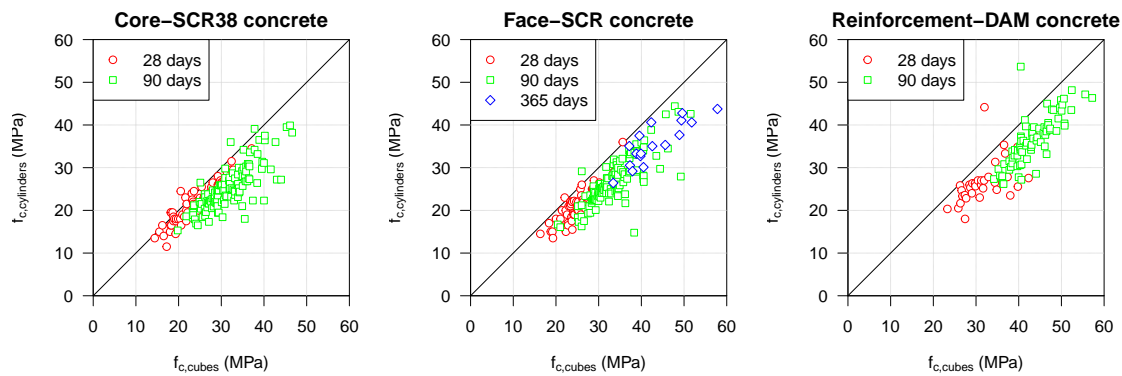


Figure 3.26: Correlation between the compressive strength obtained in cubes and the compressive strength obtained in cylinders

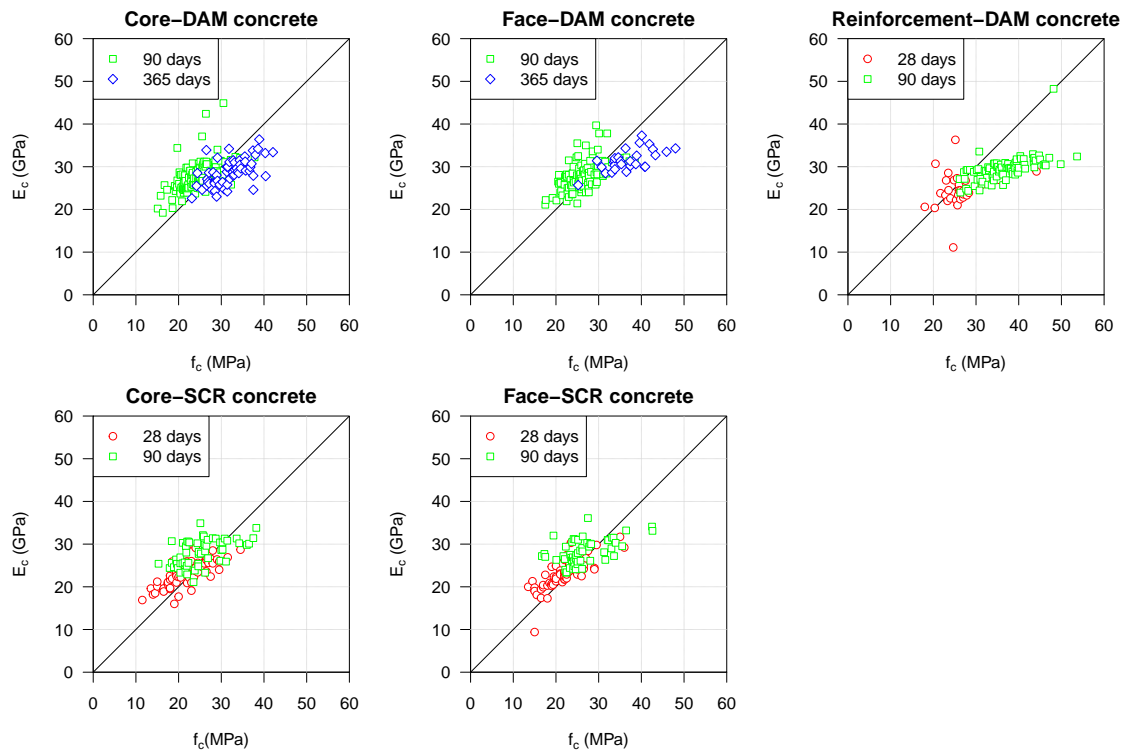


Figure 3.27: Correlation between the compressive strength and the modulus of elasticity

The second analysis concerns the correlation of the dam and the wet-screened concrete properties, separated by testing age. It is important to emphasize that dam and wet-screened results were obtained from the same concrete batch but cast in different specimen sizes. Figure 3.29 shows the relationships between each mechanical property for wet-screened concrete using small specimens and for dam concrete using large specimens. Test results show that, for both Core and Face concretes, the modulus of elasticity and the

3.7. STRUCTURAL PROPERTIES OF THE MORTAR AND CONCRETE PLACED IN THE DAM

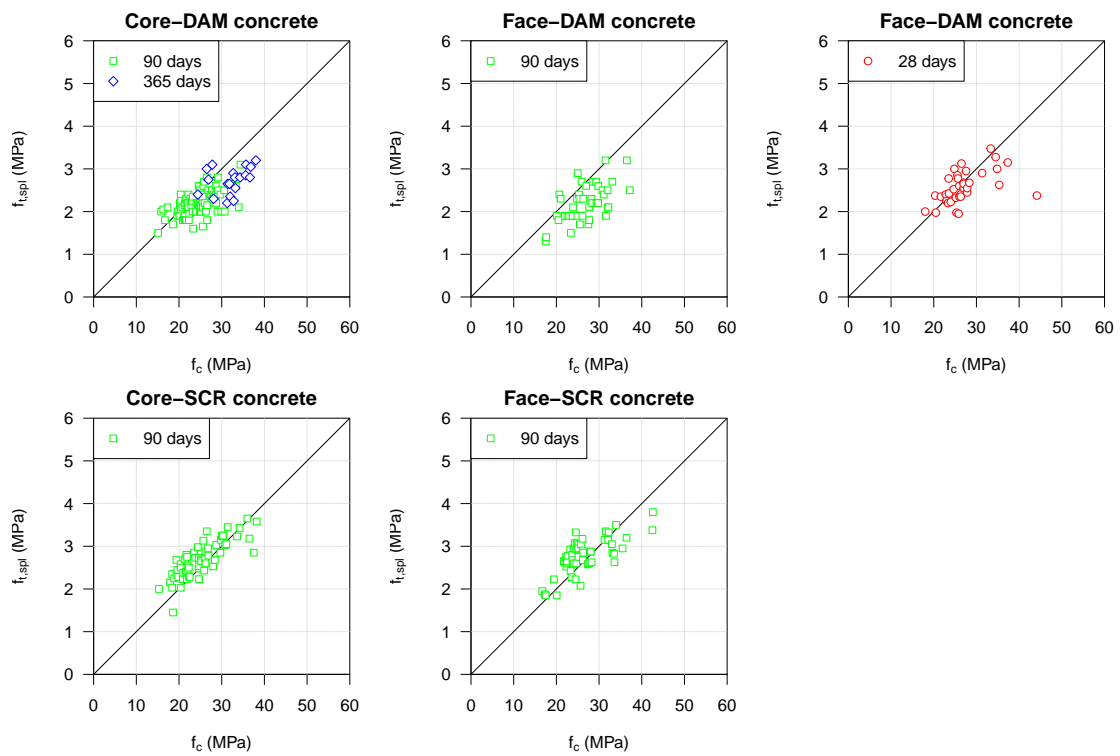


Figure 3.28: Correlation between the compressive strength and the splitting tensile strength

compressive strength of wet-screened and dam concrete are very close to each other. The splitting tensile strength shows a different behaviour, with lower strength values for the dam concrete.

CHAPTER 3. EXPERIMENTAL CHARACTERIZATION OF THE STRUCTURAL PROPERTIES OF DAM CONCRETE

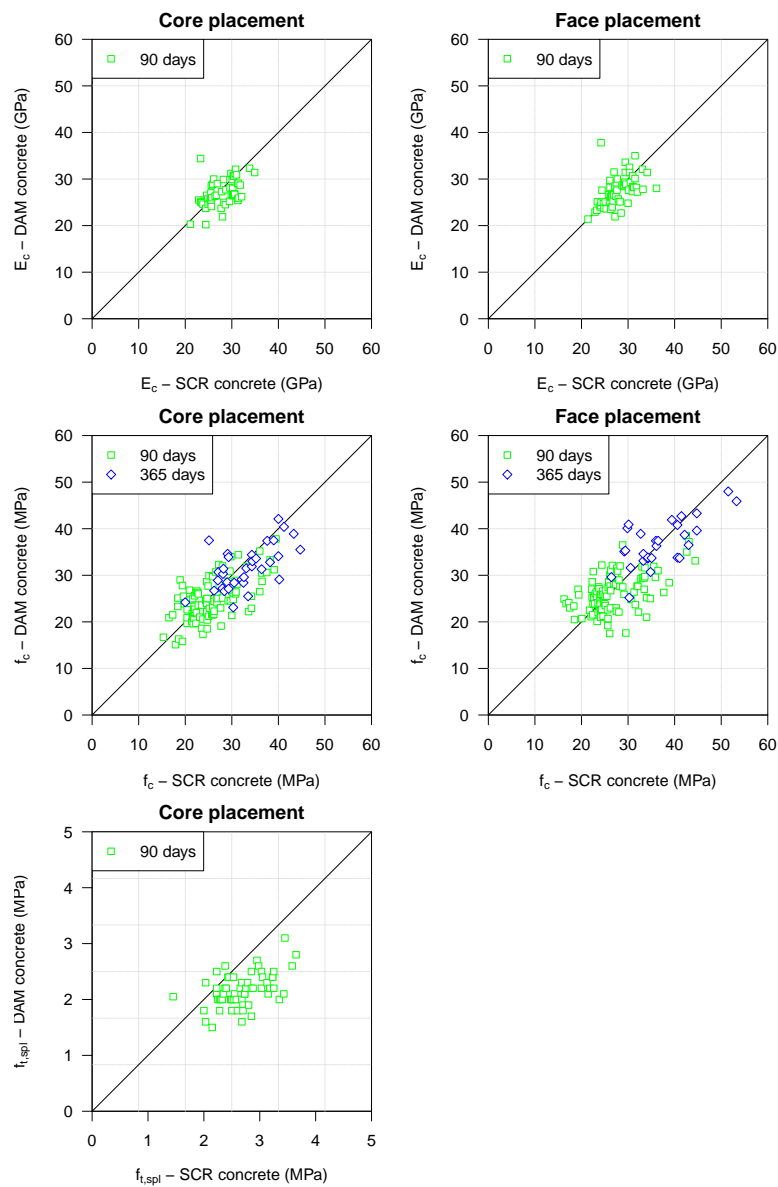


Figure 3.29: Correlation between wet-screened and dam concrete properties

3.8 Concluding remarks

The developed experimental work focused on the characterization of the main structural properties of dam and wet-screened concretes placed on Baixo Sabor dam. For this dam, three sets of results were presented: one related to the laboratory test results obtained during construction and provided by the dam's owner; another set of specific tests for the characterization of laboratory and *in situ* delayed deformability using creep cells; and, a set of laboratory tests of the aggregates and mortar binding the coarse aggregates. The studied structural properties were the modulus of elasticity and the development of creep strain over time, the compressive and the splitting tensile strengths.

One of the main difficulties of dam concrete testing is the use of large specimens, particularly for a dry consistency concrete. The cast, compaction, transport, curing and testing of large specimens with hundreds of kilograms require expertise and good quality control procedures. Wet-screened concrete testing using smaller specimens gives some insight of the quality of the placed concrete and is much easier to deal with. However, the properties of the dam concrete placed on site are different from those of wet-screened concrete and should be also assessed.

Firstly, a general overview of the development of the main structural properties in Portuguese dam concrete is presented in the beginning of the chapter. Dam concrete composition and, therefore, its mechanical properties varied significantly over the years and from dam to dam. Modulus of elasticity of dam concrete varied between 20 GPa and 40 GPa at the age of one year and the delayed strains ranged mainly between 5×10^{-6} /MPa and 25×10^{-6} /MPa. The compressive strength showed also a significant scatter, with values ranging from 28 MPa to 55 MPa. It should be noticed that the material supply is constrained to the dam's location, especially for the aggregates. The rock used for the production of aggregates is often obtained from quarries near the dam. It is known that the stiffness and the overall quality of the aggregates determine the deformability and strength properties and are one of the main reasons for the concrete variability. The analysis of this comprehensive data allowed the establishment of statistical correlations between the properties of dam and wet-screened concretes. Despite the different materials used on each Portuguese dams, it was found that there is a relationship between the properties of the two types of concrete.

Concerning the case study, the Baixo Sabor dam, this chapter presents the properties

of each concrete component, the composition data, the testing conditions and the obtained test results.

A significant part of this chapter concerns the installation, testing and analysis of *in situ* experimental results regarding compressive creep tests. A detailed description of the creep cells set up and the improvements developed during this thesis are presented. The main improvements are the increase of the specimen sizes, especially for dam concrete testing, the use of low-stiffness moulds using EPS and the use of stiff platens adjacent to the flat-jack to guarantee an uniform stress in the specimen. These features allowed for a cost reduction, an easier installation procedure and consistent test results, when compared to the traditional creep cell solution used in the past.

The analysis of the delayed deformability results, obtained from laboratory testing and from creep cells, show a stiff concrete with low creep strain development. The results of *in situ* dam concrete modulus of elasticity at early ages (< 28 days) are considered very high, motivated by the elevated temperature inside the dam's core. The development of creep strain over time is fast at early ages and slows down for later ages (long-term low rate of creep strain). The creep cell setup included two types of wet-screened concrete, the traditional concrete sieved by the 38 mm opening sieve and an intermediate concrete sieved by the 76 mm opening sieve. It was concluded that wet-screened concretes have lower modulus of elasticity and the rate of development of the creep strains increases since the coarse aggregate content is smaller.

The results obtained from the quality control procedures during construction show large deviations for each mechanical property. This deviations are fairly common for this type of concrete and can be motivated by the large aggregates and the construction duration. The replacement of cement by fly ash in large volumes had a strong influence on the property development. Although most cement hydration takes place in the first 28 days, the strength development extends greatly beyond 90 days.

The test results presented in this chapter are the basis for the development of the remaining work. The analytical and numerical model parameters are calibrated considering the characteristics of Baixo Sabor dam concrete and its wet-screened concrete.

Analytical modelling of the dam concrete structural properties

4.1 Introduction

The use of analytical or semi-empirical models can be of great aid for the interpretation of the experimental results and for the identification of large deviations and possible outliers. Well established and calibrated models can be also used for the prediction of dam concrete properties reducing the sampling frequency of this type of concrete. The prediction of dam concrete properties is especially relevant due to the cast, transport and test difficulties of very large specimens. The main purpose of the work presented in this chapter is to predict the behaviour of dam concrete using the test results of its wet-screened concrete, considering an analytical approach.

This chapter presents two types of prediction models based on analytical expressions, one related to the deformability properties and another related to the strength properties. For the deformability properties, two-phase composite models are adapted to take wet-screening into account. The strength properties were predicted using an extension of the Abrams law. The analytical models were calibrated using the presented test results of Baixo Sabor dam (§ 3).

The proposed two-phase composite models is based on the hypothesis that dam concrete is a composite of wet-screened concrete and the aggregates removed during wet-screening.

Given the deformability properties of the wet-screened concrete and the sieve analysis of dam concrete it is possible to obtain a prediction of the modulus of elasticity and creep strain development of the dam concrete. The analysis of the *in situ* test results require the use of the maturity method for obtaining an equivalent property at constant temperature. It is known that higher temperatures increase the cement hydration rate and yield higher mechanical property values. In order to compare different conditions, the modulus of elasticity and the creep strain development measured in each creep cell were converted to a reference constant temperature, taking into account the thermal history of each specimen.

The prediction of dam concrete compressive and splitting tensile strength properties used the combination of two semi-empirical laws, the size effect law and an extension of the Abrams law. Since the different types of concrete placed in the dam (Core-DAM, Core-SCR, Face-DAM, Face-SCR and Reinforcement), were produced with the same materials, a relationship between the strength properties and the composition data was obtained, using the established Abrams law. The size effect law was applied to convert the strength properties using small specimen into strength properties using large specimens (comparable with the ones used for the characterization of dam concrete).

The proposed extended Abrams laws includes not only the water to cementitious materials ratio but also the maximum size of aggregate as an input parameter due to its significance in the behaviour of this type of concrete. Taking this parameter into account, a semi-empirical expression is proposed for the prediction of dam concrete strength properties based on the wet-screened test results.

Finally, in the end of this chapter, a framework for dam concrete quality assessment is proposed. The proposed framework includes the described analytical models in order to predict the deformability and strength properties of the dam concrete and to reduce the number of tested samples once the prediction models have been properly calibrated.

4.2 Prediction of dam concrete modulus of elasticity

4.2.1 Introductory note

The content of this sub-section was published in a scientific paper in the international Journal of Materials for Civil Engineering of ASCE with the title "Effect of wet-screening in the elastic properties of dam concrete. Experimental *in situ* test results and fit to composite models" (Serra *et al.* 2016b) (Appendix B).

4.2.2 Proposed methodology

This study refers to the prediction of dam concrete modulus of elasticity over time using a two-phase composite models and the wet-screened concrete results. The obtained results, with two screening apertures (76 mm and 38 mm), were used to investigate the development of the modulus of elasticity of dam concrete (full-mixed), for *in situ* conditions.

The methodology considers the binder as the wet-screened concrete and the removed aggregates larger than the sieved used for wet-screening as the inclusions. The hypothesis supporting the methodology is that, for elastic properties, the binder properties over time determine the development of the mechanical properties of the concrete and that the relationship between binder and the concrete elastic properties can be predicted using simple composite models (Granger and Bažant 1995; Baweja *et al.* 1998).

Figure 4.1 illustrates the relations between *in situ* conditions, types of concrete and the global approach used to relate the elastic behaviour, using the maturity method and composite models. The analysis relies on three main parts: calculation of the equivalent time, t_e , for the *in situ* test results considering the measured temperature on each creep cell in order to have a reference temperature state for the comparison of different conditions (applying the maturity method) ①; fit of the modulus of elasticity results to a logarithmic development law over time for the reference temperature state ②; and, use of two-phase composite models to estimate the modulus of elasticity of the dam concrete from the wet-screened concretes results ③.

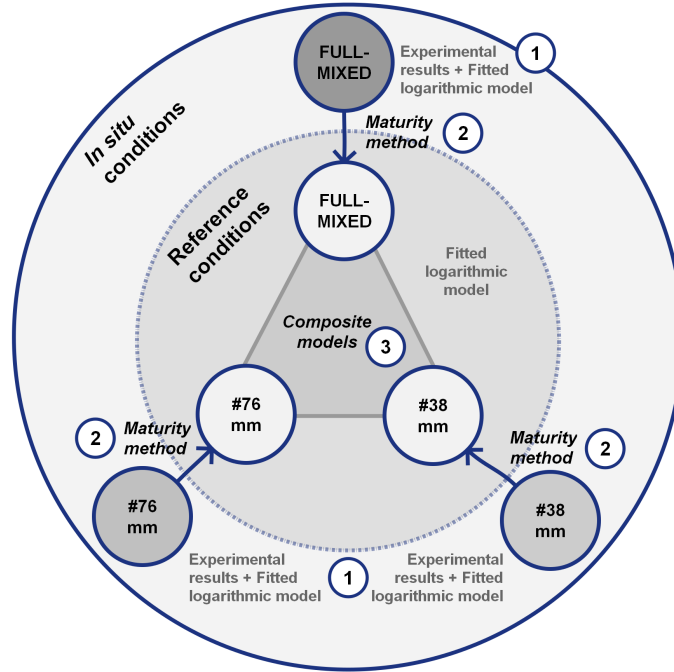


Figure 4.1: Global approach used for the prediction of dam concrete modulus of elasticity in compression

4.2.3 Maturity method application and fit to *in situ* test results

It is known from experimental studies that the properties of concrete are temperature dependent (Brooks *et al.* 2007). The development of a property at variable temperature is related to the rate of chemical reaction as a function of temperature and of reactant concentration, from which the Arrhenius law was derived. From the theoretical background for a single reaction, the Nurse-Saul maturity function to the Arrhenius temperature function (Carino and Lew 2001), the maturity method led to useful applications for the prediction of concrete behaviour under variable temperature.

Nowadays, the equivalent age method (or Arrhenius maturity) is the most commonly used function, which can be written as an equivalent age, t_e ,

$$t_e = \int_0^t e^{\left[-\frac{E_a}{R} \left(\frac{1}{273+T_{ref}} - \frac{1}{273+T_\tau} \right) \right]} d\tau \quad (4.1)$$

where T_{ref} is the reference temperature, T_τ is the measured temperature at time t , R is the gas constant ($8.31JK^{-1}mol^{-1}$) and E_a is called the apparent activation energy. When using this concept for the complex reactions of cementitious materials is important to point out that E_a reflects the minimum amount of kinetic energy needed to form products,

relates to an homogeneous reaction and its use implies an Arrhenius behaviour. Atkins and Paula (2006) calls E_a as "purely empirical quantity that enable us to discuss the variation of rate constants with temperature" and other authors reinforce this statement highlighting the complex behaviour involved in the hydration of calcium silicates (Zhang *et al.* 2008). The influence of maturing conditions on mechanical properties have been studied by several authors (Kim *et al.* 2002a; Kim *et al.* 2002b; Brooks *et al.* 2007).

For the cracking risk assessment it is necessary to define the real development of the mechanical properties of the concrete placed *in situ* coupled with the measured temperature variations (higher temperatures increases the hardening rate). *In situ* dam concrete temperatures can reach up to 50°C (Cervera *et al.* 2000a; Noorzaei *et al.* 2006), while in standard laboratory tests the concrete property characterization is done in constant conditions (usually at 20°C) (DIN 1991).

In Figure 4.2 the temperature history of the active dam concrete creep cell, CC1-150A, and the correspondent equivalent age are presented. This temperature profile illustrates the usual temperatures inside each lift, with higher temperatures in the first three days, followed by a decrease until, approximately, 30°C. The temperatures remain almost constant within a large period because the temperature exchanges to the environment are very slow. Due to the artificial cooling of the dam, this lift was submitted to a drastic temperature decrease to approximately 8°C. The influence of the temperature on the equivalent age can be perceived as an acceleration of time when temperatures are higher than the reference temperature, taken to be 20°C (Figure 4.2). Table 4.1 presents the calculated equivalent time of CC1 150-A, considering $E_a/R=5000^\circ\text{K}$ (Bažant and Baweja 2000).

For each creep cell and considering its equivalent age, t_e , calculated from the measured temperature, a logarithmic fit to the modulus of elasticity results was obtained, using linear regression analysis (Equation 4.2). The fit minimizes the square root of the sum of the deviations, e_j , between experimental results ($E_{c,i}^{exp}(t_{e,j})$) and the estimated values ($E_{c,i}^*(t_{e,j})$), using a weighted least square method (index i represents the type of concrete and index j refers to the age of concrete),

$$E_{c,i}^*(t_{e,j}) = a_i + b_i \log(t_{e,j}) \quad (4.2)$$

Table 4.1 presents the obtained modulus of elasticity results, the coefficients of the

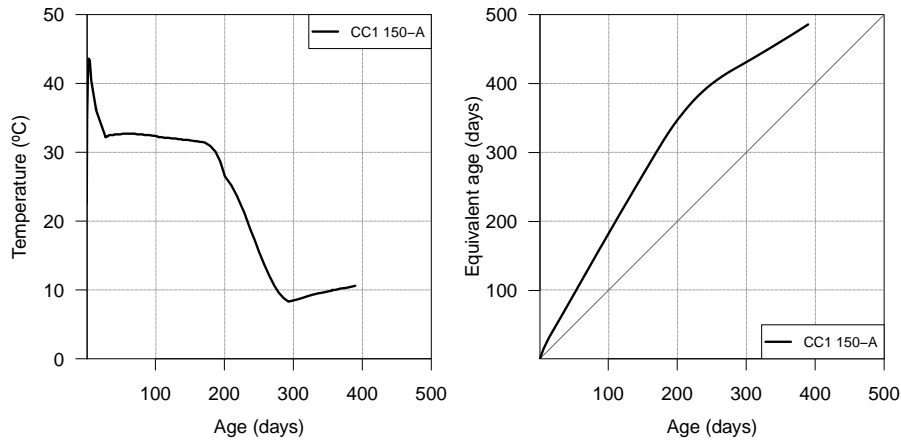


Figure 4.2: Measured temperature in CC1-150-A and the equivalent age calculated with the maturity method

logarithmic fit for each type of concrete, the estimated modulus of elasticity and the deviations to the experimental results, for the CC1 creep cell set. Table 4.1 shows that Equation 4.2 gives a good fit to experimental results in the first year of age, with a maximum absolute deviation of 4.4%. *In situ* results have larger modulus of elasticity than reference conditions, when the measured temperature is higher than the reference temperature.

Figure 4.3 shows the results and the logarithmic fit curves for the CC1 creep cell set, using the equivalent age (solid line in Figure 4.3). Considering the fitted parameters, a_i and b_i , the composite model was applied to the fit results at the reference temperature of 20°C (dashed lines in Figure 4.3).

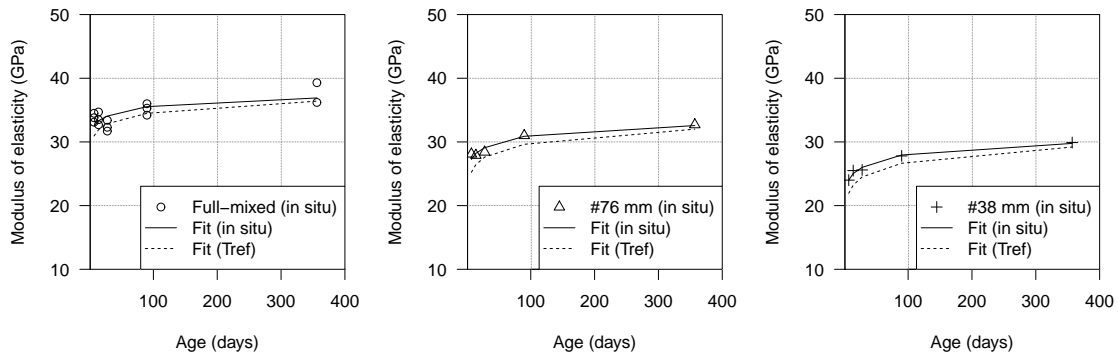


Figure 4.3: Logarithmic fit to modulus of elasticity test results obtained *in situ* and the estimate for reference conditions using maturity method (CC1)

Table 4.1: Logarithmic fit to CC1-A creep cell results

MSA (mm)	t' (days)	t_e (days)	E_c^{exp} (GPa)	a_i (GPa)	b_i (GPa/days)	$E_c^*(t_e)$ (GPa)	Deviation (%)
150	7.0	21.6	33.8	28.2	3.2	32.5	-4.0
	14.0	38.8	33.6			33.3	-0.9
	27.8	66.2	32.5			34.0	4.4
	89.9	191.2	35.2			35.5	0.8
	356.1	509.8	37.8			36.9	-2.4
76	7.0	22.7	28.1	21.9	1.7	27.3	-2.9
	14.0	39.3	27.9			28.2	1.1
	27.8	65.8	28.4			29.1	2.4
	89.8	186.4	31.0			30.9	-0.3
	357.0	496.3	32.7			32.6	-0.3
38	7.0	21.5	24.0	18.3	1.9	24.0	0.0
	14.0	37.6	25.5			25.0	-2.0
	28.0	63.3	25.6			26.0	1.5
	89.9	181.3	27.8			27.9	0.4
	357.0	485.6	29.9			29.7	-0.7

4.2.4 Composite models for the characterization of the elastic properties

Two-phase composite models are usually used to estimate the dam concrete properties when few information is available (Vilardell *et al.* 1998; Topçu 2005; ICOLD 2008). Concrete can be seen as coarse and fine aggregate particles embedded in a matrix of paste or as coarse aggregates embedded in a matrix of mortar. The models used in this study are the Counto model (Counto 1964), the spherical model (Hansen 1965), the Granger's model (Granger and Bažant 1995) and the Reuss model (Counto 1964).

Counto proposed a model considering the aggregate as a cylinder or prism embedded on mortar (Counto 1964), for which the composite modulus of elasticity is given by,

$$\frac{1}{E_c} = \frac{1 - \sqrt{V_{agg}}}{E_m} + \frac{1}{\left(\frac{1 - \sqrt{V_{agg}}}{\sqrt{V_{agg}}}\right) E_m + E_{agg}} \quad (4.3)$$

where E_c , E_m and E_{agg} are the modulus of elasticity of concrete, matrix and aggregate, respectively. V_m and V_{agg} are the fraction volume of matrix and aggregate, respectively.

Hashin derived the bulk modulus of elasticity, E_c , with a two-phase material, considered as spherical particles surrounded by matrix (Hansen 1965), taking the same Poisson's ratio for aggregate and matrix ($\nu = 0.2$),

$$E_c = \left[\frac{(1 - V_{agg}) E_m + (1 + V_{agg}) E_{agg}}{(1 + V_{agg}) E_m + (1 - V_{agg}) E_{agg}} \right] E_m \quad (4.4)$$

Granger and Bažant (Granger and Bažant 1995) considered a simple model taking the mortar phase both series and parallel,

$$\frac{1}{E_c} = \frac{1-\beta}{E_m} + \frac{\beta}{\alpha E_{agg} + (1-\alpha) E_m} \quad (4.5)$$

The physical meaning of the free parameter β is related to the amount of paste coupled in series. The product $\alpha\beta$ is taken as the volume of aggregate per unit volume of concrete, A_g .

When β is equal to 1.0, the Granger's model turns into the Voigt model ($E_c = V_m E_m + V_{agg} E_{agg}$) which can be related to the maximum amount of aggregate, $A_{g,max}$ and gives the upper bound of the modulus of elasticity value. When β is between zero and one, there is no perfect compaction of the coarse aggregates and the binding paste fills the remaining areas between aggregates (mortar portion in series with aggregates). On the other hand, when β is equal to 0.0, the Granger's model turns into the Reuss model ($E_c = \frac{1}{\frac{V_m}{E_m} + \frac{V_{agg}}{E_{agg}}}$) which gives the lower bound of the composite modulus of elasticity.

4.2.5 Prediction of the dam concrete modulus of elasticity based on experimental tests of wet-screened concrete

Following the proposed methodology, the maturity method and the two-phase composite models can be used to predict the modulus of elasticity of the dam concrete based on the wet-screened concrete test results. For that, one can consider the dam concrete as a composite of wet-screened concrete and the sieved coarse aggregate, instead of considering the binding mortar (as usually considered in composite models). Provided that the volume, $V_{equiv.binder}$, and modulus of elasticity, $E_{equiv.binder}$, of the wet-screened concrete (taken as the "equivalent binder") and the volume, V_{agg} , and modulus of elasticity, E_{agg} , of the sieved coarse aggregate (taken as the "inclusion") are known, a prediction of the modulus of elasticity, $E_{c,dam}$, of the dam concrete (full-mixed concrete) can be obtained, using the adequate composite model. In Tables 4.2 and 4.3 results for each type of composite model and for the two types of wet-screened concretes are presented.

Figure 4.4 shows the use of the two types of wet-screened concrete and the correspondence between the dam concrete and the composite model in each case (composite 1 and composite 2). Composite 1 is considered to be composed by elastic inclusions of aggregates with MSA larger than 76 mm and an equivalent binder of wet-screened concrete with MSA

4.2. PREDICTION OF DAM CONCRETE MODULUS OF ELASTICITY

smaller than 76 mm. Composite 2 is considered to be composed by elastic inclusions of aggregates with MSA larger than 38 mm and an equivalent binder of wet-screened concrete with MSA smaller than 38 mm. The composite models presented previously were used to evaluate its applicability to the proposed methodology.

Table 4.2: Composite data for the estimation of the modulus of elasticity of dam concrete (part 1)

MSA eq. binder (mm)	$V_{eq.binder}$	V_{agg}
76	0.86	0.14
38	0.72	0.28

Table 4.3: Composite data for the estimation of the modulus of elasticity of dam concrete (part 2)

MSA eq. binder (mm)	t' (days)	$E_{c,eq.bin.}^*$ (GPa)	$E_{c,dam}^{*,exp}$ (GPa)	$E_{c,dam}^{*,R.}$ (GPa)	$\omega^R.$	$E_{c,dam}^{*,C.}$ (GPa)	$\omega^C.$	$E_{c,dam}^{*,sph.}$ (GPa)	$\omega^{sph.}$	$E_{c,dam}^{*,G.}$ (GPa)	$\omega^G.$
76	7	24.5	28.8	25.5	0.48	26.4	0.36	26.0	0.42	27.0	0.30
	14	25.8	29.9	26.8		27.6		27.2			
	28	27.0	31.0	28.0		28.7		28.4			
	90	29.1	32.9	30.1		30.7		30.4			
	365	31.6	35.1	32.6		33.0		32.8			
38	7	23.3	28.8	26.9	0.35	28.3	0.17	27.9	0.22	29.6	0.10
	14	24.2	29.9	27.9		29.2		28.8			
	28	25.1	31.0	28.9		30.1		29.7			
	90	26.6	32.9	30.5		31.5		31.2			
	365	28.5	35.1	32.5		33.3		33.0			

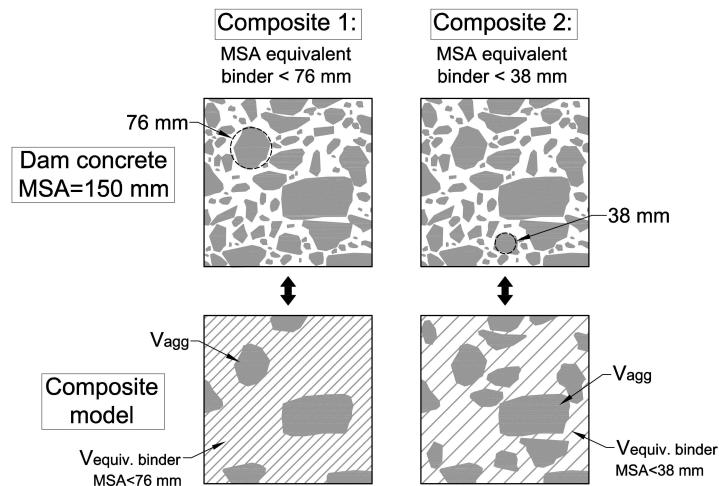


Figure 4.4: Adapted composite model for wet-screening procedure

The adopted composite models were the Reuss model (R.), the Counto model (C.), the spherical model (sph.) and the model proposed by Granger and Bažant (G.). The modulus

of elasticity of the granitic rock used for the production of the coarse aggregates was considered to be 46.3 GPa (Table 3.10). This average mechanical property was obtained from experimental tests for the characterization of the quarry from which the aggregates were extracted.

The best fit was considered the one with the lowest standardized deviation, ω , obtained from the difference between the fit to experimental results, E_c^* , and the prediction of the composite model, $E_c^{*,composite}$, at a given age, t_j ,

$$e_j^{model} = E_c^*(t_j) - E_c^{*,composite}(t_j) \quad (4.6)$$

$$\omega^{model} = \sum_{j=1}^N \frac{|e_j^{model}|}{E_c^*(t_j)} \quad (4.7)$$

Figures 4.5 and 4.6 show the fit of composite model prediction using the average test results from SCR38 (#76 mm) and SCR76 (#38 mm) wet-screened concretes, respectively. Table 4.4 present the coefficients of the logarithmic fit for each type of composite model.

The parameter β of Granger's model was determined to insure an adequate prediction by minimizing the difference between predicted values and dam concrete test results. This optimization led to a parameter $\beta=1.0$ and to a parallel composite model (Voigt model), which represents the upper bound for the predicted values (Hansen 1965). This can be physically interpreted as the optimum coarse aggregate packing according to Caquot's law and maximum aggregate compactness (for the aggregates larger than the sieved used) (Granger and Bažant 1995). This conclusion is compatible with the high values of the modulus of elasticity of the dam concrete.

The large amount of aggregate of the dam concrete associated with a good compaction leads to high values of modulus of elasticity in which several aggregates are assumed to be touching each other and creating an aggregate network surrounded by mortar where the forces are transmitted.

The use of a composite model considering the matrix as the SCR38 wet-screened concrete gave a better agreement with the experimental results of dam concrete with lower values of standard deviation, ω (Table 4.3 and Figure 4.6). This can be due to a better estimate of the volume fractions for the SCR38 wet-screened concrete (for the SCR76 concrete the volume fraction of aggregate considered in the analysis is relatively low which can lead to large deviations in the estimates).

4.2. PREDICTION OF DAM CONCRETE MODULUS OF ELASTICITY

It is shown that the Granger and Bažant's model, by considering the parameter β gives the best agreement to the experimental results. The inherent flexibility of this model makes it more suitable for different types of wet-screening (using different sieves), as the parameter β can be adjusted to give the best fit for each sieve aperture.

Table 4.4: Fitted parameters for the dam concrete modulus of elasticity prediction using the two types of adopted composite models

Composite	MSA equiv. binder (mm)	Model	$a_{dam}^{*,comp}$ (GPa)	$b_{dam}^{*,comp}$ (GPa/days)
1	76	Reuss (R.)	22.1	4.08
		Counto (C.)	23.2	3.83
		Spherical (sph.)	22.7	3.94
		Granger (G.) ($\beta = 1.0$)	23.9	3.63
2	38	Reuss (R.)	24.2	3.22
		Counto (C.)	25.9	2.87
		Spherical (sph.)	25.4	2.98
		Granger (G.) ($\beta = 1.0$)	27.5	2.48

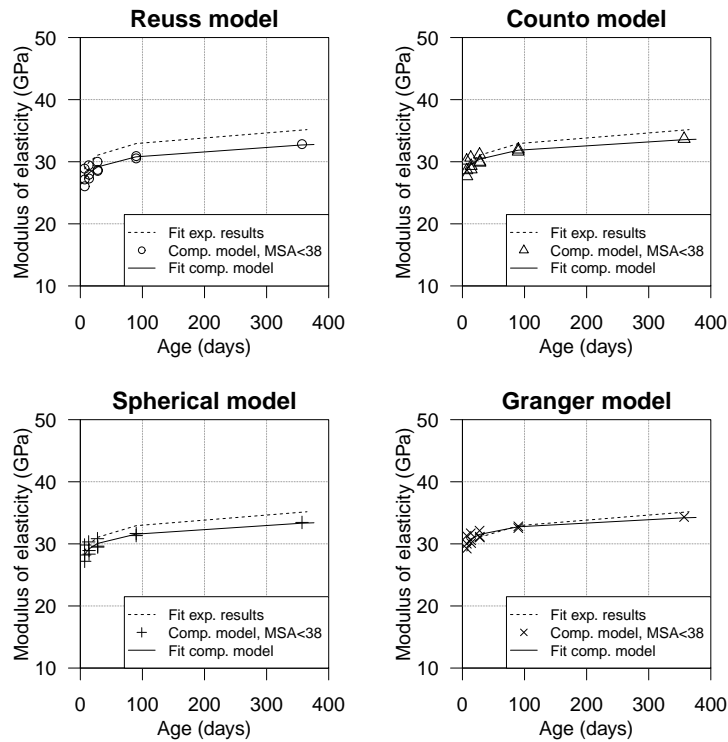


Figure 4.5: Prediction of dam concrete modulus of elasticity development using experimental results of SCR76 wet-screened concrete (composite 1)

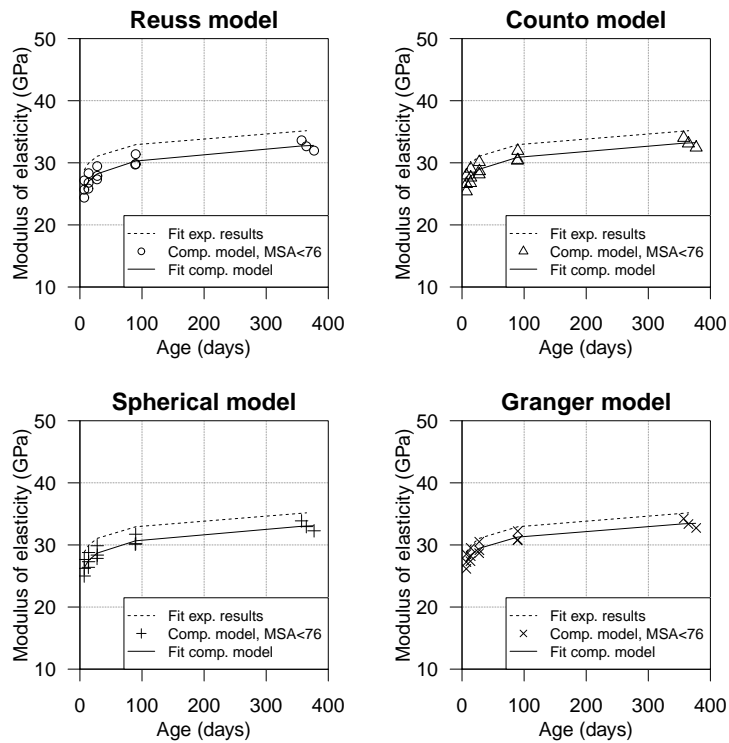


Figure 4.6: Prediction of dam concrete modulus of elasticity development using experimental results of SCR38 wet-screened concrete (composite 2)

4.3 Prediction of dam concrete creep in compression

4.3.1 Introductory note

The content of this sub-section was published in a scientific paper in the international journal *Materials and Structures* with the title "Dam and wet-screened concrete creep in compression: *in situ* experimental results and creep strains prediction using model B3 and composite models" (Serra *et al.* 2016a) (Appendix B). This paper was awarded with the *Materials and Structures: Outstanding Paper 2016 Award* (Appendix B).

4.3.2 Proposed methodology

The proposed methodology for the prediction of *in situ* dam concrete creep strains in compression is similar to the one described previously for the modulus of elasticity which used an adaptation of the usual two-phase composite model to represent the dam and the wet-screened concrete. The prediction of dam concrete creep strains is divided into three main stages: i) an experimental study for the evaluation of the compressive creep strains obtained *in situ* of the dam concrete and the two wet-screened concretes, SCR76

(#76) and SCR38 (#38) concretes); ii) the fit of the experimental results to model B3 considering the measured temperature for each type of concrete to obtain a reference temperature state; and, iii) the prediction of the dam concrete compressive creep strains based on the compressive creep strains of the wet-screened concrete using an equivalent two-phase composite model (Composite #76-Dam and Composite #38-Dam). Figure 4.7 presents the schematic view of the proposed procedure for the validation of the equivalent composite model for the prediction of dam concrete compressive creep strains.

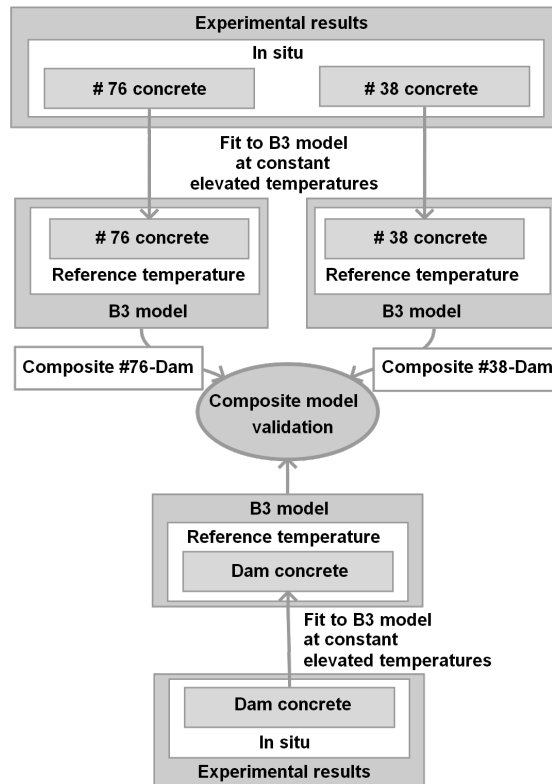


Figure 4.7: Procedure for the validation of the equivalent composite model for dam concrete compressive creep strains

The experimental programme was defined in order to measure the development of the *in situ* compressive creep strains of dam concrete and of two wet-screened concretes, the concrete with MSA=76 mm (SCR76 concrete) and the concrete with MSA=38 mm (SCR38 concrete). The SCR76 and SCR38 concretes or #76 and #38 concretes were obtained by removing the aggregates larger than 76 mm and 38 mm, respectively. The compressive creep strains were measured in creep cells (§ 3.7.3), concrete specimens embedded in the dam's core (§ 3.5).

The comparison between the different test conditions (such as the temperature variations) was achieved by fitting the test results to the model B3 at constant elevated temperatures considering the equivalent age method (§ 4.3.3). An optimization procedure considering the equivalent age method allowed for evaluation of the model parameters at reference temperature state, since the temperature variations are taken into account.

Following the work of Granger and Bažant (1995), a simple parallel and series two-phase composite model (§ 4.3.5) and its adaptation to aging materials considering the age-adjusted effective modulus method was used (§ 4.3.4).

The prediction of dam concrete delayed behaviour was obtained using an equivalent two-phase composite model which considers the wet-screened concrete, obtained from the dam concrete, as an equivalent aging viscoelastic matrix and the removed aggregates as the elastic inclusions. The input parameters are the volume fractions of equivalent matrix (wet-screened concrete) and the inclusions (removed aggregates) and the creep compliance of each wet-screened concrete. Since two type of wet-screened concretes were tested, two composite models were developed: Composite #76-Dam, using the test results of the concrete obtained from sieving the aggregates larger than 76 mm, and Composite #38-Dam, using the #38 mm wet-screened concrete test results. Each composite prediction was compared with the model B3 fit of the experimental results of dam concrete.

4.3.3 Prediction model for the concrete creep strains

Model B3, proposed by Bažant and Baweja (Bažant and Baweja 1995a; Bažant and Baweja 2000), describes the creep compliance as the sum of the asymptotic elastic strains due to unit stress, q_1 , the basic creep compliance, $C_0(t, t')$, and the drying creep compliance, $C_d(t, t_0, t')$ (Equation 4.8). Its strong points are related to the fact that the creep compliance rate, $\dot{C}_0(t, t')$, is derived according to the guidelines of RILEM TC 107 (1995), has been fitted from multi-decade laboratory tests (Bažant and Li 2008), is based on the micromechanics of aging considered in the solidification theory (Bažant and Prasannan 1989a; Bažant and Prasannan 1989b) and has been shown to have lower coefficients of variation of errors for dam concrete (Bažant and Baweja 2000).

$$J(t, t') = q_1 + C_0(t, t') + C_d(t, t', t_0) \quad (4.8)$$

For the dam body, due to the large thickness of the dam and the slow water diffusion

in concrete, only a small layer of the upstream and downstream (during construction) is subjected to cyclic drying and wetting (Bažant and Baweja 1995b) and the moisture exchange with the environment is small. For this reason, in this study, drying creep strains can be considered negligible (Bentur 2002; Schrefler *et al.* 2010). The basic creep compliance, $C_0(t, t')$, can be expressed as a linear combination of material parameters and time-dependent variables.

$$C_0(t, t') = q_2 Q(t, t') + q_3 \ln [1 + (t - t')^n] + q_4 \ln \left(\frac{t}{t'} \right) \quad (4.9)$$

where $Q(t, t')$ is a binomial integral with no analytical expression but can be approximated by Equations 4.10 to 4.13, with an error less than 1% for $n = 0.1$ and $m = 0.5$ for a large range of loading age and time under loading (Bažant and Baweja 1995a; Bažant and Baweja 2000).

$$Q(t, t') = Q_f(t') \left[1 + \left(\frac{Q_f(t')}{Z(t, t')} \right)^{r(t')} \right]^{-1/r(t')} \quad (4.10)$$

$$r(t') = 1.7 (t')^{0.12} + 8 \quad (4.11)$$

$$Z(t, t') = (t')^{-m} \ln [1 + (t - t')^n] \quad (4.12)$$

$$Q_f(t') = \left[0.086 (t')^{2/9} + 1.21 (t')^{4/9} \right]^{-1} \quad (4.13)$$

Considering a load duration, Δt , usually taken to be 0.01 days, the static modulus of elasticity yields from the creep compliance (Equation 6.27),

$$E(t') = \frac{1}{A_0 + \frac{A_1}{\sqrt{t'}}} \quad (4.14)$$

where $A_0 = q_1 + q_3 \ln(1 + \Delta t^n)$ and $A_1 = q_2 \ln(1 + \Delta t^n)$.

Each term of the sum has a physical meaning: q_1 is the asymptotic elastic part, q_2 refers to aging viscoelasticity, q_3 refers to non-aging viscoelasticity and q_4 refers to aging flow. Since it is a linear combination of time-dependent variables, the fit to experimental data is easier than other creep models. The replacement of cement by fly ash is known to

decrease the rate of property development (Popovics 1993; Kim *et al.* 2002a; Brooks *et al.* 2007) due to the late chemical reactions with the calcium silicates.

The temperature and moisture conditions have an important role in the development of the mechanical properties, especially on creep strains. The influence of temperature on the properties development is mainly ruled by the composition of the binder due to changes of cement hydration rate.

To model the effect of temperature variations in the hardening of concrete, several authors use the equivalent age method (or Arrhenius maturity) (Carino and Lew 2001) with equivalent or apparent activation energies, calibrated for tests at different temperatures, for different mechanical properties and different types of concrete (Carino and Tank 1992; Kim *et al.* 2002b; Han *et al.* 2003; Zhang *et al.* 2008). Particularly for the investigation of temperature effect on the creep of concrete, some experimental studies have been done (Browne and Blundell 1969; Bažant and Osman 1976; McDonald 1978; Vandewalle 2000).

According to this method the original compliance (Equation 4.9) yields a new expression (Equation 4.15) to take into account constant elevated temperatures, $T(t)$, in degrees Celsius (Bažant and Baweja 2000).

$$C_0(t, t', T) = R_T \left[q_2 Q(t_T, t'_e) + q_3 \ln \left[1 + (t_T - t'_e)^n \right] + q_4 \ln \left(\frac{t_T}{t'_e} \right) \right] \quad (4.15)$$

where t'_e and $t_T - t'_e$ are the equivalent age and the equivalent loading time both with the respective apparent activation energy, U_h , for the cement hydration reactions and U_c , for describing the acceleration of creep rate. U'_c refers to magnification of creep due to temperature increase, defined by the Equations 4.21 to 4.23.

$$t'_e = \int_0^{t'} \beta_T(\tau) d\tau \quad (4.16)$$

$$t_T - t'_e = \int_{t'}^t \beta'_T(\tau') d\tau' \quad (4.17)$$

$$\beta_T = \exp \left[\frac{U_h}{R} \left(\frac{1}{T_{ref} + 273} - \frac{1}{T + 273} \right) \right] \quad (4.18)$$

$$\beta'_T = \exp \left[\frac{U_c}{R} \left(\frac{1}{T_{ref} + 273} - \frac{1}{T + 273} \right) \right] \quad (4.19)$$

$$R_T = \exp \left[\frac{U'_c}{R} \left(\frac{1}{T_{ref} + 273} - \frac{1}{T + 273} \right) \right] \quad (4.20)$$

where T_{ref} is the reference temperature in degrees Celsius, T is the measured temperature in degrees Celsius and R is the gas constant ($8.31JK^{-1}mol^{-1}$) and, according to experimental fit to laboratory tests (Bažant and Baweja 2000), the apparent activation energies, U_h , U'_c and U_c , can be predicted by the following expressions:

$$\frac{U_h}{R} = 5000 \text{ } ^\circ K \quad (4.21)$$

$$\frac{U_c}{R} = 3418 \left[(w/c) (c) \right]^{-0.27} (f_{c,28})^{0.54} \quad (4.22)$$

$$\frac{U'_c}{R} = 0.18 \frac{U_c}{R} \quad (4.23)$$

where the w , c and $f_{c,28}$ are the water content, the cement content and the compressive strength at the age of 28 days. In order to take into account the temperature effect of a specific concrete composition on the creep development, the apparent activation energies can be adjusted to the obtained experimental results (Carino and Lew 2001; Zhang *et al.* 2008).

4.3.4 Age-adjusted effective modulus method

Generally, the delayed behaviour of concrete is described as a total strain, $\varepsilon(t, t')$, resultant of a stress, $\sigma(t')$, applied at the age of t' and kept constant until t , and an hygrothermal strain, $\varepsilon^0(t)$, such as drying shrinkage, thermal or chemical strains.

$$\varepsilon(t, t') = \varepsilon^i(t') + \varepsilon^c(t, t') + \varepsilon^0(t) \quad (4.24)$$

Considering that no cracking occurs, the stress-dependent strain can be expressed as the sum of an instantaneous strain, $\varepsilon^i(t')$ and of a creep strain, $\varepsilon^c(t, t')$. The instantaneous and creep strains can be expressed as a function of stress, obtaining the creep compliance, $J(t, t')$.

$$\varepsilon(t, t') = J(t, t')\sigma(t') = \varepsilon^i(t') + \varepsilon^c(t, t') \quad (4.25)$$

$$J(t, t') = \frac{1}{E(t')} + \frac{\varepsilon^c(t, t')}{\sigma(t')} \quad (4.26)$$

The stress, $\sigma(t, t')$, obtained from a given strain, $\varepsilon(t')$ is related to the relaxation function.

$$\sigma(t, t') = R(t, t')\varepsilon(t') \quad (4.27)$$

which can be approximated, as proposed by Bažant *et al.* (1979), by,

$$R(t, t') = \frac{0.992}{J(t, t')} - \frac{0.15}{J(t, t-1)} \left[\frac{J(t - \Delta t, t')}{J(t, t' + \Delta t)} - 1 \right], \quad \Delta t = \frac{t - t'}{2} \quad (4.28)$$

The age-adjusted effective modulus method, age-adjusted effective modulus (AAEM) method (Bažant 1972), based on the linear principle of superposition, is used for obtaining an approximate solution of the creep strains development by assuming that,

$$\begin{aligned} \varepsilon(t, t') - \varepsilon^0(t) &= \varepsilon_0 + \varepsilon_1 \phi(t, t'), \quad t > t' \\ \sigma(t') &= 0, \quad t < t' \end{aligned} \quad (4.29)$$

where ε_0 and ε_1 are given constants. The advantage of this method is that the creep analysis converts into an elastic analysis considering an incremental form,

$$\Delta\sigma(t) = E''(t, t') \left(\Delta\varepsilon(t, t') - \Delta\varepsilon''(t, t') \right) \quad (4.30)$$

in which,

$$\Delta\varepsilon(t, t') = \varepsilon(t) - \varepsilon(t'), \quad \Delta\sigma(t, t') = \sigma(t) - \sigma(t') \quad (4.31)$$

$$\Delta\varepsilon''(t, t') = \frac{\sigma(t')}{E(t')} \phi(t, t') + \varepsilon^0(t) - \varepsilon^0(t') \quad (4.32)$$

$$E''(t, t') = \frac{E(t')}{1 + \chi(t, t')\phi(t, t')} \quad (4.33)$$

$$\phi(t, t') = J(t, t')E(t') - 1 \quad (4.34)$$

$$\chi(t, t') = \left(1 - \frac{R(t, t')}{E(t')}\right)^{-1} - \frac{1}{\phi(t, t')} \quad (4.35)$$

where $\phi(t, t')$ and $\chi(t, t')$ are, respectively, the creep coefficient and the age coefficient and $E''(t, t')$ is the age-adjusted effective modulus.

This method was used by Granger and Bažant (1995) to introduce the aging viscoelasticity of concrete into a composite two-phase model (§ 4.3.5).

4.3.5 Composite model for the characterization of the long-term properties

The second part of the study concerns the use of composite models to predict the delayed behaviour of concrete with different coarse aggregate contents.

The heterogeneity of concrete can be studied using models where the meso-structure is taken into account. The first composite models applied to concrete concerned the elastic behaviour using approaches based on uniaxial rheological models (Hirsch 1962; Counto 1964; Hansen 1965) and on homogenization models, such as the variational approach considering spherical inclusions (Hashin-Shtrickman bounds) (Hashin 1963), the self-consistent model considering ellipsoidal inclusions (Hill 1965) and the Mori-Tanaka method (Benveniste 1987). The prediction of the aging viscoelastic behaviour of the materials using composite model was developed with the work of Counto (1964) and Popovics (1987) and later with Granger and Bažant (1995) and Baweja *et al.* (1998), based on the uniaxial rheological models, and, more recently using homogenization concepts, by Sanahuja (2013) and Lavergne *et al.* (2015).

The chosen model is the two-phase coupled series and parallel composite model, described by Granger and Bažant (Granger and Bažant 1995), which considers the mortar as the aging viscoelastic material and the coarse aggregates as the elastic inclusions. The model is based in a simple uniaxial rheological model which is strongly related to the physical behaviour of the material. The extension to triaxial behaviour was developed later by Baweja *et al.* (Baweja *et al.* 1998). It is considered that a part of the mortar is placed in series with the aggregates (related with parameter α) and another part is placed in parallel (related with parameter β) (Figure 4.8 b)). The series portion can be perceived

as the amount of mortar that separates the coarse aggregates avoiding their direct contact and the parallel portion corresponds to the remaining volume between the aggregates.

The composite model estimates the modulus of elasticity of the composite material based on the modulus of elasticity of the mortar, E_m , the modulus of elasticity of the aggregate, E_{agg} , its respective unit volume, V_{agg} and the proportion of mortar placed in series and in parallel defined by β (Equation 4.36).

$$\frac{1}{E_c} = \frac{1 - \beta}{E_m} + \frac{\beta}{\alpha E_{agg} + (1 - \alpha) E_m} \quad (4.36)$$

where $\alpha\beta = V_{agg}$.

The physical meaning of the free parameter β is related to the amount of paste coupled in series and the product $\alpha\beta$ is the volume of aggregate per unit volume of concrete, V_{agg} . When β is equal to 1.0 (Figure 4.8 a)), the model derives into Voigt model (purely parallel model (Counto 1964)) which can be related the maximum compactness, $V_{a,max}$. The maximum compactness of aggregate is related to the aggregate size distribution and corresponds to the volume of aggregate in the mix necessary to obtain the most compact packing (Larrard and Roy 1992). If the aggregates are in contact with each other, it is expected that the series portion is null and that the composite model turns into a parallel model ($\beta = 1$, Figure 4.8 b)). An example of this type of concrete is the prepacked or preplaced aggregate concrete in which the aggregates are first placed in the formworks and then the empty spaces are filled with a fluid mortar. In this case, the aggregates are in direct contact with each other and, since there is no compaction procedure, no mortar is coupled in series with the aggregates.

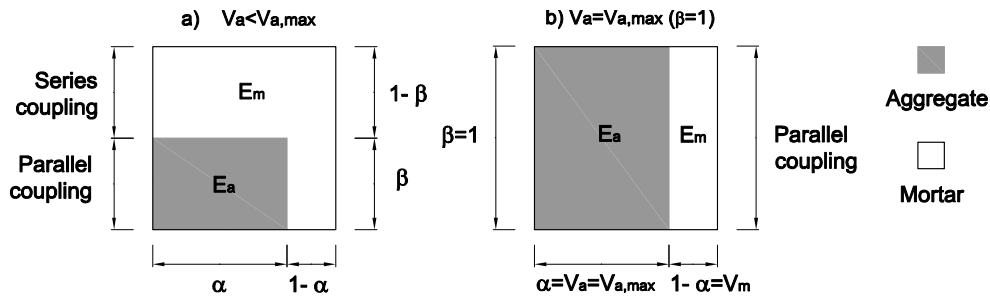


Figure 4.8: Schematic representation of the composite model: (a) volume of aggregate, V_a , lower than the maximum compactness of aggregate, $V_{a,max}$ considered as a model with a series and parallel portions; b) volume of aggregate, V_a , equal to the maximum compactness of aggregate, $V_{a,max}$ yielding a model with parallel coupling

The aging viscoelastic behaviour and the continuous stress transfer from the mortar to

the stiffer aggregates are modelled using the AAEM method (Bažant 1972) (Equations 4.29 to 4.35), described earlier in § 4.3.4, in which the stress-strain behaviour is related the coupled series and parallel two-phase composite model conditions.

The total strain, $\varepsilon(t, t')$, due to a stress, $\sigma(t')$, is obtained by the sum of the strain of mortar placed in series, $\varepsilon_m(t, t')$, and the strain of the parallel coupling of mortar and aggregates, $\varepsilon_{am}(t, t')$. Considering firstly the strain of the parallel coupling of the composite model, $\varepsilon_{am}(t, t')$, the stresses variations in both the mortar, $\Delta\sigma_m$, and the aggregates, $\Delta\sigma_a$, which yield the stress transfer from the mortar to the aggregates over time, can be obtained by

$$\Delta\sigma_a(t, t') = E_{agg}\Delta\varepsilon_{par}(t, t') \quad (4.37)$$

$$\Delta\sigma_m(t, t') = E''(t, t') \left[\Delta\varepsilon_m(t, t') - \frac{\sigma_m(t')}{E_m(t')} \phi(t, t') \right] \quad (4.38)$$

and the total stress in the mortar is ruled by the parallel model stress-strain relationships,

$$\alpha\Delta\sigma_a(t, t') + (1 - \alpha)\Delta\sigma_m = 0 \quad (4.39)$$

yielding,

$$\sigma_m(t') = \sigma(t') \frac{E_m(t')}{\alpha E_{agg} + (1 - \alpha) E_m(t')} \quad (4.40)$$

Considering an unit stress to obtain the concrete's creep compliance $J(t, t')$, it is possible to derive the expression for the proposed composite model, taking into account the creep compliance of the mortar placed in series, $J_m(t, t')$.

$$J(t, t') = \frac{\beta}{\alpha E_{agg} + (1 - \alpha) E_m(t')} \left[1 + (1 - \alpha) \frac{E_m''}{E_{am}''} \phi(t, t') \right] + (1 - \beta) J_m(t, t') \quad (4.41)$$

in which,

$$\phi_m(t, t') = E_m(t') J_m(t, t') - 1 \quad (4.42)$$

$$E_m''(t, t') = \frac{E_m(t') - R_m(t, t')}{\phi_m(t, t')} \quad (4.43)$$

$$E''_{am}(t, t') = \alpha E_a + (1 - \alpha) E''_m(t, t') \quad (4.44)$$

where $\phi_m(t, t')$ is the creep coefficient of the mortar, $E''_m(t, t')$ is the age-adjusted modulus of elasticity of the mortar and $E''_{am}(t, t')$ is the age-adjusted modulus of elasticity of the parallel portion of aggregate and mortar.

In conclusion, given the mortar's creep compliance, $J_m(t, t')$, the modulus of elasticity of the inclusions, E_a , the fraction volumes of each component, V_a and V_m , and the appropriate parameter β is possible to predict the creep compliance of the concrete, $J(t, t')$, using simple analytical expressions.

4.3.6 Prediction of dam concrete creep strains under compression based on experimental tests of wet-screened concrete

4.3.6.1 Fit of the creep test results to B3 model considering *in situ* and laboratory conditions

An optimization procedure based on genetic algorithm (GA) (Scrucca 2013) was applied to obtain the aging viscoelastic parameters q_1 , q_2 , q_3 and q_4 , following the methodology proposed by Wendner *et al.* (2015). The optimization procedure defined constraints for the fitting parameters (only positive values were allowed). The fit considered the data obtained in creep cells for the three available loading ages, 28, 90 and 365 days, simultaneously. Only the results equally spaced in logarithmic scale were considered in order to ensure a proper weight in the analysed loading time scale. Also, only the periods of time where the temperature was approximately constant were taken into account in the optimization procedure. The choice of the equally spaced values was based on expert judgement, starting with the first available measurement.

The obtained parameters minimize the sum of the square difference between the experimental results, $J_{exp}(t_{T,j}, t'_{e,i})$, and the theoretical creep compliance, $J_{B3}(t_j, t'_i, T_j, q_1, q_2, q_3, q_4)$ (Equation 4.45), considering the measured temperature in each creep cell according to the extension of the model B3 to constant elevated temperature (§4.3.3).

$$\min \left[\sum_{i=1}^m \sum_{j=1}^n \left(J_{exp}(t_{T,j}, t'_{e,i}) - J_{B3}(t_j, t'_i, T_j, q_1, q_2, q_3, q_4) \right)^2 \right] \quad (4.45)$$

where the n and m are the number of loading ages and the number of measured values

over the loading time, respectively, and T_j is the measured temperature.

The equivalent loading age, t'_e , and the equivalent loading time, $t_T - t'_e$, are calculated using the equivalent age method and the correspondent apparent activation energies, U_h/R , U_c/R and U'_c/R (§ 4.3.3). An accurate estimate for these apparent activation energies for this concrete is not possible to obtain using the limited experimental results. Some work have been done regarding the development of the strength of concrete with large fly ash content (Bamforth 1980; Sennour and Carrasquillo 1989; Han *et al.* 2003; Brooks *et al.* 2007; Trebuña *et al.* 2012) but an extensive evaluation of the effect on the apparent activation energies related to creep, U_h/R , U_c/R and U'_c/R , is still to be done.

The empirical values for U_h/R and U_c/R were calculated with the average composition data (Table 3.3) and the strength test results provided from quality control, during construction, for the #38 concrete: $w = w_{add} + w_{agg} = 172.2 \text{ kg/m}^3$ and $f_{c,90} = 25.2 \text{ MPa}$ (Table 4.5). At a loading age of 28 days, the compressive creep strains obtained *in situ* are, in average, 5% lower than compressive creep strains obtained in laboratory at 20°C (Figure 4.9, $t'=28$ days).

Table 4.5: Coefficients for the extension of model B3 to basic creep at constant elevated temperature

Type of concrete	w (kg/m^3)	t' (days)	$f_c(t')$ (MPa)	U_h/R (°K)	U_c/R (°K) (°K)	U'_c/R
Dam	120.1	90	24.7		5300.9	954.2
#76 (SCR76)	137.6	90	24.7*	5000	5109.8	919.8
#38 (SCR38)	162.0	90	25.2		4942.6	889.7

Note: The compressive strength of #76 concrete was considered to be the same as dam concrete

Tables 4.6 and 4.7 present the parameters and the obtained coefficient of determination, R^2 . The obtained determination coefficients show a good agreement between the model and the experimental results. The lower determination coefficients correspond to the optimization of the creep compliance for three loading ages (dam and #76 concretes).

Figure 4.9 shows the *in situ* (total results and the values used for the optimization process) and the laboratory results, the fit considering the *in situ* temperatures, $J_{\#38}(t_T, t'_e)$, and model B3 creep compliance for the reference temperature (20°C), using the fitted parameters q_1 , q_2 , q_3 and q_4 , $J_{\#38}(t, t')$.

Figures 4.10 and 4.11 show the results and fit obtained for the dam and #76 concretes, respectively, including the measured *in situ* creep strains (#76, *in situ*), the experimental

CHAPTER 4. ANALYTICAL MODELLING OF THE DAM CONCRETE STRUCTURAL PROPERTIES

Table 4.6: Equivalent age and equivalent loading time used in the analysis

Type of concrete	Creep Cell	t' (days)	$t - t'$ (days)	t'_e (days)	$t_T - t'_e$ (days)
Dam	CC1	27.5	159.1	65.6	182.8
	CC2	89.0	83.0	215.8	93.8
	CC3	364.4	33.0	505.2	29.1
#76 (SCR76)	CC1	27.8	152.0	66.6	185.8
	CC2	89.1	56.9	205.5	67.4
	CC3	364.6	33.0	502.2	27.2
#38 (SCR38)	CC1	27.79	152.0	64.1	169.8

Table 4.7: Parameters obtained by the optimization procedure

Creep	q_1 ($\times 10^{-6}/\text{MPa}$)	q_2 ($\times 10^{-6}/\text{MPa}$)	q_3 ($\times 10^{-6}/\text{MPa}$)	q_4 ($\times 10^{-6}/\text{MPa}$)	R^2
DAM	26.47	13.87	8.21	5.87	0.837
#76 (SCR76)	30.40	60.16	4.61	4.89	0.796
#38 (SCR38)	24.17	82.75	17.40	5.54	0.986

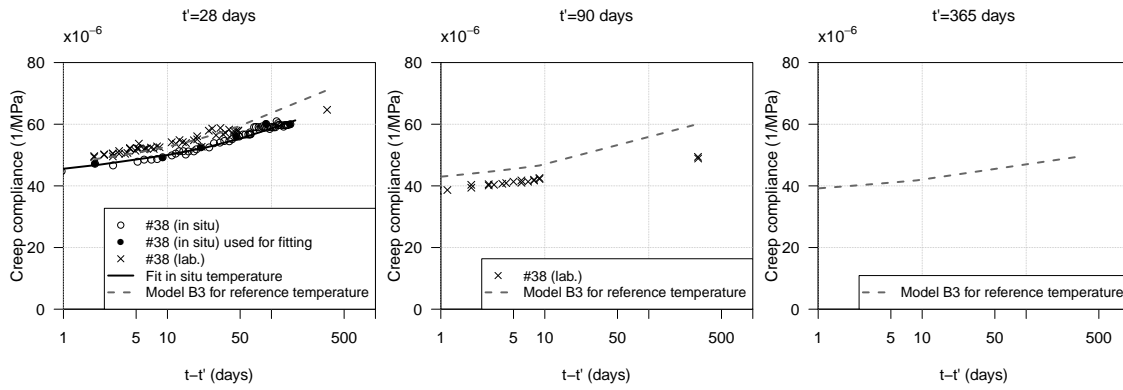


Figure 4.9: Compressive creep test results of #38 concrete at several ages and fit to model B3 for elevated constant temperature (*in situ* conditions) and constant reference temperature conditions

values used for obtaining the model B3 parameters (equally spaced in log-scale), the fitted creep compliance considering the measured temperatures, $J_{\#76}(t_T, t'_e)$ and $J_{Dam}(t_T, t'_e)$, and the fitted creep compliance for the reference temperature (20°C), $J_{\#76}(t, t')$ and $J_{Dam}(t, t')$. The differences between the *in situ* and laboratory conditions for these types of concretes are less significant, especially for the early loading times, $t - t'$.

The obtained creep strains for each concrete show a decrease of rate of development for later loading ages, due to aging, and for larger coarse aggregate contents. The aggregates restraint the development of the creep strains over time, due to a transfer of stress from the mortar to the aggregate skeleton.

4.3. PREDICTION OF DAM CONCRETE CREEP IN COMPRESSION

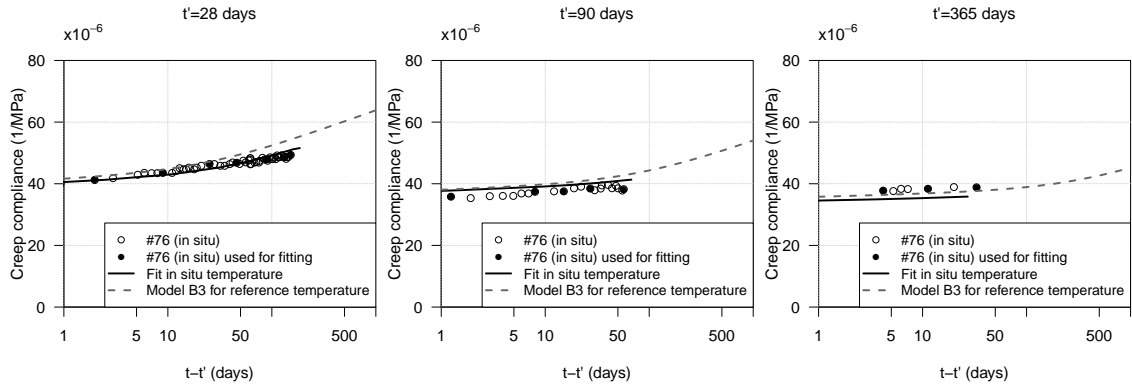


Figure 4.10: Compressive creep test results of #76 concrete at several ages and fit to model B3 for elevated constant temperature (*in situ* conditions) and constant reference temperature conditions

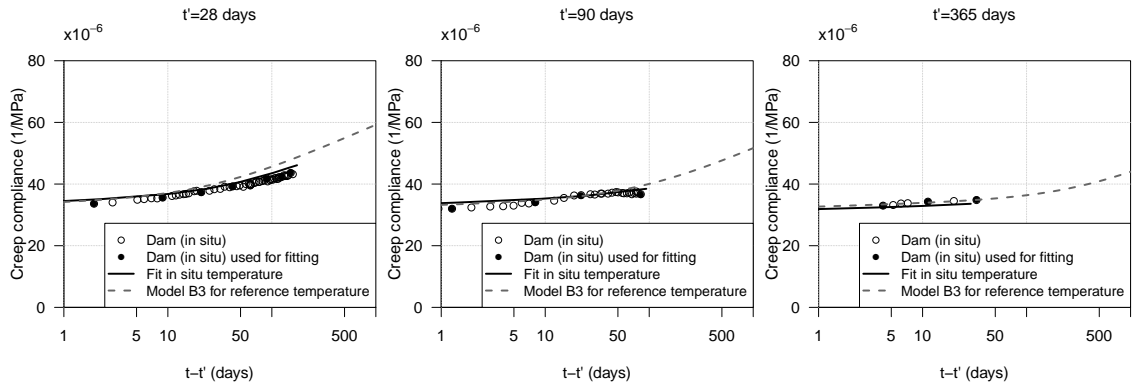


Figure 4.11: Compressive creep test results of dam concrete at several ages and fit to model B3 for elevated constant temperature (*in situ* conditions) and constant reference temperature conditions

4.3.6.2 Prediction of the dam concrete creep strains under compression using composite models

The proposed prediction of dam concrete creep under compression is based on the experimental results of wet-screened concrete measured *in situ*. The methodology relies, firstly, on the equivalence between *in situ* and laboratory results, described in § 4.3.6.1 to take into account the elevated constant temperature measured *in situ*. Secondly, it is proposed the use of the composite model theory (§ 4.3.5) to predict the effects of the changes on composition, in particular, the variations of coarse aggregate content.

Similarly to the methodology used in the previous section, the composite model described in § 4.3.5 was adapted to consider dam concrete a composite material in which the wet-screened concrete works as an equivalent matrix and the remaining aggregate as the inclusions. Two composite models, Composite #76-Dam and Composite #38-Dam,

were considered. The compressive creep test results of both types of wet-screened concrete, $J_{\#76}(t, t')$ and $J_{\#38}(t, t')$, its fraction volumes with respect to the volume of the dam concrete, $V_{\#76}$ and $V_{\#38}$, the modulus of elasticity of the removed aggregate, E_{agg} , and the fraction volumes of the removed aggregate, $V_{a>76 \text{ mm}}$ and $V_{a>38 \text{ mm}}$, were considered. An additional composite model, Composite #38-#76, was used to validate the application of the proposed methodology. Table 4.8 summarizes the properties used in the equivalent composite model analysis.

The wet-screening procedure implies a change in the matrix composition since some mortar is removed with the larger aggregates (Table 3.3 in § 3.3.3). This mortar is considered to be a very small portion of volume when compared with the equivalent matrix (considered, in this case, to be the wet-screened concrete).

Table 4.8: Properties used for the equivalent composite model analysis

Composite model	Creep compliance of equiv. matrix ($10^{-6}/\text{MPa}$)	E_{agg} (GPa)	$V_{eq.matrix=} = V_{wet-scr. concrete}$	$V_{a>MSA}$
#76-Dam	$J_{\#76}$ (Table 4.7)		0.86	0.14
#38-Dam		46.3	0.72	0.28
#38-#76	$J_{\#38}$ (Table 4.7)		0.84	0.16

Figure 4.12 shows a representation of the considered composite models (Composite #76-Dam, Composite #38-Dam and Composite #38-#76), and the involved different parameters ($\alpha_{\#76-Dam}$, $\beta_{\#76-Dam}$, $\alpha_{\#38-Dam}$, $\beta_{\#38-Dam}$, $\alpha_{\#38-\#76}$ and $\beta_{\#38-\#76}$). For the Composite #76-Dam the volume fraction of the wet-screened aggregates is lower than for the Composite #38-Dam (Table 4.8) and, therefore, the involved parameters can be different for each case.

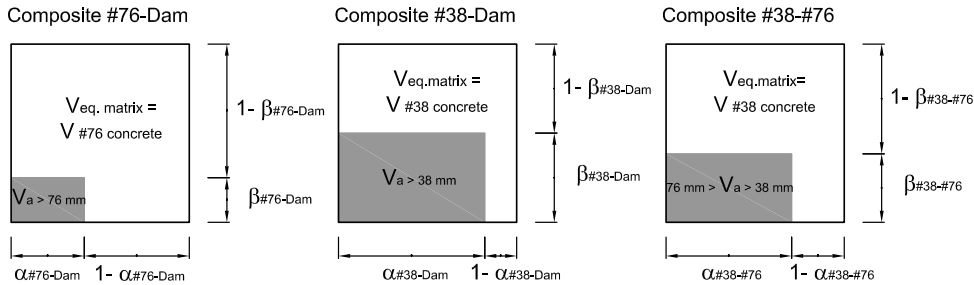


Figure 4.12: Adapted composite model for wet-screening procedure

Firstly, the procedure described in §4.3.6.1 leads to the creep compliance under compression at a reference constant temperature, $J_{Dam}(t, t')$, $J_{\#76}(t, t')$ and $J_{\#38}(t, t')$. Therefore,

the comparison of the results for each type of concrete, dam, #76 and #38 concretes, independently from the maturing conditions, was possible. Considering the composition data and the creep compliance under compression of both wet-screened concretes for reference temperatures, $J_{\#76}(t, t')$ and $J_{\#38}(t, t')$, the equivalent composite model was used to predict the compressive creep compliance of dam concrete, $J_{composite}^{\beta}(t, t')$ and compare it with $J_{Dam}(t, t')$.

The optimum β was obtained by calculating the percentage difference, $\% \Delta_{composite}^{\beta}$, between the composite prediction and the experimental result for the range of possible β , varying from 0.1 to 1.0. The percentage different, $\% \Delta_{composite}^{\beta}$, represents the average relative error of a prediction and was calculated using the range of available loading times for each composite model, n (Equation 4.46).

$$\% \Delta_{composite}^{\beta}(t') = \frac{\sum_{j=1}^n \frac{|J_{composite}^{\beta}(t_j, t') - J_{Dam}(t_j, t')|}{J_{Dam}(t_j, t')}}{n} \quad (4.46)$$

The influence of the composite model free parameters, $\beta_{\#76-Dam}$, $\beta_{\#38-Dam}$ and $\beta_{\#38-\#76}$ on the obtained predictions of dam concrete is presented in Figure 4.13 (Equation 4.46).

The percentage difference for the three loading ages, varies significantly with β . The β value with the lowest value of $\% \Delta_{composite}^{\beta}$ corresponds to the prediction model to be used. For the Composite #76-Dam and the Composite #38-#76, the value of β that gives the best fit for the three loading ages are, $\beta = 0.5$ and $\beta = 0.3$, respectively (Figure 4.14). The Composite #38-Dam has its lowest percentage difference for a $\beta = 0.6$. The existence of a minimum for almost every loading age and for the validation example (Composite #38-#76), shows the consistency of the proposed methodology and that the model is able to accurately predict the composite creep strains, for a given β .

Considering the average differences of the available loading ages, the results show a better agreement for a low value of β for the composite model using the #76 composite model and for a higher value of β for the #38 composite model (Figure 4.13). The higher the β , the least is the volume of matrix that is coupled in series with the aggregates. The Composite #76-Dam has, therefore, more equivalent matrix placed in series with the inclusions than the Composite #38-Dam due to the small amount of inclusions, $V_{a>76mm}$, and due to the fact that the larger aggregates ($MSA > 76 \text{ mm}$) are sparser in the wet-screened concrete matrix.

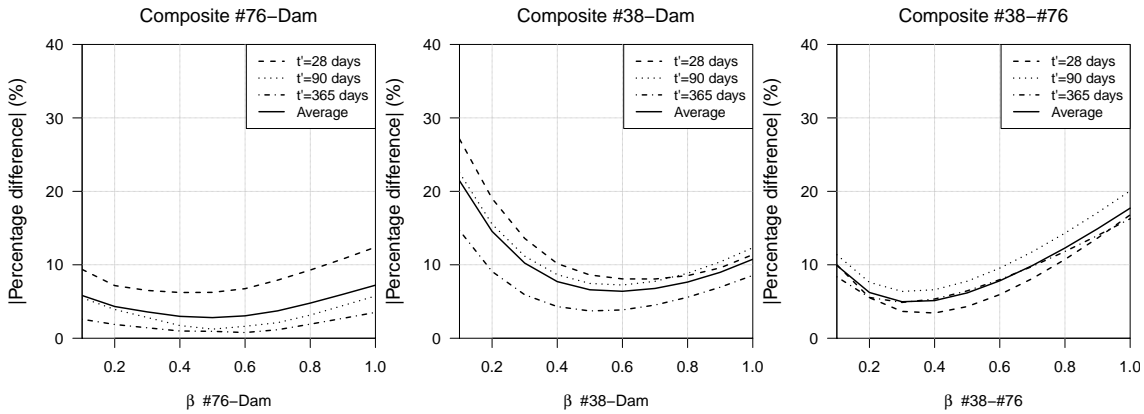


Figure 4.13: Percentage difference between the prediction using the equivalent composite and the experimental results for several values of β

Figures 4.14 and 4.15 show the development of the creep strains of the wet-screened concrete (grey solid lines) and the dam concrete (black dashed lines) and the dam concrete prediction using the respective composite model (black solid lines).

It can be concluded that the predictions of dam concrete creep strains are good, given the complexity of the phenomena and the limited test results. The higher deviations occur for the Composite #38-Dam at the loading age of 28 days and for the early ages after loading. These deviations can be due to limited compressive creep strain results and its implications on the optimization procedures to fit the model B3 parameters.

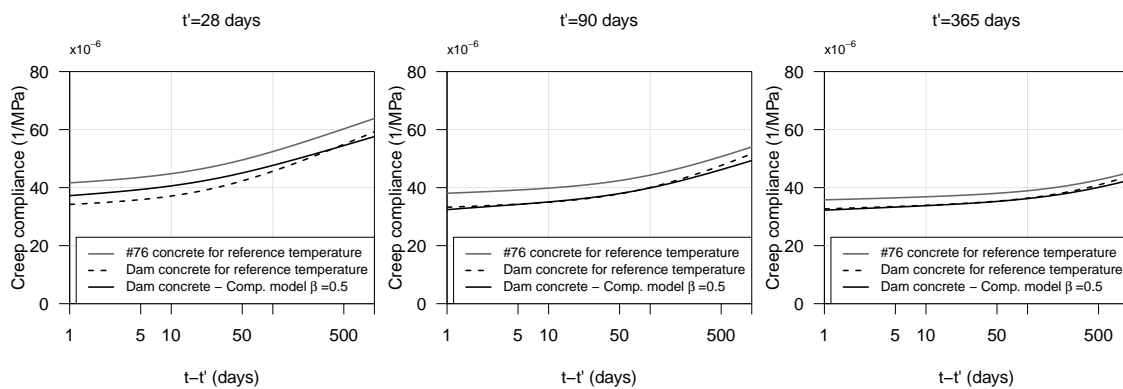


Figure 4.14: Prediction of full-mixed concrete creep compliance under compression using #76 mm equivalent composite model ($\beta = 0.5$)

The β values are related to the amount of equivalent matrix placed parallel in the composite model and can be related to the maximum amount of aggregate, $V_{a,max}$. The maximum amount of aggregate in the composite model is obtained for $\beta = 1.0$. According to the theoretical Caquot law, the maximum amount of aggregate can be given by,

4.3. PREDICTION OF DAM CONCRETE CREEP IN COMPRESSION

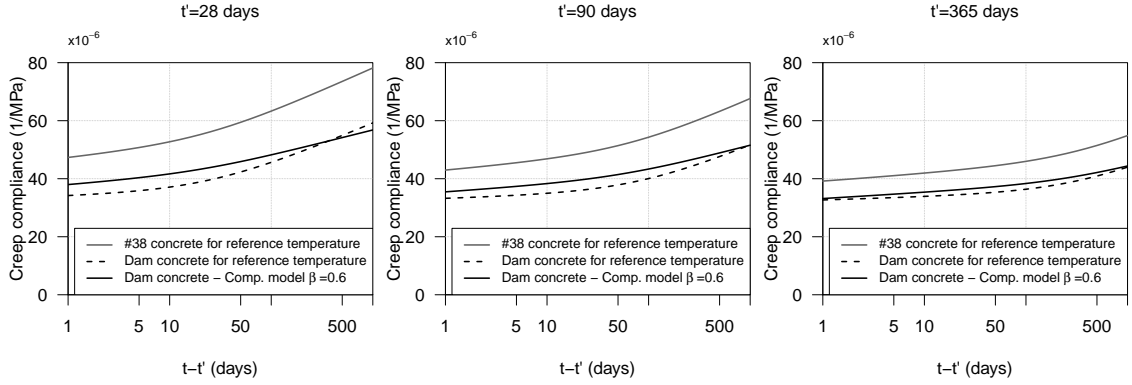


Figure 4.15: Prediction of full-mixed concrete creep compliance under compression using #38 mm equivalent composite model ($\beta = 0.6$)

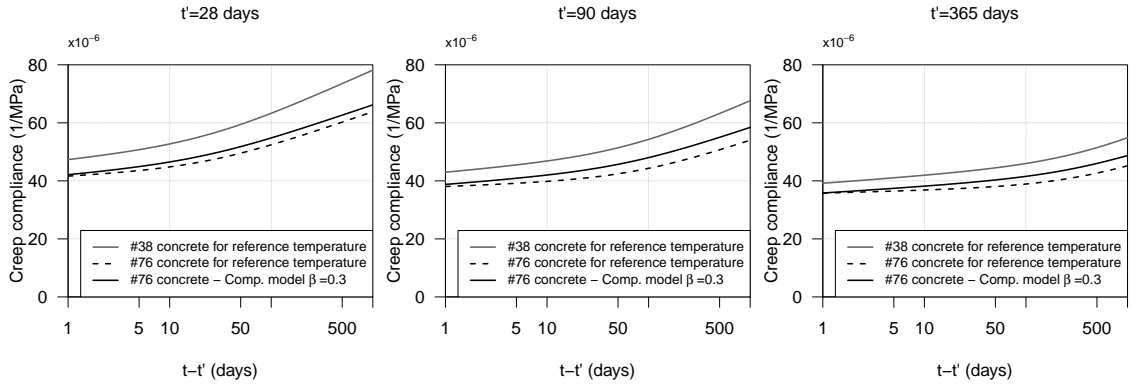


Figure 4.16: Prediction of #76 concrete creep compliance under compression using #38 mm equivalent composite model ($\beta = 0.3$)

$$V_{a,max} = 1 - 0.47 \left(\frac{d_{min}}{d_{max}} \right)^{\frac{1}{5}} \quad (4.47)$$

where d_{min} and d_{max} are the minimum and maximum size of the aggregates. This estimate can be used to compare the obtained β_{Caquot} coefficients for each composite, given the hypothesis of the equivalent composite model (Table 4.9).

Table 4.9: Comparison between estimate of β given by Caquot law and the by the fit to the experimental results

Composite model	d_{min} (mm)	d_{max} (mm)	$V_{a,max}$	$\beta_{Caquot} = V_a/V_{a,max}$	β_{fit}
#76-Dam	76	150	0.59	0.27	0.5
#38-Dam	38	150	0.64	0.44	0.6
#38-#76	38	76	0.59	0.27	0.3

Although the β estimates are lower than the ones obtained by the optimization of the percentage difference to the experimental results, the relationship between them are

consistent.

4.4 Prediction of dam concrete compressive and splitting tensile strength

4.4.1 Introductory note

The content of this sub-section was published in a scientific paper in the international Journal of Materials for Civil Engineering of ASCE with the title "Prediction of dam concrete compressive and splitting tensile strength based on wet-screened concrete test results" (Serra *et al.* 2017b) (Appendix B).

4.4.2 Proposed methodology

The proposed methodology aims the prediction of dam concrete compressive and splitting tensile strengths based on the test results of the wet-screened concrete and using structural concepts, such as the size effect law and an extension of the established Abrams law taking into account the influence of the maximum size of the aggregate. A practical expression is developed for the ratio between dam and wet-screened concrete strengths containing the influence size of the specimen and composition of the concrete.

Figure 4.17 illustrates the steps used to predict the compressive, f_c , and splitting tensile strength, $f_{t,spl}$, of DAM concrete based on the test results of SCR concrete.

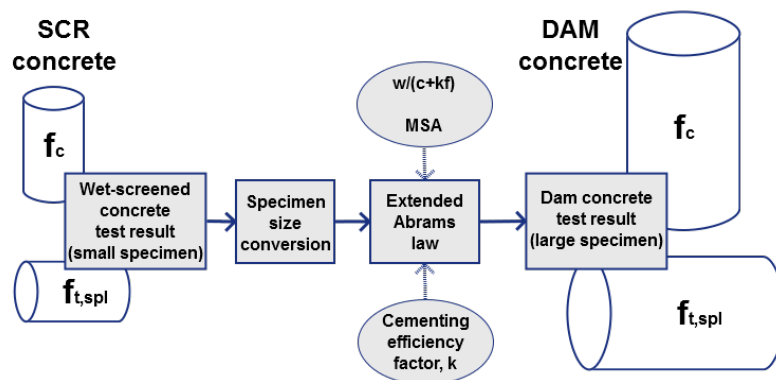


Figure 4.17: Schematic view of the proposed methodology for the prediction of the dam concrete strength properties

Since the strength of concrete is size dependent, a direct comparison between two types of concrete is only possible considering equal specimens. A size effect law is used

to convert the strength results of wet-screened concrete obtained in smaller specimens into compatible results in larger specimens. The obtained corrected strength results of wet-screened concrete can thus be compared with the results of dam concrete with larger aggregates. The application of the methodology is done with the established size effect laws (Kim *et al.* 1999; Kim *et al.* 1990) and with the mean strength results of dam and wet-screened of several types of concrete placed in Baixo Sabor dam (core, downstream and upstream face concretes and the concrete used in the reinforced areas).

Afterwards, an extension of the Abrams law, incorporating the maximum size of the aggregate (MSA), is proposed to predicted the strength of concrete based on the water to cementitious materials and the maximum size of the aggregates. The diversity of concretes produced during construction (§ 3.3.3) with the same materials allowed for the calibration of the extended Abrams law and for the development of the relationship between dam and wet-screened concrete strength results. The influence of the fly ash was taken into account using the cementing efficiency factor, k , in the water-cementitious material ratio ($w/(c + kf)$).

Furthermore, to validate the proposed methodology, a specific testing program was also carried out for the characterization of the mortar. The validation procedure consists in converting the test results of the mortar to equivalent large specimens values and then compared with the predicted extended Abrams law.

As a result of the proposed methodology, a practical expression for the ratio between dam concrete and wet-screened strengths as a function of the age of wet-screened concrete is obtained.

4.4.3 Conversion of specimen size based on size effect law

Based on the work of Bažant concerning the size effect on quasi-brittle materials (Bažant 1984), Kim *et al.* updated the proposed law introducing a size-independent strength (Kim *et al.* 1990; Kim 1990). Fitting that expression to several experimental data, Kim *et al.* obtained a generic function for compressive strength (Equation 4.48) in which the effect of the maximum aggregate size could be neglected (Kim *et al.* 1999),

$$f_{c,\Phi} = 0.8f_{c,\Phi_0} + \frac{0.4f_{c,\Phi_0}}{\sqrt{1 + \frac{(H-\Phi)}{50}}} \quad (4.48)$$

where $f_{c,\Phi}$ is the uniaxial compressive strength given in MPa obtained in a cylinder with

diameter Φ and height H , both given in mm, and f_{c,Φ_0} is the uniaxial compressive strength given in MPa obtained in a reference cylinder with diameter Φ_0 , given in mm.

Likewise, for the splitting tensile strength, Kim *et al.* (1990) developed a similar expression (Equation 4.49) fitted to specific test results .

$$f_{t,spl,\Phi} = \frac{59.76f_{t,spl,\Phi_0}}{\sqrt{1+86.6\Phi}} + 0.5f_{t,spl,\Phi_0} \quad (4.49)$$

Figure 4.18 presents Kim *et al.*'s size effect laws. The conversion from small specimens ($\Phi = 103 \text{ mm}$ for MORTAR and $\Phi = 150 \text{ mm}$ for wet-screened concrete) into larger specimens ($\Phi = 450 \text{ mm}$) is based on the relationship given by the former expressions. Both the compressive and splitting tensile strength decrease as the specimen size increases, which implies a reduction of the wet-screened concrete and mortar properties for larger specimens.

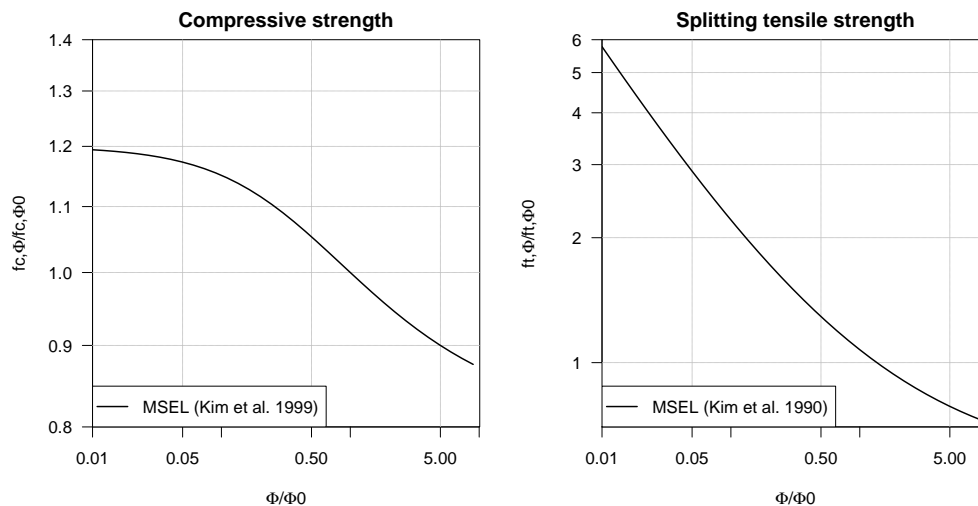


Figure 4.18: Size effect laws for the compressive and splitting tensile strengths

4.4.4 Abrams law for the prediction of concrete strength

Analytical models to predict the strength of concrete are often used to establish the water-cement ratio of a given concrete in order to achieve a required strength (ACI Committee 211.1-91 2002). The Abrams law is one of the most common expressions for this purpose but considers only the "quality" of the matrix while the "quantity" of the cement, cement paste or aggregate are not taken into account (Popovics and Ujhelyi 2008). The original Abrams law (Abrams 1918) relates the compressive strength with the water-cement ratio and can be described as a linear combination of this variable (Equation 4.50),

$$f_c = \frac{A}{B \frac{w}{c}} \Rightarrow \log f_c = \log A - \frac{w}{c} \log B = b_0 + b_1 \frac{w}{c} \quad (4.50)$$

where f_c is the concrete compressive strength, w/c is the water-cement ratio and A and B are parameters that depend on the type of strength, cement and aggregate type, admixtures, curing and testing conditions and the age of concrete.

Based on the original Abrams law, a more comprehensive expression is developed in order to take into account the specific characteristics of dam concrete, namely the large replacement of cement by fly ash and the large aggregate sizes.

4.4.4.1 Influence of the fly ash content in concrete

The fly ash cementing efficiency factor is used for proportioning fly ash concrete (Smith and Hammons 1993) and is obtained by considering that the relationship between water-cement ratio and strength of normal concretes is equivalent to the water-effective cementitious material ratio and strength relationship. The former hypothesis can be represented by the following expression,

$$\frac{w}{c_0} \equiv \frac{w}{c + kf} \quad (4.51)$$

where c_0 is the reference cement content for normal concretes, k is the overall cementing efficiency and f is the fly ash content.

Ganesh Babu and Siva Nageswara Rao (1996) proposed a general expression for the overall cementing efficiency, k , for the age of 90 days (Equation 4.52), based on the replacement ratios of fly ash. The study used concrete results from several other experimental works, considering a wide range of water-cementitious material ratios and of fly ash replacements. Although the results can be used for different types of fly ash, the size of the aggregate used was less than 20 mm, significantly lower than the sizes used in dam concrete.

$$k_{90} = 2.50p^2 - 3.59p + 1.73, \quad p = \frac{f}{c + f} \quad (4.52)$$

Since the replacement ratios in the present case study were equal to 0.5 for every type of concrete (dam and wet-screened, core, upstream and downstream and reinforcement concretes), the value of k_{90} for the studied concretes is 0.56.

4.4.4.2 Extended Abrams law for the study of effect of maximum size aggregate

This study proposes an extension of the original Abrams law for the prediction of dam concrete over time, based on the test results of wet-screened concrete. This extended Abrams law (Equation 4.53) considers the water-effective cementitious material ratio and the maximum size of aggregate (MSA) used in the concrete or mortar (Φ_{max}). Due to the lack of information, the overall cementing factor, described previously, will be used for both compressive and tensile strength predictions.

$$f_c = \frac{A}{B \left(\frac{w}{c+kf} + \alpha_d \log \frac{\Phi_{max}}{\Phi_{max}^0} \right)} \quad (4.53)$$

where f_c is the compressive strength, k is the efficiency factor of the fly ash, w is the water content, c is the cement content, f is the fly ash content, Φ_{max} is the maximum size of aggregate (MSA), Φ_{max}^0 is the reference maximum size of aggregate and A , B and α_d are parameters to be determined.

This type of expression allows the analysis of the strength as linear combination of the main parameters.

$$\log f_c = b_0 + b_1 \frac{w}{c+kf} + b_2 \log \frac{\Phi_{max}}{\Phi_{max}^0} \quad (4.54)$$

where $b_0 = \log A$, $b_1 = -\log B$ and $b_2 = \alpha_d b_1$.

Table 4.10 shows the concrete data and the test results of each type of concrete used for the fit of Equation 4.54, in which MSA is the maximum size of aggregate, $w/(c+f)$ is the water-cementitious material ratio, $w/(c+kf)$, is the water-effective cementitious material ratio, $f_{c,\Phi=450}$ is the compressive strength obtained from a cylinder with 450 mm of diameter and $f_{t,spl,\Phi=450}$ is the splitting tensile strength obtained from a cylinder with 450 mm of diameter.

Table 4.10: Baixo Sabor dam data for the fit to the extended Abrams law

Type of concrete	MSA (mm)	$\frac{w}{c+f}$	$\frac{w}{c+kf}$	$f_{c,\Phi=450}$ (MPa)			$f_{t,spl,\Phi=450}$ (MPa)		
				28 days	90 days	365 days	28 days	90 days	365 days
Core-DAM	152	0.56	0.72	-	24.7	32.1	-	2.19	2.8
Core-SCR	38	0.56	0.72	20.4	23.4	30.6	-	2.16	-
Face-DAM	76	0.55	0.71	-	26.3	36.9	-	2.21	-
Face-SCR	38	0.55	0.70	20.3	24.9	34.49	-	2.25	-
Reinf.-DAM	38	0.50	0.64	25.0	34.0	-	-	2.77	-
MORTAR	4.75	0.52	0.67	18.9	30.4	-	1.6	2.15	-

4.4. PREDICTION OF DAM CONCRETE COMPRESSIVE AND SPLITTING TENSILE STRENGTH

The fit of the proposed extended Abrams law to the available test results of different types of concretes is based on fact that they were produced with the same components and cast with the same conditions. The results related to the concretes (Core-SCR, Core-DAM, Face-SCR, Face-DAM and Reinf.-DAM) are used to find the parameters A , B and α_d by minimizing the square difference between Equation 4.53 and the compressive and splitting tensile test results obtained or estimated for the large specimen size, $\Phi = 450 \text{ mm}$. The obtained parameters are presented in Table 4.11, as well as the adjusted determination coefficients obtained by the linear regression. The R_{adj}^2 values close to the unit indicate a good fit and a statistical analysis shows that each parameter is meaningful to the prediction (p -values lower than 0.05). Other parameters, such as the cement content and the water content (Popovics 1982) were introduced into the extended Abrams law in addition to Φ_{max} but their contribution to the model was not statistically significant.

The MORTAR results are used for the validation of the proposed law since the mortar specimens were produced and cast, independently from the concretes but with the same type of components used in the concretes, after the dam construction.

Table 4.11: Parameters of the extended Abrams law

Reference	Parameter	f_c			$f_{t,spl}$
		28 days	90 days	365 days	90 days
	k_{90}	0.56			
This work (Baixo Sabor dam)	A (MPa)	-	705.3 ^(***)	19389.3 ^(.)	20.4 ^(*)
	B	-	102.2 ^(**)	6958.8 ^(.)	22.6 ^(*)
	α_d	-	-12.8×10^{-3} ^(**)	-7.7×10^{-3} ^(.)	10.2×10^{-3} ^(*)
	R_{adj}^2	-	0.99	0.84	0.89
	k_{90}	-			
(Blanks and McNamara 1935) ($w/c = 0.54$)	A (MPa)	62.1 ^(***)	58.1 ^(***)	60.0 ^(***)	-
	B	8.0 ^(***)	5.2 ^(***)	4.3 ^(***)	-
	α_d	28.0×10^{-3} ^(*)	46.6×10^{-3} ^(***)	63.7×10^{-3} ^(***)	-
	R_{adj}^2	0.81	0.79	0.79	-
	k_{90}	-			
(Higginson <i>et al.</i> 1962) (Series IV)	A (MPa)	61.7 ^(***)	66.1 ^(***)	83.6 ^(***)	-
	B	7.5 ^(***)	5.6 ^(***)	7.8 ^(***)	-
	α_d	42.5×10^{-3} ^(**)	25.6×10^{-3} ^(**)	42.1×10^{-3} ^(***)	-
	R_{adj}^2	0.96	0.95	0.96	-

Note: p -values (***) 0.001, (**) 0.01, (*) 0.05, (.) 0.1, () 1

Figures 4.19 and 4.20 show the fit of the proposed extended Abrams law to the concrete test results and the validation with the mortar test results, concerning the compressive strength and the splitting tensile strength, respectively.

The results show that the proposed extended Abrams law can describe the influence

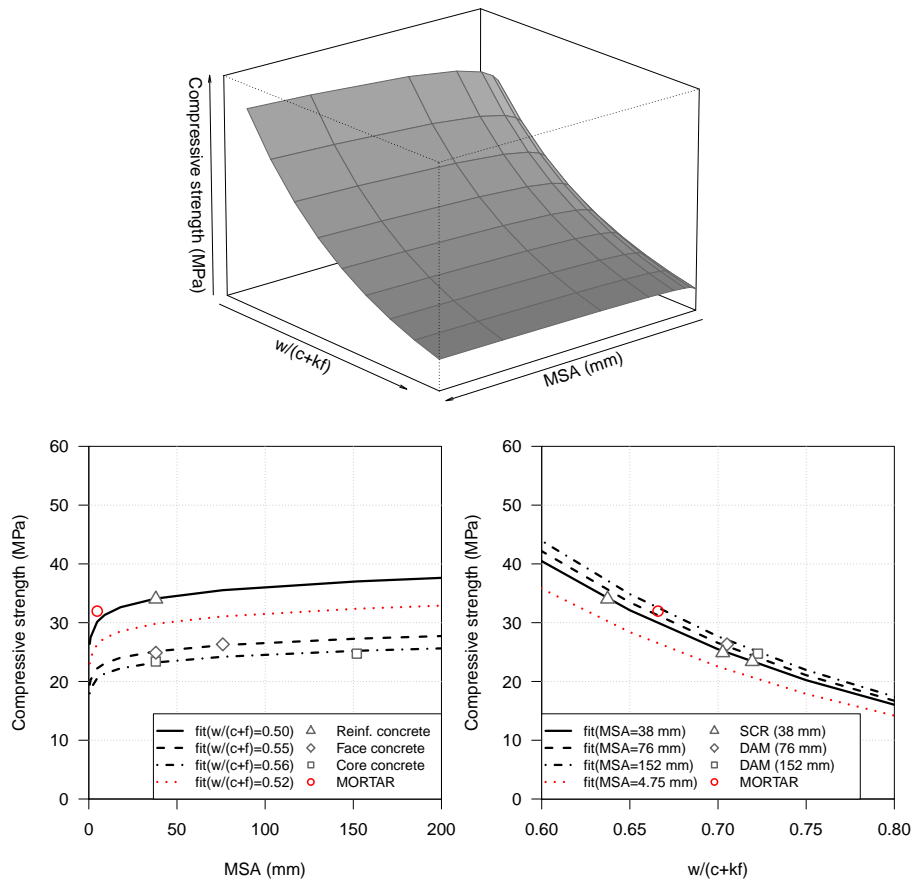


Figure 4.19: Extended Abrams law for the compressive strength at the age of 90 days of Baixo Sabor dam concrete

of the maximum size of aggregate (MSA) on the strength properties of concrete and that it has a role in the development of strength. Similar results were obtained by Akçaoğlu *et al.* (2004) but considering smaller aggregates, namely up to 32 mm and without fly ash replacement.

The experimental study of Higginson *et al.* (1962) shows that, for constant low cement contents the compressive strength increases as MSA increases. For this study and considering the concrete used in Baixo Sabor dam with low cementitious content, the strength increases as MSA increases for a given constant water to cementitious ratio. This behavior is explained by the fact that a low cement content and good quality aggregates yield failure paths through the mortar and around the aggregates and, as the aggregates get larger, the failure surface increases as well as the compressive strength (Zhou *et al.* 2010; Yang *et al.* 2016). This type of failure mode is also strongly related to the quality of the ITZ, which is lower for concretes with larger aggregates (Elsharief *et al.* 2003; Akçaoğlu *et al.* 2004).

4.4. PREDICTION OF DAM CONCRETE COMPRESSIVE AND SPLITTING TENSILE STRENGTH

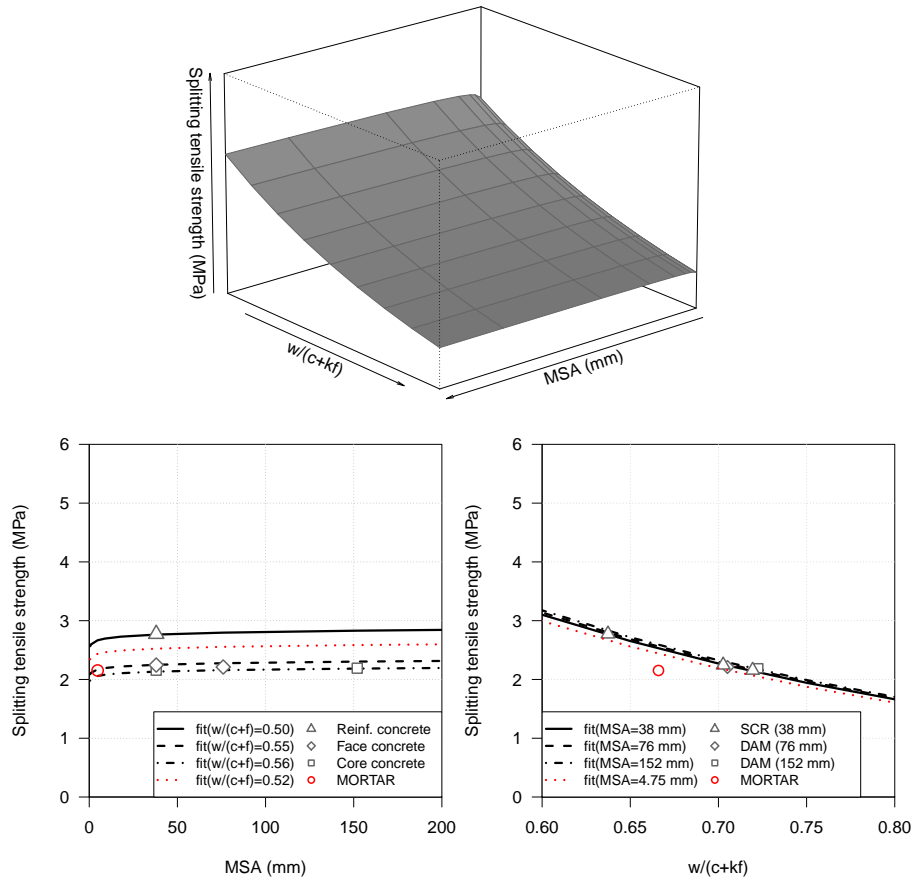


Figure 4.20: Extended Abrams law for the splitting tensile strength at the age of 90 days of Baixo Sabor dam concrete

The extended Abrams law for splitting tensile strength yields a small increase in strength as the MSA increases. Compared to the compression failure mode, the splitting failure is mainly due to the opening of a single crack, making the aggregate size less relevant to the final cracking pattern. Moreover, larger aggregates may introduce more imperfections which can explain the lower increase of tensile strength Yang *et al.* 2016.

4.4.5 Prediction of dam concrete strength based on wet-screened test results

Based on the proposed extended Abrams law, the ratio between dam and wet-screened concrete strengths for a given age and a given specimen size can be determined relying on the intrinsic properties of each type of concrete, namely the effective water-cementitious material ratio ($w/(c+kf)$) and the MSA (Φ_{max}).

Considering the conversion between specimen sizes, given by Kim's size effect law, and the proposed extended Abrams law for a given age, Equation 4.55 yields both effects for

the specific case of wet-screening dam concrete (from DAM concrete to SCR concrete). The effects are divided, respectively, into two different coefficients, k_{Φ} and k_{Abrams} . This expression, fitted to experimental results, allows for the prediction of the dam concrete strength obtained using a large specimen ($\Phi = 450$ mm) based on the strength of wet-screened concrete obtained using a smaller specimen ($\Phi = 150$ mm).

$$\frac{f_{\Phi = 450}^{DAM}}{f_{\Phi = 150}^{SCR}} = k_{\Phi} \times k_{Abrams} = k_T \quad (4.55)$$

$$k_{\Phi} = 0.8 + \frac{0.4}{\sqrt{1 + \frac{(H-\Phi)}{50}}} = 0.93 \quad (4.56)$$

$$k_{Abrams} = B \left\{ \left(\frac{w}{c+kf} \right)_{SCR} - \left(\frac{w}{c+kf} \right)_{DAM} + \alpha_d \log \left(\frac{\Phi_{max}}{\Phi_{max}^0} \right)_{SCR} - \alpha_d \log \left(\frac{\Phi_{max}}{\Phi_{max}^0} \right)_{DAM} \right\} \quad (4.57)$$

The application of the size effect law was only required for the Baixo Sabor dam and for Blanks and McNamara results since full-mixed and wet-screened concretes were tested using different specimen sizes. Higginson *et al.* results can be directly compared and only the extended Abrams law needs to be applied as same specimen size was used in the compressive strength tests. Table 4.12 and 4.13 presents the average experimental and predicted strength values and the effect of both size of the specimen, k_{Φ} , and of the composition, k_{Abrams} , in which SCR38, ϕ_{small} , SCR38, ϕ_{large} and DAM, ϕ_{large} refer to the test results of wet-screened concrete obtained using small specimens, test results of wet-screened concrete obtained using large specimens and test results of dam concrete obtained using large specimens. The comparison between the experimental and the predicted values show a maximum difference of 12% for the Higginson results at the age of 365 days.

Figure 4.21 shows the ratio between compressive and splitting tensile strengths of the full-mixed concrete obtained in large specimens and the compressive and splitting tensile strengths of the wet-screened concrete obtained in small specimens. The prediction ratios were plotted against the range of values available in the literature and presented in Table 2.1 in § 2.3.7. The large ratio range are mainly related to the diversity of concretes used in dams and to the difficulties associated to testing conditions. These results indicate that specific experimental programs are required in order to better understand the test results. It also reinforces the need to have physically-based predictive tools.

4.4. PREDICTION OF DAM CONCRETE COMPRESSIVE AND SPLITTING TENSILE STRENGTH

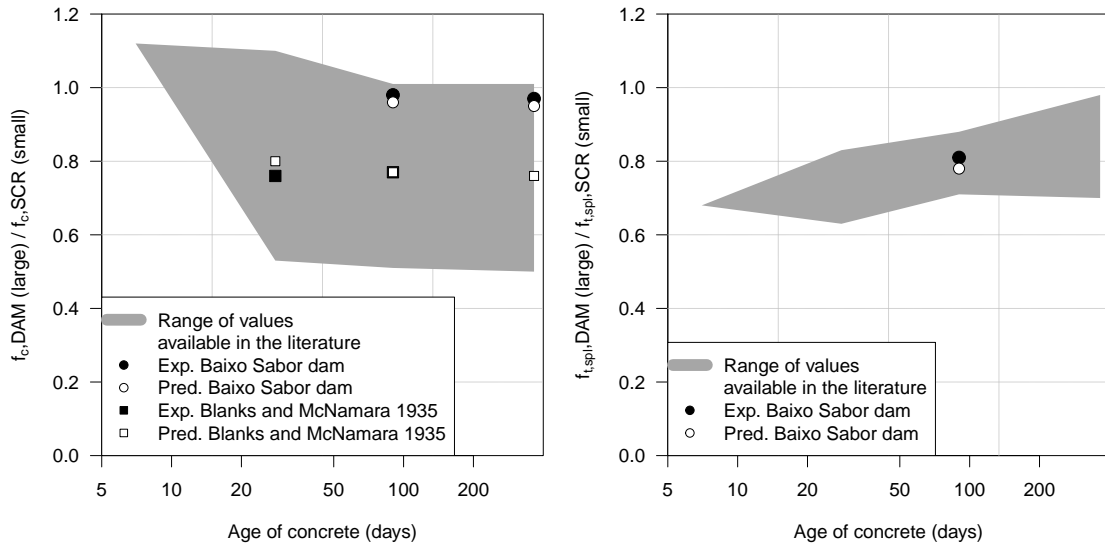


Figure 4.21: Ratios between full-mixed and wet-screened compressive and splitting tensile strength

Although the ratios are close to unit in the latter ages, the proposed relationship between dam and wet-screened concrete strength is able to capture the general trend described by the test results of USBR (1988) (Figure 2.18 in § 2.3.7). The ratio between the compressive test results of dam concrete, obtained from large specimens, and the compressive test results of wet-screened concrete, obtained from small specimens, decreases as the age of the concrete increases.

Table 4.12: Prediction of the dam concrete based on the proposed relationship and on the test results of wet-screened concrete (part 1)

Reference	Property	Age (days)	Experimental values		
			SCR38, ϕ_{small}	SCR38, ϕ_{large}	DAM, ϕ_{large}
This work Baixo Sabor dam	f_c	90	25.2	-	24.7
		365	33.1	-	32.1
(Blanks and McNamara 1935) ($w/c = 0.54$)	f_c	28	27.9	-	21.3
		90	33.2	-	25.4
		365	41.2	-	-
(Higginson <i>et al.</i> 1962) (Series IV)	f_c	28	-	27.7	24.8
		90	-	32.0	29.1
		365	-	40.7	32.8

Table 4.13: Prediction of the dam concrete based on the proposed relationship and on the test results of wet-screened concrete (part 2)

Reference	Property	Age (days)	k_{Φ}	k_{Abrams}	$\frac{f_{\Phi}^{DAM}}{f_{\Phi}^{SCR}} = k_T$	Predicted values DAM, Φ large	Difference (%)
This work Baixo Sabor	f_c	90	0.93	1.03	0.96	24.2	2.0
		365		1.02	0.95	31.4	2.2
dam	$f_{t,spl}$	90	0.80	0.97	0.78	2.1	4.5
(Blanks and McNamara 1935) ($w/c = 0.54$)	f_c	28	0.89	0.90	0.80	22.3	4.6
		90		0.87	0.77	25.6	0.8
		365		0.85	0.76	31.3	-
(Higginson <i>et al.</i> 1962) (Series IV)	f_c	28	-	0.87	0.91	25.2	1.6
		90		0.86	0.96	30.7	5.5
		365		0.89	0.91	37.0	12.8

4.5 Proposed framework for dam concrete quality control based on analytical models

Concrete quality control implies the conformity check of the mechanical properties of the concrete placed on site. Quality control procedures verify that the main mechanical properties of the placed concrete meet the minimum requirements or recommended limits defined by the designer. Strength values below a given limit and deformability results that fall out of a given range are labelled as non-conform, the test results should be rejected and special measurements should be taken into account in order to identify and correct the reason for the deviation. The limits are obtained from trial testing prior to the construction when the material components and the concrete design are already established. An accepted test result will be included into the database and used for the definition of more accurate acceptance limits (ICOLD 2008).

Since the costs of testing dam concrete are high, its sampling frequency is limited. Thus, the wet-screened concrete, used as a reference for the quality control assessments, is tested with a much higher sampling frequency. It is common practice to evaluate the statistical correlation between the two types of concrete by testing two sets from the same batch. The statistical correlation is currently used for the conversion of wet-screened concrete test results into dam concrete test results. A simple statistical correlation encloses different physical effects which can be taken into account for the analysis of each concrete test result and, ultimately, aid the identification and correction of deviations of the prescribed structural properties.

Taking into account the presented analytical tools used for the prediction of dam concrete and based on the experimental results of wet-screened concrete, a new framework

4.5. PROPOSED FRAMEWORK FOR DAM CONCRETE QUALITY CONTROL BASED ON ANALYTICAL MODELS

for dam concrete quality control is proposed. The motivation is the establishment of physically-based relationships between the two types of concrete. The effect of the size of the structural elements and the environmental conditions should also be taken into account in order to evaluate the real *in situ* structural properties.

The goal is to obtain an accurate estimate of the main mechanical properties of the placed dam structural concrete, by means of testing the actual dam concrete (DAM) using large specimens ($\Phi_{spec}=450$ mm) or testing the wet-screened concrete (SCR) using conventional size specimens ($\Phi_{spec}=150$ mm) and converting these results into the equivalent dam concrete results. The main mechanical properties are the uniaxial compressive strength, f_c , the splitting tensile strength, f_t , the modulus of elasticity under compression, E_c , and the creep compliance under compression, J_c .

The framework relates to determination of the mechanical properties through laboratory testing and the conformity check based on:

- Dam concrete test results - The main mechanical properties are evaluated using large specimens ($E_{c,450}^{DAM}$, $J_{c,450}^{DAM}$, $f_{c,450}^{DAM}$, $f_{t,450}^{DAM}$) and can be directly checked using the usual conformity criteria;
- Wet-screened concrete test results - The main mechanical properties, evaluated using small specimens ($E_{c,150}^{SCR}$, $J_{c,150}^{SCR}$, $f_{c,150}^{SCR}$ and $f_{t,150}^{SCR}$), have to be converted into its equivalent dam concrete test result in order to be compared with the designer's requirements.

Figure 4.22 illustrates the general procedure of the proposed quality control framework, including the use of dam concrete results and wet-screened concrete results. The approach relies on two separate conversion procedures, one for the deformability properties and other for the strength properties, which are based on the analytical models developed in this chapter.

The first type of conversion procedure predicts the modulus of elasticity, $E_c(t)$, and the creep compliance, $J_c(t)$, of dam concrete based on the wet-screened test results (usually determined at 20°C, using small specimens, $\Phi_{spec} = 150$ mm, and screened by the 38 mm aperture sieve), on the composition of each concrete (mainly its relative proportions, V_{SCR} and V_{DAM}), on the modulus of elasticity of the aggregates and on the use of the proposed composite model (Figure 4.23). The use of the composite models require the calibration of the parameter that defines the parallel and series proportion, β^{MSA} , and determination

of the proportions of wet-screened concrete, V^{SCR} , and sieved aggregates, V^{AGG} . As described in Figure 4.24, the composite model parameter, β^{MSA} , can be evaluated from equal specimens maintained at a reference temperature but cast with different types of wet-screened concretes (SCR19 screened using 19 mm aperture sieve, MSA=19 mm, SCR38 screened using 38 mm aperture sieve, MSA=38 mm, and SCR76 screened using 76 mm aperture sieve, MSA=76 mm) and with the dam concrete (MSA=150 mm). The second type of conversion concerns the wet-screened concrete strength properties measured in small specimens, $f_{c,150}^{SCR}$ and $f_{t,150}^{SCR}$. The prediction of dam concrete strength properties measured in large specimens, $f_{c,450}^{DAM}$ and $f_{t,450}^{DAM}$, requires the calibration of the size effect parameters (K_1 and K_2) and extended Abrams law parameters (A , B and α_d) and the determination of the water to cementitious materials of each type of concrete (w/c^{SCR} and w/c^{DAM}). Figure 4.25 presents the main effects and parameters for the strength conversion.

The extended Abrams law parameters should be determined using controlled strength tests in which equal size specimens are cast with different wet-screened concretes (SCR19 screened using 19 mm aperture sieve, MSA=19 mm, SCR38 screened using 38 mm aperture sieve, MSA=38 mm, and SCR76 screened using 76 mm aperture sieve, MSA=76 mm) and with the dam concrete (MSA=150 mm), as illustrated in Figure 4.24. The size effect should also be accounted for through specific experimental testing, varying only the size of the specimen ($\Phi=120$ mm, $\Phi=150$ mm, $\Phi=450$ mm). Figure 4.26 shows a proposal for the number and size of specimens for the calibration of the size effect law. If supplementary cementitious materials are being used in the mix, the overall cementing efficiency should also be determined for different replacement ratios (10%, 30%, 50% and 70%) and loading ages (k_7 , k_{28} , k_{90} and k_{365}) through specific testing (Ganesh Babu and Siva Nageswara Rao 1996).

After the conversion procedure, the predicted properties are compared with past dam concrete test results and checked for conformity, in order to be accepted or rejected. Similarly to the direct dam concrete test results, a rejected value should trigger corrective measures in design and/or in the production procedures. In order to assess the real structural properties, the on site effect should be considered, namely: the size effect; the temperature history effect; and the tridimensional stress state effect inside the dam's core (Figure 4.22). This structural size effect relates to the conversion from the specimen size to the structural element.

4.5. PROPOSED FRAMEWORK FOR DAM CONCRETE QUALITY CONTROL BASED ON ANALYTICAL MODELS

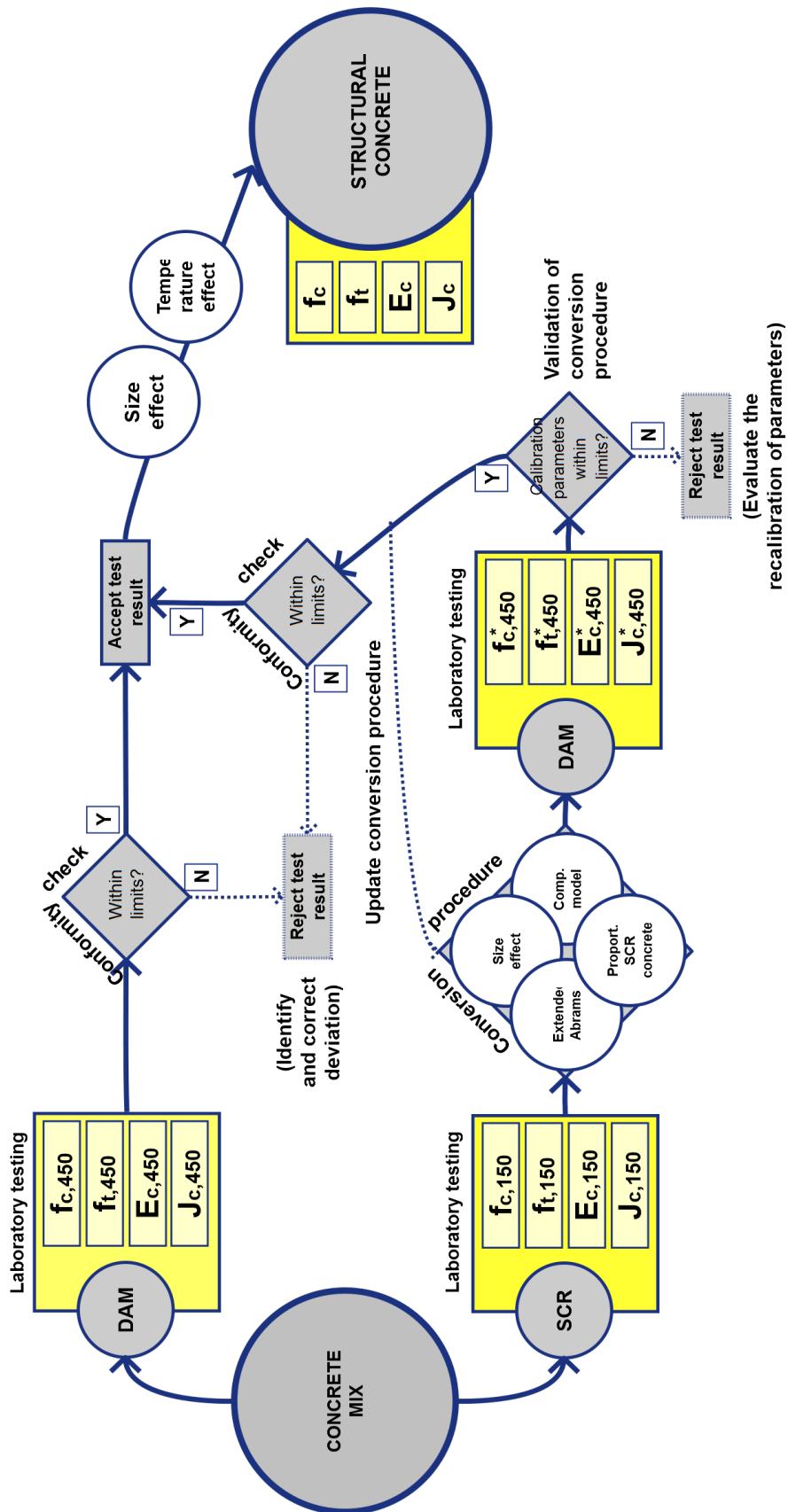


Figure 4.22: Proposed procedure for dam concrete quality control concerning the comparison between dam and wet-screened results

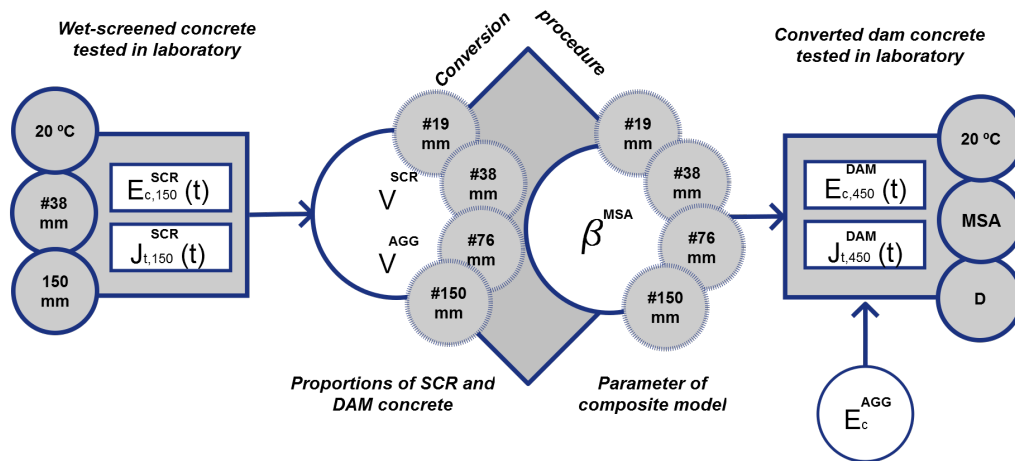


Figure 4.23: Illustration of the conversion procedure for the deformability properties including the determination of the proportions of wet-screened (SCR) and full-mixed (DAM) concretes and of the composite model parameters

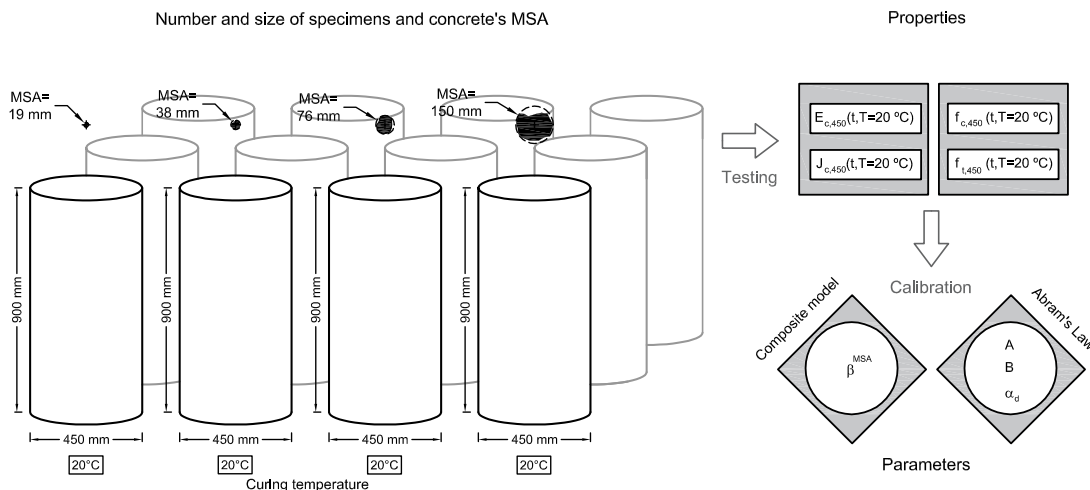


Figure 4.24: Number and size of specimens for the calibration of the composite model parameter, β^{MSA} and of the extended Abrams law's parameters, A, B and α_d

Early cracking of large concrete placements is the main concern during construction and determines the overall durability over time. The prediction of the actual mechanical properties at a given time, based on its temperature history is very important for the safety and durability assessment of each lift. The effect of temperature history can be taken into account using the maturity method and the adequate apparent activation energies, E_a/R , U_h/R , U_c/R and U'_c/R . In order to determine the apparent activation energies of the tested concrete, several specimens should be tested at different curing temperatures (10°C, 20°C, 30°C and 40°C), similarly to the procedure described in (Carino and Lew 2001).

4.5. PROPOSED FRAMEWORK FOR DAM CONCRETE QUALITY CONTROL BASED ON ANALYTICAL MODELS

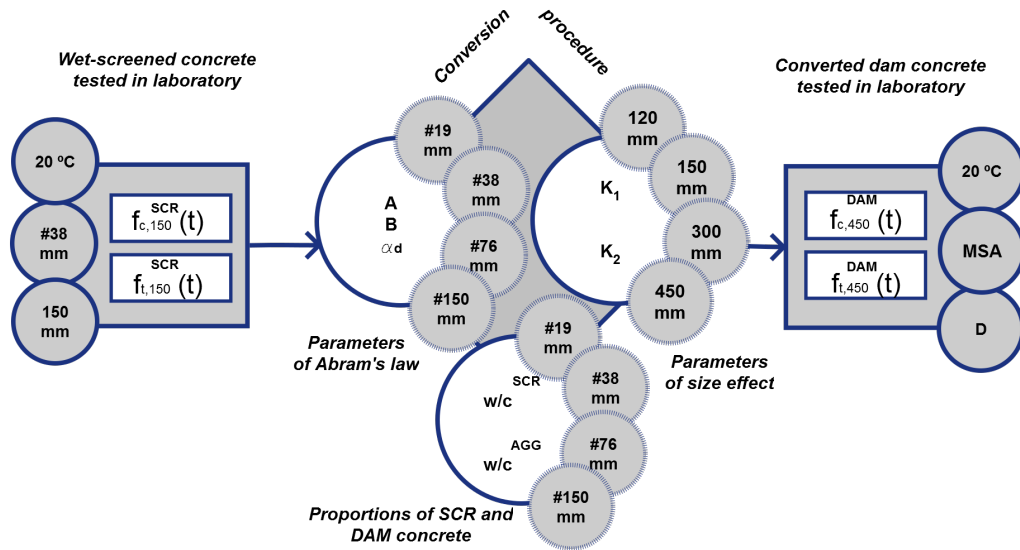


Figure 4.25: Illustration of the conversion procedure for the strength properties including the determination of the the water-cement ratio of wet-screened (SCR) and full-mixed (DAM) concretes, of the Abram's law parameters and of the size effect parameters

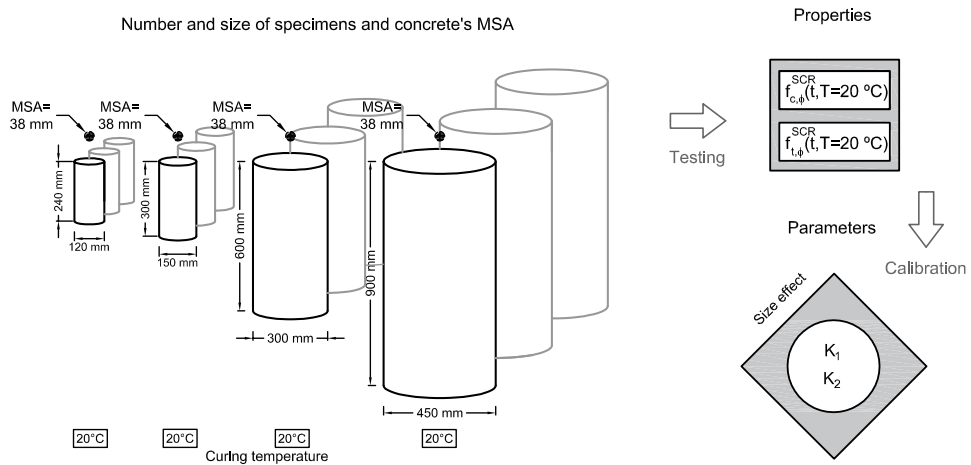


Figure 4.26: Number and size of specimens for the calibration of the size effect law parameters, K_1 and K_2

CHAPTER 4. ANALYTICAL MODELLING OF THE DAM CONCRETE STRUCTURAL PROPERTIES

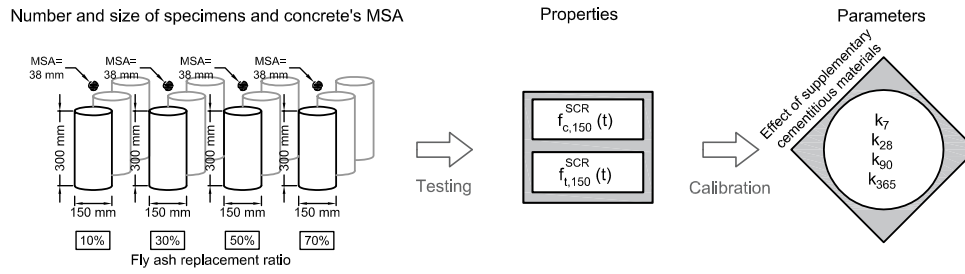


Figure 4.27: Number and size of specimens for the determination of the effect of the supplementary cementitious materials

Figure 4.28 illustrates minimum number of specimens for the calibration of the apparent activation energies.

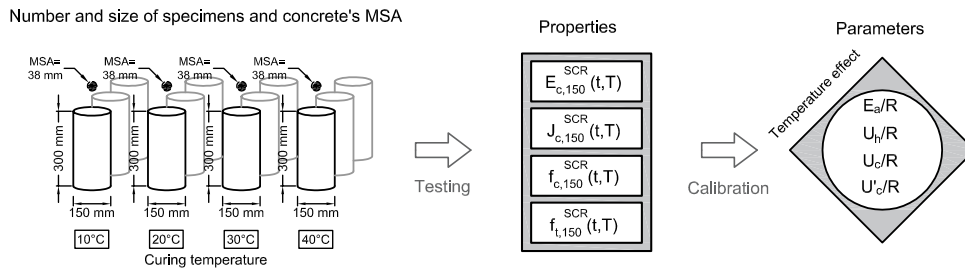


Figure 4.28: Number and size of specimens for the calibration of the equivalent age method

Inside a concrete dam, specially an arch dam, different stress states can occur, including triaxial and biaxial stress states. For example, near the up and downstream faces biaxial tension-compressive and tension-tension states can develop, while inside of the dam a triaxial compressive state is usually the most common (Mehta and Monteiro 2006). Since conventional laboratory tests are uniaxial, a reduction or amplification factor is needed in order to compare it directly with the calculated or measured stress state.

Tables 4.14 and 4.15 summarizes the list of parameters, variables, type and number of specimens proposed for the calibration of the different effects and analytical models used in the conversion procedure. It is proposed that this calibration programme occurs during the trial tests, before the dam's construction.

4.5. PROPOSED FRAMEWORK FOR DAM CONCRETE QUALITY CONTROL BASED ON ANALYTICAL MODELS

Table 4.14: List of parameters, variables, type and number of specimens proposed for the calibration of the different effects

Type of effect	Property	Parameter to determine	Variable under study	Variable range for testing	Type of specimen	Number of specimen
Temperature	f_c	$E_a/R(f_c)$	Curing temperature	10°C, 20°C, 30°C, 40°C	SCR concrete $\Phi=150$ mm, H=300 mm	3-5 samples \times 4 testing temperatures
	$f_{t,spl}$	$E_a/R(f_{t,spl})$	Curing temperature	10°C, 20°C, 30°C, 40°C	SCR concrete $\Phi=150$ mm, H=300 mm	3-5 samples \times 4 testing temperatures
	E_c	$E_a/R(E_c)$	Curing temperature	10°C, 20°C, 30°C, 40°C	SCR concrete $\Phi=150$ mm, H=300 mm	3-5 samples \times 4 testing temperatures
	J_c	$U_h/R, U_c/R, U'_c/R$	Curing temperature	10°C, 20°C, 30°C, 40°C	SCR concrete $\Phi=150$ mm, H=300 mm	3-5 samples \times 4 testing temperatures
Size effect	f_c	$K_1(f_c)$ $K_2(f_c)$	Specimen diameter	120 mm, 150 mm 300 mm, 450 mm	SCR concrete $\Phi=var$ mm, H=2 \times Φ mm	3-5 samples \times 4 specimen diameters
	$f_{t,spl}$	$K_1(f_{t,spl})$ $K_2(f_{t,spl})$	Specimen diameter	120 mm, 150 mm 300 mm, 450 mm	SCR concrete $\Phi=var$ mm, H=2 \times Φ mm	3-5 samples \times 4 specimen diameters
Supplementary cementitious materials	f_c	$k_7, k_{28}, k_{90}, k_{365}$	Fly ash replacement	10%, 30%, 50%, 70%	SCR concrete $\Phi=150$ mm, H=300 mm	3-5 samples \times 4 fly ash replacements \times 4 testing ages
	$f_{t,spl}$	$k_7, k_{28}, k_{90}, k_{365}$	Fly ash replacement	10%, 30%, 50%, 70%	SCR concrete $\Phi=150$ mm, H=300 mm	3-5 samples \times 4 fly ash replacements \times 4 testing ages
Effect of wet-screening on composition	$w/(c+kf)$	a, s	Sieve aperture used for wet-screening	#19 mm, #38 mm, #76 mm, #150 mm	-	-
	V^{SCR}, V^{AGG}	V^{AGG}	Sieve aperture used for wet-screening	#76 mm, #150 mm	-	-

Table 4.15: List of parameters, variables, type and number of specimens proposed for the calibration of the different models

Type of conversion	Property	Age (days)	Parameter to determine	Variable under study	Variable range for testing	Type of specimen	Number of specimen
Composite model	E_c	7, 28, 90, 365	β^{MSA}	Sieve aperture used for wet-screening	19 mm, 38 mm, 76 mm, 150 mm	$\Phi=150$ mm, H=300 mm $\Phi=450$ mm, H=900 mm	3-5 samples \times 4 types of concrete \times 4 testing ages
	f_c	7, 28, 90, 365	A, B, α_d	Sieve aperture used for wet-screening	19 mm, 38 mm, 76 mm, 150 mm	$\Phi=450$ mm, H=900 mm	3-5 samples \times 4 types of concrete \times 4 testing ages
Extended Abrams law	$f_{t,spl}$	7, 28, 90, 365	$A(f_{t,spl}), B(f_{t,spl}), \alpha_d(f_{t,spl})$	Sieve aperture used for wet-screening	19 mm, 38 mm, 76 mm, 150 mm	$\Phi=450$ mm, H=900 mm	3-5 samples \times 4 types of concrete \times 4 testing ages

4.6 Concluding remarks

The first part of this chapter proposes a methodology for the prediction of the dam concrete instantaneous and delayed deformability properties based on the experimental *in situ* results of the wet-screened concrete.

Due to the different temperature conditions of each creep cell, the maturity method was applied to set a comparable reference state with the equivalent age. A two-phase composite model, considering the sieved coarse aggregates as the inclusions and the wet-screened concrete as the binder, was used to predict the modulus of elasticity of the dam concrete considering two type of wet-screening sizes. The best fit to the dam test results was obtained with the Granger and Bažant model taking β as 1.0, which is the particular case of a purely parallel model (Voigt model). A similar methodology was applied to the creep strain development using the results obtained in the Baixo Sabor creep cells. The comparison between the dam concrete compressive creep strains prediction and the obtained experimental results, at reference temperature conditions, show an overall good agreement. The main deviations between the predictions and the measurement seem to be related to the fit to experimental results to the model B3 at a large range of loading ages and loading durations and to the different compaction conditions related to the two types of wet-screened concrete. A sensitivity analysis was made, using the composite model parameter β , related to the aggregate compaction conditions of the concrete, to obtain a good agreement with the experimental results of dam concrete and the optimum composite model parameters.

In the second part of the chapter it is proposed a physically-based expression for the relationship between strength properties of dam concrete obtained in large specimens and of wet-screened concrete obtained in small specimens, for a given age of concrete. The parameters were calibrated for the compressive and splitting tensile strength results of Baixo Sabor dam concrete obtained during the construction. The strength results used in the analysis concern the concretes placed in the dam's core, in the upstream and downstream faces and in the areas with reinforcement, which have different maximum size of aggregate (MSA).

A size effect law for both compressive and splitting tensile strength was used to convert the test results obtained in small specimens into results obtained in large specimens and the direct comparison between concrete test results. Then, an extended Abrams law,

proposed in this chapter, allowed for the differentiation of each type of concrete used in dams through an important intrinsic characteristic, the size of the aggregates used. The validation of the obtained expression with the test results of the mortar reinforced the good fit and its potential for several types of wet-screenings. It is shown that the maximum size of aggregate has statistical significance in the strength prediction, indicating that this parameter should be taken into account. The results obtained from the prediction model are in agreement with other experimental results available in literature (Higginson *et al.* 1962). The Baixo Sabor test results show that there is an increase of compressive strength as the maximum size of aggregate increases. It is also shown that the increase of splitting tensile strength with the maximum size of aggregate is less pronounced.

The further understanding of the relationship between dam and wet-screened concrete structural properties and the development of prediction models will contribute towards the improvement of design guidelines and of monitoring and safety control practices, regarding the assessment of long-term lifetime deterioration scenarios. These type of methodologies can be applied when designing the composition mix in the trial phase, for the optimization of the concrete quality control during construction and for test results interpretation. The proposed approaches can also improve service life prediction analysis because, due to the lack of information with few experimental data available, the abnormal behaviour of concrete due to deterioration processes is difficult to be assessed (USBR 2005).

Finally, a new framework for the dam concrete quality control is proposed, which is based on the developed prediction tools for each type of structural property. The main purpose of this framework is to obtain reliable predictions of dam concrete properties based on the test results of wet-screened concrete. Each model and method used in each prediction tool (composite models, maturity method, size effect law and Abrams law) requires the calibration of parameters in order to describe the behaviour of each specific concrete. The framework can reduce the number of dam concrete test sampling using large specimen and reduce the obtained standard deviations once the main parameters are calibrated and the prediction results are validated. It can also help the interpretation of new test results and the identification of outlier results based on well-established physically based models.

Numerical modelling of the concrete structural properties using particle models

5.1 Introduction

Detailed numerical models of concrete's mesostructure are useful to understand the interactions between its components and to predict complex deterioration scenarios. This chapter describes the use of discrete element method (DEM) applied to particle models (PM) to the prediction of concrete behaviour at the mesoscale level and considering its aggregate mesostructure.

Firstly, the two-dimensional discrete element method formulation for rigid particle models is presented, including the detailed procedure for the implementation of the method. The formulation relies on an explicit finite-difference integration scheme and on damping in order to obtain a steady-state solution equivalent to the static response of the structural system.

Four types of contact models are presented. The Hooke's model and the aging viscoelastic model, based on the solidification theory, relate to the deformability properties of contact. The contact failure is simulated following a Mohr-Coulomb model with a tension cut-off and a Mohr-Coulomb model with tensile/shear softening.

In order to simulate the long-term behaviour of cementitious materials, an explicit formulation of a DEM contact model that includes aging viscoelastic behaviour based

on the solidification theory is presented. Due to the timestep constraints of the DEM, a fast numerical procedure for the analysis of long-term aging viscoelastic behaviour of concrete is also proposed. The contact aging model validation tests using larger regular and random particle assemblies show that the fast numerical procedure significantly reduces the computational costs by introducing large timesteps in which the solution is computed, while giving the same accuracy of the fully explicit procedure.

A calibration procedure for the contact model parameters of each concrete component at the mesolevel (mortar and aggregate) is also presented, including new expressions that relate the delayed deformability macro properties with the aging viscoelastic contact properties.

Two separate analysis are described in detail concerning the deformability properties over time and the strength properties at a given loading age. The DEM aging concrete model is validated using Ward's test results (Ward *et al.* 1969) for both mortar and concrete, whereas the failure behaviour is validated using the concrete behaviour described by Vonk (1992).

The proposed DEM aging particle model was implemented in C++ for two-dimensional analysis due to the computational costs associated with this type of detailed models. Note that both the proposed aging contact model and the fast numerical procedure can be readily extended to 3D and incorporated in both commercial and open source DEM based programs.

The part of this section related to the development of the aging viscoelastic model and to the analysis of the long-term behaviour of concrete using DEM has been accepted for publishing in the international Journal of Engineering Mechanics of ASCE in October, 11 2017, with the title "Discrete element method for modelling the long-term aging viscoelastic behavior of concrete considering its mesostructure" (Serra *et al.* 2017a) (Appendix B).

5.2 Discrete element method applied to rigid particle

5.3 General aspects

The discrete element method (DEM) can be described as a numerical method for solving structural systems of individual elements, blocks (polygons) or particles (circular or

spherical) interacting with each other at contact points or interfaces. Each element, usually considered to be rigid, is ruled by a motion law and each contact by an interaction law. The motion law defines the differential equation that governs the kinematic of the elements. This differential equation is given by the Newton's second law of motion. The interaction law, known as the force-displacement law, determines the interaction forces between particles at the contact point, according with their relative displacement. The unbalanced force of each element at a given time is used for setting new velocities and positions using the law of motion, and, therefore, new interaction forces.

The advantages of this type of method is the possibility to have large displacements and rotations, the complete detachment of two elements when their contact reaches its strength capacity and consider new contacts during the simulation (Monteiro Azevedo 2003). Figure 5.1 illustrates a complete DEM cycle with the update of the forces and displacements of each element, in between the force-displacement law and the law of motion.

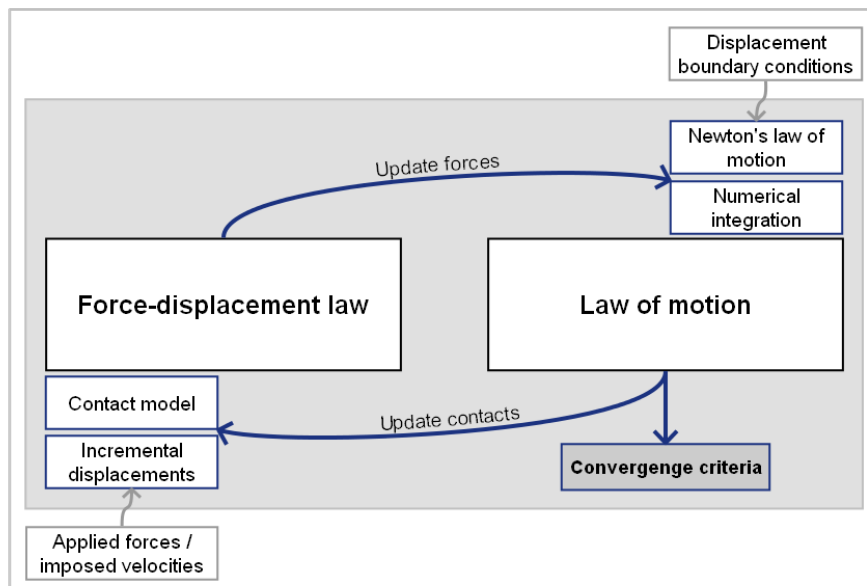


Figure 5.1: General DEM cycle

Considering external applied forces or imposed deformations and predefined boundary conditions it is possible to calculate the response of the system using a method for solving the differential equation in each cycle. The numerical methods commonly used for this type of problems rely on explicit integration schemes, where the solution at a given time is predicted from the response at the former time-step. In DEM, the explicit integration

scheme is used for the integration of accelerations into velocities.

The elements interacting with each other are therefore circular rigid particles defined by a position in space and a given radius (Figure 5.2). With this type of element, the contact detection and the general cycle calculations are easier to implement and require less computational time.

5.3.1 Force-displacement law

The force-displacement law defines the behaviour of each contact between particles. When a contact between two particles is identified, the subsequent incremental relative displacements generates a contact force increment, which is applied to the centre of the particles. A contact between two particles is defined by a line segment perpendicular to the line connecting both particle centres (point A and Point B in Figure 5.2). The intersection between those two lines is the contact point (point C in Figure 5.2). The contact overlap is the superposition of each particle on another particle. The general convention considers compression forces related to positive contact overlap and tension forces for negative contact overlap.

The distance between particle A and particle B, d , is given by Euclidean distance between the two centres of gravity, $\mathbf{x}^{[A]}$ and $\mathbf{x}^{[B]}$, and the contact overlap, U_n , is obtained by the difference of the sum of both radius, $R^{[A]}$ and $R^{[B]}$, and the distance between particles.

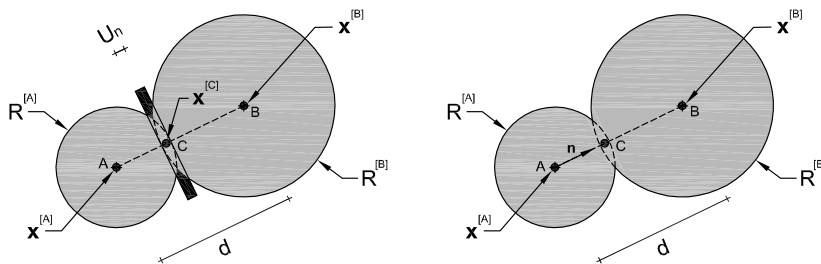


Figure 5.2: Contact point definition in particle models

$$d = \sqrt{\sum_{i=1}^2 \left(x_i^{[B]} - x_i^{[A]} \right)^2} \quad (5.1)$$

$$U_n = R^{[A]} + R^{[B]} - d \quad (5.2)$$

With the definition of the contact overlap and calculating the unit normal to the contact plane, \mathbf{n} , one can obtain the contact point location, $\mathbf{x}^{[C]}$.

$$n_i = \frac{\left(x_i^{[B]} - x_i^{[A]}\right)}{d} \quad (5.3)$$

$$x_i^{[C]} = x_i^{[A]} + \left(R^{[A]} - \frac{1}{2}U^n\right) n_i \quad (5.4)$$

The contact velocity, $\dot{\mathbf{x}}^{[C]}$, is defined by the relative velocity of both particles involved, A and B , at the contact point, $\left(\dot{\mathbf{x}}^{[C]}\right)_A$ and $\left(\dot{\mathbf{x}}^{[C]}\right)_B$. The dot above the position, \mathbf{x} , denotes the first derivative with respect to time and the bold refers to a vector with two components.

$$\dot{\mathbf{x}}^{[C]} = \left(\dot{\mathbf{x}}^{[C]}\right)_B - \left(\dot{\mathbf{x}}^{[C]}\right)_A \quad (5.5)$$

The velocity of the particle Φ at the contact point, $\left(\dot{\mathbf{x}}^{[C]}\right)_\Phi$, (translational velocity) is given by,

$$\left(\dot{x}_i^{[C]}\right)_\Phi = \dot{x}_i^{[\Phi]} + \epsilon_{i3k} \omega_3^{[\Phi]} \left(x_k^{[C]} - x_k^{[\Phi]}\right) \quad (5.6)$$

$$\epsilon_{ijk} = \begin{cases} 0 & \text{if two indices coincide} \\ +1 & \text{if i,j,k permute like 1.2.3} \\ -1 & \text{otherwise} \end{cases} \quad (5.7)$$

where ϵ_{ijk} is the permutation symbol and $\omega_3^{[\Phi]}$ is the rotational velocity of particle Φ . In Figure 5.3 the velocities of each particle and of the contact are represented.

The displacement increment of the contact, $\Delta\mathbf{x}^{[C]}$, for a given time increment, Δt , is, by integration,

$$\Delta\mathbf{x}^{[C]} = \dot{\mathbf{x}}^{[C]} \Delta t \quad (5.8)$$

and can be decomposed into the normal, $\Delta x_n^{[C]}$, and the shear, $\Delta\mathbf{x}_s^{[C]}$, components:

$$\Delta x_n^{[C]} = \sum_{i=1}^2 \left(\Delta x_i^{[C]} n_i\right) \quad (5.9)$$

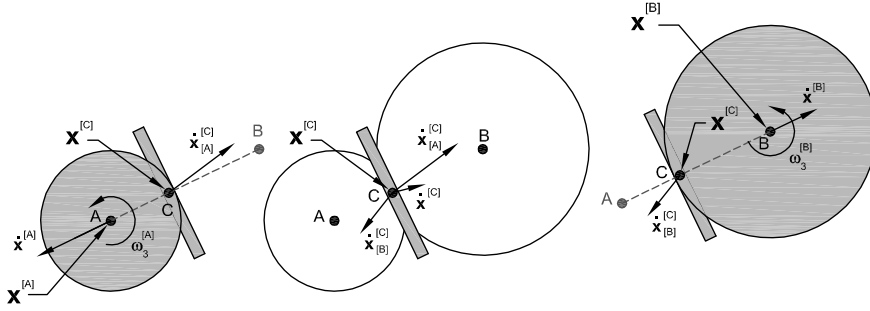


Figure 5.3: Contact point velocity definition in particle models

$$\Delta \mathbf{x}_s^{[C]} = \Delta \mathbf{x}^{[C]} - \Delta x_n^{[C]} \mathbf{n} \quad (5.10)$$

The normal and shear contact force increments, $\Delta F_n^{[C]}$ and $\Delta \mathbf{F}_s^{[C]}$, are obtained from the linear constitutive law of the contact and the normal and shear contact stiffness, k_n and k_s , respectively (Figure 5.4).

$$\Delta F_n^{[C]} = -k_n \Delta x_n^{[C]} \quad (5.11)$$

$$\Delta \mathbf{F}_s^{[C]} = -k_s \Delta \mathbf{x}_s^{[C]} \quad (5.12)$$

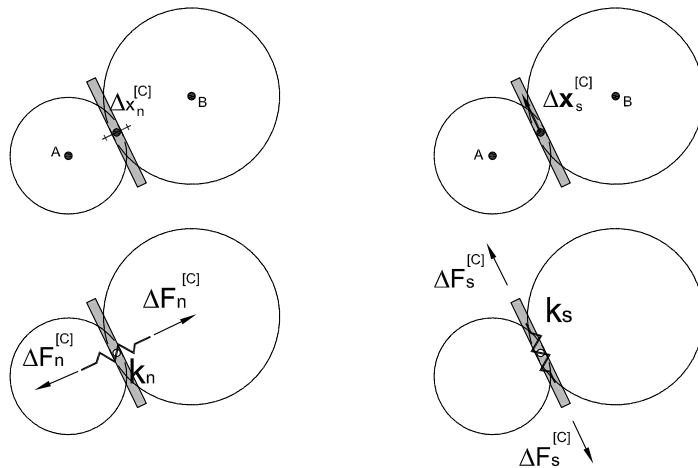


Figure 5.4: Incremental linear contact model in particle models

Since the shear contact force is defined in global coordinates and to take into account

large displacements, its necessary the correction of the shear contact force to refer it to the new contact plane, between each timestep, assuming infinitesimal rotations. Figure 5.5 shows the corrected shear force referred to the new contact plane.

$$\Delta F_{s,i}^{[C],corrected} = \Delta F_{s,i}^{[C],old} - \epsilon_{ij3} \epsilon_{3mn} \Delta F_j^{[C],old} n_m^{old} n_n \quad (5.13)$$

and, therefore, the updated predicted normal and shear forces at contact point are obtained from,

$$F_n^{[C]} = F_n^{[C],old} + \Delta F_n^{[C]} \quad (5.14)$$

$$\mathbf{F}_s^{[C]} = \mathbf{F}_s^{[C],corrected} + \Delta \mathbf{F}_s^{[C]} \quad (5.15)$$

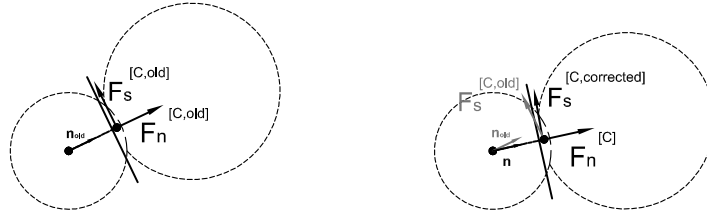


Figure 5.5: Correction of shear contact force in particle models

The contact model is applied and then the new contact force, $\mathbf{F}^{[C]}$, is given by the vectorial sum of normal and shear components,

$$\mathbf{F}_i^{[C]} = F_n^{[C]} n_i + \mathbf{F}_{s,i}^{[C]} \quad (5.16)$$

The contact forces, from each contact, are then transmitted and summed to both particles, obtaining the resultant internal forces and moments acting at particle centre, $\mathbf{F}_{t+1}^{[\Phi]}$ and $M_{3,t+1}^{[\Phi]}$ (Figure 5.6),

$$\mathbf{F}_{t+1}^{[A]} = \mathbf{F}_t^{[A]} - \mathbf{F}_t^{[C]} \quad (5.17)$$

$$\mathbf{F}_{t+1}^{[B]} = \mathbf{F}_t^{[B]} + \mathbf{F}_t^{[C]} \quad (5.18)$$

$$M_{3,t+1}^{[A]} = M_{3,t}^{[A]} - \epsilon_{3jk} \left(x_j^{[C]} - x_j^{[A]} \right) F_{k,t}^{[C]} \quad (5.19)$$

$$M_{3,t+1}^{[B]} = M_{3,t}^{[B]} + \epsilon_{3jk} \left(x_j^{[C]} - x_j^{[B]} \right) F_{k,t}^{[C]} \quad (5.20)$$

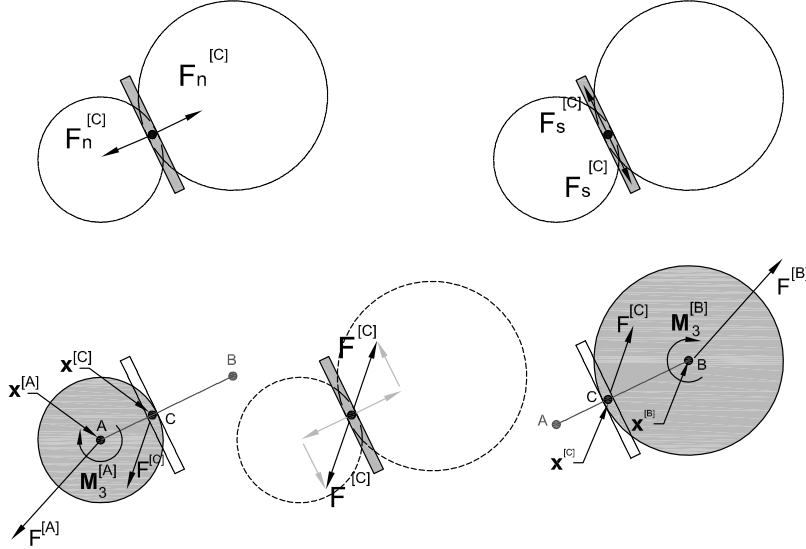


Figure 5.6: Transmission of contact force to particle forces and moments in particle models

5.3.2 Law of motion

5.3.2.1 Newton's second law

Newton's second law of motion defines the response of a single particle with applied forces or moments,

$$\mathbf{F}(t) = m\ddot{\mathbf{x}}(t) \quad (5.21)$$

$$M_3(t) = I\dot{\omega}_3(t) \quad (5.22)$$

where $\mathbf{F}(t)$ and $M_3(t)$ are the total applied force and moment at time t , m and I are the total mass and inertia of the particle, and $\ddot{\mathbf{x}}(t)$ and $\dot{\omega}_3(t)$ are the particle translational and angular accelerations. The inertia is βmR^2 , where β is $2/5$ for spherical shaped particles and $1/2$ for disk shaped particles.

There are several numerical techniques for solving differential equations based on time discretization into timesteps, Δt , and approximating derivatives within that discretization. Explicit methods calculate a solution at time $t + \Delta t$ based only on the previous solution in t and the derivative using a time increment. The updated velocities are obtained from the accelerations using centred difference scheme for calculating derivatives.

5.3.2.2 Centred difference time-integration scheme

Differential equations can be numerically solved using finite difference approximations for each derivative. A derivative of the function $f(t)$ in time, t , $\dot{f}(t) = \frac{df(t)}{dt}$, can be defined as limit of the slope of f within a predefined interval, Δt , when Δt tends to zero.

$$\dot{f}(t) = \frac{df(t)}{dt} = \lim_{\Delta t \rightarrow 0} \frac{f(t + \Delta t) - f(t)}{\Delta t} \quad (5.23)$$

One can see that, as Δt gets smaller, more accurate is the value of the derivative.

The development of a given variable, $x(t)$, in a Taylor series at time, t_0 , follows,

$$x(t) = x(t_0)(t - t_0)^0 + \frac{\dot{x}(t_0)(t - t_0)^1}{1!} + \frac{\ddot{x}(t_0)(t - t_0)^2}{2!} + \frac{\dddot{x}(t_0)(t - t_0)^3}{3!} + \dots \quad (5.24)$$

Taking $t = t_0 + \Delta t$ and considering $O(\Delta t^n)$ the truncated Δt^n terms of the Taylor series one can write the following expression,

$$x(t) = x(t_0)(\Delta t)^0 + \frac{\dot{x}(t_0)(\Delta t)^1}{1!} + \frac{\ddot{x}(t_0)(\Delta t)^2}{2!} + \frac{\dddot{x}(t_0)(\Delta t)^3}{3!} + \dots \quad (5.25)$$

From which follow the derivative, $\dot{x}(t_0)$,

$$\dot{x}(t_0) = \frac{x(t_0 + \Delta t) - x(t_0)}{\Delta t} + O(\Delta t^2) \quad (5.26)$$

and, therefore, the smaller the Δt , smaller the error, $O(\Delta t)$, obtained from discarding the remaining terms.

The centred difference scheme for the first derivative of $x(t)$ uses two points, $x(t - \Delta t)$ and $x(t + \Delta t)$,

$$x(t - \Delta t) = x(t_0) - \dot{x}(t_0)(\Delta t) + \frac{\ddot{x}(t_0)(\Delta t)^2}{2} - \frac{\dddot{x}(t_0)(\Delta t)^3}{6} + O(\Delta t^4) \quad (5.27)$$

$$x(t + \Delta t) = x(t_0) + \dot{x}(t_0)(\Delta t) + \frac{\ddot{x}(t_0)(\Delta t)^2}{2} + \frac{\dddot{x}(t_0)(\Delta t)^3}{6} + O(\Delta t^4) \quad (5.28)$$

The derivative, using these two points, is,

$$\begin{aligned} \dot{x}(t_0) &= \frac{x(t_0 + \Delta t) - x(t_0 - \Delta t)}{2\Delta t} + \frac{1}{3}\ddot{x}(t_0)\Delta t^2 + O(\Delta t^4) \\ &= \frac{x(t_0 + \Delta t) - x(t_0 - \Delta t)}{2\Delta t} + O(\Delta t^2) \end{aligned} \quad (5.29)$$

from which can be concluded that centred difference scheme gives an accuracy of $O(\Delta t^2)$ (by disregarding the Δt^2 and further terms).

For this work it will be considered that the accelerations at time t , $\ddot{\mathbf{x}}(t)$, are related to former and future velocities evaluated at mid-interval, $\dot{\mathbf{x}}(t - \Delta t/2)$ and $\dot{\mathbf{x}}(t + \Delta t/2)$, as stated by the centred difference time-integration scheme,

$$\ddot{\mathbf{x}}(t) = \frac{\dot{\mathbf{x}}^{t+\Delta t/2} - \dot{\mathbf{x}}^{t-\Delta t/2}}{2 \times \Delta t/2} \quad (5.30)$$

Considering Newton's second law of motion (Equation 5.21 and Equation 5.22), the velocities $\dot{x}(t + \Delta t/2)$ are obtained from,

$$\dot{\mathbf{x}}^{t+\Delta t/2} = \dot{\mathbf{x}}^{t-\Delta t/2} + \left(\frac{\mathbf{F}(t)}{m} \right) \Delta t \quad (5.31)$$

$$\omega_3^{t+\Delta t/2} = \omega_3^{t-\Delta t/2} + \left(\frac{\mathbf{M}_3(t)}{I} \right) \Delta t \quad (5.32)$$

The future position, $\mathbf{x}(t + \Delta t)$, and future rotation, $\theta(t + \Delta t)$, are given by,

$$\mathbf{x}^{t+\Delta t} = \mathbf{x}^t + \dot{\mathbf{x}}^{t+\Delta t/2} \Delta t \quad (5.33)$$

$$\theta^{t+\Delta t} = \theta^t + \omega_3^{t+\Delta t/2} \Delta t \quad (5.34)$$

Figure 5.7 shows a graphical representation of the adopted central finite difference scheme. Velocities are determined at mid-interval ($t \pm \Delta t/2$) and positions are determined at primary intervals ($t \pm \Delta t$). The numerical scheme starts by considering an initial value for the particle velocity at the time $t - \Delta t$, $\dot{\mathbf{x}}^{t+\Delta t/2}$ and a given external force, $F(t)$, applied to one or several particles. The unbalanced force, due to the external force, is converted

into an acceleration, and using Equations 5.31 and 5.32 the new velocities can be calculated. The new positions are given by Equations 5.33 and 5.34 based on the velocities at mid-interval and the former position. The overlap is recalculated, new contact forces are derived from the contact model and new particle forces are obtained. If there are unbalanced forces, the accelerations are not null and the numerical procedure continues until convergence.

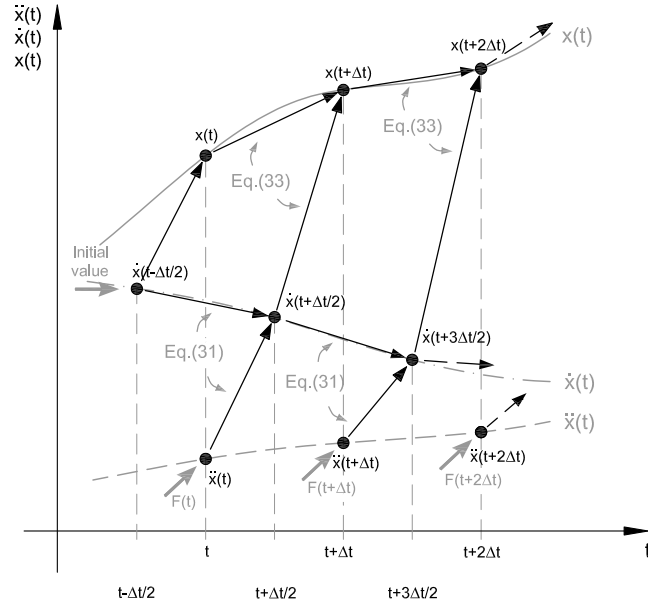


Figure 5.7: Graphical representation of the central difference scheme

5.3.2.3 Global viscous damping

For a single degree of freedom damped system, with mass, m , stiffness, k , and c as the damping coefficient, the dynamic equation of motion is,

$$m\ddot{x}(t) + c\dot{x}(t) + kx(t) = 0 \quad (5.35)$$

Critical damping occurs when,

$$c = c_c = 2\omega m \quad (5.36)$$

where ω is the natural angular frequency (Clough and Penzien 1993). A damping ratio can be defined as the ratio between damping, c , and critical damping, c_c ,

$$\xi = \frac{c}{c_c} \quad (5.37)$$

Usually dynamic systems are undercritically-damped ($c < c_c$) and, therefore, the damping ratio, ξ , is lower than 1. One can choose the value of c equal to c_c and ξ equal to unity, in order to ensure that the vibration mode is critically damped and, therefore, obtain a response that does not include oscillatory behaviour and converges faster to the steady-state position, where the unbalanced forces are null.

In N degree of freedom systems, there are N natural angular frequencies and it is difficult to choose the value of damping coefficient that ensures maximum damping efficiency. For complex systems it is usual to estimate the damping coefficient value for the lowest circular frequency, considering an undamped system,

$$c = 2\omega_0 m \xi \quad (5.38)$$

The equilibrium is obtained from a sum of the inertial forces and damping forces,

$$\mathbf{F}(t) = m\ddot{\mathbf{x}}(t) + c\dot{\mathbf{x}}(t) \quad (5.39)$$

$$M_3(t) = I\dot{\omega}_3(t) + c\omega_3(t) \quad (5.40)$$

For damped systems the law of motion has a viscous term in the right hand sides of Equation 5.31 and Equation 5.32 and the linear and angular velocities, $\dot{\mathbf{x}}(t)$ and $\omega_3(t)$, can be obtained from,

$$\dot{\mathbf{x}}^{t+\Delta t/2} = \left(D_1 \dot{\mathbf{x}}^{t-\Delta t/2} + \left(\frac{\mathbf{F}(t)}{m} \right) \Delta t \right) D_2 \quad (5.41)$$

$$\omega_3^{t+\Delta t/2} = \left(D_1 \omega_3^{t-\Delta t/2} + \left(\frac{\mathbf{M}_3(t)}{I} \right) \Delta t \right) D_2 \quad (5.42)$$

where $D_1 = 1 - (c/m)\Delta t/2$ and $D_2 = \frac{1}{1+(c/m)\Delta t/2}$.

5.3.2.4 Local non-viscous damping

Another type of damping, proposed by (Cundall 1987), is the local non-viscous damping in which the damping force is proportional to the absolute value of the unbalanced force.

This results in the following expressions for the law of motion,

$$\mathbf{F}(t) + \mathbf{F}^d(t) = m\dot{\mathbf{x}}(t) \quad (5.43)$$

$$M_3(t) + M_3^d(t) = I\omega_3(t) \quad (5.44)$$

where $\mathbf{F}^d(t)$ and $M_3^d(t)$ are, respectively, the translational and the rotational damping forces, which can be obtained from,

$$\mathbf{F}^d(t) = -\alpha |\mathbf{F}(t)| \frac{\dot{\mathbf{x}}(t)}{\|\dot{\mathbf{x}}(t)\|} \quad (5.45)$$

$$M_3^d(t) = -\alpha |M_3(t)| \frac{\omega_3(t)}{|\omega_3(t)|} \quad (5.46)$$

where α is the non-local damping coefficient. The linear and angular velocities, $\dot{\mathbf{x}}(t)$ and $\omega_3(t)$, can be obtained from,

$$\dot{\mathbf{x}}^{t+\Delta t/2} = \dot{\mathbf{x}}^{t-\Delta t/2} + \left(\frac{\mathbf{F}(t) + \mathbf{F}^d(t)}{m} \right) \Delta t \quad (5.47)$$

$$\omega_3^{t+\Delta t/2} = \omega_3^{t-\Delta t/2} + \left(\frac{\mathbf{M}_3(t) + \mathbf{M}_3^d(t)}{I} \right) \Delta t \quad (5.48)$$

5.3.3 Stability of the solution in explicit integration schemes

5.3.3.1 Mechanical critical timestep determination

When considering explicit time integration schemes the solution is more accurate and stable for infinitesimal timestep increments and there is a critical timestep for which error do not grow along the simulation. The stability of the solution along time is obtained if the chosen timestep, Δt , is under this critical value, Δt_{crit} (Belytschko and Hughes 1983).

If mass proportional damping is applied, the critical timestep should be corrected to take into account the amount of damping used,

$$\Delta t \leq \Delta t_{crit} = \frac{2}{\omega^{max}} \left(\sqrt{1 + \xi^2} - \xi \right) \quad (5.49)$$

where ω^{max} is the highest angular frequency of the undamped structural system and ξ is a fraction of the critical damping in the maximum frequency.

5.3.3.2 Gerschgorin theorem for highest circular frequency estimate

An upper bound of the maximum frequency, ω^{max} , and therefore a lower value of the critical timestep can be obtained using Gerschgorin's theorem (Underwood 1983), which guarantees that the highest frequency of a structural system is less than or equal to the absolute ratio between the sum of the stiffness row to the sum of the mass row,

$$\omega^{max} \leq \max \left\{ \sqrt{\frac{\sum_{j=1}^n |k_{ij}|}{m_i}} \right\} \quad (5.50)$$

$$\Delta t_{crit} \approx \min \left\{ 2 \sqrt{\frac{m_i}{\sum_{j=1}^n |k_{ij}|}} \right\} \quad (5.51)$$

where i, j are the degrees of freedom of a row and a column of the stiffness matrix, n is the maximum number of degrees of freedom, $\sum_{j=1}^n |k_{ij}|$ is the absolute sum of the i^{th} row of the stiffness matrix and m_i is the generalized mass of the particle with the degree of freedom i .

A simplified approach for calculating $\sum_{j=1}^n |k_{ij}|$ is to consider the sum of translational (Equation 5.52) or rotational (Equation 5.54) stiffness of each particle, taking those values as the maximum bounds,

$$k^{trans} = \sum_{j=1}^n |k_{ij}| < \sum_{c=1}^{N_c} 2(k_{n,c} + k_{s,c}) \quad (5.52)$$

$$\Delta t_{crit} \approx \min \left\{ 2 \sqrt{\frac{m_i}{k^{trans}}} \right\} \quad (5.53)$$

$$k^{rot} = \sum_{j=1}^n |k_{ij}| < \sum_{c=1}^{N_c} \left(R^{[B]^2} k_{s,c} + R^{[B]} R^{[A]} k_{s,c} \right) \quad (5.54)$$

$$\Delta t_{crit} \approx \min \left\{ 2 \sqrt{\frac{I_i}{k^{rot}}} \right\} \quad (5.55)$$

where $(k_{n,c} + k_{s,c})$ is the sum of normal and shear stiffness of the particle, N_c is the number of contacts of the particle and R is the radius of the particle.

5.3.3.3 Density scaling

The mechanical critical timestep, related to the maximum frequency and required for explicit time integration schemes, is usually very small which can be time consuming and computationally demanding. A way to overcome this is to use density scaling or mass scaling.

This approach simulates an equivalent system were these properties are calculated to maximize the ratio between the lowest frequency, ω_0 , and the maximum frequency, ω_{max} , $\frac{\omega_0}{\omega_{max}}$, which, as stated by (Underwood 1983), maximizes the convergence rate to the steady state solution, by minimizing the spectral radius, ρ^* ,

$$\rho^* = \left| 1 - 2 \frac{\omega_0}{\omega_{max}} \right| \quad (5.56)$$

For this work, the timestep was chosen as the unity ($\Delta t = 1.0$) and, therefore, from Equation 5.51, one can obtain the equivalent mass and inertia of the scaled system,

$$1.0 = 2 \sqrt{\frac{m_{scaled}}{k_{trans}}} \Leftrightarrow m_{scaled} = \left(\frac{1.0}{2} \right)^2 k^{trans} \quad (5.57)$$

$$1.0 = 2 \sqrt{\frac{I_{scaled}}{k_{rot}}} \Leftrightarrow I_{scaled} = \left(\frac{1.0}{2} \right)^2 k^{rot} \quad (5.58)$$

The highest frequency, ω_{max} , is mesh and material dependent and the lowest frequency, ω_0 , corresponds to the lowest participating mode of the structure, related to the load distribution (Tavarez and Plesha 2007).

Sauvé and Metzger (1995) guarantee a level of tolerance for the stability of the algorithm by increasing the critical timestep by a safety factor of 10% and obtaining the corresponding scaled mass and inertia (safety factor, SF).

Table 5.1 shows the model properties for the case of using real masses or scaled masses (density scaling).

Table 5.1: Real and scaled system properties

Real properties	Properties using density scaling
m_{real}, I_{real}	$m_{scaled} = \left(\frac{1.0 \times SF}{2}\right)^2 k^{trans} *$ $I_{scaled} = \left(\frac{1.0 \times SF}{2}\right)^2 k^{rot}$
k^{trans}, k^{rot}	k^{trans}, k^{rot}
$\xi = \frac{c}{c_c}$	$\xi = \frac{c}{c_c}$
$c = c_c \xi$	$c = c_c \xi$
$c_c = 2\omega_0^{real} m_{real}$	$c_c = 2\omega_0^{scaled} m_{scaled}$
$\omega_0^{real} \approx \{\text{Equation 5.59}\}$	$\omega_0^{scaled} \approx \{\text{Equation 5.59}\}$
$\omega_{max}^{real} \approx \{\text{Equation 5.50}\}$	
$\Delta t^{real} = 2\sqrt{\frac{m}{k}}, \text{ (Equation 5.51)}$	$\Delta t^{scaled} = 1.0$
* where SF is a safety factor in order to guarantee convergence.	

5.3.4 Adaptive dynamic relaxation

For damping the whole range of frequencies in an efficient way, a method, called dynamic relaxation (DR), is usually used (Underwood 1983; Petrinic 1996). This method calculates an equivalent frequency, ω_0 , through the Rayleigh's quotient. The advantage is that there is no need to determine the natural frequencies at each timestep. This circular frequency, ω_0 , is upper bounded by the maximum frequency, ω_{max} . Note that, when density scaling algorithm is adopted and timestep is set to unity, $\omega_{max} < 2$ which results in $\omega_0 < \omega_{max} < 2$ (Underwood 1983; Monteiro Azevedo 2003).

The goal of DR is to avoid overshooting the solution. For this, an adaptive DR algorithm (ADR) is used in which the global damping coefficient, the mass and the inertia are updated at each time increment.

At each timestep, the approximate fundamental frequency, ω_0 , is recalculated using the diagonal matrix that approximates the global stiffness matrix, K^{diag} (non-assembled stiffness matrix).

An approximation of the lowest circular frequency, ω_0 , associated to a loading condition is based on the principle of energy conservation, by the Rayleigh's quotient,

$$\omega_0^2 \approx \frac{u^T K u}{u^T M u} \quad (5.59)$$

where u^T and u are the current displacement vector and its transpose and K and M are the current tangent stiffness and mass matrix.

In this work, the adopted approach for the Rayleigh quotient is incremental based, using displacement increments, Δu^t , and the internal forces at each timestep, $F_{i,t}^{int}$ (Underwood 1983),

$$\omega_0^2 \approx \frac{\Delta u_i^T K_{ij}^{diag} \Delta u_j}{\Delta u_k^T M_{kl} \Delta u_l} \quad (5.60)$$

$$K_{ii}^{diag} = \frac{F_{i,t}^{int} - F_{i,t-\Delta t}^{int}}{u_{i,t} - u_{i,t-\Delta t}} \quad (5.61)$$

5.3.5 Convergence criteria

When converging to the steady state solution, a stopping criteria is needed to terminate the DR iterations.

Force and displacement tolerances, f_{tol} and u_{tol} , are defined for this convergence criteria. Within this work a tolerance of 0.001 was considered for the ratio between the mean of the unbalanced force norm, $\|F_t^{unbalanced}\|_{mean}$, and the mean contact force norm, $\|F_t^C\|_{mean}$, and for the ratio between the average displacement increment norm, $\|\Delta u_t\|_{mean}$, and the total displacement norm, $\|u_t\|_{mean}$, at a given timestep,

$$\frac{\|F_t^{unbalanced}\|_{mean}}{\|F_t^C\|_{mean}} < f_{tol} \quad (5.62)$$

$$\frac{\|\Delta u_t\|_{mean}}{\|u_t\|_{mean}} < u_{tol} \quad (5.63)$$

5.3.6 Micro-macro approximations

The behaviour of a contact can be related to the behaviour of an equivalent beam and a general equivalence between contact micro properties, normal and shear stiffness, k_n and k_s , and material macro properties, elastic modulus, E , can be obtained.

The height of the equivalent beam, \bar{R} , is determined by the average radius of the particles, $R^{[A]}$ and $R^{[B]}$, and the beam length, L , is defined as the sum of both radius,

$$\bar{R} = \frac{R^{[A]} + R^{[B]}}{2} \quad (5.64)$$

$$L = 2\bar{R} = R^{[A]} + R^{[B]} \quad (5.65)$$

For 2D particle models, with t thickness, the equivalent cross-sectional area, A_{eq} , and moment of inertia, I_{eq} , is given by,

$$A_{eq} = 2.0\bar{R}t \quad (5.66)$$

$$I_{eq} = \frac{(2.0\bar{R})^3 t}{12} \quad (5.67)$$

The equivalence between micro and macro properties follows,

$$k^n = \frac{EA_{eq}}{L} \quad (5.68)$$

$$k^s = \frac{12EI_{eq}}{L^3} \quad (5.69)$$

which for pure axial load and pure shear load follows that,

$$k^n = k^s = Et \quad (5.70)$$

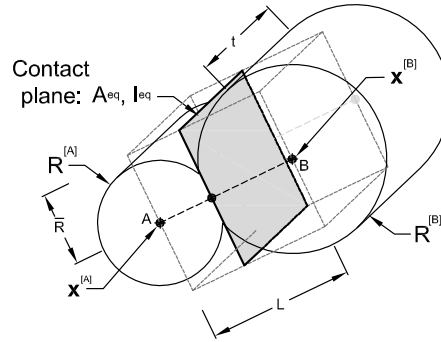


Figure 5.8: Equivalent elastic beam in particle models

5.3.7 Energy terms

The use of explicit integration schemes in nonlinear analysis can introduce numerical instabilities which can influence the structural response. The monitoring of the energy balance controls the eventual generation of spurious energy (Monteiro Azevedo 2003).

The energy balance at a given time is,

$$|U^k + U^{el} + U^{inel} + W^{damp} - W^{ext}| \leq \delta \|W\| \quad (5.71)$$

$$\|W\| = \|U^k\| + \|U^{el}\| + \|W^{ext}\| \quad (5.72)$$

where U^k is the kinetic energy of the particles, U^{el} is the internal elastic strain energy of the particles, U^{inel} is the internal energy dissipated by inelastic deformation of each contact, W^{ext} is the work done by external forces, W^{damp} is the work done by the damping forces, the parameter, δ , specifies the tolerance and the energy term $\|W\|$ is the norm of the total energy of the system.

The internal kinetic energy is given by the sum of the individual kinetic energy of each particle,

$$U^k = \frac{1}{2} \sum_{i=1}^{N_p} \sum_{j=1}^3 M_i \dot{x}_{ij}^2 \quad (5.73)$$

where N_p is the number of particles in the assembly, M_i is the mass of particle "i" and \dot{x}_{ij} is the component "j" of the velocity of particle "i".

The internal elastic strain energy of the assembly is obtained by,

$$U^{el} = \frac{1}{2} \sum_{i=1}^{N_c} \left(\frac{|F_{n_i}^{[C]}|^2}{k_n} + \sum_{j=1}^2 \frac{|F_{s_{ij}}^{[C]}|^2}{k_s} \right) \quad (5.74)$$

where N_c is the number of contacts in the assembly, $|F_{n_i}^{[C]}|$ and $|F_{s_{ij}}^{[C]}|$ are the norm of normal and shear components of the contact force.

The internal energy dissipated by inelastic deformation can be obtained directly by the inelastic contact displacements, ΔU_n^{inel} and $\Delta \mathbf{U}_s^{inel}$,

$$U^{inel} = \frac{1}{2} \sum_{i=1}^{N_c} \left(|F_{n_i}^{[C]}| \Delta U_{n_i}^{inel} + \sum_{j=1}^2 |F_{s_{ij}}^{[C]}| \Delta U_{s_{ij}}^{inel} \right) \quad (5.75)$$

The work associated with the damping forces at a given timestep, t , is the sum of the work of local damping forces, W^{local} , and the work of the global damping forces, W^{global} ,

$$W^{damp} = W^{local} + W^{global} \quad (5.76)$$

$$W_t^{local} = W_{t-1}^{local} + \sum_{i=1}^{N_p} \left(\mathbf{F}_{ti}^{local} \Delta \mathbf{u}_i \right) \quad (5.77)$$

$$W_t^{global} = W_{t-1}^{global} + \sum_{i=1}^{N_p} (\mathbf{F}_{ti}^{global} \Delta \mathbf{u}_i) \quad (5.78)$$

where \mathbf{F}^{local} is the local damping force, \mathbf{F}^{global} is the global damping force ($\mathbf{F}^{global} = cM\dot{x}$) and $\Delta \mathbf{u}$ is the displacement increment of each particle

5.4 Random assemblies of concrete

It is known that the main heterogeneity of concrete is due to the "stiff" coarse aggregates randomly distributed inside the specimen and completely embedded in a "soft" mortar (Coutinho and Gonçalves 1994). In order to simulate the behaviour of heterogeneous cementitious materials using particle models it is strongly recommended that each material is represented inside the particle assembly considering their main mechanical properties. In the case of conventional concrete, the mortar and the coarse aggregates will be considered as homogeneous materials with specific deformability properties.

The particle assembly of concrete includes the shape, aspect ratio and distribution of the coarse aggregates according to Wang *et al.* (1999). The initial aggregate particle assembly is created by first inserting the aggregate particles from the largest sieve aperture to smallest sieve aperture ensuring that the particles do not overlap with each other. As each circular particle representing the aggregate is placed, the particle boundary contour is redefined using an harmonic function of the polar angle. After all the aggregate particles are placed, the inner area of each aggregate particle given by its polygonal contour is discretized with inner circular particles (Monteiro Azevedo *et al.* 2008). Later, the outer boundary of the aggregate particles is discretized with particles representing the particle size adopted for the cement paste, including an initial reduction radius prior to the particle insertion. After the particle insertion, the real particle radius is adopted and a DEM cohesionless type solution is carried out, leading to a redistribution of the particle overlap throughout the assembly. At the end of this stage, the initial particle overlap and the particle contact forces are set to zero and the described incremental contact approach presented is adopted.

The aggregate generation procedure allows for the definition of an arbitrary aggregate distribution, which, in this particular case, follows the properties of the tested concrete and the proportion of each one in the concrete mix. More details concerning the concrete

used for the numerical modelling are described further in the next section, including the concrete's aggregate distribution and the obtained particle assembly.

5.5 Contact constitutive models for the analysis of long-term behaviour of concrete

5.5.1 Hooke's model

The elastic model is shown in § 5.3.1 (Equations 5.11 and 5.12) as an incremental linear model, relating the incremental contact forces and the incremental relative displacement, for both normal and shear behaviours. Figure 5.9 illustrates the contact model properties for normal and shear behaviour, for both instantaneous and over time response. The normal and shear stiffness at contact interface are given by k_n and k_s , respectively, which do not change over time and yields a constant response over time for constant applied forces.

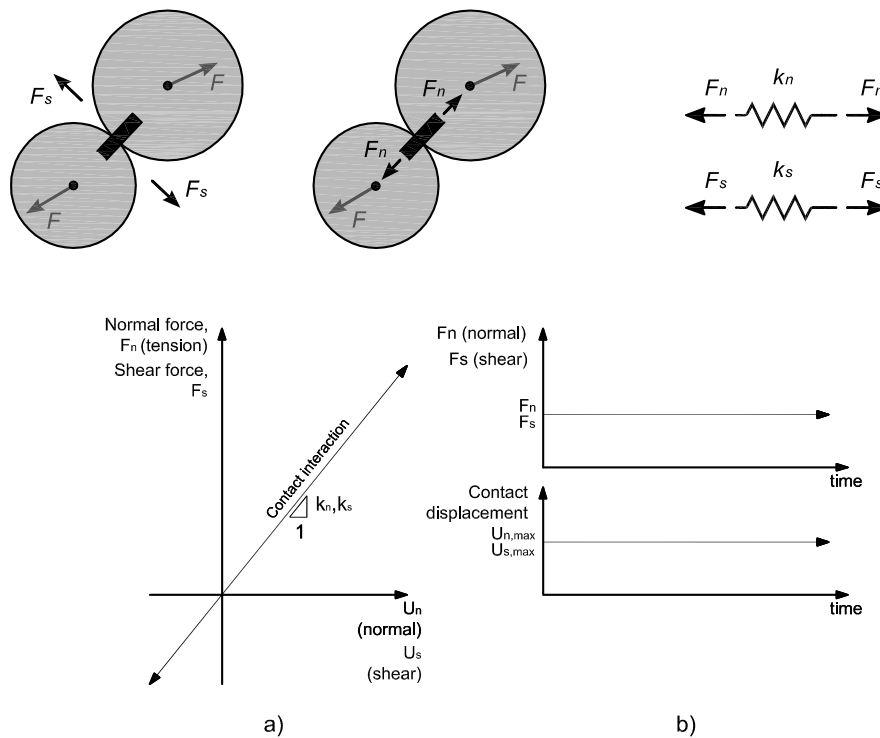


Figure 5.9: Mechanical representation of the elastic model: a) Force-overlap diagram; b) Development of contact forces and overlap over time

5.5.2 Numerical formulation of solidification theory

Since particle models are described by the displacements and forces of each particle, the implementation of the aging viscoelastic constitutive model based on the solidification theory requires an equivalence from an uniaxial model described by a strain-stress constitutive law to a displacement-force constitutive law. This equivalence is obtained by approximating the normal relative displacement, $\Delta x_n^{[C]}$, at the contact to a normal contact strain, $\Delta \varepsilon_n$ ($\Delta x_n^{[C]} = \Delta \varepsilon_n (R^{[A]} + R^{[B]})$), and the normal contact force, $F_n^{[C]}$, is approximated to a normal contact stress, $\sigma_n^{[C]}$ ($F_n^{[C]} = \sigma_n^{[C]} R_{min} t$). $R^{[A]}$ and $R^{[B]}$ are the radius of the particle A and B in contact, R_{min} is the minimum radius and t is the thickness of the contact plane, taken to be a disk for two-dimensional analysis. An approximated relationship between the modulus of elasticity in the normal direction, E_n , and the normal stiffness, k_n ($k_n = E_n R_{min} t / (R^{[A]} + R^{[B]})$), is also adopted. Similarly to other DEM models (Potyondy and Cundall 2004; Plassiard *et al.* 2009; Nitka and Tejchman 2015; Oñate *et al.* 2015), the shear contact stiffness is assumed to be proportional to the normal contact stiffness.

The aging viscoelastic model is based on Bažant and Prasannan (1989a)'s solidification theory. According to the model, aging is due to cement hydration (formation of new calcium hydrates) and, probably, due to gradual formation of bonds as a result of polymerization. The model considers the viscoelastic strain, ε^v , a consequence of the volume fraction growth associated to the viscoelastic behaviour, $v(t)$, and the viscous strain, ε^f , a consequence of the volume fraction growth associated with the viscous behaviour, $h(t)$, and are mathematically formulated in its early formulation in (Bažant 1977) and further developed in (Bažant and Prasannan 1989b).

Considering only the stress-dependent contact normal displacement, $x_n^F(t)$, as a function of contact normal force, $F_n(t')$, applied at the age t' , a constitutive relation can be obtained as follows,

$$x_n^F(t) = x_n^{inst}(t) + x_n^{creep}(t) = \int_0^t J_n(t, t') dF_n(t') \quad (5.79)$$

where $x_n^{inst}(t)$ is the normal contact instantaneous displacement, $x_n^{creep}(t, t')$ is the normal contact creep displacement and $J_n(t, t')$ is the normal compliance function (normal contact displacement at the time t due to a constant unit normal force, $F_n(t')$, applied at time t').

Similarly to the stress-strain-based solidification theory and considering a discretization of time, t_i , each displacement increment is related to a type of deformation. The

5.5. CONTACT CONSTITUTIVE MODELS FOR THE ANALYSIS OF
LONG-TERM BEHAVIOUR OF CONCRETE

instantaneous displacement increment is given by $\Delta x_n^{inst}(t_i) = q_{1,n} \Delta F_n(t_i)$, where $q_{1,n}$ is a material parameter defined for the normal direction of the contact plane (equivalent to q_1 in the original formulation).

The normal contact creep displacement is given by the sum of the viscoelastic contact displacement increment, $\Delta x_n^v(t_i)$, and the viscous contact displacement increment, $\Delta x_n^f(t_i)$, which are modeled, respectively by,

$$\Delta x_n^v(t_i) = \dot{\gamma}_n(t) / v_n(t_i) = \int_0^t \left(\dot{\Phi}_n(t_i - t') dF_n(t') \right) / v_n(t_i) \quad (5.80)$$

$$\Delta x_n^f(t_i) = \int_0^t \left(\dot{\Psi}_n(t_i - t') dF_n(t') \right) / h_n(t_i) \quad (5.81)$$

where $\Phi_n(t_i - t')$ is the non-aging microscopic compliance of the binder, which can be represented analytically by,

$$\Phi_n(t - t') = q_{2,n} \ln \left(1 + \left(\frac{(t - t')}{\lambda_0} \right) \right), \quad n = 0.1, \lambda_0 = 1 \text{ day} \quad (5.82)$$

and rheologically by a non-aging Kelvin chain of N elements, represented by Dirichlet series,

$$\Phi_n(t - t') = \frac{1}{k_{0,n}} + \sum_{\mu=1}^N \frac{1}{k_{\mu,n}} \left(1 - e^{-(t-t')/\tau_{\mu,n}} \right), \quad \tau_{\mu,n} = \frac{\eta_{\mu,n}}{k_{\mu,n}} \quad (5.83)$$

where $\eta_{\mu,n}$ are the normal viscosities of the Kelvin chains, $k_{\mu,n}$ are the normal stiffness of the Kelvin chain, defined for a predefined retardation times, $\tau_{\mu,n}$. Bažant and Xi recommend the use of the continuous retardation spectra, $L_n(\tau_{\mu,n})$, and a logarithmic discretization of retardation times for the determination of the $\frac{1}{k_{\mu,n}}$ coefficients (n is, as previously stated, equal to 0.1) (Bažant and Xi 1995). The additional term $\frac{1}{k_{0,n}}$ is related to the instantaneous tail of the continuous retardation spectra, L_n (Bažant *et al.* 2004).

In Equation 5.84, $\Psi_n(t_i - t')$ is the microscopic compliance function for incremental normal displacements of non-aging material related to the viscous deformation and with the development law, $h_n(t) = \eta_n(t) / \eta_{0,n}$, where $\eta(t)$ is the effective macroscopic viscosity given by $\eta_n(t) = t / q_{4,n}$.

The aging is given by the variable $v_n(t)$ defined by,

$$v_n(t) = \left(\frac{1}{t}\right)^m + \frac{q_{3,n}}{q_{2,n}} \quad (5.84)$$

which represents the development of volume fraction of the binder that contributes to the viscoelastic deformation ($q_{2,n}$ and $q_{3,n}$ are material parameters defined in the normal direction of the contact plane and m is also a material constant which can be considered equal to 0.5 (Bažant and Prasanna 1989a)).

Considering a time discretization, t_i , that the stress is constant in a given timestep (t_i, t_{i+1}), and that it varies at the beginning of the timestep, the total increment of viscoelastic microstrain, given by the sum of each Kelvin unit, $\Delta\gamma_n = \sum_{\mu=1}^N (\gamma_{n,i+1} - \gamma_{n,i})$, can be written as,

$$\Delta\gamma_n = \sum_{\mu=0}^N \left(\frac{1 - \lambda_{\mu,n}}{k_{\mu,n}} \right) \Delta F_{n,i} + \Delta\gamma''_{n,i}, \quad \lambda_{\mu,n} = \frac{1 - e^{-\frac{\Delta t}{\tau_{\mu,n}}}}{\frac{\Delta t}{\tau_{\mu,n}}} \quad (5.85)$$

$$\Delta\gamma''_{n,i} = \sum_{\mu=0}^N \Delta\gamma''_{\mu,n} = \sum_{\mu=0}^N \left(\frac{F_{n,i}}{k_{\mu,n}} - \gamma_{\mu,n,i} \right) (1 - e^{-\Delta\gamma_{\mu,n}}) \quad (5.86)$$

For each timestep, the viscoelastic normal displacement increment, Δx_n^v , is given by Equation 5.87,

$$\Delta x_n^v = \frac{1}{v_n(t^*)} \Delta\gamma_n = \frac{1}{v_n(t^*)} \left[\sum_{\mu=0}^N \left(\frac{1 - \lambda_{\mu,n}}{k_{\mu,n}} \right) \Delta F_n + \Delta\gamma''_n \right] \quad (5.87)$$

where $t^* = t' + [(t_{i+1} - t')(t_i - t')]^{1/2}$, which represents the middle of the timestep in the logarithmic time scale.

Taking into account the flow strain increment, $\Delta x_n^f = q_{4,n} F_n \Delta t / t^*$, and the increment of instantaneous elastic strain, $q_1 \Delta F_n$, one can write the quasi-elastic incremental contact normal force, F_n ,

$$\Delta F_{n,i} = k_n'' (\Delta x_n(t_i) - \Delta x_{n,i}'') \quad (5.88)$$

in which,

$$\frac{1}{k_n''} = q_{1,n} + \frac{1}{v_n(t_i^*)} \sum_{\mu=0}^N \left(\frac{1 - \lambda_{\mu,n}}{k_{\mu,n}} \right), \quad \Delta x_{n,i}'' = \frac{\Delta\gamma''_{n,i}}{v_n(t_i^*)} + \frac{q_{4,n} F_{n,i}(t_i^*) \Delta t_i}{t_i^*} \quad (5.89)$$

The shear contact behaviour follows the same formulation as the one previously described for the normal direction,

$$\Delta \mathbf{F}_{s,i} = k_s'' \left(\Delta \mathbf{x}_s(t_i) - \Delta \mathbf{x}_{s,i}'' \right) \quad (5.90)$$

in which,

$$\frac{1}{k_s''} = q_{1,s} + \frac{1}{v_s(t_i^*)} \sum_{\mu=0}^N \left(\frac{1 - \lambda_{\mu,s}}{k_{\mu,s}} \right), \quad \Delta \mathbf{x}_{s,i}'' = \frac{\Delta \gamma_{s,i}''}{v_s(t_i^*)} + \frac{q_{4,s} \mathbf{F}_{s,i}(t_i^*) \Delta t_i}{t_i^*} \quad (5.91)$$

5.5.3 Proposed calibration procedure for the macro-micro relationship of elastic and aging viscoelastic properties

Considering the behaviour at the contact to be similar to a beam, a general equivalence between contact micro properties and material's macro properties can be obtained. The height of the equivalent beam is determined by the minimum radius of the two particles in contact, R_{min} , and the beam length is defined as the distance between particle centres, d . In two dimensional analysis, t^{disk} defines the thickness of the disks.

For elastic materials, the macroscopic behaviour is defined by the normal and shear contact stiffnesses, k_n and k_s , respectively. Therefore, the equivalence for the definition of the micro-parameters of the aggregate contact is given by,

$$k_{n,agg} = \alpha_{n,agg} \frac{2R_{min}t}{d} E_{agg}^{macro}, \quad k_{s,agg} = \alpha_{s,agg} k_{n,agg} \quad (5.92)$$

where the $\alpha_{n,agg}$ and $\alpha_{s,agg}$ are two calibration parameters.

Following the solidification theory, the macroscopic response of the material, defined by the macro-creep compliance, J^{macro} , is dependent of the parameters q_i^{macro} (i=1, 2, 3 and 4) which are amplifiers of the instantaneous, viscoelastic, viscous and flow strains of the aging viscoelastic material. The aging viscoelastic micro-parameters at the contact point are defined as $q_{n,i}^{micro}$ for the normal direction and $q_{s,i}^{micro}$ for the shear direction (i=1, 2, 3 and 4). For the calibration of the micro-parameters, it is proposed that the micro-creep compliance in the normal direction, J_n^{micro} , is proportional to the macro-creep compliance, J^{macro} , and that the shear behaviour, described by the micro-creep compliance in the shear direction, J_s^{micro} , is proportional to the normal behaviour,

$$J_n^{micro} = \frac{1}{\alpha_n} \frac{2R_{min}t^{disk}}{d} J^{macro}, \quad J_s^{micro} = \frac{1}{\alpha_s} J_n^{micro} = \frac{1}{\alpha_s \alpha_n} \frac{2R_{min}t^{disk}}{d} J^{macro} \quad (5.93)$$

Considering this simplification it is possible to define only two calibration parameters, $\alpha_{n,mortar}$ and $\alpha_{s,mortar}$, for each type of material.

Based on the work of Wang and Tonon (2009), the elastic micro-parameters, which yield the macro properties of the aggregate, Poisson's ratio, $\nu_{agg}^{DEM}(\alpha_{s,agg})$, and modulus of elasticity, $E_{agg}^{DEM}(t, \alpha_{s,agg})$, were obtained adjusting the results of a parametric study to the following expressions, using the calibration procedure proposed by (Kazerani and Zhao 2010),

$$\nu_{agg}^{DEM}(\alpha_{s,agg}) = A_{agg} \left[\frac{a_{1,agg} - a_{2,agg} (\alpha_{s,agg} - \alpha_{s,agg,0})}{1 + b_{1,agg} (\alpha_{s,agg} - \alpha_{s,agg,0})} \right] \quad (5.94)$$

$$E_{agg}^{DEM}(\alpha_{s,agg}) = c_{0,agg} + c_{1,agg} \alpha_{n,agg} \quad (5.95)$$

where A_{agg} , $a_{1,agg}$, $a_{2,agg}$, $b_{1,agg}$, and $\alpha_{s,agg,0}$ are the calibration coefficients to fit the parametric study for the determination the Poisson's ratio of the aggregates using the calibration parameter, $\alpha_{s,agg}$, $c_{0,agg}$ and $c_{1,agg}$ are the calibration coefficients to fit the parametric study for the determination the modulus of elasticity of the aggregates using the calibration parameter, $\alpha_{n,agg}$.

For the study of delayed deformability properties over time, namely the Poisson's ratio, $\nu_{mortar}^{DEM}(t, \alpha_{s,mortar})$, and the creep compliance, $J_{mortar}^{DEM}(t, \alpha_{n,mortar})$, it is proposed an adaptation of the former expressions for the development of the Poisson's ratio over time as a function of the contact stiffness ratio (equivalent to the calibration parameter, α_s , Equation 5.96) and for the inverse of the creep compliance as a function of the normal stiffness (equivalent to the calibration parameter, α_n , Equation 5.97). These equations were developed to obtain the optimum calibration parameters for the entire range of time under analysis, t , and are expressed by,

$$\nu_{mortar}^{DEM}(t, \alpha_{s,mortar}) = A_{mortar} \left[\frac{a_{1,mortar} - a_{2,mortar} (\alpha_{s,mortar} - \alpha_{s,mortar,0})}{1 + b_{1,mortar} (\alpha_{s,mortar} - \alpha_{s,mortar,0}) \log t} \right] \quad (5.96)$$

$$\frac{1}{J_{mortar}^{DEM}}(t, \alpha_{n,mortar}) = c_{0,mortar} + c_{1,mortar}\alpha_{n,mortar} + c_{2,mortar}\frac{1}{\log t} + c_{3,mortar}\frac{\alpha_{n,mortar}}{\log t} \quad (5.97)$$

where A_{mortar} , $a_{1,mortar}$, $a_{2,mortar}$, $b_{1,mortar}$, and $\alpha_{s,mortar,0}$ are the calibration coefficients to fit the parametric study for the determination the Poisson's ratio of the aggregates using the calibration parameter, $\alpha_{s,agg}$, $c_{0,mortar}$, $c_{1,mortar}$, $c_{2,mortar}$ and $c_{3,mortar}$ are the calibration coefficients to fit the parametric study for the determination the modulus of elasticity of the aggregates using the calibration parameter, $\alpha_{n,agg}$.

The proposed calibration procedure for the mortar's micro parameters can be described in the following steps, provided that the particle size remains the same:

1. For a given loading age, t' , and time under loading, $(t - t')$, run a parametric test, varying the calibration parameter α_s , maintaining the calibration parameter $\alpha_n = 1.0$;
2. Fit the DEM's Poisson's ratio to the proposed Eq. 5.96 using an optimization procedure to find the coefficients a_1 , a_2 , $\alpha_{s,0}$ and b_1 minimizing the square difference between the fit and the Poisson's ratio obtained from the parametric study;
3. Obtain the optimum calibration parameter, α_s^{opt} , using an optimization procedure that minimized the square difference between the fit and the Poisson's ratio, $\min\{(\nu - \nu^{DEM}(t, \alpha_s))^2\}$;
4. For the loading age, t' , and time under loading, $(t - t')$, run a parametric test, varying the calibration parameter α_n , maintaining the calibration parameter $\alpha_s = \alpha_s^{opt}$ constant;
5. Fit the DEM's creep compliance for all the times under loading $(t - t')$ to the proposed Eq. 5.97 using an optimization procedure to find the coefficients c_0 , c_1 and c_2 minimizing the square difference between the fit and the creep compliance at all times under loading obtained from the parametric study;
6. Obtain the optimum calibration parameter, α_n^{opt} , minimizing the square difference between the fit and the creep compliance, $\min\{(1/J(t, t') - 1/J^{DEM}(t, \alpha_n))^2\}$.

5.5.4 Proposed fast numerical procedure for long-term analysis using DEM and validation of the aging viscoelastic contact model

The numerical stability of explicit integration procedures rely on a maximum timestep value which can be very small. To simulate the creep behaviour of structural systems, such as rock or concrete, the total calculation time can be very long. Feng *et al.* (2003) proposed a numerical procedure for overcoming the need of a large number of steps based on equivalent incremental contact forces related to the expected creep deformation using a non-aging viscoelastic model, the Burger's model.

This fast numerical procedure for the long-term behaviour was adapted for cementitious materials and makes use of both the adaptive dynamic relaxation method, to obtain a fast equilibrium without overshooting, and the aging viscoelastic contact model. The procedure is divided into two main steps as shown in Figure 5.10. The first step uses the dynamic relaxation in order to converge to the static solution at a given age of concrete considering scaled masses and $\Delta t = 1.0$. In the second step, considering large time increments, ΔT , the equivalent incremental contact forces are computed based on the aging viscoelastic constitutive model. The large time increments are the real time increments associated with the age of concrete and can be chosen in order to have a fine or sparse time discretization.

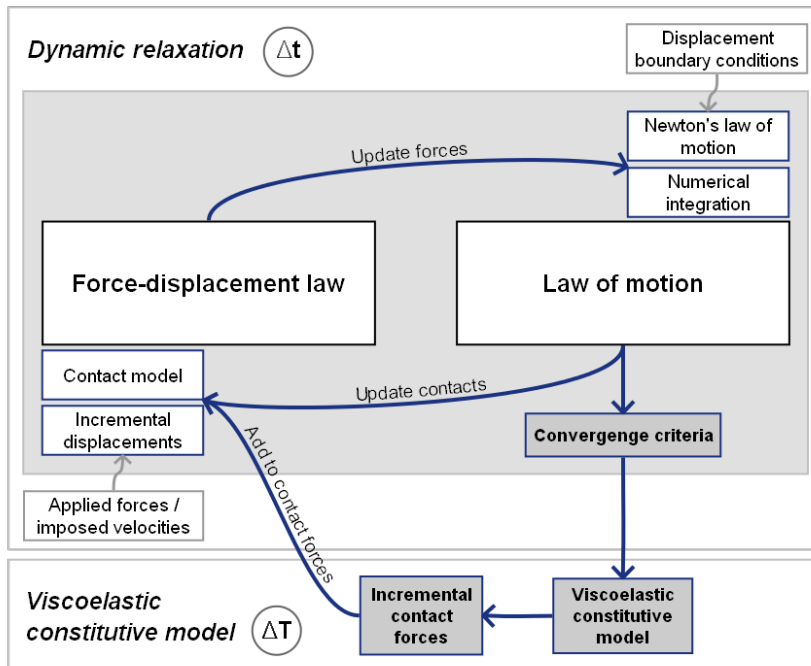


Figure 5.10: DEM cycle with the proposed numerical scheme for viscoelastic behaviour with incremental contact forces

5.5. CONTACT CONSTITUTIVE MODELS FOR THE ANALYSIS OF LONG-TERM BEHAVIOUR OF CONCRETE

For the simulation of a creep test, a loading is applied at the age of $T_1 = t'$, the initial real time, and the first step of the fast numerical procedure converges to the steady-state solution, through dynamic relaxation and scaled masses ($\Delta t = 1.0$) and considering the properties of the material at that age. The first displacement increment, $x_{n,elastic}(T_1 = t')$, is obtained using a DEM dynamic relaxation considering the time under loading equal to 0.01 days and its correspondent stiffness, $k_n(T_1 = t')$.

After convergence is obtained, the real time is incremented by ΔT_i , the incremental aging viscoelastic displacements, $\Delta x_{n,visco}(T_i)$ and $\Delta \mathbf{x}_{s,visco}(T_i)$, and the equivalent incremental contact forces, $\Delta F_n^{eq}(T_i)$ and $\Delta \mathbf{F}_s^{eq}(T_i)$, are obtained considering the aging viscoelastic model, which are added to the existing contact forces introducing an unbalanced state. The new steady-state solution for $T_2 = T_1 + \Delta T_1$ is again obtained by considering the pseudo-elastic normal and shear stiffnesses, $k_n''(T_i)$ and $k_s''(T_i)$ for that age and loading time,

$$\Delta F_n^{eq}(T_i) = \Delta x_{n,visco}(T_i)k_n''(T_i), \quad \Delta \mathbf{F}_s^{eq}(T_i) = \Delta \mathbf{x}_{s,visco}(T_i)k_s''(T_i) \quad (5.98)$$

Once the equilibrium is obtained for the timestep, T_i , a new real time increment is imposed, ΔT_i , the new incremental aging viscoelastic displacements, $\Delta x_{n,visco}(T_{i+1})$ and $\Delta \mathbf{x}_{s,visco}(T_{i+1})$, is calculated and the incremental contact forces, $\Delta F_n^{eq}(T_{i+1})$ and $\Delta \mathbf{F}_s^{eq}(T_{i+1})$, are added to each contact forces.

The Appendix C presents the structure of the fully-explicit and the numerical procedure algorithm developed in C++.

5.5.5 Validation of the aging viscoelastic contact model using the proposed fast numerical procedure

Figure 5.11 shows the particle assemblies used for the validation of the aging viscoelastic contact model and Table 5.2 presents the main parameters used in the analysis. It was considered that the contacts related to the applied force are time-dependent (grey dots in Figure 5.11) and the boundary wall contacts and the remaining contacts are kept elastic (black dots in Figure 5.11). For this type of model only the normal direction was validated, since the shear behaviour is assumed to be proportional to the normal behaviour.

Two types of analysis were done and compared with the analytical solution. The first analysis is based on the fully explicit DEM formulation and is divided in order to

Table 5.2: Parameters for the particle model validation

Model parameter	Aging viscoelastic model
R (m)	0.00048
q_1 (1/GPa)	0.007 *
q_2 (1/GPa)	0.108 *
q_3 (1/GPa)	0.044 *
q_4 (1/GPa)	0.014 *
N_{chains}	13
t' (days)	7.0
$t - t'$ (days)	10.0

* Fit to Granger's creep test results (§ 5.6.1)

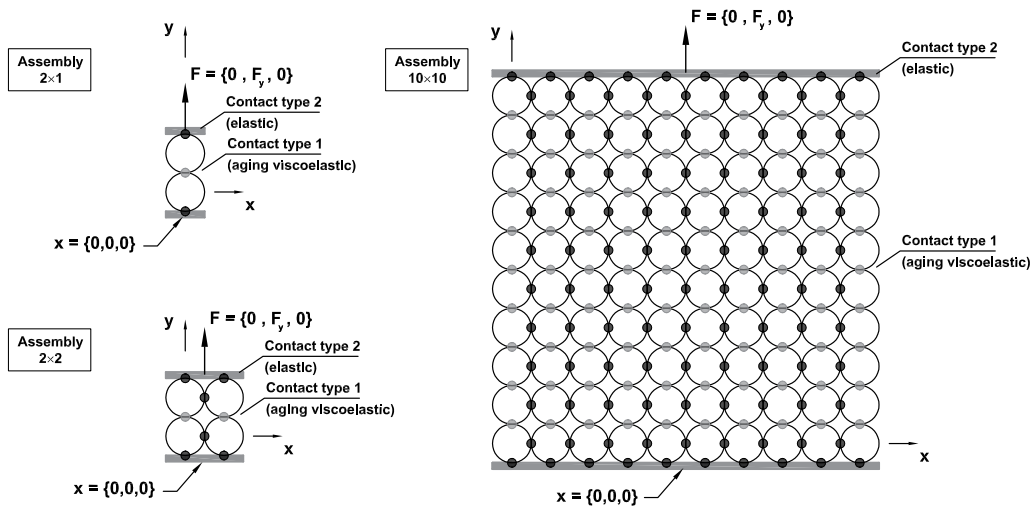


Figure 5.11: Assemblies for the validation of the aging viscoelastic models

calculate the static instantaneous deformation and the aging viscoelastic deformation for each timestep, set to the critical value for the structural system. For the delayed deformation, the real time is equal to the calculation time. The separation between the instantaneous and delayed deformation is needed to reach the equilibrium on every contact of the assembly and, therefore, accurately estimate the delayed deformation for the next timestep. Since the delayed behaviour is stress dependent, the contact model requires that the internal and external forces are equilibrated. If the original DEM formulation was used since the first timestep using the viscoelastic model (real time equal to the calculation time), an error would be made since the forces on the contacts would not be balanced with the applied forces. Recently, Abdellatef *et al.* (2015) presented similar results of numerical creep tests using lattice models considering an aging viscoelastic model.

The second analysis is based on the proposed fast numerical procedure for the long-term behaviour of concrete, previously described. With this proposal, for each real timestep the

5.5. CONTACT CONSTITUTIVE MODELS FOR THE ANALYSIS OF LONG-TERM BEHAVIOUR OF CONCRETE

equilibrium is obtained using dynamic relaxation, ensuring that the delayed strains and forces are accurately calculated, during the period of analysis. Three analysis were done considering different magnitude of large timesteps, ΔT . The period of analysis was divided into 10, 5 and 2 large timesteps (N), equally spaced in the logarithmic scale. The results show that the fast numerical procedure is suited for both short and large discretization of time. At each real timestep, T_i , the contact forces are accurately calculated in order to obtain the aging-viscoelastic response.

The results of the fast numerical procedure match the fully explicit DEM solution using the aging viscoelastic contact model and real masses ($\Delta t = \Delta t_{critical}$) and the analytical solution throughout the entire analysis. Using the fully explicit DEM formulation, the numerical critical timestep and the real timestep (age of concrete) is considered the same and, therefore, it is not possible to use the scaled masses. The analysis of the assembly of 2×1 particles has a computational cost of around 15 minutes, since the timestep is very small, and the proposed fast numerical procedure takes only 15 seconds, using 10 large timesteps over the loading time of 10 days.

Table 5.4 presents the description of the three types of particle assemblies, including number of particles, $N_{particles}$, number of contacts, $N_{contacts}$, maximum radius, R_{max} , ratio between minimum and maximum particle radius, $\frac{R_{max}}{R_{min}}$, and the normal and shear contact viscoelastic properties, $q_{i,n}$ and $q_{i,s}$ ($i=1,2,3$ and 4).

Figure 5.12 shows the validation results of the proposed fast numerical procedure for three types of particle assemblies (2×1 particle, 2×2 particles and 10×10 particles). The results were obtained considering the creep compliance of a mortar loaded at the age of 7 days and fitted to experimental tests (Ward *et al.* 1969). The load duration, $t - t'$, was 10 days.

Figure 5.13 presents the normal contact force development over time for the two type of approaches. While the original DEM formulation using aging viscoelastic contact model maintains the normal contact forces constant, the proposed numerical procedure only insures that the contact forces are constant once the particle assembly is in equilibrium with the applied force, after the dynamic relaxation of the incremental viscoelastic contact forces.

Figure 5.14 shows the additional validation results of the fully-explicit solution and the proposed fast numerical procedure for a two particle-one contact system against the analytical creep compliance obtained from the fit to Ward *et al.* (1969) experimental tests

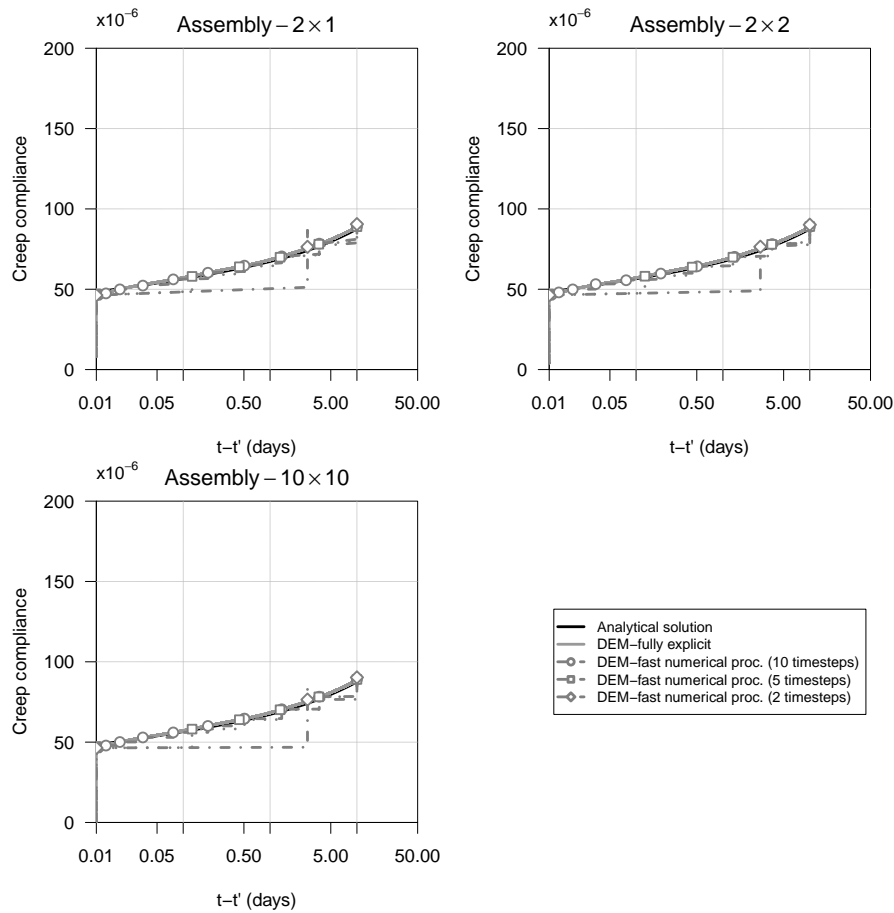


Figure 5.12: Comparison between the analytical solution of the creep compliance based on the solidification theory, the numerical solution obtained from the fully explicit DEM formulation with damping and the numerical solution using the proposed fast numerical procedure and three different time discretizations

Table 5.3: Comparison of performance results of the original DEM formulation without damping, with local non-viscous damping and using the adaptive dynamic relaxation method (ADR) and of the numerical incremental procedure for creep model applied to the solidification theory

Assembly: 2×1 particles, 1 contact		
	Adaptive dynamic relaxation (ADR)	Proposed numerical procedure
Total loading time (days)	10	10
Time step (days)	5.5×10^{-6}	1
Total steps	1815475	304^2
Total calculation time (min.)	13.5	0.25

¹ The numerical procedure divides the loading time into 10 large time steps, ΔT , equally spaced in the logarithmic scale and converges to the solution using ADR and scaled masses ($\Delta t=1$ day).

² Total number of steps divided into 10 large timesteps, ΔT .

5.5. CONTACT CONSTITUTIVE MODELS FOR THE ANALYSIS OF LONG-TERM BEHAVIOUR OF CONCRETE

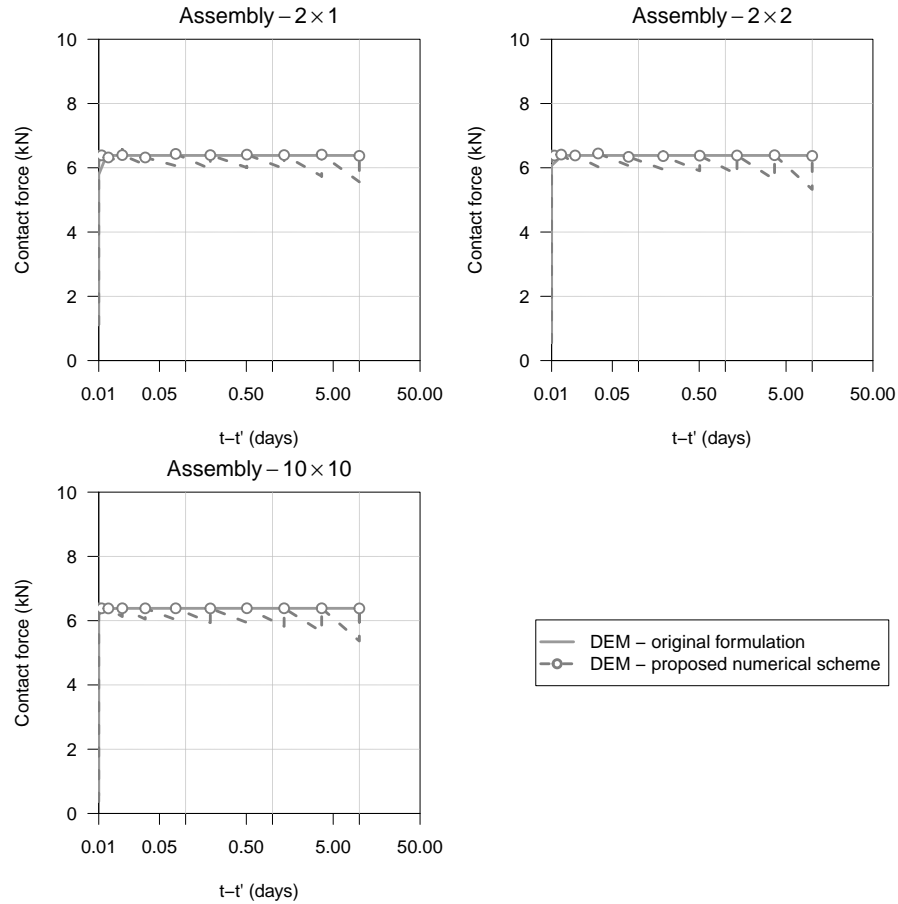


Figure 5.13: Contact force development for the numerical solution obtained from the original DEM formulation using the adaptive dynamic relaxation method (ADR) for the instantaneous deformation and the aging viscoelastic constitutive model for the delayed deformation and the numerical solution using the numerical incremental procedure for creep model applied to the solidification theory

(black lines in Figure 5.14). The results show an excellent agreement is obtained between both numerical responses and the analytical creep compliance solution for several loading ages, for the unloading case and for several fast procedure time intervals discretization (N).

In order to further validate the proposed fast numerical procedure for more complex assemblies, its results were compared with the fully-explicit DEM numerical solution for a 10×10 regular assembly with a hexagonal arrangement and for a large random assembly (1280 particles). In the random particle assembly the external forces are applied through a rigid wall (Figure 5.15).

As shown in Figure 5.15 the fast numerical procedure results closely match the fully-explicit DEM solution adopting real masses ($\Delta t = \Delta t_{critical}$) throughout the entire analysis

for several loading ages and different fast procedure time intervals discretization.

Table 5.5 presents the number of steps, N_{steps} , and calculation times, $T_{calc.}$, for each numerical analysis that was carried out. The calculation times presented in Table 5.5 clearly show that when compared with the fully-explicit DEM solution the proposed fast numerical procedure significantly reduces the computational time.

The presented results show that the fast numerical procedure is suited for both short and large discretization of time. At each real timestep, T_i , the contact forces are accurately calculated in order to obtain the aging-viscoelastic response at the given age for any loading history. The fast procedure computational time reduction is especially relevant for detailed particle DEM base models when applied to long-term analysis. The long term concrete analysis that is presented in the next section is only possible using the proposed fast procedure.

Table 5.4: Description of the three types of particle assemblies and contact properties

Assembly	Particle arrangement	$N_{particles}$ $N_{contacts}$	R_{max} (mm)	$\frac{R_{min}}{R_{max}}$	Contact properties*		
					$q_i, (i=1,2,3,4)$ ($1 \times 10^{-6}/\text{MPa}$)	α_n	α_s
2×1	Regular	2 1	0.48	1.0	$q_1 = 66.6$ $q_2 = 108.1$ $q_3 = 44.2$ $q_4 = 14.3$	1.0	0.5
10×10	Hexagonal	100 261	0.48	1.0	$q_1 = 66.6$ $q_2 = 108.1$ $q_3 = 44.2$ $q_4 = 14.3$	1.0	0.5
Random	Irregular	1280 3730	0.48	$\frac{2}{3}$	$q_1 = 66.6$ $q_2 = 108.1$ $q_3 = 44.2$ $q_4 = 14.3$	1.0	0.5

*Aging viscoelastic contact properties were obtained from a fit to the experimental results of mortar samples as described in this work

5.5. CONTACT CONSTITUTIVE MODELS FOR THE ANALYSIS OF LONG-TERM BEHAVIOUR OF CONCRETE

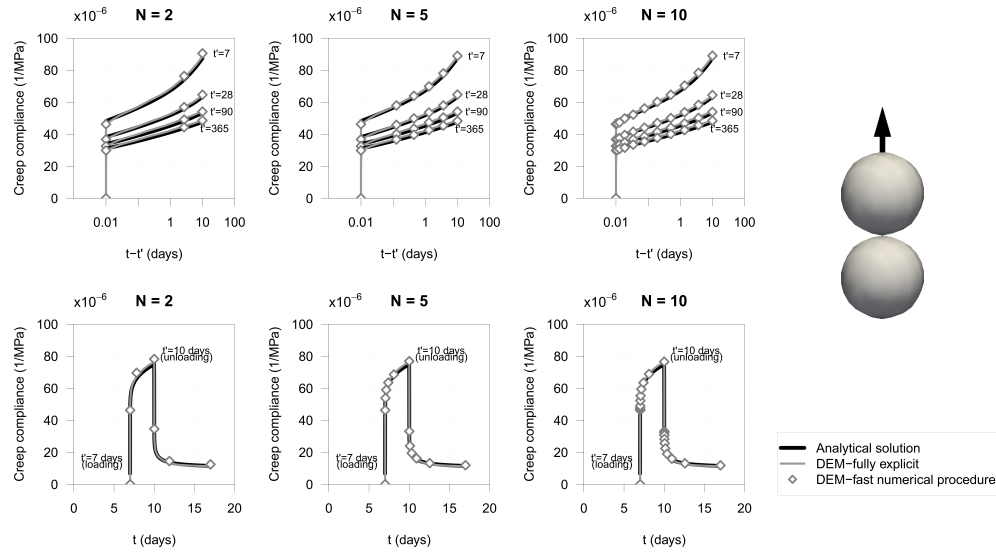


Figure 5.14: Comparison between the solidification theory analytical solution, the fully explicit DEM formulation with ADR and the proposed fast numerical procedure considering three time internals ($N=2, 5$ and 10) for a two particle, one contact assembly

Table 5.5: Comparison of calculation times for three types of particle assemblies for both fully explicit DEM and the proposed fast numerical procedure

Assembly	$N_{particles}$	t' (days)	$t - t'$ (days)	Fully-explicit			Fast numerical proc.		
				Δt_{crit} (days)	N_{steps}	T_{calc} (sec.)	N	N_{steps}	T_{calc} (sec.)
2×1	2	7	10	5.5×10^{-6}	1815475	147	2	70	1
							5	116	1
							10	142	1
10×10 (hexagonal arrangement)	100	7	10	3.9×10^{-6}	2567470	965	2	538	2
							5	1033	6
							10	1481	8
Random	1280	7	10	2.1×10^{-6}	4842672	63378	2	1752	15
							5	2999	17
							10	4443	27

CHAPTER 5. NUMERICAL MODELLING OF THE CONCRETE STRUCTURAL PROPERTIES USING PARTICLE MODELS

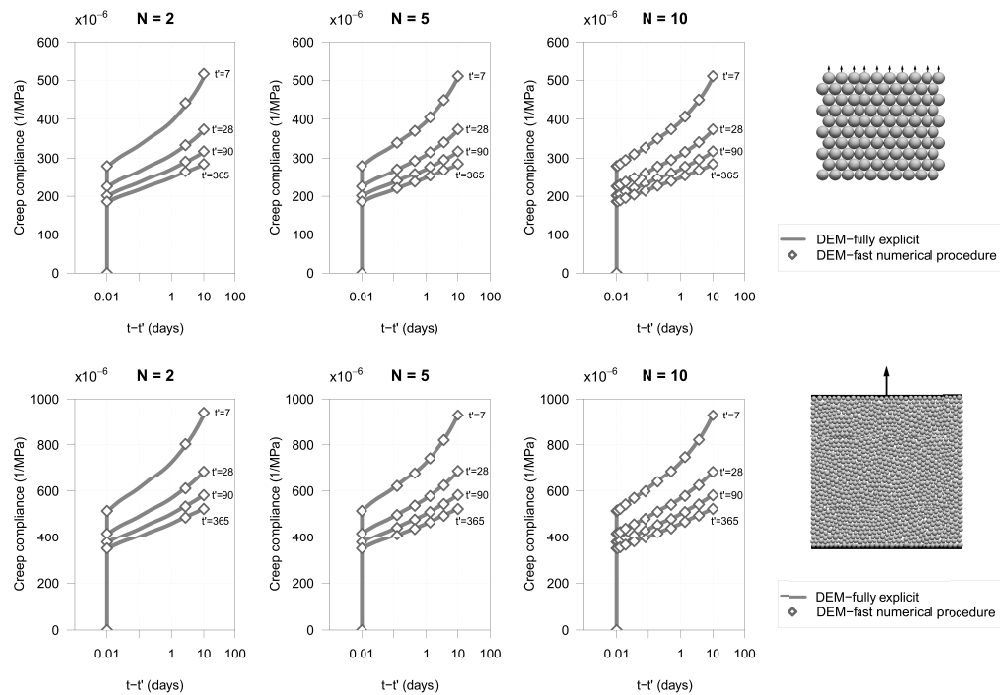


Figure 5.15: Comparison between the solidification theory analytical solution, the fully explicit DEM formulation with ADR and the proposed fast numerical procedure considering three time internals ($N=2, 5$ and 10) for 10×10 particle assembly with hexagonal arrangement and for a large random assembly

5.6 Analysis of the long-term behaviour of concrete considering its mesostructure

5.6.1 Mortar, aggregate and concrete test results and fit to B3 model

B3 model, proposed by Bažant and Baweja (1995a) and supported by the solidification theory (Bažant and Prasannan 1989a), describes the basic creep compliance, $J(t, t')$, as the sum of the asymptotic elastic strains due to unit stress, q_1 and a linear combination of material parameters, q_2 , q_3 and q_4 , and time-dependent variables,

$$J(t, t') = q_1 + q_2 Q(t, t') + q_3 \ln [1 + (t - t')^n] + q_4 \ln \left(\frac{t}{t'} \right) \quad (5.99)$$

where t is time since casting, t' is age of loading and $Q(t, t')$ is a binomial integral with no analytical expression. The expressions for the approximated solution of $Q(t, t')$ can be obtained in (Bažant and Prasannan 1989a). In this study only basic creep will be considered.

In order to validate the use of detailed DEM particle models for the prediction of long-term behaviour of concrete considering its mesostructure, the mortar and concrete creep test results of Ward *et al.* (1969) were used. These results allow the comparison between the development of concrete and mortar basic creep strains. The basic creep tests were performed at the age of 7 days and considering 76 mm-diameter cylinders loaded with an uniaxial stress of 30% of the compressive strength of the material.

Table 5.6 presents the main properties of the mortar (mortar M6), the aggregates and the concrete produced with those components (concrete C4). The volume of aggregate, V_{agg} , is taken as the total aggregate, considered as the sum of the fine, $V_{fine\ agg}$, and coarse aggregate, $V_{coarse\ agg}$, and is calculated from the available data of the ratio of sand content to gravel content, (s/g) , given by weight. The coarse and fine aggregate unit weight were considered to be 2650 and 2600 kg/m³, respectively. The compressive strength, f_c , and modulus of elasticity, E_c , of each material at the age of 7 days are also presented in Table 5.6.

The best fit parameters, q_1 , q_2 , q_3 and q_4 , related to the mortar and concrete creep test results were obtained using an optimization procedure based on a genetic algorithm (GA), following the methodology proposed by Serra *et al.* (2016a). The obtained parameters minimize the sum of the square difference between Ward's experimental results, $J_{exp}(t, t')$,

CHAPTER 5. NUMERICAL MODELLING OF THE CONCRETE STRUCTURAL PROPERTIES USING PARTICLE MODELS

Table 5.6: Properties and composition of the aggregate, the mortar and of the concrete

Material	f_c (MPa)	E_c (GPa)	V_{agg}	$\left(\frac{s}{g}\right)^{mass}$	$\left(\frac{s}{g}\right)^{volume}$	$V_{coarse\ agg.}$	V_{mortar}
Aggregate	-*	70.0**	1.00	-	-	1.00	-
Mortar M6	40.0***	18.8***	-	-	-	-	1.00
Concrete C4	34.1***	24.2***	0.69	0.78	0.80	0.38	0.62

*The compressive strength of the aggregate is not available
 **The modulus of elasticity was obtained from Ward's work
 ***The mechanical properties of the mortar and of the concrete were obtained for the age of 7 days

and the B3 model creep compliance, $J_{B3}(t, t', q_1, q_2, q_3, q_4)$. Table 5.7 presents the obtained parameters and the macroscopic results of each aging material and the adjusted coefficient of determination, R_{adj}^2 . Figure 5.16 shows the fit of the B3 model to the test results of mortar M6 and of concrete C4. The experimental results show that the stiff aggregates restrain the development of the mortar's creep strains and contributes to higher modulus of elasticity and lower creep rate.

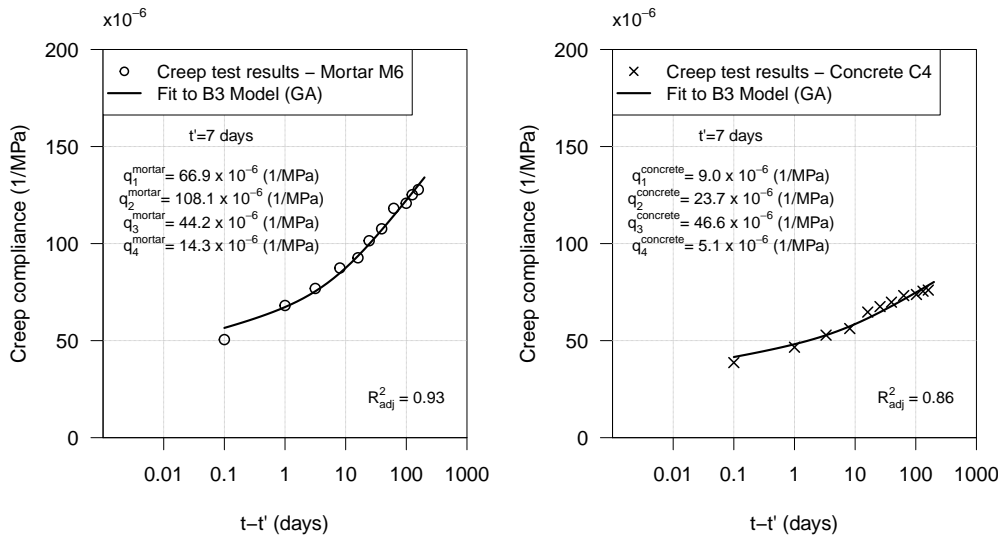


Figure 5.16: Fit of B3 model to Ward's creep test results of mortar and concrete using genetic algorithm (GA) (Ward *et al.* 1969)

Table 5.7: Parameters of B3 model fit to Ward's creep test results of mortar and concrete using genetic algorithm (GA)

Material	q_1 (1×10^{-6} /MPa)	q_2 (1×10^{-6} /MPa)	q_3 (1×10^{-6} /MPa)	q_4 (1×10^{-6} /MPa)	R_{adj}^2
Mortar M6	66.6	108.1	44.2	14.3	0.93
Concrete C4	9.0	23.7	46.6	5.1	0.86

5.6.2 Modelling the instantaneous behaviour of the aggregates and the long-term behaviour of the mortar

In order to model the composite effect of concrete, first it is necessary to calibrate the micro-parameters related to the individual behaviour of the aggregates and the mortar.

The calibration procedure was done using a 76 mm (A) square particle assembly of mortar and a 10 mm (A) square particle assembly of aggregate. These dimensions were chosen to match the concrete specimen and the largest aggregate, respectively. The size of the particles used for the calibration of the mortar's and aggregate's properties calibration has to take into account the concrete's mesostructure. It should be small enough to represent the contribution of the smallest aggregate in the concrete behaviour maintaining a reasonable computational cost. The maximum particle radius was considered to be one fifth of the minimum size of the coarse sand, ϕ_{min}^{agg} ($R_{max} = \phi_{min}^{agg}/5 = 2.4/5 = 0.48$ mm). The ratio between the minimum and the maximum particle radius, R_{min} and R_{max} , was considered to be two thirds ($R_{min} = 2/3R_{max} = 0.32$ mm), in order to obtain a compact assembly.

Figure 5.17 shows the results of the two step calibration procedure of the micro-parameters of aging viscoelastic behaviour of the mortar, $\alpha_{s,mortar}$ and $\alpha_{n,mortar}$, at a loading age of 7 days for a loading time of 365 days.

In Figure 5.17 the first two plots (top line) refer to the parametric study for different times under loading, $t - t'$, concerning the stiffness of the contact in the shear direction controlled by the parameter, α_s , and the determination of its optimum value, α_s^{opt} , to fit the mortar's Poisson's ratio of 0.2. The two last plots (bottom line) show the influence of the contact stiffness in the normal direction, defined by α_n , on the axial response over time, $t - t'$, and the fit of α_n^{opt} to the analytical values. As previously described, the fit to the macroscopic properties was done considering a minimization procedure that averages the deviations between the results of the model and the analytical values over the full loading time.

With the Equations 5.94, 5.95, 5.96 and 5.97 it is possible to fit the calibration parameters, α_n and α_s , to obtain the long-term properties of the material, for any particle dimensions and size of the specimen. Table 5.8 shows the optimum calibration parameters, α_n^{opt} and α_s^{opt} that yield the aging viscoelastic behaviour of mortar and the elastic behaviour of the aggregate.

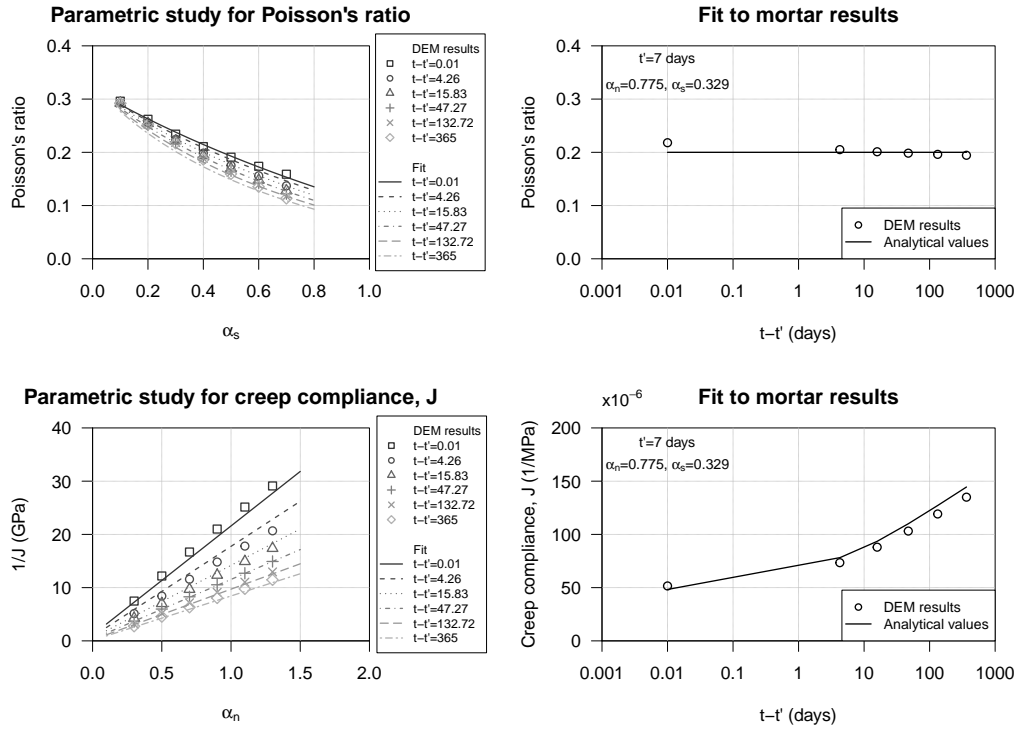


Figure 5.17: Results of the calibration procedure of the $\alpha_{n,mortar}$ and $\alpha_{s,mortar}$ for a loading age of 7 days

Table 5.8: Optimum parameters α_n^{opt} and α_s^{opt} of the mortar and the aggregate

Material	t' (days)	$t-t'$ (days)	$E_{eff}^{M6}(t, t')$ (GPa)	ν	α_s^{opt}	α_n^{opt}	$E_{eff}^{DEM}(t, t')$ (GPa)	ν^{DEM}
Mortar M6	7	0.01	20.7	0.20	0.329	0.775	21.0	0.20
		4.3	12.8				12.6	0.20
		15.8	10.7				10.5	0.20
		47.3	9.1				9.0	0.20
		132.7	7.9				7.8	0.20
		365.0	6.9				6.9	0.20
Mortar M6	28	0.01	26.1	0.20	0.317	0.770	26.1	0.21
		4.3	17.2				17.3	0.20
		15.8	14.9				15.0	0.20
		47.3	12.7				12.8	0.20
		132.7	10.8				10.8	0.20
		365	9.2				9.2	0.20
Mortar M6	90	0.01	29.5	0.20	0.319	0.766	29.4	0.21
		4.3	20.0				20.2	0.20
		15.8	18.0				18.1	0.20
		47.3	15.9				16.0	0.20
		132.7	13.7				13.6	0.20
		365	11.6				11.5	0.20
Mortar M6	365	0.01	32.2	0.20	0.318	0.764	31.9	0.21
		4.3	22.2				22.1	0.20
		15.8	20.3				20.4	0.20
		47.3	18.7				18.8	0.20
		132.7	16.9				16.8	0.20
		365	14.7				14.8	0.20
Aggregate	-	-	70.0	0.15	0.449	0.678	70.0	0.15

5.6.3 Modelling the long-term behaviour of the concrete considering the effect of the interfacial transition zone (ITZ)

The mesoscale models are particularly relevant for the study of different types of concrete deterioration since the aggregate structure of concrete and the interfacial transition zone (ITZ) are explicitly taken into account (Scrivener *et al.* 2004). The interfacial transition zone (ITZ) between the cement paste and the aggregates is known to have an important role in the mechanical properties of concrete. Reference values for the deformability of the ITZ have been considered in other numerical studies but limited to the instantaneous deformation:

- $E_{ITZ}/E_{mortar} = 8.8/11.0 = 0.8$ (Suchorzewski *et al.* 2017);
- $E_{ITZ}/E_{mortar} = 19.2/24.0 = 0.8$ (Sinaie *et al.* 2016);
- $E_{ITZ}/E_{mortar} = 16.0/19.0 = 0.8$ (Sun and Li 2015);
- $E_{ITZ}/E_{cement\ paste} = 0.6$ (Zheng and Zhou 2006; Lutz *et al.* 1997);
- $E_{ITZ}/E_{mortar} = 0.447 - 5.01/E_{mortar}$ (Ghebrab and Soroushian 2011).

The following procedure was used to obtain a prediction of the ITZ's creep compliance based on the fitted mortar creep compliance, $J_{mortar}(t, t')$ and concrete numerical results, $J_{concrete}^{DEM}(t, t')$. Firstly, it was considered that the contact between an aggregate particle and a mortar particle has a specific creep compliance, $J_{ITZ}(t, t')$, with the parameters, $q_{i,ITZ}$, is given by,

$$J_{ITZ}(t, t') = q_{1,ITZ} + q_{2,ITZ} Q(t, t') + q_{3,ITZ} \ln [1 + (t - t')^n] + q_{4,ITZ} \ln \left(\frac{t}{t'} \right) \quad (5.100)$$

Secondly, it was also considered that the parameters, $q_{i,ITZ}$, are proportional to the mortar's creep compliance parameters, $q_{i,mortar}$ ($i=1, 2, 3, 4$):

$$q_{i,ITZ} = K_{ITZ} q_{i,mortar} \quad i = 1, 2, 3, 4 \quad (5.101)$$

where the coefficients $K_{ITZ} q_{i,mortar}$ define the relationship between the ITZ's and the mortar's creep compliance.

The effect of the ITZ's creep compliance, $J_{ITZ}(t, t')$, defined by the coefficients $K_{ITZ} q_{i,mortar}$ was considered using a quadratic model for the prediction of the concrete's creep compliance, $J_{concrete}^{DEM}(t, t')$,

$$\begin{aligned}
 J_{concrete}^{DEM}(t, t') = & a_0 + \sum_{i=1}^4 a_i \times KITZ_{q_i} + \\
 & \sum_{i=1}^4 \sum_{j=1}^4 a_{ij} \times KITZ_{q_i} \times KITZ_{q_j} + \\
 & \sum_{i=1}^4 a_{it} \times KITZ_{q_i} \times \log(t - t' + 1) + \\
 & \sum_{i=1}^4 \sum_{j=1}^4 a_{ijt} \times KITZ_{q_i} \times KITZ_{q_j} \times \log(t - t' + 1)
 \end{aligned} \tag{5.102}$$

$i = 1, 2, 3, 4; j = 1, 2, 3, 4$

where a_i , a_{ij} , a_{it} and a_{ijt} are the coefficients to be fitted to the concrete numerical creep compliance results, $J_{concrete}^{DEM}(t, t')$.

Based on the Central Composite Design (CCD) method (Yoon 2007), several numerical tests ranging the values of $KITZ_{q_i}$ between 0.1 and 3.0 and for several loading ages, t' and loading times, t , were performed in order to obtain the best fit coefficients, a_i^{opt} , a_{ij}^{opt} , a_{it}^{opt} and a_{ijt}^{opt} . These coefficients define the relationship between the DEM particle model response and the coefficients, $KITZ_{q_i}$. The influence of each parameter on the concrete creep compliance for the age of 7 days and the fit of the proposed quadratic model are presented in Figure 5.18. It is possible to perceive that $KITZ_{q_2}$, $KITZ_{q_3}$ and $KITZ_{q_4}$ are the parameter that have the larger effect on the development of concrete creep strains.

Considering the fitted quadratic model, the optimum values of the coefficients, $KITZ_{q_i}^{opt}$, were obtained by minimizing the quadratic difference between the experimental concrete's creep compliance, J_{exp}^{C4} , and the DEM result, $J_{concrete}^{DEM}(t_j, t', KITZ_{q_i})$, obtained from Equation 5.102, using the optimum parameters,

$$\min \left[\sum_{j=1}^n \left(J_{exp}^{C4}(t_j) - J_{concrete}^{DEM}(t_j, t', KITZ_{q_i}) \right)^2 \right] \rightarrow KITZ_{q_i}^{opt}, i = 1, 2, 3, 4 \tag{5.103}$$

where n is the number of measured values over the loading time.

The results of the minimization of the quadratic model are presented in Table 5.9 which are the average $KITZ_{q_i}$ coefficients for several loading ages and for 5 random particle assemblies. These coefficients, especially due to the influence of $KITZ_{q_1}$ and $KITZ_{q_2}$ which are mostly related to the instantaneous deformation, increase the values of the ITZ's

5.6. ANALYSIS OF THE LONG-TERM BEHAVIOUR OF CONCRETE CONSIDERING ITS MESOSTRUCTURE

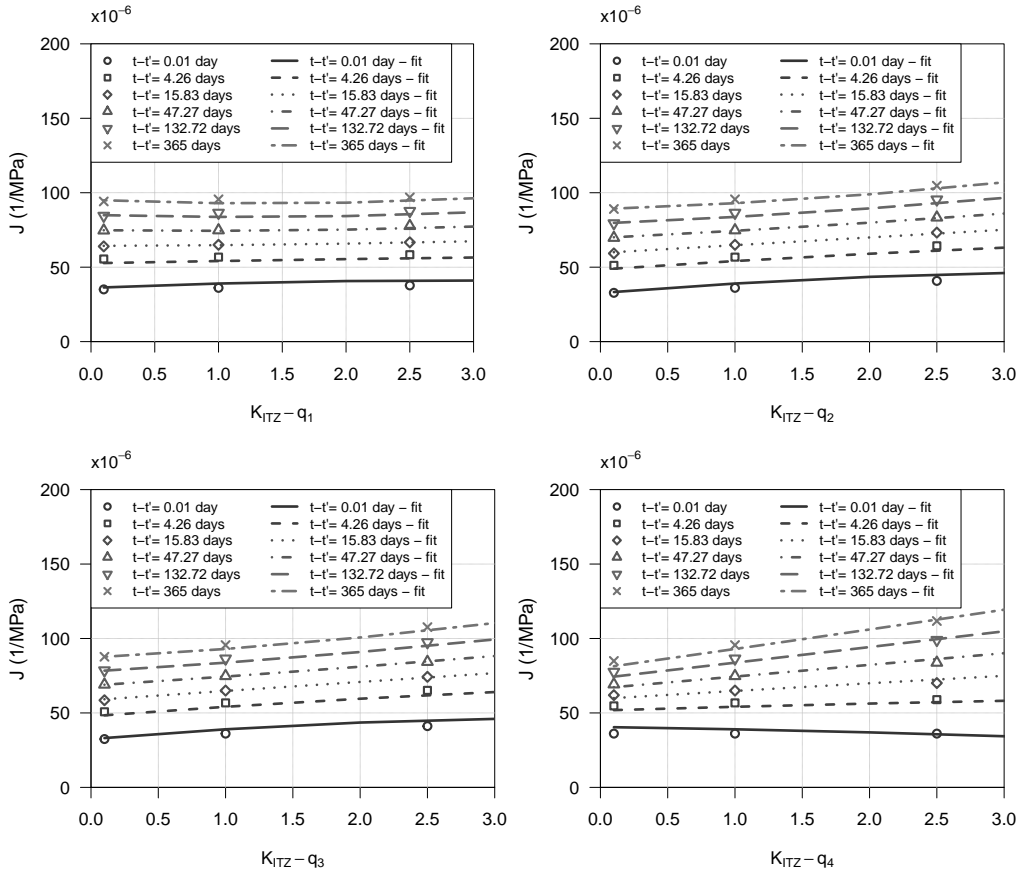


Figure 5.18: Results of the parametric study for the determination of the influence of ITZ on the behaviour of concrete

creep compliance when compared with the mortar's creep compliance.

Table 5.9: Optimum coefficients obtained from the minimization of the quadratic model to fit the concrete behaviour

Age (days)	$KITZ_{q1}^{opt}$	$KITZ_{q2}^{opt}$	$KITZ_{q3}^{opt}$	$KITZ_{q4}^{opt}$
7	2.2	0.9	0.6	0.6
28	2.9	2.1	1.1	0.2
90	3.5	2.0	2.1	0.1
365	3.0	2.2	2.8	1.2

Figure 5.19 shows an overview of the study of concrete's long-term behaviour using DEM particle model regarding the main components and its mesostructure and illustrates the refinement used in the concrete DEM particle model. The main variables of the long-term analysis of concrete using a DEM particle model are the size of the specimen, the boundary conditions, the maximum particle size, defined earlier as one fifth of the smallest coarse sand ($R_{max} = 0.48 \text{ mm}$), the arrangement of the coarse aggregates in the specimen,

the arrangement of the particle assembly inside each aggregate and of the mortar around the aggregate and the micro properties of each type of contact: MORTAR-MORTAR; MORTAR-AGG (ITZ); and, AGG-AGG. MORTAR represents a particle of mortar (grey circle in Figure 5.19) and AGG represents a particle of coarse aggregate (white circle in Figure 5.19).

This degree of refinement, both inside the aggregates, the ITZ and the mortar, allows for the study of local interactions between each component over time. A detailed DEM particle model including the particles representing the mortar allows for the contact constitutive models to be less complex when compared with other particle models that do not have the same degree of discretization (Alnaggar *et al.* 2013; Pan *et al.* 2017). The fact that the laws are simpler makes it easier to understand the obtained macroscopic behaviour and the influence that each individual contact behaviour has on the macroscopic response of concrete.

The particle model includes two rigid walls, one on the top of the specimen to transfer the load uniformly and another in the bottom to establish the zero displacement boundary condition. The specimen is laterally unconfined. The particle assembly simulates concrete cylinders with 76 mm in diameter and 228 mm of height. The axial and lateral strains were calculated based on the average relative displacements of the particles crossed by the horizontal and vertical dashed lines drawn inside the specimen in Figure 5.19. For elastic and viscoelastic behaviour the strain measurements can be considered independent of the adopted measurement length and location. Similar results would be obtained if the total specimen geometry was used. Given that fracture studies are also intended to be carried out in the near future, different deformability behaviours at the different locations can be identified with the adopted measurement procedure.

The optimum parameters of the mortar, α_n^{mortar} and α_s^{mortar} , were taken as the average values of the several loading ages.

The analysis included five randomly generated samples of concrete considering the same properties but with different random seeds and, therefore, different aggregate and particle arrangements. Table 5.10 presents the total aggregate volumes in the planar section used in the generation of the particle assembly, $V_{2.4-4.75}^{2D}$ and $V_{4.75-10.0}^{2D}$, the two-dimensional volume of mortar, V_{mortar}^{2D} and the average number of particles, $N_{particles}$, of five randomly generated concrete assemblies, divided into coarse aggregate particles and mortar particles (the fine aggregate).

5.6. ANALYSIS OF THE LONG-TERM BEHAVIOUR OF CONCRETE
CONSIDERING ITS MESOSTRUCTURE

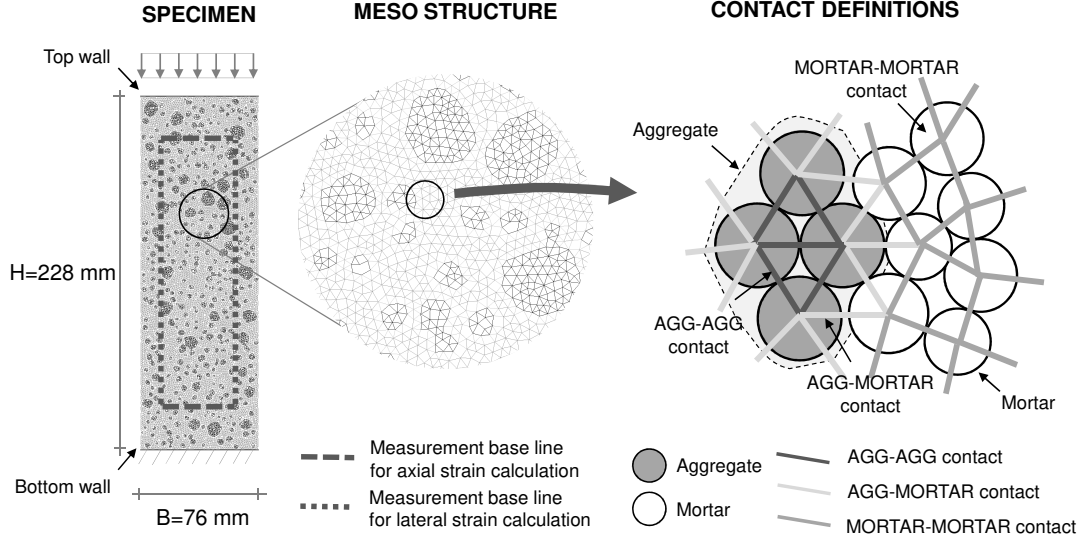


Figure 5.19: Description of the detailed particle model for the study of concrete's long-term behaviour

The mesostructure of concrete was represented using the procedures described earlier and considering the volumes of aggregate passing through a specific sieve. The volumes of aggregate were corrected to take into account the two-dimensional analysis. An equation, derived by Walraven (1980), defines the particle radius on a planar section using the probability, P_c , that an arbitrary point on the concrete body of the planar section is located in a circle with diameter, D , lower than a specific diameter, D_0 (defined as each sieve aperture),

$$\begin{aligned}
 P_c(D < D_0) = & P_k(1.455D_0^{0.5}D_{max}^{-0.5} - 0.50D_0^{2.0}D_{max}^{-2.0} + 0.036D_0^{4.0}D_{max}^{-4.0} \\
 & + 0.006D_0^{6.0}D_{max}^{-6.0} + 0.002D_0^{8.0}D_{max}^{-8.0} \\
 & + 0.001D_0^{10.0}D_{max}^{-10.0})
 \end{aligned} \tag{5.104}$$

where P_k is the ratio of the total volume of the aggregate to the concrete volume and D_{max} is the maximum size of aggregate in the concrete, equal to 10 mm.

Table 5.10: Aggregate distribution, total aggregate volumes and number of particles of the concrete compact assemblies (average of five numerical samples)

Material	$V_{coarse\ agg.}^{2D}$		V_{mortar}^{2D}	$N_{particles}$	
	$V_{2.4-4.75}^{2D}$	$V_{4.75-10}^{2D}$		Coarse agg.	Mortar
Concrete C4	0.236	0.119	0.645	12269	23133

CHAPTER 5. NUMERICAL MODELLING OF THE CONCRETE
STRUCTURAL PROPERTIES USING PARTICLE MODELS

Table 5.11 presents the average results obtained in the five random concrete assemblies using five time intervals ($N=5$) and a loading time of one year ($t-t' = 365 \text{ days}$). Figure 5.20 shows average results of the DEM numerical creep compliance for several loading ages using five and ten time intervals discretization ($N=5$ and 10), the comparison with Ward's experimental results and the fitted creep compliance. For each large timestep the solution is obtained by the convergence of the viscoelastic contact forces using the proposed fast numerical procedure, as previously described (§ 5.5.4). The extension of the loading time to 10 years ($t-t' = 3650 \text{ days}$) shows that the model is able to predict the long-term behaviour of concrete beyond the period used for the calibration of the components, without large deviations.

Table 5.11: Results of the long-term analysis of concrete using DEM particle model and five time intervals ($N=5$)

Material	t' (days)	$t-t'$ (days)	$E_{eff}^{CA}(t,t')$ (GPa)	ν^{C4}	$E_{eff}^{DEM}(t,t')$ (mean(st.dev.)) (GPa)	$\nu^{DEM}(t,t')$ (mean(st.dev.))
Concrete C4	7	0.01	27.6	0.20	28.4 (0.1)	0.20 (0.001)
		4.3	18.5		18.7 (0.1)	0.20 (0.002)
		15.8	16.3		16.4 (0.2)	0.20 (0.002)
		47.3	14.5		14.3 (0.2)	0.20 (0.003)
		132.7	13.0		12.7 (0.1)	0.21 (0.003)
		365.0	11.8		11.5 (0.1)	0.21 (0.003)
Concrete C4	28	0.01	29.4	0.20	29.5 (0.1)	0.20 (0.001)
		4.3	20.4		20.6 (0.1)	0.20 (0.002)
		15.8	18.5		19.0 (0.2)	0.20 (0.002)
		47.3	16.6		17.0 (0.2)	0.20 (0.002)
		132.7	14.9		15.1 (0.1)	0.20 (0.002)
		365.0	13.4		13.5 (0.2)	0.20 (0.002)
Concrete C4	90	0.01	30.3	0.20	30.3 (0.1)	0.19 (0.001)
		4.3	21.3		21.4 (0.1)	0.19 (0.002)
		15.8	19.6		20.3 (0.1)	0.19 (0.002)
		47.3	18.0		18.5 (0.2)	0.19 (0.002)
		132.7	16.4		16.4 (0.2)	0.19 (0.002)
		365.0	14.7		14.9 (0.1)	0.19 (0.002)
Concrete C4	365	0.01	30.9	0.20	30.1 (0.1)	0.19 (0.002)
		4.3	21.8		21.4 (0.1)	0.18 (0.002)
		15.8	20.2		20.6 (0.1)	0.18 (0.002)
		47.3	18.9		18.9 (0.1)	0.19 (0.002)
		132.7	17.6		17.8 (0.2)	0.19 (0.002)
		365.0	16.2		16.4 (0.1)	0.19 (0.002)

The results show a good agreement between the B3 model creep compliance (grey continuous lines in Figure 5.20) fitted to the experimental results ("×" grey mark in Figure 5.20) and the range and mean of numerical results obtained with DEM particle model for the behaviour of concrete (grey area and black diamonds in Figure 5.20), for

5.6. ANALYSIS OF THE LONG-TERM BEHAVIOUR OF CONCRETE CONSIDERING ITS MESOSTRUCTURE

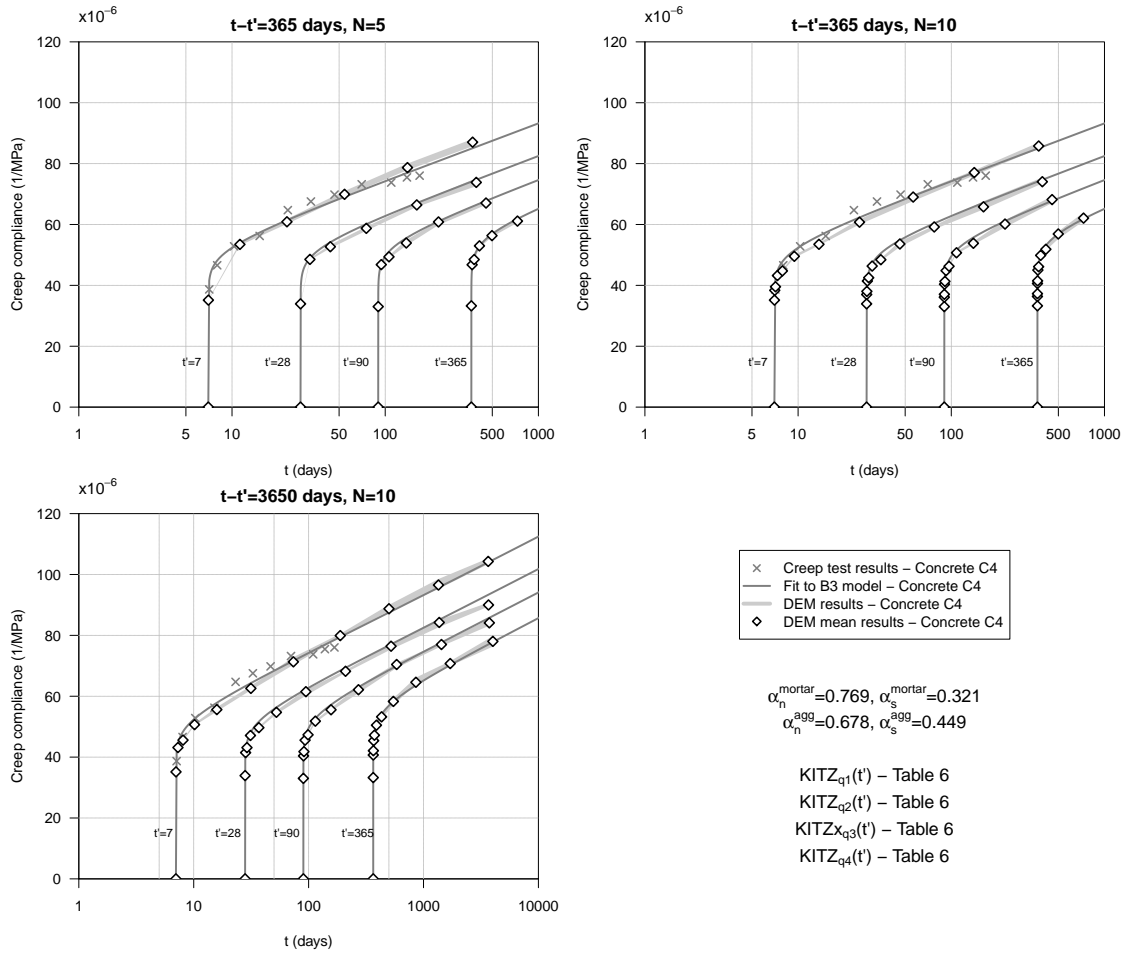


Figure 5.20: Comparison between the experimental concrete creep test results by Ward, the fit to B3 model and the results of the long-term analysis of concrete using the DEM applied to particle model using the proposed fast numerical procedure with five and ten time intervals ($N=5$ and 10) and for two loading times ($t-t'=365$ and 3650 days) (average of 5 numerical samples)

each loading age. The Poisson's ratio of the concrete is 0.20 immediately after loading ($t-t'=0.01$ days) and presents a small increase over time (Table 5.11).

The fact that the mortar parameters were calibrated using a large uniform specimen and, inside the concrete mesostructure, the mortar is interleaved with aggregate, can influence the effect of the optimal parameters in the model results. The effect of the different sizes of the coarse aggregates in the concrete can also imply a specific calibration of each aggregate size.

The proposed DEM based particle model is able to simulate the different long-term behaviour of mortar and concrete. The model also predicts the decrease of creep strains development over time due to the addition of the stiff elastic coarse aggregates when compared with the creep strain development of the particle model of the mortar. The

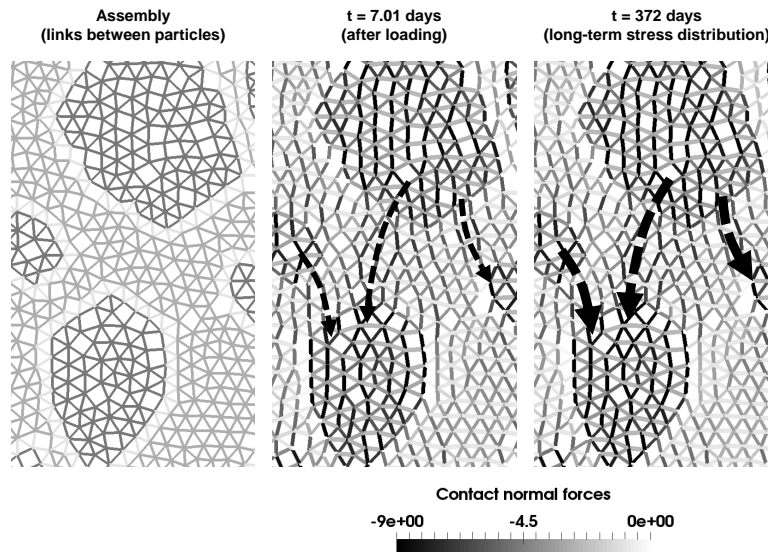


Figure 5.21: Normal contact force distributions after loading ($t=7.01$ days) and after one year under constant loading ($t=372$ days)

influence of different aggregate arrangements is not very significant.

Figure 5.21 shows the development of normal contact forces in a section of the concrete where two coarse aggregates are close to each other. Contacts aligned with the loading direction have compressive forces and contacts perpendicular to the loading direction have tensile forces. The results indicate that the force chain inside the concrete structure develop gradually overtime due to the creep properties of the mortar and the stiff elastic aggregates. Over time, the mortar between two coarse aggregates aligned in the loading direction tends to increase their compressive force due to the transfer of forces into the stiffer aggregates.

The analysis that was carried out clearly shows the potential of DEM based particle models to the study of concrete long-term behaviour. Due to the associated computational costs it is important to point out that the long-term analyses are only possible using the proposed fast numerical procedure. This type of models and approach can be particularly important for the prediction of slow deterioration scenarios in which the interaction of the cementitious materials and the aggregate over time has an important role in the behaviour of concrete, such as the development of internal stresses inside large placements of dam concrete and the development of alkali-aggregate reactions over several decades.

5.7 Contact constitutive models for the analysis of failure behaviour of concrete

5.7.1 Mohr-Coulomb model with a tension cut-off (brittle model)

Although the Mohr-Coulomb model is traditionally defined in stresses, the failure of the contact between particles is usually defined in forces, therefore, the Mohr-Coulomb failure equation is multiplied by the contact areas in order to obtain forces instead of stresses.

The Mohr-Coulomb model defines the behaviour for the normal and shear directions at a contact level in which the tensile force is limited by a maximum tensile normal strength, $F_{n,t,max}$. The force-displacement model in the normal direction is brittle for tensile forces.

The normal failure criteria at the contact is presented in Figure 5.22 and is defined by,¹

$$F_n = \begin{cases} 0, & \text{if } F_{n,predicted} > -F_{n,t,max} \\ F_{n,predicted}, & \text{otherwise} \end{cases} \quad (5.105)$$

where F_n is the normal contact force to consider in the calculation at the current timestep, $F_{n,predicted}$ is the predicted normal contact force before failure and $F_{n,t,max}$ is the maximum tensile normal strength.

For the shear direction, the maximum shear strength is given by the classical Mohr-Coulomb criteria,

$$F_{s,max} = C + F_n \tan \phi \quad (5.106)$$

where $F_{s,max}$ is the maximum shear contact force, C is the contact cohesion and ϕ is the contact friction angle.

Figure 5.22 also presents the shear failure criteria which can be described as,

$$\mathbf{F}_{si} = \begin{cases} \mathbf{F}_{s,predicted} \frac{F_{s,residual}}{F_{s,predicted}}, & \text{if } F_{s,predicted} > F_{s,max} \\ \mathbf{F}_{s,predicted}, & \text{otherwise} \end{cases} \quad (5.107)$$

$$F_{s,residual} = C_{residual} + F_n \tan \phi_2 \quad (5.108)$$

¹the normal compression forces are positive and normal tension forces are negative

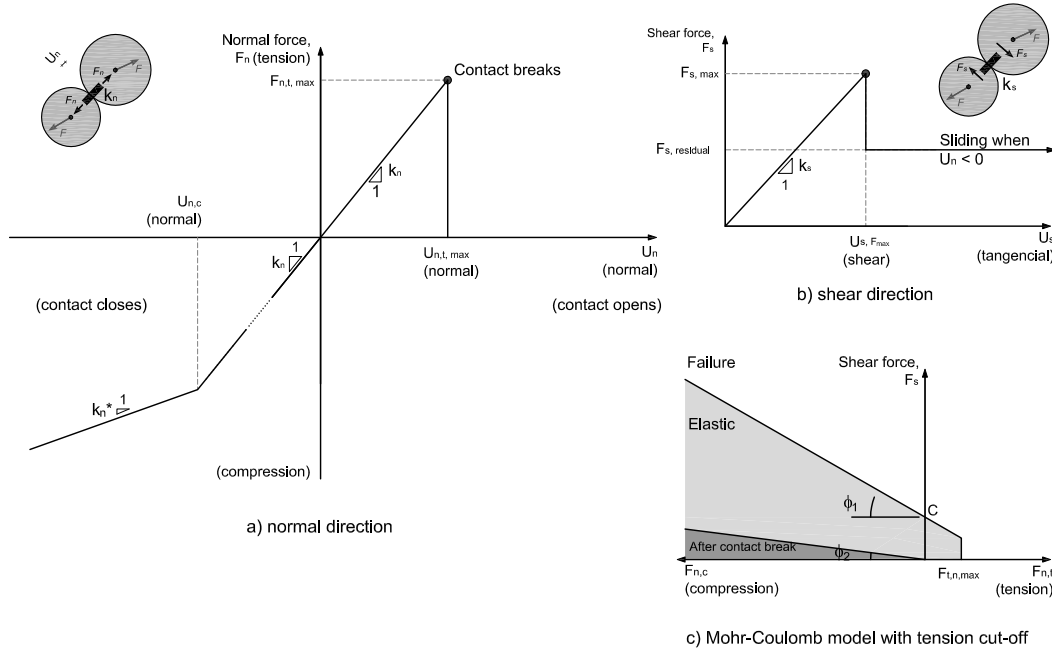


Figure 5.22: Mohr-Coulomb model with tension cut-off

$$F_{s,predicted} = \|\mathbf{F}_{s,predicted}\| \quad (5.109)$$

Until the contact is elastic, *i.e.* until the normal contact force and the shear force is below their maximum values, the contact is elastic. Once one of the failure conditions is met, the contact breaks and behaves as a Mohr-Coulomb model with residual cohesion, $C_{residual}$ (which can be null) for the shear sliding at the contact, the contact friction angle could also change to a different value, ϕ_2 , and the contact only bears compressive forces. In order to take into account the decrease of stiffness due to high compression stresses, a bilinear law was implemented in the compressive behaviour, in which the contact normal stiffness is reduced from k_n to k_n^* , after the predefined value of $U_{n,c}$ is reached (Oñate *et al.* 2015). Figure 5.22 shows the normal and shear behaviour of the brittle model and the normal-shear representation of the failure surface.

5.7.2 Mohr-Coulomb model with softening in tension and shear

As described by Monteiro Azevedo (2003), the use of a contact tensile and shear fracture energy using a softening model can reduce the fracture propagation velocities and the particle size dependency.

5.7. CONTACT CONSTITUTIVE MODELS FOR THE ANALYSIS OF FAILURE BEHAVIOUR OF CONCRETE

Similarly to the brittle model, the model is elastic until the contact forces are below the maximum strengths (for both tension and shear). Once one of the maximum strength is reached, a linear softening allows for a gradual reduction of the contact forces. The softening was adopted for the normal and shear directions and the global damage takes into account the two types of softening. After the maximum tensile strength is reached, the normal contact force is reduced using the global contact damage. If the maximum shear strength is reached, the initial cohesion is reduced using also the global contact damage. The global contact damage, d , varies between 0, for an undamaged contact, and 1, for completely damaged contact.

In order to take into account the normal and shear fracture energies at the contact, $G_{f,t}$ and $G_{f,s}$, the maximum overlaps, $U_{n,t,max}$ and $U_{s,max}$, after the complete softening, is given by,

$$U_{n,t,max} = \frac{2G_{f,n}}{F_{n,t,max}} \quad (5.110)$$

$$U_{s,max} = \frac{2G_{f,s}}{C} \quad (5.111)$$

The overlaps at maximum contact forces, $U_{n,t,max}$ and $U_{s,max}$, are obtained using the elastic energy, $G_{e,t}$ and $G_{e,s}$,

$$U_{n,t,Fmax} = \frac{2G_{e,n}}{F_{n,t,max}} \quad (5.112)$$

$$U_{s,Fmax} = \frac{2G_{e,s}}{C} \quad (5.113)$$

Beyond the maximum normal contact force and cohesion, the softening law defines a normal tensile and shear damage coefficients, d_n^+ and d_s , which relates to the overlap values after yielding, $U_{n,t,i}$ and $U_{s,i}$,

$$d_n^+ = \frac{U_{n,t,i} - U_{n,t,max}}{U_{n,t,Fmax} - U_{n,t,max}} \quad (5.114)$$

$$d_s = \frac{U_{s,i} - U_{s,max}}{U_{s,Fmax} - U_{s,max}} \quad (5.115)$$

It is assumed that the normal and shear damage are coupled and that the global contact

damage, d , is a linear combination of two components, d_n^+ and d_s (considering a maximum of one for the global contact damage). The actual tensile strength, $F_{n,t}^{actual}$, and the actual cohesion, C^{actual} , are obtained from the global contact damage, d , and the correspondent contact forces are updated,

$$F_{n,t,max}^{actual} = F_{n,t}d = F_{n,t} (d_n^+ + d_s) \quad (5.116)$$

$$C^{actual} = Cd = C (d_n^+ + d_s) \rightarrow F_{s,max}^{actual} = C^{actual} + F_n \tan \phi \quad (5.117)$$

$$F_n = \begin{cases} F_{n,t}^{actual}, & \text{if } F_{n,predicted} > -F_{n,t,max}^{actual} \\ F_{n,predicted}, & \text{otherwise} \end{cases} \quad (5.118)$$

$$\mathbf{F}_{si} = \begin{cases} \mathbf{F}_{s,predicted} \frac{F_{s,max}^{actual}}{F_{s,predicted}}, & \text{if } F_{s,predicted} > F_{s,max}^{actual} \\ \mathbf{F}_{s,predicted}, & \text{otherwise} \end{cases} \quad (5.119)$$

$$F_{s,predicted} = \|\mathbf{F}_{s,predicted}\| \quad (5.120)$$

Similarly to the brittle contact model, once the maximum overlap is reached the contact breaks and the cohesion is set to zero and the residual shear force relies only on final friction value, ϕ_f . Also, if the global contact damage is higher than 1, only a friction model is left for the maximum shear strength.

Figure 5.23 shows the normal and shear behaviour of the softening model and the normal-shear representation of the failure surface at different stages of loading. Figures 5.24 and 5.25 illustrate an example of the stress path of a normal tensile contact failure and of a shear contact failure, respectively. In both cases, as soon as the contact force exceeds the maximum forces, the new updated contact force is obtained in order to be at the failure surface, defined by the softening law. As the displacements increase, the contact force drops smoothly until zero, the damage increases until its maximum value, $d = 1$, and the normal and shear stiffnesses also decrease, $k_n > k_n^d$ and $k_s > k_s^d$.

5.7. CONTACT CONSTITUTIVE MODELS FOR THE ANALYSIS OF FAILURE BEHAVIOUR OF CONCRETE

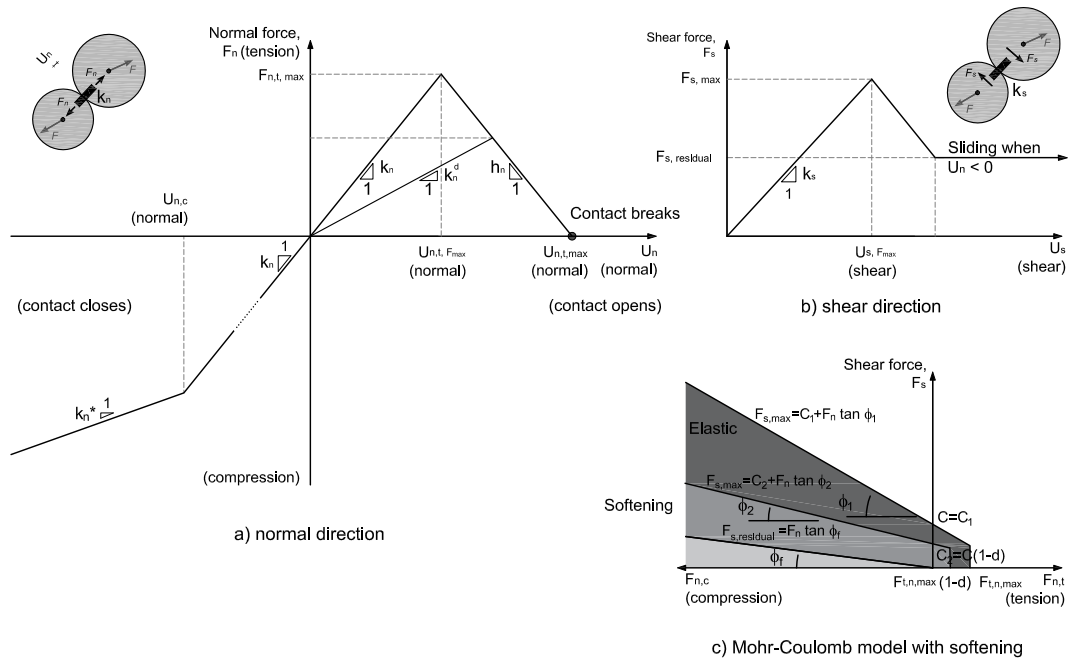


Figure 5.23: Mohr-Coulomb model with softening in tension and shear

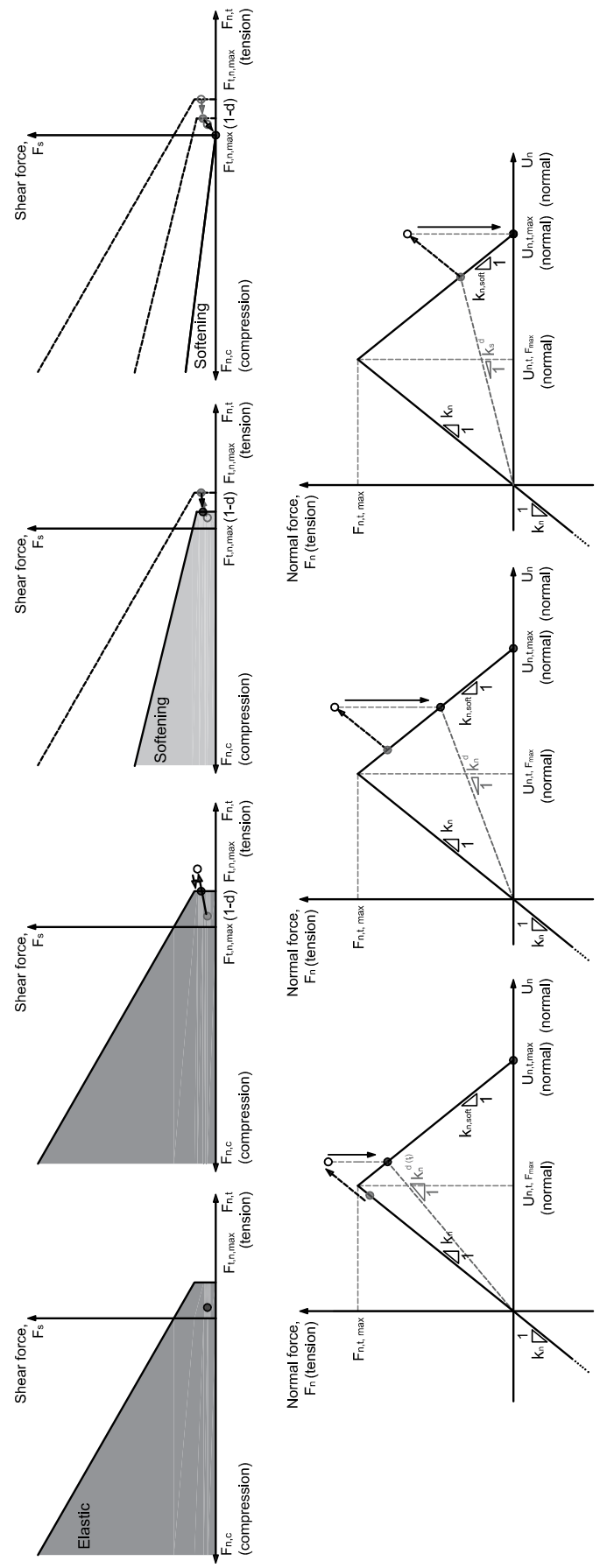


Figure 5.24: Description of the normal contact force path under softening

5.7. CONTACT CONSTITUTIVE MODELS FOR THE ANALYSIS OF FAILURE BEHAVIOUR OF CONCRETE

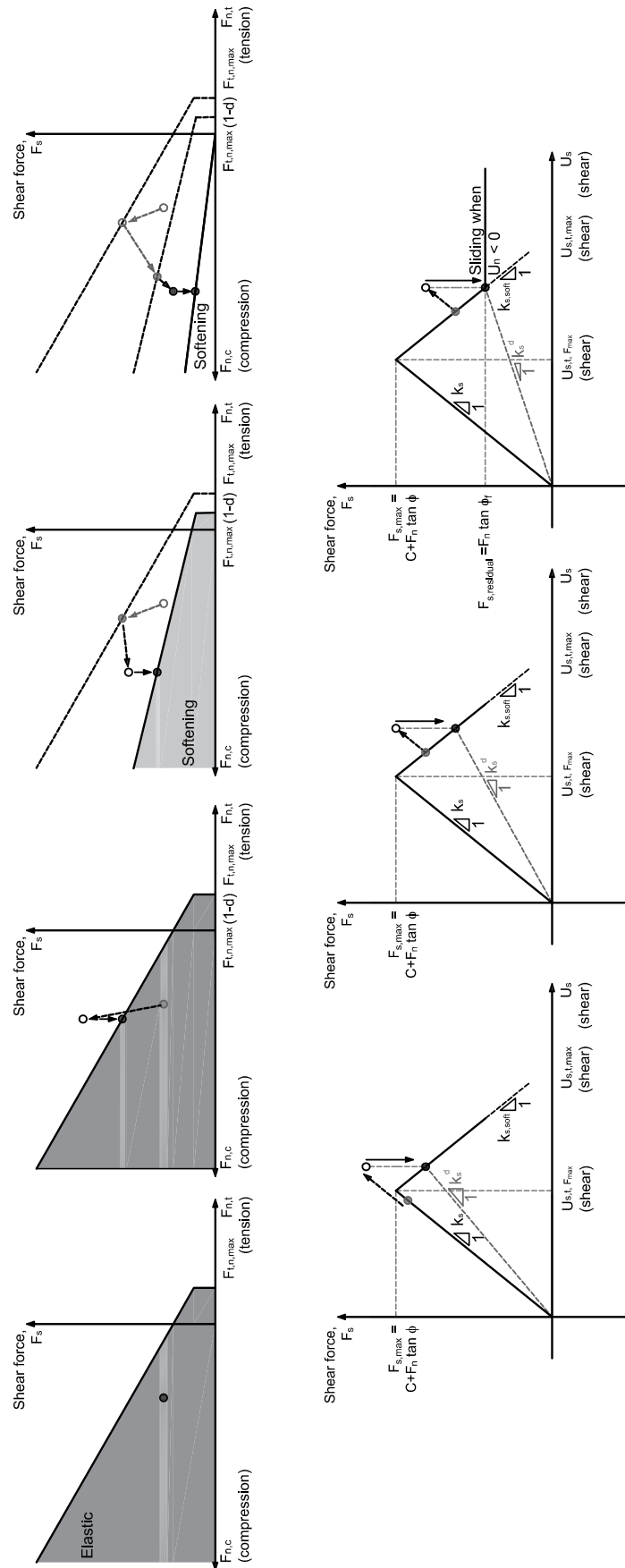


Figure 5.25: Description of the shear contact forces path under softening

5.7.3 Validation of Mohr-Coulomb contact models (brittle and softening)

In order to validate the model implementation on the computational code, simple testing examples were used for tension and shear loadings in which the failure mode is previously known. The full description of failure behaviour was obtained for a constant boundary wall velocity. A set of hypothetical micro properties were used for the analysis of these examples (Table 5.12). Figure 5.26 shows the particle assemblies used for the validation of the Mohr-Coulomb contact model. For the 2×1 assembly the contact between particles has a Mohr-Coulomb model and the wall contacts are kept elastic. For the 2×2 and 10×10 particle assemblies, the central contacts have a Mohr-Coulomb model and the remaining contacts are elastic. The normal and shear behaviours of the contact models are validated considering different types of loading under constant velocity control.

Table 5.12

Model parameter	Mohr-Coulomb model with cut-off	Mohr-Coulomb model with softening
R (m)		0.00048
k_n (N/m)		10×10^6
k_s/k_n		1.0
k_n^* (in compression)		$0.3 k_n$
$F_{n,t,max}$ (N)		1×10^5
C (N)		5×10^4
$\tan \phi$		0.3
$G_{e,n}$ (N/m)		$\frac{F_{n,t,max}}{2k_n}$
$G_{e,s}$ (N/m)		$\frac{F_{s,t,max}}{2k_s}$
$G_{f,n}$ (N/m)	-	$4 G_{e,n}$
$G_{f,s}$ (N/m)	-	$4 G_{e,s}$

The validation tests of the two particle model included a specific force path in order to describe the complete behaviour of the contact brittle and softening model: firstly, a vertical wall velocity, v_y , is set to introduce only tension forces into the contact until the contact breaks and the two particles separate; secondly, the wall velocity is inverted in order to approximate the two particles, which after failure do not undergo forces; as the two particles touch, the compressive stiffness and the model in compression is activated. Figure 5.27 shows the result of the validation test for the two particles model and for the brittle and softening models. A similar test was done for the 10×10 assembly under tension loading considering brittle and softening contact model (Figure 5.28).

In order to validate the shear behaviour of the contact model, a 2×2 assembly was tested considering a constant horizontal wall velocity, v_x , with and without an applied

5.7. CONTACT CONSTITUTIVE MODELS FOR THE ANALYSIS OF FAILURE BEHAVIOUR OF CONCRETE

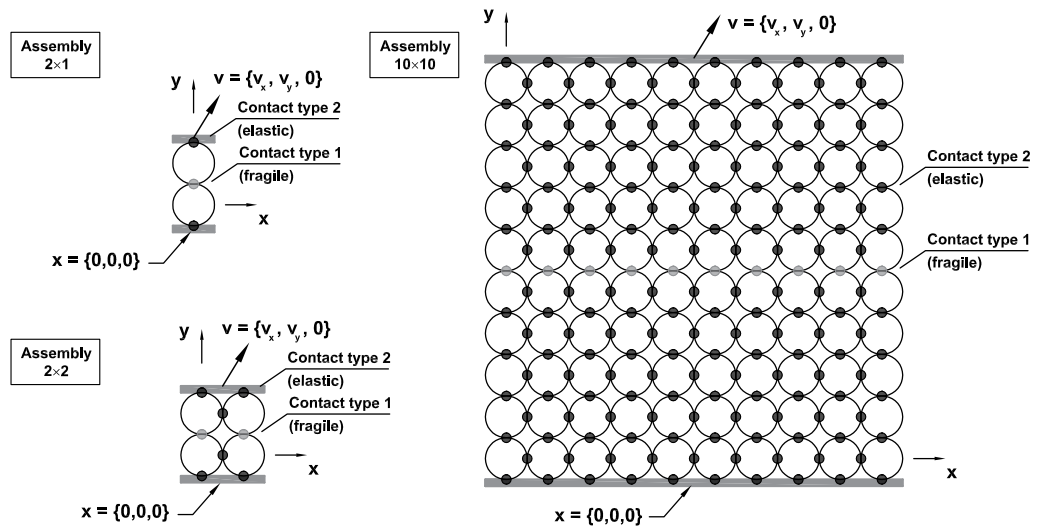


Figure 5.26: Assemblies for the validation of the Mohr-coulomb models

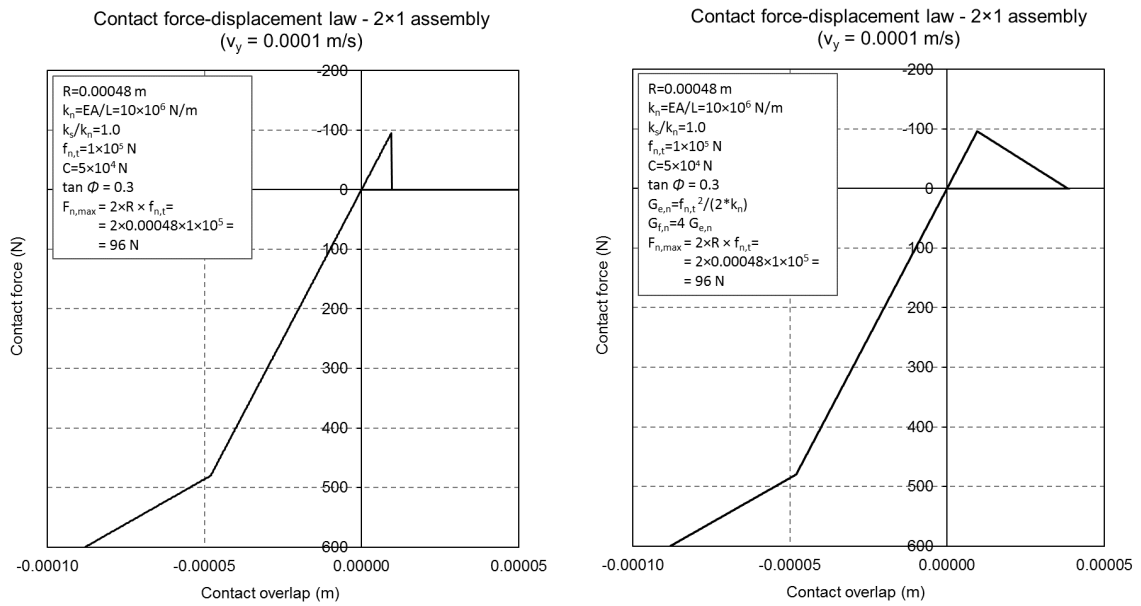


Figure 5.27: Contact force-displacement law for the 2x1 assembly under tension and compression loading considering brittle (left) and softening (right) contact model

CHAPTER 5. NUMERICAL MODELLING OF THE CONCRETE STRUCTURAL PROPERTIES USING PARTICLE MODELS

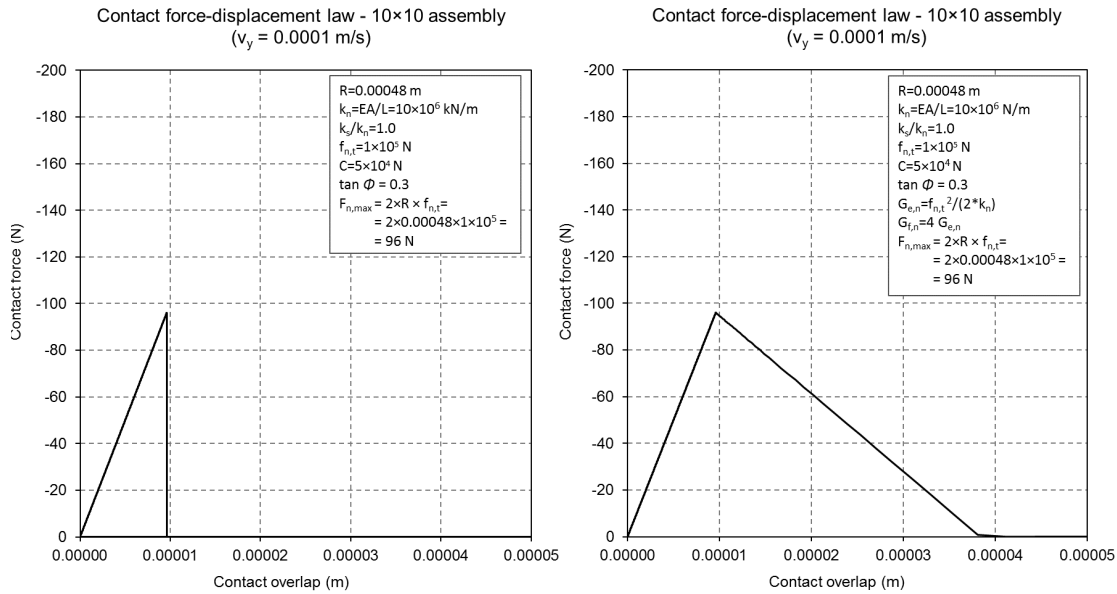


Figure 5.28: Contact force-displacement law for the 10×10 assembly under tension loading considering brittle (left) and softening (right) contact model

compressive force and for brittle and softening models. A pure shear test yields the results shown in Figure 5.29, without any residual shear force in the contact. If the contact has a compressive force, a residual shear force derived from the friction coefficient still remains after the contact is broken (Figure 5.30).

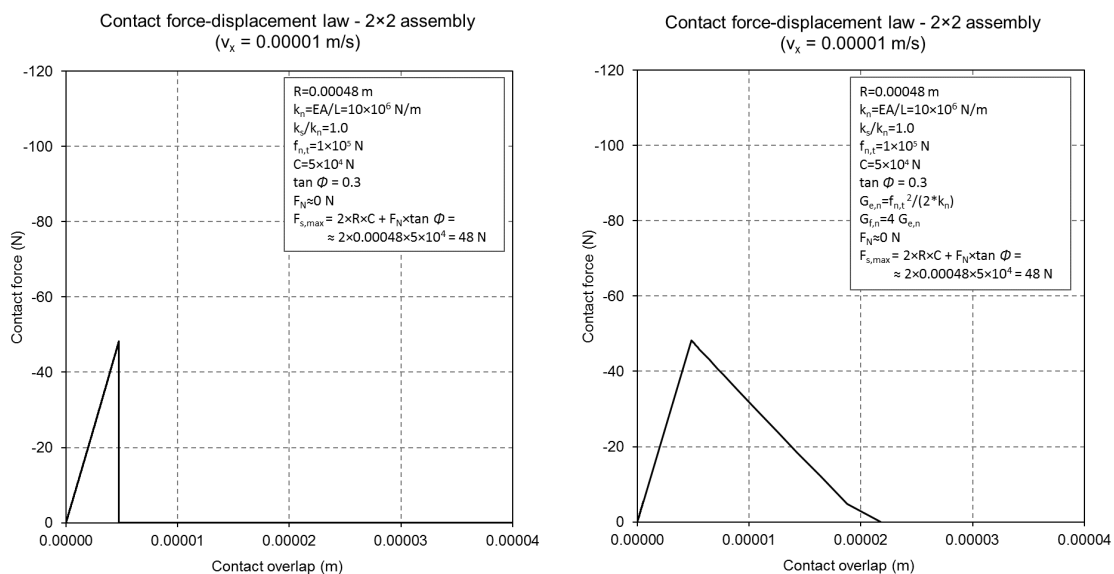


Figure 5.29: Global and contact force-displacement law for the 2×2 assembly under shear loading considering brittle (left) and softening (right) contact model

5.8. ANALYSIS OF THE FAILURE BEHAVIOUR OF CONCRETE CONSIDERING ITS MESOSTRUCTURE

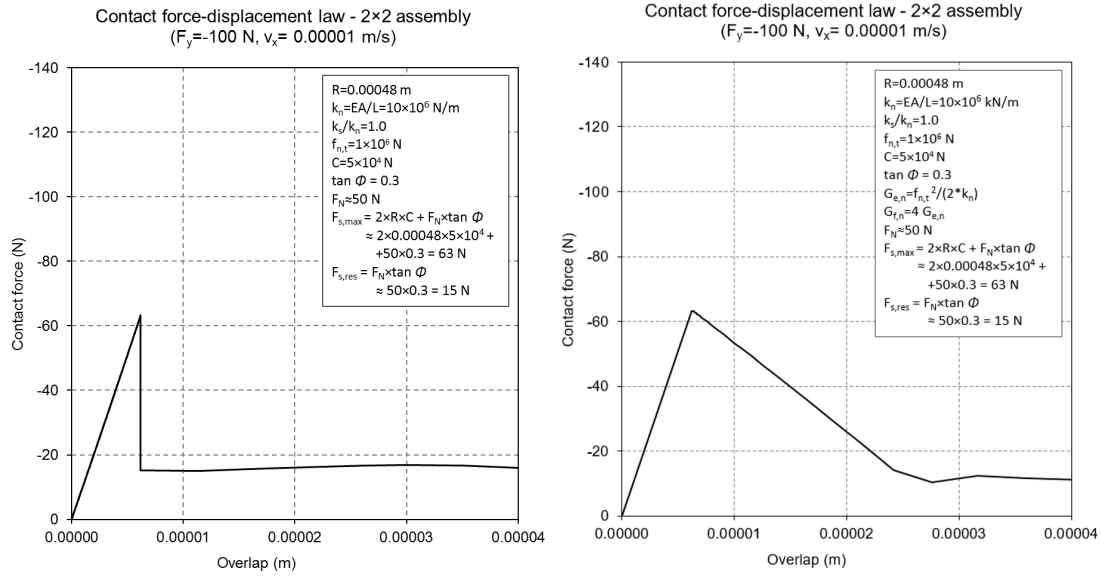


Figure 5.30: Global and contact force-displacement law for the 2×2 assembly under compression and shear loading considering brittle (left) and softening (right) contact model

5.8 Analysis of the failure behaviour of concrete considering its mesostructure

5.8.1 Particle model properties and parametric study

In order to validate the particle model for the prediction of concrete behaviour taking into account the coarse aggregate distribution inside the specimen, 5 random particle models were generated for both tensile and compressive loadings. The tests follow the work of Vonk (1992) which describes the experimental conditions and results. Vonk (1992) tested conventional concrete in tension and in compression considering different lateral restraints in the platens, presents the obtained stress-strain results and the numerical simulations using a micromechanical approach based on the discrete element method in which the domain is divided into deformable polygonal elements. The numerical tests using a concrete particle model are directly compared to the Vonk's numerical results.

The generation of concrete mesostructure using particle models follow the description in § 5.4 and the composition data presented in Table 5.13. The specimens used for tensile strength tests have 50 mm in height and 100 mm-width and the compressive strength is obtained in 100 mm \times 100 mm specimens. The maximum radius, R_{max} , and ratio between minimum and maximum particle radius, $\frac{R_{max}}{R_{min}}$, are equal to 1.0 and 2/3, respectively. The generated assemblies have around of 2500 particles and 7000 contacts for the tensile

strength tests and around 4700 particles and 14000 contacts for the compressive strength tests.

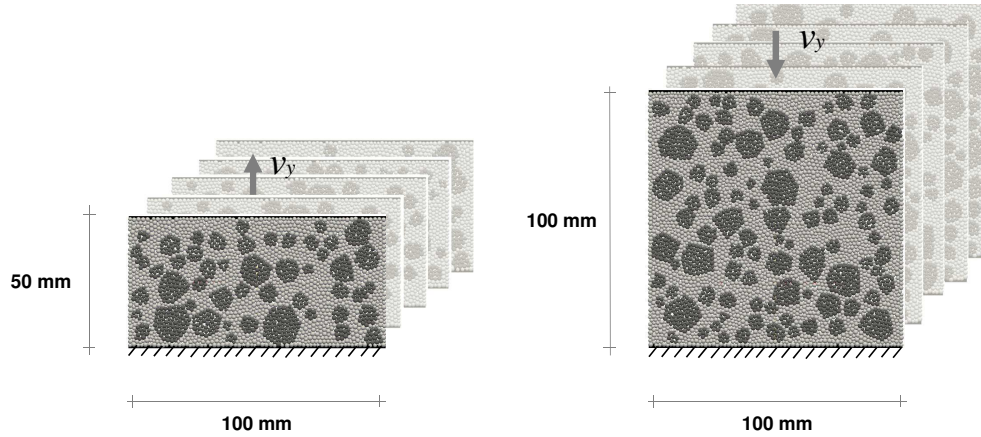


Figure 5.31: Specimen size and type of loading of the concrete particle models

Two rigid walls simulate the platens in which the external loading is applied (Figure 5.31). The external loading is an imposed constant velocity of the top wall of 5×10^{-5} m/s. In order to validate the model using Vonk's numerical results, the rigid wall do not restrain the lateral displacements of the particles. The forces are damped by local non-viscous damping, as described in § 5.3.2.4, using non-viscous damping coefficient, $\alpha = 0.7$.

Table 5.13: Concrete composition of Vonk (1992) tests

Component	Content (kg/m ³)	
Cement (Portland A)	330.0	
Water	165.0	
Fine aggregate	0.0 - 0.25	150.3
	0.25 - 0.5	225.5
	0.5 - 1.0	225.5
	1.0 - 2.0	187.9
	2.0 - 4.0	263.1
Coarse aggregate	4.0 - 8.0	375.8
	8.0 - 16.0	451.0

Prior to the calibration of the micro parameters and fit to Vonk's numerical results, a sensitivity study is presented in order to evaluate the influence of the main factors on the tensile and compressive behaviour of concrete. The factors under study are the modulus of elasticity of the aggregates, the contact strength parameters of the mortar in the normal and tangential directions, $F_{n,t,max}^{mortar}$, C^{mortar} , $\tan \phi^{mortar}$, the ratio between contact properties of the ITZ and the mortar, $r_F = \frac{F_{n,t,max}^{ITZ}}{F_{n,t,max}^{mortar}}$, $r_C = \frac{C^{ITZ}}{C^{mortar}}$, the ratio between the contact's

5.8. ANALYSIS OF THE FAILURE BEHAVIOUR OF CONCRETE CONSIDERING ITS MESOSTRUCTURE

total and elastic fracture energy in both directions, $r_{G,n} = \frac{G_{f,n}}{G_{e,n}}$ and $r_{G,s} = \frac{G_{f,s}}{G_{e,s}}$, the wall imposed velocity, v_y^{wall} , and the lateral restraint of the walls, k_s^{wall} . Table 5.14 describes the variation of the influencing parameters on each factor and Figures 5.32 to 5.37 show the effect of the stress-strain response for tensile and compressive stresses. The bold values in Table 5.14 refer to the reference state for the direct comparison between each analysis.

The imposed wall velocity is an important factor in this type of numerical models using DEM. In order to evaluate the quasi-static response of concrete the wall velocity should be as small as possible. High wall velocities introduce large contact force variations which can be difficult to balance and yield an apparent global softening behaviour. The adopted wall velocity for all the sensitivity study cases was $v_y = 5 \times 10^{-4}$ m/s for compression tests and $v_y = 5 \times 10^{-5}$ m/s for tension tests. The criteria for establishing the quasi-static wall velocity concerned the energy balance between work and kinetic energy during the test. If the kinetic energy differs from the work done in the system there are significant dynamic effects that not being taken into account in the constitutive model and, therefore, the wall velocity should decrease in order for the system to dissipate the excessive contact velocities during the calculation and obtain a quasi-static solution.

Figure 5.32 shows the effect of aggregate's modulus of elasticity variations on the global stress-strain behaviour for both direct tensile strength tests and compressive tests. The most significant effect is the decrease of the modulus of elasticity of concrete and the small increase of peak strength in tension and compression as the modulus of elasticity of the aggregate decreases. The concrete with softer aggregates ($E_{agg}=35$ GPa) have less internal heterogeneity which can imply also less stress concentration around the aggregates and can lead to a delay in the development of large cracks and an increase of the peak strength.

It is shown that higher maximum normal contact forces of mortar yield higher concrete tensile and slightly higher compressive strengths (Figure 5.33) and more brittle responses, considering the ratio between ITZ and mortar contact strength properties is maintained equal to 0.5. The variation of the ratio between ITZ and mortar contact strength properties shows that the tensile strength is more sensitive to the ITZ properties than the compressive strength (Figure 5.35). Higher ITZ strength properties also yield brittle responses. When the ITZ strength properties are reduced, the first cracks around the aggregates develop very early but the large inter-aggregate cracks, which imply the failure of the mortar with much higher strength, occur later in time.

Figure 5.34 shows also the influence of mortar's contact cohesion on the macroscopic

CHAPTER 5. NUMERICAL MODELLING OF THE CONCRETE
STRUCTURAL PROPERTIES USING PARTICLE MODELS

Table 5.14: Definition of variables for the sensitivity study

Parameter under study	Type of loading	Value
Modulus of elasticity of the aggregate (E_{agg})	Tension	$E_{agg} = 35 \text{ GPa}$ $E_{agg} = 70 \text{ GPa}$ $E_{agg} = 105 \text{ GPa}$
	Compression	$E_{agg} = 35 \text{ GPa}$ $E_{agg} = 70 \text{ GPa}$ $E_{agg} = 105 \text{ GPa}$
Maximum contact force of mortar $(F_{n,t,max}^{mortar})$	Tension	$F_{n,t,max}^{mortar} = 4500 \text{ kN}, C^{mortar} = 15000 \text{ kN}$ $F_{n,t,max}^{mortar} = 9000 \text{ kN}, C^{mortar} = 15000 \text{ kN}$ $F_{n,t,max}^{mortar} = 13500 \text{ kN}, C^{mortar} = 15000 \text{ kN}$
	Compression	$F_{n,t,max}^{mortar} = 4500 \text{ kN}, C^{mortar} = 15000 \text{ kN}$ $F_{n,t,max}^{mortar} = 9000 \text{ kN}, C^{mortar} = 15000 \text{ kN}$ $F_{n,t,max}^{mortar} = 13500 \text{ kN}, C^{mortar} = 15000 \text{ kN}$
Contact cohesion of mortar (C^{mortar})	Tension	$F_{n,t,max}^{mortar} = 9000 \text{ kN}, C^{mortar} = 7500 \text{ kN}$ $F_{n,t,max}^{mortar} = 9000 \text{ kN}, C^{mortar} = 15000 \text{ kN}$ $F_{n,t,max}^{mortar} = 9000 \text{ kN}, C^{mortar} = 22500 \text{ kN}$
	Compression	$F_{n,t,max}^{mortar} = 9000 \text{ kN}, C^{mortar} = 7500 \text{ kN}$ $F_{n,t,max}^{mortar} = 9000 \text{ kN}, C^{mortar} = 15000 \text{ kN}$ $F_{n,t,max}^{mortar} = 9000 \text{ kN}, C^{mortar} = 22500 \text{ kN}$
Ratio between contact properties of ITZ and mortar $\left(r_f = \frac{f_{n,t,max}^{ITZ}}{f_{n,t,max}^{mortar}}, r_C = \frac{C^{ITZ}}{C^{mortar}} \right)$ $, r_\phi = \frac{\tan\phi^{ITZ}}{\tan\phi^{mortar}}$	Tension	$r_f = 0.25, r_C = 0.25, r_\phi = 0.25$ $r_f = 0.5, r_C = 0.5, r_\phi = 0.5$ $r_f = 1.0, r_C = 1.0, r_\phi = 1.0$
	Compression	$r_f = 0.25, r_C = 0.25, r_\phi = 0.25$ $r_f = 0.5, r_C = 0.5, r_\phi = 0.5$ $r_f = 1.0, r_C = 1.0, r_\phi = 1.0$
Ratio between total and elastic contact fracture energy $\left(r_{G,n} = \frac{G_{f,n}}{G_{e,n}}, r_{G,s} = \frac{G_{f,s}}{G_{e,s}} \right)$	Tension	$r_{G,n} = r_{G,s} = 1.0$ (brittle) $r_{G,n} = r_{G,s} = 4.0$ $r_{G,n} = r_{G,s} = 10.0$
	Compression	$r_{G,n} = r_{G,s} = 1.0$ (brittle) $r_{G,n} = r_{G,s} = 4.0$ $r_{G,n} = r_{G,s} = 10.0$
Lateral restraint of the walls (k_s^{wall})	Tension	$k_s^{wall} = 0 \text{ kN/m}$ $k_s^{wall} = 0.5 k_s^{mortar}$ $k_s^{wall} = 1.0 k_s^{mortar}$
	Compression	$k_s^{wall} = 0 \text{ kN/m}$ $k_s^{wall} = 0.5 k_s^{mortar}$ $k_s^{wall} = 1.0 k_s^{mortar}$

5.8. ANALYSIS OF THE FAILURE BEHAVIOUR OF CONCRETE CONSIDERING ITS MESOSTRUCTURE

strength properties of concrete. It is shown that, due to the type of failure of tensile strength tests, contact cohesion does not affect the tensile strength behaviour since there is no shear involved. In compression, large shear displacements take place across the specimen and around the coarse aggregates and, therefore the contact cohesion has a great effect on the ultimate compressive strength values.

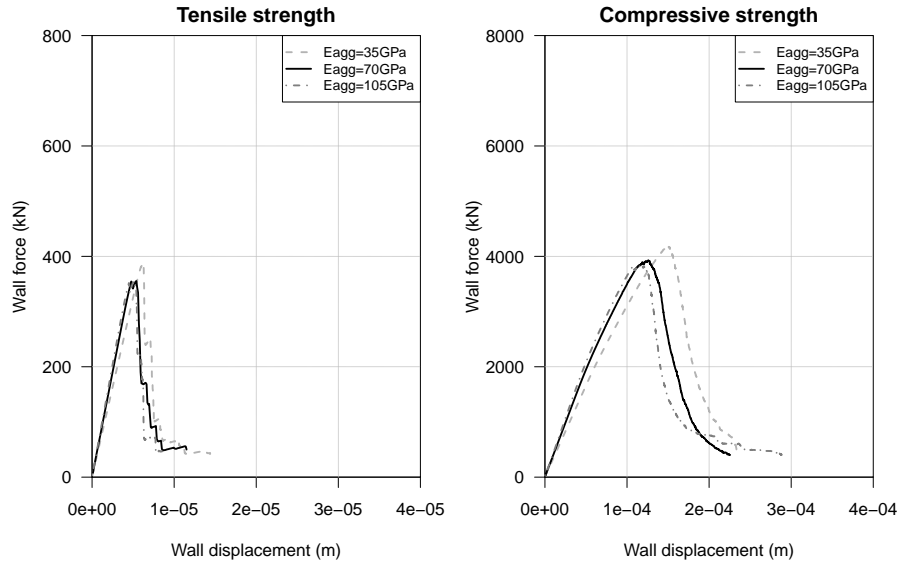


Figure 5.32: Influence of the modulus of elasticity of the aggregate in the stress-strain behaviour in tension and compression

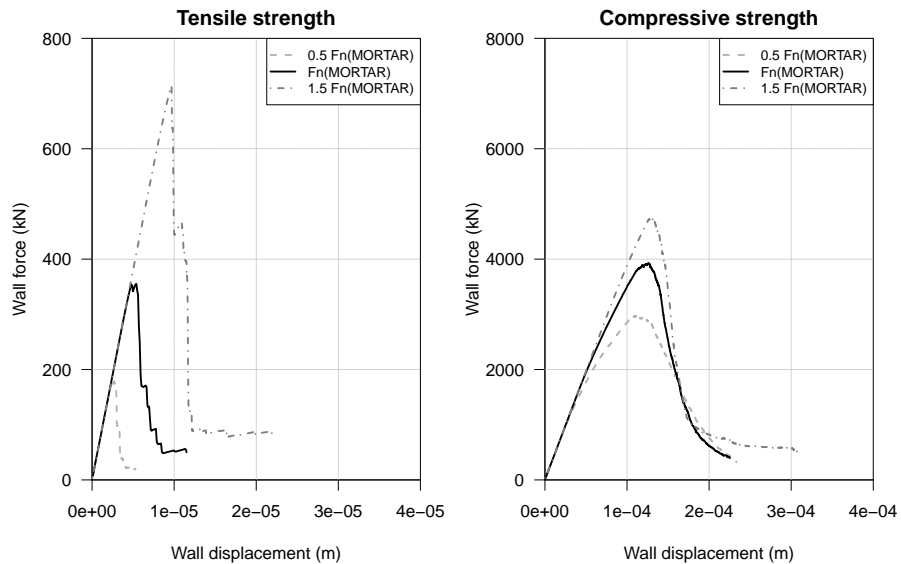


Figure 5.33: Influence of the contact strength properties of the mortar in the stress-strain behaviour in tension and compression

The effect of the contact fracture energy is presented in Figure 5.36 in which the total

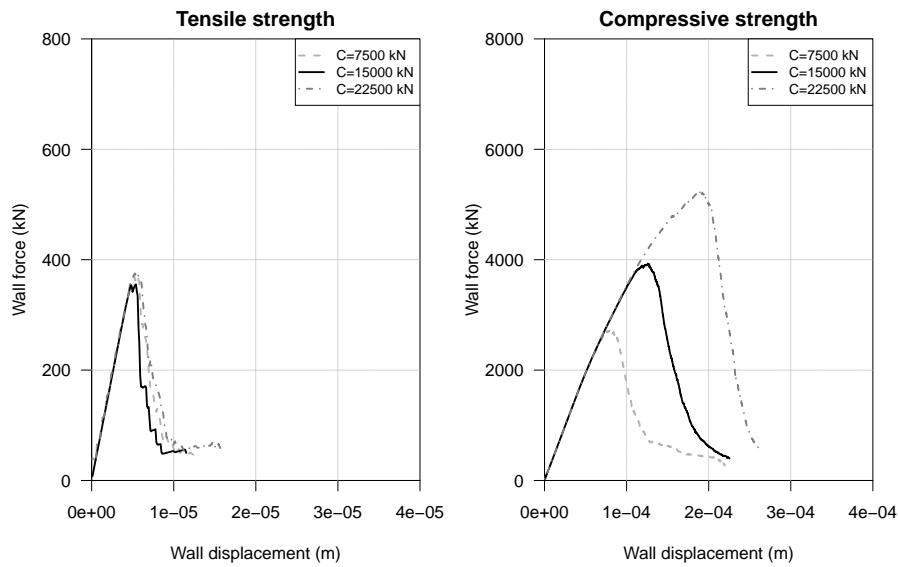


Figure 5.34: Influence of the contact cohesion of the mortar in the stress-strain behaviour in tension and compression

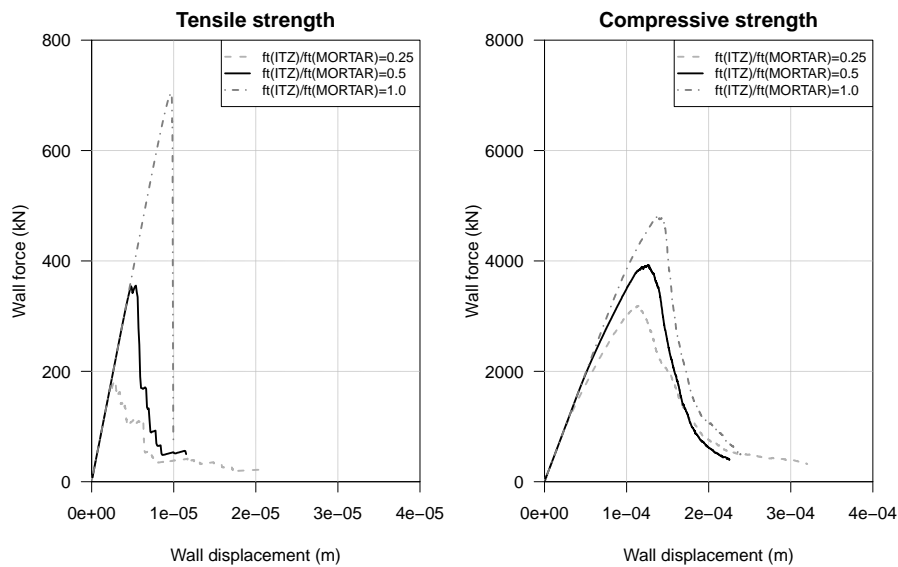


Figure 5.35: Influence of the ratio between contact strength properties of the ITZ and the mortar in the stress-strain behaviour in tension and compression

5.8. ANALYSIS OF THE FAILURE BEHAVIOUR OF CONCRETE CONSIDERING ITS MESOSTRUCTURE

contact fracture energy is varied from a brittle behaviour ($G_f = G_e$) to a large softening behaviour ($G_f = 10G_e$). The influence of the brittle behaviour is more pronounced for tensile loadings. Larger total contact fracture energies yield higher tensile and compressive peak strengths.

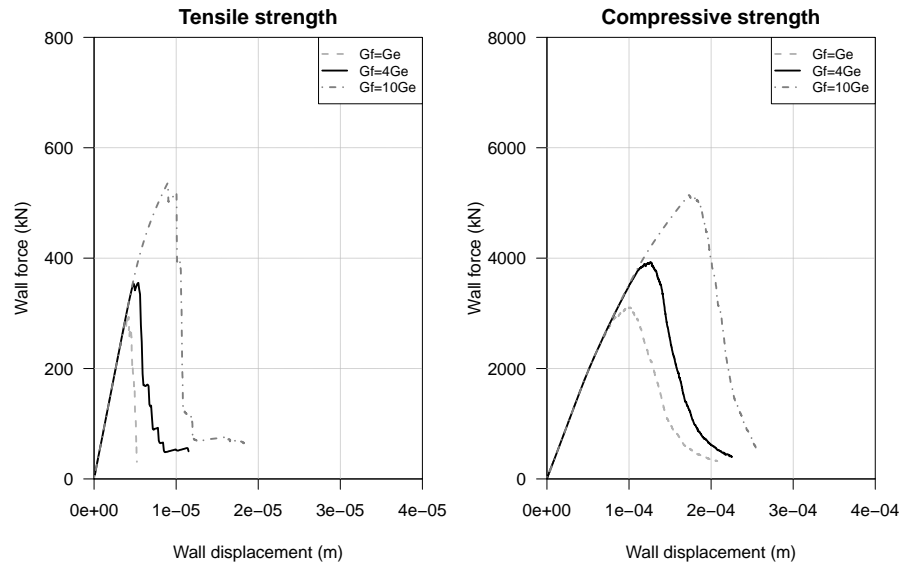


Figure 5.36: Influence of the contact fracture energy in the stress-strain behaviour in tension and compression

The effect of the lateral restraint of the wall was also studied and Figure 5.37 shows the stress-strain responses considering no lateral restrictions and two degrees of restraint. Several studies refer to the study of concrete softening considering zero lateral restraints in order to evaluate the concrete material properties without the influence of the testing conditions (Vonk 1992; Mier 1998). The platens introduce a lateral restrictions which influences the failure mode and, therefore, the stress strain response. Figure 5.37 show a significant increase on the peak strength and on the softening response of concrete when some lateral restraint is considered.

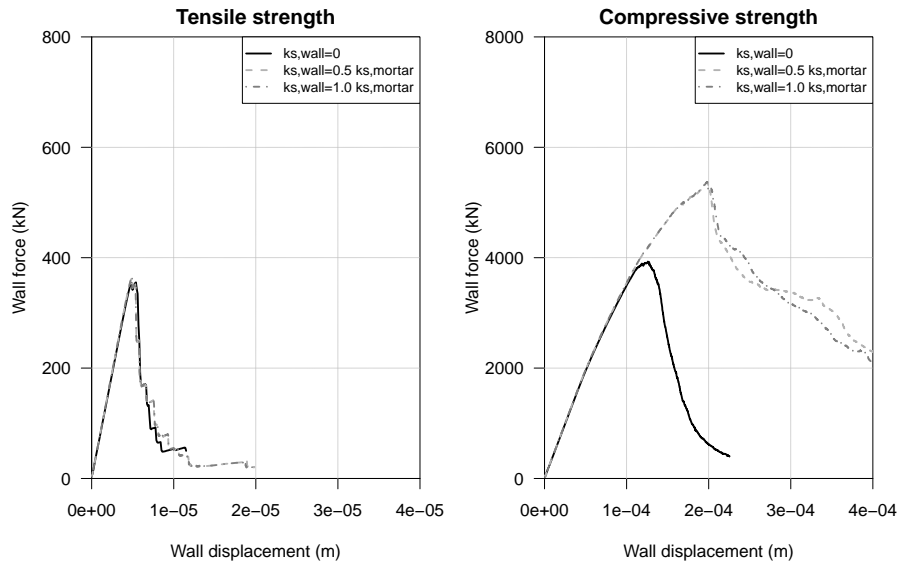


Figure 5.37: Influence of the lateral restraint of the walls in the stress-strain behaviour in tension and compression

5.8.2 Modelling the tensile and compressive instantaneous stress-strain behaviour

For the fit to Vonk's results, the tensile and compressive tests are simulated using a Mohr-Coulomb model with softening in which the contact's total fracture energy for the normal direction, $G_{f,n}$, and for the tangential direction, $G_{f,s}$, are taken as 10 times larger than the respective contact's elastic energy, $G_{e,n}$ and $G_{e,s}$. It is assumed that the aggregate contacts (AGG-AGG) are elastic and do not break. The calibration of the elastic micro-parameters followed the procedure previously described (§ 5.5.3) and the main strength parameters were obtained from trial-and-error in order to fit the stress-strain response to the Vonk's tests. Table 5.15 and Table 5.16 present the main parameters and results. Figures 5.39 and 5.40 present the complete stress-strain behaviour for both tensile and compressive loadings and the development of the modulus of elasticity and Poisson's ratio, of the number of normal and shear contact breaks and of the work and kinetic energy (range of 5 numerical simulations for randomly generated assemblies).

The obtained results show a good prediction of the tensile and compressive peak strengths although with a much higher brittle response (Figures 5.39 and 5.41).

The direct tensile strength tests of the concrete particle model show that the work of the boundary walls and the kinetic energy are equal and the elastic properties remain the same until some inelastic displacement occurs (after 50000 steps and at 80% of the peak

5.8. ANALYSIS OF THE FAILURE BEHAVIOUR OF CONCRETE
CONSIDERING ITS MESOSTRUCTURE

Table 5.15: Parameters used for the concrete particle model

Type of loading	E^{agg} (GPa) α_n^{agg} α_s^{agg}	E^{mortar} (GPa) α_n^{mortar} α_s^{mortar}	E^{ITZ} (GPa) α_n^{ITZ} α_s^{ITZ}	$F_{n,t,max}^{mortar}$ (N) C^{mortar} (N) $\tan\phi^{mortar}$	$F_{n,t,max}^{ITZ}$ (N) C^{ITZ} (N) $\tan\phi^{ITZ}$
Tension	70×10^6	25×10^6	25×10^6	7.5×10^3	3.75×10^3
	1.15	1.15	1.15	13.0×10^3	6.5×10^3
	0.30	0.30	0.30	0.3	0.3
Compression	70×10^6	25×10^6	25×10^6	7.5×10^3	3.75×10^3
	1.50	1.50	1.50	13.0×10^3	6.5×10^3
	0.30	0.30	0.30	0.3	0.3

Table 5.16: Results of tensile and compressive numerical tests of concrete particle models

Type of loading	v^{wall} (m/s)	$\frac{G_{f,n}}{G_{e,n}} = \frac{G_{f,s}}{G_{e,s}}$	E^{DEM} (mean(st.dev.)) (GPa) ν^{DEM} (mean(st.dev.)) F^{DEM} (mean(st.dev.)) (kN)	E^{exp} (GPa) ν^{exp} F^{exp} (kN)
Tension	5×10^{-5}	10	31.0 (0.2)	30.6
			0.22 (0.002)	0.2
			421.9 (19.9)	369.6
Compression	5×10^{-5}	10	40.7 (0.2)	40.7
			0.20 (0.003)	0.2
			4349.4 (242.6)	4221.1

strength). After this point, the tensile modulus of elasticity drops as a consequence of internal damage. It should be noted that normal and shear breaks refer to the end of the softening path. Just before the peak strength is reached, the number of normal breaks increase rapidly since several softening contacts are not capable of withstanding more load. In tensile failure the number of shear breaks are very small which indicates that the shear behaviour is not dominant for this type of loading (Figure 5.39). The lines in the plots refer to the mean values of the 5 random assemblies, where as the grey areas show the variation of each test result.

Figure 5.38 presents three stages of the failure process due to tensile loading: ① with no damage; ② at peak strength; and, ③ at the end of the softening curve. At peak strength the main cracks are already formed on the ITZ and across some aggregates and, as the upper wall moves, these cracks bridge with each other and propagate through the mortar until all cross section of the specimen has failed.

Figure 5.40 presents the compressive strength test results including the development of the external work and kinetic energy, the decrease of the modulus of elasticity and the brittle stress-strain response. Figure 5.41 shows the failure patterns in compressive loading at peak strength and at the end of the softening curve. At peak strength large vertical cracks are already developed across the specimen and only very narrow concrete

columns remain intact. After peak strength, these vertical cracks increase their width and propagate into several ramifications very quickly.

The progressive reduction of the modulus of elasticity is due to both the decrease of the compressive contact stiffness (from k_n and k_s to $k_n^* = 0.3k_n$ and $k_s^* = 0.3k_s$, § 5.7.2 and § 5.7.1) and the development of softening of some contacts. This decrease of global stiffness occurs at approximately 40% of the peak strength and introduces the nonlinear behaviour of concrete before the maximum strength is reached (Coutinho and Gonçalves 1994). Since the stiff coarse aggregates introduce nonuniform stressed areas, there are some contacts that change to the reduced stiffness earlier than others, which allows for a progressive reduction of the global stiffness. Despite the progressive stiffness reduction, the concrete particle model still yield a brittle failure after the peak strength is reached.

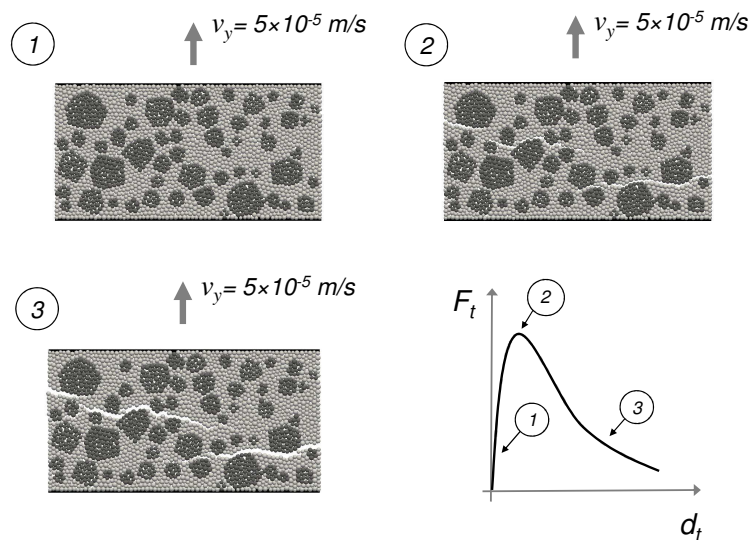


Figure 5.38: Development of cracking pattern and correspondence to the stress-strain behaviour under tensile stress

5.8. ANALYSIS OF THE FAILURE BEHAVIOUR OF CONCRETE CONSIDERING ITS MESOSTRUCTURE

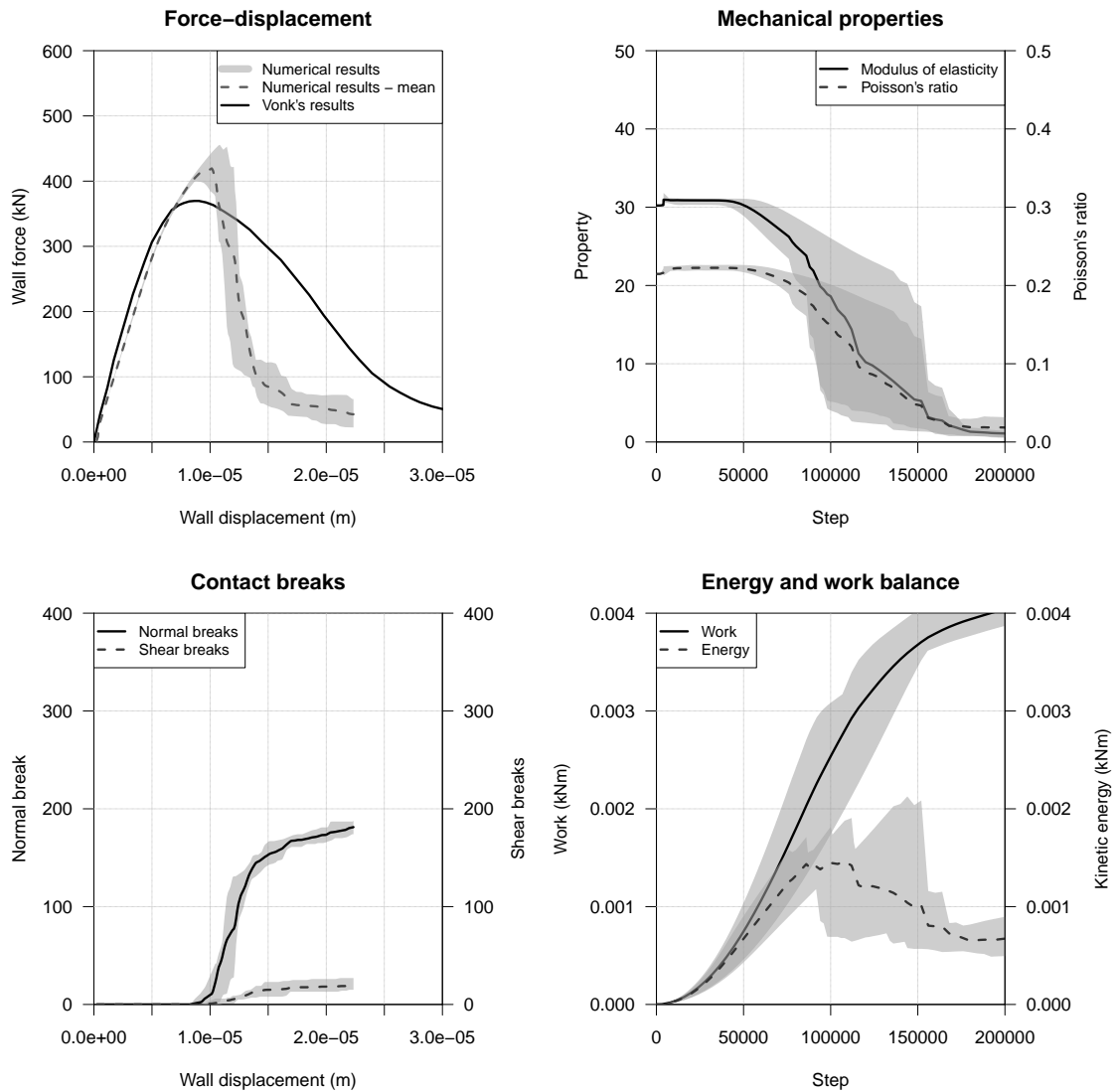


Figure 5.39: Results of direct tensile strength tests of the concrete particle model including the stress-strain behaviour and the development of the modulus of elasticity and Poisson's ratio, of the number of normal and shear contact breaks and of the work and kinetic energy

CHAPTER 5. NUMERICAL MODELLING OF THE CONCRETE STRUCTURAL PROPERTIES USING PARTICLE MODELS

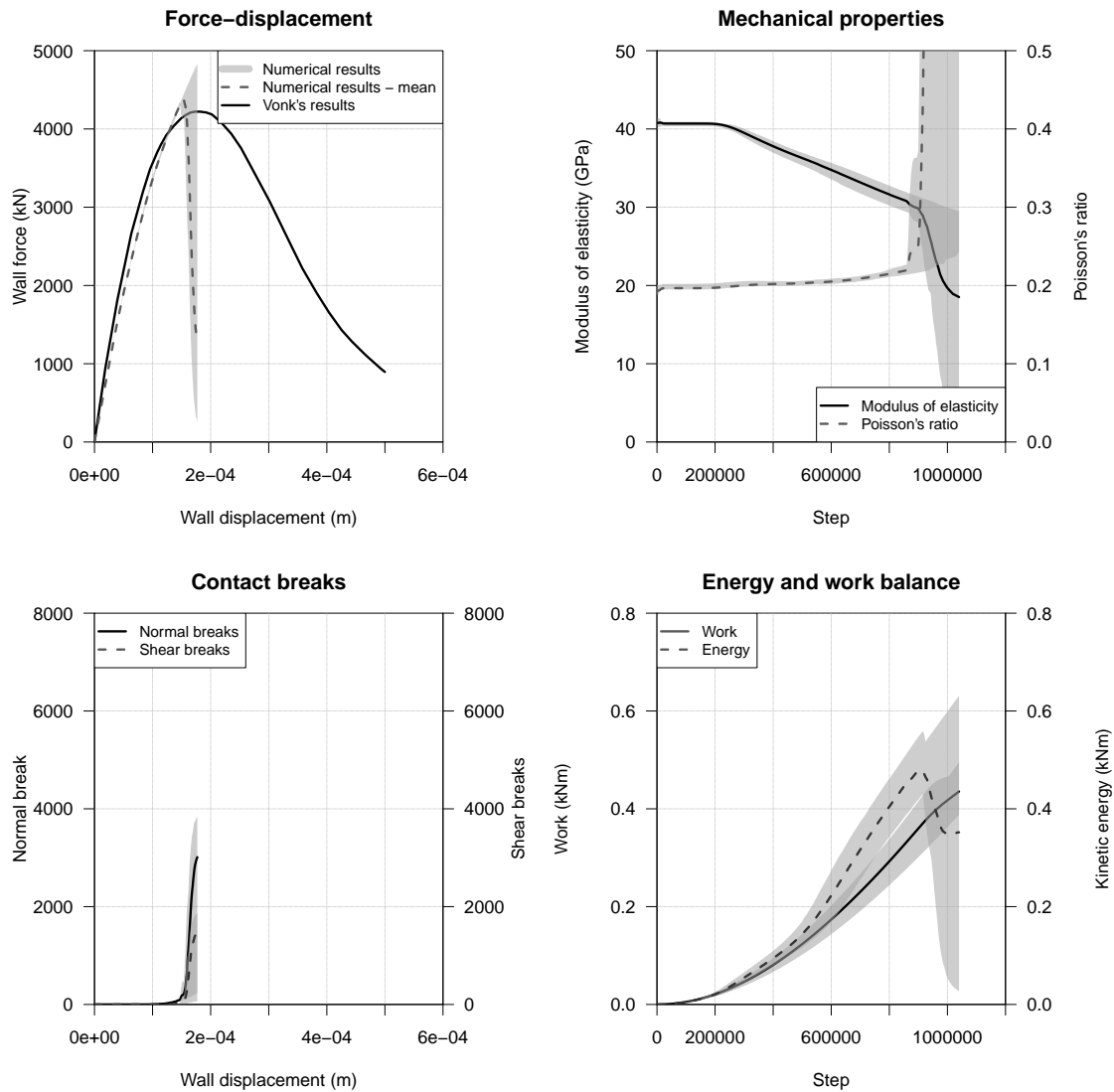


Figure 5.40: Results of compressive strength tests of the concrete particle model including the stress-strain behaviour and the development of the modulus of elasticity and Poisson's ratio, of the number of normal and shear contact breaks and of the work and kinetic energy

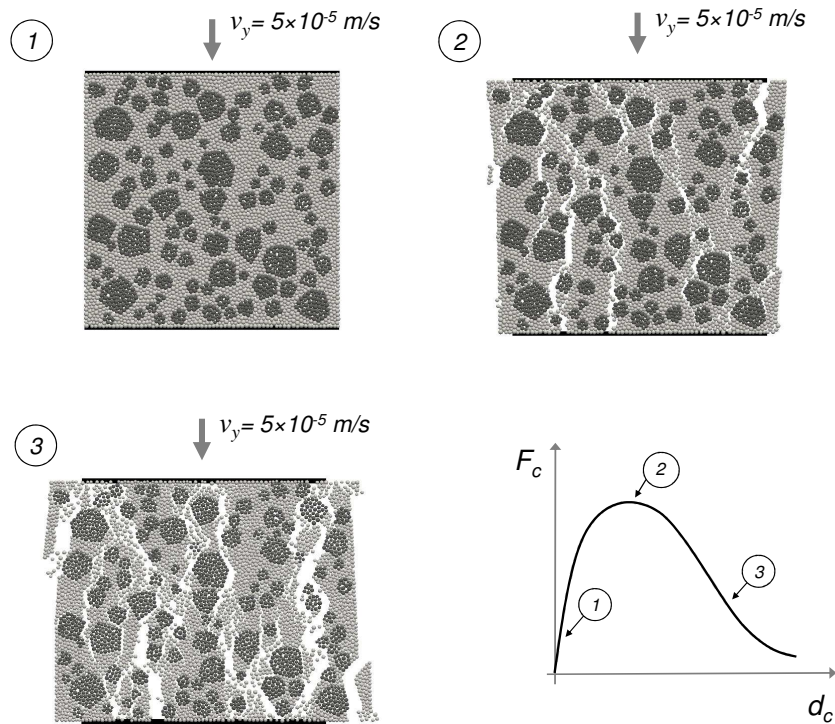


Figure 5.41: Development of cracking pattern and correspondence to the stress-strain behaviour under compressive stress

5.9 Concluding remarks

This chapter describes the discrete element method (DEM) formulation and its application to 2D particle models (PM) for the instantaneous and long-term analysis of quasi-brittle material behaviour with particular focus on concrete behaviour. The instantaneous and long-term analysis regarding the deformation properties require that the model reproduces the aging viscoelastic behaviour of cementitious materials considering a computationally efficient procedure. The prediction of the instantaneous stress-strain behaviour until failure for the prediction of concrete strength properties is based on a quasi-static test using the Mohr-Coulomb model at the contact level.

Firstly, an explicit formulation of a DEM particle model that includes aging viscoelastic contact behaviour based on the solidification theory is presented. Due to the computational costs associated with timestep constraints of DEM based particle model, a fast numerical procedure for the analysis of long-term aging viscoelastic behaviour of concrete is proposed. The fast numerical procedure separates the real time, related to the age since casting, and the numerical time, related to the convergence of the DEM model to a steady state

solution. A calibration procedure for the aging viscoelastic contact model parameters is presented, including new expressions for the delayed deformability macro properties.

The aging viscoelastic contact model based on the solidification theory is validated using a simple one contact particle assembly and other simple assemblies. It is shown that both the fully explicit DEM procedure response with small timestep and the fast numerical procedure response match the creep compliance analytical solution. The contact aging model validation tests using larger regular and random particle assemblies showed that the fast numerical procedure significantly reduces the computational time by introducing large timesteps in which the solution is computed, while giving the same accuracy of the fully explicit procedure.

The DEM aging concrete model was validated using Ward's experimental results and a B3 model fit to the Ward's experimental results for different loading ages. The aging viscoelastic contact properties of the mortar and of the interfacial transition zone (ITZ) and the elastic contact properties of the aggregate were determined during the particle model calibration procedure. The obtained numerical results show that the DEM aging viscoelastic particle model considering the concrete mesostructure can predict the long-term behaviour of concrete.

The second part of the chapter relates to the implementation and validation of failure contact models for the analysis of the stress-strain behaviour of cementitious material in quasi-static conditions. The Mohr-Coulomb model with tensile cut-off (brittle) and the Mohr-Coulomb model with linear softening were implemented into the DEM code at the contact level (normal and shear directions). A contact stiffness reduction for high compressive loadings was also implemented in order to have some control on the damage in compressed areas and increase the stress-strain curvature before the peak strength, as measured in normal strength concrete tests. The contact behaviour was validated using simple particle assemblies, predefined failure areas and controlled loading conditions, both pure tension and pure shear loadings.

A more complex model validation was done regarding realistic concrete particle models with explicit representation of the coarse aggregates. Prior to the calibration of the micro parameters, a sensitivity analysis for the main parameters was presented. This sensitivity analysis helped to understand the effect of the main input parameters and model properties on the macroscopic structural response. The main conclusions relate to the effect of normal contact strength and cohesion of the mortar and of the ITZ, the effect of the contact fracture

energy and the effect of lateral stiffness of the boundary wall. The validation of the model was based on the examples described by Vonk (1992) and on its numerical results using a polygonal DEM model for both tensile and compressive strength tests. The obtained results show that the concrete particle model has a much brittle response than Vonk (1992)'s model but it is able to reproduce the peak strength, the stiffness reduction before the strength maximum value and the expected failure patterns, both in tension and in compression.

Although the validation examples adopt a two-dimensional DEM particle model that has been implemented in C++, the proposed aging contact model, the proposed fast numerical procedure and the Mohr-Coulomb contact models can be readily incorporated in tridimensional DEM based codes.

The proposed numerical tool can be used to improve the prediction of long-term deterioration processes of concrete in which the properties of the coarse aggregate are relevant, for example for the prediction of early-age cracking due to hydration and temperature variations and for the study of alkali-aggregate reaction effect on the development of the mechanical properties.

Numerical modelling of the dam concrete structural properties using particle models

6.1 Introduction

The particle models can be used to predict the behaviour of heterogeneous materials considering different contact properties. For the modelling of concrete, the main heterogeneity is due to the aggregates, mainly because the rock used for the aggregates and the cement paste have very different mechanical properties and due to the weaker properties of the interfacial transition zone (ITZ).

This chapter presents the prediction of dam concrete mechanical properties using particle models. The behaviour of dam concrete depends mainly on the properties of the mortar and the aggregate obtained from the presented experimental results (§ 3) and on the content of each component in the concrete mixture. The computational costs limits the use of large number of particles and the refinement of the particle model relates to the minimum particle radius. The physical representation of the fine aggregates would require the use of very small particles when compared with the size of the specimen and would significantly increase the number of particles in the model. Therefore, for this work, concrete is represented by a mortar (cement paste and fine aggregates) and the coarse aggregates. The smallest coarse aggregate defines the radius of the particles used in throughout the specimen model.

The proposed approach is to characterize and model both the mortar and the coarse aggregates separately in order to control their behaviour in the heterogeneous model of concrete. The contact micro properties are calibrated using small homogeneous numerical specimens and following the procedure described in the previous chapter (§ 5.5.3). For the mortar, a long-term analysis is required for modelling the aging viscoelastic properties. For the aggregates, an elastic analysis defines the contact micro properties in order to obtain the macro properties of the intact rock.

The second part of this chapter presents the calibration of mortar's compressive and tensile strengths for several loading ages using the Mohr-Coulomb model with linear softening and the incorporation of these results on the prediction of wet-screened and dam concrete fracture behaviour.

The particle model of concrete considers the mortar and the coarse aggregates, which are explicitly taken into account. The aggregate's structure is built using an algorithm for the placement of coarse aggregates in the specimen based on a given sieve analysis (Monteiro Azevedo 2003).

Figure 6.1 shows the overall proposed approach for the prediction of wet-screened (SCR38 and SCR76) and dam (DAM) concretes using particle models. After the calibration of the properties of each component, they are used for modelling the different types of concrete, namely the wet-screened concrete and the dam concrete. The model prediction results are then compared with the available test results in order to evaluate the accuracy of the prediction.

The main difference between the two types of concrete is the aggregate's structure. The maximum size of aggregate of wet-screened concrete is 38 mm or 76 mm and the fraction volume of mortar is higher. The dam concrete has larger aggregates and, therefore, a large coarse aggregate content. It is considered that the mortar around the aggregates has the same properties in both concretes.

The numerical results obtained from the wet-screened and dam concrete particle model using DEM are compared with the experimental results.

6.2. PREDICTION OF DAM CONCRETE DEFORMABILITY PROPERTIES USING PARTICLE MODELS

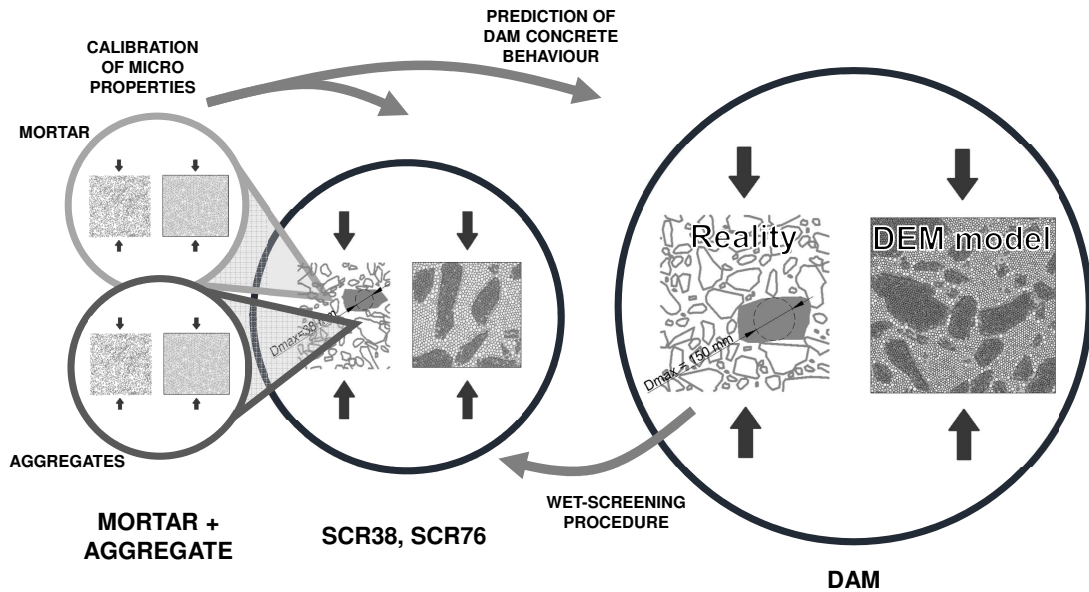


Figure 6.1: Schematic representation of the proposed approach for the prediction of dam concrete properties using particle models

6.2 Prediction of dam concrete deformability properties using particle models

6.2.1 Particle model definitions

The goal of this type of analysis is to explicitly take into account the deformability and strength properties of each component of concrete. Therefore, the particle model definitions should reflect, as much as possible, the internal structure of the different types of concrete.

It is assumed that the maximum particle radius, R_{max} and the same ratio between maximum and minimum particle radius, R_{min}/R_{max} is the same for each type of material across the entire particle assembly. This option is important due to the sensitivity of the results to the size of particles. The same discretization was used for the calibration procedure of the mortar and the aggregate.

The size of the particles have to take into consideration the size of the smallest coarse aggregate. On the other hand, the model refinement is constraint to the computational costs, especially when testing large specimens of dam concrete. The maximum particle radius definition is a combination of these two factors. By trial and error procedure, the maximum particle size was set to 1.5 mm, which is a fraction of the smallest coarse aggregate (4.75 mm). This value insures reasonable number of particles for testing the larger specimen within the smaller aggregates. The use of a ratio between maximum and

minimum particle radius, R_{min}/R_{max} , equal to $2/3$ increases the number of interactions between particles and increasing the number of contacts per particle, the coordination number, N_{coord} .

It has been shown that higher coordination number increases the internal material friction which can lead to more accurate stress-strain responses (Wang and Tonon 2009; Monteiro Azevedo and Lemos 2011). For the prediction of dam concrete behaviour using particle models, the definition of the contact points between particles and the contact area is obtained by a Voronoi tessellation, similarly to the work of Monteiro Azevedo *et al.* (2015). This type of contact detection increases the number of contacts when compared with the traditional contact detection scheme in which only real particle interactions are considered (Potyondy and Cundall 2004).

In order to reproduce the testing conditions, the particle model includes two rigid boundary walls, at the top and bottom of the specimen, which represent the rigid platens of the testing equipments and sets the same loading conditions for each boundary particle. Since only unconfined conditions will be considered, no lateral confinement is taken into account (Figure 6.2).

The loading conditions can be an applied force vector or an imposed velocity vector. The external applied force is distributed into contact force for each boundary particle according to the stiffness of the wall contact. When an imposed velocity is applied to the wall, all the boundary particles are affected with the same velocity. The boundary conditions are also defined by the walls, which can be restrained or unrestrained in the horizontal and vertical direction and for rigid body rotations. Although the wall can be fixed in all directions, the wall contacts define the actual boundary conditions between the platen and the specimen. The wall contacts are defined to link the wall to the assembly, transferring the loading and setting the restrains, and also to introduce the type of lateral interaction between the wall and the assembly. This lateral interaction can be defined as a shear stiffness in order to simulate the lateral forces developed during standard tests due to the friction between the platen and the concrete specimen or as a completely shear-free wall, for specific tests in which there is no lateral restraint to the specimen deformation (Vonk 1992).

Table 6.1 presents the definition of the model properties including each type of contact and its micro-properties for the prediction of aging viscoelastic and strength properties

6.2. PREDICTION OF DAM CONCRETE DEFORMABILITY
PROPERTIES USING PARTICLE MODELS

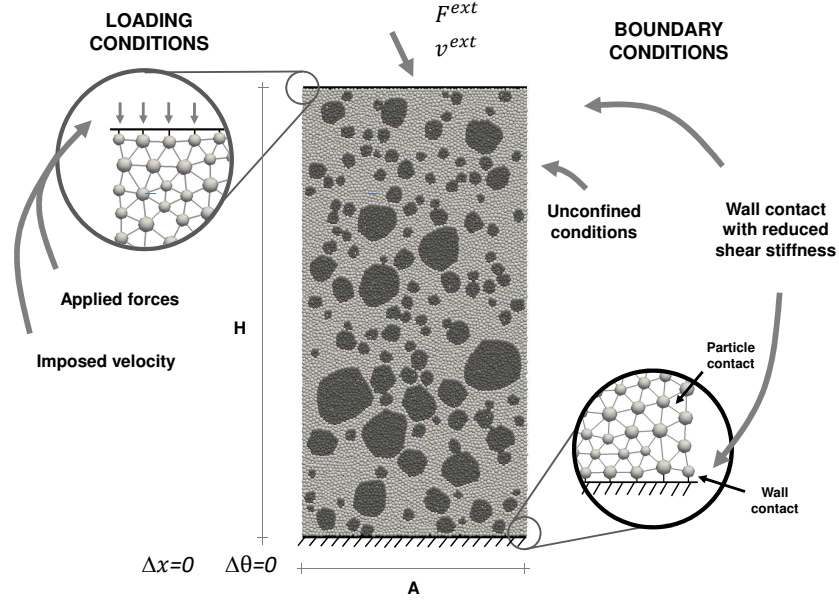


Figure 6.2: Representation of the loading conditions at the top wall and the boundary conditions of the particle model

of concrete. Five types of contacts are defined for interactions inside each type of aggregate (AGG150-AGG150, AGG76-AGG76, AGG38-AGG38, AGG19-AGG19 and AGG9.5-AGG9.5) and five types are also defined for the interactions between the mortar particles and each type of aggregate (MORTAR-AGG150, MORTAR-AGG76, MORTAR-AGG38, MORTAR-AGG19 and MORTAR-AGG9.5). The contacts between a given particle and a rigid wall (MORTAR/AGG i -WALL k) is always considered elastic, without the possibility of failure. The behaviour of each type of ITZ is taken into account using a serial model of the elastic properties of the aggregate (E_{agg}) and the aging viscoelastic properties of the ITZ ($q_{i,ITZ}$). Since the aggregates only have elastic behaviour, the asymptotic elastic part of the aging viscoelastic model of ITZ, $q_{1,ITZ}$, is affected by the aggregate's stiffness and the other aging coefficients, $q_{2,ITZ}$, $q_{3,ITZ}$ and $q_{4,ITZ}$, remain equal to the mortar properties,

$$\begin{aligned}
 q_{1,ITZ} &= \frac{1}{2E_{agg}} + \frac{q_{1,mortar}}{2} \\
 q_{2,ITZ} &= q_{2,mortar} \\
 q_{3,ITZ} &= q_{3,mortar} \\
 q_{4,ITZ} &= q_{4,mortar}
 \end{aligned} \tag{6.1}$$

Table 6.1: Particle model properties for the representation of concrete behaviour

Type of contact	Element A	Element B	Contact model	Contact micro-properties
AGG150-AGG150	Particle AGG150	Particle AGG150	Elastic model + Failure	$k_n^{agg150}, k_s^{agg150}, F_{n,max}^{agg150}, F_{s,max}^{agg150}$
AGG76-AGG76	Particle AGG76	Particle AGG76	Elastic model + Failure	$k_n^{agg76}, k_s^{agg76}, F_{n,max}^{agg76}, F_{s,max}^{agg76}$
AGG38-AGG38	Particle AGG38	Particle AGG38	Elastic model + Failure	$k_n^{agg38}, k_s^{agg38}, F_{n,max}^{agg38}, F_{s,max}^{agg38}$
AGG19-AGG19	Particle AGG19	Particle AGG19	Elastic model + Failure	$k_n^{agg19}, k_s^{agg19}, F_{n,max}^{agg19}, F_{s,max}^{agg19}$
AGG9.5-AGG9.5	Particle AGG9.5	Particle AGG9.5	Elastic model + Failure	$k_n^{agg9.5}, k_s^{agg9.5}, F_{n,max}^{agg9.5}, F_{s,max}^{agg9.5}$
AGG i - AGG j	Particle AGG i	Particle AGG j	Elastic serial model + Failure model	$k_n^{agg i}, k_s^{agg i}, k_n^{agg j}, k_s^{agg j}, F_{n,max}^{agg i}, F_{n,max}^{agg j}, F_{s,max}^{agg i}, F_{s,max}^{agg j}$
MORTAR-MORTAR	Particle MORTAR	Particle MORTAR	Aging viscoelastic model + Failure model	$q_n^{mortar}, q_s^{mortar}, F_{n,max}^{mortar}, F_{s,max}^{mortar}, G_{f,n}^{mortar}, G_{f,s}^{mortar}$
MORTAR-AGG150	Particle MORTAR	Particle AGG150	Aging viscoelastic model + Failure model	$k_n^{agg150}, k_s^{agg150}, q_n^{ITZ}, q_s^{ITZ}, F_{n,max}^{ITZ}, F_{s,max}^{ITZ}, G_{f,n}^{ITZ}, G_{f,s}^{ITZ}$
MORTAR-AGG76	Particle MORTAR	Particle AGG76	Aging viscoelastic model + Failure model	$k_n^{agg76}, k_s^{agg76}, q_n^{ITZ}, q_s^{ITZ}, F_{n,max}^{ITZ}, F_{s,max}^{ITZ}, G_{f,n}^{ITZ}, G_{f,s}^{ITZ}$
MORTAR-AGG38	Particle MORTAR	Particle AGG38	Aging viscoelastic model + Failure model	$k_n^{agg38}, k_s^{agg38}, q_n^{ITZ}, q_s^{ITZ}, F_{n,max}^{ITZ}, F_{s,max}^{ITZ}, G_{f,n}^{ITZ}, G_{f,s}^{ITZ}$
MORTAR-AGG19	Particle MORTAR	Particle AGG19	Aging viscoelastic model + Failure model	$k_n^{agg19}, k_s^{agg19}, q_n^{ITZ}, q_s^{ITZ}, F_{n,max}^{ITZ}, F_{s,max}^{ITZ}, G_{f,n}^{ITZ}, G_{f,s}^{ITZ}$
MORTAR-AGG9.5	Particle MORTAR	Particle AGG9.5	Aging viscoelastic model + Failure model	$k_n^{agg9.5}, k_s^{agg9.5}, q_n^{ITZ}, q_s^{ITZ}, F_{n,max}^{ITZ}, F_{s,max}^{ITZ}, G_{f,n}^{ITZ}, G_{f,s}^{ITZ}$
MORTAR/AGG i-WALL k	Particle MORTAR/AGG i	WALL k	Elastic model	$k_n^{wall k}, k_s^{wall k}$

6.2. PREDICTION OF DAM CONCRETE DEFORMABILITY PROPERTIES USING PARTICLE MODELS

As previously described in § 5.5.3, the prediction of concrete long-term behaviour using particle models requires the calibration of the microproperties of the main components of this heterogeneous material. Figures 6.3 and 6.4 show each calibration specimen and properties used for the prediction of wet-screened concrete and dam concrete. Table 6.2 presents the calibration scheme for each type of concrete considering its different components and the specimen sizes used for each test.

Figure 6.3 refers to the prediction of wet-screened concrete, where the maximum size of aggregate is 38 mm and only three coarse aggregate sizes are used, 38 mm, 19 mm and 9.5 mm. The contact behaviour for the three types of aggregates and for the mortar were calibrated to yield their macroscopic properties. For a concrete particle assembly, the particles inside the aggregates are classified as aggregate particles and the particles surrounding the aggregates are classified as mortar particles. The type of contact is defined by the classification of the two particles in contact. For example, a contact of two mortar particles is a mortar particle. The special case of the contact between an aggregate particle and a mortar particle is defined by a serial model of both the aggregate contact model and the interfacial transition zone contact model.

In order to compare the predicted results with the ones obtained in creep cells, the temperature history and its influence on the mechanical properties were taken into account in the contact model. This effect was considered using the maturity method, as previously used for the analytical composite models, considering uniform temperature field over the specimen. This effect is known to accelerate the mechanical property development as the temperature before testing increases. For each real time, T , the equivalent time, T_e , is calculated based on the previous temperature history and then used for the determination of the stiffness of each contact properties (§ 5.5.4).

Figure 6.4 illustrates the same calibration procedure for the dam concrete prediction including the larger aggregates that were removed during the wet-screening procedure ($MSA > 38$ mm) and the actual dam concrete specimen size. The properties of mortar and the ITZ's equivalent stiffness are considered the same as the SCR38 and SCR76 particle models. The effect of temperature on the development of the creep strains of viscoelastic materials is also considered.

CHAPTER 6. NUMERICAL MODELLING OF THE DAM CONCRETE STRUCTURAL PROPERTIES USING PARTICLE MODELS

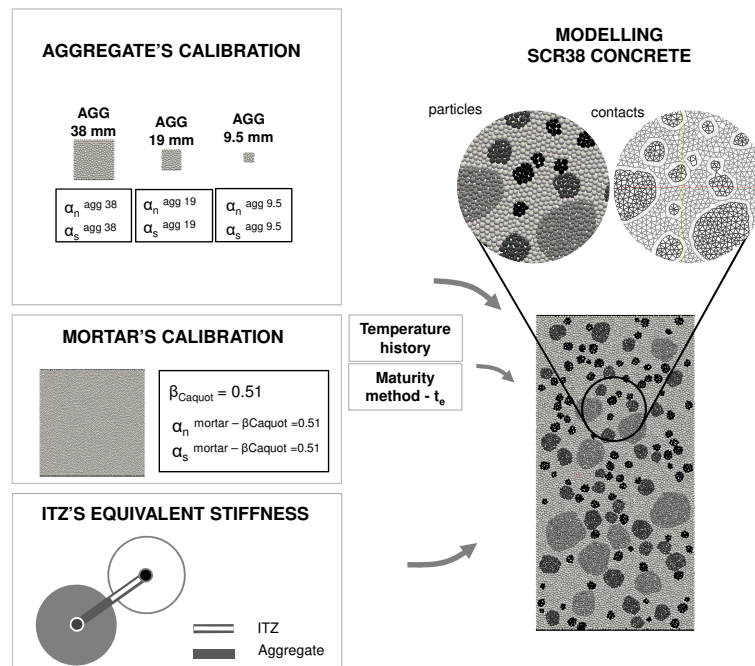


Figure 6.3: Calibration of the deformability properties of each component of concrete and modelling of #38 wet-screened concrete

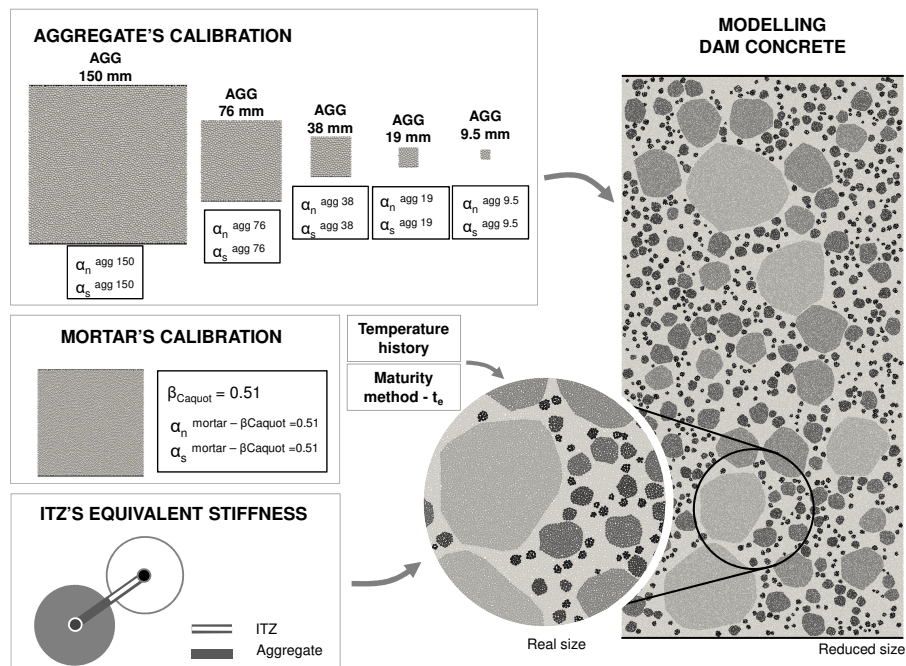


Figure 6.4: Calibration of the deformability properties of each component of concrete and modelling of dam concrete

6.2. PREDICTION OF DAM CONCRETE DEFORMABILITY PROPERTIES USING PARTICLE MODELS

Table 6.2: Calibration scheme for each type of concrete considering its different components

Type of concrete	Specimen size (mm × mm)	Macro properties	Type of component	Specimen size (mm × mm)	Macro properties	Micro parameters
SCR38	150 × 300	J_{SCR38} , ν_{SCR38}	AGG38	38 × 38	E_{agg}, ν_{agg}	$\alpha_n^{agg38}, \alpha_s^{agg38}$
			AGG19	19 × 19	E_{agg}, ν_{agg}	$\alpha_n^{agg19}, \alpha_s^{agg19}$
			AGG9.5	9.5 × 9.5	E_{agg}, ν_{agg}	$\alpha_n^{agg9.5}, \alpha_s^{agg9.5}$
			MORTAR	100 × 100	J_{mortar}, ν_{mortar}	$\alpha_n^{mortar}, \alpha_s^{mortar}$
SCR76	300 × 600	J_{SCR76} , ν_{SCR76}	AGG76	76 × 76	E_{agg}, ν_{agg}	$\alpha_n^{agg76}, \alpha_s^{agg76}$
			AGG38	38 × 38	E_{agg}, ν_{agg}	$\alpha_n^{agg38}, \alpha_s^{agg38}$
			AGG19	19 × 19	E_{agg}, ν_{agg}	$\alpha_n^{agg19}, \alpha_s^{agg19}$
			AGG9.5	9.5 × 9.5	E_{agg}, ν_{agg}	$\alpha_n^{agg9.5}, \alpha_s^{agg9.5}$
			MORTAR	100 × 100	J_{mortar}, ν_{mortar}	$\alpha_n^{mortar}, \alpha_s^{mortar}$
DAM	450 × 900	J_{DAM} , ν_{DAM}	AGG150	150 × 150	E_{agg}, ν_{agg}	$\alpha_n^{agg150}, \alpha_s^{agg150}$
			AGG76	76 × 76	E_{agg}, ν_{agg}	$\alpha_n^{agg76}, \alpha_s^{agg76}$
			AGG38	38 × 38	E_{agg}, ν_{agg}	$\alpha_n^{agg38}, \alpha_s^{agg38}$
			AGG19	19 × 19	E_{agg}, ν_{agg}	$\alpha_n^{agg19}, \alpha_s^{agg19}$
			AGG9.5	9.5 × 9.5	E_{agg}, ν_{agg}	$\alpha_n^{agg9.5}, \alpha_s^{agg9.5}$
MORTAR	100 × 100	J_{mortar}, ν_{mortar}	$\alpha_n^{mortar}, \alpha_s^{mortar}$			

6.2.2 Prediction of mortar's creep compliance based on the concrete properties

Due to several types of constraints, the experimental characterization of the long-term properties of the mortar was not possible. In order to obtain the aging viscoelastic properties of the mortar, the composite model, proposed by Granger and Bažant (1995) and described in § 4.3.5, was used.

The composite model gives a prediction of the concrete behaviour based on the properties of the aging viscoelastic matrix and of the elastic inclusions and their proportion in a unit volume (Equations 6.3 to 6.6). An inverse procedure using genetic algorithms was used to find the aging viscoelastic parameters of the mortar, $q_1^{Mortar,SCR38}$, $q_2^{Mortar,SCR38}$, $q_3^{Mortar,SCR38}$ and $q_4^{Mortar,SCR38}$. The inverse procedure optimizes the goal function defined by Equation 6.2, which minimizes the difference between the wet-screened creep compliance fitted to experimental results, $J^{SCR38}(t, t')$ (defined in Table 6.3), and the creep compliance prediction of the composite model, $J_{composite}(t, t')$ (defined by the Equation 6.3),

$$\min \left[\sum_{i=1}^m \sum_{j=1}^n \left(J_{Core-SCR38}(t_j, t'_i) - J_{composite}(t_j, t'_i, q_1^{Mortar, SCR38}, q_2^{Mortar, SCR38}, q_3^{Mortar, SCR38}, q_4^{Mortar, SCR38}) \right)^2 \right] \quad (6.2)$$

where the n and m are the number of loading ages and the number of measured values over the loading time, respectively,

$$J_{composite}(t, t') = \frac{\beta}{\alpha E_a + (1 - \alpha) E_m(t')} \left[1 + (1 - \alpha) \frac{E_m''}{E_{am}''} \phi(t, t') \right] + (1 - \beta) J_m(t, t') \quad (6.3)$$

in which,

$$\phi_m(t, t') = E_m(t') J_m(t, t') - 1 \quad (6.4)$$

$$E_m''(t, t') = \frac{E_m(t') - R_m(t, t')}{\phi_m(t, t')} \quad (6.5)$$

$$E_{am}''(t, t') = \alpha E_a + (1 - \alpha) E_m''(t, t') \quad (6.6)$$

where $\phi_m(t, t')$ is the creep coefficient of the mortar, $E_m''(t, t')$ is the age-adjusted modulus of elasticity of the mortar and $E_{am}''(t, t')$ is the age-adjusted modulus of elasticity of the parallel portion of aggregate and mortar.

Table 6.3: Parameters of B3 model for Core-SCR38 wet-screened concrete (#38)

Material	q_1^{SCR38} (1×10^{-6} /MPa)	q_2^{SCR38} (1×10^{-6} /MPa)	q_3^{SCR38} (1×10^{-6} /MPa)	q_4^{SCR38} (1×10^{-6} /MPa)
Core-SCR38 concrete	24.17	82.75	17.4	5.54

The composite model parameter, β , was obtained using the Caquot law for the prediction of the maximum aggregate volume, $V_{a,max}$ (Equation 6.7) applied to the wet-screened concrete. Table 6.4 presents the calculation of β_{Caquot} based on the properties of Core-SCR38 concrete.

6.2. PREDICTION OF DAM CONCRETE DEFORMABILITY
PROPERTIES USING PARTICLE MODELS

$$V_{a,max} = 1 - 0.47 \left(\frac{d_{min}}{d_{max}} \right)^{\frac{1}{5}} \quad (6.7)$$

Table 6.4: Calculation of β_{Caquot} based on the properties of Core-SCR38 concrete

Composite model	d_{min} (mm)	d_{max} (mm)	V_a (m^2/m^2)	$V_{a,max}$ (m^2/m^2)	β_{Caquot}
Mortar Core-SCR38	4.75	38	0.35	0.69	0.51

The optimization procedure using genetic algorithms yield the B3 model parameters presented in Table 6.5, which was validated using the composite model, for several loading ages. Figure 6.5 shows the validation of the fit with the comparison between the concrete creep compliance obtained from the experimental results and the creep compliance obtained from the composite model using the fitted parameters of the mortar.

Table 6.5: Parameters of B3 model for the mortar

Concrete	q_1^{mortar} ($1 \times 10^{-6}/\text{MPa}$)	q_2^{mortar} ($1 \times 10^{-6}/\text{MPa}$)	q_3^{mortar} ($1 \times 10^{-6}/\text{MPa}$)	q_4^{mortar} ($1 \times 10^{-6}/\text{MPa}$)
Mortar Core-SCR38	27.2	164.7	26.0	11.6

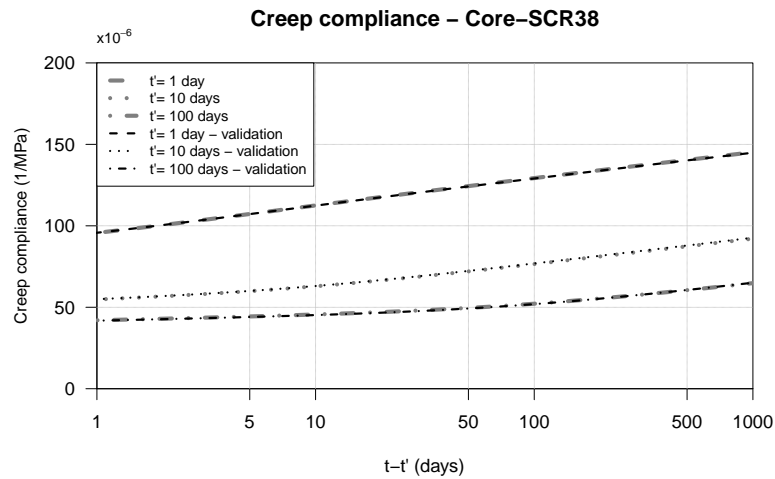


Figure 6.5: Validation of the composite model for the prediction of mortar's creep compliance based on the #38 wet-screened concrete

As discussed in the previous chapter, test results of the ITZ are difficult to obtain and its effect on the concrete behaviour is complex. For the case study example, the ITZ properties were obtained by fitting the results of the particle model to the experimental values of concrete deformability, using the mortar and the aggregate properties.

The use of the two-phase composite model implies that the matrix embedding the inclusions includes both the mortar's and the ITZ's deformability properties, for this type of concrete. The estimated mortar's creep compliance using this methodology reflects the proportion of these two materials and its effect on the long-term properties of concrete.

After the validation of the particle model, the mortar Core-SCR38, which includes the contribution of the ITZ, is then used for the prediction of both SCR76 wet-screened (#76) and dam concrete.

6.2.3 Calibration of micro parameters of the contacts for the aggregates and for the mortar

As described in the previous chapter, the discrete element method implies the calibration of the micro-properties for the interaction law at the contact between elements. For a given discrete element assembly, the macroscopic response is determined by each set of micro-properties.

Following the proposed procedure for particle models (§ 5.4), the aging viscoelastic micro-properties and the elastic micro-properties were fitted to the creep compliance of the mortar and of the aggregates, respectively.

The elastic macroscopic properties of the aggregate are the modulus of elasticity, $E^{macro,agg}$ and the Poisson's ratio, $\nu^{macro,agg}$, which are known to be proportional to the elastic normal contact stiffness, k_n , and to the ratio between the shear and normal contact stiffness, k_s/k_n ,

$$k_n^{agg} = \alpha_n^{agg} \frac{E^{macro,agg} A}{d} \quad (6.8)$$

$$\nu^{macro,agg} \propto \frac{k_s^{agg}}{k_n^{agg}} = \alpha_s^{agg}, \quad k_s^{agg} = \alpha_s^{agg} k_n^{agg} \quad (6.9)$$

where α_n^{agg} and α_s^{agg} are calibrated micro-parameters. A and d are the contact area and the distance between particle centers. As described in the previous chapter, different values of A can be used. For the study of dam and wet-screened concrete the value is the contact area provided by the Voronoi tessellation (§ 6.2.1).

Table 6.6 presents the obtained micro-parameters calibrated to fit the mean modulus of elasticity and Poisson's ratio of the aggregate. As shown in Figures 6.3 and 6.4, the calibration models for each aggregate are square homogeneous particle assemblies with

6.2. PREDICTION OF DAM CONCRETE DEFORMABILITY
PROPERTIES USING PARTICLE MODELS

sides of $A_{specimen}$ equal to the size of the aggregate. The micro-parameters, α_n^{agg} and α_s^{agg} , of the different aggregates are very similar to each other.

Table 6.6: Calibration micro parameters for the modelling of each aggregate's deformability properties

Calibration model	E^{macro} (GPa)	ν^{macro}	$A_{specimen}$ (mm)	R_{max} (mm)	α_n	α_s
AGG150			150		1.318	0.220
AGG76			76		1.339	0.209
AGG38	46.3	0.25	38	1.5	1.376	0.171
AGG19			19		1.331	0.169
AGG9.5			9.5		1.283	0.378

The calibration procedure of the mortar aims to find the micro-parameters, α_n^{mortar} and α_s^{mortar} , which relates the macroscopic creep compliance, $J^{macro,mortar}$, and Poisson's ratio, $\nu^{macro,mortar}$, of the mortar with the microscopic normal and shear creep compliances, J_n^{micro} and J_s^{micro} . The macroscopic creep compliance yields the development of the modulus of elasticity and of the creep strains over time.

$$J_n^{micro} = \frac{1}{\alpha_n^{mortar}} J^{macro,mortar} \quad (6.10)$$

$$\nu^{macro,mortar} \propto \frac{J_s^{mortar}}{J_n^{mortar}} = \alpha_s^{mortar}, \quad J_s^{micro} = \frac{1}{\alpha_s^{mortar}} J_n^{micro} = \frac{1}{\alpha_s^{mortar} \alpha_n^{mortar}} J^{macro} \quad (6.11)$$

Table 6.7 presents the mortar calibration results for each loading age. For a given particle assembly, the micro-parameters, α_n^{mortar} and α_s^{mortar} , do not vary significantly with loading age and the mean value was used for numerical simulations.

Table 6.7: Calibration micro parameters for the modelling of mortar's deformability properties

Calibration model	J^{macro} (GPa)	ν^{macro}	R_{max} (mm)	β	Age (days)	α_n	α_s	α_n (mean)	α_s (mean)
Mortar					7	0.418	0.318		
Core-SCR38	Table 6.5	0.20	1.5	0.51	28	0.405	0.340	0.408	0.325
					90	0.405	0.320		
					365	0.402	0.323		

6.2.4 Generation of wet-screened and dam concrete's aggregate structure

The procedures for the generation of a particle assembly is already described in the previous chapter (§ 5.4) and published in specific documents (Wang *et al.* 1999; Monteiro Azevedo *et al.* 2008). This section aims to give some insight on the generation of particle assemblies of wet-screened and dam concretes and to discuss the difficulties associated to the construction of realistic models.

In order to have a refined particle model throughout the entire specimen and a realistic contribution of each coarse aggregate, the size of the particle had to take into account the size of the smallest aggregate and the computational limitations. The use of very small particles would represent the smallest coarse aggregate but with a high computational cost, especially for the case of large specimen tests.

Three particle sizes were tested in order to evaluate the computational time of each particle model considering the maximum radius, R_{max} , equal to 1.0, 1.2 and 1.5 mm. The ratio between the minimum and the maximum radius was considered equal to $2/3$. Table 6.8 presents the discretization of the smallest coarse aggregate and the estimated size of the concrete particle assembly for each specimen and for each maximum particle radius.

It was considered that the value of 1.5 mm for the maximum radius was sufficiently small to include the influence of the deformability of the smallest coarse aggregate ($\Phi_{4.75} = 4.75$ mm) without compromising the size of the structural problem with an excessive number of particles and contacts, especially for the analysis of Core-DAM concrete. In average, the smallest aggregate includes two particles in each direction, *i.e.*, one contact in each direction ($\Phi_{4.75}/R_{mean} \times 2$, R_{mean} is the mean radius).

Table 6.8: Influence of the minimum particle radius on the size of the concrete particle assembly

Type of concrete	Type of specimen	V_{spec} (m ²)	$\frac{R_{min}}{R_{max}}$	R_{max} (mm)	R_{min} (mm)	R_{mean} (mm)	$\frac{\Phi_{4.75}}{R_{med} \times 2}$	Number of particles	Number of contacts
Core-DAM	450 × 900	0.405	$\frac{2}{3}$	1.00	0.67	0.84	2.83	± 182703	± 1096218
				1.20	0.80	1.00	2.38	± 128916	± 773496
				1.50	1.00	1.25	1.90	± 82506	± 495036
Core-SCR76	300 × 600	0.180	$\frac{2}{3}$	1.00	0.67	0.84	2.83	± 81202	± 487212
				1.20	0.80	1.00	2.38	± 57296	± 343776
				1.50	1.00	1.25	1.90	± 36669	± 220014
Core-SCR38	150 × 300	0.045	$\frac{2}{3}$	1.00	0.67	0.84	2.83	± 20300	± 121800
				1.20	0.80	1.00	2.38	± 14324	± 85944
				1.50	1.00	1.25	1.90	± 9167	± 55002

6.2. PREDICTION OF DAM CONCRETE DEFORMABILITY PROPERTIES USING PARTICLE MODELS

The particle assembly procedure starts by defining the largest coarse aggregates areas inside the specimen geometry and generating a compact assembly for each aggregate. The placement of one type of aggregate is defined by the upper and lower sieve and follows a uniform distribution within that aperture range (for example, MSA=150 mm aggregate area is defined between the 150 mm and the 76 mm sieve aperture). After the prescribed volume is placed and the compact particle assembly is completed inside each placed aggregate, the next type of aggregate is defined and so forth for the remaining aggregates. Finally, after all the aggregate types are placed, the remaining specimen volume is filled following a similar algorithm. Figure 6.6 shows the aggregate placement procedure for each type of concrete and specimen.

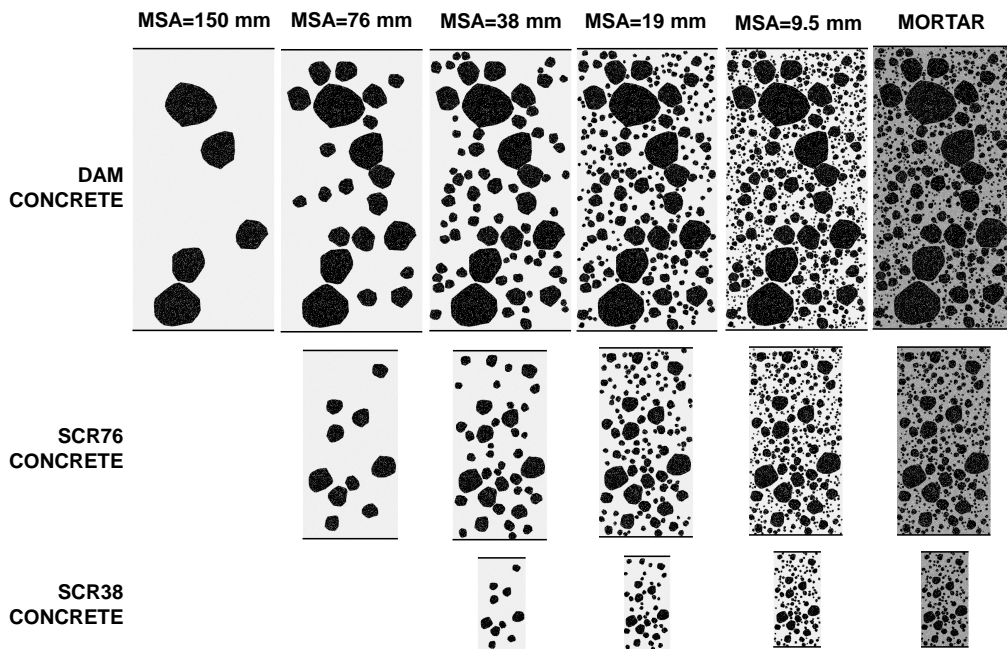


Figure 6.6: Generation of concrete's aggregate structure for the analysis of particle models

Tables 6.9 and 6.10 present the sieve analysis for the studied concretes considering the unit volume of each type of coarse aggregate (between sieves) and the properties of the particle models including the volume of the specimen, the volume of fine aggregate and coarse aggregates. The aggregate fraction volume can reach up to 68% of the specimen volume, for the Core-DAM concrete and 50% are coarse aggregates.

Figure 6.7 shows the comparison between the sieve analysis of the coarse aggregates placed in the concretes and in particle models (DEM), in cumulative weight percent retained in each sieve. The coarse aggregate distributions in the concrete particle models (dots in Figure 6.7) are very close to ones in the real concrete specimens (lines in Figure 6.7).

CHAPTER 6. NUMERICAL MODELLING OF THE DAM CONCRETE
STRUCTURAL PROPERTIES USING PARTICLE MODELS

Beside presenting the aggregate placement procedure, Figure 6.6 illustrates the size of each specimen and its relationship with the maximum size of the aggregate. This figure clearly shows the differences between the SCR38 wet-screened concrete and the dam concrete.

Table 6.9: Sieve analysis for each type of concrete placed in Baixo Sabor dam

Material	V_a (coarse aggregate) (m^2/m^2)					Total
	4.75/9.5 mm	9.5/19 mm	19/37.5 mm	37.5/75 mm	75/150 mm	
Core-DAM	0.065	0.082	0.096	0.123	0.133	0.499
Core-SCR76	0.076	0.096	0.112	0.144	-	0.428
Core-SCR38	0.093	0.117	0.136	-	-	0.346

Table 6.10: Properties of each type of concrete and of concrete particle models

Type of concrete	Type of specimen	V_{spec} (m^2)	$V_{a,fine}$ (m^2)	$V_{a,coarse}$ (m^2)	$V_{a,total}/V_{spec}$	$V_{a,coarse}/V_{spec}$
Core-DAM	450 × 900	0.405	0.075	0.202	0.68	0.50
Core-SCR76	300 × 600	0.180	0.038	0.077	0.64	0.43
Core-SCR38	150 × 300	0.045	0.011	0.016	0.58	0.35
Core-DAM (DEM-random #1)	450 × 900	0.405	-*	0.202	-*	0.50
Core-SCR76 (DEM-random #1)	300 × 600	0.180	-*	0.074	-*	0.41
Core-SCR38 (DEM-random #1)	150 × 300	0.045	-*	0.015	-*	0.33

* The fine aggregates are not represented in the concrete particle models

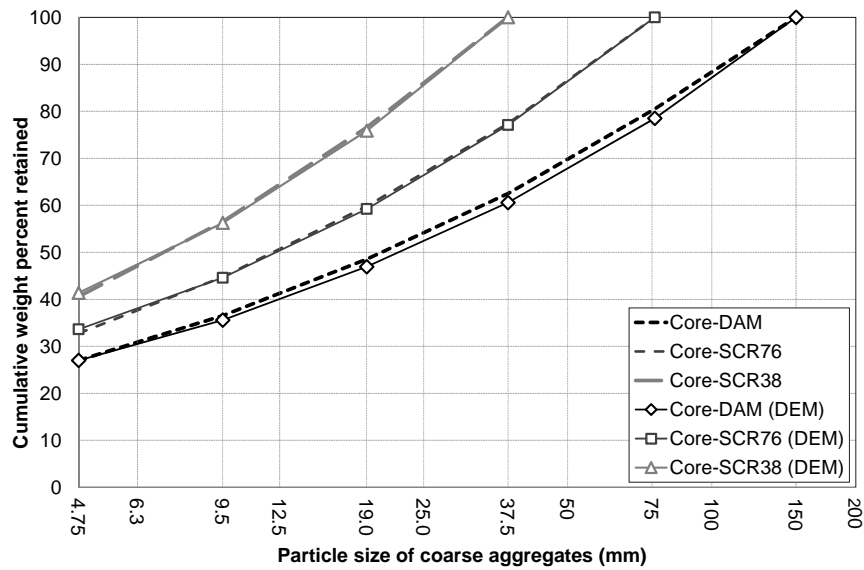


Figure 6.7: Comparison between the sieve analysis of DAM and SCR38 concretes and of the generated assemblies for the DEM analysis

6.2.5 Influence of the aggregate content and maximum size of aggregate on the behaviour of concrete

Most of the studies involving the concrete mesostructure are applied to conventional concrete, in which the coarse aggregate size ranges from 4.75 mm to 25-32 mm. In the special case of dam concrete the range of coarse aggregate sizes is very wide, from 4.75 mm to 150 mm. The heterogeneity of dam concrete and the aggregate distribution inside the mortar matrix is expected to be higher than conventional concretes. Additionally, since the minimum radius used in the concrete assembly is fixed, the ratio between the size of the aggregate and the particle radius is also very different, for each sieve size.

In order to investigate the behaviour of each type of aggregate embedded in a mortar matrix, a series of simple particle assemblies were generated. Each particle model has only one type of aggregate and three aggregate fraction volume (V_a/V_t). The particle models were tested in compression and the macroscopic modulus of elasticity was determined. The results were compared with the results of Granger's composite model.

The particle models were generated using square specimens around each type of aggregate according to the aggregate fraction: four aggregate sizes ($\Phi = 150 \text{ mm}$, $\Phi = 76 \text{ mm}$, $\Phi = 38 \text{ mm}$, $\Phi = 19 \text{ mm}$ and $\Phi = 9.5 \text{ mm}$); and three fraction volumes ($V_a/V_t = 0.2$, $V_a/V_t = 0.4$ and $V_a/V_t = 0.6$). Three random assemblies were generated for each type

of particle model. Figure 6.8 shows the twelve types of particle models and the micro properties of each type of material.

The macroscopic modulus of elasticity of each individual material was obtained using an uniform particle model for the aggregate and for the mortar. The macroscopic modulus of elasticity of the aggregates and of the mortar yield reasonably close values to the mean aggregate's and mortar's modulus of elasticity (46.3 and 14.9 GPa at the age of 28 days, respectively). The micro properties of each type of contact were fixed to values similar to the obtained previously in the calibration process ($\alpha_n^{mortar} = 0.5$, $\alpha_s^{mortar} = 0.3$, $\alpha_n^{agg} = 1.3$, $\alpha_n^{agg} = 0.15$). The results of the uniform particle models are presented in Table 6.11.

Considering the individual macroscopic modulus of elasticity of each material, Granger's composite model was used to obtain an estimate of the concrete modulus of elasticity for each aggregate's fraction volume. It is assumed that the value of β is the square root of the unit volume of aggregate, which is the most usual case in a concrete mix. The comparison between the prediction of the particle model and the estimate of the composite model is presented in Table 6.11 and Figure 6.9.

The comparison shows that the particle model follows the expected elastic behaviour of concrete. The maximum percentual deviation (Equation 6.12) is approximately 10% of the composite modulus of elasticity. These deviations can be explained by the randomness of the shape and position of the aggregate inside the square specimen of the particle model. For example, particle models with aggregate fraction volume equal to 0.6 have larger predicted values than the composite estimate. This can be due to a very small portion of mortar in parallel in the particle assembly, yielding higher larger modulus of elasticity. Despite that, the particle models capture the overall behaviour.

$$\epsilon_E = \frac{E_{concrete}^{DEM} - E_{concrete}^{composite}}{E_{concrete}^{composite}} \times 100 \quad (6.12)$$

Although similar situations can occur inside the concrete mix it is considered that the particle models are adequate to simulate the composite behaviour even for the specific case of dam concrete with a large ratio between the size of larger and the smaller aggregate.

6.2. PREDICTION OF DAM CONCRETE DEFORMABILITY PROPERTIES USING PARTICLE MODELS

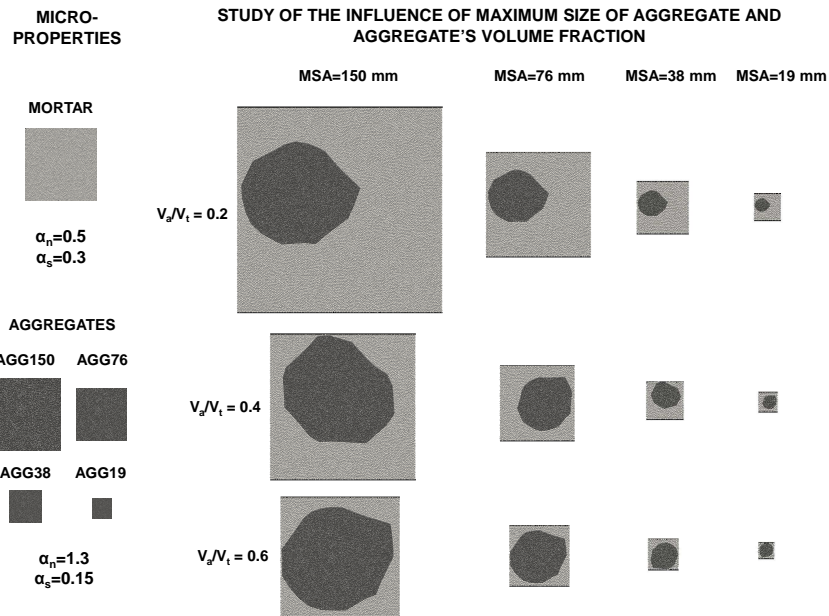


Figure 6.8: Types of simple particle models for the studying the influence of the aggregate content and maximum size of aggregate

Table 6.11: Results of each type of single aggregate particle model

MSA (mm)	V_a/V_t	V_a/V_t (DEM)	$\beta = \alpha$	E_{mortar}^{DEM} (GPa)	E_{agg}^{DEM} (GPa)	$E_{concrete}^{composite}$ (GPa)	$E_{concrete}^{DEM}$ (GPa)	ϵ_E (%)
19	0.2	0.23	0.48	16.1	43.2	20.5	18.9 (0.2)	-8.0
19	0.4	0.43	0.65	16.1	43.2	24.5	26.2 (0.4)	3.4
19	0.6	0.63	0.79	16.1	43.2	29.4	31.7 (0.6)	11.4
38	0.2	0.23	0.48	16.1	43.2	20.4	19.9 (0.1)	-3.4
38	0.4	0.43	0.66	16.1	43.2	24.6	24.4 (0.2)	2.9
38	0.6	0.64	0.80	16.1	43.2	29.7	32.5 (0.1)	12.8
76	0.2	0.23	0.48	16.1	43.7	20.5	20.0 (0.0)	-2.8
76	0.4	0.45	0.67	16.1	43.7	25.1	26.3 (0.0)	4.5
76	0.6	0.66	0.81	16.1	43.7	30.6	34.2 (0.1)	10.8
150	0.2	0.23	0.48	16.1	43.7	20.5	20.8 (0.0)	-0.5
150	0.4	0.46	0.68	16.1	43.7	25.3	25.3 (0.1)	3.0
150	0.6	0.66	0.81	16.1	43.7	30.4	33.6 (0.1)	10.9

Note: The presented DEM results are the mean and standard deviation (inside the parenthesis) of three random particle generations

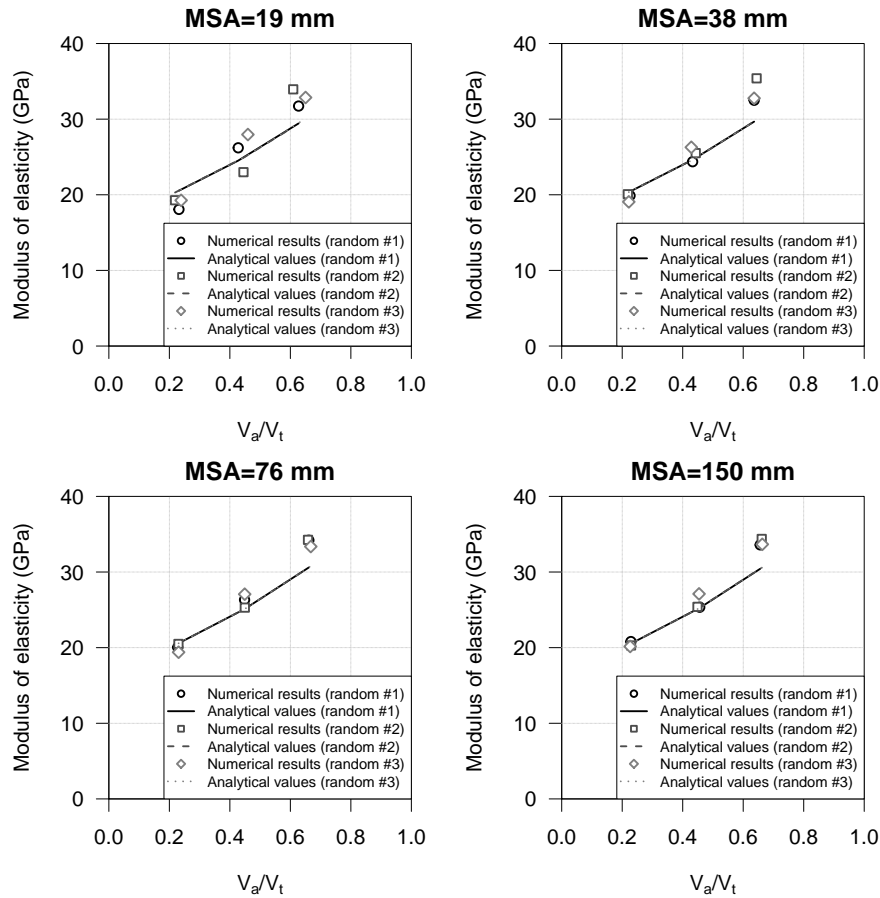


Figure 6.9: Results of each type of simple particle model

6.2.6 Influence of temperature on the development of the mechanical properties

As previously discussed, temperature has a dual effect on concrete deformability: higher temperatures increases the mechanical property rate of development, decreasing the creep rate; and it increases the movement of water inside the cement structure and the rate of bond breakage and, therefore, increasing the creep strains (Bažant and Baweja 2000). The effect of temperature can be taken into account by converting both the loading age and the time under loading into equivalent values, based on the measured temperature and maturity concepts. This mechanism is especially relevant for the interpretation of the experimental results obtained in creep cells (§ 3.7.3).

The equivalent time, t'_e , and the reduced time, t_r , can be obtained, respectively, by Equations 6.13 and 6.14. Both times are applied to the aging viscoelastic model at each contact, discussed in § 5.5.2.

$$t'_e = \int_0^{t'} \beta_T(\tau) d\tau \quad (6.13)$$

$$t_r = \int_{t'}^t \psi_T(\tau) d\tau \quad (6.14)$$

$$\beta_T = \exp \left[\frac{Q_h}{R} \left(\frac{1}{T_{ref} + 273} - \frac{1}{T + 273} \right) \right] \quad (6.15)$$

$$\psi_T = \exp \left[\frac{Q_v}{R} \left(\frac{1}{T_{ref} + 273} - \frac{1}{T + 273} \right) \right] \quad (6.16)$$

where T_{ref} is the reference temperature in degrees Celsius, T is the measured temperature in degrees Celsius and R is the gas constant ($8.31JK^{-1}mol^{-1}$) and, according to experimental fit to laboratory tests (Bažant and Baweja 2000), the apparent activation energies for hydration, Q_h/R , and viscous processes, Q_v are, respectively, $2700^\circ K$ and $5000^\circ K$.

In order to validate the temperature effect on creep strains, an uniform particle assembly was tested using the concrete properties and results available in (Bažant and Baweja 2000) from Kommendat, in 1976. Kommendat's creep tests included a reference test at a temperature of $23^\circ C$ and two validation tests at temperatures of $43^\circ C$ and $71^\circ C$. The creep compliance macro-properties were obtained from literature ($q_1^{macro} = 20.0 \times 10^{-6}/MPa$, $q_2^{macro} = 70.0 \times 10^{-6}/MPa$, $q_3^{macro} = 5.6 \times 10^{-6}/MPa$, $q_4^{macro} = 7.0 \times 10^{-6}/MPa$, $\nu^{macro} = 0.20$) (Bažant and Baweja 2000) and the micro-properties were calibrated yielding the following micro-parameters, $\alpha_n = 0.402$ and $\alpha_s = 0.323$, considering a minimum particle radius equal to 1.5×10^{-4} m.

Figure 6.10 show the comparison between Kommendat's creep test results and the numerical results obtained using the uniform particle model. The dashed lines are the fit to the reference temperature results ($23^\circ C$). The continuous lines are the numerical results using the fitted macro-properties, the calibrated micro-parameters and considering the testing temperatures of $43^\circ C$ (left plot) and of $71^\circ C$ (right plot).

The results show that the maturity concepts using the equivalent time, t'_e , and the reduced time, t_r , applied to the particle model are able to represent the main effect of temperature on creep strains, *i.e.* as the temperature increases there is an acceleration of the creep strain development.

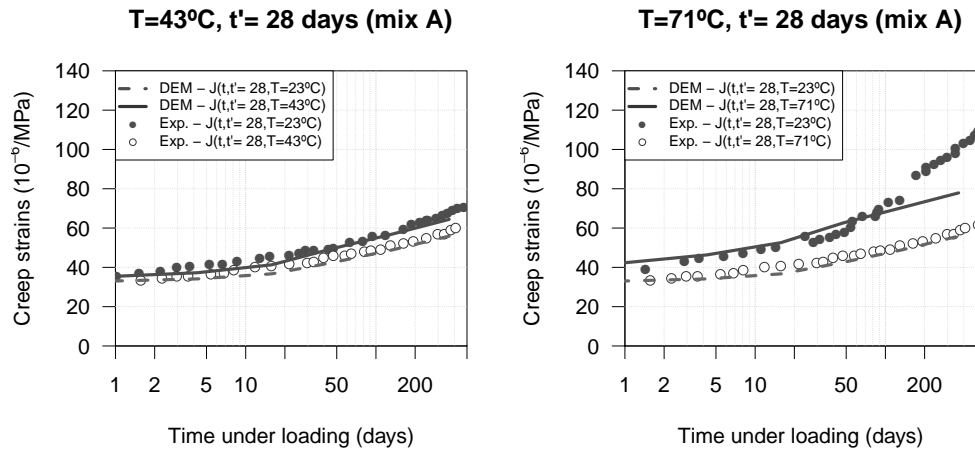


Figure 6.10: Validation of the temperature effect on the development of the creep strains

6.2.7 Prediction of wet-screened concrete long-term deformability properties

6.2.7.1 Validation of the particle model

The prediction of wet-screened concrete properties using particle models is based on the micro-properties obtained from the calibration procedure of each component of concrete and on the particle assembly considering the concrete mesostructure. The two types of wet-screened concretes, SCR38 and SCR76, were used to validate the results obtained using the two-phase composite models, discussed in § 4. The analysis includes the development of over time of the modulus of elasticity of concrete and of the creep strains for several loading ages, t' , and a loading duration of one year, $t - t' = 365$ days.

Table 6.12 and Figures 6.11 and 6.12 present the obtained results of the SCR76 and SCR38 concrete particle models. The left side of the Figures 6.11 and 6.12 show the comparison between the mortar's and the SCR38 and SCR76 concrete's modulus of elasticity. The prediction of the two-phase composite model shows a good agreement with the experimental results obtained in laboratory (§ 3.7). It should be noted that the mortar's modulus of elasticity prediction was obtained from the wet-screened concrete results and, therefore, it includes the effect of the ITZ's properties (§ 6.2.2). The numerical results of the concrete particle models show also a good agreement with the results obtained using the two-phase composite model. This comparison validates the calibration procedure applied to each component and the generation of the concrete's internal aggregate structure. The numerical results were obtained from five different random particle assemblies, with the same aggregate sieve distribution input.

6.2. PREDICTION OF DAM CONCRETE DEFORMABILITY PROPERTIES USING PARTICLE MODELS

The right side of Figures 6.11 and 6.12 show the same comparison for the development of the creep strains over time, for four different loading ages, 7, 28, 90 and 365 days. The prediction of the particle model is very close to the analytical result for the two types of concrete studied for both instantaneous and delayed behaviour (modulus of elasticity and creep compliance, respectively). The particle models are able to reproduce the reduction of creep strains of the mortar (dashed lines in Figures 6.11 and 6.12) due to the effect of the elastic restraint of the stiff aggregates.

Table 6.12 presents the obtained values, including the mean and standard deviation of the particle model results and a measurement of the error between numerical and analytical results for both the modulus of elasticity, ϵ_E , and the creep compliance, ϵ_J (Equations 6.17). The percentage deviations between analytical (Composite) and numerical models (DEM) vary between 0.7% and 5.8%. The standard deviations of the numerical results of the five random assemblies are also very small compared with the average values (for example, for the SCR38 concrete, 0.4 GPa for the modulus of elasticity at the age of 365 days (28.6 GPa) and 2.9×10^{-6} /MPa for the creep compliance at the age of 372 days). The results show a constant difference of approximately 8 and 10 GPa between the modulus of elastic of mortar and SCR38 and SCR76 concretes, respectively.

Table 6.12: Results of SCR76 and SCR38 concrete particle model based on the mortar's and aggregate's deformability mean properties and considering a constant temperature of 20 °C

Concrete	t' (days)	t (days)	$E_{composite}$ (GPa)	$J_{composite}$ ($\times 10^{-6}$ /MPa)	E_{DEM} (GPa)	ϵ_E (%)	J_{DEM} ($\times 10^{-6}$ /MPa)	ϵ_J (%)
SCR76	7	372	22.8	74.2	21.5 (0.3)	5.7	78.4 (2.0)	5.7
	28	393	26.2	58.6	25.8 (0.3)	1.5	61.3 (1.3)	4.6
	90	455	28.0	49.2	28.3 (0.3)	1.1	51.3 (0.9)	4.3
	365	730	29.2	41.7	30.2 (0.3)	3.4	43.2 (0.6)	3.6
SCR38	7	372	20.6	91.6	19.7 (0.4)	4.3	89.3 (2.9)	2.5
	28	393	24.6	71.7	24.0 (0.4)	2.4	68.7 (1.9)	4.2
	90	455	27	59.6	26.6 (0.4)	1.5	56.6 (1.3)	5.0
	365	730	28.8	49.8	28.6 (0.4)	0.7	46.9 (0.9)	5.8

Note: The presented DEM results are the mean and standard deviation (inside the parenthesis) of five random particle generations

$$\epsilon_E = \left| \frac{E_{DEM} - E_{composite}}{E_{composite}} \right| \times 100, \quad \epsilon_J = \left| \frac{J_{DEM} - J_{composite}}{J_{composite}} \right| \times 100 \quad (6.17)$$

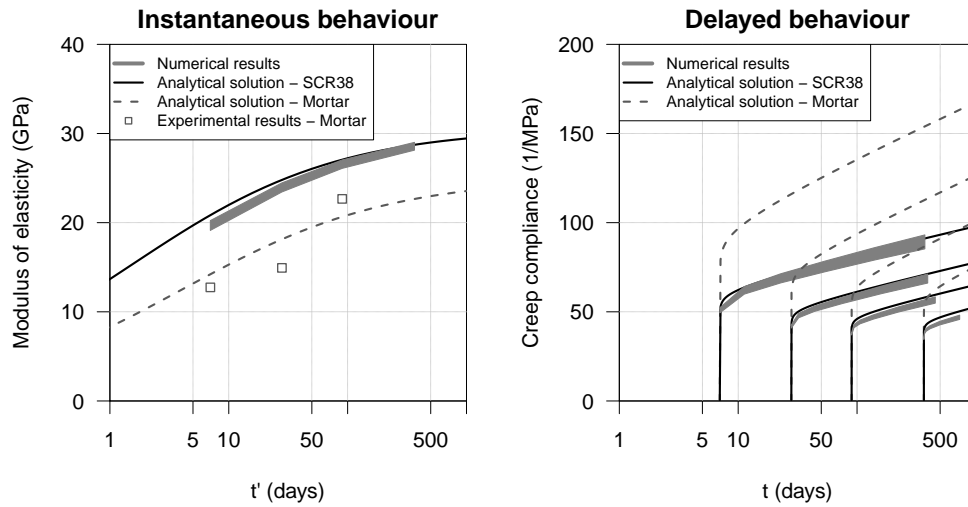


Figure 6.11: Results of SCR38 concrete particle model based on the mortar’s and aggregate’s deformability mean properties and considering a constant temperature of 20 °C

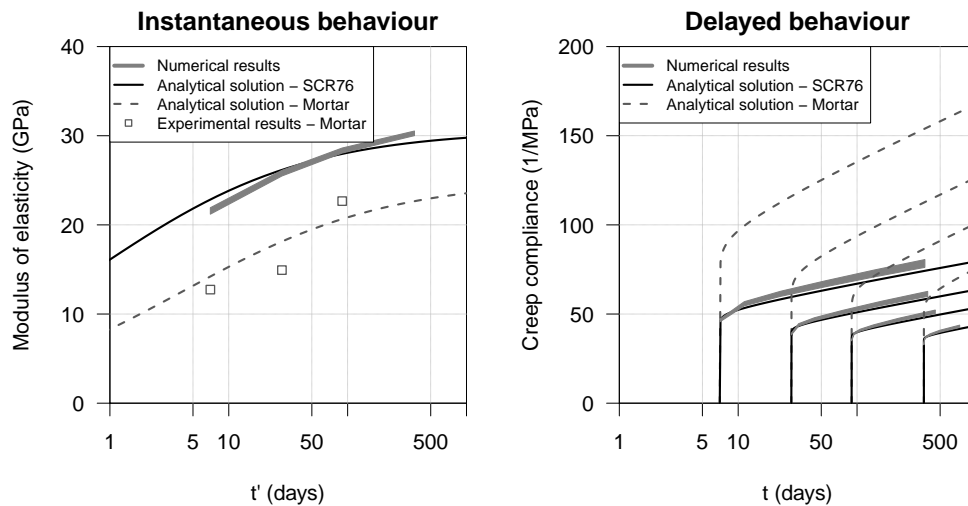


Figure 6.12: Results of SCR76 concrete particle model based on the mortar’s and aggregate’s deformability mean properties and considering a constant temperature of 20 °C

6.2.7.2 Prediction of wet-screened concrete test results obtained in creep cells

In order to compare the numerical results with the experimental results obtained in the creep cells, the effect of temperature on the instantaneous and long-term properties should be taken into account. The temperature inside the creep cells, which are embedded in a dam lift, varies with the placement temperature, the development of the hydration reactions and the different boundary conditions over time. A typical temperature profile includes a sharp temperature increase in the first days, followed by a slow decrease which can last several months. Figure 3.22 in Chapter 3 shows an example of the measured

temperature inside a creep cell.

Taking into account the validated particle model for the reference temperature of 20°C, the equivalent times, described previously in § 6.2.6, and the measured temperatures inside each creep cell, a numerical prediction of the *in situ* measured behaviour for both SCR76 and SCR38 concrete was obtained. As it would be expected, the high initial temperatures accelerates the hydration processes and yield an increase of the modulus of elasticity. The grey area in the left plot of Figures 6.13 and 6.14 is the particle model prediction which are in agreement with the measured modulus of elasticity in creep cells (diamond points).

This effect is also present in the development of the creep strains, since its initial values are lower mainly due to higher modulus of elasticity at loading age (right plot in Figures 6.13 and 6.14). The creep development over time has a misfit for the younger ages after loading, especially for the loading age of 28 days.

The percentage deviations between the numerical prediction and the experimental results are presented in Table 6.13, for both types of concrete and for the instantaneous, ϵ_E^{exp} , and long-term properties, ϵ_J^{exp} (Equations 6.18). Unfortunately, it was not possible to have full experimental description of the concrete properties, including the several ages, especially for the SCR38 concrete (Chapter 3) but the maximum percentage deviations are 4.1% for the modulus of elasticity and 11.1% for the creep strains.

The results show that this type of model is capable of accurately simulate the concrete deformability including not only the internal mesostructure of concrete but also the effect of temperature. The typical high temperatures in the early ages and rapid temperature variations, besides introducing differential imposed strains are known to increase the concrete stiffness and, therefore, influence the development of stresses over time.

$$\epsilon_E^{exp} = \left| \frac{E_{DEM} - E_{exp}}{E_{exp}} \right| \times 100, \quad \epsilon_\epsilon^{exp} = \left| \frac{\epsilon_{DEM} - \epsilon_{exp}}{\epsilon_{exp}} \right| \times 100 \quad (6.18)$$

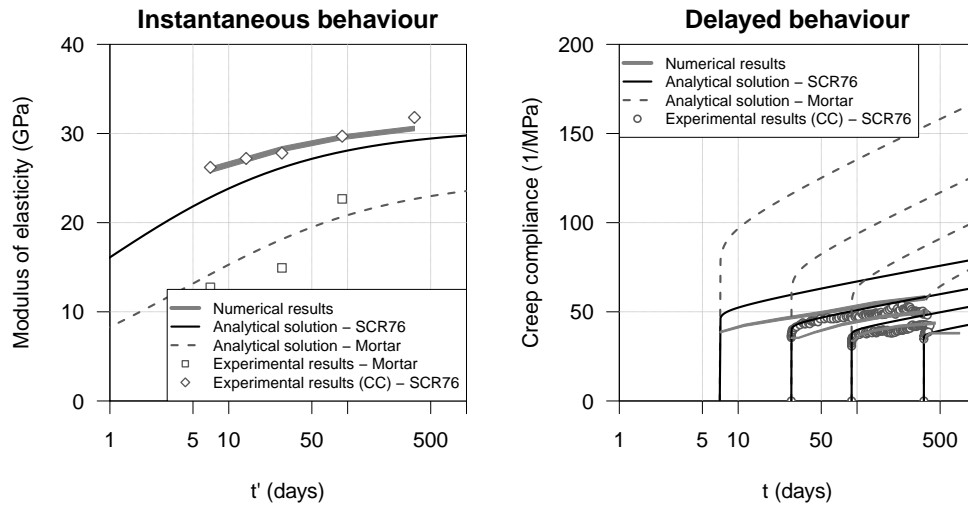


Figure 6.13: Results of SCR76 concrete particle model based on the mortar's and aggregate's deformability mean properties and considering the measured temperature inside the creep cell

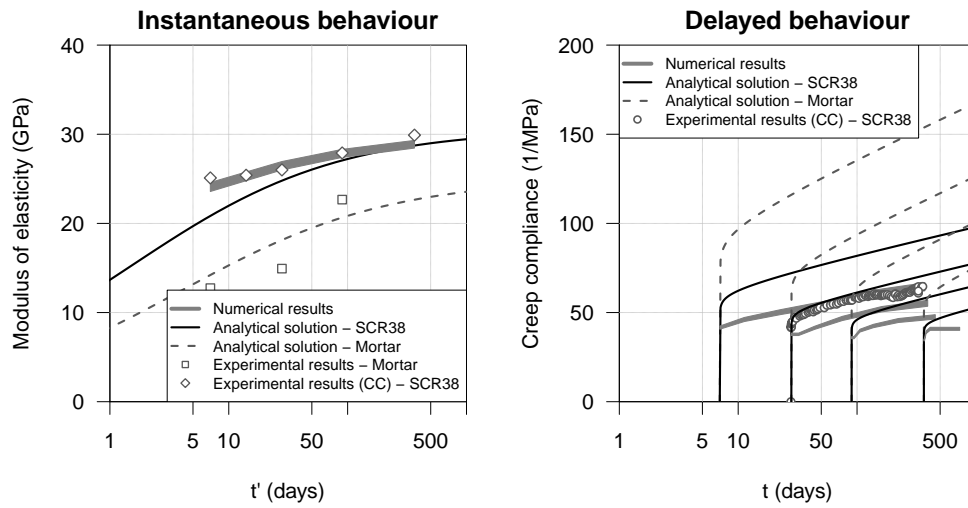


Figure 6.14: Results of SCR38 concrete particle model based on the mortar's and aggregate's deformability mean properties and considering the measured temperature inside the creep cell

6.2. PREDICTION OF DAM CONCRETE DEFORMABILITY PROPERTIES USING PARTICLE MODELS

Table 6.13: Results of SCR76 and SCR38 concrete particle model based on the mortar's and aggregate's deformability mean properties and considering the measured temperature inside the creep cells

Concrete	t' (days)	t (days)	E_{exp} (GPa)	ε_{exp} ($\times 10^{-6}$ /MPa)	E_{DEM} (GPa)	$\epsilon_{E,exp}$ (%)	ε_{DEM} ($\times 10^{-6}$ /MPa)	$\epsilon_{\varepsilon,exp}$ (%)
SCR76	7	372	26.2	-	25.9 (0.3)	1.1	57.8 (1.2)	-
	28	393	27.8	48.2	28.2 (0.3)	1.4	50.1 (0.9)	3.9
	90	455	29.7	42.2	29.6 (0.3)	0.3	43.7 (0.6)	3.6
	365	730	31.8	38.6	30.5 (0.3)	4.1	38.0 (0.4)	1.6
SCR38	7	372	25.1	-	24.1 (0.4)	4.0	64.4 (1.7)	-
	28	393	26.0	62.1	26.0 (0.4)	0.0	55.2 (1.3)	11.1
	90	455	27.9	-	27.9 (0.4)	0.0	47.5 (0.9)	-
	365	730	29.9	-	28.9 (0.4)	3.3	40.8 (0.7)	-

Note: The presented DEM results are the mean and standard deviation (inside the parenthesis) of five random particle generations

6.2.8 Prediction of dam concrete long-term deformability properties

6.2.8.1 Validation of the particle model and sensitivity studies

Similarly to the wet-screened concrete validation, this section compares the dam concrete behaviour prediction using the two-phase composite models (Chapter 4) and the results of the dam concrete particle model, taking into account the remaining aggregate sizes into the concrete mesostructure and the calibrated micro-properties of the mortar and of each type of aggregate.

Table 6.14 and Figure 6.15 show the results of both analysis, using analytical and numerical models, and the results of the mortar's deformability. The numerical results are compatible with the ones obtained from the composite model, which validates the hypothesis assumed for this type of analysis. The maximum percentage deviations between analytical and numerical results are 1.3% for the modulus of elasticity and 8.1% for the creep compliance.

Table 6.14: Results of DAM concrete particle model based on the mortar's and aggregate's deformability mean properties and considering a constant temperature of 20 °C

Concrete	t' (days)	t (days)	$E_{composite}$ (GPa)	$J_{composite}$ ($\times 10^{-6}$ /MPa)	E_{DEM} (GPa)	ϵ_E (%)	J_{DEM} ($\times 10^{-6}$ /MPa)	ϵ_J (%)
DAM	7	372	24.1	71.9	23.9 (0.2)	0.8	66.8 (0.7)	7.1
	28	393	28.0	58.0	28.0 (0.2)	0.0	53.6 (0.5)	7.6
	90	455	30.1	49.6	30.4 (0.2)	0.9	45.6 (0.4)	8.1
	365	730	31.7	42.6	32.1 (0.2)	1.3	39.2 (0.3)	8.0

Note: The presented DEM results are the mean and standard deviation (inside the parenthesis) of five random particle generations

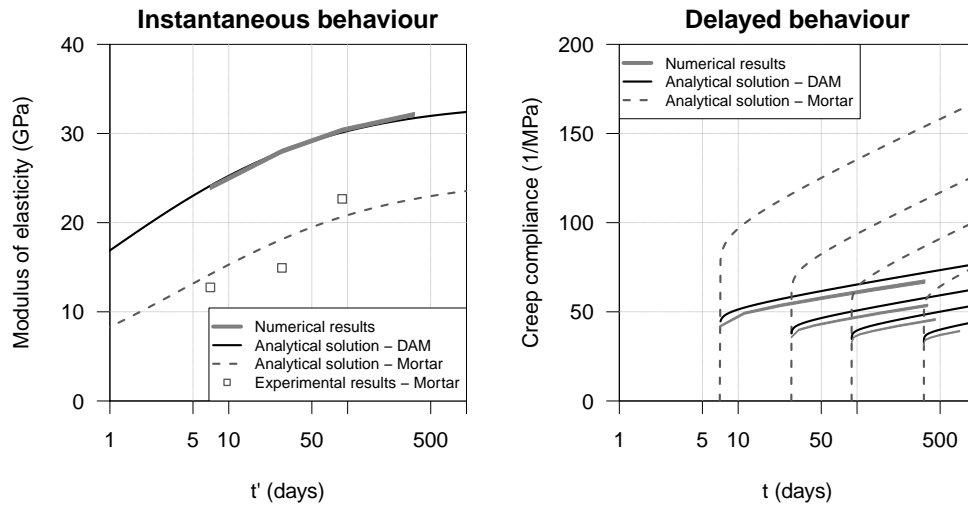


Figure 6.15: Results of DAM concrete particle model based on the mortar’s and aggregate’s deformability mean properties and considering a constant temperature of 20 °C

As previously stated, due to several reasons, mechanical properties of dam concrete placed on site are known to have a large scatter. It is also known that the aggregate’s modulus of elasticity test results show large standard deviations (5.1 GPa, 11% of the mean value). This section studies the influence of the coarse aggregate modulus of elasticity on DAM concrete particle model results.

Three scenarios were tested to evaluate range of concrete property prediction based on the results of the particle model: the case where the modulus of elasticity of the coarse aggregates is taken as the mean value ($\mu(E_{agg})$) obtained from specific laboratory tests to the granitic rock (§ 3.6); the case where the modulus of elasticity of the coarse aggregates is a lower bound of the tested samples ($\mu(E_{agg}) - \sigma(E_{agg})$), where $\sigma(E_{agg})$ is the standard deviation of the results; and, the case where the modulus of elasticity of the coarse aggregates is an upper bound of the tested samples ($\mu(E_{agg}) + \sigma(E_{agg})$).

The five random particle generations used in the three cases show that effect of the large variation of the coarse aggregate modulus of elasticity results on the deformability properties of concrete (Figure 6.16). The results show that a range of 10.2 GPa (22% of the average values) in the aggregate’s modulus of elasticity, between $\mu(E_{agg}) - \sigma(E_{agg})=46.3-5.1=41.2$ GPa and $\mu(E_{agg}) + \sigma(E_{agg})=46.3+5.1=51.4$ GPa, yields a maximum range of $|-1.6|+1.6=3.2$ GPa (10% of the average value) at the age of 365 days. Tables 6.15 and 6.16 presents the obtained results and the absolute, $\Delta E_{\sigma(E_{agg})}$ and $\Delta J_{\sigma(E_{agg})}$, and percentage deviations, $\epsilon_{E,\sigma(E_{agg})}$ and $\epsilon_{J,\sigma(E_{agg})}$, for each sensitivity case study (Equations 6.19 to 6.22)

6.2. PREDICTION OF DAM CONCRETE DEFORMABILITY
PROPERTIES USING PARTICLE MODELS

Table 6.15: Results of DAM concrete particle model using different aggregate's modulus of elasticity (part 1)

E_{agg} (GPa)	t' (days)	t (days)	E_{DEM} (GPa)	$\Delta E_{\sigma(E_{agg})}$ (GPa)	$\epsilon_{E,\sigma(E_{agg})}$ (%)
46.3	7	372	23.9 (0.2)	-	-
	28	393	28.0 (0.2)	-	-
	90	455	30.4 (0.2)	-	-
	365	730	32.1 (0.2)	-	-
41.2	7	372	22.9 (0.3)	-1.0	-4.2
	28	393	26.7 (0.2)	-1.3	-4.6
	90	455	28.9 (0.2)	-1.5	-4.9
	365	730	30.5 (0.2)	-1.6	-5
51.4	7	372	24.9 (0.2)	1.0	4.2
	28	393	29.3 (0.2)	1.3	4.6
	90	455	31.8 (0.2)	1.4	4.6
	365	730	33.7 (0.2)	1.6	5

Note: The presented DEM results are the mean and standard deviation (inside the parenthesis) of five random particle generations

Table 6.16: Results of DAM concrete particle model using different aggregate's modulus of elasticity (part 2)

E_{agg} (GPa)	t' (days)	t (days)	J_{DEM} ($\times 10^{-6}$ /MPa)	$\Delta J_{\sigma(E_{agg})}$ ($\times 10^{-6}$ /MPa)	$\epsilon_{J,\sigma(E_{agg})}$ (%)
46.3	7	372	66.8 (0.7)	-	-
	28	393	53.6 (0.5)	-	-
	90	455	45.6 (0.4)	-	-
	365	730	39.2 (0.3)	-	-
41.2	7	372	68.8 (1.2)	2.0	3
	28	393	55.5 (0.8)	1.9	3.5
	90	455	47.5 (0.6)	1.9	4.2
	365	730	41.0 (0.4)	1.8	4.6
51.4	7	372	64.9 (0.7)	-1.9	-2.8
	28	393	51.7 (0.5)	-1.9	-3.5
	90	455	43.9 (0.4)	-1.7	-3.7
	365	730	37.6 (0.3)	-1.6	-4.1

Note: The presented DEM results are the mean and standard deviation (inside the parenthesis) of five random particle generations

$$\Delta E_{\sigma(E_{agg})} = E_{DEM}^{\mu(E_{agg}) \pm \sigma(E_{agg})} - E_{DEM}^{\mu(E_{agg})} \quad (6.19)$$

$$\Delta J_{\sigma(E_{agg})} = J_{DEM}^{\mu(E_{agg}) \pm \sigma(E_{agg})} - J_{DEM}^{\mu(E_{agg})} \quad (6.20)$$

$$\epsilon_{E,\sigma(E_{agg})} = \frac{E_{DEM}^{\mu(E_{agg}) \pm \sigma(E_{agg})} - E_{DEM}^{\mu(E_{agg})}}{E_{DEM}^{\mu(E_{agg})}} \times 100 \quad (6.21)$$

$$\epsilon_{J,\sigma(E_{agg})} = \frac{J_{DEM}^{\mu(E_{agg}) \pm \sigma(E_{agg})} - J_{DEM}^{\mu(E_{agg})}}{J_{DEM}^{\mu(E_{agg})}} \times 100 \quad (6.22)$$

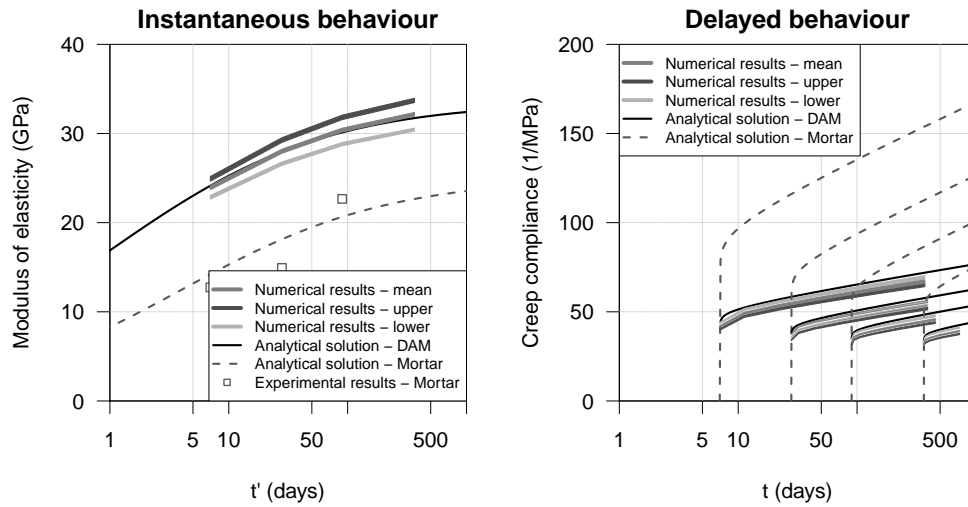


Figure 6.16: Results of DAM concrete particle model using different aggregate's modulus of elasticity

Although it is assumed that the composite model prediction of the mortar's creep compliance includes the ITZ's contribution (§ 6.2.2), a sensitivity study was also done in order to evaluate the influence of the ITZ's deformability properties on the behaviour of dam concrete. It is known that the ITZ has smaller modulus of elasticity (§ 2.4.2) and an expected higher creep compliance when compared with the mortar properties but a full characterization of this local material is very difficult. The ITZ's thickness has also a great influence on the deformability properties of concrete and it does not vary with the size of the aggregate (Bentz *et al.* 1993).

For this sensitivity study two scenarios were tested in order to evaluate the influence of the ITZ's deformability on the macroscopic behaviour of concrete. The first is the reference state in which the ITZ and the MORTAR have the same properties and in the second scenario it was assumed that the ITZ's macro-creep compliance is twice as much as the mortar's creep compliance ($J_{ITZ} = 2 \times J_{MORTAR}$). This second scenario is taken as an extreme case of a poor quality ITZ and it is considered that the ITZ's thickness is the same for every type of aggregate.

The effect of the highly deformable ITZ is shown in Figure 6.17 and the results are presented in Table 6.17. The percentage reduction of the modulus of elasticity and of the creep compliance can be as much as 7.9% and 12.0%, respectively. This variability, although not very significant, can explain some misfit between the numerical results and the experimental results and should be taken into account in the interpretation of the predicted values.

6.2. PREDICTION OF DAM CONCRETE DEFORMABILITY PROPERTIES USING PARTICLE MODELS

Table 6.17: Results of DAM concrete particle model using different ITZ's modulus of elasticity

J_{ITZ}	t' (days)	t (days)	E_{DEM} (GPa)	ΔE (GPa)	ϵ_E (%)	J_{DEM} ($\times 10^{-6}/\text{MPa}$)	ΔJ (GPa)	ϵ_J (%)
J_{MORTAR}	7	372	23.9 (0.2)	-	-	66.8 (0.7)	-	-
	28	393	28.0 (0.2)	-	-	53.6 (0.5)	-	-
	90	455	30.4 (0.2)	-	-	45.6 (0.4)	-	-
	365	730	32.1 (0.2)	-	-	39.2 (0.3)	-	-
$2 \times J_{MORTAR}$	7	372	22.0 (0.3)	-1.9	-7.9	74.8 (1.3)	8.0	12.0
	28	393	25.9 (0.3)	-2.1	-7.5	59.3 (0.9)	5.7	10.6
	90	455	28.2 (0.2)	-2.2	-7.2	50.1 (0.6)	4.5	9.9
	365	730	30.0 (0.2)	-2.1	-6.5	42.6 (0.5)	3.4	8.7

Note: The presented DEM results are the mean and standard deviation (inside the parenthesis) of five random particle generations

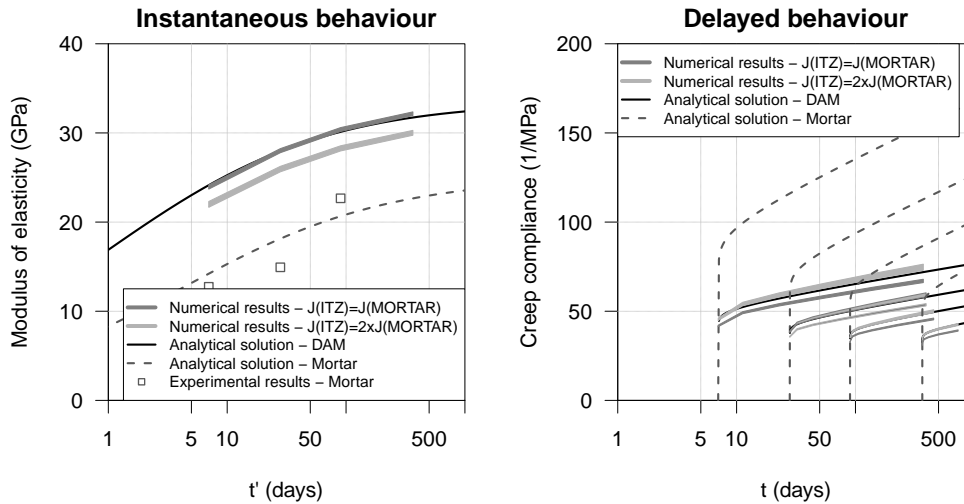


Figure 6.17: Results of DAM concrete particle model using different aggregate's modulus of elasticity

The effect of crushed aggregates with elongated shapes is also compared with the concrete particle model results using rounded aggregates. The properties of the crushed aggregate structure are similar to the one used for the rounded aggregate structure. The difference, as described in § 6.2.4 is the shape of the aggregates. Table 6.18 and Figure 6.18 show the comparison between the two types of aggregate shape. The average values of crushed aggregate structure modulus of elasticity are slightly higher than the ones obtained for the rounded aggregate structure. The scatter of both the modulus of elasticity and creep compliance is larger for the concrete with crushed aggregate which indicates a more non-uniform distribution of the forces inside the specimen.

Table 6.18: Results of DAM concrete particle model based on the mortar’s deformability properties and considering crushed aggregates

Type of aggregate	t' (days)	t (days)	E_{DEM} (GPa)	ΔE (GPa)	ϵ_E (%)	ϵ_{DEM} ($\times 10^{-6}/\text{MPa}$)	ΔJ (GPa)	ϵ_J (%)
Rounded	7	372	23.9 (0.2)	-	-	66.8 (0.7)	-	-
	28	393	28.0 (0.2)	-	-	53.6 (0.5)	-	-
	90	455	30.4 (0.2)	-	-	45.6 (0.4)	-	-
	365	730	32.1 (0.2)	-	-	39.2 (0.3)	-	-
Crushed	7	372	24.2 (0.8)	0.3	1.3	65.9 (3.0)	-0.9	-1.3
	28	393	28.3 (0.7)	0.3	1.1	52.9 (2.1)	-0.7	-1.3
	90	455	30.6 (0.7)	0.2	0.7	45.1 (1.6)	-0.5	-1.1
	365	730	32.4 (0.6)	0.3	0.9	38.8 (1.1)	-0.4	-1.0

Note: The presented DEM results are the mean and standard deviation (inside the parenthesis) of five random particle generations

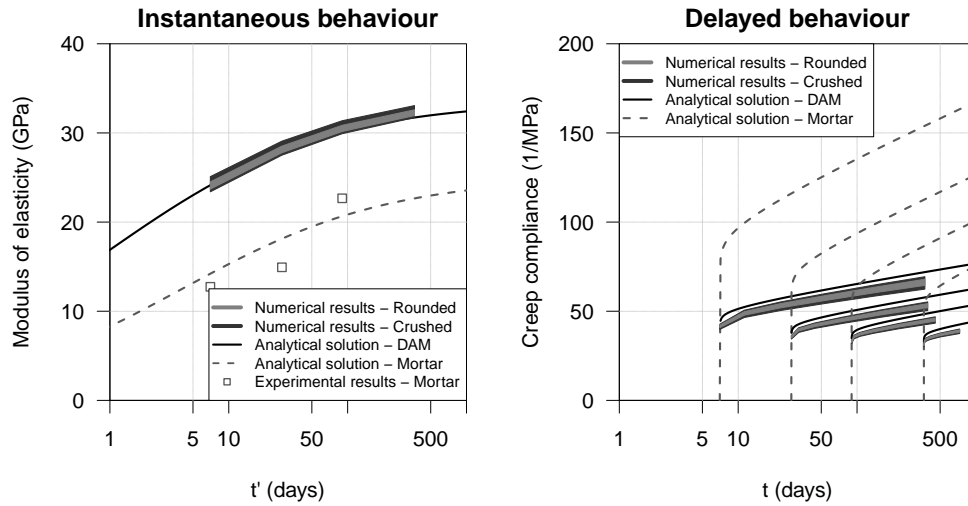


Figure 6.18: Results of DAM concrete particle model based on the mortar’s deformability, considering the crushed aggregates

6.2.8.2 Prediction of dam concrete test results obtained in creep cells

Figure 6.19 and Table 6.19 present the dam concrete particle model results considering the variability of the aggregate’s modulus of elasticity and the measured temperature inside the creep cells. By taking into account the *in situ* conditions, it is possible to compare this prediction with the test results obtained in the dam concrete creep cells.

As previously stated, the prediction of dam concrete deformability properties is greatly related to the aggregate’s modulus of elasticity. Due to its large scatter, the presented numerical results include three scenarios, considering: the mean value of the aggregate’s modulus of elasticity ($\mu(E_{agg})$); an upper bound value of the aggregate’s modulus of elasticity ($\mu(E_{agg}) + \sigma(E_{agg})$); and, a lower bound value of the aggregate’s modulus of

6.2. PREDICTION OF DAM CONCRETE DEFORMABILITY
PROPERTIES USING PARTICLE MODELS

elasticity ($\mu(E_{agg}) - \sigma(E_{agg})$), similarly to the sensitivity study in § 6.2.8.1.

The percentage deviations between numerical and experimental results are higher for dam concrete than for the wet-screened concrete. The percentage deviation of the modulus of elasticity and of the creep strains are as high as 11% and 33%, respectively (using the aggregate's mean modulus of elasticity of 46.3 GPa). The difference between the prediction of the composite model at reference constant temperature (continuous black line in Figure 6.19) and the experimental results (diamond points in Figure 6.19) is partially due to the acceleration of hydration processes, which is very significant at the younger ages. For the latter ages, the deviation between the numerical results and the experimental results can be due to the variability of the aggregate's modulus of elasticity. Figure 6.19 shows that this variability can introduce significant scatter to the concrete prediction since the coarse aggregate volume is high and the size of the aggregates is large. The scatter is less pronounced for the concrete creep strains. The large percentage deviation of the creep strain for the loading age of 28 days (Table 6.19) can be due to the difficulty of the maturity concepts under heating and cooling conditions applied to the creep rate. Some studies indicate that creep increases under cooling while other show the opposite effect (Bažant and Baweja 2000).

Table 6.19: Results of DAM concrete particle model based on the mortar's and aggregate's deformability properties and considering the measured temperature inside the creep cells

E_{agg} (GPa)	t' (days)	t (days)	E_{exp} (GPa)	ε_{exp} ($\times 10^{-6}/\text{MPa}$)	E_{DEM} (GPa)	ϵ_E^{exp} (%)	ε_{DEM} ($\times 10^{-6}/\text{MPa}$)	$\epsilon_\varepsilon^{exp}$ (%)
46.3 (mean)	7	372	31.3	-	28.2 (0.3)	9.9	50.5 (0.8)	-
	28	393	31.5	33.4	30.4 (0.3)	3.5	44.5 (0.6)	33.2
	90	455	33.5	41.0	31.6 (0.3)	5.7	39.4 (0.5)	3.9
	365	730	36.3	-	32.5 (0.3)	10.5	35.0 (0.3)	-
41.2 (lower)	7	372	31.3	-	27.1 (0.6)	13.4	52.2 (1.1)	-
	28	393	31.5	33.4	29.1 (0.6)	7.6	46.1 (0.9)	38.0
	90	455	33.5	41.0	30.3 (0.7)	9.6	41.0 (0.8)	0.0
	365	730	36.3	-	31.1 (0.7)	14.3	36.5 (0.8)	-
51.4 (upper)	7	372	31.3	-	29.3 (0.7)	6.4	49.1 (1.3)	-
	28	393	31.5	33.4	31.5 (0.8)	0.0	43.1 (1.1)	29.0
	90	455	33.5	41.0	32.8 (0.8)	2.1	38.1 (1.0)	7.1
	365	730	36.3	-	33.8 (0.9)	6.9	33.8 (0.9)	-

Note: The presented DEM results are the mean and standard deviation (inside the parenthesis) of five random particle generations

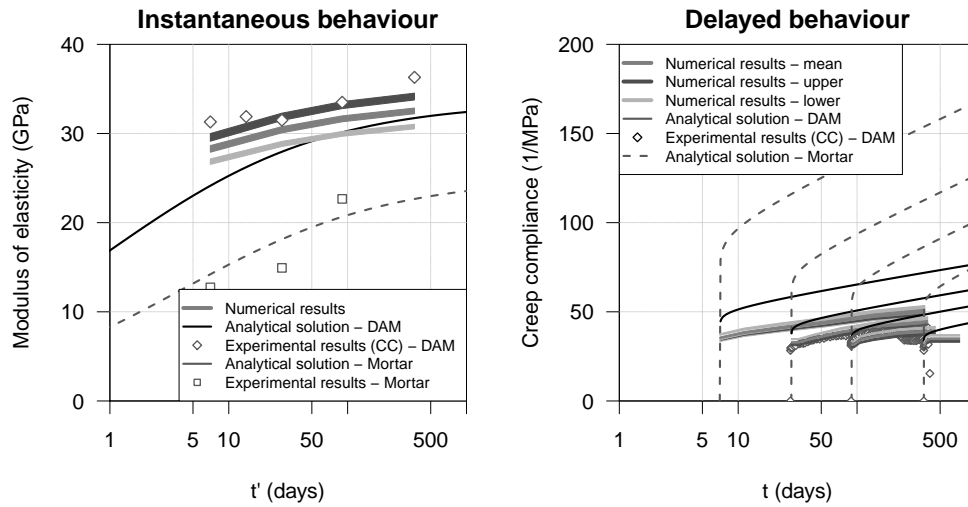


Figure 6.19: Results of DAM concrete particle model based on the mortar’s deformability, considering the aggregate’s deformability variability and the measured temperature inside the creep cells

6.2.9 Study of the normal and shear force distribution inside the concrete mesostructure

The analysis of concrete considering its mesostructure enables the study of the interactions between the aging mortar and the aggregate inclusions and introduces new insight into the stress and force distribution inside a concrete specimen and its development over time. The main features of concrete’s mesostructure are the coarse aggregate distribution, including content and arrangement inside the specimen, and the stiffness differences between the mortar, the aggregate and the interfacial transition zone (ITZ).

The discrete element method applied to particle models allows for the analysis of large assemblies with a fine refinement which is especially relevant for modelling dam concrete behaviour using large specimens. In order to fully represent the deformability properties of the coarse aggregate structure, the smaller coarse aggregate has to be considered into the particle model.

Dam concrete is usually made with stiff aggregates and the binding matrix has lower modulus of elasticity than the aggregates, especially in the younger ages. The mesostructure of concrete behaves as structural system a random combination of different aggregate sizes and shapes placed in series and in parallel with each other. The force distribution follows the stiffer elements of the system and, therefore, introduces local areas of higher stresses and strains which lead to a non-uniform stress state.

The stress distribution is highly dependent of the aggregate structure and, in the case

6.2. PREDICTION OF DAM CONCRETE DEFORMABILITY PROPERTIES USING PARTICLE MODELS

of dam concrete, the range of coarse aggregate sizes introduces a complex stiff structure in which the applied forces are drawn to. This type of representation highlights the areas where the normal and shear contact forces are higher and illustrates the "force path" from the top to the bottom of the specimen. An accurate physical representation of the stiffness distribution enables a realistic stress localization. Figure 6.20 illustrates the compressive and tensile normal contact forces for the case of a concrete particle model with rounded aggregates. In the detailed area of each particle assembly the links between particles show the intensity of the normal contact force. For compressive contact forces, darker links have larger compressive forces (in the center of Figure 6.20). For tensile contact forces, darker links have larger tensile forces (in the right of Figure 6.20). The arrows represent qualitatively the "force path" and the areas which have higher forces.

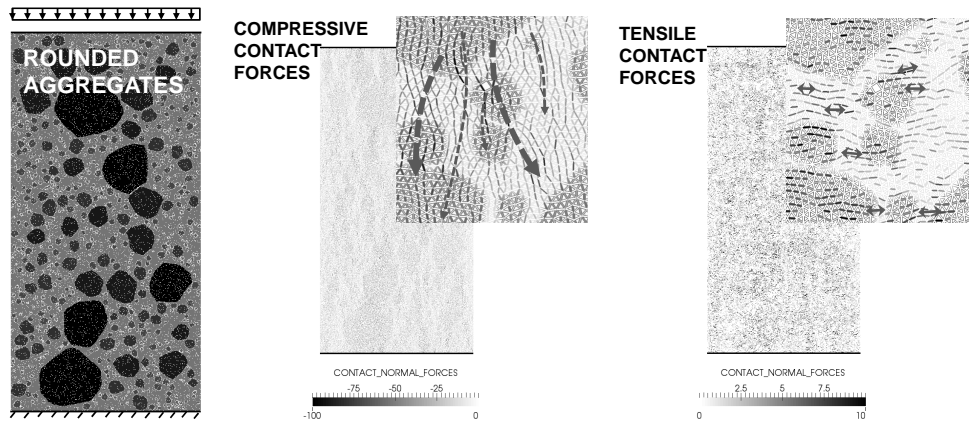


Figure 6.20: Comparison between compressive and tensile normal contact forces in rounded coarse aggregate structure and crushed coarse aggregate structure for the DAM concrete particle model

Figure 6.21 presents the development over time of the maximum and minimum normal contact forces over time for each contact type considering a rounded particle model and the measured temperature inside the creep cells. The plotted values are related to every contact in the concrete assembly. These graphs show that the range of normal contact forces is significant for the compressive values and very narrow for the tensile contact forces and that every type of contact, aggregate-aggregate, mortar-mortar and aggregate-mortar have similar maximum and minimum normal contact values. The mortar and the ITZ work as the filling between the aggregate skeleton and, therefore, it is also likely to undertake high stresses. This phenomena can be especially relevant for mortar areas between large aggregates where tensile stresses can develop. Although tensile strength is the weak link

in cement-based materials, compressive stresses can be relevant in the ITZ around the aggregates. Van Mier refers to the potential crushing of the ITZ in local stressed areas around the aggregates (Mier 1998).

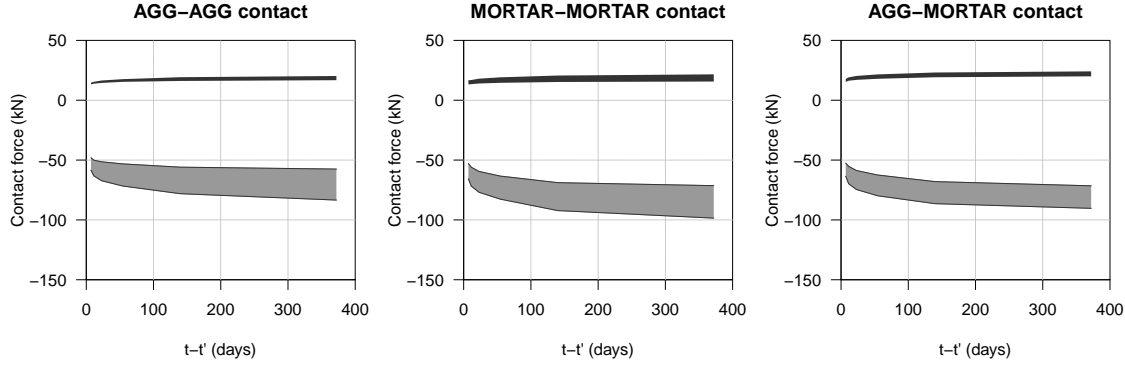


Figure 6.21: Development of the maximum and minimum normal contact forces over time for each contact type considering a rounded particle model and the measured temperature inside the creep cells

Following the measurement logic adopted in the commercial program *PFC^{2D}* (Itasca Consulting Group Inc. 2008), the stresses inside the specimens can be approximated by an averaging procedure within a given region. The measurement region is usually a circle large enough to include a representative number of contacts. The approximated stresses are given by the Equation 6.23,

$$\sigma_{ij} = \left(\frac{1-n}{\sum_{N_p} V^{(p)}} \right) \left(\sum_{N_p} \sum_{N_c^{(p)}} \left(x_i^{(c)} - x_i^{(p)} \right) F_j^{c,p} \right) \quad (6.23)$$

where $V^{(p)}$ is the volume of the particle inside the measurement region, n is the porosity inside the measurement region (Equation 6.24), $N_c^{(p)}$ is the number of contacts inside the measurement region, $x_i^{(p)}$ and $x_i^{(c)}$ are, respectively, the locations of the particle and of its contact and $F_j^{c,p}$ is the force acting on particle (p) at contact (c).

$$n = 1 - \frac{V_{mat}}{V_{reg}} = 1 - \frac{\sum_{N_p} V^{(p)}}{V_{reg}} \quad (6.24)$$

Two different cross sections, composed by consecutive uniform measurement circles (MC), were considered to obtain the stress distribution variations inside the specimen. The identification and properties of each analyzed cross section are presented in Table 6.20 and in Figure 6.22. CS-H-1 and CS-V-2 represent generic cross sections over the width and the height of the specimen.

6.2. PREDICTION OF DAM CONCRETE DEFORMABILITY PROPERTIES USING PARTICLE MODELS

Table 6.20: Identification and properties of each analysed cross section of DAM concrete specimen

Type of concrete	Cross section	Direction	Number of MC	Location of MC		Radius of MC (m)
				x direction (m)	y direction (m)	
Core-DAM	CS-H-1	Horizontal	49	0-0.45	0.30	0.009
	CS-V-2	Vertical	99	0.225	0.0-0.90	0.009

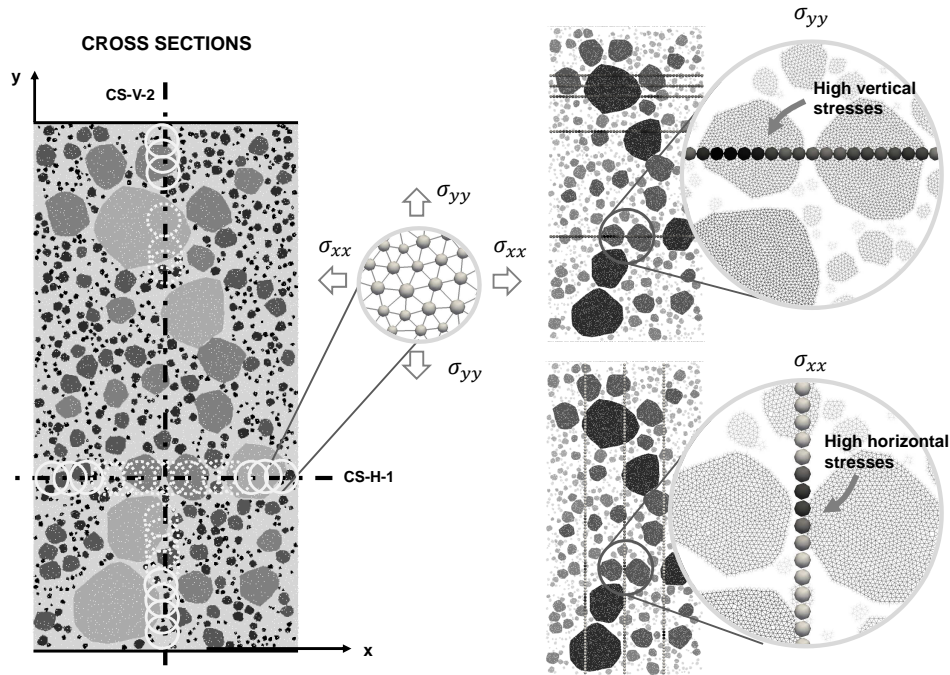


Figure 6.22: Localization and results of each analyzed cross section of DAM concrete specimen

Figures 6.23 and 6.24 shows the normal contact stiffness and the stress distribution over the cross sections CS-H-1 and CS-V-2 of the DAM concrete specimen, immediately after loading ($t - t' = 0.01$ days) and after one year of loading ($t - t' = 365$ days). The most significant result is the variation of stress inside the specimen, both for the vertical and horizontal stresses.

Although the vertical compressive "stress path" is very much dependent of the aggregate's structure, the vertical compressive stresses, σ_{yy} , are mainly correlated with the average normal contact stiffness. CS-H-1 crosses two side-by-side aggregates (between the 0.15 m and 0.30 m) but the "stress path" is more pronounced in the aggregate in the left (between 0.15 m and 0.20 m). This reason is due to the fact that there is a vertical chain of aggregates, which introduces a stiffer path for the development of stress (Figure 6.22). This example shows the importance of a global analysis of the results for the interpretation of

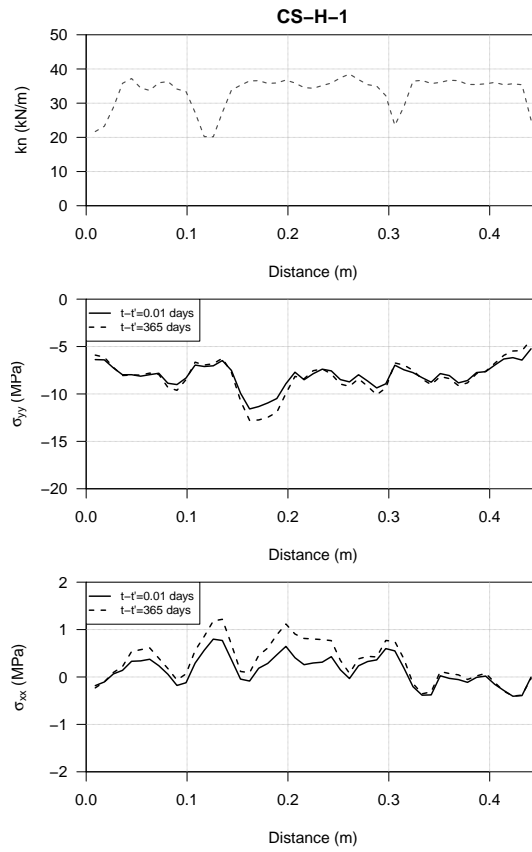


Figure 6.23: Stress distribution over the cross section CS-H-1 of the DAM concrete specimen loaded at the age of 7 days

local effects, since each specimen has a random aggregate arrangement. Local high stresses can be due to specific patterns which can occur inside a concrete specimen, especially when a large range of aggregate sizes is used.

The stress development over time in Figures 6.23 and 6.24 show that the areas in which the stress is higher for $t - t' = 0.01$ days tend to increase their stress over time ($t - t' = 365$ days) and that the areas in which the stress is lower for $t - t' = 0.01$ days tend to decrease their stress over time ($t - t' = 365$ days), highlighting the stress transfer between soft and stiff material. The horizontal stresses, σ_{xx} , are mainly tensile stresses and are due to the internal structure of both mortar and aggregates. The Poisson's ratio effect introduces a complex local behaviour inside the concrete specimen and significant stress variations over time. Deviations on direction of the compressive "stress path" can also generate horizontal tensile forces. Over the vertical cross section, CS-V-2, the horizontal stresses vary significantly, ranging between 1 MPa in tension to -1 MPa in compression.

The combination of highly stressed areas and local weaker areas, such as the ITZ, can

6.3. PREDICTION OF DAM CONCRETE STRENGTH PROPERTIES USING PARTICLE MODELS

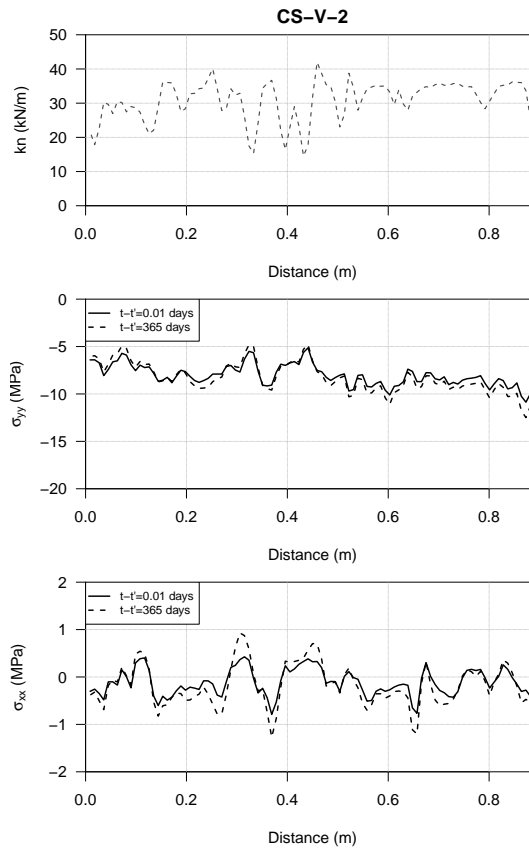


Figure 6.24: Stress distribution over the cross section CS-V-2 of the DAM concrete specimen loaded at the age of 7 days

be the focus of initial damage which can lead to damage and cracking. Understanding the beginning of damage and the development of cracking patterns for several types of loading or deterioration scenarios is key for the accurate prediction of material properties.

6.3 Prediction of dam concrete strength properties using particle models

6.3.1 Correlation between modulus of elasticity and strength results of mortar and aggregate

The prediction of the contact strength parameters is based on the statistical correlation between the strength properties and the modulus of elasticity of the mortar and the aggregates. It is assumed that this statistical correlation obtained from test results of mortar and aggregate is valid for the contact properties. Additionally, since the deformability contact properties were previously calibrated for these two materials and for different loading ages,

it is possible to obtain a first estimate of the development of strength contact properties. The implemented contact models only allow tensile failures, therefore only splitting tensile strength results were predicted.

Based on the aggregate and mortar test results, presented in § 3.6 and § 3.7 respectively, and on the correlation expression proposed by the ACI Committee 318 (ACI Committee 318 1995) and the FIB (Fib 2010). The parameters of the correlation were fitted to the experimental results for different loading ages.

$$E^{mortar}(t') = K_1^{mortar} \left(f_{t,spl}^{mortar}(t') \right)^{\frac{1}{n_1^{mortar}}} \Leftrightarrow f_{t,spl}^{mortar}(t') = K_2^{mortar} \left(E^{mortar}(t') \right)^{n_1^{mortar}} \quad (6.25)$$

$$E^{agg} = K_1^{agg} \left(f_{t,spl}^{agg} \right)^{\frac{1}{n_1^{agg}}} \Leftrightarrow f_{t,spl}^{agg} = K_2^{agg} \left(E^{agg} \right)^{n_1^{agg}} \quad (6.26)$$

Figure 6.25 shows the test results and the fitted correlation for both mortar and aggregate, using nonlinear regression model. Table 6.21 presents the obtained correlation parameters.

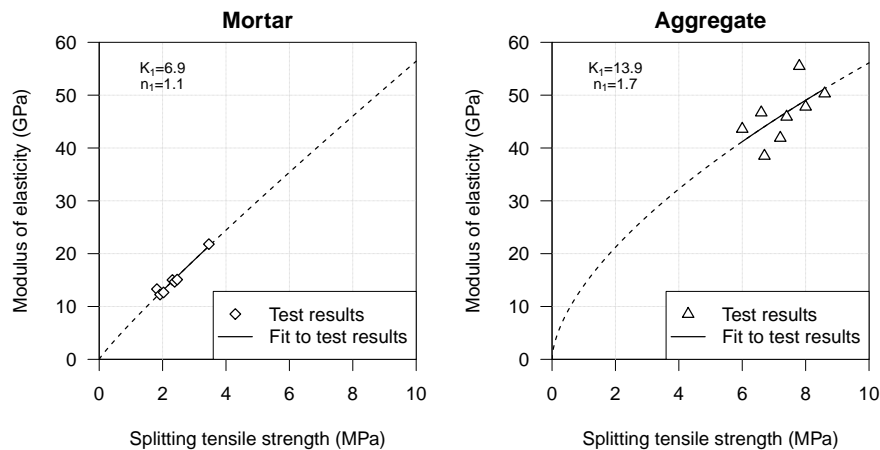


Figure 6.25: Correlation between splitting tensile strength and the modulus of elasticity and fit to mortar and aggregate test results

Table 6.21: Correlation parameters fitted to experimental results of mortar and aggregate

Material	K_1 (GPa)	K_2 (MPa)	n_1	R^2
Mortar	6.9	0.12	1.1	0.96
Aggregate	13.9	0.11	1.7	0.46

6.3. PREDICTION OF DAM CONCRETE STRENGTH PROPERTIES USING PARTICLE MODELS

As previously described, considering a load duration, Δt , usually taken to be 0.01 days, the static modulus of elasticity yields from the creep compliance, $J(t, t')$,

$$E(t') = \frac{1}{A_0 + \frac{A_1}{\sqrt{t'}}} \quad (6.27)$$

where $A_0 = q_1 + q_3 \ln(1 + \Delta t^n)$ and $A_1 = q_2 \ln(1 + \Delta t^n)$.

Taking into account the correlation between the modulus of elasticity and the splitting tensile strength and the hypothesis that direct tensile strength, $f_t(t')$ is equal to 0.9 $f_{t,spl}$, the development of direct tensile strength over time can be predicted using the proposed equation for both mortar and aggregate,

$$\begin{aligned} f_t^{mortar}(t') &= 0.9 f_{t,spl}^{mortar} = 0.9 K_2^{mortar} E^{mortar}(t') n_1^{mortar} = \\ &= 0.9 K_2^{mortar} \left(\frac{1}{A_0^{mortar} + \frac{A_1^{mortar}}{\sqrt{t'}}} \right)^{n_1^{mortar}} \end{aligned} \quad (6.28)$$

$$\begin{aligned} f_t^{agg} &= 0.9 f_{t,spl}^{agg} = \\ &= 0.9 K_2^{agg} (E^{agg}) n_1^{agg} \end{aligned} \quad (6.29)$$

6.3.2 Micro-macro approximations for contact strength

Similarly to the criteria used for the viscoelastic properties, a beam equivalence can be used between contact micro properties and material macro properties,

$$F_{n,t,max} = 2.0 f_t A \quad (6.30)$$

where $F_{n,t,max}$ is the normal contact ultimate force, f_t is the material's direct tensile strength and A is the area of the contact, respectively.

This equivalence yields for both mortar and aggregate contacts:

$$F_{n,t,max}^{mortar} = \alpha_{f_t}^{mortar} 1.8 A K_2^{mortar} \left(\frac{1}{A_0^{mortar} + \frac{A_1^{mortar}}{\sqrt{t'}}} \right)^{n_1^{mortar}} \quad (6.31)$$

$$F_{n,t,max}^{agg} = \alpha_{f_t}^{agg} 1.8 A K_2^{agg} (E^{agg}) n_1^{agg} \quad (6.32)$$

where $\alpha_{f_t}^{mortar}$ and $\alpha_{f_t}^{agg}$ are coefficients to be calibrated. The shear contact behaviour, defined by the contact cohesion, C^{mortar} and C^{agg} , and the contact friction angle, ϕ^{mortar}

and ϕ^{agg} , are obtained by trial-and-error procedures.

6.3.3 Calibration of micro parameters of the contacts for the mortar and aggregates

Taking into account the proposed micro-macro relationship based on the development of the modulus of elasticity over time, the main micro parameters and coefficients are calibrated to fit the measured behaviour of the mortar and the aggregates. For this practical example, the aggregates have infinite strength. This hypothesis simplifies the calibration process and follows the observed behaviour of normal strength concrete produced with good quality aggregates in which the cracking pattern develops around the aggregates (Piotrowska 2013; Wang *et al.* 2016). Dam concrete failure mode is especially bound to have this type of behaviour due to the use of very good quality aggregates and low cement content. Similarly to other studies, the contact strength properties of the ITZ are taken as half of the contact strength properties of the mortar (Grassl *et al.* 2012; Suchorzewski *et al.* 2017).

The calibration procedure starts with the fit of the coefficient α_{f_t} (Equations 6.31 and 6.32), maintaining the parameters of the shear behaviour constant, in order to predict the tensile strength of concrete for different loading ages. Once the model predicts the tensile strength, compressive tests are done to fit the contact cohesion and the contact friction angle for several loading ages.

Tables 6.22 and 6.23 present the obtained parameters and coefficients for describing the mortar and aggregate behaviour. The deformability properties were calibrated previously in the chapter and are presented in Tables 6.7 and 6.6.

Figure 6.26 presents the stress-strain curves for both tensile and compressive tests of mortar particle models for three different loading ages. The numerical results fit well with the experimental results and show the brittle response of mortar specimens. As described in § 2, the nonlinear behaviour is mainly due to the coarse aggregates which introduce a residual resistance to failure after the peak strength is reached.

Figures 6.27 and 6.28 show the cracking patterns and the damage coefficients for tensile and compressive strength tests, respectively. The direct tensile strength test results show the development of an almost horizontal crack across the specimen width in which the contact softening fully develops. Despite that, it is possible to observe that there are other random contacts within the specimen which also undergo damage (normal and shear) representing an overall microcracking. The amount of damaged contacts in the

6.3. PREDICTION OF DAM CONCRETE STRENGTH PROPERTIES USING PARTICLE MODELS

compressive strength test is much higher than the tensile strength test. The microcracking related to the normal contact damage develop almost vertically but the failure pattern is the shear band across the specimen, related to the shear damage in both directions.

Table 6.22: Parameters of MORTAR particle model for the prediction of strength properties

Material	Age (days)	Deformability properties	α_n, α_s	K_2 (MPa)	n_1	$F_{t,n,max}$ (kN)	α_{ft}	$C, \tan\phi$ (kN)
Mortar	7	Table 6.7		0.12	1.1	Equation 6.31	1.3	$4.1 \times 10^3, 0.3$
	28							$5.3 \times 10^3, 0.3$
	90							$8.1 \times 10^3, 0.3$
Aggregate	-	Table 6.6		0.11	1.7	Equation 6.32	1.0	$8.1 \times 10^3, 0.3$

Table 6.23: Strength results of MORTAR particle model

Material	Age (days)	E^{exp} (GPa)	ν	f_t^{exp} (MPa)	f_c^{exp} (MPa)	E^{DEM} (GPa/m)	ν^{DEM}	f_t^{DEM} (MPa)	f_c^{DEM} (MPa)
Mortar	7	14.2	0.20	1.73	14.6	14.7	0.20	1.74	15.0
	28	18.1	0.20	2.14	20.1	18.9	0.21	2.29	19.6
	90	20.7	0.20	2.57	32.9	21.6	0.21	2.67	30.4

Note: The direct tensile strength, f_t^{exp} was considered to be 0.9 of the splitting tensile strength, $f_{t,spl}^{exp}$, § 3.7.5

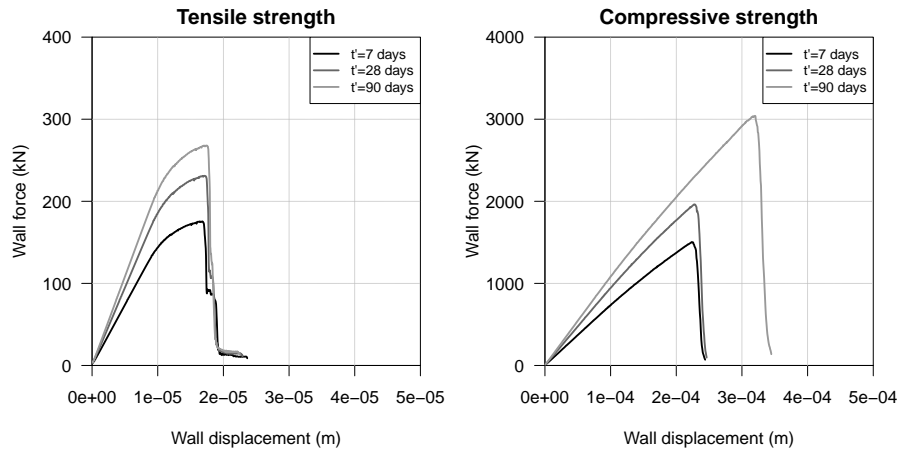


Figure 6.26: Tensile and compressive stress-strain curves of mortar for three different loading ages

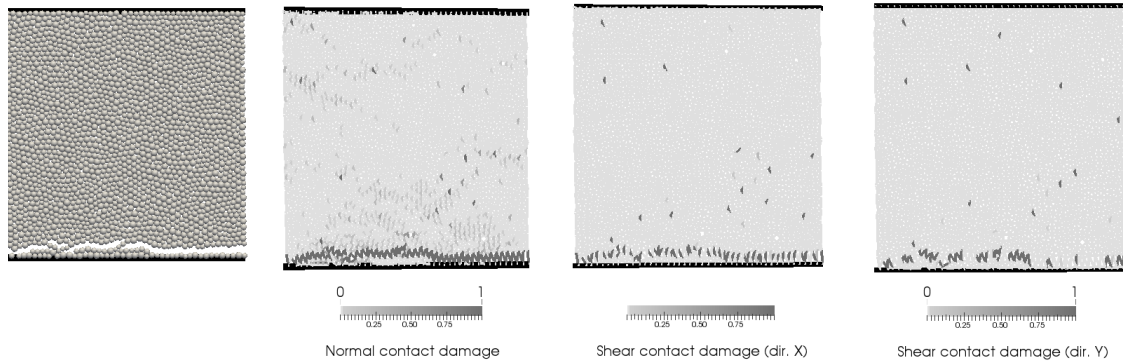


Figure 6.27: Cracking pattern, normal and shear contact damage for direct tensile test of mortar at the age of 7 days

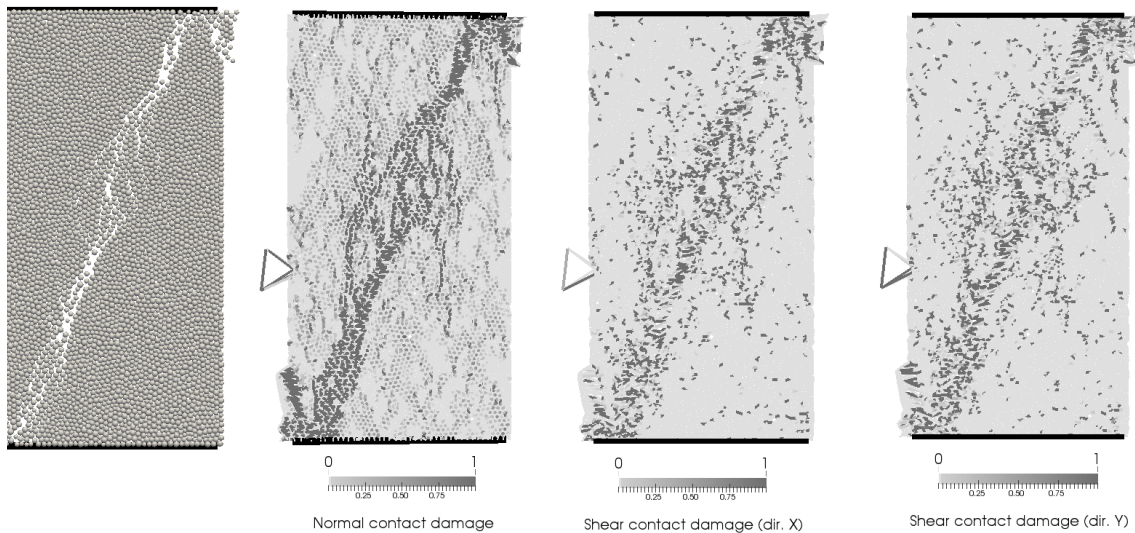


Figure 6.28: Cracking pattern, normal and shear contact damage for compressive test of mortar at the age of 7 days

6.3.4 Prediction of wet-screened and dam concrete strength properties

The prediction of wet-screened and dam concrete is firstly based on the ultimate properties of the mortar and on a trial-and-error calibration process for the determination of the ultimate properties of the ITZ assuming that they are lower than the mortar. In order to simplify the calibration process and due to the good quality of the aggregates, the coarse aggregates are not allowed to fail.

The experimental results show that the mortar and SCR38 concrete splitting tensile strengths are very similar (Table 6.24). As described in § 5.8, the ITZ properties has a large influence on the stress-strain behaviour of concrete, mainly for tensile loadings

(Grassl and Jirásek 2010). Since it is known that tensile strength is mainly influenced by the properties of ITZ, the obtained test results indicate that the ITZ and the mortar of SCR38 concrete have similar strengths. This conclusion do not agree with experimental evidence (Scrivener *et al.* 2004) and numerical studies (Suchorzewski *et al.* 2017) that the ITZ has higher porosity and lower bearing capacity.

An explanation for the obtained results can be the different compaction conditions of the mortar specimens. As described in chapter 3.7, the characterization of the mortar was based on a specific experimental programme using the materials and contents of the mortar binding the coarse aggregates of dam concrete. However, due to compaction conditions in a small specimen and without the aid of aggregates, the tested mortar could yield low strength than the mortar that actually is binding the coarse aggregates.

In order to simulate the behaviour of SCR38 concrete using particle models three cases studies are tested, combining the calibrated strength parameters using the mortar's test results (Table 6.22) and a given strength of the ITZ. The first uses the low maximum normal contact forces for the ITZ's contacts and high contact cohesion, the second uses ITZ with high maximum normal contact properties but lower contact cohesion and the third uses reduced values of ITZ's maximum normal contact force and contact cohesion. The SCR38 concrete particle model is described in § 6.2.1.

The results of first two cases studies yield similar compressive strengths but very different tensile behaviour (Table 6.25). The use of the maximum contact force from the mortar's calibration, $\alpha_{f_t}^{mortar}$, and half the maximum contact force for the properties of the ITZ, $\alpha_{f_t}^{ITZ}$, yields, as expected, very low values of macroscopic tensile strength of the wet-screened concrete but adequate macroscopic compressive strength. The use of the maximum contact force from the mortar's calibration for both the mortar and the ITZ, $\alpha_{f_t}^{mortar} = \alpha_{f_t}^{ITZ}$, and lower values of contact cohesion of the ITZ, C^{ITZ} gives more suitable values of macroscopic tensile and compressive strengths (Table 6.25) but tensile strength below what would be expected suggesting that both the ITZ contact strength parameters should be reduced. Figure 6.29 shows the stress-strain behaviour for both study cases in which the higher maximum normal contact force and lower contact cohesion give larger tensile strengths and similar compressive strengths.

In third case study both the values of maximum contact normal force and cohesion of the mortar and of the ITZ were calibrated in order to fit the SCR38 concrete test results using small specimens. The relationship between the mortar's and the ITZ's strength parameters

Table 6.24: Parameters of mortar, ITZ and aggregate contact model for the prediction of strength properties of concrete

Case study	Material	Age (days)	K_2 (MPa)	n_1	$F_{t,n,max}$ (kN)	α_{ft}	C, $\tan\phi$ (kN)
Reduced $F_{t,n,max}^{ITZ}$	Mortar	90	0.12	1.1	Eq. 6.31	1.3	8.1×10^3 , 0.3
	ITZ					0.7	8.1×10^3 , 0.3
Reduced C^{ITZ}	Mortar	90	0.12	1.1	Eq. 6.31	1.3	8.1×10^3 , 0.3
	ITZ					1.3	4.0×10^3 , 0.3
Reduced $F_{t,n,max}^{ITZ}$ and C^{ITZ}	Mortar	90	0.12	1.1	Eq. 6.31	3.4	4.7×10^3 , 0.3
ITZ	1.7					2.4×10^3 , 0.3	

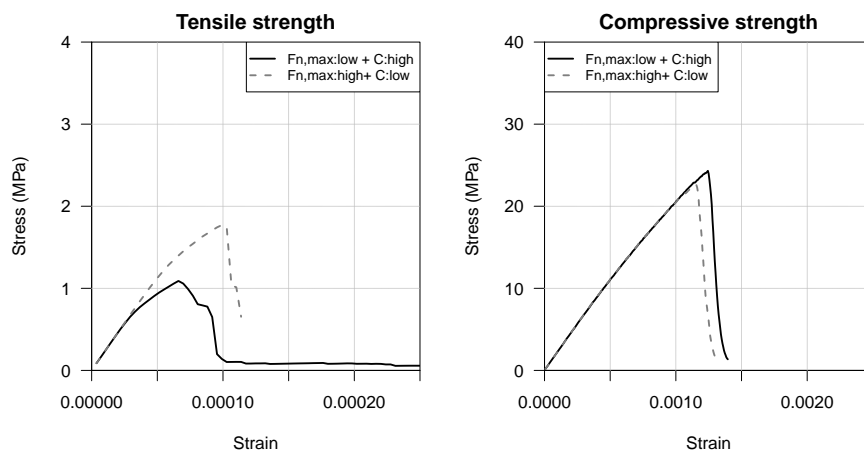


Figure 6.29: Comparison between stress-strain curves of the two sets of strength properties of ITZ (reduced $F_{t,n,max}^{ITZ}$ and reduced C^{ITZ}) for the prediction compressive strength of SCR38 concrete

was fixed: $\frac{\alpha_{ft}^{ITZ}}{\alpha_{ft}^{mortar}} = 0.5$, $\frac{C^{ITZ}}{C^{mortar}} = 0.5$. The numerical results of SCR38 particle model using the third approach, considering higher contact strength values for mortar and reduced contact strength values for ITZ show a good agreement with the experimental results of SCR38 concrete for both tensile and compressive strengths (Table 6.25). The deformability contact properties of each component were obtained from the numerical results, presented in § 6.2.8.2.

Figure 6.30 shows the stress-strain behaviour and number of normal and shear contact breaks for tensile and compressive loadings of SCR38 concrete in small specimen using three random particle assemblies. Additionally, Figures 6.31 and 6.32 present, respectively, the tensile and compressive fracture patterns for the three random concrete particle assemblies. The figures show that the stress-strain results of the three random examples are very similar although its different failure mechanisms. The tensile stress-strain results show a

6.3. PREDICTION OF DAM CONCRETE STRENGTH PROPERTIES
USING PARTICLE MODELS

Table 6.25: Strength results of SCR38 and DAM concrete particle model

Case study	Material	ϕ (mm)	Age (days)	E^{exp} (GPa)	f_t^{exp} (MPa)	f_c^{exp} (MPa)	E^{DEM} (GPa)	f_t^{DEM} (MPa)	f_c^{DEM} (MPa)
Reduced $F_{t,n,max}^{ITZ}$	SCR38	150	90	25.4	2.4	25.3	23.5	1.1	24.3
Reduced C^{ITZ}	SCR38	150	90	25.4	2.4	25.3	23.4	1.8	22.6
Reduced	SCR38	150	90	25.4	2.4	25.3	23.0	2.3	26.0
$F_{t,n,max}^{ITZ}$	SCR38	450	90	-	-	-	24.0	1.9	26.3
and C^{ITZ}	DAM	450	90	27.6	2.0	24.7	27.9	1.9	24.9

Note: The direct tensile strength, f_t^{exp} was considered to be 0.9 of the splitting tensile strength, $f_{t,spl}^{exp}$, § 3.7.5

progressive damage until peak strength and some softening. The tensile failures illustrate some of the observed phenomena, namely, the crack localization and some generalized microcracking around the larger aggregates, the bridging of the main cracks on the ITZ across the mortar, the development of two main cracks from each side of the specimen (random #2) and the complete debonding of a coarse aggregate (random #3). The numerical results of SCR38 concrete particle model show a continuous increase of broken contacts both in tension and shear directions (microcracking) but with a small decrease of global stiffness until the peak strength is reached. The microcracking occurs not only due to the internal heterogeneity of concrete (higher stress concentration and lower properties of ITZ) but also due to the use of Voronoi contact area which introduces additional randomness to the particle assembly (the contact area is related to the particle radius and to the distance between particles). Small contact areas with low strength capacity are scattered throughout the assembly, introducing local weakness similar to voids in the cement paste or mortar (see, for example, the damage obtained in mortar particle model in Figures 6.27 and 6.28).

At peak strength, local damage develop into large macrocracks which lead to instability and failure. Similarly to the work of Monteiro Azevedo *et al.* (2008), the post-peak response of SCR38 concrete particle model is more brittle than it would be expected, as reported in different experimental and numerical results concerning conventional concrete (Vonk 1992; Wendner *et al.* 2014) and dam concrete (Deng *et al.* 2008). The softening and fracture toughness can be enhanced not only by increasing the contact softening but also by increasing the capacity for load redistribution inside the particle assembly. The contact friction, the roughness and shape of the aggregates, the aggregate interlocking, the

strength properties of the ITZ and mortar, the lateral restraint of the walls, the minimum size of the particles and the use of 3D analysis are known to influence the post-peak load redistribution (Monteiro Azevedo *et al.* 2008; Sinaie *et al.* 2016; Suchorzewski *et al.* 2017).

Figure 6.32 shows the deformed shape and distribution of normal contact damage of SCR38 concrete particle models under uniaxial compressive strength tests with constant wall velocity. The model predicts crack localization across the height of the specimen which can be divided into main cracks that lead to failure and secondary cracks that do not develop in their full extent. The phenomena of crack bridging and crack branching, which is particularly important for the prediction of large specimens (Mier *et al.* 2002), is fairly modelled.

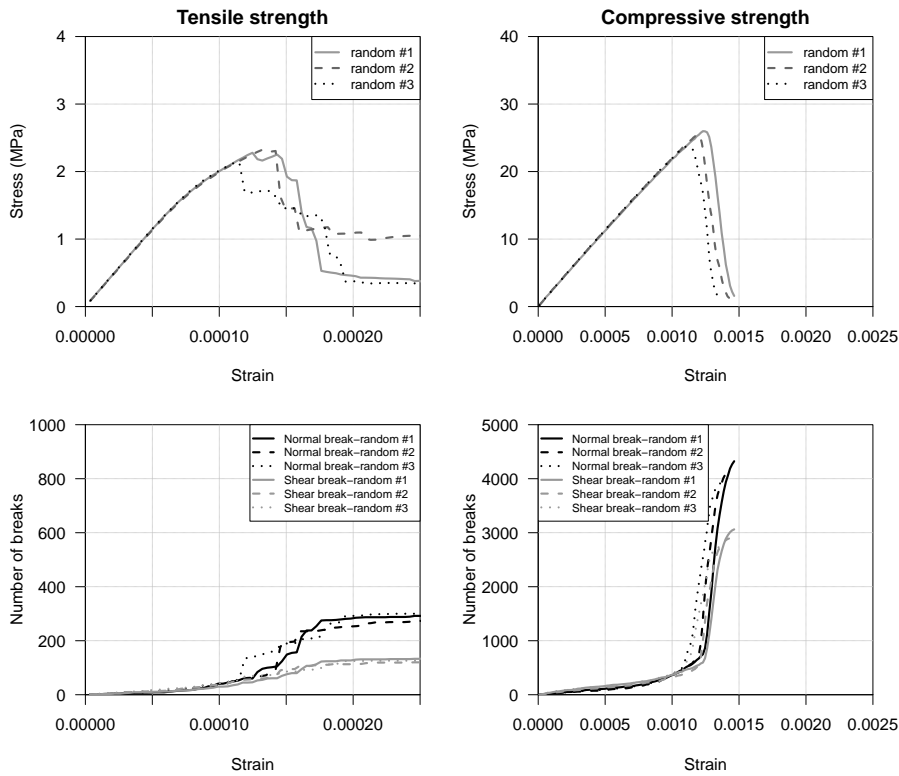


Figure 6.30: Stress-strain curves of SCR38 concrete considering ITZ's properties half of mortar's properties

6.3. PREDICTION OF DAM CONCRETE STRENGTH PROPERTIES USING PARTICLE MODELS

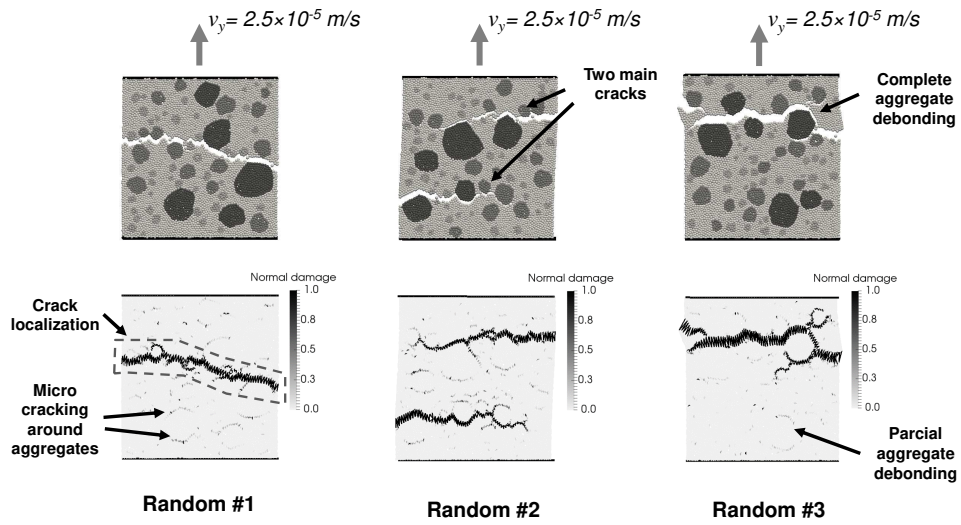


Figure 6.31: Cracking pattern and normal contact damage for tensile test of SCR38 concrete at the age of 90 days considering ITZ's properties half of mortar's properties

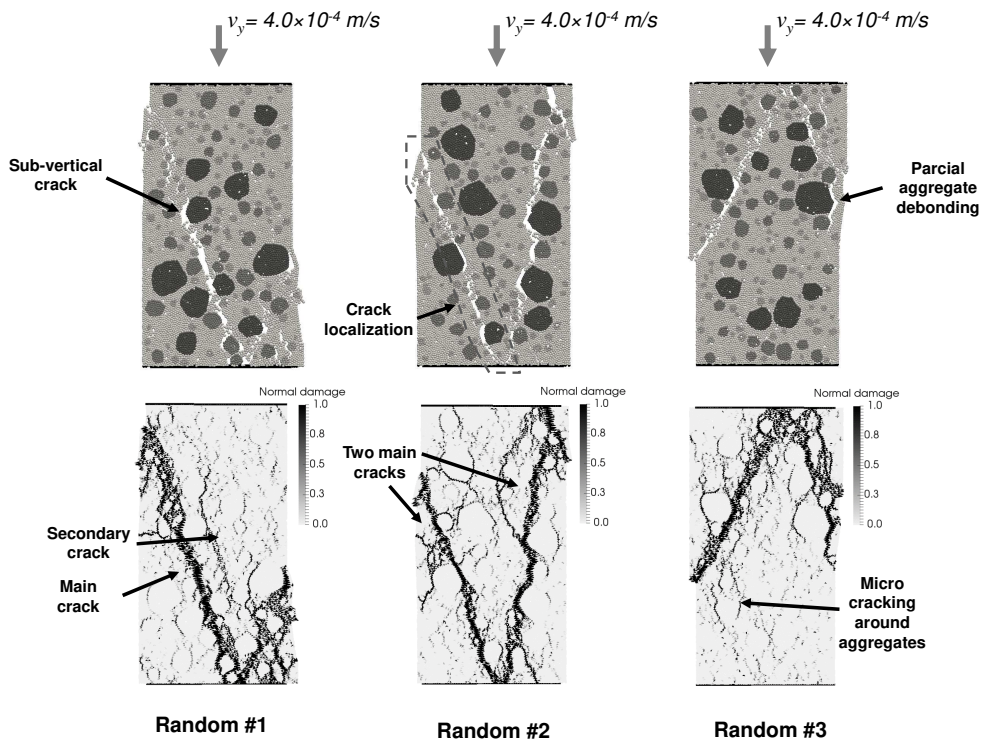


Figure 6.32: Cracking pattern and normal contact damage for compressive test of SCR38 concrete at the age of 90 days considering ITZ's properties half of mortar's properties

CHAPTER 6. NUMERICAL MODELLING OF THE DAM CONCRETE
STRUCTURAL PROPERTIES USING PARTICLE MODELS

The influence of the lateral restraint of the walls was also studied. Figures 6.33 and 6.34 show the comparison between the stress-stain curves and failure patterns under compressive load considering no lateral restraint of the wall and considering 20% of the shear stiffness of the mortar in the particle-wall contacts. The results show a similar stress-strain response but a significant difference in failure patterns. The restraint of the top and walls yield the development of diagonal cracks and two almost undamaged areas next to the walls, similarly to what is usual obtained in standard laboratory tests.

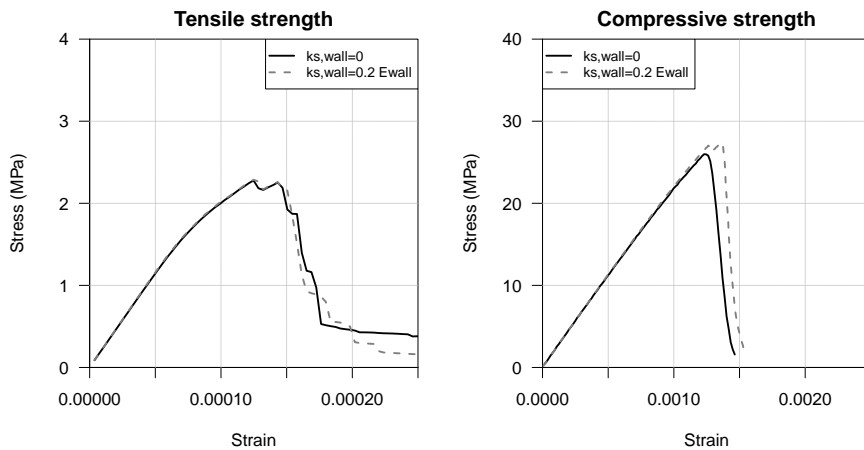


Figure 6.33: Stress-strain curves of SCR38 concrete considering ITZ's properties half of mortar's properties with and without lateral restraint

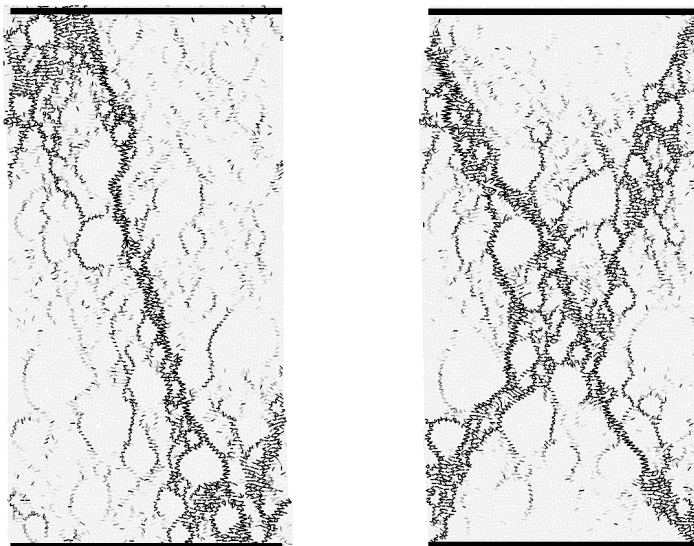


Figure 6.34: Comparison of failure patterns for compressive loading with (right) and without (left) lateral restraint of the walls

The strength contact properties of mortar and ITZ fitted to agree with the SCR38 concrete's tensile and compressive macroscopic strengths obtained in small specimens

were used for the prediction of SCR38 concrete behaviour in large specimens and for the prediction of DAM concrete behaviour in large specimens (third row on Table 6.24). The DAM concrete particle model is described in § 6.2.1.

The DAM concrete particle model results show a good agreement with the experimental results predicting the lower tensile and compressive strengths of DAM concrete obtained in large specimens ($\phi = 450$ mm) when compared with the strength values of SCR38 obtained in small specimens ($\phi = 150$ mm). Figure 6.35 presents the predicted stress-strain curves which shows the brittle behaviour for both tensile and compressive loadings. The cracking patterns of DAM concrete particle model are close to the ones obtained for SCR38 concrete particle model, with similar phenomena as previously described (Figures 6.37 and 6.38). It is noteworthy the extent of damaged areas around the large coarse aggregates in the compressive strength test and the thickness of the main cracks, embedding the smaller coarse aggregates (Figure 6.38).

The effect of the shear stiffness of the wall contacts is also captured for the DAM concrete simulations (Figure 6.39). The stress-strain results show an almost identical result for tensile loading and an increase of the peak-strength and softening when some lateral restraint occurs between the specimen and the walls (Figure 6.36).

Figures 6.40 and 6.41 illustrates the tensile force distribution and normal contact damage inside the DAM concrete particle assembly near peak strength and after peak strength for compressive loading (black lines are higher tensile forces and higher damage). The tensile force distribution shows a slightly higher stress concentrations in the larger aggregates but also significant in the mortar and in the ITZ. In the tensile force distribution, the white line around the side of the larger aggregates indicates that the damaged areas do not withstand any tensile load and there is a complete detachment of the aggregate. After failure, there is a crack localization between the larger aggregates and a further debonding of the aggregates (Figure 6.41).

Figures 6.42 and 6.43 show the same type of result for the compressive force distribution at peak compressive strength and after peak compressive strength. As discussed previously in this chapter, the stiff coarse aggregates work as stress concentrators and influences the force distribution inside the concrete specimen. Figure 6.42 shows that the ITZ and the mortar between the aggregates is highly compressed when compared to other areas of the specimen and shows the lateral deviation of the vertical compressive forces which generates horizontal tensile forces. After failure, the load in the aggregates completely unloads and

CHAPTER 6. NUMERICAL MODELLING OF THE DAM CONCRETE STRUCTURAL PROPERTIES USING PARTICLE MODELS

some residual forces remain in the mortar between the main cracks (Figure 6.43).

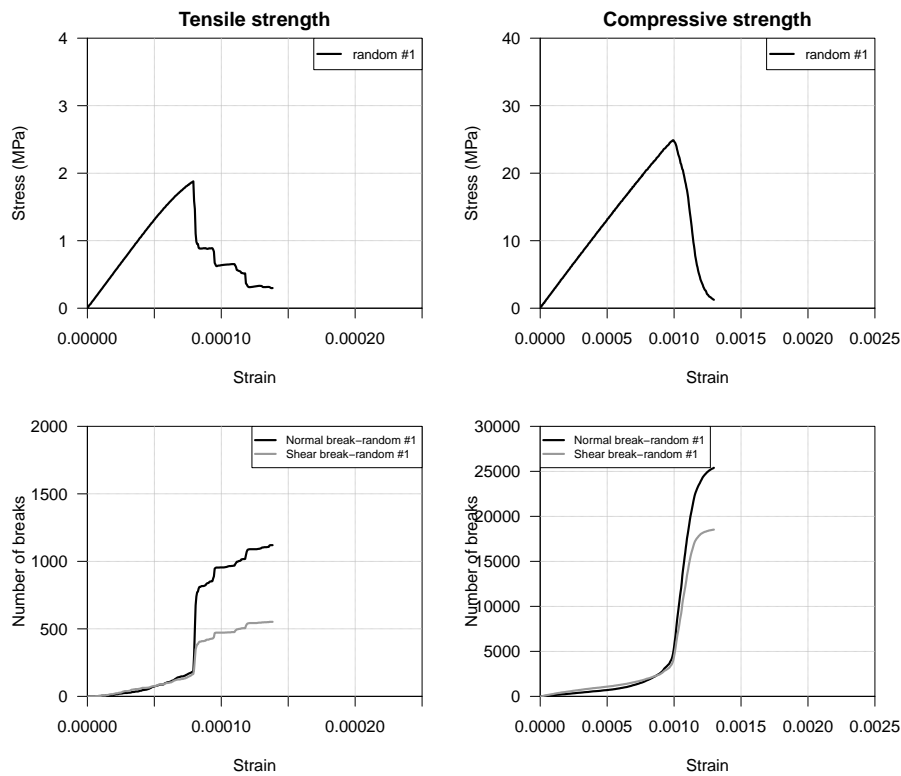


Figure 6.35: Stress-strain curves of DAM concrete considering ITZ's properties half of mortar's properties and no lateral restraint

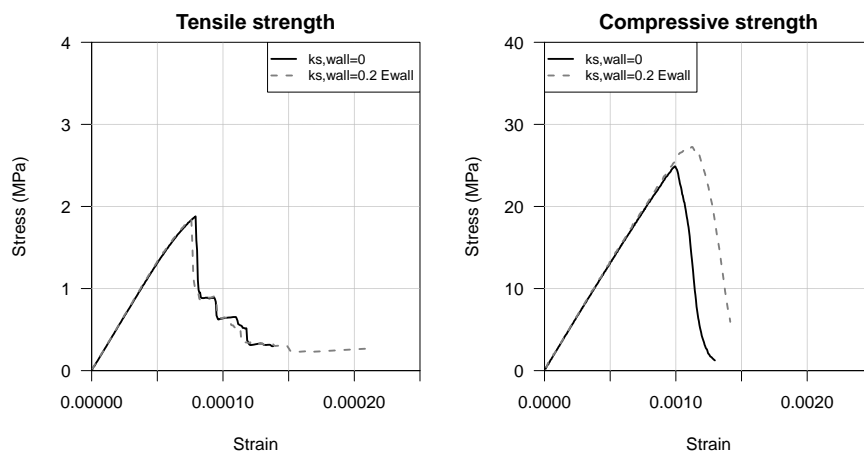


Figure 6.36: Stress-strain curves of DAM concrete considering ITZ's properties half of mortar's properties with and without lateral restraint

6.3. PREDICTION OF DAM CONCRETE STRENGTH PROPERTIES USING PARTICLE MODELS

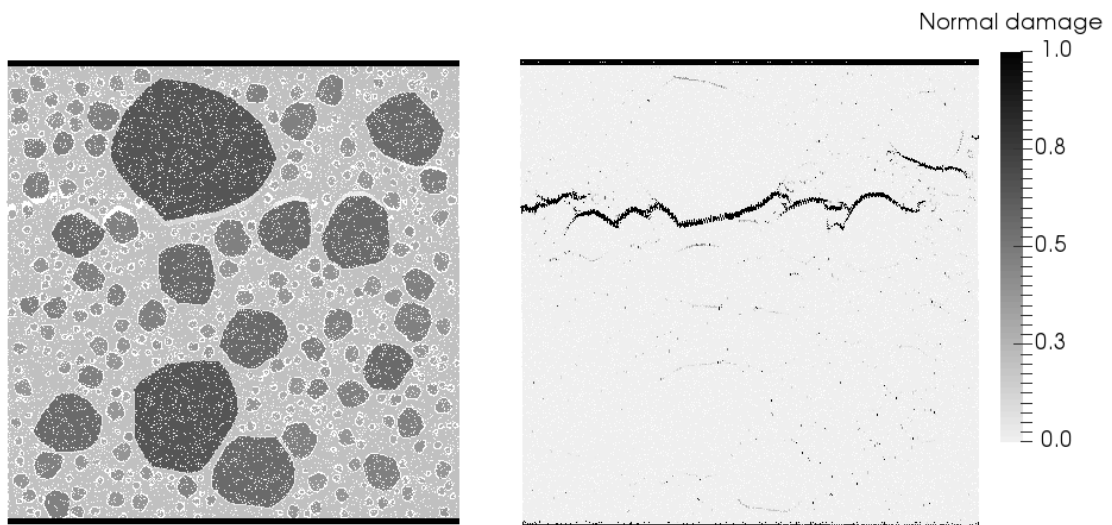


Figure 6.37: Cracking pattern and normal contact damage for tensile test of DAM concrete at the age of 90 days considering ITZ's properties half of mortar's properties

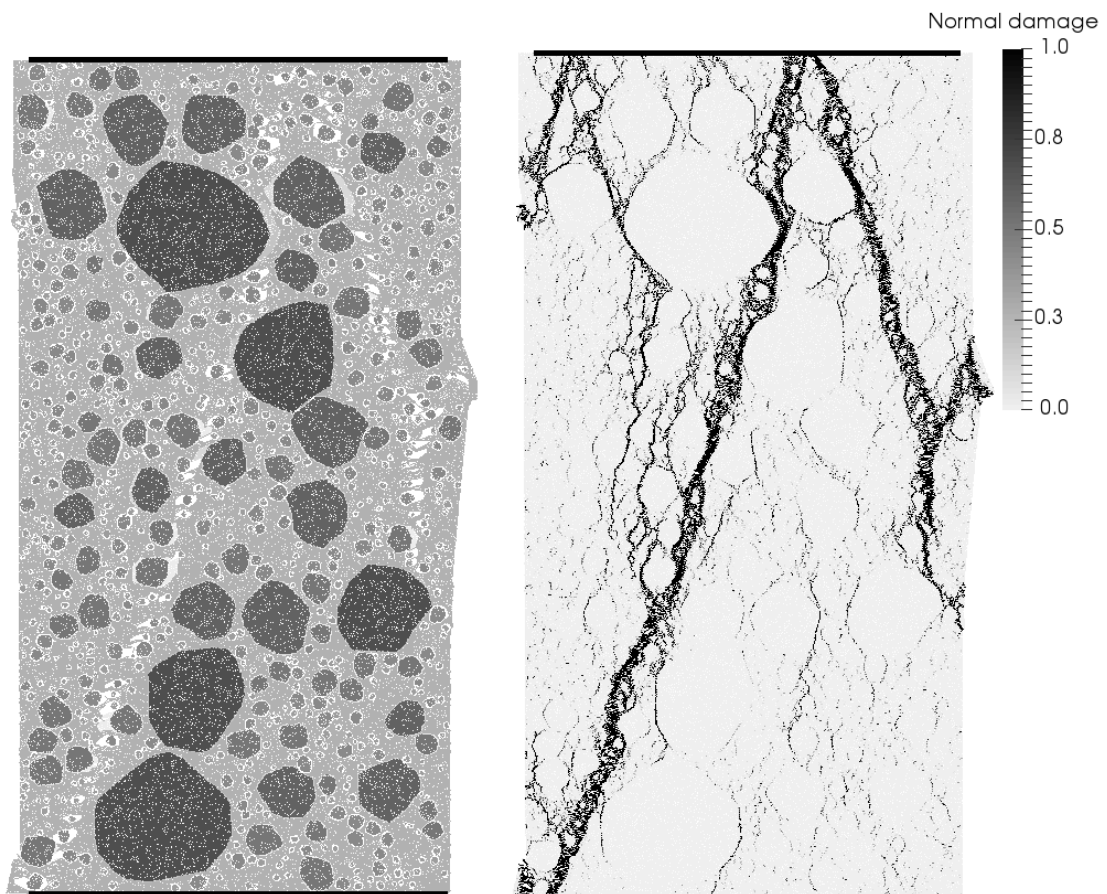


Figure 6.38: Cracking pattern and normal contact damage for compressive test of DAM concrete at the age of 90 days considering ITZ's properties half of mortar's properties and without lateral restraint of the walls

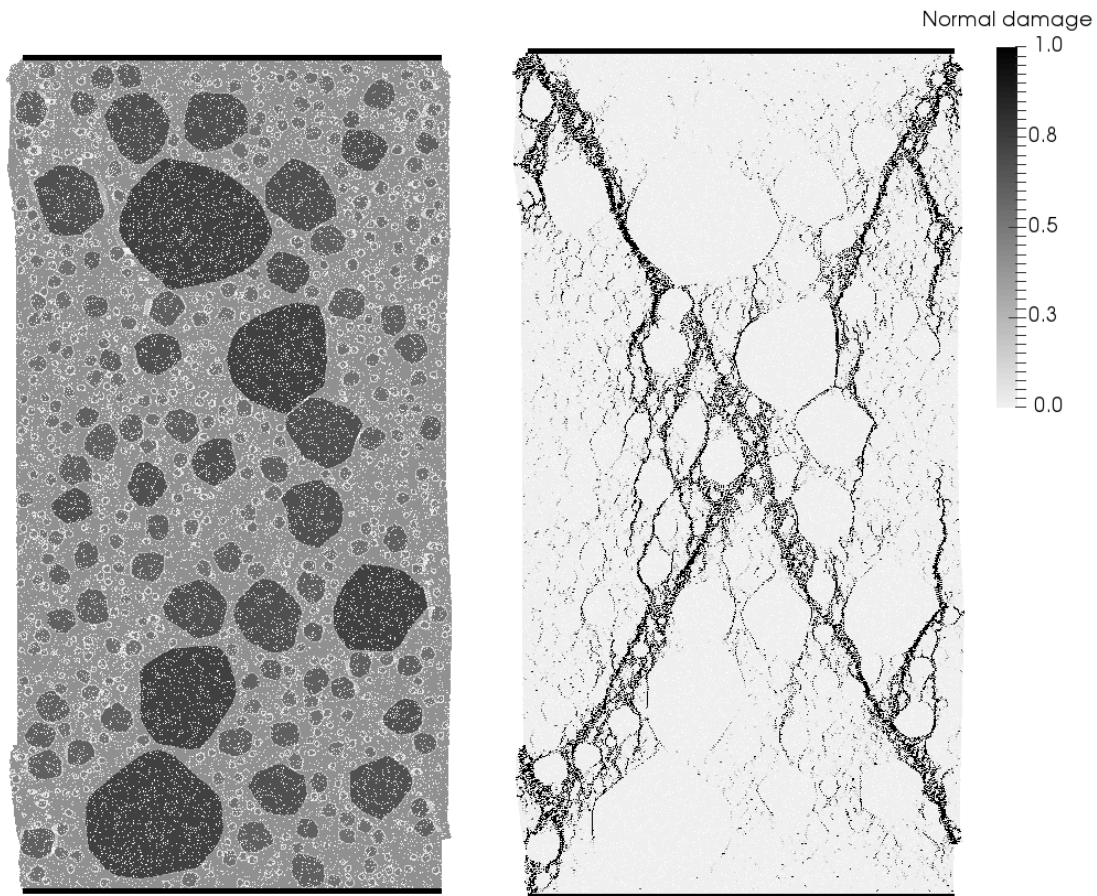


Figure 6.39: Cracking pattern and normal contact damage for compressive test of DAM concrete at the age of 90 days considering ITZ's properties half of mortar's properties and with lateral restrain of the walls

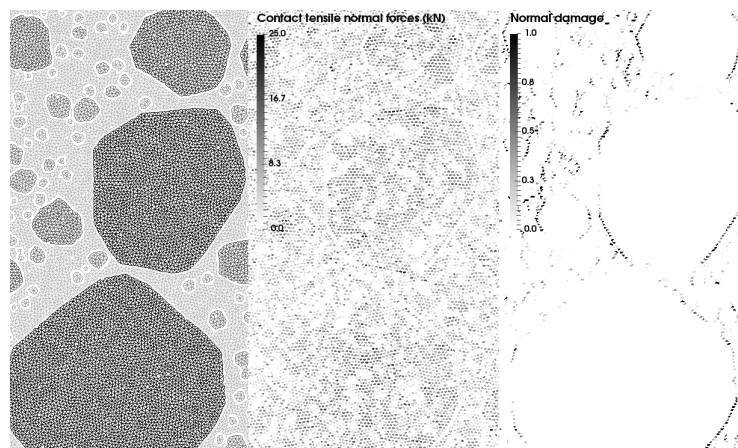


Figure 6.40: Distribution of tensile contact forces of DAM concrete near the peak strength

6.3. PREDICTION OF DAM CONCRETE STRENGTH PROPERTIES USING PARTICLE MODELS

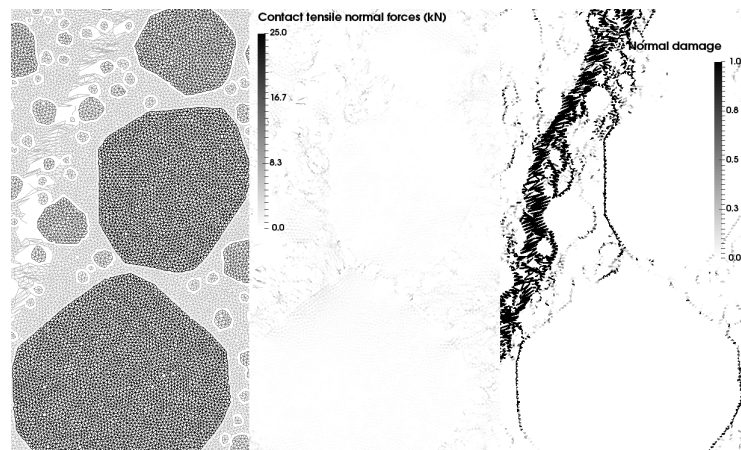


Figure 6.41: Distribution of tensile contact forces of DAM concrete after peak strength

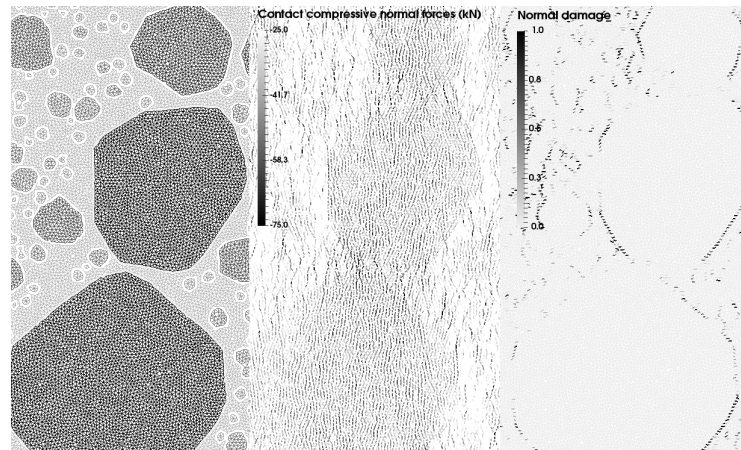


Figure 6.42: Distribution of compressive contact forces of DAM concrete near the peak strength

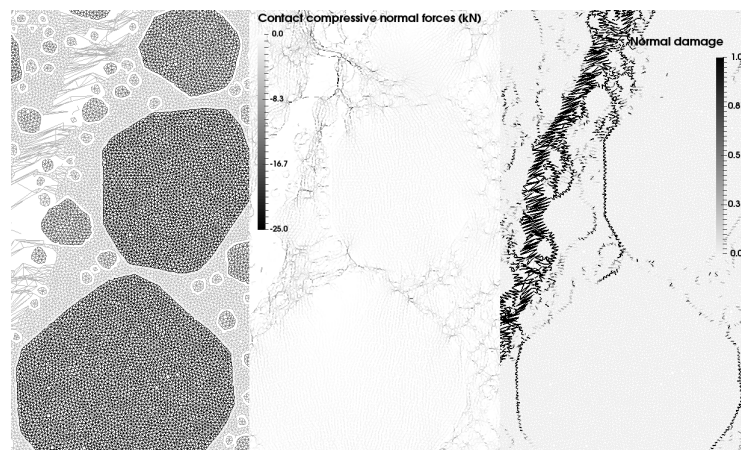


Figure 6.43: Distribution of compressive contact forces of DAM concrete after peak strength

In order to study the influence of the effect of specimen size on strength of wet-screened concrete, to separate this effect from the effect of the composition and to compare with the results obtained using the analytical models in § 4.4, a two large particle assemblies of wet-screened concrete were also tested. The size of the numerical specimens are 450×450 mm cube and 450×900 mm rectangle of wet-screened concrete, for tensile and compressive loadings, respectively. The simulations considered the same contact properties as the previous examples (Table 6.24). The peak strength values are presented in Tables 6.25 and 6.26 and Figure 6.44. The size effect on wet-screened concrete specimens is properly described with a decrease of tensile strength as the size of the specimen increases: $f_{t,\phi=150}^{DEM}=1.1$ MPa; $f_{t,\phi=450}^{DEM}=1.0$ MPa (Table 6.25). The size effect is not predicted for compressive strength behaviour. This could be due to the fact that there is lateral no restraint of the walls in the particle model, which reduces the influence of specimen aspect ratio and size and to the lack of more random assembly results.

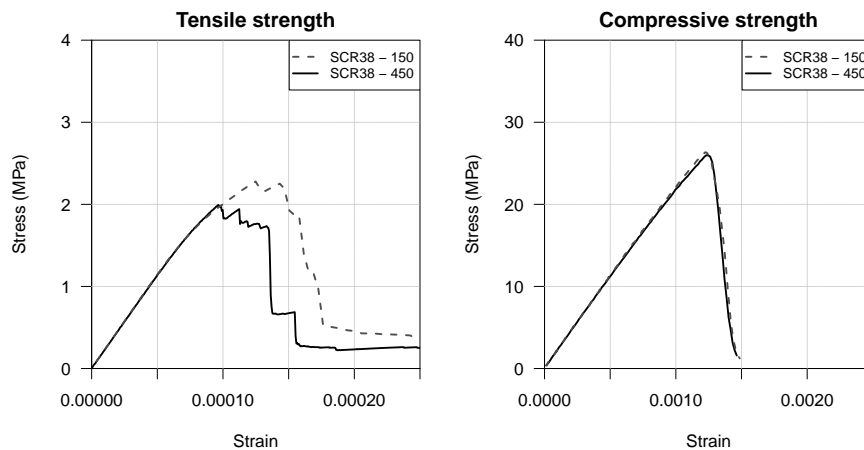


Figure 6.44: Comparison between stress-strain curves of SCR38 concrete tested in small and large specimens

Figures 6.45, 6.46 and 6.47 show the comparison between the results obtained using large particle assemblies for the study of SCR38 and DAM concretes. The stress-strain behaviour predicts a decrease of tensile and compressive peak strengths and a decrease of ductility for both loading conditions due to the addition of large aggregates (Figure 6.45). The higher strain development and ductility before complete failure is due to higher generalized microcracking and secondary cracks throughout the specimen of SCR38 concrete when in comparison to DAM concrete (Figure 6.46 for tensile loading and Figure 6.47 for compressive loading).

Table 6.26 compares the results obtained using analytical and numerical models for the

6.3. PREDICTION OF DAM CONCRETE STRENGTH PROPERTIES USING PARTICLE MODELS

different effects: the size effect, considering the parameter k_Φ , and the effect of composition, considering the parameter, k_{Abrams} (§ 4.4). Both effects are well represented for tensile strength but, although the particle model captures the lower strength values of DAM concrete, the size effect and the composition effect are not in agreement with the analytical prediction. This results could be due to the fact that, as previously described, the size effect is more relevant when there is some lateral restraint of the boundary walls and that there is low internal friction due to the presence of the coarse aggregates which leads to early and brittle failure. The large aggregates also influences the shear and friction behaviour of the ITZ contacts, before and after peak-strength. ITZ and mortar properties in DAM concrete could be different from those present in the SCR38 concrete since experimental results show that larger aggregates allow for better packing and can increase the quality of the matrix (Walker and Bloem 1960; Higginson *et al.* 1962; Stock *et al.* 1979).

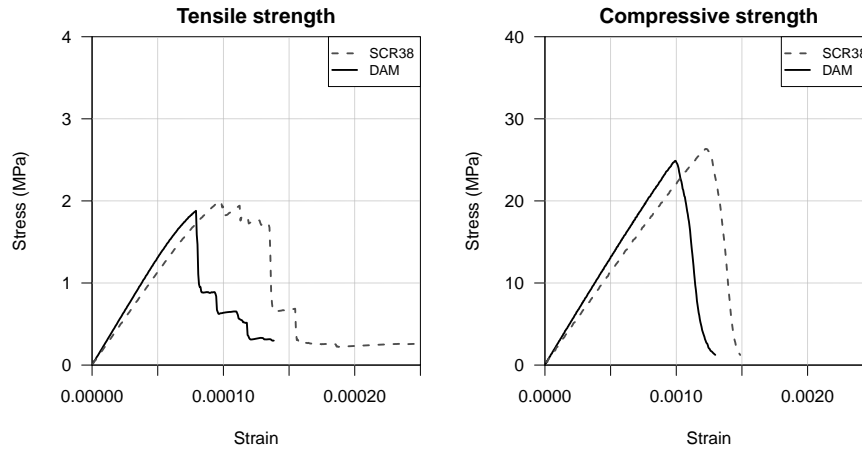


Figure 6.45: Comparison between stress-strain curves of SCR38 and DAM concrete tested in large specimens

Table 6.26: Comparison between analytical and numerical predictions

Type of model	Property	Age (days)	k_Φ	k_{Abrams}	$\frac{f_\Phi^{DAM}}{f_\Phi^{SCR}} = k_T$	Predicted values DAM, Φ large	Diff. (%)
Analytical model	f_c	90	0.93	1.03	0.96	24.2	2.0
	$f_{t,spl}$	90	0.80	0.97	0.78	2.1	4.5
Numerical model (no lateral restraint)	f_c	90	1.01	0.95	0.96	24.9	-0.8
	$f_{t,spl}$	90	0.83	1.00	0.83	1.9	13.0
Numerical model (lateral restraint)	f_c	90	1.05	0.97	1.00	27.3	-10.5
	$f_{t,spl}$	90	0.90	0.90	0.80	1.8	18.0

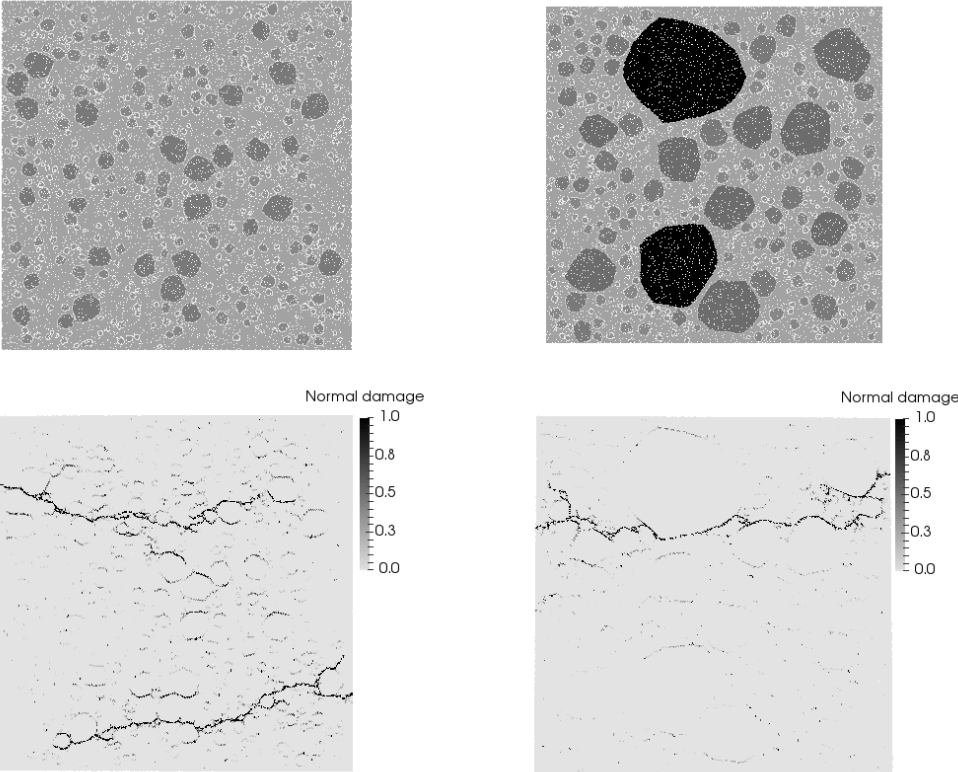


Figure 6.46: Comparison between cracking patterns of tensile tests of SCR38 concrete (left) and DAM concrete (right) using the same specimen size

6.3. PREDICTION OF DAM CONCRETE STRENGTH PROPERTIES
USING PARTICLE MODELS

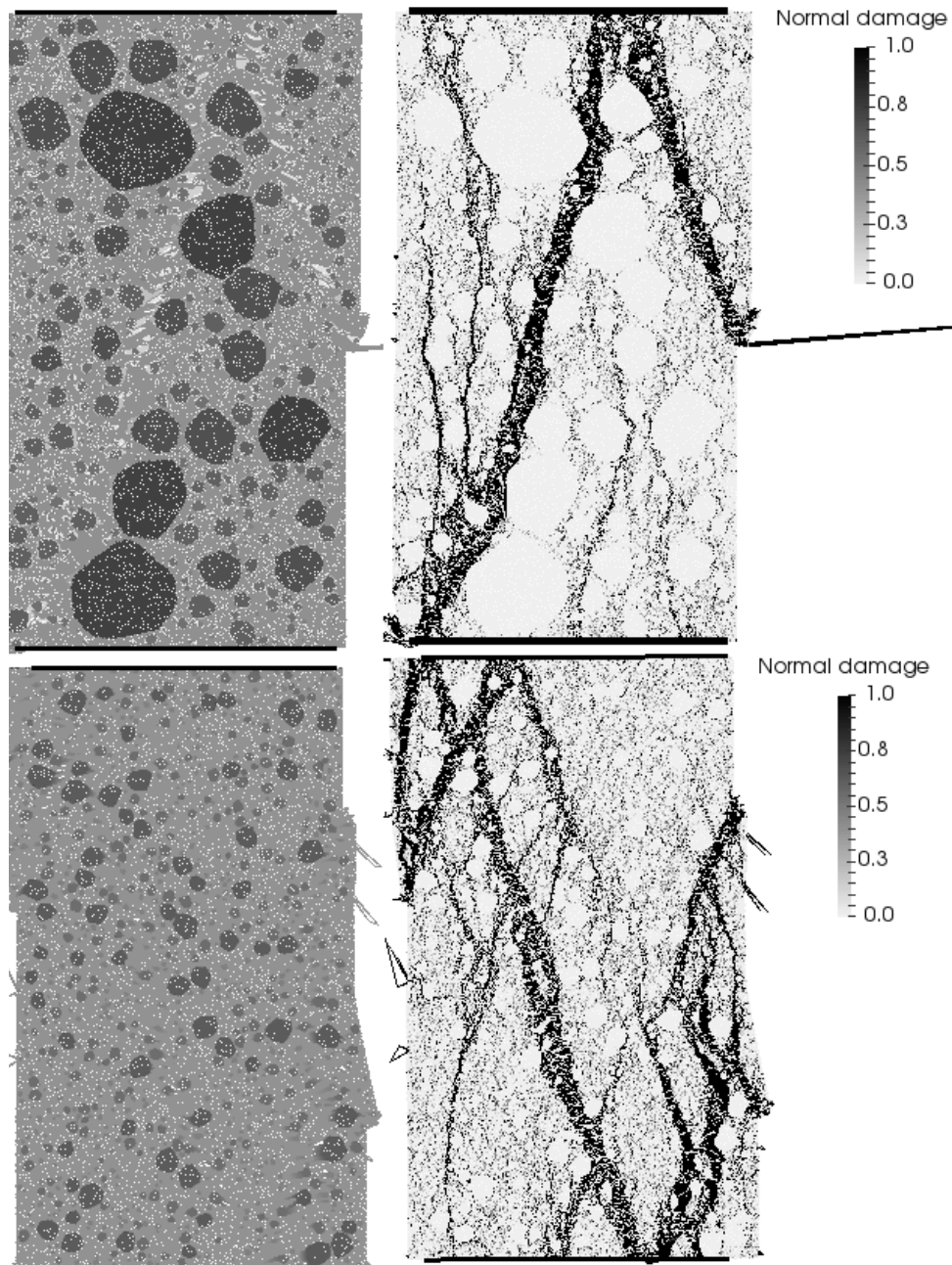


Figure 6.47: Comparison between cracking patterns of compressive tests of DAM concrete (top) and SCR38 concrete (bottom) using the same specimen size

6.4 Concluding remarks

Based on the particle model developed in chapter 5 and taking advantage of its capabilities, chapter 6 presents a practical application for the prediction of dam concrete behaviour using the available results of wet-screened concrete and the properties of each material components, namely the mortar, the aggregates and the ITZ. The complexity of the dam concrete particle models are mainly related to the accurate representation of each component, to the calibration of each component, especially of the ITZ, and its relationship with the available test results. Other main difficulty is the size of particle assembly since, similarly to the previous validation examples, the particle size is constraint by the size of the smallest coarse aggregate. In order to have an uniform particle discretization throughout the specimen and a detailed representation of the material, the larger aggregates and the mortar have the same discretization as the smaller aggregates. The large size aggregates and the large specimens of dam concrete imply a significant number of particles and contacts and a high computational analysis time.

The advantage of this type of detailed particle models is the possibility of studying the several complex interactions inside the concrete mesostructure without discretization assumptions and using simple contact models and a direct micro properties calibration using smaller homogeneous assemblies for each type of material. The ITZ representation is directly obtained by the contact between an aggregate particle and a mortar particle and the thickness of the ITZ can easily be predefined using the series model.

Previously to the prediction of dam concrete using this type of particle models, the elastic behaviour of an each individual aggregate and its interaction with the surrounding mortar was validated. This analysis ensured the expected behaviour for very large aggregates and considering different aggregate contents. Additionally, the effect of temperature was also taken into account using the maturity method in order to model the *in situ* behaviour of dam and wet-screened concretes measured in creep cells.

Firstly, homogeneous particle models were used to calibrate the contact properties of each component, namely the mortar and ITZ as a combined material and each aggregate. Secondly, the instantaneous elastic and long-term aging viscoelastic behaviour of wet-screened concrete was validated by the fitted analytical models, namely the B3 model, for standard constant temperature conditions and by the creep test results for variable temperature conditions. This preliminary analysis ensured the physical representation of

not only the reduction of the mortar creep strains over time due to the restraint of the aggregates but also the gain in stiffness at early ages due to the temperature rise in the first months. Once the response of wet-screened concrete long-term behaviour was fitted to the experimental results and the concrete particle model was validated, the long-term behaviour of *in situ* dam concrete was predicted and compared with the measured test results obtained in creep cells. The prediction showed a good agreement with the test results and allowed for the interpretation of the high values of dam concrete modulus of elasticity at early ages which is mainly due to the high coarse aggregate content and to the sustained high temperatures.

The same procedure was adopted for the prediction of strength properties of dam concrete: calibration of micro parameters of each concrete component; validation and further adjustment of micro properties based on wet-screened concrete results; and, prediction of dam concrete behaviour under extreme tensile and compressive loadings. A correlation law between the modulus of elasticity and the tensile strength of both the mortar and the aggregates, fitted to experimental results, was used to obtain a first estimate of the contact tensile strength of these concrete components. Since the deformability properties of the concrete particle model were already well established and the strength results are scarce, the correlation law allowed for the definition of the strength development over time at the contact level.

The prediction of fracture concrete was divided into modelling of tensile and compressive tests of both wet-screened concrete (SCR38) and full-mixed concrete (DAM). The micro properties fitted to describe the behaviour of SCR38 concrete were used for the prediction of DAM concrete macroscopic properties with good global results. Although only the experimental peak strengths are available, the complete stress-strain curve and the failure modes were analysed. The concrete particle models allowed for the representation of complex fracture behaviours, such as microcracking, localization, crack bridging and branching and global softening of the material.

Conclusions and future developments

7.1 Summary and main conclusions

The main goal of the presented work was to study the behaviour of dam concrete and to develop physically-based models for the prediction of its structural properties based on the properties of wet-screened concrete. The proposed methodologies featured: results of the developed experimental work that characterized the development of main structural properties over time; analytical models based on semi-empirical expressions tailored for the study the effect of dam concrete wet-screening; and, complex numerical tools based on particle models in which the concrete mesostructure is explicitly taken into account.

Firstly, a literature review was presented in the second chapter. The objective was to present the main structural properties of hardened dam concrete, the influence of composition data, the most relevant approaches for the study of concrete behaviour and the available correlations between the properties of dam and wet-screened concretes. This review set the foundation for this work and showed the need for the use of physically-based approaches to study not only the effect of wet-screening on dam concrete structural properties but also the influence of the internal aggregate mesostructure on the overall behaviour of concrete.

A comprehensive study of the properties of dam concrete placed on Portuguese dams established an overview of the composition and properties of different types of concretes, from 1951 to 2014. One of the main differences between past and present concretes is the

use of large percentages of other cementitious materials introduced during the mix instead of blended cements, the use of highly effective superplasticizers and the new production and compaction procedures on site. The results of both deformability and strength properties show a large scatter mainly due to the different types of aggregates used but it was possible to establish a general relationship between the properties of dam concrete and wet-screened concrete, considering the results of four dams, in which granitic aggregates were used.

The *in situ* experimental installation in Baixo Sabor dam presented several technical improvements favouring the creep cell installation procedures, reducing the stiffness of lost moulds and reducing the production costs. The improvements related to the redesign of the flat-jack allowed for a more uniform and effective load application and, ultimately, to better results. The results of this specific experimental study concluded that the deformability properties of dam concrete are different from the wet-screened deformability properties, with higher modulus of elasticity and lower creep strain development over time and lower creep rate. This results could be explained by the coarse aggregate content and also by the effect of elevated temperature during the first months which increases the rate of development of the main structural properties.

The experimental laboratory results obtained during construction, provided by the dam's owner, revealed a large scatter at each testing age, a significant rate of development even for later ages and that the ratio between dam and wet-screened concrete structural properties is close to the unit. Although the obtained strength results agree with the available results in the literature, the modulus of elasticity test results differs from what would be expected. Both dam and wet-screened concrete yielded similar modulus of elasticity laboratory test results. It would be expected that the large aggregate content of dam concrete would yield higher modulus of elasticity values, as it was obtained for the *in situ* test results.

In order to include some type of physical meaning into the analysis of the test results and to enhance the interpretation of the behaviour of concrete, several semi-empirical or analytical models were developed to predict the main structural properties based on the obtained results of wet-screened concrete and composition data. The work concerning these analytical models was divided into two main parts, the first relates to the instantaneous and delayed properties of concrete and the second relates to the strength properties.

The prediction of deformability properties of dam concrete relied on different two-phase

composite models and on the equivalent age method. An innovative adaptation of two-phase composite models to the wet-screening procedure established a direct correlations between the two types of concrete showing a good fit between the model results and the experimental results. It was concluded that the high modulus of elasticity results were better fitted by the Granger's composite model using the β parameter equal to 1.0, equivalent to the Voigt composite model, which gives the upper bound of modulus of elasticity values. Similarly, the dam concrete creep strain prediction relied on the use of Granger's composite model and to the fit of the free parameter β . The best fit was obtained using values of β of 0.5 and 0.6 for the prediction using SCR76 and SCR38 wet-screened concretes, respectively. This result relates mainly to the amount of equivalent creeping matrix placed in parallel in the composite model and to the maximum amount of aggregate for this type of concrete. The differences between the β results for instantaneous and delayed properties can be due to the temperature effect which is more pronounced before 28 days of age.

In order to establish a correlation between dam and wet-screened concrete creep strain development over time and interpret the test results obtained in the creep cells, it was necessary to incorporate the temperature effect into the prediction model. Each of the creep cell test results are influenced by a different temperature history, usually above 30°C during the first month. The effect of elevated temperature was corrected in order to estimate the creep strain development at a constant temperature and, therefore have a comparable base for the correlation between each type of concrete. This approach validated the use of maturity method to take into account the effect of temperature on creep strain and can be used for the interpretation of *in situ* test results or global safety assessments during construction.

The prediction of compressive and splitting tensile strengths of dam concrete was also obtained considering the size effect, an adaptation of the Abrams law in order to take into account the maximum size of aggregate (MSA) and the water to cementitious materials ratio. The extended Abrams law was fitted to the experimental results of the different types of concrete placed in Baixo Sabor dam. It was concluded that the influence of MSA is statistically significant and it has an important role on the prediction of these types of concretes produced with large aggregates. It was also concluded that the separation between the size effect and the influence of composition data is crucial for the analysis of the strength results of dam and wet-screened concrete.

Two different methodologies were proposed and validated using the available test results, concerning the deformability properties and the strength properties. It was successfully shown that different models and methods can be adapted and combined to predict the behaviour of dam concrete.

When calibrated with a trial experimental programme, these models can be used for the prediction of dam concrete structural properties and help the main quality control procedures concerning conformity check and for obtaining estimates when dam concrete test results are not available. A new framework for the dam concrete quality control is proposed in chapter 4 based on the developed analytical models.

Although the analytical models successfully describe the behaviour of dam concrete based on concrete's composition data, namely the aggregate content, the MSA and the water to cement ratio, and on results of mortar and aggregate, it should be bear in mind that only the macroscopic behaviour is described. Only the global effect of "stiff" coarse aggregate inclusions on the "soft" and aging viscoelastic mortar is described and local effects are averaged and resumed in an global law. It is known that, for example, the prediction of concrete strength is a complex task and it is influenced by both intrinsic factors, such as the type and content of each component, and external factors, such as the type of loading. Tensile and compressive strengths involve different failure mechanisms which are intimately related to composite nature of concrete and to the properties of the interfacial transition zone (ITZ). Additionally, the effect of coarse aggregate's content and maximum size are known to have contradictory effects on concrete strength (§ 2.3.7). The developed analytical relations between strength properties of dam and wet-screened concretes does not take every factor into consideration but describes the global behaviour of concrete fitted to experimental results.

For example, the extended Abrams law for strength properties evaluation includes the effect of the maximum size of the aggregate and the water to cementitious materials ratio but failed to predict the ultimate behaviour of mortar based on the test results of concrete. This could be due to the higher porosity or more entrapped air in mortar specimens (Neville *et al.* 1983), to the different testing conditions of the mortar specimens and/or to the effect of the ITZ on the concrete specimens. The obtained results enhance the fact that coarse aggregates have a significant effect on the properties of concrete, affecting both the composition and the failure mechanisms.

In order to study the effect of the internal aggregate structure of concrete and to

predict the behaviour of dam concrete, a numerical model was developed considering the Discrete Element Method (DEM). For this work, DEM is based on rigid particle models for the representation of both aggregates and surrounding mortar. In each contact between two circular particles a constitutive model defines the behaviour of a specific material (aggregate, mortar or ITZ) and the global assembly defines the complex behaviour of concrete.

Chapter 5 defines the general DEM numerical scheme and the rigid particle model formulation. Based on DEM, it is also described the implementation of the constitutive contact models which includes the proposed aging viscoelastic model based on the solidification theory and its adaptation for long-term analysis and the Mohr-Coulomb model with and without softening. Due to numerical constraints, the numerical time step is linked to the stiffness of the assembly and is often very small. This limitation is a major difficulty for long-term analyses using DEM and, therefore, a new fast numerical procedure was developed for the implementation of the aging viscoelastic contact model.

The proposed fast numerical procedure defines two different times, one related to the real time and age of concrete and other related to the calculation time. By doing so, it is possible to have large real time increments in which equivalent aging viscoelastic forces are introduced into the model. The unbalanced system reaches equilibrium with DEM cycling, using the small time step necessary for convergence of the structural system and equivalent elastic properties. It is shown that this fast numerical procedure significantly reduces the computational time allowing for the study of the macroscopic concrete creep compliance and the interactions between aging viscoelastic mortar and the stiff elastic aggregates over time.

Additionally, a calibration procedure was proposed for the determination of long-term micro properties in order for the particle model to describe the macroscopic behaviour of the material. Taking into account that the calibration of the micro parameters is pointed out as one of the main drawbacks of particle models, this procedure insures a direct relation between the contact properties and the material's macroscopic properties, for the deformability properties.

The DEM aging concrete model was validated using a B3 model fit to Ward *et al.* (1969) experimental results for different loading ages. The aging viscoelastic contact properties of the mortar and of the interfacial transition zone (ITZ) and the elastic contact properties of the aggregate were determined during the particle model calibration procedure.

The obtained numerical results show that the DEM aging viscoelastic particle model considering the concrete mesostructure can predict long-term behaviour of concrete. The obtained results revealed high creep strain development for the ITZ, which agrees with the experimental results and other numerical studies for the prediction of ITZ properties.

In the second part of chapter 5 the failure contact model, based on the brittle and linear softening Mohr-Coulomb models, was validated using simple particle assemblies for both tensile and shear loadings.

A sensitivity study was also carried out to better understand the effect of the main input parameters on the macroscopic stress-strain behaviour of concrete. The main parameters were the modulus of elasticity of the aggregate, the maximum normal contact force of the mortar contacts, the cohesion of the mortar contacts, the ratio between contact strength properties of ITZ and mortar, the ratio between total and elastic contact fracture energy and the lateral restraint of the boundary walls. The results show that: similarly to the previous results concerning the aging viscoelastic behaviour, the ITZ has a great influence on the strength properties, especially on the tensile strength; the contact cohesion has a much higher influence on the compressive strength; and, the lateral restraint of the boundary walls changes the global failure pattern and increases the model's ductility. Although this type of concrete particle models yield lower fracture energy than the models based on deformable polygons (Vonk 1992), the developed particle models are capable of reproducing the global macroscopic behaviour of concrete, including the main cracking patterns, and the peak strength values.

The development of a C++ computational code of DEM applied to particle models for the study of instantaneous and delayed behaviour of concrete allowed for the implementation of tailored solutions for the main numerical difficulties and a complete control of the input parameters for the analysis. The development of the concrete particle models focused on the prediction of concrete behaviour considering a detailed mesostructure, using faithful representations of reality and physically-based input parameters. For example, although the model is always constraint by the minimum particle radius, this model property was taken as a portion of the size of the smallest coarse aggregate insuring that its properties were represented in the model.

Chapter 6 presents the practical application of DEM concrete particle models to the prediction of dam concrete considering the mortar, aggregate and wet-screened concrete test results and the analytical models developed in chapter 4. The proposed approach was

to determine the micro properties of contacts related to the mortar and to each coarse aggregate size and, based on those input parameters, predict the behaviour of wet-screened and dam concrete using a concrete particle model and a realistic representation of the coarse aggregates and the mortar within the model.

This analysis ensured the physical representation of, not only the reduction of the mortar creep strains over time due to the restraint of the aggregates, but also the gain in stiffness at early ages due to the temperature rise in the first months. The dam concrete prediction showed a good agreement with the test results and allowed for the interpretation of the high values of dam concrete modulus of elasticity at early ages which is mainly due to the high coarse aggregate content and to the sustained high temperatures.

The modelling of quasi-static behaviour of cementitious materials requires the representation of its micro and meso structure in order to obtain a realistic response and to capture the different fracture mechanisms. Based on the work presented in chapter 5, in which the basis for fracture behaviour of concrete was developed and validated, it was possible to establish a prediction approach for modelling dam concrete based on the wet-screened results, similarly to what was presented for the deformability properties.

The detailed particle model of DAM concrete shows a good global agreement with the experimental tensile and compressive strength results, using the same micro properties as the ones used for the validation of SCR38 concrete. The numerical results were also compared directly to the ones obtained by the analytical models developed in § 4. Although the obtained tensile strength results for small and large specimens follow the size effect law (decrease of tensile strength as the size of the specimen increases), the compressive strength results remains approximately the same as the specimen size increases.

The concrete particle model is also able to simulate different fracture mechanisms of concrete, such as generalized microcracking around the larger aggregates, crack localization, bridging of the main cracks on the ITZ across the mortar, the development of main and secondary cracks and the partial or complete debonding of a coarse aggregate. This behaviour is captured for both SCR38 and DAM concretes, although SCR38 yields higher microcracking and ductility in tension and compression.

7.2 General recommendations and future developments

During the progression of this study it was possible to better understand the main difficulties of dam concrete testing and to develop methodologies to tackle those difficulties. The recommendations presented in this section are focused on the improvement of the experimental procedures concerning dam concrete characterization, both in laboratory and *in situ*, namely:

- The increase of the number of laboratory creep tests of wet-screened concrete in order to have a more representative sample of the concrete placed on site and to study the effect of composition variations that occur during construction;
- A rigorous control of the specimen curing, transport and testing conditions, especially during the first days of curing and for dam concrete specimens;
- Each main structural properties should be obtained at several ages of concrete (at least four testing ages) in order to fit to a time development law capable of providing information on intermediate ages and accurate predictions of the ultimate structural properties;
- Testing of early age properties of dam and wet-screened concrete into the quality control procedures in order to have early alerts of concrete non-conformities and to have a better characterization of the early age behaviour;
- The improvement of creep strain measurement, including more measurement points, internal and external measurements (other type of embedded strainmeter), both *in situ* and in laboratory;
- The implementation of an automatic acquisition system for strain and pressure measurements would also improve the overall quality of the results.

Regarding creep tests, although recognizing that it is very difficult to increase the number of *in situ* testing using creep cells, due to its cost and schedule constraints. As recommended in standard concrete testing procedures (NP EN 206 2005; ASTM 2006), the number of specimens from the same batch should be at least 3 to 5 specimens in order to have statistical representation of the results. Additionally, it is known that small differences in curing conditions, temperature and moisture variations, have a great influence on the strength development of concrete over time.

Regarding future developments, due to the diversity of the developed work, the proposals are divided into three main parts, related to: the experimental developments and

research topics; analytical models for the prediction of concrete behaviour; and, concrete particle models.

Future work concerning experimental programmes should include:

- The characterization of the strength properties of mortar, aggregates and concrete, measuring the stress-strain curves with controlled displacements for tensile and compressive loadings and the characterization of its deformability properties based on compressive creep tests at several ages;
- The study the effect of wet-screening of dam concrete on the main structural properties using more types of wet-screened concretes;
- The characterization of the early age properties of dam and wet-screened concrete and the mortar binding the coarse aggregates;
- The study of the temperature variations on the development of the main structural properties.

The early age behaviour of concrete placed in dams is of the foremost importance due to high temperature gradients, the low strength development and, therefore the high cracking risk at early ages (JCI-RILEM 2017). In order to extend the analysis of dam concrete to its early age behaviour, it is necessary to define experimental setups for the first ages after setting. Combined with standard tests, specific experimental programmes can be used to determine the structural properties of dam concrete, for example, the new EMM-ARM (Elasticity Modulus Measurement through Ambient Response Method) which is being used for obtaining a continuous measurement of the modulus of elasticity of cement paste and concrete (Azenha *et al.* 2009; Granja and Azenha 2017) and tensile creep tests of dam concrete.

The analytical and numerical tools developed for the prediction of concrete structural behaviour are bound to have limitations which can be reduced or overcome in future developments. The analytical models based on semi-empirical expressions can be further developed considering research focused on:

- Studying the magnitude of parameter β of Granger's model for other sets of experimental results, for both instantaneous and delayed properties;
- Developing three or four-phase composite models that would be helpful to include the effect of the ITZ on the prediction of dam concrete deformability properties;

- Testing the accuracy of other prediction models, such as the Bolomey law and the recommendation of USBR based on Feret formula, in the proposed methodology for the prediction of dam concrete based on wet-screened test results;
- Extending the developed analytical models for the prediction of strength of concrete to take into account the effect of the age of concrete;
- Studying the significance of other composition data and properties on the strength properties of concrete using a comprehensive test result database;
- Establishing a procedure for the conversion of strain histories measured on site in wet-screened concrete into strain histories that would develop in dam concrete and the calculation of the stress development over time.

The effect of temperature on the development of the main structural properties of dam concrete has been a concern at LNEC. The experimental work of (Silveira and Florentino 1971; Silveira *et al.* 1981; Soares de Pinho *et al.* 1988; Serra *et al.* 2012) on creep strain development is still of great importance but there is the need for the development of numerical tools that include not only the effect of elevated temperature taking into account the maturity method (Bažant and Baweja 2000) but also to include large temperature variations (higher temperatures during hydration and, for some cases, significant temperature drops during forced cooling).

It would be important to test and implement the proposed framework for the dam concrete quality control during the construction (§ 4.5) of a new dam in order to validate the proposed analytical models. The framework includes extensive experimental work, the adjustment of prediction laws and the study of the effect of temperature on the development of the main structural properties *in situ*.

Concerning the concrete particle models, the main proposed future developments are:

- The implementation of the extension of the DEM to 3D analysis, particularly the proposed fast numerical procedure for long-term analysis using the aging viscoelastic contact model;
- The implementation of imposed deformations, such as thermal strains, shrinkage strains and expansion strains due to internal expansion reactions (IER), into the DEM computational code;
- The development of specific studies focusing on other types of tests, such as: biaxial/triaxial tests; 3-point bending test; brazilian or tensile splitting test; stiffness

damage test (SDT); and, tensile creep tests;

- The development of specific studies of tertiary creep and nonlinear creep, of the coupling between creep and damage, size effect and the influence of the specimen height-width ratio, the effect of the ratio between MSA and specimen width, the effect of the ratio between MSA and the embedded measurement devices and the hysteretic properties of concrete;
- The development of specific studies concerning the behaviour of different types of concretes in which the interaction between the each component has particular interest, such as, reinforced concrete, high strength concrete, recycled aggregate concrete, fiber concrete, asphalt concrete and pre-placed aggregate concrete.

Mesoscale analyses are being used for the study of the behaviour of concrete focusing on the interactions between coarse or fine aggregates and the maturing mortar or cement paste in order to evaluate the main mechanical properties and their deterioration (Pan *et al.* 2012; Alnagar *et al.* 2013; Giorla *et al.* 2015). At early ages, the self-induced stresses due to hydration and shrinkage can introduce local damage and reduce the potential mechanical properties (Aydin *et al.* 2007; Azenha *et al.* 2017; Xu *et al.* 2017). These types of models are particularly relevant for the study of internal expansion reactions (IER) since the aggregate structure of concrete and the interfacial transition zone (ITZ) are explicitly taken into account (Scrivener *et al.* 2004). Since the swelling reactions occur relatively slow over a large period of time, creep and relaxation properties of concrete have an important role in the development of stress and in the progress of damage (Dunant and Scrivener 2010). Limited numerical work has been done considering the interaction between creep and damage of swelling concrete at the mesoscale (Giorla *et al.* 2015) and in a practical application at the macroscale (Saouma *et al.* 2015; Esposito *et al.* 2016).

The implementation of imposed deformations, such as thermal strains, shrinkage strains and expansion strains due to IER, into the DEM computational code is also expected to be done in the near future. This feature would allow to simulate the behaviour of concrete since cast for several types of internal and external "loadings" and would be a important tool for the study of the self-induced or self-balanced stresses that develop during hydration. It would be possible also to simulate the behaviour of concrete for controlled and *in situ* conditions, since cast and for long-term analysis. The implementation of the expansion strain development on specific materials (in the ITZ for the alkali-silica reactions (ASR))

and in the mortar for the internal sulfate reaction (ISR)) would allow to study the behaviour of the mesostructure over the years due to IER and to better interpret the experimental results, which are often executed in accelerated testing conditions.

The development of these types of concrete particle models set the foundations for the study of concrete behaviour at the specimen level, including the explicit influence of its mesostructure. The presented work focused only on standard laboratory tests (uniaxial compressive modulus of elasticity test, uniaxial compressive creep test, uniaxial direct tensile strength test and uniaxial compressive strength test) and further studies can be done focusing on other types of tests, previously listed.

Finally, a significant future development would be the study of the influence of dam concrete structural properties on the strain and stress fields of a dam since construction, considering the different types of concrete, the casting schedule, the curing process (temperature and moisture variations), the effect of curing on the development of the main structural properties. The accurate prediction of creep strains and tensile strength over time for *in situ* conditions is key for determining the cracking risk during construction but also for lifetime predictions and assessment of deterioration scenarios.

7.3 List of publications during the development of the Ph.D. thesis

7.3.1 Technical papers in international journals (with peer review)

- **Serra, C.;** Monteiro Azevedo, N.; Batista, A. L.; Schclar, N. – Discrete element method for modelling the long-term aging viscoelastic behaviour of concrete considering its mesostructure. *Journal of Engineering Mechanics*, 2017 (accepted for publication);
- **Serra, C.;** Batista, A. L.; Monteiro Azevedo, N.; Custódio, J. – Prediction of Dam Concrete Compressive and Splitting Tensile Strength on Wet-Screened Concrete Test Results. *Journal of Materials in Civil Engineering*, v. 29, n. 10, 2017 (DOI: 10.1061/(ASCE)MT.1943-5533.0002012);
- **Serra, C.;** Batista, A. L.; Monteiro Azevedo, N. - Effect of Wet Screening in the Elastic Properties of Dam Concrete: Experimental In Situ Test Results and Fit to Composite Models. *Journal of Materials in Civil Engineering*, v. 28, n. 12, 2016 (DOI: 10.1061/(ASCE)MT.1943-5533.0001672);
- **Serra, C.;** Batista, A. L.; Monteiro Azevedo, N. - Dam and wet-screened concrete creep in compression: in situ experimental results and creep strains prediction using model B3 and composite models. *Materials and Structures*, v. 49, n. 11, pp 4831–4851, 2016 (DOI: 10.1617/s11527-016-0828-2);

7.3.2 Technical papers in national journals

- **Serra, C.;** Batista, A. L.; Monteiro Azevedo, N. - Análise integrada dos resultados dos ensaios de deformabilidade do betão de grandes barragens portuguesas. *Revista Portuguesa de Engenharia de Estruturas*, n. 15, p. 27-38, 2015.

7.3.3 International proceedings papers

- **Serra, C.;** Batista, A. L.; Monteiro Azevedo, N. - Comprehensive analysis of the concrete deformability test results of Portuguese large dams. *Second International Conference Dam World*, 2015. Lisboa;
- **Serra, C.,** Monteiro Azevedo, N., Batista, A. L. - Viscoelastic concrete behaviour analysis using rigid particle detailed modelling. *Congresso de Métodos Numéricos*

em Engenharia, 2015. Lisboa. Congresso de Métodos Numéricos em Engenharia. 2015;

- Mata, J., Martins, L.; Ribeiro, A., Tavares de Castro, A., **Serra, C.** -. Contributions of applied metrology for concrete dam monitoring. HYDROPOWER'15, 2015. Stavanger. Hydropower'15. 2015;

7.3.4 National proceedings papers

- **Serra, C.**, Monteiro Azevedo, N., Batista, A. L. - Representação do comportamento viscoelástico com endurecimento com modelos detalhados de partículas: calibração dos parâmetros das leis constitutivas, Encontro Nacional Betão Estrutural - BE2016, Coimbra, 2016;
- **Serra, C.**; Batista, A. L., Monteiro Azevedo, N. - Utilização de modelos compósitos na determinação da deformabilidade do betão de barragens, Encontro Nacional Betão Estrutural - BE2016, Coimbra, 2016;
- **Serra, C.**; Batista, A. L., Monteiro Azevedo, N. - Melhoramentos recentes no projeto e instalação de células de fluência em barragens de betão, 10^o Congresso Nacional de Mecânica Experimental, pp. 205 -206, Lisboa, 2016;
- **Serra, C.**, Batista, A. L. - Experiência de utilização de uma prensa na verificação do funcionamento de dispositivos de resistência elétrica tipo carlson para a monitorização de barragens de betão, 10 Congresso Nacional de Mecânica Experimental, pp. 207 -208, Lisboa, 2016;
- Pereira, R., Batista, A. L., **Serra, C.** - Análise e interpretação do comportamento observado da barragem de Rebordelo durante o primeiro enchimento da albufeira e primeiro período de exploração, 5^{as} Jornadas Portuguesas de Engenharia de Estruturas 2014, Lisboa, 2014;
- **Serra, C.**; Batista, A. L., Monteiro Azevedo, N. - Estudos de avaliação da deformabilidade do betão da barragem de montante do Baixo Sabor, 5^{as} Jornadas de Engenharia de Estruturas 2014, Lisboa, 2014;
- **Serra, C.**; Batista, A. L., Monteiro Azevedo, N. - Análise integrada dos resultados dos ensaios de deformabilidade do betão de grandes barragens portuguesas, 5^{as} Jornadas de Engenharia de Estruturas 2014, Lisboa, 2014.

7.3.5 Technical reports

- LNEC - Analysis of the concrete test results obtained during the Baixo Sabor dam construction, Relatório 236/2017 – DBB/NO, Laboratório Nacional de Engenharia Civil, Lisboa, 2017.
- LNEC - Code implementation of particle based discrete element method for concrete viscoelastic modelling, Laboratório Nacional de Engenharia Civil, Relatório 333/2015 – DBB/NO, Laboratório Nacional de Engenharia Civil, Lisboa, 2015;
- LNEC - Barragem de Rebordelo - Análise e interpretação do comportamento observado durante o primeiro enchimento da albufeira e primeiro período de exploração, Relatório 477/2014 – DBB/NO, Laboratório Nacional de Engenharia Civil, Lisboa, Lisboa, 2014;
- LNEC - Barragem de montante do aproveitamento hidroelétrico do Baixo Sabor - Instalação de células de fluência e ensaios nas primeiras idades, Relatório 311/2014 – DBB/NO, Laboratório Nacional de Engenharia Civil, Lisboa, Lisboa, 2014;
- LNEC - Procedimentos e recomendações para a realização de ensaios de deformabilidade em betão de barragens, efectuados in situ e em laboratório, Relatório 455/2013 – DBB/NO, Laboratório Nacional de Engenharia Civil, Lisboa, 2013;
- LNEC - Caracterização experimental e modelação numérica das propriedades reológicas do betão de barragens. Plano de tese de doutoramento do Bolseiro de Iniciação à Investigação Científica Carlos Serra, Relatório 284/2013 – DBB/NO/Chefia/NMMR, Laboratório Nacional de Engenharia Civil, Lisboa, 2013.

Bibliography

- Abd elaty, M. abd allah (2014). “Compressive strength prediction of Portland cement concrete with age using a new model.” In: *HBRC Journal* 10.2, pp. 145–155. ISSN: 16874048. DOI: 10.1016/j.hbrcj.2013.09.005.
- Abdellatef, M., M. Alnaggar, G. Boumakis, G. Cusatis, G. Di-Luzio, and R. Wendner (2015). “Lattice Discrete Particle Modeling for Coupled Concrete Creep and Shrinkage Using the Solidification Microprestess Theory.” In: *CONCREEP 10*. Reston, VA: American Society of Civil Engineers, pp. 184–193. ISBN: 978-0-7844-7934-6. DOI: 10.1061/9780784479346.022.
- Abrams, D. (1918). *Design of concrete mixtures*. Chicago: Lewis Institute, p. 20.
- ACI Committee 207 (1997). *ACI 207.1R-96: Mass concrete*. Tech. rep. Detroit: American Concrete Institute, p. 30.
- ACI Committee 207 (2005). *ACI 207.1R-05: Guide to mass concrete*. Detroit: American Concrete Institute.
- ACI Committee 209 (1992). *ACI 209R-92: Prediction of Creep, Shrinkage, and Temperature Effects in Concrete Structures (Reapproved 2008)*. Tech. rep. Detroit: American Concrete Institute, p. 47.
- ACI Committee 211.1-91 (2002). *ACI 211.1-91: Standard practice for selecting proportions for normal, heavyweight and mass concrete (Reapproved 2002)*. Tech. rep. American Concrete Institute, p. 37.
- ACI Committee 221 (2001). *ACI 221.R-96: Guide for Use of Normal Weight and Heavy-weight Aggregates in Concrete*. Detroit: American Concrete Institute, p. 29.
- ACI Committee 318 (1995). *Building code requirements for reinforced concrete (ACI 318-95) and comentary (ACI318R-95)*. Tech. rep. Detroit: American Concrete Institute, p. 369.
- ACI Committee 363 (1992). *State-of-the-art report on high-strength concrete*. Tech. rep. Detroit: American Concrete Institute, p. 55.

BIBLIOGRAPHY

- Acker, P (2001). “Creep and shrinkage of concrete: physical origins and practical measurements.” In: *Nuclear Engineering and Design* 203.2-3, pp. 143–158. ISSN: 00295493. DOI: 10.1016/S0029-5493(00)00304-6.
- Akçaoğlu, T., M. Tokyay, and T. Çelik (2004). “Effect of coarse aggregate size and matrix quality on ITZ and failure behavior of concrete under uniaxial compression.” In: *Cement and Concrete Composites* 26.6, pp. 633–638. ISSN: 09589465. DOI: 10.1016/S0958-9465(03)00092-1.
- Alexander, M. and S. Mindess (2010). *Aggregates in Concrete*. Taylor & Francis, p. 435. ISBN: ISBN0-415-25839-1.
- Alnaggar, M., G. Cusatis, and G. D. Luzzo (2013). “Lattice Discrete Particle Modeling (LDPM) of Alkali Silica Reaction (ASR) deterioration of concrete structures.” In: *Cement and Concrete Composites* 41.August, pp. 45–59. ISSN: 09589465. DOI: 10.1016/j.cemconcomp.2013.04.015.
- Antoniou, A., L. Daudeville, P. Marin, and S. Potapov (2017). “Discrete element modelling of concrete structures under hard impact.” In: *V International Conference on Particle-based Methods - Fundamentals and Applications*. Ed. by P. Wriggers, M. Bischoff, E. Oñate, D. Owen, and T. Zohdi. Hannover, Germany, pp. 261–272.
- Arıoğlu, N., Z. C. Girgin, and E. Arıoğlu (2006). “Evaluation of Ratio between Splitting Tensile Strength and Compressive Strength for Concretes up to 120 MPa and its Application in Strength Criterion.” English. In: *Materials Journal* 103.1, pp. 18–24. ISSN: 0889-325X.
- ASTM (2006). *Significance of tests and properties of concrete & Concrete-making materials*. Ed. by J. F. Lamond and J. H. Pielert. Bridgeport, NJ: ASTM International, p. 219.
- ASTM (2009). *ASTM C150 / C150M - 09 Standard Specification for Portland Cement*. West Conshohocken, PA.
- ASTM (2012). *ASTM C618-12a Standard Specification for coal fly ash and raw or calcined natural pozzolan for use in concrete*. West Conshohocken, PA.
- ASTM (2014). *ASTM C1778-14 Standard guide for reducing the risk of deleterious alkali-aggregate reaction in concrete*. West Conshohocken, PA.
- ASTM (2017). *ASTM C150 / C150M-17, Standard Specification for Portland Cement*. West Conshohocken, PA.
- Atkins, P. and J. de Paula (2006). *Physical Chemistry*. 8th Editio. Oxford University Press, p. 1053.

- Autodesk (2016). *AutoCAD*.
- Ayachit, U. (2005). *The ParaView Guide: A Parallel Visualization Application*.
- Ayachit, U. (2015). *The ParaView Guide: A Parallel Visualization Application*.
- Aydin, A. C., A. Arslan, and R. Gül (2007). “Mesoscale simulation of cement based materials’ time-dependent behavior.” In: *Computational Materials Science* 41.1, pp. 20–26. ISSN: 09270256. DOI: 10.1016/j.commatsci.2007.02.012.
- Azenha, M., R. Faria, and D. Ferreira (2009). “Identification of early-age concrete temperatures and strains: Monitoring and numerical simulation.” In: *Cement and Concrete Composites* 31.6, pp. 369–378. ISSN: 09589465. DOI: 10.1016/j.cemconcomp.2009.03.004.
- Azenha, M., L. Leitão, J. L. Granja, C. de Sousa, R. Faria, and J. A. Barros (2017). “Experimental validation of a framework for hygro-mechanical simulation of self-induced stresses in concrete.” In: *Cement and Concrete Composites* 80, pp. 41–54. ISSN: 09589465. DOI: 10.1016/j.cemconcomp.2017.02.008.
- Bamforth, P. B. (1980). “In situ measurement of the effect of partial Portland cement replacement using either fly ash or ground granulated blast-furnace slag on the performance of mass concrete.” In: *Proc. Instn Civ. Engrs* 69, pp. 777–800.
- Bartojay, K. and W. Joy (2010). “Long-Term Properties of Hoover Dam Mass Concrete.” In: ed. by R. L. Wiltshire, D. R. Gilbert, and J. R. Rogers. Vol. 390. 41141. Las Vegas, NV: ASCE, p. 6.
- Batista, A. L. (1998). “Análise do comportamento ao longo do tempo de barragens de abóbada.” Ph. D. Universidade Técnica de Lisboa, Instituto Superior Técnico, p. 240.
- Baweja, S., G. J. Dvorak, and Z. P. Bažant (1998). “Triaxial Composite Model for Basic Creep of Concrete.” In: *Journal of Engineering Mechanics* 124.9, pp. 959–965. ISSN: 0733-9399. DOI: 10.1061/(ASCE)0733-9399(1998)124:9(959).
- Bažant, Z. P. (1972). “Numerical determination of long-range stress history from strain history in concrete.” In: *Matériaux et Constructions* 5.27, pp. 135–141.
- Bažant, Z. P. (1975). “Theory of creep and shrinkage in concrete structures: a précis of recent development.” In: *Mechanics Today*. Pergamon Press. Chap. Vol.2, pp. 1–93.
- Bažant, Z. P. (1977). “Viscoelasticity of solidifying porous material - Concrete.” eng. In: *Journal of the Engineering Mechanics Division* 103.6, pp. 1049–1067. ISSN: 0044-7951.
- Bažant, Z. P. (1984). “Size effect in blunt fracture: Concrete, rock , metal.” In: *Journal of Engineering Mechanics* 110.4, pp. 518–535.

- Bažant, Z. P. (1988). “Material models for structural creep analysis.” In: *Mathematical Modeling of Creep and Shrinkage of Concrete*. Ed. by Z. P. Bažant. Evanston: Wiley & Sons. Chap. 2, pp. 99–215.
- Bažant, Z. P. (1994). “Recent advances in fracture mechanics, size effect and rate dependence of concrete: Implication for dams.” In: *International Workshop on Dam Fracture and Damage*. Ed. by E. Bourdarot, J. Mazars, and V. Saouma. Chambéry, France: A. A. Balkema, Rotterdam, pp. 41–54.
- Bažant, Z. P. (2000). “Criteria for rational prediction of creep and shrinkage of concrete.” In: *Adam Neville Symposium: Creep and Shrinkage - Structural Design Effects*. Ed. by A. Al-Manaseers. Vol. 3. Farmington Hills: Am. Concrete Institute, pp. 237–260.
- Bažant, Z. P. (2002). *Scaling of structural strength*. First edit. London: Hermes-Penton Science, p. 280.
- Bažant, Z. P. and S. Baweja (1995a). “Creep and shrinkage prediction model for analysis and design of concrete structures - model B3.” In: *Materials and Structures* 28.6, pp. 357–365.
- Bažant, Z. P. and S. Baweja (1995b). “Justification and refinements of model B3 for concrete creep and shrinkage 2. Updating and theoretical basis.” In: *Materials and Structures* 28.8, pp. 488–495. ISSN: 0025-5432. DOI: 10.1007/BF02473171.
- Bažant, Z. P. and S. Baweja (2000). “Creep and shrinkage prediction model for analysis and design of concrete structures - model B3.” In: *Adam Neville Symposium: Creep and Shrinkage - Structural Design Effects*. Ed. by A. Al-Manaseer. Vol. 28. 6. Michigan: American Concrete Institute, Michigan, pp. 1–83. DOI: 10.1007/BF02473152.
- Bažant, Z. P. and J. Kim (1991). “Improved prediction model for time-dependent deformations of concrete: Part 2—Basic creep.” In: *Materials and Structures* 24.6, pp. 409–421. ISSN: 0025-5432. DOI: 10.1007/BF02472014.
- Bažant, Z. P. and J. Kim (1992). “Improved prediction model for time-dependent deformations of concrete: Part 4—Temperature effects.” In: *Materials and Structures* 25.2, pp. 84–94. ISSN: 0025-5432. DOI: 10.1007/BF02472461.
- Bažant, Z. P. and G. Li (2008). *Comprehensive database on concrete creep and shrinkage*. Tech. rep. 08. Evanston: Infrastructure Technology Institute, McCormick School of Engineering and Applied Science, Northwestern University, p. 10.
- Bažant, Z. P. and E. Osman (1976). “Double power law for basic creep of concrete.” In: *Materials and Structures (RILEM, Paris)* 9.49, pp. 3–11.

- Bažant, Z. P. and S. Prasannan (1989a). “Solidification theory for concrete creep. I: Formulation.” en. In: *Journal of Engineering Mechanics* 115.8, pp. 1691–1703. ISSN: 0733-9399. DOI: 10.1061/(ASCE)0733-9399(1989)115:8(1691).
- Bažant, Z. P. and S. Prasannan (1989b). “Solidification theory for concrete creep. II: Verification and application.” en. In: *Journal of Engineering Mechanics* 115.8, pp. 1704–1725. ISSN: 0733-9399. DOI: 10.1061/(ASCE)0733-9399(1989)115:8(1704).
- Bažant, Z. P. and Y. Xi (1995). “Continuous retardation spectrum for solidification theory of concrete creep.” In: *Journal of Engineering Mechanics* 121.2, pp. 281–288.
- Bažant, Z. P., S.-S. Kim, and F. ASCE (1979). “Approximate relaxation function for concrete.” In: *Journal of Structural Division* 105, pp. 2695–2705.
- Bažant, Z. P., Y. Xiang, and P. C. Prat (1996). “Microplane model for concrete. I: Stress-strain boundaries and finite strain.” In: *Journal of Engineering Mechanics* 122.245-254.
- Bažant, Z. P., G. Cusatis, and L. Cedolin (2004). “Temperature Effect on Concrete Creep Modeled by Microprestress-Solidification Theory.” en. In: *Journal of Engineering Mechanics* 130.6, p. 691. ISSN: 07339399. DOI: 10.1061/(ASCE)0733-9399(2004)130:6(691).
- Bažant, Z. P., Q. Yu, and G. Li (2009). *Excessive Long-Time Deflections of Prestressed Box Girders*. Tech. rep. Evanston: Northwestern University.
- Bažant, Z. P., Q. Yu, M. Hubler, V. Kristek, and Z. Bittnar (2011). “Wake-up call for creep, mith about size effect and black holes in safety: what to improve in fib model code draft.” In: *fib Symposium Prague 2011*. Praga: Czech Concrete Society, Prague, Czech Republic, pp. 731–746. ISBN: 9788087158296.
- Bažant, Z. P., M. R. Tabbara, M. T. Kazemi, and G. Pijaudier-Cabot (1990). “Random Particle Model for Fracture of Aggregate or Fiber Composites.” en. In: *Journal of Engineering Mechanics* 116.8, pp. 1686–1705. ISSN: 0733-9399. DOI: 10.1061/(ASCE)0733-9399(1990)116:8(1686).
- Bažant, Z. P., M. H. Hubler, and M. Jirásek (2013). “Improved Estimation of Long-Term Relaxation Function from Compliance Function of Aging Concrete.” EN. In: *Journal of Engineering Mechanics* 139.2, pp. 146–152. ISSN: 0733-9399. DOI: 10.1061/(ASCE)EM.1943-7889.0000339.
- Belytschko, T. and T. J. R. Hughes (1983). “Computational methods for transient analysis.” In: *Mechanics and Mathematical Methods*. Ed. by T. Belytschko and T. J. R. Hughes. North Holland, p. 536. ISBN: 0444864792.

- Benboudjema, F., E. Guillon, and J.-M. Torrenti (2004). “Effect of interfacial transition zone and aggregates on the time-dependent behaviour of mortar and concrete.” In: *Fifth International Conference on Fracture Mechanics of Concrete and Concrete Structures—FraMCoS-5*. Vail (USA).
- Bentur, A. (2002). “Cementitious Materials—Nine Millennia and A New Century: Past, Present, and Future.” en. In: *Journal of Materials in Civil Engineering* 14.1, p. 2. ISSN: 08991561. DOI: 10.1061/(ASCE)0899-1561(2002)14:1(2).
- Bentz, D., J. Garboczi, and P. Stutzman (1993). “Computer Modelling of the Interfacial Transition Zone in Concrete.” In: *Interfaces in Cementitious Composites*. Ed. by J. C. Maso. F.N. Spon, London, pp. 259–268.
- Benveniste, Y. (1987). “A new approach to the application of Mori-Tanaka’s theory in composite materials.” In: *Mechanics of Materials* 6.2, pp. 147–157. ISSN: 01676636. DOI: 10.1016/0167-6636(87)90005-6.
- Beygi, M. H., M. T. Kazemi, J. Vaseghi Amiri, I. M. Nikbin, S. Rabbanifar, and E. Rahmani (2014). “Evaluation of the effect of maximum aggregate size on fracture behavior of self compacting concrete.” In: *Construction and Building Materials* 55, pp. 202–211. ISSN: 09500618. DOI: 10.1016/j.conbuildmat.2014.01.065.
- Blanks, R. F. and C. C. McNamara (1935). “Mass Concrete Tests In Large Cylinders.” English. In: *Journal Proceedings* 31.1, pp. 280–303. ISSN: 0002-8061.
- Bolander, J. and S. Saito (1998). “Fracture analyses using spring networks with random geometry.” In: *Engineering Fracture Mechanics* 61.5-6, pp. 569–591. ISSN: 00137944. DOI: 10.1016/S0013-7944(98)00069-1.
- Bolomey, J. (1936). “Granulation et prévision de la résistance probable des béton.” In: *Bulletin technique de la Suisse romande* 7, pp. 73–78.
- Briffaut, M., F. Benboudjema, C. Laborderie, and J. M. Torrenti (2013). “Consequences of Internal Stresses Generated by Hydration on the Concrete Mechanical Behaviour.” In: *FraMCoS-8 - VIII International Conference on Fracture of Concrete and Concrete Structures*. Ed. by J. van Mier, G. Ruiz, C. Andrade, R. C. Yu, and X. X. Zhang. Toledo, p. 12.
- Briffaut, M., F. Benboudjema, J.-M. Torrenti, and G. Nahas (2012). “Concrete early age basic creep: Experiments and test of rheological modelling approaches.” In: *Construction and Building Materials* 36, pp. 373–380. ISSN: 09500618. DOI: 10.1016/j.conbuildmat.2012.04.101.

- Brooks, A. G., A. K. Schindler, and R. W. Barnes (2007). “Maturity method evaluated for various cementitious materials.” en. In: *Journal of Materials in Civil Engineering* 19.12, pp. 1017–1025. ISSN: 0899-1561. DOI: 10.1061/(ASCE)0899-1561(2007)19:12(1017).
- Browne, R. D. and R. Blundell (1969). “The influence of loading age and temperature on the long term creep behaviour of concrete in a sealed, moisture stable, state.” In: *Matériaux et Constructions* 2.2, pp. 133–143. ISSN: 0025-5432. DOI: 10.1007/BF02475101.
- Burlion, N., F. Bourgeois, and J.-F. Shao (2005). “Effects of desiccation on mechanical behaviour of concrete.” In: *Cement and Concrete Composites* 27.3, pp. 367–379. ISSN: 0958-9465. DOI: 10.1016/J.CEMCONCOMP.2004.05.004.
- Carino, N. J. and H. S. Lew (2001). “The maturity method: from theory to application.” In: *2001 Structures Congress & Exposition*. Ed. by P. Chang. Washington D. C.: American Society of Civil Engineers, p. 19.
- Carino, N. J. and R. C. Tank (1992). “Maturity function for concretes made with various cements and admixtures.” In: *Materials Journal* 89.2, pp. 188–196.
- Carino, N. J. and H. S. Lew (1982). “Re-examination of the Relation Between Splitting Tensile and Compressive Strength of Normal Weight Concrete.” English. In: *Journal Proceedings* 79.3, pp. 214–219. ISSN: 0002-8061.
- Carol, I., C. M. López, and O. Roa (2001). “Micromechanical analysis of quasi-brittle materials using fracture-based interface elements.” In: *International Journal for Numerical Methods in Engineering* 52.12, pp. 193–215. ISSN: 00295981. DOI: 10.1002/nme.277.
- CEB-FIP (1990). *Model Code 1990*. Lausanne.
- CEN (2005). *Concrete — Part 1: Specification, performance, production and conformity (EN 206-1)*. Brussels.
- CEN (2012). *NP EN 197-1:2012 - Cement. Part 1: Composition, specifications and conformity criteria for common cements*.
- Cervera, M. and M. Chiumenti (2006). “Smearred crack approach: back to the original track.” In: *International Journal for Numerical and Analytical Methods in Geomechanics* 30.12, pp. 1173–1199. ISSN: 0363-9061. DOI: 10.1002/nag.518.
- Cervera, M., J. Oliver, and T. Prato (1999). “Thermo-chemo-mechanical model for concrete. I: Hydration and aging.” en. In: *Journal of Engineering Mechanics* 125.9, pp. 1018–1027. ISSN: 07339399. DOI: 10.1061/(ASCE)0733-9399(1999)125:9(1018).

- Cervera, M., J. Oliver, and T. Prato (2000a). “Simulation of construction of RCC dams. I: Temperature and aging.” en. In: *Journal of Structural Engineering* 126.9, pp. 1053–1061. ISSN: 0733-9445. DOI: 10.1061/(ASCE)0733-9445(2000)126:9(1053).
- Cervera, M., J. Oliver, and T. Prato (2000b). “Simulation of construction of RCC dams. II: Stress and damage.” en. In: *Journal of Structural Engineering* 126.9, pp. 1062–1069. ISSN: 0733-9445. DOI: 10.1061/(ASCE)0733-9445(2000)126:9(1062).
- Charlwood, R. (2009). “Predicting the long term behaviour and service life of concrete dams.” In: *2nd International Conference Long term behavior of dams*. Ed. by E. Bauer, S. Semprich, and G. Zenz. Graz: Verl. der Techn. Univ. Graz, pp. 39–49.
- Cho, N., C. Martin, and D. Segol (2007). “A clumped particle model for rock.” In: *International Journal of Rock Mechanics and Mining Sciences* 44.7, pp. 997–1010. ISSN: 13651609. DOI: 10.1016/j.ijrmms.2007.02.002.
- Clough, R. W. and J. Penzien (1993). *Dynamics of structures*. Ed. by B. J. Clack. 2nd ed. McGraw-Hill International Editions, p. 738. ISBN: 0070113920.
- Çolak, A. (2006). “A new model for the estimation of compressive strength of Portland cement concrete.” In: *Cement and Concrete Research* 36.7, pp. 1409–1413. ISSN: 00088846. DOI: 10.1016/j.cemconres.2006.03.002.
- Cordon, W. A. and H. A. Gillespie (1963). “Variables in Concrete Aggregates and Portland Cement Paste which Influence the Strength of Concrete.” English. In: *Journal Proceedings* 60.8, pp. 1029–1052. ISSN: 0002-8061.
- Costa, D. Dias-da, J. Alfaiate, L. J. Sluys, and E. Júlio (2010). “A comparative study on the modelling of discontinuous fracture by means of enriched nodal and element techniques and interface elements.” In: *Int J Fract* 161, pp. 97–119. DOI: 10.1007/s10704-009-9432-6.
- Counto, U. J. (1964). “The effect of the elastic modulus of the aggregate on the elastic modulus, creep and creep recovery of concrete.” en. In: *Magazine of Concrete Research* 16.48, pp. 129–138. ISSN: 0024-9831. DOI: 10.1680/macr.1964.16.48.129.
- Coutinho, A. (1977). “A contribution to the mechanism of concrete creep.” In: *Matériaux et Constructions* 10.1, pp. 3–16. ISSN: 0025-5432. DOI: 10.1007/BF02473583.
- Coutinho, A. (1988). *Fabrico e propriedades do betão. Volume II*. 2nd. Lisboa: Laboratório Nacional de Engenharia Civil, p. 219.
- Coutinho, A. and A. Gonçalves (1994). *Fabrico e propriedades do betão. Volume III*. 2nd. Lisboa: Laboratório Nacional de Engenharia Civil, p. 368.

- Cundall, P. A. (1971). “A computer model for simulating progressive large scale movements in blocky rock systems.” In: *Proceedings of the international symposium on rock fracture*. Ed. by International Society for Rock Mechanics. Nancy, pp. 129–136.
- Cundall, P. A. (1987). “Distinct element models of rock and soil structure.” In: *Analytical and computational methods in engineering rock mechanics*. Ed. by E. T. Brown. London: Allen & Unwin. Chap. 4, pp. 129–163.
- Cundall, P. A. and O. D. L. Strack (1979). “A discrete numerical model for granular assemblies.” en. In: *Géotechnique* 29.1, pp. 47–65. ISSN: 0016-8505. DOI: 10.1680/geot.1979.29.1.47.
- Cusatis, G., Z. P. Bazant, and L. Cedolin (2001). “3D Lattice Model for Dynamic Simulations of Creep, Fracturing and Rate Effect in Concrete.” In: *CONCREEP- 6 - Creep, Shrinkage and Durability Mechanics of Concrete and Other Quasi-Brittle Materials*. Ed. by F.-J. Ulm, Z. P. Bazant, and F. H. Wittmann. Elsevier, pp. 113–118.
- Cusatis, G. (2001). “Tridimensional random particle model for concrete.” Ph.D. Politecnico di Milano, Milano, p. 130.
- Deng, Z., Q. Li, and H. Fu (2008). “Comparison between Mechanical Properties of Dam and Sieved Concretes.” In: *Journal of Materials in Civil Engineering* 20.4, pp. 321–326. ISSN: 0899-1561. DOI: 10.1061/(ASCE)0899-1561(2008)20:4(321).
- Dias, I. F., J. Oliver, and A. E. Huespe (2017). *Strain Injection Techniques in Numerical Modeling of Propagating Material Failure*.
- DIN (1991). *Testing concrete: testing of hardened concrete (specimens prepared in mould). Part 5. Volume 1048*. Berlin.
- Dolado, J. and K. van Breugel (2011). “Recent advances in modeling for cementitious materials.” In: *Cement and Concrete Research* 41.7, pp. 711–726. ISSN: 00088846. DOI: 10.1016/j.cemconres.2011.03.014.
- Dolen, T. P. (2010). “Advances in Mass Concrete Technology - The Hoover Dam Studies.” In: ed. by R. L. Wiltshire, D. R. Gilbert, and J. R. Rogers. Vol. 390. 41141. Las Vegas, NV: ASCE, p. 5.
- Donzé, F. and S.-A. Magnier (1995). “Formulation of a 3-D numerical model of brittle behaviour.” In: *Geophysical Journal International* 122.3, pp. 790–802. ISSN: 0956540X. DOI: 10.1111/j.1365-246X.1995.tb06838.x.
- Dunant, C. F. and K. L. Scrivener (2010). “Micro-mechanical modelling of alkali-silica-reaction-induced degradation using the AMIE framework.” In: *Cement and Concrete*

BIBLIOGRAPHY

- Research* 40.4, pp. 517–525. ISSN: 00088846. DOI: 10.1016/j.cemconres.2009.07.024.
- Eddy, L., A. Awasthi, K. Matsumoto, K. Nagai, and S. Asamoto (2017). “Mesoscopic analysis of different expansion causes in concrete by 3D Rigid Body Spring Model.” In: *Seisan Kenkyu* 69.4, pp. 181–185. ISSN: 0037-105X. DOI: 10.11188/SEISANKENKYU.69.181.
- EDP (2005). *Aproveitamento Hidroelétrico do Baixo Sabor. Projecto. Memória Geral e Apêndices*. Porto.
- Elices, M and C Rocco (2008). “Effect of aggregate size on the fracture and mechanical properties of a simple concrete.” In: *Engineering Fracture Mechanics* 75.13, pp. 3839–3851. ISSN: 00137944. DOI: 10.1016/j.engfracmech.2008.02.011.
- Elsharief, A., M. D. Cohen, and J. Olek (2003). “Influence of aggregate size, water cement ratio and age on the microstructure of the interfacial transition zone.” In: *Cement and Concrete Research* 33.11, pp. 1837–1849. ISSN: 00088846. DOI: 10.1016/S0008-8846(03)00205-9.
- Esposito, R., C. Anaç, M. A. N. Hendriks, and O. Çopuroğlu (2016). “Influence of the Alkali-Silica Reaction on the Mechanical Degradation of Concrete.” In: *Journal of Materials in Civil Engineering* 28.6, p. 04016007. ISSN: 0899-1561. DOI: 10.1061/(ASCE)MT.1943-5533.0001486.
- Feng, J., Z. Chuhan, W. Gang, and W. Guanglun (2003). “Creep Modeling in Excavation Analysis of a High Rock Slope.” eng. In: *Journal of Geotechnical and Geoenvironmental Engineering* 129.9, pp. 849–857. ISSN: 1090-0241@e1943-5606.
- Fib (2010). *Model Code 2010*. Lausanne.
- Flatt, R. J., N. Roussel, and C. R. Cheeseman (2012). “Concrete: An eco material that needs to be improved.” In: *Journal of European Ceramic Society*, p. 12.
- Ganesh Babu, K. and G. Siva Nageswara Rao (1996). “Efficiency of fly ash in concrete with age.” In: *Cement and Concrete Research* 26.3, pp. 465–474. ISSN: 00088846. DOI: 10.1016/S0008-8846(96)85034-4.
- Gardner, N. J. and M. J. Lockman (2001). “Design Provisions for Drying Shrinkage and Creep of Normal-Strength Concrete.” In: *Materials Journal* 98.2, pp. 159–167.
- Ghaemmaghani, A. and M. Ghaemian (2006). “Large-scale testing on specific fracture energy determination of dam concrete.” In: *International Journal of Fracture* 141.1-2, pp. 247–254. ISSN: 0376-9429. DOI: 10.1007/s10704-006-0078-3.

- Ghebrab, T. T. and P. Soroushian (2011). “Development of Structure-Property Relationships for Concrete.” In: *Journal of Advanced Concrete Technology* 9.1, pp. 5–14. ISSN: 1346-8014. DOI: 10.3151/jact.9.5.
- Ghosh, R. S. and J. Timusk (1981). “Creep of fly ash concrete.” In: *ACI Journal* 78.5, pp. 351–357.
- Gilkey, H. J. (1961). “Water-Cement Ratio Versus Strength-Another Look.” English. In: *Journal Proceedings* 57.4, pp. 1287–1312. ISSN: 0002-8061.
- Giorla, A. B., K. L. Scrivener, and C. F. Dunant (2015). “Influence of visco-elasticity on the stress development induced by alkali–silica reaction.” In: *Cement and Concrete Research* 70.April, pp. 1–8. ISSN: 00088846. DOI: 10.1016/j.cemconres.2014.09.006.
- Gopalakrishnan, K. S., A. M. Neville, and A. Ghali (1969). “Creep Poisson’s Ratio of Concrete Under Multiaxial Compression.” In: *ACI Journal Proceedings* 66.12, pp. 1008–1019. ISSN: 0002-8061. DOI: 10.14359/7451.
- Granger, L. and Z. P. Bažant (1995). “Effect of composition on basic creep of concrete and cement paste.” en. In: *Journal of Engineering Mechanics* 121.11, pp. 1261–1270. ISSN: 07339399. DOI: 10.1061/(ASCE)0733-9399(1995)121:11(1261).
- Granja, J. and M. Azenha (2017). “Towards a robust and versatile method for monitoring E-modulus of concrete since casting: Enhancements and extensions of EMM-ARM.” In: *Strain* 53.4, e12232. ISSN: 00392103. DOI: 10.1111/str.12232.
- Grassl, P. and M. Jirásek (2010). “Meso-scale approach to modelling the fracture process zone of concrete subjected to uniaxial tension.” In: *International Journal of Solids and Structures* 47.7-8, pp. 957–968. ISSN: 00207683. DOI: 10.1016/j.ijsolstr.2009.12.010.
- Grassl, P., D. Grégoire, L. Rojas Solano, and G. Pijaudier-Cabot (2012). “Meso-scale modelling of the size effect on the fracture process zone of concrete.” In: *International Journal of Solids and Structures* 49.13, pp. 1818–1827. ISSN: 00207683. DOI: 10.1016/j.ijsolstr.2012.03.023.
- Gronidin, F. and M. Matallah (2014). “How to consider the Interfacial Transition Zones in the finite element modelling of concrete?” In: *Cement and Concrete Research* 58, pp. 67–75. ISSN: 00088846. DOI: 10.1016/j.cemconres.2014.01.009.
- Guan, J., Q. Li, Z. Wu, S. Zhao, W. Dong, and S. Zhou (2016). “Fracture parameters of site-cast dam and sieved concrete.” In: *Magazine of Concrete Research* 68.1, pp. 43–54. ISSN: 0024-9831. DOI: 10.1680/macr.15.00008.

- Han, S.-H., J.-K. Kim, and Y.-D. Park (2003). "Prediction of compressive strength of fly ash concrete by new apparent activation energy function." In: *Cement and Concrete Research* 33.7, pp. 965–971.
- Hannant, D. J., K. J. Buckley, and J. Croft (1973). "The effect of aggregate size on the use of the cylinder splitting test as a measure of tensile strength." In: *Matériaux et Constructions* 6.1, pp. 15–21. ISSN: 0025-5432. DOI: 10.1007/BF02474838.
- Hansen, T. (1965). "Influence of aggregate and voids on modulus of elasticity of concrete, cement mortar, and cement paste." In: *ACI Journal* 62.2, pp. 193–216.
- Hashin, Z. (1962). "The Elastic Moduli of Heterogeneous Materials." In: *Journal of Applied Mechanics* 29.1, p. 143. ISSN: 00218936. DOI: 10.1115/1.3636446.
- Hashin, Z. (1963). "A variational approach to the theory of the elastic behaviour of multiphase materials." In: *Journal of Mechanics Physics Solids* 11, pp. 127–140. ISSN: 00225096. DOI: 10.1016/0022-5096(63)90060-7.
- Hashin, Z. and P. Monteiro (2002). "An inverse method to determine the elastic properties of the interphase between the aggregate and the cement paste." In: *Cement and Concrete Research* 32.8, pp. 1291–1300. ISSN: 00088846. DOI: 10.1016/S0008-8846(02)00792-5.
- Hassani, N. (1998). "An experimental-numerical study for the determination of concrete fracture physical parameters in DEM." In: *Fracture Mechanics of Concrete Structures*. Freiburg, Germany: AEDIFICATIO.
- Havlásek, P. and M. Jirásek (2015). "Modeling Drying Shrinkage and the Creep of Concrete at the Meso-Level." In: *CONCREEP 10*. Reston, VA: American Society of Civil Engineers, pp. 287–295. ISBN: 9780784479346. DOI: 10.1061/9780784479346.033.
- Higginson, E., G. Wallace, and E. Ore (1962). "Effect of maximum size of aggregate upon compressive strength of concrete." In: *Symposium on mass concrete*. Ed. by A. C. Institute. Denver, Colorado: U.S. Dept. of the Interior Bureau of Reclamation, p. 23.
- Hill, R. (1965). "A self-consistent mechanics of composite materials." In: *Journal of the Mechanics and Physics of Solids* 13.March 1962, pp. 213–222. ISSN: 00225096. DOI: 10.1016/0022-5096(65)90010-4.
- Hirsch, T. J. (1962). "Modulus of elasticity of concrete affected by elastic moduli of cement paste matrix and aggregate." In: *Journal Proceedings* 59.3, pp. 427–452.

- Ho, M., U. Lall, M. Allaire, N. Devineni, H. H. Kwon, I. Pal, D. Raff, and D. Wegner (2017). “The future role of dams in the United States of America.” In: *Water Resources Research* 53.2, pp. 982–998. ISSN: 00431397. DOI: 10.1002/2016WR019905.
- Honorio, T., B. Bary, and F. Benboudjema (2016). “Multiscale estimation of ageing viscoelastic properties of cement-based materials: A combined analytical and numerical approach to estimate the behaviour at early age.” In: *Cement and Concrete Research* 85, pp. 137–155. ISSN: 00088846. DOI: 10.1016/j.cemconres.2016.03.010.
- Hudson, J. (1993). “Rock testing and site characterization.” In: *Comprehensive rock engineering. Principles, practice & projects*. Ed. by J Hudson. First Edit. Oxford: Pergamon Press. Chap. Volume 3, p. 982.
- Hudson, J., S. Crouch, and C. Fairhurst (1972). “Soft, stiff and servo-controlled testing machines: a review with reference to rock failure.” In: *Engineering Geology*, pp. 155–189.
- Hwang, K., T. Noguchi, and F. Tomosawa (2004). “Prediction model of compressive strength development of fly-ash concrete.” In: *Cement and Concrete Research* 34.12, pp. 2269–2276.
- ICOLD (2008). *Bulletin 145 - The physical properties of hardened conventional concrete in dams (Preprint)*.
- ICOLD (2009). *Bulletin 136 - The specification and quality control of concrete for dams*. Tech. rep. Paris: ICOLD, p. 122.
- IPQ (2001). *NP EN 934-2:2001 - Adjuvantes para betão, argamassa e caldas de injeção - Parte 2: Adjuvantes para betão - Definições, requisitos, conformidade, marcação e rotulagem*. Caparica.
- IPQ (2012a). *NP EN 197-1:2012 Cimento. Parte 1: Composição, especificações e critérios de conformidade para cimentos correntes (Cement. Composition, specifications and conformity criteria for common cements)*. Caparica.
- IPQ (2012b). *NP EN 450-1:2012 Cinzas volantes para betão. Parte 1: Definição, especificações e critérios de conformidade*. Caparica.
- IPQ (2014). *NP EN 196-2:2014 - Métodos de ensaio de cimentos. Parte 2: Análise química dos cimentos*. Caparica.
- Itasca Consulting Group Inc. (2008). *PFC2D (Particle Flow Code in 2 Dimensions)*. Minnesota.

- Jansen, R. (2012). *Advanced Dam Engineering for Design, Construction, and Rehabilitation*. Ed. by R. B. Jansen. New York: Springer US, p. 811. ISBN: 978-1-4612-8205-1.
- JCI-RILEM (2017). *JCI-RILEM International Workshop on Control of Cracking of Mass Concrete and Related Issues concerning Early Age Cracking of Concrete Structures*. Tokyo, Japan.
- Jennings, H. and J. Bullard (2011). “From electrons to infrastructure: Engineering concrete from the bottom up.” In: *Cement and Concrete Research* 44.727-735. ISSN: 00088846. DOI: 10.1016/j.cemconres.2011.03.025.
- Jennings, H. M., J. W. Bullard, J. J. Thomas, J. E. Andrade, J. J. Chen, and G. W. Scherer (2008). “Characterization and Modeling of Pores and Surfaces in Cement Paste: Correlations to Processing and Properties.” In: *Journal Of Advanced Concrete Technology* 6.1, pp. 5–29.
- Jensen, R. P., P. J. Bosscher, M. E. Plesha, and T. B. Edil (1999). “DEM simulation of granular media—structure interface: effects of surface roughness and particle shape.” In: *International Journal for Numerical and Analytical Methods in Geomechanics* 23.6, pp. 531–547. ISSN: 0363-9061. DOI: 10.1002/(SICI)1096-9853(199905)23:6<531::AID-NAG980>3.0.CO;2-V.
- Jia, J. (2010). “Several issues to be considered for long-term better behavior of concrete gravity dams.” In: *Frontiers of Architecture and Civil Engineering in China* 4.1, pp. 40–46. ISSN: 1673-7407. DOI: 10.1007/s11709-010-0006-5.
- Kaplan, M. F. (1959). “Flexural and Compressive Strength of Concrete as Affected by the Properties of Coarse Aggregates.” English. In: *Journal Proceedings* 55.5, pp. 1193–1208. ISSN: 0002-8061.
- Kar, A., I. Ray, A. Unnikrishnan, and J. F. Davalos (2013). “Composite modeling to predict shrinkage of concretes containing supplementary cementitious materials from paste volumes.” In: *Construction and Building Materials* 43.null, pp. 139–155. ISSN: 09500618. DOI: 10.1016/j.conbuildmat.2013.01.002.
- Kawai, T. (1978). “New discrete models and their application to seismic response analysis of structures.” In: *Nuclear Engineering and Design* 48.1, pp. 207–229. ISSN: 00295493. DOI: 10.1016/0029-5493(78)90217-0.
- Kazerani, T. and J. Zhao (2010). “Micromechanical parameters in bonded particle method for modelling of brittle material failure.” In: *International Journal for Numerical and*

- Analytical Methods in Geomechanics* 34.18, pp. 1877–1895. ISSN: 03639061. DOI: 10.1002/nag.884.
- Khaloo, A. R., M. R. Mohamadi Shooreh, and S. M. Askari (2009). “Size influence of specimens and maximum aggregate on dam concrete: Compressive strength.” en. In: *Journal of Materials in Civil Engineering* 21.8, pp. 349–355. ISSN: 0899-1561. DOI: 10.1061/(ASCE)0899-1561(2009)21:8(349).
- Kim, J., S. Han, and Y. Song (2002a). “Effect of temperature and aging on the mechanical properties of concrete. Part I - Experimental results.” In: *Cement and Concrete Research* 32.7, pp. 1087–1094. ISSN: 00088846. DOI: 10.1016/S0008-8846(02)00744-5.
- Kim, J., S. Hunhan, and S. Kyunpark (2002b). “Effect of temperature and aging on the mechanical properties of concrete. Part II - Prediction model.” In: *Cement and Concrete Research* 32.7, pp. 1095–1100. ISSN: 00088846. DOI: 10.1016/S0008-8846(02)00745-7.
- Kim, J.-K., S.-H. Eo, and H.-K. Park (1990). “Size Effect in Concrete Structures Without Initial Crack.” English. In: *Special Publication* 118, pp. 179–196.
- Kim, J.-K. (1990). “Size effect in concrete specimens with dissimilar initial cracks.” en. In: *Magazine of Concrete Research* 42.153, pp. 233–238. ISSN: 0024-9831. DOI: 10.1680/mac.1990.42.153.233.
- Kim, J.-K., S.-T. Yi, C.-K. Park, and S.-H. Eo (1999). “Size Effect on Compressive Strength of Plain and Spirally Reinforced Concrete Cylinders.” English. In: *Structural Journal* 96.1, pp. 88–94. ISSN: 0889-3241.
- Kozul, R. and D. Darwin (1997). *Effects of aggregate type, size, and content on concrete strength and fracture energy*. Tech. rep. Lawrence, Kansas: University of Kansas Center for Research, Inc., p. 85.
- Kumar, R., N. V. Mahure, R. Gupta, P. K. Jha, S. L. Gupta, and M. Ratnam (2015). “Establishing the correlation between compressive strength of small sized wet screened concrete cubes and full size large concrete cubes for mass concrete of dam.” In: *Engg. Sci. & Mgmt. (IJESM)* 5.2, pp. 26–31.
- Labra, C. and E. Oñate (2009). “High-density sphere packing for discrete element method simulations.” In: *Communications in Numerical Methods in Engineering* 25.7, pp. 837–849. ISSN: 10698299. DOI: 10.1002/cnm.1193.

BIBLIOGRAPHY

- Larrard, F. and R. Roy (1992). “Relation entre formulation et quelques propriétés mécaniques des bétons à hautes performances.” In: *Materials and Structures* 25.8, pp. 464–475. ISSN: 0025-5432. DOI: 10.1007/BF02472636.
- Larrard, F. de (1999). *Concrete Mixture Proportioning: A Scientific Approach*. ISBN: 0419235000.
- Larrard, F. de and A. Belloc (1997). “The Influence of Aggregate on the Compressive Strength of Normal and High-Strength Concrete.” In: *ACI Materials Journal* 94.5, pp. 417–426. ISSN: 0889-325X. DOI: 10.14359/326.
- Lavergne, F., K. Sab, J. Sanahuja, M. Bornert, and C. Toulemonde (2015). “Homogenization schemes for aging linear viscoelastic matrix-inclusion composite materials with elongated inclusions.” In: *International Journal of Solids and Structures*. ISSN: 00207683. DOI: 10.1016/j.ijsolstr.2015.10.014.
- Li, G., Y. Zhao, and S.-S. Pang (1999). “Four-phase sphere modeling of effective bulk modulus of concrete.” In: *Cement and Concrete Research* 29.6, pp. 839–845. ISSN: 00088846. DOI: 10.1016/S0008-8846(99)00040-X.
- Li, Q., Z. Deng, and H. Fu (2004). “Effect of Aggregate Type on Mechanical Behavior of Dam Concrete.” In: *ACI Materials Journal* 101.6, pp. 483–492.
- Lilliu, G and J. van Mier (2003a). “3D lattice type fracture model for concrete.” In: *Engineering Fracture Mechanics* 70.7-8, pp. 927–941. ISSN: 00137944. DOI: 10.1016/S0013-7944(02)00158-3.
- Lilliu, G and J. van Mier (2003b). “3D lattice type fracture model for concrete.” In: *Engineering Fracture Mechanics* 70.7-8, pp. 927–941. ISSN: 00137944. DOI: 10.1016/S0013-7944(02)00158-3.
- Liu, Y., Q. Dai, and Z. You (2009). “Viscoelastic model for discrete element simulation of asphalt mixtures.” In: *Journal of Engineering Mechanics* 135.4, p. 324. ISSN: 07339399. DOI: 10.1061/(ASCE)0733-9399(2009)135:4(324).
- LNEC (1968). *Efeito da temperatura sobre a fluência do betão em massa - Relatório final*. Lisboa.
- LNEC (1993a). *Especificação LNEC E 397:1993 Betões. Determinação do módulo de elasticidade em compressão*. Lisboa.
- LNEC (1993b). *Especificação LNEC E 406:1993 Cimentos. Determinação do teor de óxido de ferro. Método espectrofotométrico com a 1,10 Fenantrolina*. Lisboa: Laboratório Nacional de Engenharia Civil, I. P. (LNEC).

- LNEC (1993c). *LNEC Specification E 406: 1993 - Cement; Determination of the iron content; Spectrophotometric method with 1,10 phenanthroline*. Lisboa: Laboratório Nacional de Engenharia Civil, I. P. (LNEC).
- LNEC (1993d). *LNEC Specification E 407:1993 Cement; Determination of the soluble silica content; Molybdate Spectrophotometric method*. Lisboa: Laboratório Nacional de Engenharia Civil, I. P. (LNEC).
- LNEC (2013). *Procedimentos e recomendações para a realização de ensaios de deformabilidade do betão de barragens, in situ e em laboratório*. Lisboa.
- LNEC (2014a). *Barragem de montante do aproveitamento hidroelétrico do Baixo Sabor*. Tech. rep. Lisboa: Laboratório Nacional de Engenharia Civil, p. 64.
- LNEC (2014b). *Barragem de montante do aproveitamento hidroelétrico do Baixo Sabor. Instalação de células de fluência e ensaios nas primeiras idades*. Lisboa.
- LNEC (2017). *Analysis of the concrete test results obtained during the Baixo Sabor dam construction*. Tech. rep. Lisboa: Laboratório Nacional de Engenharia Civil, p. 101.
- LNEC (Laboratório Nacional de Engenharia Civil) (1993). *Especificação LNEC E 407:1993 Cimentos. Determinação do teor de sílica remanescente. Método Espectrofotométrico com o molibdato*. Lisboa: Laboratório Nacional de Engenharia Civil.
- López-Moreno, J. I., S. M. Vicente-Serrano, S. Beguería, J. M. García-Ruiz, M. M. Portela, and A. B. Almeida (2009). “Dam effects on droughts magnitude and duration in a transboundary basin: The Lower River Tagus, Spain and Portugal.” In: *Water Resources Research* 45.2. ISSN: 00431397. DOI: 10.1029/2008WR007198.
- Luković, M., B. Šavija, E. Schlangen, G. Ye, and K. van Breugel (2016). “A 3D Lattice Modelling Study of Drying Shrinkage Damage in Concrete Repair Systems.” In: *Materials* 9.7, p. 575. DOI: 10.3390/ma9070575.
- Lutz, M. P., P. J. Monteiro, and R. W. Zimmerman (1997). “Inhomogeneous interfacial transition zone model for the bulk modulus of mortar.” In: *Cement and Concrete Research* 27.7, pp. 1113–1122. ISSN: 00088846. DOI: 10.1016/S0008-8846(97)00086-0.
- Ma, T., Y. Zhang, D. Zhang, J. Yan, and Q. Ye (2016). “Influences by air voids on fatigue life of asphalt mixture based on discrete element method.” In: *Construction and Building Materials* 126, pp. 785–799. ISSN: 09500618. DOI: 10.1016/j.conbuildmat.2016.09.045.

- Mas Ivars, D., M. E. Pierce, C. Darcel, J. Reyes-Montes, D. O. Potyondy, R. Paul Young, and P. A. Cundall (2011). “The synthetic rock mass approach for jointed rock mass modelling.” In: *International Journal of Rock Mechanics and Mining Sciences* 48.2, pp. 219–244. ISSN: 13651609. DOI: 10.1016/j.ijrmms.2010.11.014.
- McDonald, J. (1978). “Creep of Concrete under Various Temperature, Moisture, and Loading Conditions.” English. In: *ACI Special Publication* 55, pp. 31–54. DOI: 10.14359/6608.
- Meguro, K. and M. Hakuno (1989). “Fracture analysis of concrete structures by the modified distinct element method.” In: *Structural Engineering / Earthquake Engineering* 6.2, pp. 283–294.
- Mehta, P. K. and P. Monteiro (2006). *Concrete: microstructure, properties and materials*. Third Edit. McGraw-Hill, p. 659. ISBN: 0071462899.
- Microsoft Corporation (2010a). *Microsoft Visual C++ 2010 Express*.
- Microsoft Corporation (2010b). *Visual Studio C++ 2010 Express*.
- Mier, J. van, S. Shah, M. Arnaud, J. Balayssac, A. Bascoul, S. Choi, D. Dasenbrock, G. Ferrara, C. French, M. E. Gobbi, B. L. Karihaloo, G. König, M. D. Kotsovos, J. Labuz, D. Lange-Kornbak, G. Markeset, M. N. Pavlovic, G. Simsch, K.-C. Thienel, A. Turatsinze, M. Ulmer, H. J.G. M. van Geel, M. R. A. van Vliet, and D. Zissopoulos (1997). “Strain-softening of concrete in uniaxial compression.” In: *Materials and Structures* 30.4, pp. 195–209. ISSN: 1871-6873. DOI: 10.1007/BF02486177.
- Mier, J. G. van, M. R. van Vliet, and T. K. Wang (2002). “Fracture mechanisms in particle composites: statistical aspects in lattice type analysis.” In: *Mechanics of Materials* 34.11, pp. 705–724. ISSN: 01676636. DOI: 10.1016/S0167-6636(02)00170-9.
- Mier, J. van (1998). “Failure of concrete under uniaxial compression: an overview.” In: *Fracture Mechanics of Concrete Structures. Proceedings FraMCoS-3*. Gifu (Japan): AEDIFICATIO Publishers, pp. 1169–1182.
- Mitsui, K., Z. Li, D. Lange, and S. Shah (1994). “Relationship between microstructure and mechanical properties of paste-aggregate interface.” In: *ACI Materials Journal* 91.1, pp. 30–39.
- Moës, N. and T. Belytschko (2002). “Extended finite element method for cohesive crack growth.” In: *Engineering Fracture Mechanics* 69.7, pp. 813–833. DOI: 10.1016/S0013-7944(01)00128-X.

- Monteiro Azevedo, N. (2003). “A rigid particle discrete element model for the fracture analysis of plain and reinforced concrete.” Ph.D. Heriot-Watt University, p. 301.
- Monteiro Azevedo, N. and J. V. Lemos (2011). “A 3D generalized rigid particle contact model for fracture analysis.” In: *Particles 2011 - II International Conference on Particle-based Methods*. Ed. by E. Oñate and D. Owen. Barcelona, p. 12.
- Monteiro Azevedo, N. and J. Vieira de Lemos (2006). “Aggregate shape influence on the fracture behaviour of concrete.” eng. In: *Structural Engineering and Mechanics* 24.4, pp. 411–427. ISSN: 1225-4568. DOI: 10.12989/sem.2006.24.4.411.
- Monteiro Azevedo, N., J. Vieira de Lemos, and J. R. de Almeida (2008). “Influence of aggregate deformation and contact behaviour on discrete particle modelling of fracture of concrete.” In: *Engineering Fracture Mechanics* 75.6, pp. 1569–1586. ISSN: 00137944. DOI: 10.1016/j.engfracmech.2007.06.008.
- Monteiro Azevedo, N., M. Candeias, and F. Gouveia (2015). “A Rigid Particle Model for Rock Fracture Following the Voronoi Tessellation of the Grain Structure: Formulation and Validation.” In: *Rock Mechanics and Rock Engineering* 48.2, pp. 535–557. ISSN: 0723-2632. DOI: 10.1007/s00603-014-0601-1.
- Nagai, K., Y. Sato, and T. Ueda (2004). “Mesoscopic Simulation of Failure of Mortar and Concrete by 2D RBSM.” In: *Journal of Advanced Concrete Technology* 2.3, pp. 359–374. DOI: 10.3151/jact.2.359.
- Nasser, K. W. and A. M. Neville (1967). “Creep of Old Concrete at Normal and Elevated Temperatures.” In: *ACI Journal Proceedings* 64.2, pp. 97–103. ISSN: 0002-8061. DOI: 10.14359/7546.
- Naus, D. J. and M. W. Johnston (2001). “International RILEM Workshop on Life Prediction and Aging Management of Concrete Structures.” In: *Materials and Structures* 34.8, pp. 458–466. ISSN: 1359-5997. DOI: 10.1007/BF02486493.
- Neville, A. (1983). *Properties of concrete*. Third edit. Harlow Essex: Longman Scientific & Technical.
- Neville, A., W. Dilger, and J. Brooks (1983). *Creep of plain and structural concrete*. New York: Longman Inc.
- Neville, A. M. (1959). “Role of Cement in the Creep of Mortar.” In: *ACI Journal Proceedings* 55.3, pp. 963–984. ISSN: 0002-8061. DOI: 10.14359/11405.
- Neville, A. M. and J. J. Brooks (2010). *Concrete technology*. 2nd. Harlow Essex: Pearson Education Limited, p. 442.

- Neville, A. and B. L. Meyers (1964). “Creep of Concrete: Influencing Factors and Prediction.” In: *Special Publication 9*, pp. 1–33.
- Nikbin, I., M. Beygi, M. Kazemi, J. Vaseghi Amiri, E. Rahmani, S. Rabbanifar, and M. Eslami (2014). “Effect of coarse aggregate volume on fracture behavior of self compacting concrete.” In: *Construction and Building Materials* 52, pp. 137–145. ISSN: 09500618. DOI: 10.1016/j.conbuildmat.2013.11.041.
- Nitka, M. and J. Tejchman (2015). “Modelling of concrete behaviour in uniaxial compression and tension with DEM.” In: *Granular Matter* 17.1, pp. 145–164. ISSN: 1434-5021. DOI: 10.1007/s10035-015-0546-4.
- Nitka, M. and J. Tejchman (2017). “DEM analysis of effect of interfacial transitional zones on fracture in concrete.” In: *V International Conference on Particle-based Methods - Fundamentals and Applications*. Ed. by P. Wriggers, M. Bischoff, E. Oñate, D. Owen, and T. Zohdi. Hannover, Germany, pp. 249–260.
- Nixon, P. J. and I. Sims (2016). *RILEM Recommendations for the Prevention of Damage by Alkali-Aggregate Reactions in New Concrete Structures (State-of-the-Art Report of the RILEM Technical Committee 219-ACS)*. Dordrecht.
- Noguchi, T., F. Tomosawa, K. M. Nemat, B. M. Chiaia, and A. P. Fantilli (2009). “A Practical Equation for Elastic Modulus of Concrete.” In: *ACI Structural Journal* 106.5, pp. 690–696. ISSN: 08893241.
- Noorzaei, J., K. Bayagoob, W. Thanoon, and M. Jaafar (2006). “Thermal and stress analysis of Kinta RCC dam.” In: *Engineering Structures* 28.13, pp. 1795–1802. ISSN: 01410296. DOI: 10.1016/j.engstruct.2006.03.027.
- Novais Ferreira (1952). “Discussion of Novais Ferreira after Nunes J. presentation.” In: *Simposium de betões em grandes massas*. Lisbon: Ordem dos Engenheiros, pp. 133–143.
- NP EN 206 (2005). *NP EN 206-1: Especificação, desempenho, produção e conformidade*. Tech. rep. Lisboa: Instituto Português da Qualidade, p. 84.
- Oliveira Santos, T. (2006). “Retração do betão em pontes. Observação e análise.” Ph. D. Universidade Nova de Lisboa, Faculdade de Ciências e Tecnologia, p. 285.
- Ollivier, J., J. Maso, and B. Bourdette (1995). “Interfacial transition zone in concrete.” In: *Advanced Cement Based Materials* 2.1, pp. 30–38. ISSN: 10657355. DOI: 10.1016/1065-7355(95)90037-3.

- Oluokun, F. A., E. G. Burdette, and J. H. Deatherage (1991). “Splitting Tensile Strength and Compressive Strength Relationships at Early Ages.” English. In: *Materials Journal* 88.2, pp. 115–121. ISSN: 0889-325X.
- Oñate, E., F. Zárate, J. Miquel, M. Santasusana, M. A. Celigueta, F. Arrufat, R. Gandikota, K. Valiullin, and L. Ring (2015). “A local constitutive model for the discrete element method. Application to geomaterials and concrete.” In: *Computational Particle Mechanics* 2.2, pp. 139–160. ISSN: 2196-4378. DOI: 10.1007/s40571-015-0044-9.
- Özturan, T. and C. Çeçen (1997). “Effect of coarse aggregate type on mechanical properties of concretes with different strengths.” In: *Cement and Concrete Research* 27.2, pp. 165–170. ISSN: 00088846. DOI: 10.1016/S0008-8846(97)00006-9.
- Pan, J., Y. T. Feng, F. Jin, Y. Xu, Q. Sun, C. Zhang, and D. R. J. Owen (2012). “Meso-scale particle modeling of concrete deterioration caused by alkali-aggregate reaction.” In: *International Journal for Numerical and Analytical Methods in Geomechanics*, n/a–n/a. ISSN: 03639061. DOI: 10.1002/nag.2157.
- Pan, Y., A. Prado, R. Porras, O. Hafez, and J. Bolander (2017). “Lattice Modeling of Early-Age Behavior of Structural Concrete.” In: *Materials* 10.3, p. 231. ISSN: 1996-1944. DOI: 10.3390/ma10030231.
- Petricin, N. (1996). “Aspects of Discrete Element Modelling Involving Facet-to-facet Contact Detection and Interaction.” Ph.D. University of Wales Swansea, p. 183.
- Piotrowska, E. (2013). “Role of coarse aggregates in the triaxial behavior of concrete: experimental and numerical analysis.” Ph.D. Université de Grenoble, p. 146.
- Plassiard, J.-P., N. Belheine, and F.-V. Donzé (2009). “A spherical discrete element model: calibration procedure and incremental response.” In: *Granular Matter* 11.5, pp. 293–306. ISSN: 1434-5021. DOI: 10.1007/s10035-009-0130-x.
- Plesha, M. E. (1983). “On the modeling of rocks with microstructure.” In: *24th U.S. Symposium on Rock Mechanics*. Station, Texas: American Rock Mechanics Association.
- Popovics, S. (1982). “Strength relationships for fly ash concrete.” In: *Journal Proceedings* 79.1, pp. 43–49.
- Popovics, S. (1986). “Effect of curing method and final moisture condition on compressive strength of concrete.” In: *Journal Proceedings* 83.4, pp. 650–657.
- Popovics, S. (1987). “Quantitative deformation model for two-phase composites including concrete.” In: *Materials and Structures* 20.3, pp. 171–179. ISSN: 0025-5432. DOI: 10.1007/BF02472733.

BIBLIOGRAPHY

- Popovics, S. and J. Ujhelyi (2008). “Contribution to the concrete strength versus water-cement ratio relationship.” en. In: *Journal of Materials in Civil Engineering* 20.7, pp. 459–463. ISSN: 0899-1561. DOI: 10.1061/(ASCE)0899-1561(2008)20:7(459).
- Popovics, S. (1993). “Portland cement-fly ash-silica fume systems in concrete.” In: *Advanced Cement Based Materials* 1.2, pp. 83–91. ISSN: 10657355. DOI: 10.1016/1065-7355(93)90013-E.
- Potyondy, D. (2010). “A grain-based model for rock: Approaching the true microstructure.” In: *Rock Mechanics in the Nordic Countries 2010*. Kongsberg, Norway.
- Potyondy, D. and P. Cundall (2004). “A bonded-particle model for rock.” In: *International Journal of Rock Mechanics and Mining Sciences* 41.8, pp. 1329–1364. ISSN: 13651609. DOI: 10.1016/j.ijrmms.2004.09.011.
- Pukhov, I. E. (1978). “Results of investigating creep of concrete in the Toktogul dam.” In: *Hydrotechnical Construction* 12.4, pp. 356–362. ISSN: 0018-8220. DOI: 10.1007/BF02304342.
- Pukhov, I. E. and G. N. Kuleshov (1981). “Investigations of the characteristics of elasticity and creep of concrete in the Andizhan reservoir dam.” In: *Hydrotechnical Construction* 15.12, pp. 743–749. ISSN: 0018-8220. DOI: 10.1007/BF01432797.
- Qian, Z. and E. Schlangen (2013). “Lattice modeling of fracture processes in numerical concrete with irregular shape aggregates.” In: *VIII International Conference on Fracture Mechanics of Concrete and Concrete Structures, FraMCoS-8*. Ed. by J. van Mier, G. Ruiz, C. Andrade, R. C. Yu, and X. X. Zhang. Toledo (Spain), pp. 1539–1545.
- Qin, C. and C. Zhang (2011). “Numerical study of dynamic behavior of concrete by meso-scale particle element modeling.” In: *International Journal of Impact Engineering* 2 38.12, pp. 1011–1021.
- Qiu, Y. and G. Zhang (2017). “Stress and damage in concrete induced by pipe cooling at mesoscopic scale.” In: *Advances in Mechanical Engineering* 9.2, p. 168781401769050. ISSN: 1687-8140. DOI: 10.1177/1687814017690509.
- R Development Core Team (2017). *R: A Language and Environment for Statistical Computing*. Vienna, Austria.
- Rajabipour, F., E. Giannini, C. Dunant, J. H. Ideker, and M. D. A. Thomas (2015). “Alkali-silica reaction: Current understanding of the reaction mechanisms and the knowledge gaps.” In: *Cement and Concrete Research* 76. ISSN: 00088846. DOI: 10.1016/j.cemconres.2015.05.024.

- Rajamane, N. P., J. Annie Peter, and P. S. Ambily (2007). “Prediction of compressive strength of concrete with fly ash as sand replacement material.” In: *Cement and Concrete Composites* 29.3, pp. 218–223. ISSN: 0958-9465. DOI: 10.1016/J.CEMCONCOMP.2006.10.001.
- Ramos, J. (1985). *Consideração da reologia do betão no comportamento de barragens*. PhD. Lisboa.
- Ramos, J. and J. Soares de Pinho (1981). *Deformabilidade do betão de barragens (Determinações laboratoriais e in situ)*. Lisboa.
- Ramos, J. and J. Soares de Pinho (1983). *Deformabilidade do betão de barragens - Tratamento automático dos resultados dos ensaios laboratoriais*. Lisboa.
- Rao, G. (2001). “Generalization of Abrams’ law for cement mortars.” In: *Cement and Concrete Research* 31.3, pp. 495–502. ISSN: 00088846. DOI: 10.1016/S0008-8846(00)00473-7.
- RILEM TC 107 (1995). “Guidelines for characterizing concrete creep and shrinkage in structural design codes or recommendations.” In: *Materials and Structures* 28, pp. 52–55.
- RILEM TC 107-CSP (1998). “Measurement of time-dependent strains of concrete.” In: *Materials and Structures* 31.8, pp. 507–512. ISSN: 1359-5997. DOI: 10.1007/BF02481530.
- RILEM TC-242-MDC (2015). “RILEM draft recommendation: TC-242-MDC multi-decade creep and shrinkage of concrete: material model and structural analysis*.” In: *Materials and Structures* 48.4, pp. 753–770. ISSN: 1359-5997. DOI: 10.1617/s11527-014-0485-2.
- Rocco, C. and M. Elices (2009). “Effect of aggregate shape on the mechanical properties of a simple concrete.” In: *Engineering Fracture Mechanics* 76.2, pp. 286–298. ISSN: 00137944. DOI: 10.1016/j.engfracmech.2008.10.010.
- Roelfstra, P. E., H. Sadouki, and F. H. Wittmann (1985). “Le béton numérique.” In: *Materials and Structures* 18.5, pp. 327–335. ISSN: 0025-5432. DOI: 10.1007/BF02472402.
- Rojek, J., C. Labra, O. Su, and E. Oñate (2012). “Comparative study of different discrete element models and evaluation of equivalent micromechanical parameters.” In: *International Journal of Solids and Structures* 49.13, pp. 1497–1517.
- Sajna, A. and H. Linsbauer (1998). “Fracture mechanics of mass concrete - wet-screening procedure (FMWS).” In: *Fracture Mechanics of Concrete Structures*. Ed. by V. C.

- Li, K. Y. Leung, K. J. Willam, and S. L. Billington. Gifu, Japan: AEDIFICATIO, Freiburg, Germany, pp. 101–110.
- Saliba, J., F. Grondin, M. Matallah, A. Loukili, and H. Boussa (2012). “Relevance of a mesoscopic modeling for the coupling between creep and damage in concrete.” In: *Mechanics of Time-Dependent Materials* 17.3, pp. 481–499. ISSN: 1385-2000. DOI: 10.1007/s11043-012-9199-4.
- Sanahuja, J. (2013). “Effective behaviour of ageing linear viscoelastic composites: Homogenization approach.” In: *International Journal of Solids and Structures* 50.19, pp. 2846–2856. ISSN: 00207683. DOI: 10.1016/j.ijsolstr.2013.04.023.
- Santos Silva, A. (2006). “Degradação do betão por reacções álcalis-sílica. Utilização de cinzas volantes e metacaulino para a sua prevenção.” Doutoramento. Lisboa: Universidade do Minho, p. 339.
- Saouma, V. E., R. A. Martin, M. A. Hariri-Ardebili, and T. Katayama (2015). “A mathematical model for the kinetics of the alkali-silica chemical reaction.” In: *Cement and Concrete Research* 68, pp. 184–195. ISSN: 00088846. DOI: 10.1016/j.cemconres.2014.10.021.
- Sauvé, R. G. and D. R. Metzger (1995). “Advances in Dynamic Relaxation Techniques for Nonlinear Finite Element Analysis.” In: *Journal of Pressure Vessel Technology* 117.2, p. 170. ISSN: 00949930. DOI: 10.1115/1.2842106.
- Šavija, B. and E. Schlangen (2016). “Use of phase change materials (PCMs) to mitigate early age thermal cracking in concrete: Theoretical considerations.” In: *Construction and Building Materials* 126, pp. 332–344. ISSN: 09500618. DOI: 10.1016/j.conbuildmat.2016.09.046.
- Schlangen, E. and E. Garboczi (1997). “Fracture simulations of concrete using lattice models: Computational aspects.” In: *Engineering Fracture Mechanics* 57.2-3, pp. 319–332. ISSN: 00137944. DOI: 10.1016/S0013-7944(97)00010-6.
- Schlangen, E. and J. van Mier (1992). “Experimental and numerical analysis of micromechanisms of fracture of cement-based composites.” In: *Cement and Concrete Composites* 14.2, pp. 105–118. ISSN: 09589465. DOI: 10.1016/0958-9465(92)90004-F.
- Scholer, C. (1967). *The role of mortar-aggregate bond in the strength of concrete*. Tech. rep. Lafayette, Indiana: Purdue University, p. 18.

- Scholer, C. and S. Baker (1973). *Effect of variations in coarse aggregate gradation on properties of Portland cement concrete*. Tech. rep. West Lafayette, Indiana: Purdue University, p. 46.
- Schrefler, B. A., F. Pesavento, L. Sanavia, G. Sciume, S. Secchi, and L. Simoni (2010). “A general framework for modeling long-term behavior of earth and concrete dams.” In: *Frontiers of Architecture and Civil Engineering in China* 5.1, pp. 41–52. ISSN: 1673-7407. DOI: 10.1007/s11709-010-0070-x.
- Schutter, G. and L. Taerwe (1996). “Degree of hydration-based description of mechanical properties of early age concrete.” In: *Materials and Structures* 29.6, pp. 335–344. ISSN: 0025-5432. DOI: 10.1007/BF02486341.
- Scrivener, K. L., A. K. Crumbie, and P. Laugesen (2004). “The interfacial transition zone (ITZ) between cement paste and aggregate in concrete.” In: *Interface Science* 12.4, pp. 411–421. ISSN: 0927-7056. DOI: 10.1023/B:INTS.0000042339.92990.4c.
- Scrucca, L. (2013). “GA: A Package for Genetic Algorithms in R.” In: *Journal of Statistical Software* 53.4, pp. 1–37. ISSN: 1548-7660. DOI: 10.18637/jss.v053.i04.
- Sennour, M. L. and R. L. Carrasquillo (1989). *Creep and shrinkage properties in concrete containing fly ash*. Tech. rep. Austin: University of Texas, p. 112.
- Serra, C., A. L. Batista, and A. Tavares de Castro (2010). “Determinação da função de fluência do betão da barragem de Alqueva.” In: *Encontro Nacional Betão Estrutural 2010*. Ed. by M. Pipa, A. B. Ribeiro, and M. Lourenço. Lisboa, pp. 1–16.
- Serra, C., A. L. Batista, and A. Tavares de Castro (2012). “Creep of dam concrete evaluated from laboratory and in situ tests.” In: *Strain* 48.3, pp. 241–255. ISSN: 00392103. DOI: 10.1111/j.1475-1305.2011.00818.x.
- Serra, C., A. L. Batista, and N. Monteiro Azevedo (2014a). “Análise integrada dos resultados dos ensaios de deformabilidade do betão de grandes barragens portuguesas.” In: *5as Jornadas de Engenharia de Estruturas*.
- Serra, C., A. L. Batista, and N. Monteiro Azevedo (2014b). “Estudos de avaliação da deformabilidade do betão da barragem de montante do Baixo Sabor.” In: *5as Jornadas de Engenharia de Estruturas2*.
- Serra, C., A. L. Batista, and N. Monteiro Azevedo (2015a). “Análise integrada dos resultados dos ensaios de deformabilidade do betão de grandes barragens portuguesas.” In: *Revista Portuguesa de Engenharia de Estruturas* II.15, pp. 27–38.

- Serra, C., A. L. Batista, and N. Monteiro Azevedo (2015b). “Comprehensive analysis of the concrete deformability test results of Portuguese large dams.” In: *2nd International Dam World Conference*. Lisboa: Laboratório Nacional de Engenharia Civil, p. 12.
- Serra, C., A. L. Batista, and N. Monteiro Azevedo (2016a). “Dam and wet-screened concrete creep in compression: in situ experimental results and creep strains prediction using model B3 and composite models.” In: *Materials and Structures* 49.11, pp. 4831–4851. ISSN: 1359-5997. DOI: 10.1617/s11527-016-0828-2.
- Serra, C., A. L. Batista, and N. Monteiro Azevedo (2016b). “Effect of Wet Screening in the Elastic Properties of Dam Concrete: Experimental In Situ Test Results and Fit to Composite Models.” In: *Journal of Materials in Civil Engineering* 28.12, p. 10. DOI: 10.1061/(ASCE)MT.1943-5533.0001672.
- Serra, C., N. Monteiro Azevedo, A. L. Batista, and N. Schlar (2017a). “Discrete element method for modelling the long-term aging viscoelastic behavior of concrete considering its mesostructure (accepted for publication).” In: *Journal of Engineering Mechanics*.
- Serra, C., A. L. Batista, N. Monteiro Azevedo, and J. Custódio (2017b). “Prediction of Dam Concrete Compressive and Splitting Tensile Strength Based on Wet-Screened Concrete Test Results.” In: *Journal of Materials in Civil Engineering* 29.10, p. 10. ISSN: 0899-1561. DOI: 10.1061/(ASCE)MT.1943-5533.0002012.
- Shen, L., L. Wang, Y. Song, and L. Shi (2017). “Comparison between dynamic mechanical properties of dam and sieved concrete under biaxial tension-compression.” In: *Construction and Building Materials* 132, pp. 43–50. ISSN: 0950-0618. DOI: 10.1016/J.CONBUILDMAT.2016.11.113.
- Silveira, A., C. Florentino, and C. Freitas (1981). *LNEC experience in the field of concrete dam observation and of in situ tests*. Lisboa.
- Silveira, A. F. D. and C. A. Florentino (1971). “Influence of Temperature on the Creep of Mass Concrete.” In: *Special Publication* 25, pp. 173–190. DOI: 10.14359/17336.
- Simo, J. C., J. Oliver, and F. Armero (1993). “An analysis of strong discontinuities induced by strain-softening in rate-independent inelastic solids.” In: *Computational Mechanics* 12.5, pp. 277–296. ISSN: 0178-7675. DOI: 10.1007/BF00372173.
- Sinaie, S. (2017). “Application of the discrete element method for the simulation of size effects in concrete samples.” In: *International Journal of Solids and Structures* 108, pp. 244–253. ISSN: 00207683. DOI: 10.1016/j.ijsolstr.2016.12.022.

- Sinaie, S., A. Heidarpour, and X. Zhao (2016). “A micro-mechanical parametric study on the strength degradation of concrete due to temperature exposure using the discrete element method.” In: *International Journal of Solids and Structures* 88-89.June, pp. 165–177. ISSN: 00207683. DOI: 10.1016/j.ijsolstr.2016.03.009.
- Sizov, V. P. (1997). “Effect of sand content in concrete and aggregate size on cement consumption and strength of concrete.” In: *Hydrotechnical Construction* 31.3, pp. 194–196. ISSN: 0018-8220. DOI: 10.1007/BF02767203.
- Smith, D. M. and M. I. Hammons (1993). “Creep of mass concrete at early ages.” In: *Journal of Materials in Civil Engineering* 5.3, pp. 411–417. DOI: [http://dx.doi.org/10.1061/\(ASCE\)0899-1561\(1993\)5:3\(411\)](http://dx.doi.org/10.1061/(ASCE)0899-1561(1993)5:3(411)).
- Smith, J., C. Jin, D. Pelessone, and G. Cusatis (2015). “Dynamics Simulations of Concrete and Concrete Structures through the Lattice Discrete Particle Model.” In: *Structures Congress 2015*. Reston, VA: American Society of Civil Engineers, pp. 63–74. ISBN: 9780784479117. DOI: 10.1061/9780784479117.006.
- Soares de Pinho, J. (1989). *Contribuição para o estudo da deformabilidade do betão de barragens*. PhD. Lisboa.
- Soares de Pinho, J., J. Ramos, and C. Florentino (1988). “Control of mass concrete for dams. Full-mixed and wet-screened concrete tests.” In: *ICOLD Congress*. LNEC. San Francisco: International Commission On Large Dams (ICOLD), p. 8.
- Stock, A. F., D. J. Hannant, and R. I. T. Williams (1979). “The effect of aggregate concentration upon the strength and modulus of elasticity of concrete.” en. In: *Magazine of Concrete Research* 31.109, pp. 225–234. ISSN: 0024-9831. DOI: 10.1680/mac.1979.31.109.225.
- Suchorzewski, J., J. Tejchman, and M. Nitka (2017). “Discrete element method simulations of fracture in concrete under uniaxial compression based on its real internal structure.” In: *International Journal of Damage Mechanics*, p. 105678951769091. ISSN: 1056-7895. DOI: 10.1177/1056789517690915.
- Sun, B. and Z. Li (2015). “Adaptive concurrent multi-scale FEM for trans-scale damage evolution in heterogeneous concrete.” In: *Computational Materials Science* 99.March, pp. 262–273. ISSN: 09270256. DOI: 10.1016/j.commatsci.2014.12.033.
- Tavarez, F. A. and M. E. Plesha (2007). “Discrete element method for modelling solid and particulate materials.” In: *International Journal for Numerical Methods in Engineering* 70.4, pp. 379–404. ISSN: 00295981. DOI: 10.1002/nme.1881.

- Taylor, H. (1997). *Cement chemistry*. 2nd. Thomas Telford, p. 469.
- Teychenne, D. C., L. J. Parrot, and C. D. Pomeroy (1978). *The estimation of the elastic modulus of concrete for the design of structures*. Tech. rep. Wokingham, Berkshire United Kingdom: Transport and Road Research Laboratory (TRRL), p. 11.
- The Mathworks Inc. (2010). *MATLAB*. Natick, Massachusetts.
- Topçu, I. B. (2005). “Alternative estimation of the modulus of elasticity for dam concrete.” In: *Cement and Concrete Research* 35.11, pp. 2199–2202. ISSN: 00088846. DOI: 10.1016/j.cemconres.2004.08.010.
- Trebuňa, F., P. Padevět, and P. Bittnar (2012). “Influence of Fly Ash Content in Cement Paste on Size of Creep.” In: *Procedia Engineering* 48, pp. 520–524.
- Trivedi, N. and R. Singh (2014). “Assessment of in-situ concrete creep: Cylindrical specimen and prototype nuclear containment structure.” In: *Construction and Building Materials* 71.30, pp. 16–25. ISSN: 09500618. DOI: 10.1016/j.conbuildmat.2014.08.010.
- Tsiskreli, G. D. and A. N. Dzhavakhidze (1970). “The effect of aggregate size on strength and deformation of concrete.” In: *Gidrotekhnicheskoe stroitel'stvo* 5, pp. 42–45.
- Underwood, P. (1983). “Dynamic Relaxation.” In: *Computational Methods for Transient Analysis*. Oxford, United Kingdom: Elsevier Science Publishers B.V. Chap. 5, pp. 245–265.
- USBR (1955). *Investigation of creep characteristics of Shasta dam concrete*. Tech. rep. Denver, Colorado: United States Bureau of Reclamation - Department of the Interior.
- USBR (1977). *Design criteria for concrete arch and gravity dams*. Denver.
- USBR (1988). *Concrete manual. A water resources technical publication*. 8th Ed. Washington: United States Government Printing Office, p. 627.
- USBR (2005). *Materials properties model of aging concrete*. Denver, Colorado: United States Government Printing Office, p. 28.
- Van Mier, J. G. and M. B. Nooru-Mohamed (1990). “Geometrical and structural aspects of concrete fracture.” In: *Engineering Fracture Mechanics* 35.4-5, pp. 617–628. ISSN: 00137944. DOI: 10.1016/0013-7944(90)90144-6.
- Vandamme, M. and F. Ulm (2009). “Nanogranular origin of concrete creep.” In: *Proceedings of the National Academy of Sciences of the United States of America* 106.26, pp. 10552–7. ISSN: 1091-6490. DOI: 10.1073/pnas.0901033106.

- Vandewalle, L. (2000). “Concrete creep and shrinkage at cyclic ambient conditions.” In: *Cement and Concrete Composites* 22.3, pp. 201–208. ISSN: 09589465. DOI: 10.1016/S0958-9465(00)00004-4.
- Vieira, M. (2012). *Estudo de fluência do betão para a empreitada de construção da nova barragem do Alto Ceira - 3^a Colheita*. Tech. rep. Lisboa: LNEC.
- Vieira de Lemos, J. (1987). “A distinct element model for dynamic analysis of jointed rock with application to dam foundations and fault motion.” Ph.D. University of Minnesota, p. 590.
- Vilardell, J., A. Aguado, L. Agullo, and R. Gettu (1998). “Estimation of the modulus of elasticity for dam concrete.” In: *Cement and Concrete Research* 28.1, pp. 93–101. DOI: doi:10.1016/S0008-8846(97)00214-7.
- Vonk, R. (1992). “Softening of concrete loaded in compression.” Ph.D. Eindhoven University of Technology, p. 197.
- Vu, X. H., L. Daudeville, and Y. Malecot (2011). “Effect of coarse aggregate size and cement paste volume on concrete behavior under high triaxial compression loading.” In: *Construction and Building Materials* 25.10, pp. 3941–3949. ISSN: 09500618. DOI: 10.1016/j.conbuildmat.2011.04.026.
- Walker, S. and D. Bloem (1960). “Effects of aggregate size on properties of concrete.” In: *Journal Proceedings* 57.9, pp. 283–298.
- Walraven, J. (1980). “Aggregate interlock: A theoretical and experimental analysis.” Ph.D. Delft University of Technology, p. 197.
- Wang, X., M. Zhang, and A. P. Jivkov (2016). “Computational technology for analysis of 3D meso-structure effects on damage and failure of concrete.” In: *International Journal of Solids and Structures* 80, pp. 310–333. ISSN: 0020-7683. DOI: 10.1016/J.IJSOLSTR.2015.11.018.
- Wang, Y. and F. Tonon (2009). “Modeling Lac du Bonnet granite using a discrete element model.” In: *International Journal of Rock Mechanics and Mining Sciences* 46.7, pp. 1124–1135. ISSN: 13651609. DOI: 10.1016/j.ijrmms.2009.05.008.
- Wang, Z., A. Kwan, and H. Chan (1999). “Mesoscopic study of concrete I: generation of random aggregate structure and finite element mesh.” In: *Computers & Structures* 70.5, pp. 533–544. ISSN: 00457949. DOI: 10.1016/S0045-7949(98)00177-1.

- Ward, M. A., A. M. Neville, and S. P. Singh (1969). “Creep of air-entrained concrete.” en. In: *Magazine of Concrete Research* 21.69, pp. 205–210. ISSN: 0024-9831. DOI: 10.1680/mac.1969.21.69.205.
- Wendner, R., M. H. Hubler, and Z. P. Bažant (2013). “The B4 Model for Multi-decade Creep and Shrinkage Prediction.” en. In: *Mechanics and Physics of Creep, Shrinkage, and Durability of Concrete*. Ed. by F.-J. Ulm, M. H. Jennings, and J.-M. P. Roland. Cambridge, Massachusetts, United States: American Society of Civil Engineers, pp. 429–436.
- Wendner, R., J. Vorel, J. Smith, C. G. Hoover, Z. P. Bažant, and G. Cusatis (2014). “Characterization of concrete failure behavior: a comprehensive experimental database for the calibration and validation of concrete models.” In: *Materials and Structures*. ISSN: 1359-5997. DOI: 10.1617/s11527-014-0426-0.
- Wendner, R., M. H. Hubler, and Z. P. Bažant (2015). “Optimization method, choice of form and uncertainty quantification of Model B4 using laboratory and multi-decade bridge databases.” In: *Materials and Structures*. ISSN: 1359-5997. DOI: 10.1617/s11527-014-0515-0.
- Wriggers, P. and S. O. Moftah (2006). “Mesoscale models for concrete: Homogenisation and damage behaviour.” In: *Finite Elements in Analysis and Design* 42.7, pp. 623–636. DOI: 10.1016/J.FINEL.2005.11.008.
- Xotta, G., V. Salomoni, and C. Majorana (2013). “Thermo-hygro-mechanical meso-scale analysis of concrete as a viscoelastic-damaged material.” en. In: *Engineering Computations* 30.5, pp. 728–750. ISSN: 0264-4401. DOI: 10.1108/EC-08-2013-0097.
- Xu, Y., Q. Xu, S. Chen, and X. Li (2017). “Self-restraint thermal stress in early-age concrete samples and its evaluation.” In: *Construction and Building Materials* 134, pp. 104–115. ISSN: 09500618. DOI: 10.1016/j.conbuildmat.2016.12.066.
- Yamamoto, Y., S. Okazaki, H. Nakamura, M. Beppu, and T. Shibata (2016). “Crack Propagation and Local Failure Simulation of Reinforced Concrete Subjected to Projectile Impact Using RBSM.” In: *Volume 9: Prof. Norman Jones Honoring Symposium on Impact Engineering; Prof. Yukio Ueda Honoring Symposium on Idealized Nonlinear Mechanics for Welding and Strength of Structures*. ASME, V009T12A026. ISBN: 978-0-7918-5000-8. DOI: 10.1115/OMAE2016-54969.

- Yang, H., M. Rao, and Y. Dong (2016). "Influence study of extra-large stone limited size and content on full-graded concrete properties." In: *Construction and Building Materials* 127.November, pp. 774–783. ISSN: 09500618. DOI: 10.1016/j.conbuildmat.2016.10.006.
- Yeh, I.-C. (2006). "Generalization of strength versus water-cementitious ratio relationship to age." In: *Cement and Concrete Research* 36.10, pp. 1865–1873. ISSN: 00088846. DOI: 10.1016/j.cemconres.2006.05.013.
- Yoon, J (2007). "Application of experimental design and optimization to PFC model calibration in uniaxial compression simulation." In: *International Journal of Rock Mechanics and Mining Sciences* 44.6, pp. 871–889. ISSN: 13651609. DOI: 10.1016/j.ijrmms.2007.01.004.
- Yurtdas, I., N. Burlion, and F. Skoczylas (2004). "Experimental characterisation of the drying effect on uniaxial mechanical behaviour of mortar." In: *Materials and Structures* 37.3, pp. 170–176. ISSN: 1359-5997. DOI: 10.1007/bf02481616.
- Zhang, J., D. Cusson, P. Monteiro, and J. Harvey (2008). "New perspectives on maturity method and approach for high performance concrete applications." In: *Cement and Concrete Research* 38.12, pp. 1438–1446.
- Zhao, Q., X. Liu, and J. Jiang (2015). "Effect of curing temperature on creep behavior of fly ash concrete." In: *Construction and Building Materials* 96, pp. 326–333. ISSN: 09500618. DOI: 10.1016/j.conbuildmat.2015.08.030.
- Zheng, J.-j. and X.-z. Zhou (2006). "A numerical method for predicting the elastic modulus of concrete made with two different aggregates." In: *Journal of Zhejiang University SCIENCE A* 7.S2, pp. 293–296. ISSN: 1009-3095. DOI: 10.1631/jzus.2006.AS0293.
- Zheng, J., X. Zhou, and X. Jin (2012). "An n-layered spherical inclusion model for predicting the elastic moduli of concrete with inhomogeneous ITZ." In: *Cement and Concrete Composites* 34.5, pp. 716–723. ISSN: 09589465. DOI: 10.1016/j.cemconcomp.2012.01.011.
- Zhou, F. P., F. D. Lydon, and B. I. Barr (1995). "Effect of coarse aggregate on elastic modulus and compressive strength of high performance concrete." In: *Cement and Concrete Research* 25.1, pp. 177–186. ISSN: 00088846. DOI: 10.1016/0008-8846(94)00125-I.
- Zhou, S. H., H. Q. Yang, and Y. Dong (2010). "Analysis and Comparison on Mechanical Properties between Full-Graded and Wet-Screened Concretes." In: *Advanced Materials*

BIBLIOGRAPHY

Research 168-170, pp. 426–429. ISSN: 1662-8985. DOI: 10.4028/www.scientific.net/AMR.168-170.426.

Zubelewicz, A. and Z. Mróz (1983). “Numerical simulation of rock burst processes treated as problems of dynamic instability.” In: *Rock Mechanics and Rock Engineering* 16.4, pp. 253–274. ISSN: 0723-2632. DOI: 10.1007/BF01042360.



Properties of the cement and of the fly ash used in Baixo Sabor dam

A chemical analysis was performed to both the cement and fly ash used in the dam concrete. The chemical analysis of the cement was carried out according to NP EN 196-2:2014 (IPQ 2014); whilst that performed to the fly ash generally followed the methods recommended in NP EN 450-1:2012 (IPQ 2012b). The determination of the fly ash alkali content, not covered by NP EN 450-1, was done using a LNEC Internal Method. The fly ash iron oxide content was determined following LNEC Specification E 406:1993 (LNEC 1993d). The results obtained and the specific test methods used for each property are presented in Table A.1. The cement and fly ash average bulk density was also determined and is presented in TableA.1.

APPENDIX A. PROPERTIES OF THE CEMENT AND OF THE FLY ASH USED IN BAIXO SABOR DAM

Table A.1: Chemical characteristics of the cement and fly ashes

Cement			Fly ash		
Property	Value (%)	Test method	Property	Value (%)	Test method
SiO ₂	18.25	NP EN 196-2:2014 (section 5)	SiO ₂	50.12	NP EN 196-2:2014 (sections 4.5.4 and 4.5.6) ^{C,D}
Al ₂ O ₃	4.66		Al ₂ O ₃	25.21	NP EN 196-2:2014 (sections 4.5.11) ^C
Fe ₂ O ₃	3.24		Fe ₂ O ₃	8.91	LNEC E 406:1993 ^C
CaO	61.39		CaO _{total}	2.66	NP EN 196-2:2014 (sections 4.5.14) ^C
MgO	1.89		CaO _{free}	<0.1	NP EN 451-1:2006
SO ₃	3.66		CaO _{reactive}	2.62	NP EN 196-2:2014 ^{A,B,C}
K ₂ O	1.49		MgO	1.91	NP EN 196-2:2014 (sections 4.5.15) ^C
Na ₂ O	0.12		SO ₃	0.5	NP EN 196-2:2014 (section 4.4.2)
Na ₂ O _{eq.}	1.1		K ₂ O	4.11	LNEC Internal Method ^{C,E}
TiO ₂	0.3		Na ₂ O	0.8	LNEC Internal Method ^{C,E}
P ₂ O ₅	0.07		Na ₂ O _{eq.}	3.5	-
Mn ₂ O ₃	0.04		-	-	-
SrO	0.05		-	-	-
Cr ₂ O ₃	0.01		-	-	-
ZnO	0.02		-	-	-
Cl	0.02		-	-	-
L.O.I.	1.86	NP EN 196-2:2014 (section 5)	-	-	-
I.R.	1.26	NP EN 196-2:2014 (section 4)	-	-	-

NOTES: L.O.I. – loss on ignition; I.R. – insoluble residue;

A – The reactive calcium oxide content was calculated according to the definition and test method given in NP EN 197-1:2012 IPQ 2012b;

B – The carbon dioxide content was determined according to a LNEC Internal Method by treating the sample with phosphoric acid and collecting the released carbon dioxide with an ascarite absorbent;

C – The sample was fused with lithium tetraborate;

D – The soluble silica, indicated in section 4.5.9 of NP EN 196-2:2014, was determined according to LNEC Specification E 407:1993 LNEC (Laboratório Nacional de Engenharia Civil) 1993;

E – The alkali content of the solutions was determined by means of flame photometry;

Na₂O_{eq.} = Na₂O + (0.658 K₂O).

Table A.2: Physical characteristics of the cement and fly ashes

Material	Density (kg/m ³)	Test method
Cement	3120	NP EN 196-6:2010
Fly ash	2480	NP EN 1097-7:2012



**Scientific papers published in national and
international journals during the Ph.D.**

Análise integrada dos resultados dos ensaios de deformabilidade do betão de grandes barragens portuguesas

Comprehensive analysis of the concrete deformability test results of Portuguese large dams

Carlos Serra
António Lopes Batista
Nuno Monteiro Azevedo

Resumo

A caracterização das propriedades dos materiais estruturais através de ensaios é prática corrente em obras onde as deformações e tensões são elevadas, como pontes de grande vão, centrais nucleares, edifícios altos e grandes barragens.

Neste trabalho apresentam-se alguns estudos de avaliação da correlação entre a composição e as propriedades de deformabilidade dos betões integral e crivado utilizados na construção de barragens. Para isso compilaram-se os elementos relativos à composição e aos principais resultados dos ensaios de deformabilidade do betão de diversas barragens portuguesas, efetuados pelo Laboratório Nacional de Engenharia Civil desde 1951. Foi possível estabelecer correlações entre alguns dados de composição e os resultados experimentais e entre os coeficientes de fluência do betão crivado e do betão integral, considerando os resultados dos ensaios realizados em laboratório e *in situ*.

Abstract

Structural material characterization through testing is a common practice in structures such as large-span bridges, nuclear power stations, tall buildings and large dams, where the installed strains and stress take significant values.

The collected data of composition and deformability test results of the concrete of several Portuguese dams, built since 1951, properly treated, allowed the establishment of correlations between the composition and the deformability properties of the full-mixed and the wet-screened concrete used in dam construction. Taking into account the laboratory and *in situ* testing, correlations between some composition elements and the experimental test results and between creep coefficients of wet-screened and full-mixed concrete were obtained.

Palavras-chave: Betão de barragens / Deformabilidade do betão / Ensaios *in situ* e em laboratório / Correlação entre propriedades mecânicas

Keywords: Dam concrete / Concrete deformability / *In situ* and laboratory tests / Mechanical property correlation

Effect of Wet Screening in the Elastic Properties of Dam Concrete: Experimental In Situ Test Results and Fit to Composite Models

Carlos Serra¹; António Lopes Batista²; and Nuno Monteiro Azevedo³

Abstract: This paper proposes the use of the maturity method and a two-phase composite model for the prediction of dam concrete modulus of elasticity. The methodology was validated with test results obtained from experimental in situ setup using creep cells placed in the dam's body, subjected to variable environmental conditions. It is shown that composite models can be used to predict the modulus of elasticity of in situ dam concrete based on the modulus of elasticity of the wet-screened concrete. DOI: 10.1061/(ASCE)MT.1943-5533.0001672. © 2016 American Society of Civil Engineers.

Author keywords: Dam concrete; Wet-screened concrete; In situ experimental tests; Maturity method; Composite models.

Introduction

This work focuses on mass concrete, in particular on dam concrete, placed in large volumes and produced with large aggregate sizes. The size of the aggregate reduces the use of cement but it is limited by the concrete strength and by the costs associated with handling, mixing, transporting and with the consolidation of large aggregate concrete [ACI Committee 207 (ACI 2005)]. The maximum size of aggregates (MSA) can be 150 mm, the total aggregate percentage is usually 60–70% of the total volume and the binder content is low (100–300 kg/m³). Because of the thermal cracking risk, the cement content of dam concrete is customized to decrease the heat generation, considering the strength properties as a secondary requirement (ACI 2005; ICOLD 2008). Design practice often considers material properties based on coarse estimates obtained from experimental data from other works and/or based on experimental test results obtained from trial compositions (CEN 2005; ICOLD 2008).

The number of experimental tests on dam concrete is sparse due to local conditions, namely related with the source of the concrete component materials. Comprehensive experimental study of dam concrete or even mass concrete is still to be done. Generally, the elastic, viscoelastic, and strength properties of dam concrete have a slower rate of development, lower maximum strengths, and higher modulus of elasticity when compared with conventional concretes (ICOLD 2008).

Wet-screened concrete, obtained from the dam concrete (full-mixed concrete) by sieving or screening the larger aggregates after

mixing the components, is widely used for laboratory testing and for embedding the monitoring devices, such as strain and stress meters, but it has a distinct composition and different mechanical properties. Although using the same type of materials, the mix proportions change when the larger aggregates are removed by wet-screening (ICOLD 2008). Earlier research studies focused on characterizing the relation between dam and wet-screened concrete mechanical properties can be found in Sajna and Linsbauer (1998), Vilardell et al. (1998), ICOLD (2008), and Serra et al. (2012).

The wet-screening procedure changes significantly the concrete composition of dam concrete, mainly the coarse aggregate content. To take into account the wet-screening effect on the structural properties, specific studies are required. Nevertheless, the available results focused on the influence of the aggregate properties, gradation, and content on the modulus of elasticity of the concrete are relevant to the study of the wet-screening procedure (Walker and Bloem 1960; Hirsch 1962; Counto 1964; Vilardell et al. 1998; Alexander and Mindess 2010).

The prediction and modeling of the concrete behavior based on the properties of the components used in the mix is a complex task for elastic, viscoelastic (Granger and Bažant 1995; Bažant and Baweja 2000), and strength properties (Hwang et al. 2004). Several studies focused on the characterization and modeling of the cement paste in order to determine the behavior of the produced concrete, because it is responsible for the growth of mechanical properties over time. Besides, the rate of development over time is coupled with the environmental conditions (Bažant et al. 2011). Multiscale analysis and property homogenization can be used to model the behavior of concrete based on the known behavior of each component, validated with experimental results, and submitted to variable temperature and humidity conditions (Maekawa et al. 2009).

This paper shows the influence of the dam concrete wet-screening on the development of the modulus of elasticity based on a specific experimental program, using in situ creep cells. Dam and wet-screened concrete creep cells were installed in the dam's core and the modulus of elasticity was determined for several ages and for the environmental conditions inside the concrete mass. The prediction of the instantaneous deformability properties of dam concrete over time was based on the composite model theory, considering the wet-screened concrete as equivalent binder of the larger

¹Ph.D. Research Fellow, Dept. of Concrete Dams, National Laboratory for Civil Engineering, Av. Brasil 101, 1700-066 Lisboa, Portugal (corresponding author). E-mail: cserra@lnec.pt

²Head of the Department and Senior Researcher, Dept. of Concrete Dams, National Laboratory for Civil Engineering, Av. Brasil 101, 1700-066 Lisboa, Portugal. E-mail: a.l.batista@lnec.pt

³Research Officer, Dept. of Concrete Dams, National Laboratory for Civil Engineering, Av. Brasil 101, 1700-066 Lisboa, Portugal. E-mail: nazevedo@lnec.pt

Note. This manuscript was submitted on September 22, 2015; approved on April 19, 2016; published online on June 27, 2016. Discussion period open until November 27, 2016; separate discussions must be submitted for individual papers. This paper is part of the *Journal of Materials in Civil Engineering*, © ASCE, ISSN 0899-1561.

Dam and wet-screened concrete creep in compression: in situ experimental results and creep strains prediction using model B3 and composite models

C. Serra  · A. L. Batista · N. Monteiro Azevedo

Received: 20 July 2015 / Accepted: 14 February 2016
© RILEM 2016

Abstract This paper proposes a methodology for the prediction of the compressive creep strains of dam concrete based on wet-screened experimental results at constant elevated temperature conditions measured in situ. Due to its large aggregate dimensions, the experimental characterization of dam concrete has particular constraints. The wet-screened concrete, obtained by sieving the aggregates larger than a given dimension, after mixing, is used to cast standard specimens and to embed monitoring devices. An experimental in situ installation using creep cells was used to obtain the compressive creep strain development over time for the maturing conditions of the dam core. The study of the effect of wet-screening procedure on creep in compression considers three types of concrete, dam concrete and two wet-screened concretes tested at three loading ages, 28, 90 and 365 days. The comparison between different types of concrete at different maturing conditions requires the definition of a reference state given by the maturity method, using the equivalent age, and relies on the fit of compressive creep strains to the RILEM recommended model B3. To take into account the effect of the aggregate content on the deformability properties of dam concrete, an

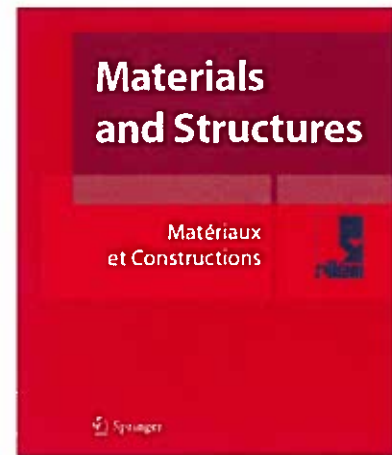
equivalent two-phase composite model was applied. The equivalent composite model considered the equivalent matrix as the wet-screened concrete and the inclusions as the larger aggregates that are removed during the wet-screening procedure. Predictions obtained with the composite model are close to the dam concrete experimental results, for the tested loading ages.

Keywords Dam concrete · Wet-screened concrete · Creep in compression · In situ tests · Model B3 · Composite models

1 Introduction

Dam concrete is considered to be a mass concrete with a poor binder content, 100–300 kg/m³, and with large admixtures dosage, up to 50 % of the cement replacement [1]. It has a large aggregate content and the maximum size of aggregate (MSA) can reach up to 150 mm [2, 3]. The combination of the temperature gradients due to heat dissipation, the slow mechanical property development and, therefore, the cracking risk at early ages are the main concerns of mass concrete [2, 3]. For an accurate cracking risk assessment it is necessary to determine the mechanical properties development, as well as the stress development during the first year [4, 6]. Moreover, to interpret the dam structural behaviour for several decades, long-term instantaneous and time-dependent properties are key

C. Serra (✉) · A. L. Batista · N. Monteiro Azevedo
National Laboratory for Civil Engineering, Av. do Brasil
101, Lisbon 1700-066, Portugal
e-mail: cserra@lnec.pt



04 November 2016

Congratulations on the Outstanding Paper 2016 Award

for the paper

*“Dam and wet-screened concrete creep in compression:
in situ experimental results and creep strains prediction
using model B3 and composite models”*

C. Serra, A. L. Batista, N. Monteiro Azevedo, *Materials and Structures* (2016) 49: 4831-4851

On behalf of the Board of Editors of Materials and Structures

A handwritten signature in blue ink, which appears to be 'Pietro Lura', is written over a light blue horizontal line.

Pietro Lura
Editor in Chief
Materials and Structures

Prediction of Dam Concrete Compressive and Splitting Tensile Strength Based on Wet-Screened Concrete Test Results

Carlos Serra¹; António Lopes Batista²; Nuno Monteiro Azevedo³; and João Custódio⁴

Abstract: The mechanical property characterization of dam concrete is a challenging task mainly due to the use of large aggregate sizes. The properties of dam concrete are often evaluated from wet-screened concrete tests using standard specimen sizes. A physically based relationship between dam concrete and wet-screened concrete strength properties is currently unavailable. A prediction methodology is proposed that can be used to obtain the compressive and the splitting tensile strength of dam concrete by taking into account the wet-screened strength results, the effect of the specimen dimensions, and the effect of the maximum size of aggregate. The predicted results are compared with test results available in the literature and with test results recently obtained during the construction of the Baixo Sabor dam. It is shown that the proposed prediction tool can be used to obtain accurate estimates of dam concrete strength. DOI: 10.1061/(ASCE)MT.1943-5533.0002012. © 2017 American Society of Civil Engineers.

Author keywords: Dam concrete; Wet-screened concrete; Compressive strength; Splitting tensile strength; Size effect; Extended Abrams law.

Introduction

This work focuses on the prediction of the compressive and splitting tensile strength properties of dam concrete. The placement of large volumes of dam concrete requires special measures to reduce the heat generation during hydration reactions, to control volume changes, and to minimize the cracking risk at early ages (ACI 2005).

The dam concrete composition is designed to decrease the heat generation by reducing the cement content. The maximum size of aggregate (MSA) can reach 150 mm, and the total coarse aggregate percentage is usually 60–70% of the total volume, which implies that the cementitious material content is low (100–300 kg/m³). The strength properties are often taken as a secondary requirement for the composition design (ACI 2005). Nevertheless, the strength properties are important for the evaluation of the cracking risk at early ages and for long-term deterioration assessment scenario, which can occur due to potentially alkali-reactive aggregates (Nixon and Sims 2016a).

¹Ph.D. Student, Dept. of Civil Engineering, Faculdade de Ciências e Tecnologia, Universidade Nova de Lisboa, 2829-516 Caparica, Portugal; Doctoral Research Fellow, National Laboratory for Civil Engineering, Concrete Dams Dept., Av. Brasil 101, 1700-066 Lisboa, Portugal (corresponding author). E-mail: cl.serra@campus.fct.unl.pt; cserra@lnec.pt

²Invited Associate Professor, Dept. of Civil Engineering, Faculdade de Ciências e Tecnologia, Universidade Nova de Lisboa, 2829-516 Caparica, Portugal; Senior Researcher, Head of the Department, National Laboratory for Civil Engineering, Concrete Dams Dept., Av. Brasil 101, 1700-066 Lisboa, Portugal. E-mail: a.l.batista@lnec.pt

³Research Officer, National Laboratory for Civil Engineering, Dept. of Concrete Dams, Av. Brasil 101, 1700-066 Lisboa, Portugal. E-mail: nazevedo@lnec.pt

⁴Assistant Researcher, National Laboratory for Civil Engineering, Dept. of Materials, Av. Brasil 101, 1700-066 Lisboa, Portugal. E-mail: jcustodio@lnec.pt

Note. This manuscript was submitted on August 3, 2016; approved on March 21, 2017; published online on July 21, 2017. Discussion period open until December 21, 2017; separate discussions must be submitted for individual papers. This paper is part of the *Journal of Materials in Civil Engineering*, © ASCE, ISSN 0899-1561.

In dam concrete the cement is replaced by fly ash to cope with the temperature rise effect and to control future swelling effects related with alkali-aggregate reactions [ACI Committee 207 (ACI 2005)]. When compared with conventional concretes, dam concrete elastic and strength properties have a slower development, lower maximum strengths, and slightly higher modulus of elasticity (ICOLD 2008).

The characterization of dam concrete (full-mixed concrete or fully graded concrete) is difficult due to its large aggregates, which imply the use of large specimens and heavy testing equipment, increasing the costs of quality-control procedures. These constraints lead to the use of wet-screened concrete to evaluate the material properties. The wet-screened concrete is obtained from the produced dam concrete by removing the aggregates larger than a given sieve aperture. The 38-mm aperture sieve is usually adopted for the wet-screening of full-mixed dam concrete. The wet-screening procedure is done after mixing, while the concrete is still fresh, changing mainly the coarse aggregate content (Blanks and McNamara 1935).

Dam structural design practice often considers material properties based on estimates provided by experimental data available in the literature or based on preliminary test results obtained from trial compositions (ICOLD 2008). A reliable concrete strength prediction tool based on the wet-screened results is relevant as it (1) will allow the reduction of the required number of tests of full-mixed concrete, which are known to be costly; (2) will guarantee, during the construction phase, that the concrete strength evaluated from wet-screened samples meets the design requirements of the full-mixed concrete; and (3) will allow an accurate assessment of full-mixed concrete's long-term strength properties for the modeling of the dam's structural behavior, especially for deterioration scenarios (USBR 2005; Nixon and Sims 2016a).

The relation between full-mixed and wet-screened concrete mechanical properties has been studied in the past mainly through experimental testing (USBR 1988; Pinho et al. 1988; Sajna and Linsbauer 1998; Vilardell et al. 1998; Li et al. 2004; Topçu 2005; ICOLD 2008; Deng et al. 2008; Khaloo et al. 2009; Zhou et al. 2010; Kumar et al. 2015; Serra et al. 2012, 2016a, b; Guan et al. 2016; Yang et al. 2016). However, a general physically

DISCRETE ELEMENT METHOD FOR MODELING THE LONG-TERM AGING VISCOELASTIC BEHAVIOR OF CONCRETE CONSIDERING ITS MESOSTRUCTURE

Carlos Serra¹, Not a member, ASCE
Nuno Monteiro Azevedo², Not a member, ASCE
António Lopes Batista³, Not a member, ASCE
Noemi Schclar⁴, Not a member, ASCE

ABSTRACT

Detailed models of concrete mesostructure can be used to understand the interactions between its components and predict complex deterioration scenarios. The discrete or distinct element method (DEM) is currently being used for modelling the fracture process of quasi-brittle materials, such as rock and concrete.

An explicit formulation of a DEM contact model that includes aging viscoelastic behaviour based on the solidification theory is proposed allowing the DEM particle model to be applied to delayed concrete analysis. Due to the time step constraints of the DEM, a fast numerical procedure for the analysis of long-term aging viscoelastic behavior of concrete is also proposed. A calibration procedure for the aging viscoelastic contact model parameters is presented, including new expressions for the delayed deformability macro properties.

The presented validation tests using a one contact particle assembly show a good agreement between the fast numerical procedure, the fully explicit DEM procedure with small timestep and the creep compliance analytical solution. The contact aging model validation tests using larger regular and random particle assemblies show that the fast numerical procedure significantly reduces the computational costs by introducing large time steps in which the solution is computed, while giving the same accuracy of the fully explicit procedure.

¹Ph.D. Student, Civil Engineering Department, Faculdade de Ciências e Tecnologia, Universidade Nova de Lisboa, 2829-516 Caparica, Portugal. E-mail: cl.serra@campus.fct.unl.pt

²Research Officer, National Laboratory for Civil Engineering, Concrete Dams Department, Av. Brasil 101, 1700-066, Lisboa. E-mail: nazevedo@lnec.pt

³Head of the Department, Senior Researcher, National Laboratory for Civil Engineering, Concrete Dams Department, Av. Brasil 101, 1700-066, Lisboa. E-mail: a.l.batista@lnec.pt

⁴Senior Researcher, National Laboratory for Civil Engineering, Concrete Dams Department, Av. Brasil 101, 1700-066, Lisboa. E-mail: nschclar@lnec.pt



C++ computational structure of the 2D particle model for the behaviour analysis

For the implementation of the DEM, the former concepts and procedures were structured into a C++ computational code (Microsoft Corporation 2010a). Figure C.1 shows a schematic view of the code's structure, divided into three main parts. The first **SETUP** part deals with the definition of properties, geometries, boundary and analysis conditions. It is possible to generate a regular, rectangular or hexagonal, mesh, and to built input data files for a generic mesh (including several types of materials). The second part, **CYCLE**, iterates over time and applies the law of motion and the law of forces to all the particles and contacts until the convergence criteria is reached and the third part, **OUTPUT**, is where the main results are written into ASCII files, including data files (.dad) and files with the undeformed and deformed meshes (using .vtk files).

The fully-explicit algorithm is summarized in the following steps:

SETUP

1. Generation of particle assembly (predefined mesh, rectangular or hexagonal, or user-defined mesh);
2. Definition of contacts;
3. Definition of boundary and loading conditions;
4. Definition of real or scaled masses;
5. Calculation of the critical timestep or the scaled masses;

6. Definition of the stopping criteria (maximum simulation time, maximum number of steps and convergence criteria using force and displacement tolerances);
7. Set type of damping;
8. Set constitutive law;
9. Calculates initial natural frequency, ω_0 ;
10. Calculation of the initial velocities and positions (obtained from an undamped system);

CYCLE

11. Law of motion:
 - a) Calculation of new velocities;
 - b) Calculation of new positions;
 - c) Calculation of displacements;
 - d) Update of the velocities and positions.
12. Law of forces:
 - a) Calculation of overlap;
 - b) Calculation of contact position;
 - c) Calculation of contact velocity;
 - d) Calculation of incremental contact displacement;
 - e) Calculation of incremental contact forces;
 - f) Calculation of total contact forces;
 - g) Calculation of total particle forces;
 - h) Updates of the total particle forces.
13. Recalculation of critical timestep or scaled masses;
14. Recalculation of natural frequency, ω_0 ;
15. Check convergence criteria (unbalanced force or displacement criteria). If convergence is reached, exit; otherwise, go to 11.

OUTPUT

The proposed fast numerical procedure is summarized in the following steps:

1. Generation of particle assembly (rectangular or hexagonal);
2. Definition of contacts;
3. Definition of boundary and loading conditions;
4. Definition of real or scaled masses;
5. Calculation of the critical timestep or the scaled masses;
6. Definition of the stopping criteria (maximum simulation time or maximum number of steps);
7. Set type of damping;
8. Set constitutive law;
9. Calculation of the initial velocities and positions (obtained from an undamped system);
10. Start the cycle for time-dependent behaviour:
 - a) Setting creep time, $T_i = 0$, creep time increment, ΔT and maximum creep time of analysis, T_{max} :

CYCLE

- b) Starting the cycle for dynamic relaxation, considering DR time, t and a DR timestep, Δt :
 - i. Law of motion:
 - A. Calculates new velocities;
 - B. Calculates new positions;
 - C. Calculates displacements;
 - D. Update velocities and positions.
 - ii. Law of forces:
 - A. Calculates overlap;
 - B. Calculates contact position;
 - C. Calculates contact velocity;
 - D. Calculates incremental contact displacement;
 - E. Calculates incremental contact forces;
 - F. Calculates total contact forces;
 - G. Calculates total particle forces;

- H. Updates total particle forces.
 - iii. Recalculation of critical timestep or scaled masses;
 - iv. Recalculation of natural frequency, ω_0 ;
 - v. Checking convergence criteria (unbalanced force or displacement criteria).
- If convergence is reached, exit. Otherwise, go to i).

OUTPUT

- c) Increase of time to T_{i+1} . If $T_{i+1} \geq T_{max}$, exit. Otherwise, return to b).
- d) Calculation of viscoelastic displacement increment, ΔU_{visco} , for T_{i+1} ;
- e) Calculation of incremental contact force, ΔF_c , add to the contact force, F_c ;

The output files are composed by ".dad" file types with the results obtained for the control particles, including particle ID, step, time, particle position, particle velocity and particle forces, a ".info" file with the information about the analysis and ".vtk" files for the graphical representation of the system.

Figure C.2 shows the structure used for the code implementation using C++. The definition of classes "Particle" and "Contact" within the "Domain" allows for the use of object-oriented programming and for each problem "Particle" and "Contact" objects are created were their properties and specific "functions" are predefined.

The Particle.cls class file includes the properties regarding the rigid particles, such as the radius, the specific mass, the position (displacements and rotations) the linear velocities and angular velocities and defines functions to deal with those properties. The Contact.cls class file defines the properties and functions related to the interaction of two particles, such as the ID of particle A and particle B, the contact normal and shear stiffness.

The global functions are defined in the Domain.cls class file which controls the SETUP, CYCLE and OUTPUT phases. In the CYCLE phase, the domain class calls the law of motion and the law of forces functions for each timestep until the convergence criteria is reached.

In the OUTPUT phase the main results for a set of particles ($ID = N$) and contacts ($ID = M$) are written into ASCII files (..._part_ID_N.dad and ..._cont_ID_M.dad). The results are also written in .vtk format for the representation into a graphical view using, for example, the ParaView software (Ayachit 2005).

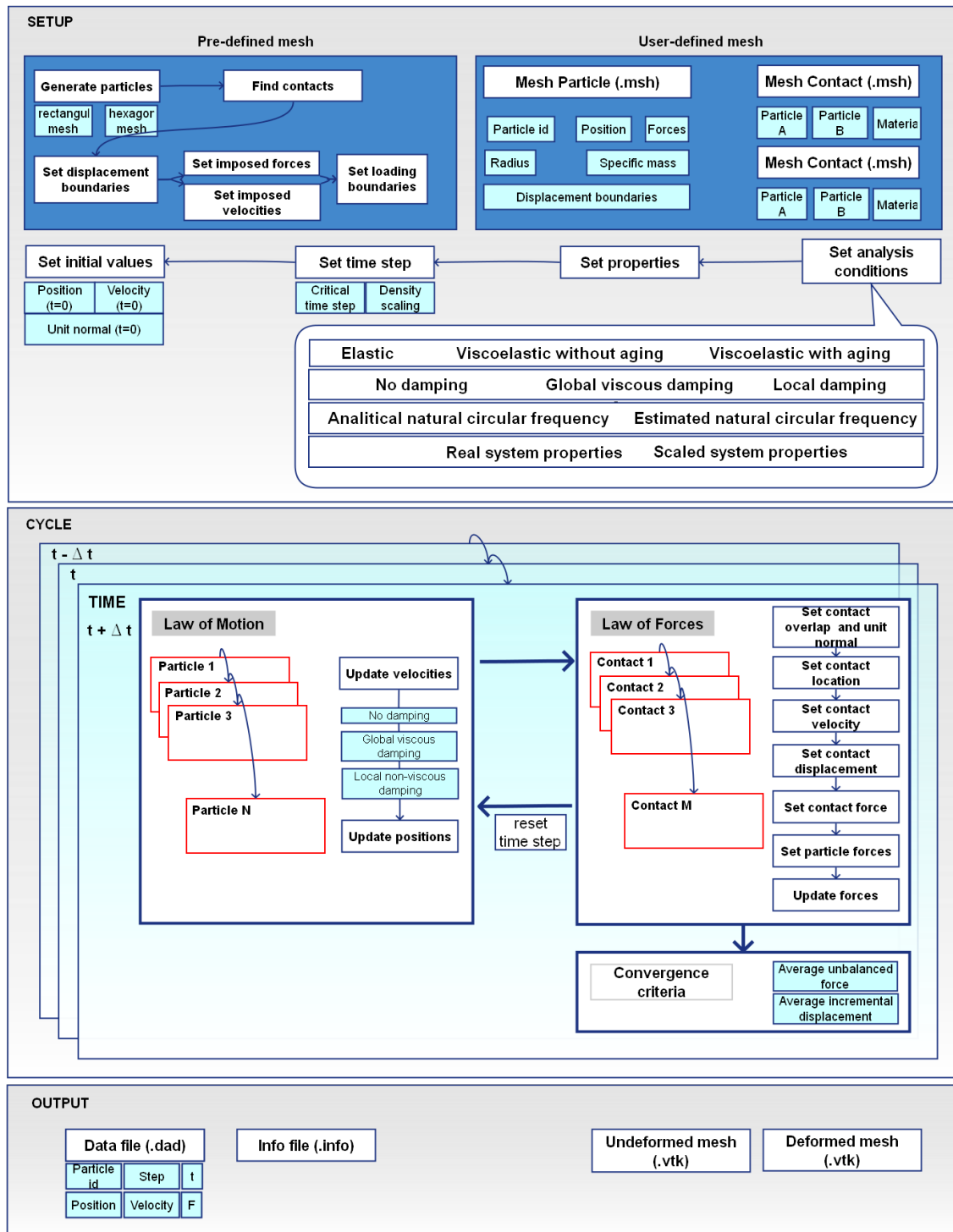


Figure C.1: C++ discrete element method code flowchart

APPENDIX C. C++ COMPUTATIONAL STRUCTURE OF THE 2D PARTICLE MODEL FOR THE BEHAVIOUR ANALYSIS

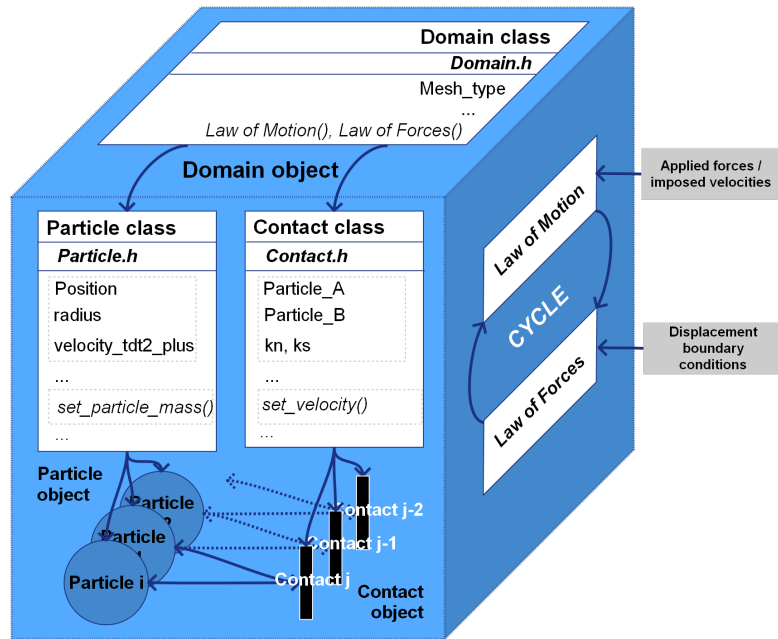


Figure C.2: C++ classes